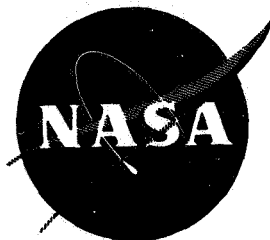


K fa #

APD

NASA CR-72555
AVSD-0306-69-RR

N69-34989



ISOTOPE REENTRY VEHICLE DESIGN STUDY
PRELIMINARY DESIGN - PHASE II - FINAL REPORT

Prepared for
NATIONAL AERONAUTICS AND SPACE ADMINISTRATION

Contract NAS 3-10938

**CASE FILE
COPY**

AVCO CORPORATION
AVCO GOVERNMENT PRODUCTS GROUP
201 Lowell Street
Wilmington, Massachusetts 01887

NOTICE

This report was prepared as an account of Government sponsored work. Neither the United States, nor the National Aeronautics and Space Administration (NASA), nor any person acting on behalf of NASA:

- A.) Makes any warranty or representation, expressed or implied, with respect to the accuracy, completeness, or usefulness of the information contained in this report, or that the use of any information, apparatus, method, or process disclosed in this report may not infringe privately owned rights; or
- B.) Assumes any liabilities with respect to the use of, or for damages resulting from the use of any information, apparatus, method or process disclosed in this report.

As used above, "person acting on behalf of NASA" includes any employee or contractor of NASA, or employee of such contractor, to the extent that such employee or contractor of NASA, or employee of such contractor prepares, disseminates, or provides access to, any information pursuant to his employment or contract with NASA, or his employment with such contractor.

Requests for copies of this report should be referred to

National Aeronautics and Space Administration
Office of Scientific and Technical Information
Attention: AFSS-A
Washington, D.C. 20546

NASA CR-72555
AVSD-0306-69-RR

ISOTOPE REENTRY VEHICLE DESIGN STUDY

PRELIMINARY DESIGN - PHASE II - FINAL REPORT

Prepared for

NATIONAL AERONAUTICS AND SPACE ADMINISTRATION

by

Richard L. Ryan
John W. Graham

August 1969

Contract NAS 3-10938

TECHNICAL MANAGEMENT
NASA LEWIS RESEARCH CENTER
Cleveland, Ohio

BRAYTON CYCLE BRANCH
LLOYD I. SHURE

AVCO CORPORATION
AVCO GOVERNMENT PRODUCTS GROUP
201 Lowell Street
Wilmington, Massachusetts 01887

ABSTRACT

This document summarizes the Phase II preliminary design effort on the Isotope Reentry Vehicle (IRV) study. The major objective of the entire study (Phases IA, IB, and II) was to develop a preliminary design of a 25 kw_t PU 238 IRV. Primary emphasis was placed on safety considerations and developability in the design.

The Phase II study followed two previous efforts of the program, i.e., Phases IA and IB. During Phase IA various IRV, heat source, and heat source exchanger concept combinations were developed and evaluated. During Phase IB, three of the more promising combinations resulting from Phase IA were further evaluated at the conceptual design level. The results were then used to select a reference concept for preliminary design in Phase II.

EDITED BY:
EDITORIAL SERVICES SECTION
W. H. Barber

ACKNOWLEDGEMENT

This report, Isotope Reentry Vehicle Design Study - Phase II - Preliminary Design Final Report, was prepared by the Applied Technology Division*, Lowell, Mass., of the Avco Government Products Group, under NASA Contract NAS 3-10938. The study was performed for the Brayton Cycle Branch of the NASA Lewis Research Center, Cleveland, Ohio. Mr. Lloyd Shure, the NASA-Lewis Program Manager, provided valuable assistance and guidance in developing the study.

This report covers the Preliminary Design work completed under Phase II of the study. R. L. Ryan, of the Space Systems Directorate, was the Avco Project Manager. The study was conducted as a cooperative effort with support furnished by various technical specialists from the division's line engineering departments. Principal contributors and their specialties areas were as follows:

S. Georgiev	- Study Management
J. Graham	- Associate Program Manager and Thermal Analysis
D. Henderson	- Systems and Safety Analysis Task Leader
A. Laber	- Vehicle Design and Spacecraft Integration
B. Morgan	- Aerodynamics Analysis
H. Steinle	- Thermal Control
R. E. Wagner	- Aerodynamics Analysis
R. Wray	- Structural Analysis
O. Zappa	- Aerodynamics Task Leader

The design and supporting analyses of the Heat Source were performed by the Westinghouse Astronuclear Laboratory under a subcontract to Avco. R. Lochbaum was the Westinghouse project engineer for the IRV study.

The Garrett Airesearch, Los Angeles Division, developed the design for the Heat Source Heat Exchanger under subcontract to Avco. Mr. Murray Coombs was the Garrett Airesearch project engineer.

Acknowledgement is also made to Goodyear Aerospace for providing support in the area of ballute design.

Avco also wishes to acknowledge the valuable assistance furnished during the study by the following NASA personnel: V. Peterson - Ames Research Center, H. S. Bloomfield - Lewis Research Center, and P. J. Bobbitt - Langley Research Center; and by Mr. R. W. Hunke, Sandia Corporation.

The Avco report number is AVSD-0306-69-RR.

Approved: R. L. Ryan
R. L. Ryan
IRV Project Manager

*Formerly the Space Systems Division

CONTENTS

1.0	INTRODUCTION	1
2.0	SUMMARY	2
2.1	Phase IA -- Conceptual Design Summary	7
2.2	Phase IB -- Conceptual Design Summary	7
2.2.1	Isotope Reentry Vehicle (IRV)	14
2.2.2	Heat Source (HS)	17
2.2.3	Heat Source Heat Exchanger (HSHX)	22
2.2.4	Summary of Conclusions and Recommendations (Phase IB)	26
2.3	Phase II -- Preliminary Design Summary	29
2.3.1	Heat Source (HS)	33
2.3.2	Isotope Reentry Vehicle (IRV)	38
2.3.3	Heat Source Heat Exchanger (HSHX)	41
2.4	Conclusions and Recommendations	49
2.5	References	49
3.0	IRV PRELIMINARY DESIGN	51
3.1	Systems Analysis	51
3.1.1	Design Requirements	52
3.1.2	Drag Augmentation System	70
3.1.3	Location Aids	72
3.1.4	Safing, Arming, and Initiation System	73
3.2	Reentry Performance Analysis	77
3.2.1	Heating and Loads Summary	79
3.2.2	Analysis and Results	83
3.2.2.1	Aerodynamic Heating	85
3.2.2.1.1	Forebody Heating	85
3.2.2.1.2	Capsule Heating	89
3.2.2.1.3	Fence Heating	95
3.2.2.2	Dynamic Stability Analysis	107
3.2.2.2.1	Vehicle Entry Dynamics	107
3.2.2.2.2	Wind and Gust Effects	112
3.3	Heat Source Design	117

CONTENTS (Cont'd)

3.3.1	Heat Source Thermal Performance	117
3.3.1.1	Introduction	117
3.3.1.2	Summary of Heat Source Thermal Analysis	118
3.3.1.3	Two Dimensional Thermal Model of Heat Source	121
3.3.1.4	Launch Pad Operation	125
3.3.1.5	Steady State -- Space Operation of IRV Heat Source	130
3.3.1.6	Transient Studies -- Space	135
3.3.2	Heat Source Mechanical Design	154
3.3.2.1	Design Environment	154
3.3.2.2	Heat Source Material Selection	156
3.3.2.3	Structural Performance -- Heat Source Plate ...	171
3.3.2.4	Dynamic Analysis of the Heat Source	174
3.3.3	ACHX Design	176
3.3.3.1	Mechanical Description	176
3.3.4	Insulation Subsystem	185
3.3.4.1	Thermal Insulation Design	185
3.3.4.2	Insulation Support Plate Structure	187
3.3.4.3	Insulation System Heat Loss	191
3.3.5	Truss Subsystem	191
3.3.5.1	Mechanical Design	191
3.3.5.2	Structural Analysis	194
3.3.6	Heat Source Preliminary Design	197
3.3.6.1	Heat Source Plate Assembly	197
3.3.6.2	Thermal Insulation Assembly	207
3.3.6.3	Heat Source Structural Support System	211
3.3.6.4	Insulation and Support Structure Assembly	211
3.4	Isotope Reentry Vehicle (IRV)	215
3.4.1	Reentry Vehicle	217
3.4.1.1	Heat Shield	217
3.4.1.1.1	Design Considerations	217
3.4.1.1.2	Reference Design	218

CONTENTS (Cont'd)

3.4.1.2	Aeroshell Structure	224
3.4.1.2.1	Structural Load Requirements	224
3.4.1.2.2	Aeroshell Structural Design	225
3.4.1.2.3	Dynamic Analysis of IRV Aeroshell ...	227
3.4.2	Thermal Control	229
3.4.2.1	Normal Operation	229
3.4.2.1.1	Summary of Ground Rules and Assumptions	232
3.4.2.1.2	Analytical Model and Expressions	232
3.4.2.1.3	Thermal Control Coating Selection ...	238
3.4.2.1.4	Summary of Results	239
3.4.2.1.5	Conclusions	239
3.4.2.2	Pad Fire Analysis	242
3.4.2.3	Upside-down Landing	242
3.4.3	Isotope Reentry Vehicle Preliminary Design	250
3.5	References	252
4.0	HEAT SOURCE HEAT EXCHANGER (HSHX)	259
4.1	HSHX Design	259
4.1.1	Description	259
4.1.2	Materials Selection	262
4.1.3	Fabrication	275
4.2	Analysis and System Performance	277
4.2.1	Pressure Drop and Flow Distribution	277
4.2.2	Heat Source	288
4.3	Insulation System	297
4.3.1	Description	297
4.3.2	Material Performance and Selection	297
4.3.3	Heat Leaks	206
4.4	Structural Considerations	306
4.4.1	Introduction	306
4.5	Engineering Drawings	320
4.6	References	320

CONTENTS (Cont'd)

5.0	IRV SYSTEM INTEGRATION	327
5.1	Brayton Cycle Power System	327
5.1.1	Cycle Description	327
5.1.2	System Components	329
5.1.3	System Performance	341
5.2	IRV/Brayton Cycle/Spacecraft Integration	341
5.2.1	General Installation Requirements	346
5.2.1.1	Component Attachment and Support	346
5.2.1.2	Abort and Deorbit Mechanization	350
5.2.1.3	Emergency Cooling Methods	356
5.2.2	MORL Installation	359
5.3	Ground Handling Requirements	361
5.3.1	Fuel Capsules	361
5.3.2	Heat Source Plate Assembly and Facilities	363
5.3.3	ACHX Requirements	364
5.3.4	Fuel Capsule Loading	364
5.3.5	Launch Vehicle Integration	367
5.3.6	ACHX Launch Pad Hook-up and Installation	370
5.4	References	373

APPENDIXES

A.	HEAT SOURCE AND SUPPORT SYSTEM	375
A1.0	STRUCTURAL ANALYSIS OF HEAT SOURCE PLATE	375
A1.1	Plate as a Whole	375
A1.2	ACHX Header Panels	377
A1.3	BeO Retension Panels	378
A1.4	Internal Ribs	378
A1.5	Retention Bolt for Top Cover	379
A1.6	Support Plate Lock Pin Assembly	379
A1.7	ACHX Header Outlet Pipe Load Limitations	380
A2.0	DYNAMIC ANALYSIS OF HEAT SOURCE AND SUPPORT SYSTEM	381
A2.1	Heat Source Plate Flexural Resonant Frequency	381
A2.2	Strut Lateral Resonant Frequency	382
A2.3	Lateral Resonance of Truss/Heat Source	382
A2.4	Vertical Vibratory Resonance of Heat Source on Truss	383
A2.5	Vibratory Stresses in IRV Strut	384

CONTENTS (Concl'd)

A3.0	STRUCTURAL ANALYSIS OF TRUSS SUBSYSTEM AND SUPPORT SYSTEM	386
A3.1	Struts	386
A3.2	Support Ring and Tie-Plate Analysis	389
A3.3	Strut-Ring-Bolts-to-Shear on Impact	395
A3.4	Truss Bending Stress Due to Heat Source Plate Expansion	396
B.	STRUT HEAT LOSS	399
C.	HEAT SOURCE FABRICATION PLAN	407
C1.0	INTRODUCTION	407
C2.0	MANUFACTURING DESCRIPTION	408
C2.1	Support Structure	408
C3.0	HEAT SOURCE PLATE	412
C3.1	Description	412
C4.0	COVER AND FUEL PLATE ASSEMBLY	417
C4.1	Description	417
C5.0	INSULATION ASSEMBLY	419
C6.0	FINAL ASSEMBLY	419

ILLUSTRATIONS

Figure	1-1	Isotope Reentry Vehicle Reference Design	2
	1-2	Cross Section of Fuel Capsules	3
	1-3	Brayton Cycle Power Conversion Module	4
	1-4	Heat Source Heat Exchanger System	4
	2-1	IRV 49-inch-Diameter Planar Array	18
	2-2	IRV 39-inch-Diameter Pin Cushion Array	19
	2-3	Cold Plate Concept with Recessed Corner	20
	2-4	Mechanical Details of Pin Cushion Array	23
	2-5	Vented Capsule Retention -- 46-inch-Diameter Planar Array	24
	2-6	IRV/Brayton Cycle/Atlas-Centaur Integration	28
	2-7	Basic IRV/Brayton Cycle System in a Typical Spacecraft Installation	31
	2-8	Exploded View of the Heat Source Plate	34
	2-9	Design Reentry Conditions	39
	2-10	IRV Preliminary Design Layout	42
	2-11	Two-Pass Involute Tubular HSHX (Final Configuration)	45
	2-12	Typical HSHX Insulation and Support Concept	46
	3-1	Deorbit and Abort Rocket Integration Concepts	56
	3-2	Deorbit System Considerations	57
	3-3	Launch Pad and Early Abort Sequence	60
	3-4	Fireball Thermal Environment	61
	3-5	Design Reentry Conditions	61
	3-6	Ascent Abort -- MORL	65
	3-7	Cold Plate Concept with Recessed Corner	67
	3-8	IRV Rotational Impact Attenuation System Concept	68

ILLUSTRATIONS (Cont'd)

Figure	3-9	Reference Design for Weight and Diameter Tradeoff Study -- With Crushup	69
	3-10	Ballute in Deployed Condition	71
	3-11	Safing, Arming, and Initiation System Schematic	75
	3-12	Phase II Aerodynamic Configuration	84
	3-13	Aeroshell Heating Factor Variation with Angle of Attack	86
	3-14	Aeroshell Station Location	87
	3-15	Forebody Heating Factors	88
	3-16	Forebody Heating -- Nominal Reentry Mode	90
	3-17	Forebody Heating -- Tumbling Reentry Mode	91
	3-18	Forebody Heating -- Rearward Reentry Mode	91
	3-19	Forebody Heating -- Nominal Spinning Reentry Mode	92
	3-20	Forebody Heating -- Rearward Spinning Reentry Mode	92
	3-21	Capsule Heating Distributions -- Phase II Fences	93
	3-22	Worst Capsule Heating Factor, Angle-of-Attack Variation -- Phase II Fences	94
	3-23	Effect of Dynamic Motion on Worst Capsule Heating Factors	94
	3-24	Worst Capsule Heating -- Nominal Reentry Mode	96
	3-25	Worst Capsule Heating -- Tumbling Reentry Mode	97
	3-26	Worst Capsule Heating -- Rearward Reentry Mode	97
	3-27	Worst Capsule Heating -- Nominal Reentry Mode (Offset c.g.)	98
	3-28	Worst Capsule Heating -- Rearward Spinning Reentry Mode	98
	3-29	Worst Capsule Heating -- Rearward Spinning Reentry Mode	99

ILLUSTRATIONS (Cont'd)

Figure	3-30	Worst Capsule Heating -- Rearward Spinning Reentry Mode	99
	3-31	Worst Capsule Heating -- Rearward Spinning Reentry Mode	100
	3-32	Worst Capsule Heating -- Deorbit Error Analysis	101
	3-33	Worst Capsule Heating Dependence on Fence Turnaround Effectiveness -- Retro System Failure Mode	102
	3-34	Maximum Worst Capsule Heating Dependence on Fence Turnaround Effectiveness -- Retro System Failure Mode	102
	3-35	Worst Capsule Heating -- Rearward Spinning Reentry Mode	103
	3-36	Fence Heating Factors -- Midpoint of the Flare and at the Hole	104
	3-37	Fence Heating Factors -- Dynamic Modes	105
	3-38	Fence Heating Factors -- Hole	105
	3-39	Fence Heating Factors -- Flare	106
	3-40	Fence Heating Factors -- Rearward Spinning	106
	3-41	IRV Aerodynamic Moment Characteristics	108
	3-42	IRV Hypersonic Axial Force Coefficient	108
	3-43	IRV Hypersonic Normal Force Coefficient	109
	3-44	Angle-of-Attack Envelope Histories -- Controlled Reentry	110
	3-45	Angle-of-Attack Envelope Histories -- Uncontrolled Reentry	111
	3-46	Angle-of-Attack Envelope Histories -- Effect of Turnaround Moment	111
	3-47	Wind Profile Data	113
	3-48	Gust Velocity Data	113
	3-49	Gust Factor Data	114

ILLUSTRATIONS (Cont'd)

Figure	3-50	Gust Duration Data	114
	3-51	Design Gust Velocity Data	115
	3-52	Effect of Wind Gust on Vehicle Attitude at Impact	116
	3-53	Two-Dimensional Thermal Model of Heat Source	119
	3-54	Heat Source Temperature History	120
	3-55	Heat Source Thermal Model	123
	3-56	ACHX Operation Temperature Distribution at Channel Exit for a 2-mil Air Gap	127
	3-57	Heat Source Temperature History after ACHX Disconnect	129
	3-58	Steady State Heat Source Radiating Temperature versus Maximum Capsule Temperature	132
	3-59	Steady State Temperature Profile at Heat Source Hot Spot	133
	3-60	HSHX Temperature Distributions (1st HSHX in Operation) ...	134
	3-61	Heat Source Steady State Temperature Distribution in Deployed State	136
	3-62	Heat Source Temperature History after Termination of HSHX Cooling without Contact Between BeO and Plate	138
	3-63	Heat Source Temperature History after Termination of HSHX Cooling	140
	3-64	Heat Source Temperature History Following Deployment from Normal Operation	142
	3-65	Worst Capsule Heat Source Temperature History -- Normal Reentry Mode	144
	3-66	Worst Capsule Heat Source Temperature History -- Tumbling Reentry Mode	146
	3-67	Worst Capsule Heat Source Temperature History -- Nominal Reentry Mode (Offset c.g.)	147
	3-68	Steady State Radiation Intensity	149
	3-69	Worst Capsule Heat Source Temperature History -- Rearward Reentry to Impact Mode (from Steady State Deployment)	150

ILLUSTRATIONS (Cont'd)

Figure	3-70	Comparison of 2D Model to the 1D Model for Calculation of IRV Reentry Temperature	152
	3-71	Tensile Strength versus Temperature for Cb-1Zr (Recrystallized Sheet)	158
	3-72	Larson-Miller Parameter Plot of Rupture Stress in Cb-1Zr	159
	3-73	Thermal Conductivity -- Cb-1Zr	160
	3-74	Specific Heat -- Cb-1Zr	161
	3-75	0.5 Percent Creep in TZM	162
	3-76	Free Energy of Formation of BeO and Columbian and Zirconium Oxides	163
	3-77	Specific Heat -- BeO	164
	3-78	Thermal Conductivity -- BeO	165
	3-79	Tensile Strength versus Temperature for Recrystallized T-111	167
	3-80	Larson-Miller Plot for T-111 -- Creep 1 Percent	168
	3-81	Specific Heat -- T-111	169
	3-82	Thermal Conductivity -- T-111	170
	3-83	Exploded View of the Heat Source Plate	172
	3-84	Schematic of ACHX	177
	3-85	Wall Effect of Orifice Pressure Drop on Channel Heat Loss	180
	3-86	Performance Map of Peak Capsule Temperature versus Total Mass Flow Rate	182
	3-87	ACHX Hydraulic Performance for a Peak Capsule Temperature of 171° F	183
	3-88	ACHX Orifice Holes Through Top Plate	184
	3-89	Heat Source Insulation Detail	186
	3-90	Planar Heat Source for Multi-foil Insulation	189

ILLUSTRATIONS (Cont'd)

Figure	3-91	Edge Thermal Losses for Multi-foil Insulation	190
	3-92	Heat Source Support Structure -- Overall View	192
	3-93	Heat Source Support Structure -- Detail View	193
	3-94	IRV Assembly	198
	3-95	Heat Source Plate Assembly	199
	3-96	Heat Source Details	200
	3-97	Cross-Section of Heat Source Plate	203
	3-98	Cover Plate	204
	3-99	Longitudinal Section Detail of Heat Source Fuel Plate Assembly	205
	3-100	Lewis Research Center Reference Fuel Capsule	206
	3-101	Typical BeO Heat Sink Section and Retaining Plate	208
	3-102	Cross-Section Detail of Heat Source Fuel Plate Assembly	209
	3-103	Thermal Insulation Assembly Barrier	210
	3-104	Heat Source Insulation Detail	212
	3-105	Heat Source Structural Support System	213
	3-106	Heat Source Support Structure -- Detail View	214
	3-107	Cross Section of Heat Source Assembly	216
	3-108	Typical Aeroshell Bondline Temperature, Avcoat 5026-39 HC-G, Stagnation Point	220
	3-109	IRV Heat Shield Requirements, Avcoat 5026-39 HC-G, Out of Orbit Reentry	220
	3-110	IRV Heat Shield Requirements, Avcoat 5026-39 HC-G, Out of Orbit Reentry	221
	3-111	Typical Temperature History, Avcoat 5026-39 HC-G, Stagnation Point, Out of Orbit Reentry	221
	3-112	3D Graphite Fence Temperatures Midpoint of Fence -- Rearward Spinning Reentry Mode	223

ILLUSTRATIONS (Cont'd)

Figure	3-113	IRV Fence Heating Midpoint of the Fence for 0.30-inch Thick Thornel 3D Graphite -- Rearward Spinning Reentry Mode	223
	3-114	IRV Aeroshell Model for Vibration Analysis	228
	3-115	Vibration Mode Description for Each Harmonic Number, n ...	230
	3-116	IRV First Natural Frequency as a Function of Harmonic Number	230
	3-117	IRV Aeroshell Modal Displacements Zeroth and First Harmonics	231
	3-118	IRV Aeroshell Modal Displacements Second and Third Harmonics	231
	3-119	Reference Design -- Normal Operation	233
	3-120	Orbital Geometry and Incident Heat Loads -- Normal Operation	234
	3-121	Incident Radiation versus True Anomaly for Reference Orbit -- Normal Operation	235
	3-122	Steady State Temperature Distribution for Aluminum Aeroshell, Reference Orbit -- Normal Operation	240
	3-123	Comparison of Aluminum and Titanium Aeroshell, Sun and Space Exposure -- Normal Operation	241
	3-124	Heat Source Temperature History -- Fireball	245
	3-125	Upside-down Landing and Post Impact Temperature History	248
	3-126	Upside-down Landing and Post Impact Temperature History -- 6-hour Exposure	249
	3-127	IRV with Ballute and Location Aids -- 68-inch Diameter Reference Design	251
	3-128	Detail of Truss Aeroshell Attachment Point	253
	4-1	Two-Pass Tubular HSHX -- Final Configuration	260
	4-2	HSHX Assembly	261
	4-3	Involute Tube Geometry	262

ILLUSTRATIONS (Cont'd)

Figure	4-4	Material Evaporation Rates in Vacuum	264
	4-5	Evaporation Problem of Materials in Vacuum Using an Evaporation Sequence for Thin Specimens of Type 316 Stainless Steel Exposed to High Vacuum Between 1475° and 1835° F as an Example	266
	4-6	Tensile Yield Strength versus Temperature of Candidate Alloys	268
	4-7	Elongation versus Temperature for Candidate Alloys	269
	4-8	Rupture Strength for Candidate Materials at 1700° F	270
	4-9	Mean Coefficient of Thermal Expansion	271
	4-10	Fabrication of Core	278
	4-11	Fabrication of Return Manifold	279
	4-12	Fabrication of Inlet Manifold	280
	4-13	Fabrication of Outlet Manifold	281
	4-14	Welding Heat Exchanger Tubes to Return Manifold	282
	4-15	Welding Heat Exchanger Tubes to Inlet and Outlet Manifolds	283
	4-16	Joining of Heat Exchanger Tubes to Form Core Brazing of Boss to Inlet Manifold	284
	4-17	Typical Fabrication and Assembly Sequence	285
	4-18	Steady-State Performance Circular Planar Heat Source	290
	4-19	Thermal Model for Involute Heat-Source Heat Exchanger	291
	4-20	Schematic of the Brayton Cycle Space Power Plant	293
	4-21	Gas Inlet Temperature to HSHX During Startup	294
	4-22	Time History of the Gas Outlet Temperature During the Startup of HSHX 2	295
	4-23	Response of the Maximum Effective Source Temperature During the Startup of HSHX 2	298

ILLUSTRATIONS (Cont'd)

Figure	4-24	Involute Heat-Source Heat Exchanger Performance (Heat Exchanger 2 in Operation)	299
	4-25	Gas Outlet Temperature During Startup of HSHX 1	300
	4-26	Response of the Maximum Effective Source Temperature During Startup of HSHX 1	300
	4-27	Heat-Source Heat Exchanger Steady-State Performance (Heat Exchanger 1 in Operation) (48-in. dia.)	302
	4-28	HSHX Component Temperature Distributions	303
	4-29	Turbine Inlet Temperature versus Power Output	304
	4-30	Assumptions for Heat Leak Estimates	305
	4-31	Planar Heat Flux Test Results (Mo-THO ₂ Insulation, Brush Coated, Zero Loading)	307
	4-32	Average Effective Thermal Conductivity Between Source and Sink Temperatures (Planar Mo-THO ₂ Insulation)	308
	4-33	Cylindrical Heat Flux Test Results (Mo-THO ₂ Insulation, Spray Coated, Zero Loading)	309
	4-34	Planar Heat Flux Test Results (W-THO ₂ Insulation, Spray Coated, Pressure Loading, 40- and 100- Layer Samples)	310
	4-35	Thermal Conductivity Comparison	311
	4-36	Heat Leak Estimates	312
	4-37	Tube-to-Header Transition Region	317
	4-38	Schematic of Time-Temperature Transient Occurring When Gas Flow is Initiated.....	318
	4-39	Assumed Tube Elastic-Plastic Cycle for 500° F Temperature Difference Between the Inlet Header and the Tube Array	319
	4-40	HSHX Assembly	321
	4-41	HSHX Tube	322
	4-42	HSHX Manifold, Inlet	323

ILLUSTRATIONS (Cont'd)

Figure	4-43	HSHX Manifold, Outlet	324
	4-44	HSHX Manifold, Return	325
	4-45	HSHX Cap, Manifold, Return	326
	5-1	Power System Schematic Diagram	328
	5-2	Schematic Diagram of Pu ²³⁸ Brayton Power Plant (Reference 25 kw _t source; Nominal 7 kw Rating)	330
	5-3	Brayton Power System Components (NASA Engine B)	331
	5-4	Brayton Cycle Heat Exchanger Unit No. 1 -- Complete Assembly	333
	5-5	Brayton Rotating Unit (BRU)	334
	5-6	Typical HSHX for Isotope Heat Source (25 kw _t)	336
	5-7	Brayton Cycle Conversion Module	337
	5-8	Brayton Cycle Power Conversion Module with Typical HSHX Installation	337
	5-9	Electrical Subsystem Schematic Diagram	338
	5-10	Heat Rejection Subsystem Schematic Diagram	340
	5-11	Typical Radiator Configuration	342
	5-12	Turbine Inlet Temperature versus Power Output	343
	5-13	Turbine Inlet Temperature versus Power Output (Typical Only)	344
	5-14	IRV/Brayton Cycle/Atlas-Centaur Integration	345
	5-15	Typical IRV/Brayton Cycle/Spacecraft Integration	347
	5-16	Perspective View of the IRV and HSHX Configuration	348
	5-17	Launch Pad and Early Abort Sequence	351
	5-18	Ascent Abort -- MORL	352
	5-19	Orbital Abort and Mission Termination -- MORL Configuration	353

ILLUSTRATIONS (Concl'd)

Figure	5-20	IRV and Support Ring Assembly	355
	5-21	IRV/Support Ring Explosive Nut Assembly	357
	5-22	Detail View of Guide Rail Assembly	358
	5-23	MORL/IRV Integral Launch Configuration	360
	5-24	Fuel Capsule Loading Installation	365
	5-25	Retention System Assembly	366
	5-26	Heat Source Storage and Transfer Equipment	368
	5-27	Transfer of Heat Source Transporter to Gantry	369
	5-28	Heat Source Installation	371
	5-29	ACHX System Schematic -- IRV Heat Source	372
	B-1	Strut Heat Loss Model	400
	B-2	Strut Heat Losses versus Cold-side Temperature	401
	C-1	Manufacturing Plan Support Structure	409
	C-2	Heat Source Structural Support System	410
	C-3	Manufacturing Plan Heat Source Plate	411
	C-4	Thermal Insulation Assembly Barrier	413
	C-5	Manufacturing Plan Cover and Fuel Plate Assembly	418
	C-6	Manufacturing Plan Final Assembly	420

TABLES

Table	2-1	Program Ground Rules	8
	2-2	IRV Design Criteria	9
	2-3	Safety Criteria	10
	2-4	Characteristics Summary of Basic IRV Concepts	11
	2-5	Summary of Weight/Diameter Characteristics	12
	2-6	Phase IB Ground Rules	13
	2-7	Reference Vehicle Performance Comparison -- Circular Planar versus Pin Cushion Heat Sources	15
	2-8	IRV Weight/Diameter Summary	16
	2-9	Heat Source Summary Comparison	21
	2-10	HSHX Design Summary -- Phase IB	25
	2-11	HSHX Summary -- Phase IB	27
	2-12	Phase II Ground Rules	30
	2-13	Weight Summary -- IRV/Brayton Cycle System MORL	32
	2-14	Heat Source Preliminary Design Summary	35
	2-15	Thermal Design Criteria	36
	2-16	System Design Requirements	38
	2-17	IRV Heat Shield Requirements -- Avcoat 5026-39 HC-G	40
	2-18	IRV Performance Summary	43
	2-19	Mass Properties Summary for Reference Design -- Vehicle Diameter 68 inches	44
	2-20	HSHX Characteristics	47
	2-21	HSHX Steady State Performance Summary	48
	2-22	Conclusions	50
	3-1	Routine Launch Equipment	53
	3-2	IRV Subsystems	53

TABLES (Cont'd)

Table	3-3	Optional IRV Subsystems	53
	3-4	Safety Mechanisms	54
	3-5	Deorbit System Considerations	58
	3-6	System Design Requirements	63
	3-7	Rotation Concept	66
	3-8	Radiation Resistance -- Effect of Exposure on Yarn Strength	70
	3-9	Location Aid Candidates	72
	3-10	Location Aid and Drag Augmentation Data	73
	3-11	Trajectory Entry Data Summary for an Altitude of 400 kilofeet	81
	3-12	Design Aerodynamic Heating Summary	82
	3-13	Design Airloads Summary	83
	3-14	Heat Source Thermal Design Criteria	117
	3-15	Typical Cooling Air Requirements versus Gap Assumptions for Constant Peak Capsule Temperature	128
	3-16	Trajectories Used in Capsule Analysis	143
	3-17	Worst Capsule Reentry Heat Balance for Trajectory 9 ($R/R_B = 0.72$)	148
	3-18	Summary of Cover and Capsule Temperatures	151
	3-19	Structural Design Parameters	155
	3-20	Materials Property Data	171
	3-21	ACHX Performance Summary	181
	3-22	Heat Source Heat Loss Summary	194
	3-23	Heat Source Weight and Moment Summary	201
	3-24	Aeroshell Heat Shield Environment	217
	3-25	Summary of Heating Data Used in Heat Shield Design	219

TABLES (Concl'd)

Table	3-26	IRV Heat Shield Requirements -- Avcoat 5026-39 HC-G	222
	3-27	IRV Structural Load Environment	224
	3-28	Summary of Structural Requirements for Major Components	226
	3-29	Thermal Model, Properties, and Dimensions -- Normal Operation	236
	3-30	Ablator Coating System Summary	238
	3-31	Pad Fire Thermal Analysis and Design Data -- Case A, Heat Source Down	243
	3-32	Pad Fire Thermal Analysis and Design Data -- Case B, Heat Source Up	244
	3-33	Upside-down and Post Impact Thermal Analysis and Design Data	247
	3-34	Mass Properties Summary for Reference Design -- Vehicle Diameter 68 inches	254
	3-35	Isotope Reentry Vehicle (IRV) Performance Summary	255
	4-1	Shear Strength of Candidate Braze Alloys	274
	4-2	Pressure Drop Summary	288
	4-3	Cb-1Zr Allowable Stresses	314
	4-4	Heat Exchanger Pressure Containment Summary	315
	5-1	Weight Summary IRV/Brayton Cycle System -- Advanced MORL	362

1.0 INTRODUCTION

This report summarizes the results of the Phase II task of the Isotope Reentry Vehicle (IRV) Design Study. The study has been performed for the NASA Lewis Research Center under Contract NAS3-10938. The major objective of this study is to develop a preliminary design of a 25 kw_t (end-of-life) Pu 238 Heat Source IRV. Required operational lifetime is 5 years, and major design emphasis has been placed on system safety and vehicle developability. In addition, the IRV has been configured for minimum diameter and weight. The IRV is comprised of two major subsystems, the heat source (HS) and the reentry vehicle (R/V). A third major element that has been considered in the design study is the heat source heat exchanger (HSHX). The design of the HSHX is to be compatible with the characteristics of the Brayton Cycle Power Supply unit presently being investigated at the NASA Lewis Research Center. Westinghouse Astronuclear Laboratory has completed the required analysis and design of the Heat Source and its structural support system under subcontract to Avco. The Heat Source Heat Exchanger preliminary design has been developed under a subcontract from Avco by the Garrett Aircor, Los Angeles Division. Results of these subcontract efforts are summarized in this report.

Figure 1-1 shows a perspective view of the Isotope Reentry Vehicle (IRV) design developed under Phase II of the study. The isotope heat source consists of a circular planar array of refractory isotope capsules containing PuO₂ fuel. Approximately 164 nonvented capsules (Figure 1-2) are required to achieve a net thermal power output of 25 kw at the end of the 5 year lifetime. The isotope fuel capsule array together with its BeO heat sink is mounted on a refractory metal support plate. A refractory truss is used to attach the heat source subsystem to the aluminum honeycomb aeroshell. Low conductivity vacuum multifoil insulation is used to minimize heat loss to the reentry vehicle and temperature-sensitive subsystems.

Transfer of heat from the isotope heat source to the HSHX is accomplished solely by radiation. There is then no hard connection between the IRV/HS unit and the HSHX.

The HSHX is a part of the closed gas loop of the Brayton-cycle power conversion system. The major elements of the Brayton-cycle gas loop are contained in a package as illustrated in Figure 1-3. These elements consist of the Brayton cycle rotating unit (BRU) and the Brayton heat exchanger unit (BHXU), which consists of the recuperator and the heat-sink heat exchanger.

The elements of the HSHX system are illustrated in Figure 1-4. It is seen that the HSHX, ducts, structure, power conversion module (PCM) package, and insulation form a single integral unit.

Redundant and independently replaceable heat exchangers are provided to accept the thermal output of the heat source capsules which radiate with a maximum hot spot capsule temperature of less than 2000° F.

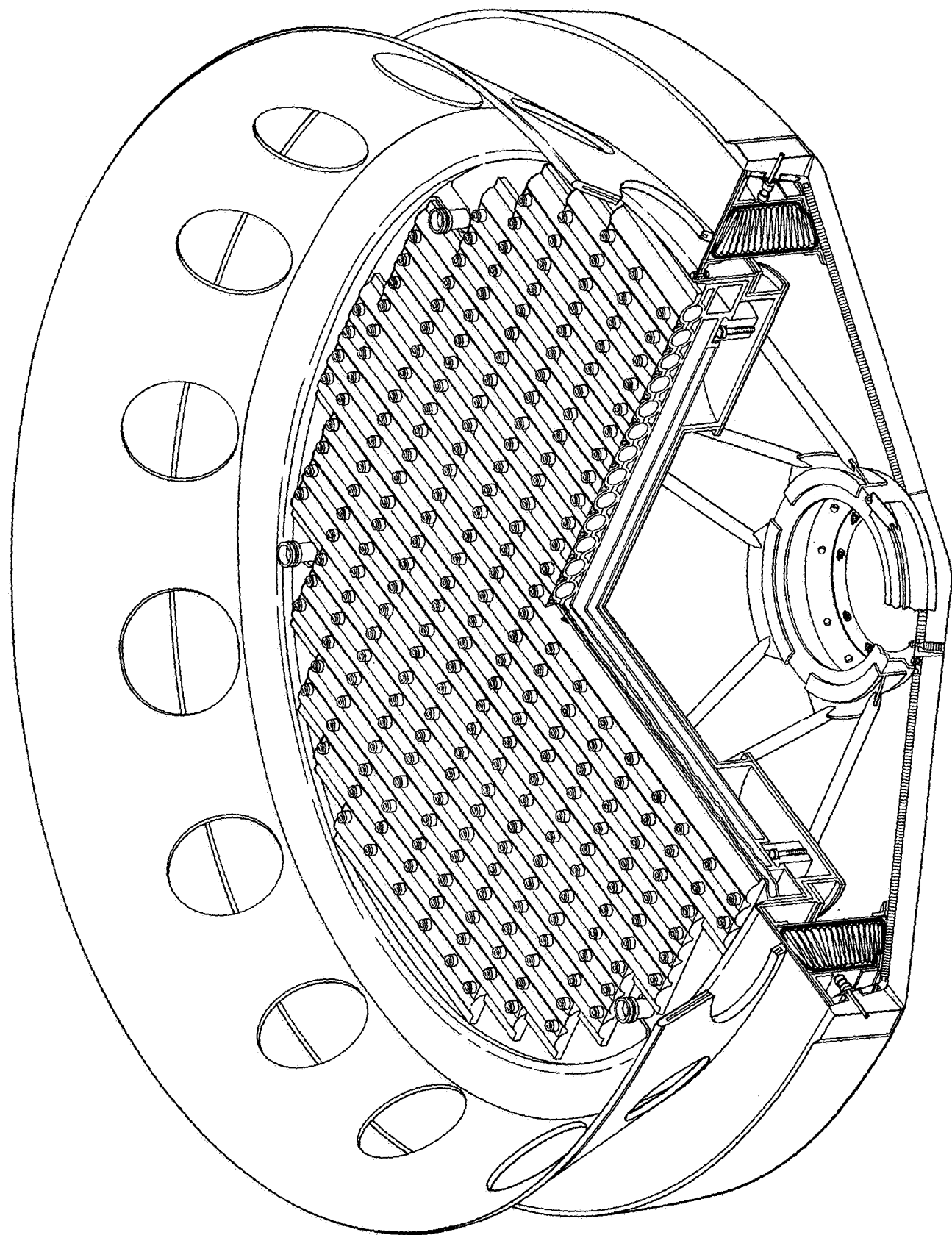
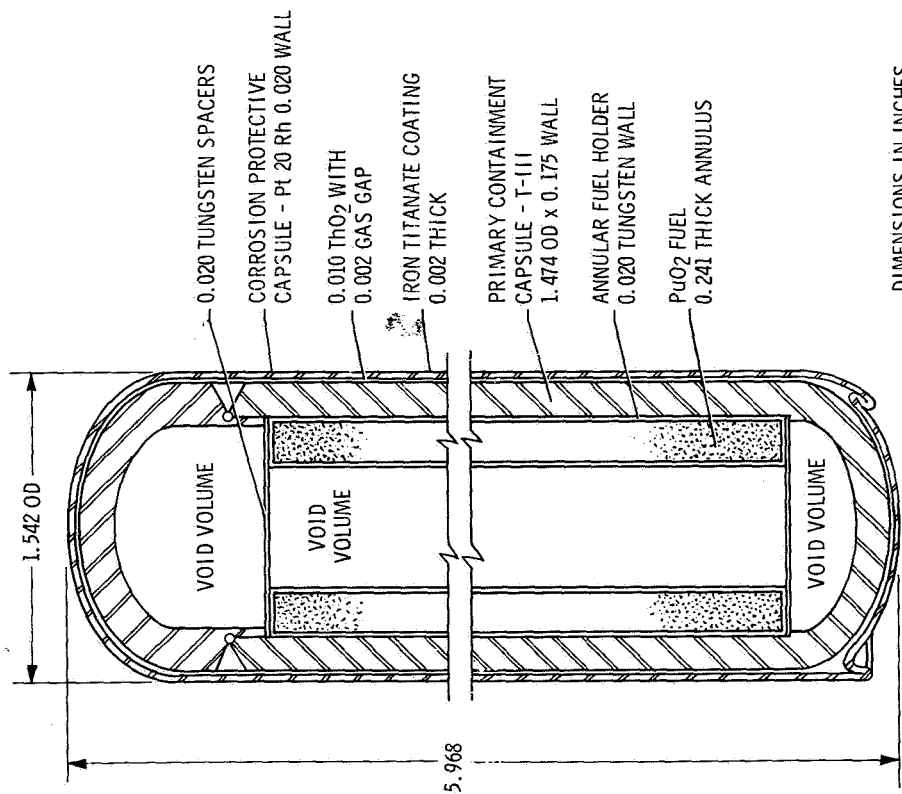
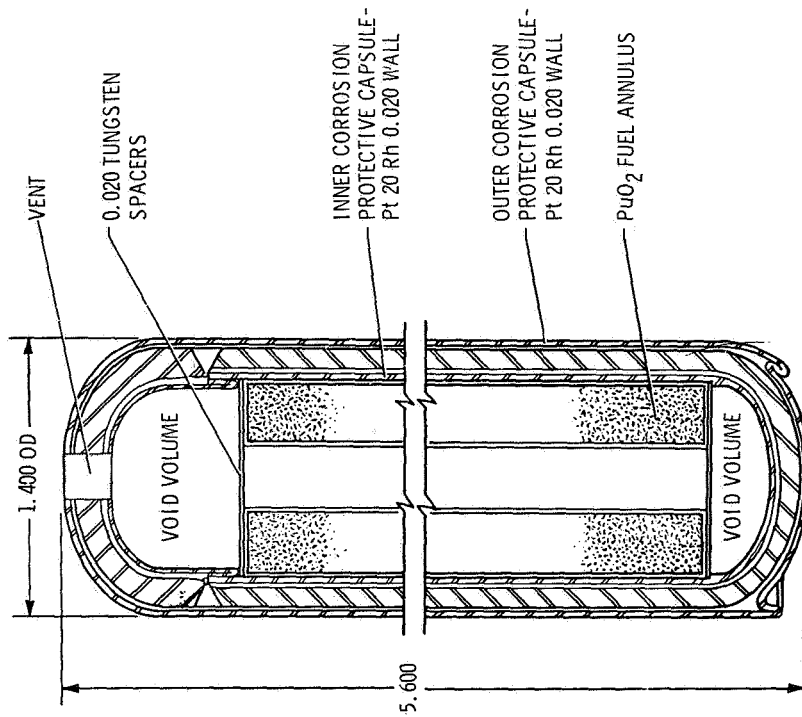


Figure 1-1 ISOTOPE REENTRY VEHICLE REFERENCE DESIGN



NON-VENTED CAPSULE DESIGN



VENTED CAPSULE DESIGN

Figure 1-2 CROSS SECTION OF FUEL CAPSULES

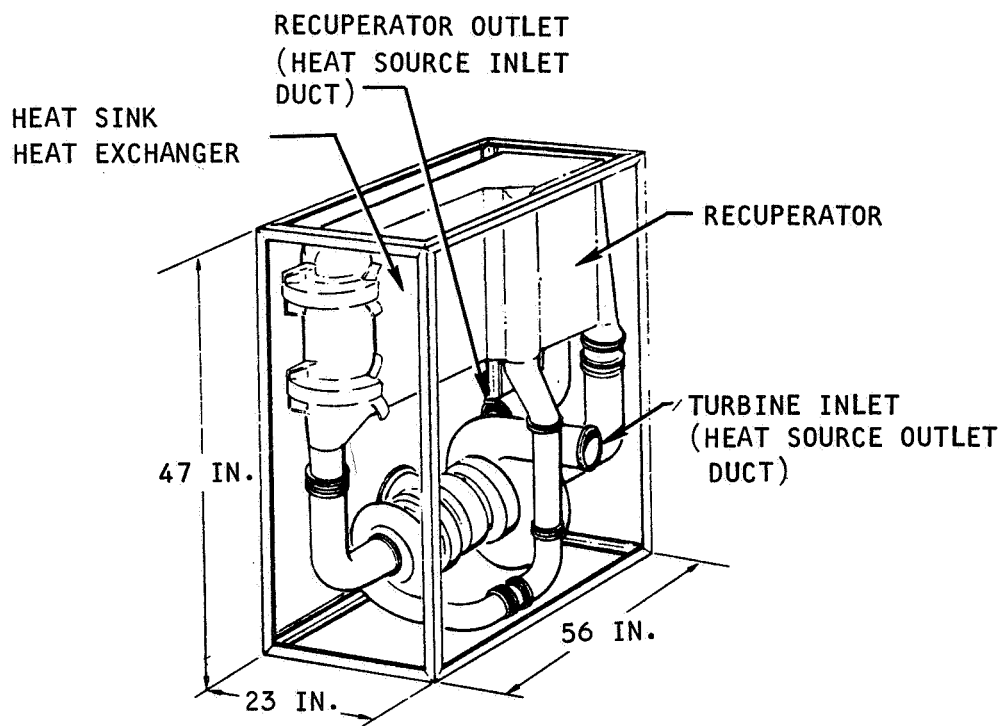
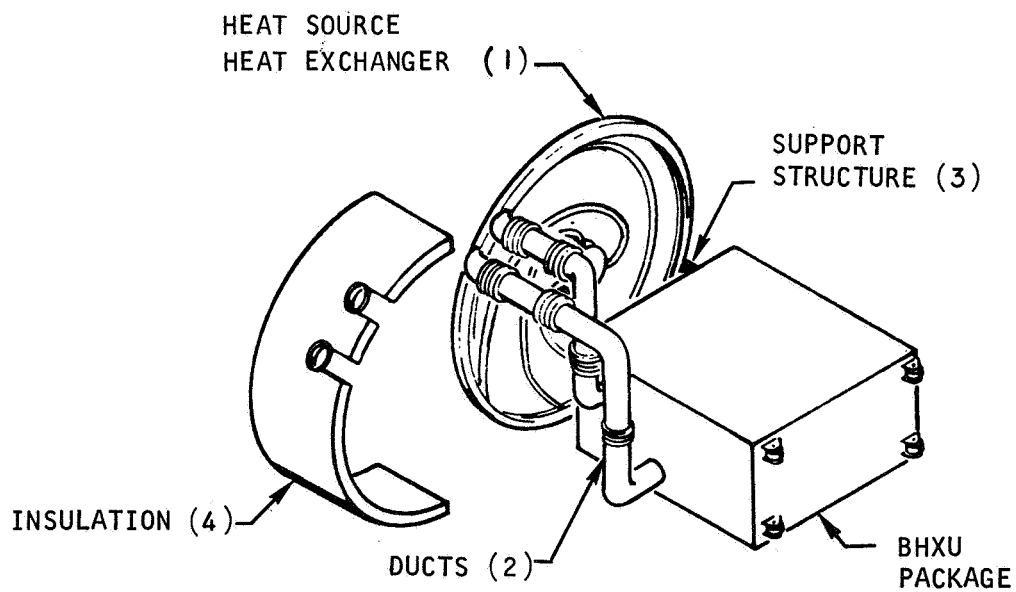


Figure 1-3 BRAYTON CYCLE POWER CONVERSION MODULE



A-33454

Figure 1-4 HEAT SOURCE HEAT EXCHANGER SYSTEM

There have been three major tasks (or phases) in the study. These have consisted of a two-part conceptual design effort, Phases 1A and 1B; and a preliminary design effort, Phase II, reported in this document. In addition to these tasks, an aerodynamic test program is being conducted by NASA Ames Research Center to develop a turnaround (destabilizing) device that ensures proper IRV attitude during all credible reentry modes.

2.0 SUMMARY

This section contains a brief review of the Phases IA and IB conceptual design study results, as well as a summary of the results and significant conclusions of the Phase II Preliminary Design Study.

Initial program ground rules are listed in Table 2-1. The basic program design criteria specified by NASA-LeRC are listed in Table 2-2. Safety criteria guidelines established at the outset of the program are contained in Table 2-3.

2.1 PHASE IA -- CONCEPTUAL DESIGN SUMMARY

During this period of the conceptual design phase, three major subtasks were completed leading to the selection of the three vehicle concepts which were evaluated in Phase IB.

First, a systems analysis was performed that resulted in the definition of the critical system design requirements for the IRV (e.g., abort requirements, reentry conditions, impact attenuation requirements, etc.). Safety considerations and examination of various failure modes played a predominant role in this analysis.

Second, a variety of conceptual designs were considered and evaluated for each of the critical IRV subsystems. Their relative advantages and disadvantages were examined and selections of preferred design alternatives were made wherever possible. The major design considerations in this analysis were aerodynamic shape, reentry performance, HS configuration, HSHX configuration, structural support and attachment, impact attenuation, recovery and location aid requirements, abort and deorbit rocket integration, and spacecraft/IRV integration. Third, a considerable number of total IRV conceptual designs were synthesized in order to examine the impact of different design alternatives on the total vehicle system. Table 2-4 summarizes the basic characteristics of the five prime generic combinations developed during this activity. The effect of inclusion of various combinations of impact attenuation, abort rockets, and location aids on these basic vehicle types is shown in Table 2-5.

At the conclusion of Phase IA, three overall vehicle concepts were selected by NASA-LeRC for further evaluation in the Phase IB conceptual design effort. The concepts, all employing 60-degree blunt cone IRV's, were:

- a minimum diameter circular planar HS nonvented fuel capsule.
- a "pin cushion" (vertical array of fuel capsules) HS in a 60-degree blunt cone R/V.
- A minimum diameter circular planar HS utilizing vented capsules.

Results of the Phase IA task are summarized in Reference 2-1.

2.2 PHASE IB -- CONCEPTUAL DESIGN SUMMARY

During Phase IB the three recommended concepts were evaluated in terms of safety, vehicle diameter, vehicle weight, reentry performance, overall reliability (simplicity) and developability, and ability of the design to allow growth potential or changes in subsystem characteristics. Phase IB ground rules are listed in Table 2-6 below.

TABLE 2-1

PROGRAM GROUND RULES

- Use nonvented isotope heat source capsule characteristics furnished by LERC
- Consider both separate IRV launch (Atlas/Centaur) and integral launch (Saturn 1B-MORL)
- Consider incorporation of recovery aids for the IRV
- Aerodynamic configurations limited to 60° half-angle blunt cone and modified Apollo shape
- HSHX to be in-place redundant and replaceable
- Intact reentry capability during all mission phases
- Design must provide for adequate heat rejection after impact

TABLE 2-2

IRV DESIGN CRITERIA

1)	Isotope Fuel	PuO_2
2)	Capsule Design	See Figure 1-2
3)	Fuel Loading	25 kw_t (EOL)
4)	IRV Ballistic Coefficient -- $\frac{W}{C_D A}$	$\leq 80 \text{ lb/ft}^2$ (Subsonic)
5)	Heat Leak -- IRV, HSHX, and ACHX	$\leq 1.5 \text{ kw}_t^*$
6)	Heat Source Temperature:	
	Max Continuous, Surface	$\leq 2000^\circ\text{F}$
	Max Transient, Surface	$\leq 2500^\circ\text{F}^*$
	Max Launch Pad Equilibrium	$\leq 1400^\circ\text{F}$ (Operation with ACHX)
7)	Emergency Heat Rejection	Passive Radiation to Space by Body Deployment
8)	Thermal Storage:	
	Material	BeO
	Requirement	60 min (1800°F to 2500°F)
9)	Launch Abort	Rocket Ejection $\leq 10g$ Acceleration
10)	Orbital Emergency Separation	Redundant Pyrotechnic


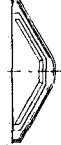

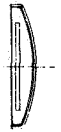

* In the event of upside-down IRV earth impact, provision must be made to destroy or otherwise overcome the insulation and permit heat rejection without exceeding heat source temperature limits.

TABLE 2-3

SAFETY CRITERIA

- Capsule design based on 10 half-life containment
- No fuel release as a result of launch pad abort, fire, or entrapment of heat source in debris
- Intact reentry of IRV from uncontrolled random reentry
- Reentry vehicle ejection in the event of catastrophic launch abort
- No burial of IRV after impact at terminal velocity
- Radiation coupling only between heat source and power conversion system - no physical connection
- No credibility for assembly of critical mass

TABLE 2-4
BASIC IRV CONCEPTS - CHARACTERISTICS SUMMARY

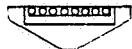
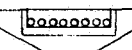

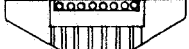


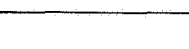
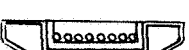

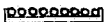

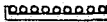
	 B. C. CIRC PLANAR	 B. C. CONICAL	 B. C. CIR. PIN CUSHION	 MOD APOLLO PLANAR	 B. C. RECT. PIN CUSHION (32 x 56)
DIAMETER (IN)	64	77	62	66	81
ENTRY WEIGHT (LBS)	1500	1660	1320	1500	1435
HEAT SOURCE WEIGHT (LBS)	1304	1416	1140	1304	1180
W/C _D A (LBS/FT ²)	43	31	41	45	25
SOURCE TEMP (°F) (NORMAL OP.)	1980	1865	2000	1980	2000
HSX WEIGHT (LBS)	200	200	200	200	200
ATTACHMENT AND SUPPORT *	G	G	F	G	F
HSX INTEGRATION *	G	G	P	G	P

78-0053

* G - GOOD
F - FAIR
P - POOR

** B.C. - BLUNT CONE

TABLE 2-5
SUMMARY OF WEIGHT/DIAMETER CHARACTERISTICS

CONFIGURATION	VEHICLE																
HEAT SOURCE		FLUSH		RECESSED (3 CAPSULE DIAMETER)		CRUSH-UP		FLUSH CRUSH-UP		FLUSH RECOVERY AIDS		RECESSED RECOVERY AIDS		RECESSED CRUSH-UP RECOVERY AIDS		CRUSH-UP RECOVERY AIDS	
		DIA.	WT.	DIA.	WT.	DIA.	WT.	DIA.	WT.	DIA.	WT.	DIA.	WT.	DIA.	WT.	DIA.	WT.
	CIRCULAR 47" DIA.	64"	1500	73"	1530	89"	1900	98"	1950	84"	1690	84"	1690	98"	2080	113"	3210
	RECTANGULAR 63" X 34"	89"	1690	92"	1710	107"	2080	116"	2140	89"	1800	92"	1830	116"	2290	-----	-----
	CONICAL 57" DIA.	77"	1660	77"	1660	91"	2030	101"	2040	94"	1860	94"	1860	101"	2190	103"	3160
	39" DIA. 4" PROTRUSION 20% CYL. 32x56 RECT. 4" PROTRUSION 20% CYL.	62"	1320	-----	-----	-----	-----	-----	-----	85"	1520	-----	-----	-----	-----	-----	-----
	CIRCULAR 47" DIA. APOLLO	66"	1500	80"	1550	102"	1950	119"	2040	92"	1710	92"	1710	119"	2180	-----	-----

78-0018

TABLE 2-6

PHASE IB GROUND RULES

- Establish design characteristics of three IRV concepts (all 60 degree blunt cones)
- Use truss support structure only
- Impact attenuation system should be based on the use of peripheral crushup to ensure heat source "flat" impact
- Ballutes are to be considered for drag augmentation
- Retro and abort rocket systems should be mounted on a tower in the Atlas/Centaur and on a minimum extension in the integral launch vehicle (Saturn I-B booster)
- Heat source and HSHX designs are to be based on maintaining a 1600° F turbine inlet temperature with the primary HSHX operating
- HSHX designs shall be developed to meet in place redundancy and separate replaceability criteria

In addition to the comparison of the three reference concepts, the major design areas encompassed in the Phase IB study were:

- determination of minimum diameter reentry survival vehicles.
- determination of impact survival system tradeoffs.
- evaluation of fuel capsule cover plate utility for reentry heating protection.
- consideration of ballutes for drag augmentation.
- examination of HSHX design considerations in terms of reducing fuel capsule maximum hot spot operating temperatures.
- IRV/launch vehicle/spacecraft integration.

The significant results and conclusions of the Phase IB study are summarized in the following discussion. Details of the Phase IB effort are contained in Reference 2-2.

2.2.1 Isotope Reentry Vehicle (IRV)

Primary emphasis during Phase IB was placed on the development of IRV systems incorporating the three reference HS configurations. Aerodynamic performance of the three vehicles is comparatively similar in that they are all 60-degree blunt cones with the same general weight, diameter, and aerodynamic coefficient characteristics.

Table 2-7 lists the comparative characteristics of the three reference IRV concepts developed during Phase IB. The two circular planar arrays incorporate an impact attenuation system based on the "Rotating Plate Concept," introduced in Phase IA and described in Subsection 7.2 of Reference 2-2. Therefore, the weight and size advantage of the pin cushion concept over the 49-inch-diameter circular planar array is illusory, in that it includes no provision for impact attenuation. (As is shown in Table 2-8, a comparison on the same basis for "bare" vehicles shows a significant weight and diameter margin for the circular planar array.) This diameter and weight margin is increased substantially when the pin cushion array is mounted in a flush (i.e., with the end of the vertically stacked capsules in the plane of the IRV base) position, to reduce reentry heating effects on the fuel capsules.

Referring again to Table 2-8, the potential weight and diameter savings possible with a vented capsule HS is indicated in the IRV reentry weight totals and vehicle diameters. Again, it should be noted that the diameter and weight totals reflect the inclusion of the impact attenuation system. The "bare" vehicle comparison is shown in Table 2-8. Table 2-8 shows IRV weights and diameters for minimum weight, minimum diameter, and optimum combination (Reference Designs) for Circular Planar HS IRV's using this intact impact concept. For comparison IRV weights are also shown for a crude attenuation system which employs isotropic crushup in the void volume below the HS.

TABLE 2-7

REFERENCE VEHICLE PERFORMANCE COMPARISON -- CIRCULAR
PLANAR VERSUS PIN CUSHION HEAT SOURCES

	Circular Planar H. S. Array (49-in. Dia.)	Circular Planar H. S. Array (46-in. Dia. Vented Capsule)	Pin Cushion H. S. Array (39-in. Dia.)
Vehicle Diameter (in.)	85	75	70.5
X _{c.g.} /D (in.)**	0.31	0.33	0.34
W/C _D A (lbs/ft ²)	29	30	38
Heat Source Weight (lbs)	1288	985	1365
IRV Aeroshell Weight (lbs)	553	480	281
IRV Entry Weight (lbs)	1841	1465	1646*
HSX Weight (lbs)	166	148	70
Number of Fuel Capsules	164	164	164
Thermal Power EOL (kw)	25	25	25
Maximum Capsule Temperature (°F) (Normal Operation)	1870	1920	1790
Inplace Redundancy and Separate Replaceability	OK	OK	Requires Rotation of HSX or IRV
Impact Attenuation	Intact Plate Concept	Intact Plate Concept	Intact Plate Con- cept not Feasible Without Large Weight Penalty (>1000 lbs)
Developability***	G	G	P
Attachment and Support***	G	G	P
Aerodynamic Heating***	G	G	P

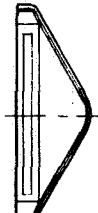

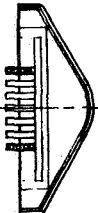
* No Impact Attenuation System

** X_{c.g.} Measured From Nose Station

*** G - Good
P - Poor

TABLE 2-8

IRV WEIGHT/DIAMETER SUMMARY

PERTURBATION (1) HEAT SOURCE CONFIGURATION		REF. DESIGN	A MIN. DIA. (BARE)		B ISOTROPIC CRUSH-UP		C CRUSH-UP		D CRUSH-UP WITH RECESS	
A	49.0 CIRC. PL 	85	66.0	66.0			MIN. WT. 90.0	MIN. DIA. 75.0	MIN. WT. 95.5	MIN. DIA. 75.0
		1841	1551	2151			1826	1986	1851	2083
B	46.0 CIRC. PL - VENTED 	75.0	62.3	62.3			75.0	70	76.2	71.1
		1464	1232	1772			1464	1540	1506	1585
C	39.0 PIN CUSHION 	70.5 (2)	70.5 (2)	70.5 (2) 82.5 (3) 1916 (2) 1893 (3)						
		1646 (2)	1646 (2)							

- (1) ALL CONFIGURATIONS HAVE BALLUTE & FLUSH HEAT SOURCE UNLESS OTHERWISE SPECIFIED
 (2) PROTRUDING (4.0") HEAT SOURCE
 (3) WITH TOP OF FUEL CAPSULES FLUSH WITH REAR SURFACE OF IRV

The normal operating temperature of the fuel capsule with the pin cushion HSHX is approximately 80 degrees lower than the nonvented fuel capsule HS array, and 130 degrees lower than the vented capsule HS. The differences are due to the more efficient usage of heat transfer area in the case of the pin cushion HS, and less conductive area availability in the case of the vented capsule HS.

Figures 2-1 and 2-2 show perspective drawings of the circular planar HS IRV and the pin cushion concepts, as developed during Phase IB. The planar array vehicle, as shown in Figure 2-1, incorporates terminal impact survival subsystems, while the smaller diameter pin cushion concept provides no impact protection provision. Utilization of the vented capsule design, shown in Figure 1-2 in the previous section, in the circular planar HS array does result in a significant reduction in IRV weight (~ 300 lb).

This comparison only attempts to evaluate the relative developability and fabricability of the two classes of systems in qualitative terms. However, the fabrication of the pin cushion system is certainly more complex than is that of the circular planar arrays. In addition, provision of a system to ensure similar impact performance with the pin cushion system to the circular planar arrays could only be achieved with large weight penalties.

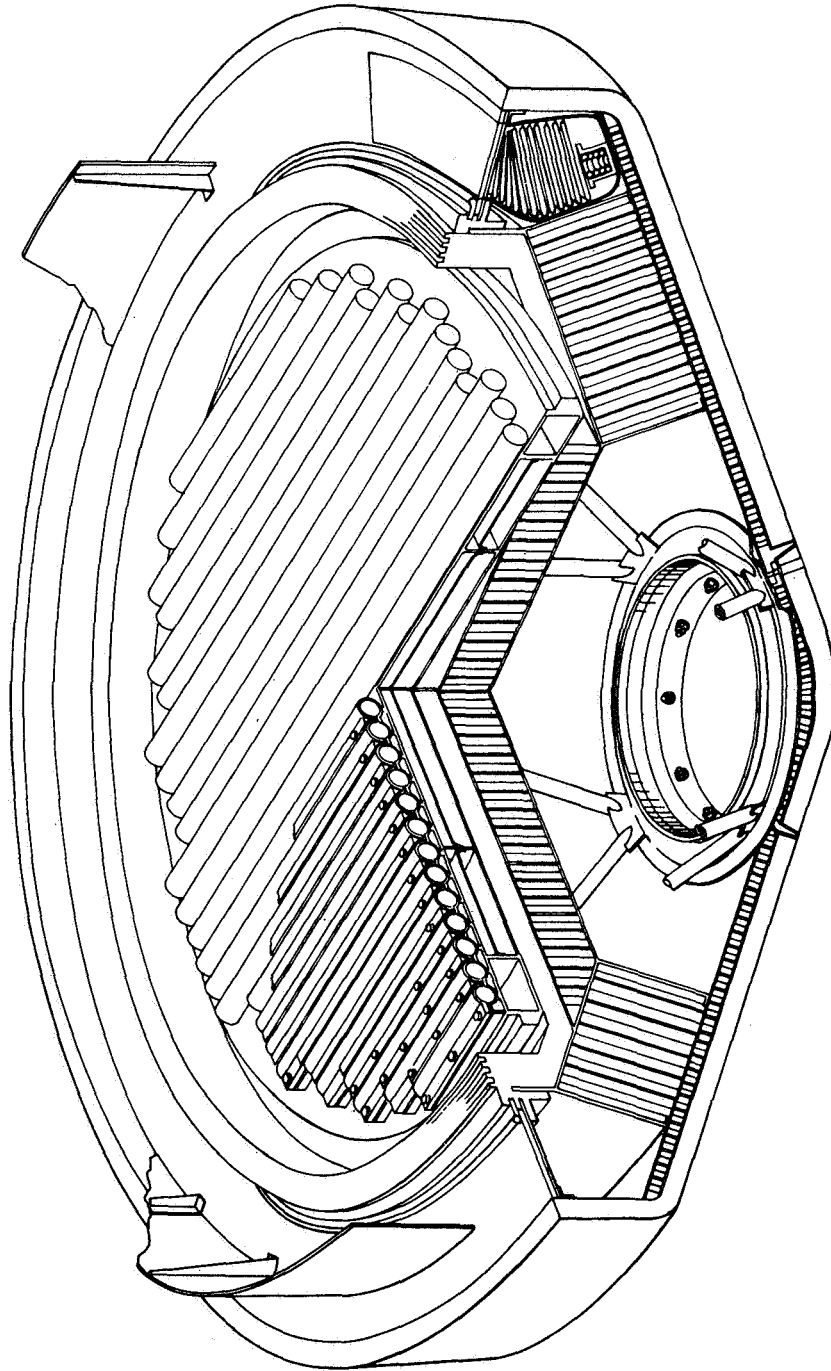
Finally, the comparative heating on the capsules during the various classes of reentry situation is much higher in the case of the complex, protruding, pin cushion array, than it is for the flush mounted circular planar arrays.

An optimization study of the intact plate, impact attenuation system has been completed during Phase IB. Figure 2-3 shows a section view of the conceptual scheme, incorporating a "cold plate" support structure to provide support for the HS during rotation during impact, and HS edge geometry modification to allow inclusion of rotational crushup at minimal cost in IRV diameter.

2.2.2 Heat Source (HS)

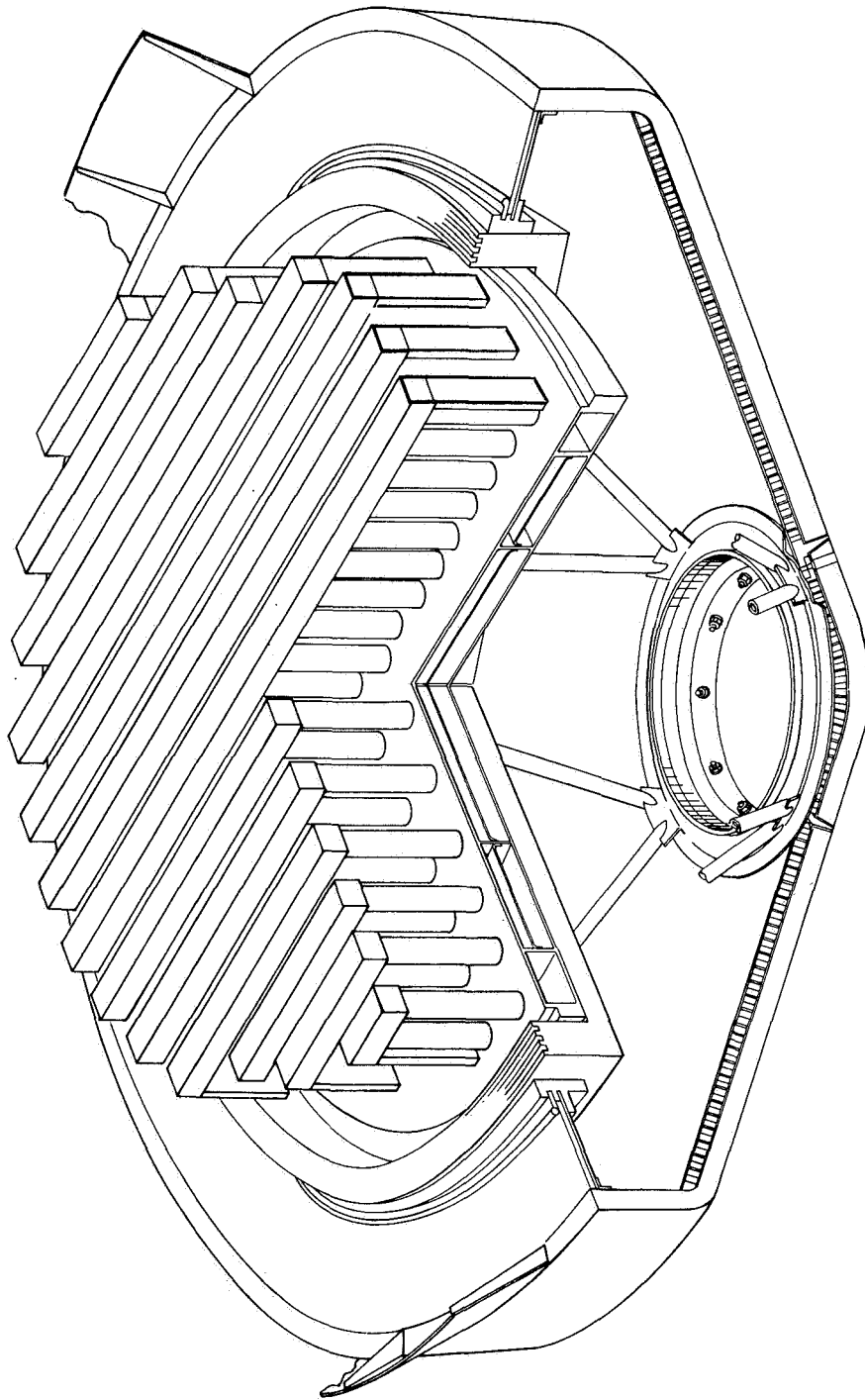
Prime emphasis was placed on the development of feasible retention of systems for both the nonvented and vented fuel capsules designs; the development minimum diameter heat sources for both the circular planar and the pin cushion or stacked log class arrays; better characterization of the thermal performance of all three types of heat sources in all required operating (or survival) modes; better definition of aeroshell/HS interface constraints; and development of ACHX and BeO location and sizing details.

Mechanical and thermal performance characteristics developed are summarized in Table 2-9. From a weight consideration, the circular planar design with vented capsules offers a substantial advantage over the other two designs. The largest weight for the pin cushion design is primarily due to the increased weight requirement of the BeO heat sink (220 pounds versus 140 pounds for the circular heat source diameter. Reduction in diameter for the circular planar design with vented capsules compared to the nonvented capsule heat source design is not as much as the reduction in capsule size may indicate (1.40-inch diameter x 5.6-inch length compared to 1.542-inch diameter x 5.968-inch length for nonvented capsule). This is primarily due to the fact that the required 164 capsules, arranged with eight capsules in a row at the center, determine the heat source diameter. It should



78-1610

Figure 2-1 IRV 49-INCH-DIAMETER PLANAR ARRAY



78-0611
Figure 2-2 IRV 39-INCH-DIAMETER PIN CUSHION ARRAY

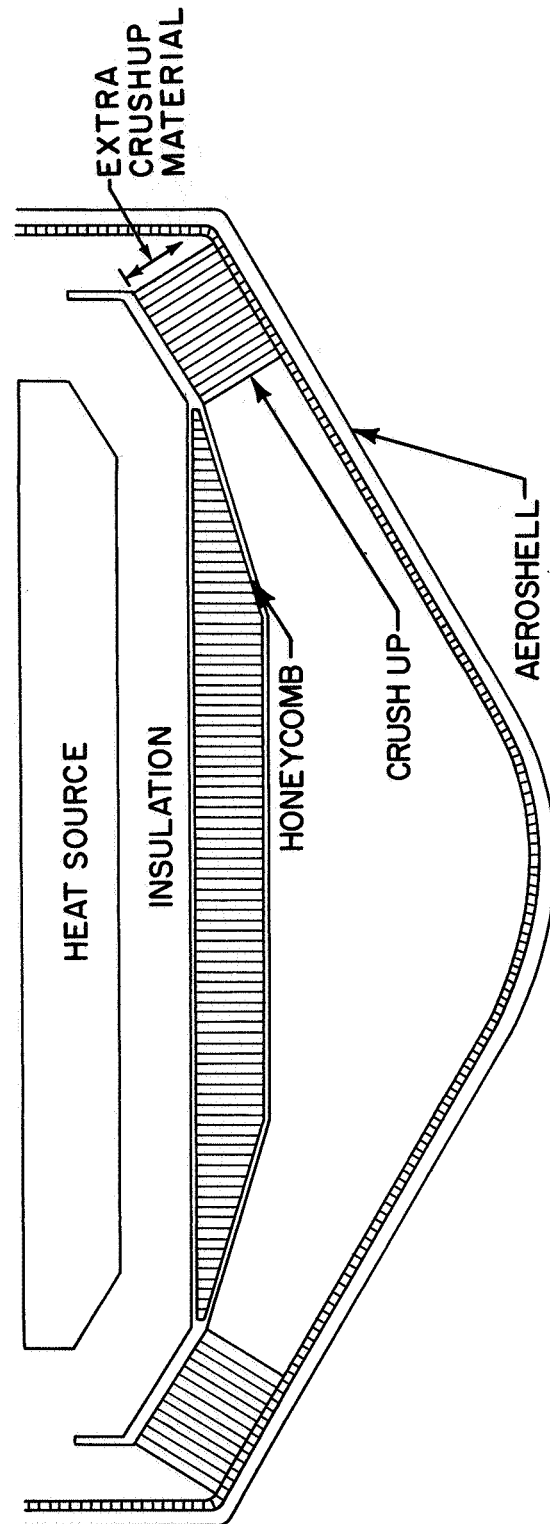


Figure 2-3 COLD PLATE CONCEPT WITH RECESSED CORNER

78-0627

TABLE 2-9

HEAT SOURCE SUMMARY COMPARISON

	Configuration		
	Planar	Planar Vented	Pin Cushion
Weight (lb)	1288	983	1365
Heat Source Diameter (in.)	49.0	46.0	39.0
Number of Capsules	164	164	165
Center-of-Gravity from Nose (in.)	27.8	27.5	26.8
Peak Capsule Temperature Gradient (°F)	120	155	70
Heat Source Radiation Area (ft ²)	13.1	11.5	17.5
Peak Capsule Temperature (°F)			
• Primary HSHX Operating	1870	1925	1790
• Secondary HSHX Operating (1600° F Turbine Inlet)	2060	2115	1790

also be noted that the radiation heat transfer area facing the HSHX cannot be reduced much without a penalty in the peak capsule temperature. A radiation heat transfer area of approximately 11.5 ft² appears to be the minimum practical.

The peak capsule temperature of the pin cushion design is not affected by the mode of HSHX operation, (i.e., with either the primary or secondary heat exchanger operating). A relatively low temperature of 1790° F is achieved compared to the other two circular designs. It is estimated that with the circular planar designs the peak capsule temperature is 200° F higher with the secondary HSHX operating if a 1600° F turbine inlet temperature was required for this operating mode.

The development of an attachment and support scheme for the pin cushion HS that met thermal and spacing constraints as set by the HSHX and fuel capsule operation temperature limits, while allowing incorporation of required ACHX channels and BeO heat sink material was a complex design problem. Figure 2-4 shows a detail of the pin cushion attachment system. It should be noted that while this system does meet basic operational requirements, its utility in limiting fuel capsule damage during terminal impact situations is not as good as the cradle retention system developed for the circular planar arrays (Figure 2-5 shows the cradle retention system with a vented capsule). This was the only basic deficiency in any of the three heat source designs considered during Phase IB.

It was concluded that the circular planar design with nonvented capsules was the preferred design for the preliminary IRV design effort during Phase II. The circular planar heat source proved to be lighter and simpler to fabricate. Its mechanical performance was also more predictable and better understood for ground impact.

Feasibility of using vented capsules in a circular planar heat source without any unsurmountable difficulty was shown. Although the vented capsule development is still in the early state compared to the nonvented capsules, it does offer an attractive potential in weight reduction and some gain in diameter reduction.

2.2.3 Heat Source Heat Exchanger (HSHX)

On the basis of the Phase IA studies, three heat sources were identified and received detailed analysis during Phase IB. These three heat sources are those described in Table 2-9 previously.

From the Phase IA studies, the most attractive approach to the HSHX's was found to be the tube-fin spiral involute, two-pass type of heat exchanger. As a result, this was the only approach considered in Phase IB of the study for each of the three heat sources listed above. While previous studies indicated that the tube-fin heat exchanger offered the lowest-weight design, elimination of the fins between the tubes and utilization of an all-tubular heat exchanger resulted in an easier fabrication approach. All-tubular heat exchangers were therefore employed, where possible, throughout the Phase IB studies.

Four HSHX designs were developed for the three heat-source geometries considered. Table 2-10 presents a summary of the physical characteristics of these four heat exchanger designs. For the planar heat exchanger designs, additional consideration was given to incorporating a heat dump system where a portion of the superinsulation forming the cavity around the heat source and HSHX would be removable to permit heat rejection to space.

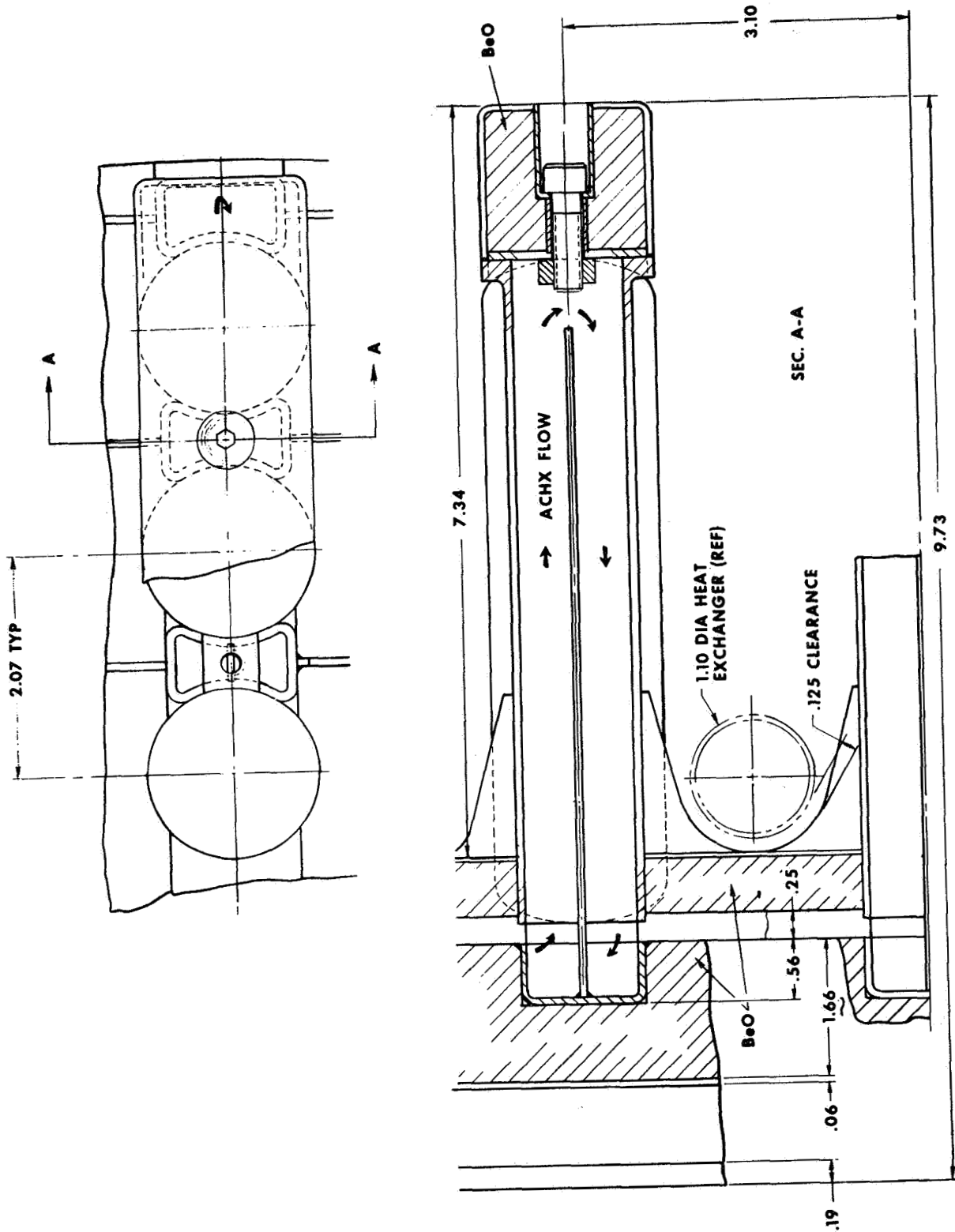
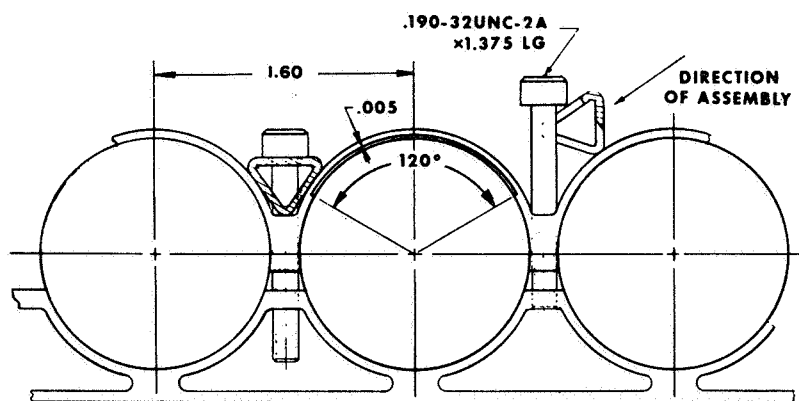
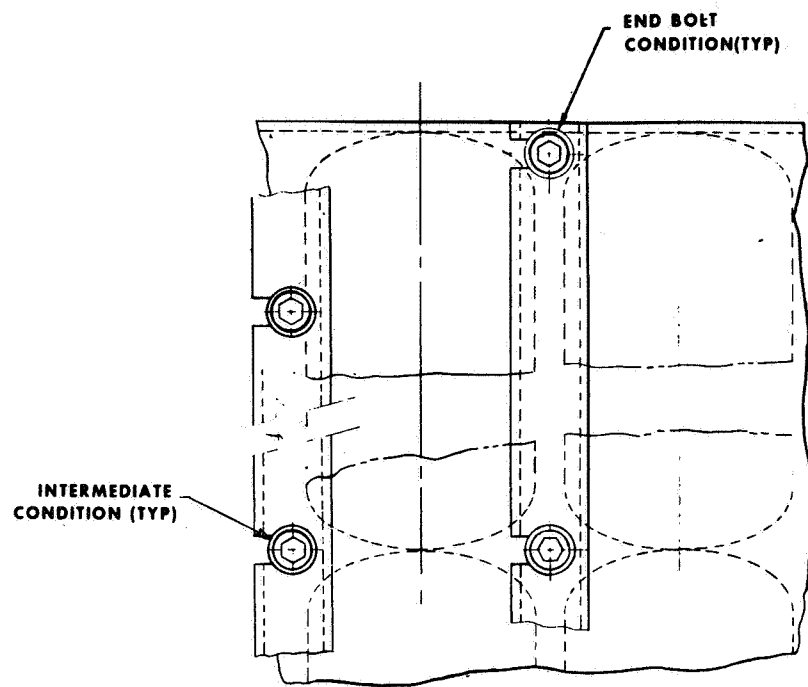


Figure 2-4 MECHANICAL DETAILS OF PIN CUSHION ARRAY

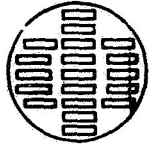

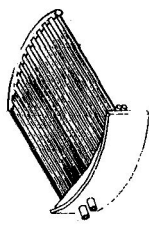

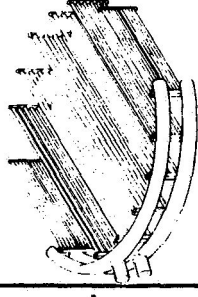
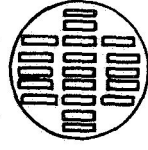



89 - 3401

Figure 2-5 VENTED CAPSULE RETENTION, 46-INCH DIAMETER PLANAR ARRAY

TABLE 2-10

HSHX DESIGN SUMMARY -- PHASE I-B

Heat Source		Heat-Source Heat Exchanger							
Geometry	Size	Geometry	Type	Dimensions, in.	Tube OD, in.	No. of Tubes	Core Weight, lb	Manifold Weight, lb	Total Weight, lb
	49-in. OD		Circular involute 2-pass tubular	Core 49 OD Overall 53.5 OD	1.34	18	54	35	89
			Rectangular 2-pass tubular	Overall 50 by 57	1.0	48	71	14	85
	39-in. OD		7-parallel rectangular legs 2-pass tube-fin	Overall 45.5 by 42.3	0.297 0.594 1.06 1.123 1.08 0.871 0.491	16 8 4 4 4 6 10	24	15	39
Circular planar (vented capsules) 	46-in. OD		Circular involute 2-pass tubular	Core 46 OD overall 50.5 OD	1.34	18	47	32	79

A-34850

The performance characteristics of the three heat sources and four HSHX designs that were developed in this phase of the study are summarized in Table 2-11. The first item is the minimum-weight HSHX design (that is, minimum material thickness), and the second item is the maximum fuel capsule temperatures associated with full power output on HSHX 2. Only the pin cushion design falls below the 2000° F temperature level. The third item is the increase in the HSHX weight required to reduce the capsule operating temperature to 2000° F under the condition of HSHX 2 delivering full power. The fourth item is the maximum source temperature associated with the minimum-weight heat exchangers for HSHX 1 in operation. If the temperatures of line 4 are set as a new maximum, the Brayton fluid outlet temperatures of the HSHX 2 are calculated, and this result is translated into a power output of PCS 2, the values listed in Item 5 emerge. For example, with an 1870° F maximum source temperature, 74.5-percent power can be achieved from the second system. Item 6 gives an estimate of the heat leaks associated with the installation of each of the systems examined, with and without heat dump capability. These heat leak estimates are necessarily approximate because the details of the supporting structure and the mechanical interfaces with the IRV had not been worked out in detail. The major problems of each HSHX are listed as comments (Item 7).

For the circular planar heat-source arrays, the maximum fuel capsule operating temperatures with PCS 2 in operation at full power (Item 2, Table 2-11) are higher than reported in the Phase IA studies. The circular planar heat source of Phase IA had a diameter of 53 inches. The two circular planar heat sources considered in this phase of the study had diameters of 49 and 46 inches, which represent a 17- and 32-percent decrease, respectively, in radiating heat transfer area. This decrease in radiating area plus a more detailed analysis of the temperature levels associated with this geometry resulted in the higher source temperatures indicated.

Conceptual designs of integrated HSHX-PCM packages suitable for integration with the Atlas/Centaur and MORL vehicles were developed for each of the four HSHX's and the three heat sources. A typical Brayton cycle package and installation concept for an Atlas/Centaur vehicle is shown in Figure 2-6. In addition, conceptual installation designs were developed for both the rectangular and the circular HSHX's employing a movable-insulation heat dump system.

2.2.4 Summary of Conclusions and Recommendations (Phase IB)

The following major conclusions and recommendations were made on the basis of the Phase I Conceptual Design Study:

1. The circular planar HS array is recommended for preliminary design. The only significant pin cushion advantages are somewhat lower capsule operating temperatures. Developability and fabricability, reentry heating, impact protection, structural support, heat source weight, and HSHX replaceability are all more favorable for the circular planar array.
2. For comparable aerodynamic vehicle performance the pin cushion results in only slightly smaller vehicle diameters. The vented capsule circular planar HS array yields significantly lower vehicle weights and diameters (since impact attenuation can be provided with smaller diameter penalties).

TABLE 2-11

HSHX SUMMARY -- PHASE IB

	49-in.-dia Source		46-in.-dia Source, Vented Capsule	39-in.-dia Source, Pin Cushion
	Circular	Rectangular		
1. HSHX weight (lb)	89	85	79	39
2. Maximum source temperature (°F) (HSHX 2 in operation)	2060	2020	2115	1790
3. ΔWT to meet 2000°F max. source temperature (HSHX 2 in operation)	100	25	--	0
4. Maximum source temperature (°F) (HSHX 1 in operation)	1870	1845	1925	1790
5. Power output of HSHX 2 with maximum source temperature of (4 percent)	74.5	76	74	100
6. Heat leaks, w No heat dump With heat dump	922 991	887 945	907 971	823 --
7. Comments	1. Complex fabrication 2. Large volume with heat dump	1. Difficult flow distribution problems 2. Simple fabrication	1. Highest temperatures 2. Complex fabrication 3. Large volume with heat dump	1. Requires movement of source to replace HSHX 2. No heat dump capability 3. Simple fabrication 4. Lowest temperatures

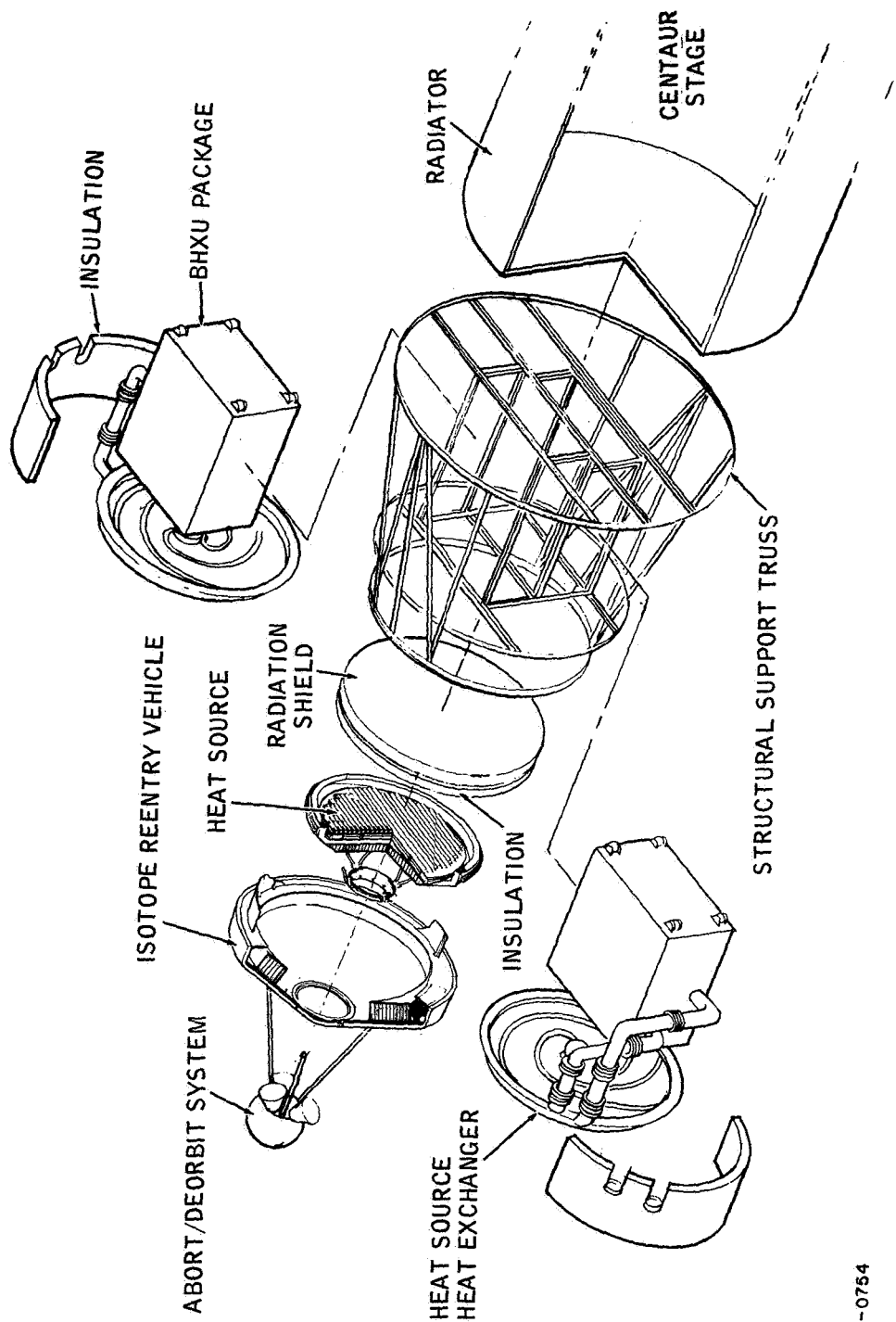


Figure 2-6 IRV/BRAYTON CYCLE/ATLAS CENTAUR INTEGRATION

78-0754

3. The HS cover plate can be used to reduce reentry peak capsule temperature.
4. Two-pass, tube fin HSHX's are recommended for preliminary design.
5. Circular planar HS maximum capsule operating temperature can be reduced to less than 1850° F by adding tube wall weight (~100 lb) to the HSHX.
6. A tower mounted deorbit system is recommended. Further work is needed on spin stabilization and reentry performance tradeoffs.
7. An intact HS concept for impact attenuation can be used with reasonably small weight and diameter penalties.
8. A practical minimum vehicle diameter with impact attenuation is about 75 inches (nonvented capsules).

2.3 PHASE II -- PRELIMINARY DESIGN SUMMARY

A detailed preliminary design of the minimum diameter circular planar HS/IRV illustrated in Figure 1-1 has been developed during Phase II. The revised study ground rules followed in Phase II are listed in Table 2-12.

During this study phase final materials choices have been made; thermal performance of the total IRV/HS/HSHX system has been defined; and structural designs, with required fabrication sequences, have been developed. In addition, a detailed reentry performance analysis has been performed to establish the performance limitations of the vehicle and its sensitivity to variation in the reentry trajectory, vehicle motions, and vehicle physical parameters.

A detailed IRV/Brayton cycle/spacecraft (S/C) integration and mounting concept has been developed. The structural support and mechanization of this installation concept has been primarily dictated by operational safety requirements. Figure 2-7 shows the basic IRV/Brayton cycle system in a typical S/C installation. Total system weight estimates for single and redundant Brayton cycle Power Conversion Module (PCM) system in a Manned Orbital Research Laboratory (MORL) class vehicle are summarized in Table 2-13.

An aerodynamic test program conducted by NASA Ames Research Center has supplied supporting test data to this study program. The major purpose of the test program is to define a passive aerodynamic device (such as a fence or fin) which ensures that the vehicle is not stable in a rearward attitude during reentry. Consequently, if the vehicle were to initially begin reentry in such an attitude (180-degree angle of attack) this device would guarantee vehicle turnaround at high altitudes prior to peak heating. Rearward (or high angle of attack) reentry is undesirable because of the increased aerodynamic heating experienced by the heat source fuel capsules which are located at the base region of the vehicle.

A number of different aerodynamic devices have been studied analytically, and the most promising configurations are undergoing testing in the free-flight 42-inch shock tunnel at the NASA Ames Research Center. This facility is capable of achieving the appropriate Reynolds number ($10^4 - 10^5$) and Mach number (> 10) conditions. Sufficient data have been collected to provide a basis for making

TABLE 2-12

PHASE II GROUND RULES

Reentry Vehicle	<ul style="list-style-type: none">- Minimum diameter, 60-degree blunt cone- Symmetrical fence, geometry based on results of NASA Ames test program- Ballute retardation system
Heat Source	<ul style="list-style-type: none">- Circular planar array- Nonvented capsule- "Close-pack" fuel capsule retention system
HSHX	<ul style="list-style-type: none">- Two-pass, circular planar, tubular involute- Turbine inlet temperature 1600° F with HSHX 1 in operation- Turbine inlet temperature with HSHX 2 in operation to be determined by heat source operating temperature requirements

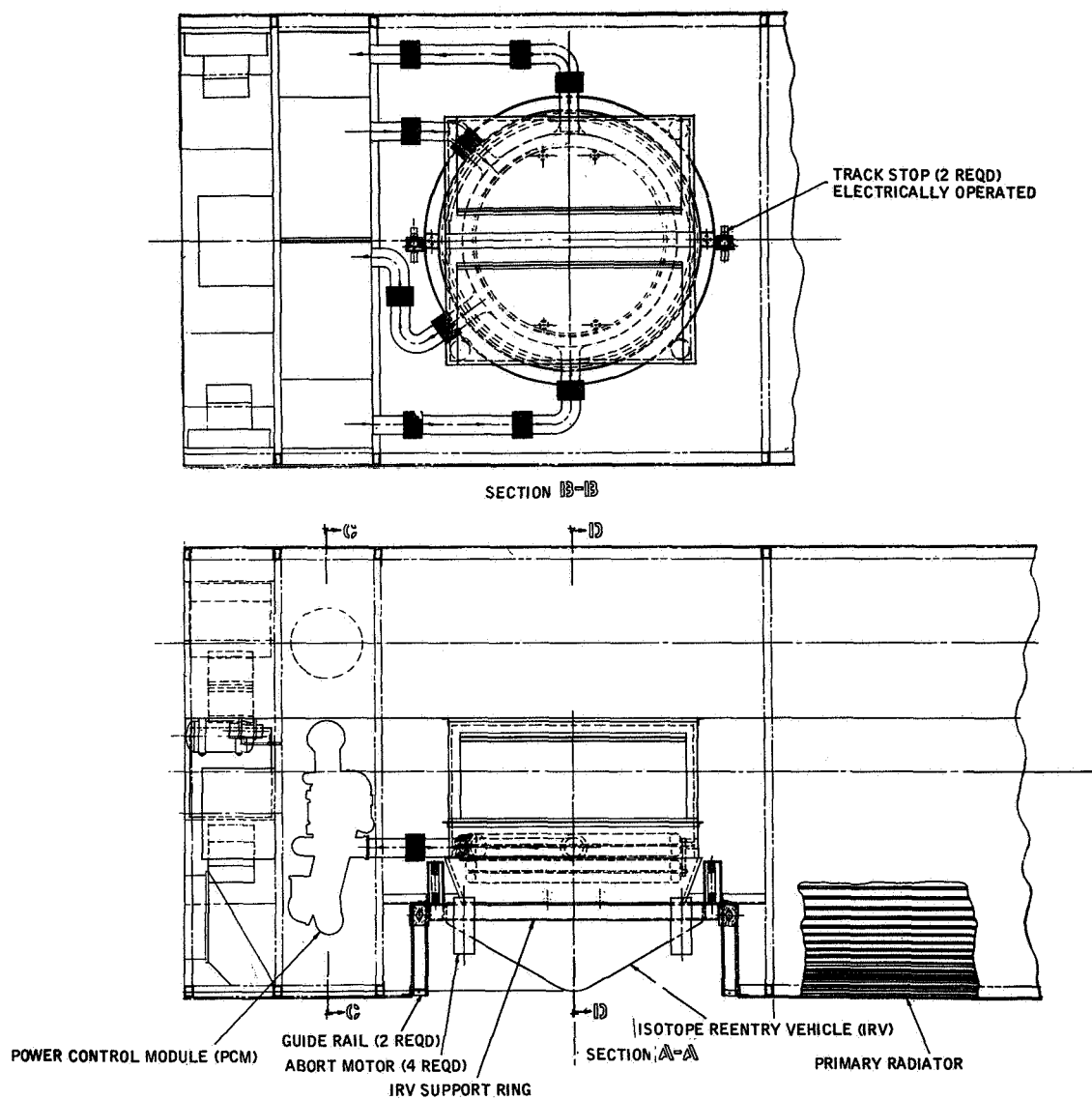


Figure 2-7 BASIC IRV/BRAYTON CYCLE SYSTEM IN A
TYPICAL SPACECRAFT INSTALLATION

TABLE 2-13

WEIGHT SUMMARY -- IRV/BRAYTON
CYCLE SYSTEM MORL

	Single PCM System (1b)	Redundant PCM System (1b)
IRV	2300	2300
HSHX	230	430
PCM	435	870
Heat Rejection	230	390
Gas Management	150	300
Electrical and Control	505	730
System Support Structure	690	690
Total System Weight*	4540	5710

* Does not include radiators and radiation shield.

a preliminary selection of an effective turnaround device together with dimensional characteristics for use during the preliminary design task. Static force and moment tests are being conducted in the NASA Ames 3.5-ft hypersonic wind tunnel.

The turnaround fence concept on the IRV configuration shown in Figure 1-1 is based on the NASA Ames preliminary recommendation.

The significant results and conclusions of the Phase II preliminary design study are summarized by major subsystems in the following subsections.

2.3.1 Heat Source (HS)

In Phase II the minimum diameter circular planar array heat source with the reference design nonvented capsules has been selected for further study to develop a preliminary design. Design features included the cover plate type capsule retention system, BeO heat sink, multilayer insulation system, support ring with truss support system, Auxiliary Coolant Heat Exchanger (ACHX) incorporated within the heat source with connections for external coolant supply and mounting of the heat source flush with the base plane of the reentry vehicle. An exploded view of the heat source preliminary design assembly is shown on Figure 2-8, indicating the major component subassemblies. Table 2-14 is a summary of the heat source characteristics.

The Cb-1Zr heat source plate is a built-up structure. Its primary function is to support the 164 fuel capsules producing 25 kw_t throughout all phases of the mission. The top of the heat source plate consists of rows of cradles to support the fuel capsules. ACHX cooling channels are incorporated in triangular-like passages formed by adjacent cradles between the capsule rows. The ACHX supply and return headers form the periphery of the heat source plate and serve as main structural members. Individual ACHX cooling channels are connected to the headers by holes in the top plate, with the connections to the return header properly sized to balance the flow between channels based on heat load.

One of the IRV design ground rules is to avoid any mechanical connection between the heat source and the Brayton power unit Heat Source Heat Exchanger (HSHX) assembly. Also, the ACHX system was to be compatible for operation with the IRV in the closed or operating position. Various alternate methods of routing the Auxiliary Cooling Heat Exchanger (ACHX) coolant were considered and, consequently, inlet and outlet connections were provided at the thermal radiation face of the heat source for mating by coolant lines which will penetrate the HSHX assembly structure. To meet this ground rule and expedite hookup and separation of coolant lines at the connectors, a quick disconnect mechanism with seals which will sublimate at the heat source operating temperature was developed.

The cover plate is Cb-1Zr with grooves to mate with the fuel capsules. It is designed to retain fuel capsules during the entire service life of the heat source, and to provide a thermal barrier to protect the fuel capsules from severe aerodynamic heating during IRV reentry. The cover plate is held in place by triangularly shaped Cb-1Zr retention bars which permit remote final assembly. T-111 bolts with Cb-1Zr lock washers are used to bolt down the retention bars and the cover plate. Cb-1Zr washers are used since this material is more compatible with the high emissivity coating used on the cover plate to enhance thermal radiation.

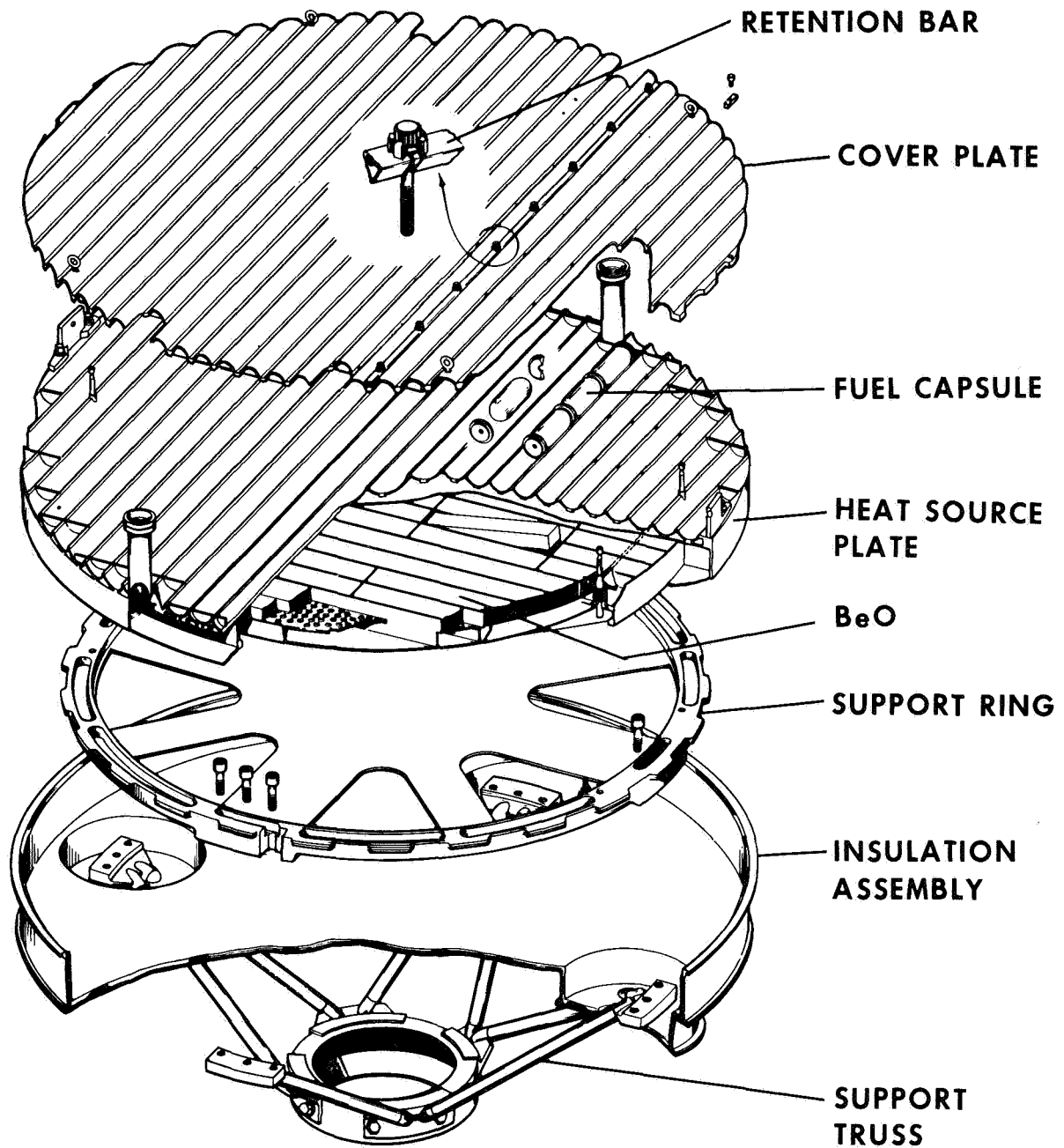


Figure 2-8 EXPLODED VIEW OF THE HEAT SOURCE PLATE

TABLE 2-14

HEAT SOURCE PRELIMINARY DESIGN SUMMARY

Configuration	Circular Planar
Overall Diameter	49.0 inches
No. of Capsules	164
Heat Source Weight	1476 lb
Fuel Capsules	755 lb
Heat Source Plate	232 lb
Cover Plate Assembly	87 lb
Support Structure	153 lb
Insulation Assembly	79 lb
BeO Heat Sink	170 lb
Thermal Performance	
Heat Source Radiation Area	13.11 ft ²
Steady-State Peak Capsule Temperature	
a) Primary HSHX Operation	1918° F
b) Secondary HSHX Operation ($T_{in} = 1600^{\circ}$ F)	2060° F
c) Deployed in Space	1455° F
Transient Heatup Rate (from 1880° F)	650° F in 1 hr
ACHX Operation	
Mass Flow Rate	3.13 lb/sec
Pressure (inlet)	90 psia
Peak Capsule Temperature	350° F

*Based on active length (fueled length) of fuel capsules. Temperature is 1300° F using total length of fuel capsules.

Thermal design criteria for the heat source are summarized in Table 2-15. These temperature criteria served to establish the BeO heat sink design. During the detailed analysis of the heat source thermal response characteristics, it became apparent that the BeO heat sink weight requirements are sensitive to the nature and extent of thermal contact between BeO and the heat source plate. An assumption of an effective contact resistance of about 100 Btu/hr-ft²-°F will enable 170 pounds of BeO to meet the design criteria. However, if a complete radiation gap is assumed, the BeO weight required to meet the thermal design criterion of a heatup of less than 700°F in 1 hour starting from 1800°F will be increased to about 300 pounds. Available reference data on the thermal contact resistance for similar materials indicate that this assumption is quite conservative. However, this assumption should be verified by testing the selected materials for the surface finish and loading conditions expected in the heat source.

A close review of the superinsulation system indicated that very little performance data were available at the higher temperatures. Because of the relative conductivities, the greater uncertainty in performance at the IRV temperatures, and the bulkier nature of this insulation, a vacuum multilayer foil system was selected.

TABLE 2-15
THERMAL DESIGN CRITERIA

• Maximum Steady-State Capsule Temperature	2000° F
• Maximum Transient Capsule Temperature	2500° F
• Maximum Capsule Temperature Rise in One Hour from 1800°F	700° F
• Maximum Launch Pad IRV Temperature	350° F
• Maximum IRV Operating Heat Loss	1500 watts

Analysis indicated that the insulation system of about 100 layers would be satisfactory, and any further increase in the number of layers would yield diminishing returns, i.e., little gain with increased weight penalty. The overall insulation system is shown in Figure 2-8. The heat loss through the heat source insulation system is 310 watts, thus resulting in a loss (including struts) of approximately 500 watts.

A vehicle diameter of 68 inches was selected for the IRV to provide integration with various candidate spacecraft. Also, the Phase IB study indicated a substantial thermal benefit for the flush or recessed heat source mounting over the exposed mounting in the reentry vehicle during reentry heating conditions. Since every inch of increase in distance between the heat source and the reentry body nose results in approximately a 4-inch increase in vehicle diameter, the heat source was placed as close to the vehicle nose as feasible. A combination of these goals and constraints on the heat source mounting in the reentry vehicle resulted in a reduced length (from a 22- to a 19.2-inch strut) support truss system

and a reduced strut angle with respect to the horizontal plane of the reentry vehicle (reduced from 45 to 34 degrees). The structural load imposed on the strut was substantially increased. More important, the horizontal components of loads acting on the support ring became so large that it was necessary to provide a tie plate (a scalloped circular plate) within the support ring to protect it and the ACHX header ring, which mates with it, from excessive deformation and yielding from reentry load. From a standpoint of mechanical simplicity and structural ruggedness, the bimetal strut design was judged less desirable and was replaced by single-piece refractory metal (T-111) struts. The reduction of strut length, increase of strut cross-sectional area over the bimetallic design and the use of T-111 throughout contributed to a substantial increase in heat loss through the support truss system, i.e., from 112 watts calculated in Phase IA to 188 watts, assuming 300° F at the cold end of the support system. However, this higher heat loss when combined with other leaks is within the limit of 1500 watts and offers a practical solution to the support problem.

Heating for several types of reentry, i.e., nominal, orbital decay-tumbling, nominal with offset c.g., and rearward, were considered. The thermal response of the heat source was calculated for each trajectory with special emphasis on the temperature of the capsule. The peak capsule temperatures were below 2420° F for the first three cases; however, the capsule temperature reached 2860° F for the rearward reentry. The rearward reentry was the worst heating case defined, and the capsule temperature exceeded the 2500° F limit defined under the design criteria; but the occurrence of such a trajectory is believed to be most improbable. Also, the excursion above 2500° F was of short duration (≈140 seconds) and the capsule material, T-111, can probably survive without difficulty.

A detailed manufacturing plan for the fabrication sequence and processes was defined. It presented no insurmountable difficulties and indicated a realistic demonstration of feasibility. Potential warpage from multiple welding of thin parts required in fabrication of the heat source plate was identified as an area requiring careful attention during final detail design and during fabrication.

The operation sequence for heat source assembly, ground handling, transportation, and integration with a launch vehicle was reviewed to assure these operations were feasible. It should be noted that the heat source assembly and handling do not require any hot cell facility other than a light local radiation shielding; however, the assembly is also thermally hot and requires handling tools. Since the emissivity coating may require rather delicate handling to avoid damaging and flaking of the coating, master-slave type handling equipment of standard design is preferred over any direct hand tool such as tongs. To avoid any oxidation damage to the heat source structure, a temporary and transportable cooling system must be connected to the ACHX as soon as fuel capsule loading starts. This temporary and transportable cooling system should be continuously active until the heat source is mounted in the launch vehicle and the launch pad cooling system is connected to the heat source ACHX. To prevent oxidation damage to the refractory structure, the ACHX is designed to keep the heat source temperature below 350° F. During transients in the oxygen atmosphere, 600° F is considered an acceptable limit without incurring oxidation contamination. The ACHX operation will be terminated when the launch vehicle liftoff is committed and the launch tower coolant lines are disconnected from the IRV. There is sufficient thermal inertia in the system so that if the cooling is terminated at liftoff, the system will be out of the oxygen atmosphere before the temperature reaches 600° F.

2.3.2 Isotope Reentry Vehicle (IRV)

The recommended IRV preliminary design is shown in Figure 1-1. This configuration is primarily a modification of the IRV concept developed during the efforts of Phases IA and IB. The IRV is designed to contain, and mate with, the heat source described in the preceding section.

The reference IRV has been designed to maintain the fuel capsule temperature below the design values listed in Table 2-15 in all possible flight regimes. Initial reentry conditions used to develop the aerodynamic environments to be encountered by the IRV are summarized in Figure 2-9. These conditions were established after a detailed review of the credible launch and flight failure modes. The reentry conditions coupled with the balance of the systems criteria, summarized in Table 2-16, combined to establish the IRV performance criteria.

TABLE 2-16

SYSTEM DESIGN REQUIREMENTS

Launch Environment	Atlas/Centaur, Saturn I-B, 20-sec Abort Delay
Reentry Initial Condition	$\alpha = 180$ degrees, Full Spin or Maximum Tumble Rate
Reentry Velocity (ft/sec)	17,000 to 26,000
Reentry Angle (degrees)	0 to -18
Spin Rate (rpm)	0 to 20
Tumble Rate (rpm)	0 to 6
Impact Velocity (ft/sec)	< 300
Pad Separation Distance (ft)	200 to 250
Maximum Fuel Capsule Temperature ($^{\circ}\text{F}$)	
Operational	2000
Reentry	2500
Fireball	3000

Aerodynamic load (structural, thermal) environment variation for the reference design, with the vented symmetrical fence was evaluated for various dynamic conditions. Those analyses included a review of vehicle stability over the flight regimes of interest and wind gust effects during the terminal descent phase. Resulting heat shield thicknesses are summarized in Table 2-17, for various locations on the vehicle. The table also notes the particular trajectory that provided maximum heating for that location.

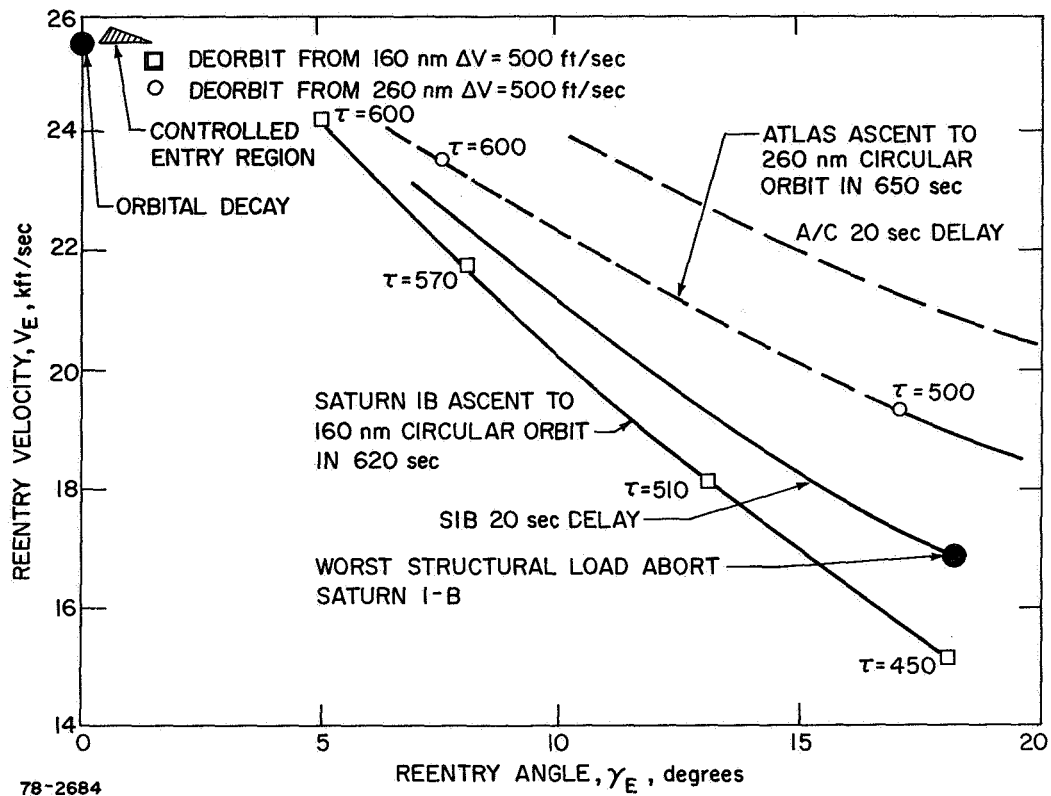
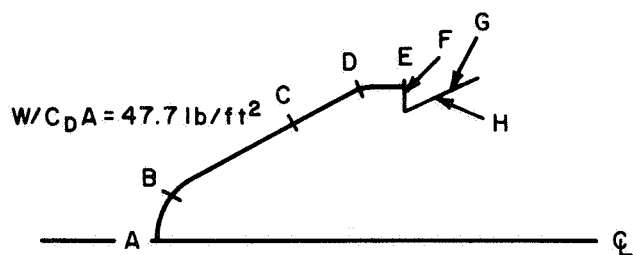


Figure 2-9 DESIGN REENTRY CONDITIONS

TABLE 2-17

IRV HEAT SHIELD REQUIREMENTS
AVCOAT 5026-39 HC-G



Location	Heat Shield Thickness (inches)	Design Trajectory	Trajectory No.	Integrated Heating (Btu/ft ²)
A	1.87	$\alpha = 180$ degrees (No spin)	8	56,200
B	1.72	$\alpha = 0$ degrees (No spin)	18	44,000
C	1.45	$\alpha = 180$ degrees (No spin)	18	17,900
D	1.87	Spinning Rearward	16	57,400
E	1.76	Spinning Rearward	16	46,900
F	1.50	Spinning Rearward	16	26,900
G	1.22	Spinning Rearward	16	23,000
H	1.12	Spinning Rearward	16	15,000

The IRV preliminary design layout, with blowups of specific fabrication details, is shown in Figure 2-10. Fabrication techniques identified in this design are similar to those employed in the Apollo heat shield program.

The vehicle is a 60-degree half-angle 25-percent blunt cone configuration. A 360-degree vented canted "fence" is employed to provide assurance of proper vehicle attitude during reentry under all credible mission nominal or failure modes. Total reentry weight of the 68-inch-diameter vehicle is 1977 pounds. The basic aeroshell is fabricated from aluminum honeycomb which is protected during reentry by a low-density ablator (Avco 5026-39) heat shield. Location aids are mounted on the vehicle to assist in recovery or to provide assurance of proper deep water burial of the reentered vehicle. A ballute located around the periphery of the vehicle is provided to limit terminal velocities prior to impact of the IRV.

Significant performance parameters of the IRV are listed in Table 2-18. Table 2-19 contains a summary of the mass characteristics of the reference IRV design.

2.3.3 Heat Source Heat Exchanger (HSHX)

The final heat source heat exchanger design configuration is illustrated in Figure 2-11. The core of the heat exchanger is composed of eighteen 1.44-inch-diameter tubes, each 68 inches long. Each tube describes an involute spiral from the outer circular ring manifolds to a central reversing header. The Brayton cycle working fluid is introduced into the top circular ring manifold where it is distributed to nine of the involute tubes, which conduct the gas across the core of the heat exchanger where it enters a central reversing header. From the central reversing header, the gas enters the nine return involute tubes where the gas is conducted back across the heat exchanger core and enters the bottom circular ring exit manifold. Thus, the major portion of the core consists of an array of tubes in which the flow in alternate tubes is in the opposite direction and the Brayton cycle working fluid makes two passes across the heat exchanger, one in and one out.

The HSHX is made entirely of Cb-1Zr. This material was selected on the basis of its high temperature stability for long-term operation in a space vacuum. Although superalloy materials were considered, they would require coatings to protect them against constituent evaporation at the elevated temperatures of interest. The long-term behavior of such coatings in a space vacuum is currently unknown. Thus, the all refractory metal approach was selected. A high-emissivity coating is applied to all surfaces of the HSHX to enhance the radiant heat transfer performance. The HSHX is supported on two ends. On one end it is supported by a flange attached to the cooler inlet manifold. On the other end, a pin attached to the inlet manifold is inserted in a retaining bracket that is part of the fixed cavity structure, as illustrated in Figure 2-12. The characteristics of the HSHX are given in Table 2-20.

The performance of the HSHX under various modes of operation is summarized in Table 2-21. Item 1 gives the temperatures throughout the system with HSHX 1 in operation at full output power. Item 2 gives the same information with HSHX 2 in operation at full output power. Item 3 presents the temperature data with HSHX 2 in operation with a maximum fuel capsule temperature of 2000° F. Under this condition, the power output from the second system drops to 6.15 kw_e.

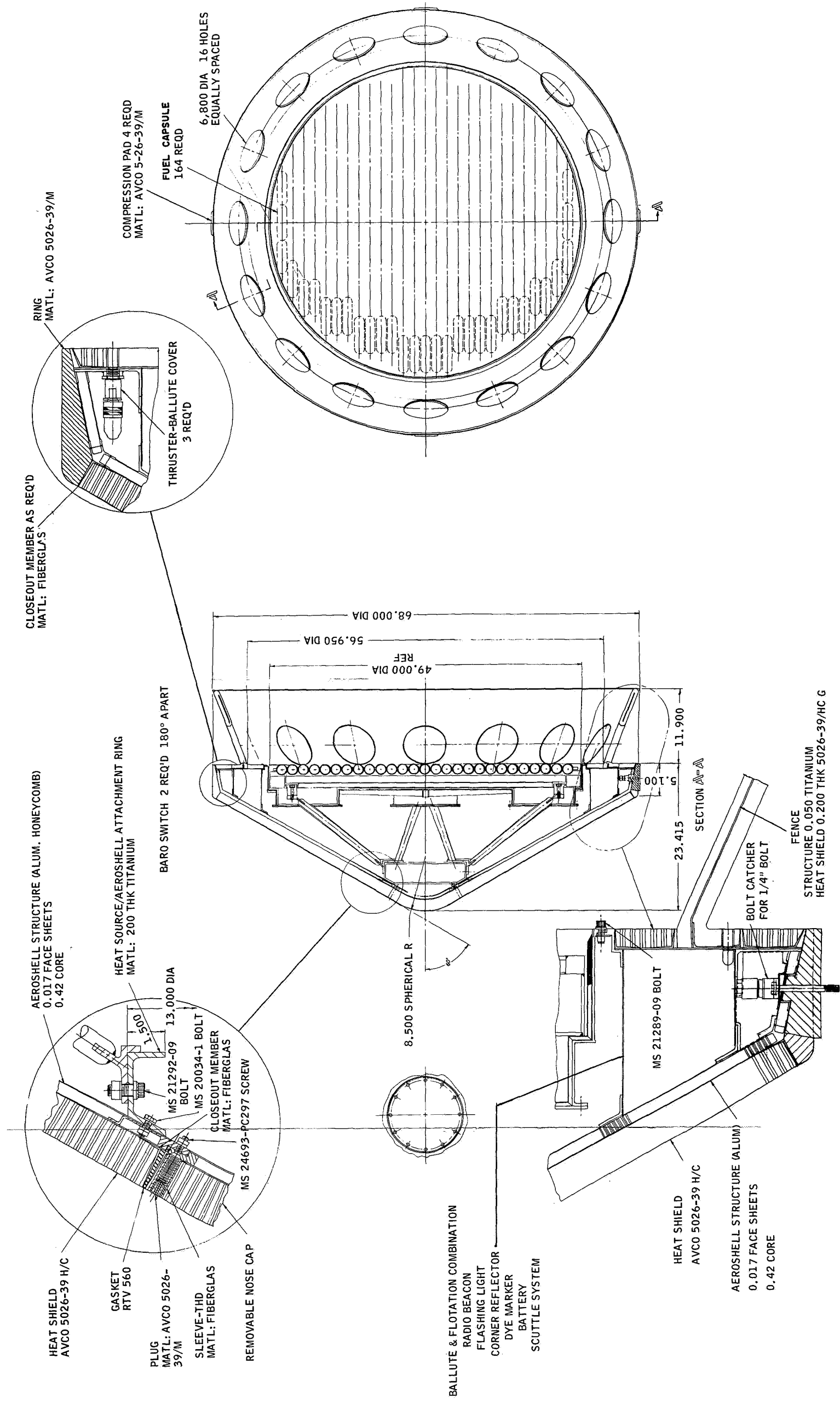


Figure 2-10 Irv PRELIMINARY DESIGN LAYOUT

TABLE 2-18

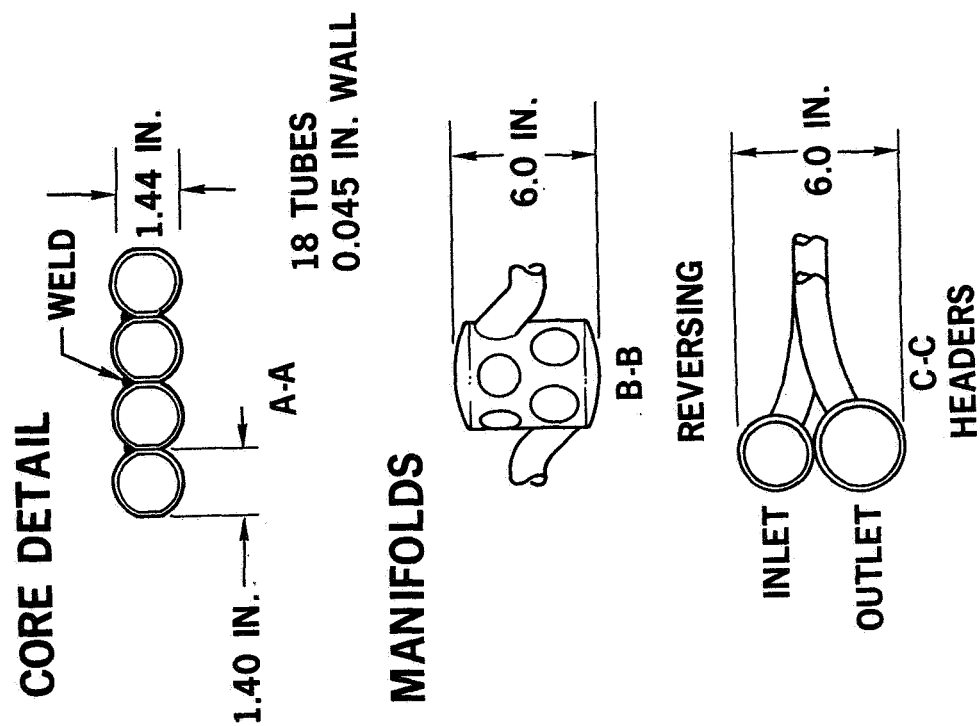
ISOTOPE REENTRY VEHICLE IRV PERFORMANCE SUMMARY

Configuration	60-degree Half-Angle Blunt Cone
Diameter (In.)	68
X_{cg}/D	0.31
$W/C_D A$ (lb/ft ²) (Hypersonic)	48
Terminal Velocity (Ft/sec)	
- = 0 degrees	266
- = 180 degrees	232
Entry wt (lb)	1980
Moments of Inertia:	
I_{xx} (Roll, Slug-ft ²)	186
I_{yy} (Pitch, Slug-ft ²)	102
Materials	
- Aeroshell	Aluminum Honeycomb
- Fence	Titanium Honeycomb
- Heat Shield	Avco 5026-39 (Apollo Heat Shield Material)

TABLE 2-19

MASS PROPERTIES SUMMARY
FOR REFERENCE DESIGN
Vehicle Diameter 68 inches

	Weight (Pounds) (1476)
A. Heat Source	
Fuel Capsules	755
Heat Source Plate	402
Cover Plate Assembly	87
Support Structure	153
Insulation Assembly	79
B. Aeroshell	(386)
Heat shield	215
Bond	4
Structure	68
Honeycomb	24
Truss Support	5
Brackets and Stiffeners	29
Hardware	10
Fence	99
Structure	15
Heat Shield	84
C. Ballute and Flotation Systems	(95)
D. Recovery Aids	(20)
E. IRV Reentry Weight	1977
F. Mass Properties of Reentry Vehicle	
Weight	1977
C.G. (Inches From Nose)	20.8
I_{xx} (Roll-Slug/ft ²)	186
I_{yy} (Pitch-Slug/ft ²)	102



S-43334

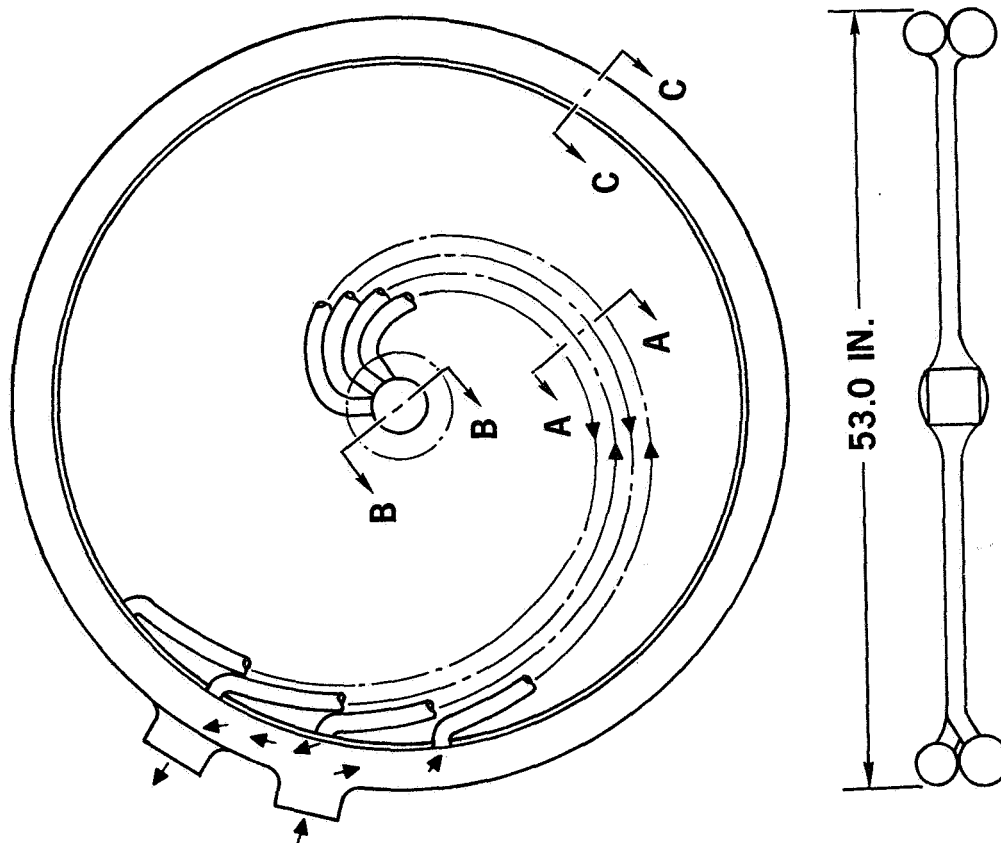
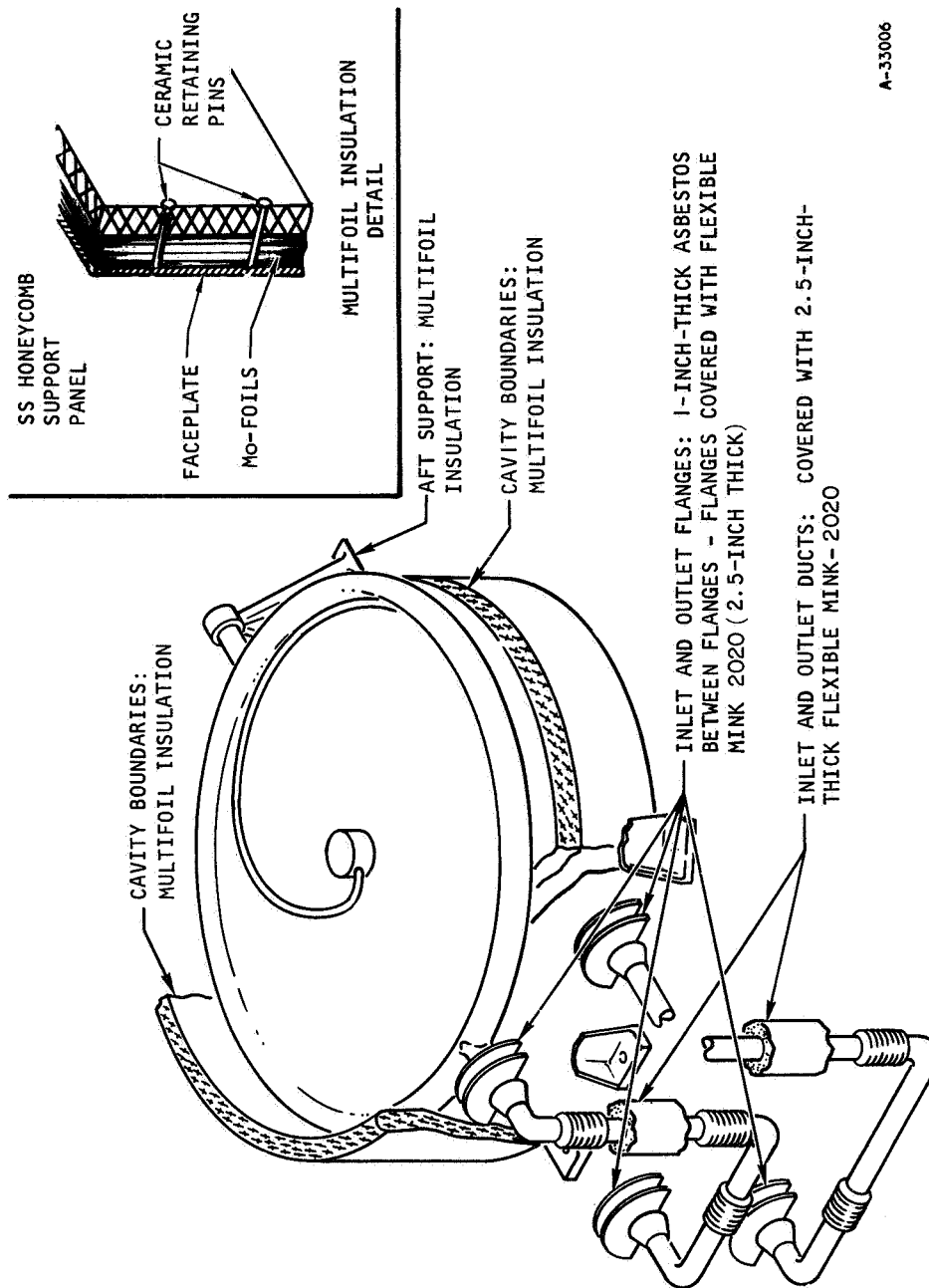


Figure 2-11 TWO-PASS INVOLUTE TUBULAR HSHX (FINAL CONFIGURATION)



A-33006

Figure 2-12 TYPICAL HSHX INSULATION AND SUPPORT CONCEPT

TABLE 2-20

HSHX CHARACTERISTICS

Core	
Number of tubes	18
Diameter of tubes (OD), in.	1.44
Length of tubes, in.	68.0
Tube wall thickness, in.	0.045
Inlet manifold	
Diameter, in.	2.40
Length, in.	160
Wall thickness, in.	0.045
Exit manifold	
Diameter, in.	3.00
Length, in.	160
Wall thickness, in.	0.045
Center header	
Diameter, in.	4.3
Height, in.	6.0
Weight, lb	
Tubes	75.5
Manifolds	41.7
Center header	3.8
Miscellaneous	6.1
Support	<u>3.2</u>
Total	130.3
Dimensions	
Overall diameter, in.	53.0
Overall height, in.	6.0
$\Delta P/P$	0.03
Flow maldistribution, percent	< 1
Thermal capacitance ($C_p W$), Btu/ $^{\circ}F$	13.0

TABLE 2-21

HSHX STEADY STATE PERFORMANCE SUMMARY

Operating Mode	Temperature, °F			
	Maximum Capsule	Maximum Effective Radiation	HSHX 1	HSHX 2
1. HSHX 1 in operation (power = 6.8 kw _e)	1916	1770	1614 to 1672	--
2. HSHX 2 in operation (power = 6.8 kw _e)	2060	1935	1780 to 1830	1630 to 1690
3. HSHX 2 in operation (power = 6.15 kw _e)*	2000	1860	1735 to 1785	1588 to 1645
4. HSHX 2 in operation (power = 5.7 kw _e)*	1916	1770	1610 to 1660	1460 to 1520

Heat Leaks	Watts
Cavity	305
Ducts	404
Support structure	263
Total	972

* Estimated on Conditions 1 and 2.

Item 4 gives the same data with the maximum fuel capsule temperature held to 1916° F (that is, the same as Item 1). Under these conditions, the power output drops to 5.7 kw_e. Item 5 presents a summary of the heat leaks associated with the HSHX system for the installation concept described in Section 5.0.

2.4 CONCLUSIONS AND RECOMMENDATIONS

The basic conclusions reached after completion of Phases I and II are summarized in Table 2-22.

In addition to these conclusions, a series of recommendations pursuant to ultimate hardware development have resulted from the completion of the two tasks. These recommendations follow:

- Turnaround device test program should continue in concurrence with investigation of geometry variation effect on IRV performance.
- Aerodynamic test programs are required to develop heating and stability coefficients over flight regimes of interest for this geometry.
- Continue analytical evaluation of vehicle reentry performance sensitivity to spin rate and moment coefficient variation.
- Advanced (Graphitic) heat shield cover and fence materials should be considered for potential weight and diameter reduction on IRV.
- Impact testing should be initiated to evaluate IRV utility on limiting impact damage to isotope fuel capsules.
- Test effort should be initiated to determine the effect of long term space exposure to the IRV operating environment on materials, components, and subsystems, e.g., low density ablator, thermal control coatings, pyrotechnics, thermal batteries, solid propellants.

2.5 REFERENCES

- 2-1 Isotope Reentry Vehicle Study Conceptual Design, Phase IA, Topical Report, AVSSD-0071-68-CR, NASA CR-72366.
- 2-2 Isotope Reentry Vehicle Design Study Conceptual Design, Phase IB, Topical Report, AVSSD-0193-68, CR-NASA CR-72463.

TABLE 2-22

CONCLUSIONS

- Preliminary design meets design objectives.
- Use of cover plate is warranted by its combined utility in capsule retention and as a thermal protection element.
- Ballute appears to be a practical and attractive retardation device.
- Heat source fuel capsules will survive all credible reentry environments to impact.
- Use of reference vented capsules could result in a significant weight reduction.
- Basic insulation system should be multifoil type because of its low conductivity.
- Tubular HSHX is preferable because of light weight and simple rugged construction.
- Avcoat 5026/39 heat shield material is preferred since its properties meet design requirements and it is extensively characterized.
- Further high temperature emissivity coating performance and materials compatibility testing should be completed.
- Insulation system development to characterize fabrication techniques, edge effects, and performance in the various operating modes (including dynamic environment) is required.
- Vehicle dynamics must be established in conjunction with fence development to determine effort on transonic and subsonic stability.
- Continued investigation of ballutes and parachutes should be conducted to firmly establish feasibility and utility.
- Vented capsules should be further evaluated in detail to explore potential significant reduction in weight and diameter.
- Heat transfer testing should be conducted to verify heat transfer coefficients for low Prandtl number flow in HSHX.
- Materials characterization should be conducted for refractory alloys response to operating environment.
- Investigate maximum acceptable short term capsule temperature limit.
- Further consideration should be given to HSHX replaceability requirement.

3.0 IRV PRELIMINARY DESIGN

During Phase II of the IRV program a preliminary design of the IRV was defined using the results of Phases IA and IB. More detailed studies were conducted relative to systems analysis, reentry performance, heat source and aeroshell designs. The aforementioned studies were integrated with each other to satisfy overall system constraints while at the same time providing a practical design.

The systems analysis consisted of defining the V_e, γ_e conditions, failure mode analysis, sequence of events and safety (including on-pad booster explosion). In addition, requirements for location aids and a ballute were developed.

The reentry performance studies included evaluation of stability effects, dynamic characteristics (spin, tumble), fence requirements, terminal and gust effects, loads and heating for both the aeroshell and heat source capsules. A strong interface exists between reentry conditions, allowable capsule temperature and fence requirements, and this effect was evaluated.

In the heat source design consideration had to be given a proper thermal analysis of the entire system during on-pad, launch, orbit and reentry. From these studies definition of insulation, structural support and heat sink requirements were established by combining the thermal and structural considerations. The analysis during reentry which determined maximum capsule temperatures was used with the performance analysis to define reentry turnaround requirements. The heat source studies also developed the design of the ACHX system used for on-pad cooling. A fabrication plan and set of drawings outlining details of the heat source were also provided.

The size of the aeroshell was defined by the diameter, weight, and configuration of the heat source. Selection of the heat shield and structural material considered the wide range of heating, shear, pressure and loads possible with the various entry modes. Location of location aids, ballute and detailed weight and moment-of-inertia values were determined for utilization in trajectory studies.

The following sections describe in detail the analysis conducted to define the complete IRV concept.

3.1 SYSTEMS ANALYSIS

The IRV has been designed to function reliably and safely under the complete range of operational and abort environments imposed on it for the two basic missions specified in the Phase IA Report (Ref. 3-1), (i.e., the Saturn I-B Integral Launch in a MORL class vehicle and the Atlas/Centaur Separate Launch). The approach used in the safety analysis to establish the adequacy of the design was to:

- a. systematically review each phase of the nominal mission profile,
- b. specify all operational and design requirements necessary to fulfillment of mission goals, and
- c. at all times satisfy the safety criteria established at the outset of their programs.

A failure mode analysis was completed to ascertain system performance under off-nominal mission conditions. This was accomplished by considering all credible malfunctions during each phase of the mission profile. Each situation was carried to either a "safe" or "unsafe" condition. In the latter case, system design or the operational procedures were modified until a "safe" condition was obtained. A "safe" condition has been arbitrarily defined in this study as a terminal event or disposal of the IRV which involved no potential criticality hazard or release of fuel in the biosphere. Deep water burial of the IRV has been assumed to be an acceptable disposal mode. The results of the study are presented in Phase 1A Report (Ref. 3-1).

Equipment requirements resulting from this analysis are listed in Tables 3-1, 3-2, and 3-3 in three categories:

- a. Routine Launch Equipment -- those equipments or subsystems normally available at the launch site or on the launch vehicle that are vital to assurance of no nuclear hazard during launch pad or launch operations.
- b. IRV Subsystems -- those IRV subsystems or interface hardware requirements dictated by mission or launch vehicle imposed constraints, that are absolutely essential to guaranteeing mission safety during all operational phases.
- c. Optional IRV Subsystems -- those equipments whose inclusion may limit fuel capsule damage potential during ground impact or facilitate IRV recovery. (An absolute requirement for inclusion of these equipments in the IRV has not, however, been demonstrated during the study.)

The results of the systems safety analysis show that during each mission phase there are several orders of safety mechanisms built into the IRV system design which act to prevent the occurrence of any potential nuclear hazard. Table 3-4 lists these mechanisms by mission phase. It is important to note that there are always at least five orders of safety barriers (six during the most critical pre-launch, ascent, and orbital phases) present in the overall system design.

The results of the Phase IA and IB systems analyses have been updated to be specifically applicable to the IRV preliminary design developed during Phase II. These modifications and final results are summarized in the following paragraphs in terms of Design Requirements (para. 3.1.1); and IRV ancillary system resulting from safety or integration interface imposed requirements (i.e., Drag Augmentation System (para. 3.1.2), Location Aids (para. 3.1.3), and Safing, Arming, and Initiation System (para. 3.1.4)).

3.1.1 Design Requirements

In view of the fact that the IRV must meet its performance and safety requirements under the most severe expected environmental conditions, only those sequences and events which lead to the critical environmental conditions will be discussed in this systems analysis review. The peak vibration and shock environments occur during ascent, while the IRV is still attached to the launch vehicle. These environments are summarized in the Aeroshell Structure section (3.4.1.2). The most severe aero-thermal and structural loads environment which must be considered during the nominal mission profile occurs as a result of reentry either from an early launch abort or from an uncontrolled decay out of orbit reentry situation.

TABLE 3-1

ROUTINE LAUNCH EQUIPMENT

1. Instrumentation	4. Telemetry
2. Ground Support Hardware and Software (GSE)	5. Rate Instrumentation (Launch Vehicle only)
3. Abort Sequencing System	6. Spacecraft Display Systems

TABLE 3-2

IRV SUBSYSTEMS

1. Redundant Active Elements in Auxiliary Coolant Heat Exchanger (ACHX)
2. Passive and Active Heat Dump
3. Shroud Jettison System
4. Disconnect and Separation Subsystem (With Redundancy)
5. Abort Rockets with Thrust Vector Control (TVC)
5. Aeroshell -- Structure and Heat Shield
7. Location Aids

TABLE 3-3

OPTIONAL IRV SUBSYSTEMS

1. Impact Attenuation System
- Crushup
- Ballute
2. Location Aids
- Parachutes
- Flotation System

TABLE 3-4

SAFETY MECHANISMS

	Ground Handling	On The Pad	Ascent	Orbital	Reentry	Descent	Impact
1st Order Safety Mechanism	Shipping Container	Redundant Auxiliary Coolant System	* Heat Sink (BeO)	Alternate Heat Rejection Systems	Aeroshell	Air Snatch	Water Impact
2nd Order Safety Mechanism	BeO	Abort and Recovery System	Abort, Reentry Aeroshell and Recovery System	Abort, Reentry Aeroshell and Recovery System	BeO	Impact Attenuation System	Impact Attenuation System
3rd Order Safety Mechanism	Fuel Plate	BeO	Impact Attenuation System	Impact Attenuation System	Fuel Plate	Fuel Plate	Fuel Plate
4th Order Safety Mechanism	Fuel Capsule	Fuel Plate	Fuel Plate	Fuel Plate	Fuel Capsule	Fuel Capsule	Fuel Capsule
5th Order Safety Mechanism	Fuel Form	Fuel Capsule	Fuel Capsules	Fuel Capsules	Fuel Form	Fuel Form	Fuel Form
6th Order Safety Mechanism	--	Fuel Form	Fuel Form	Fuel Form	--	--	--

* IRV launched in passive heat rejection mode.

Two basic reentry conditions must be considered in the analysis: (a) controlled deorbit based on employment of a retrorocket to ensure downrange impact in a pre-selected location, and (b) off-nominal reentry conditions. These two basic cases are discussed separately in the following paragraphs.

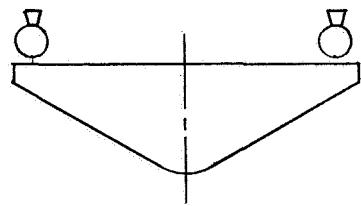
a. Controlled Deorbit

Reentry conditions resulting from a controlled deorbit maneuver are significantly influenced by the amount of deorbit ΔV , and the manner (direction) of its application. A tradeoff exists between the size of the retro package, the reentry conditions, and downrange dispersion. A large value of velocity correction (ΔV), which means a heavier retrorocket package will result in minimum downrange dispersions, higher reentry loads, higher heating rates, but lower integrated heating. A low ΔV means a smaller retro package, but results in greater downrange dispersions, lower heating rates and loads, but possibly, higher integrated heating. Parametric reentry conditions, generated for a variety of ΔV 's, and application angles, are presented in Figures 3.2-7 through 3.2-14 in the Phase IA Report (Ref. 3-1). As a result of this study, a deorbit ΔV of 500 ft/sec has been selected for a reference case. This ΔV will ensure direct reentry (i.e., no skip cases), reasonable downrange impact accuracy, and require a deorbit package size which is comparatively small.

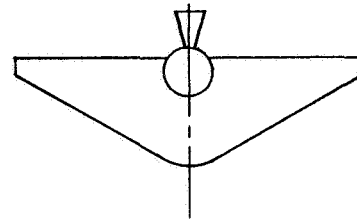
The orientation and spin rate are dependent upon the type of deorbit system used. There are four possibilities as shown in Figure 3-1. Another possibility comes from a mission class wherein the entire spacecraft is deorbited with the IRV being ejected subsequent to the deorbit action. In any case, the spacecraft provides desired orientation for IRV reentry prior to retrofire.

A tradeoff study was conducted during the Phase IB portion of the study to determine which of the four configurations presented in Figure 3-1 was preferable. The single rocket with a central internal location, although one of the best from a performance point of view, was discarded because of the integration problems associated with the HSHX, the severity of the thermal environment and the resultant weight and diameter penalty. The characteristics of the other three configurations are summarized in Table 3-5. Ease of integration and the amount of spin stabilization (for Thrust Vector Control (TVC)) are considered to be the most vital aspects of retro package system specification. As will be noted in subsection 3.3 vehicle turnaround time is a strong function of spin rate. The tower-mounted configuration is difficult to integrate (particularly into the MORL class vehicle) because of the length required to allow rocket plume expansion. It also requires the highest spin rate for TVC (Figure 3-2). The peripheral system is the easiest to integrate and implement, but it is the least reliable, requires higher spin rates than the nose-mounted configuration, and has an unacceptable tumbling failure mode in the event of a single rocket misfiring.

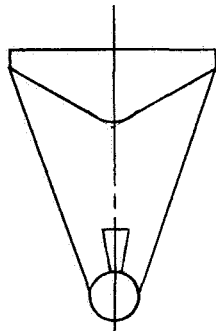
The nose-mounted configuration, therefore, has been selected for the reference design. Because of the direction of application of the retro thrust, however, the resultant reentry angle of attack is near backwards, since the vehicle is fixed inertially in space and travels approximately half an orbit before entry occurs.



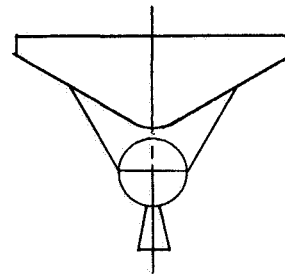
FOUR ROCKET PERIPHERAL
LOCATION



SINGLE ROCKET
CENTRAL INTERNAL
LOCATION



SINGLE ROCKET
TOWER SYSTEM



SINGLE ROCKET
HEAT SHIELD MOUNTING

776470P

Figure 3-1 DEORBIT AND ABORT ROCKET INTEGRATION CONCEPTS

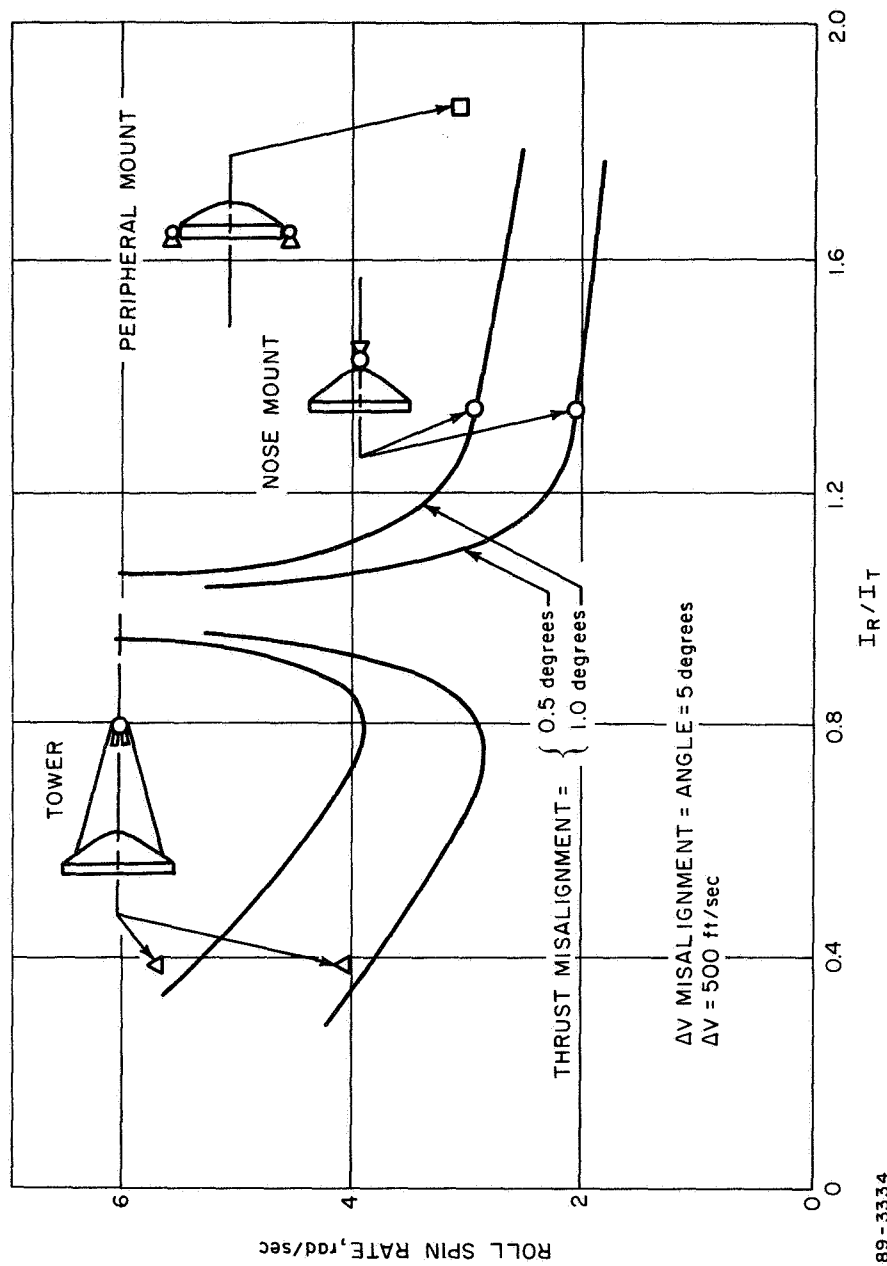


Figure 3-2 DEORBIT SYSTEM CONSIDERATIONS

TABLE 3-5

DEORBIT SYSTEM CONSIDERATIONS

Configuration	Spin Requirements	Integration	Reliability	Weight	Volume	Operation	Performance
Nose Mounted	Lowest Spin	Easiest	Best	Lowest	Lowest	Requires separate abort system	Backward entry
Tower	Highest	Most Difficult	Good	Highest	Highest	Can be used for abort mode	Low angle of attack entry
Peripheral	High	Not Bad	Very Poor	O.K.	O.K.	Can be used for abort mode	Low angle of attack entry

b. Off-Nominal Mission Profile

The most severe design environments were found to result from off-nominal mission situations, or from a mission malfunction. The failure mode analysis conducted during the Phase IA portion of the study concluded that the critical failure modes were:

- Pad Fire
- Ascent Abort and Reentry
- Ground Impact

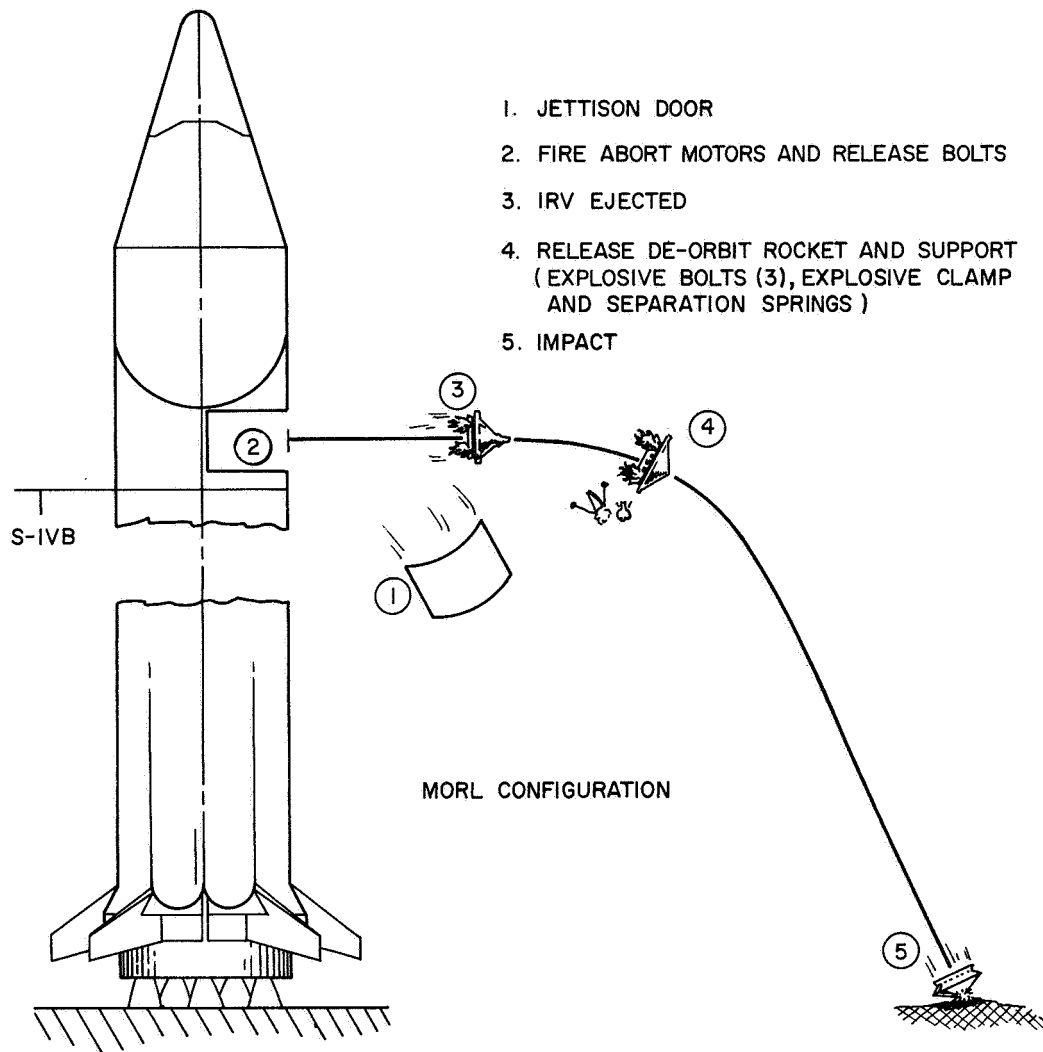
The effect these failure modes have on system design and operational characteristics are discussed in the following paragraphs.

Pad Fire

The abort system described in the Phase IB study was designed to achieve a safe separation distance from the launch vehicle. This distance is assumed to be a minimum of 200 feet in the horizontal direction. The distance choice is based on an arbitrary requirement to escape falling debris from the launch vehicle or the gantry on the pad. It is activated in the case of a launch vehicle malfunction which is assumed capable of terminating in booster detonation or fire. A complete description of the abort and separation system is presented in subsection 4.2.

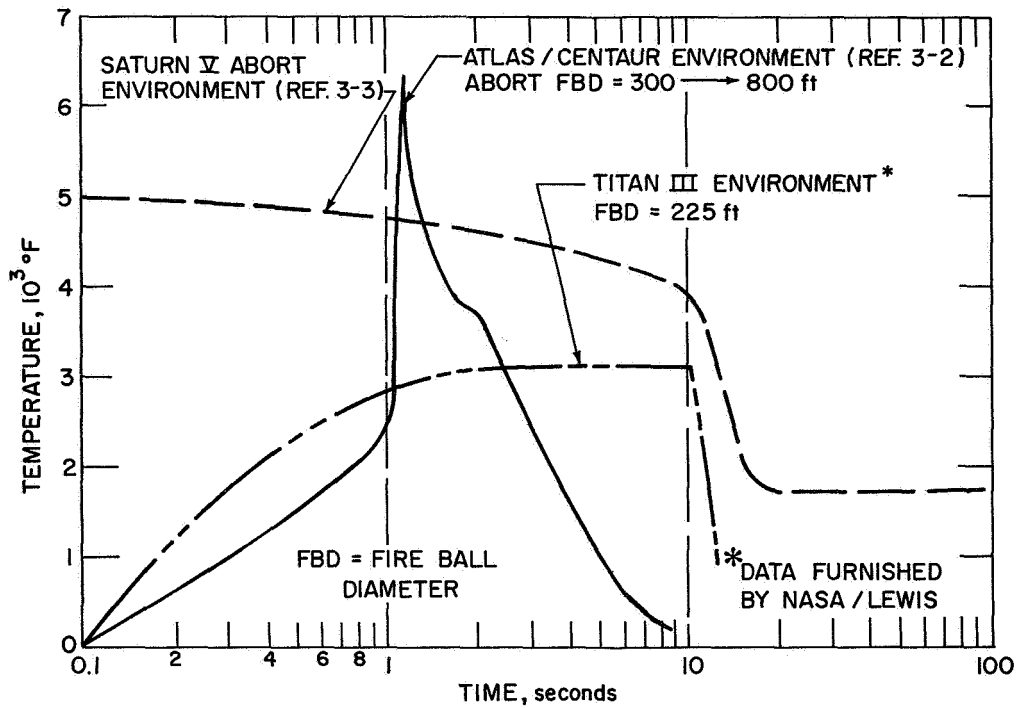
In a typical pad abort situation the rockets which are attached to the support ring, are not fully fired before the IRV/support ring reaches the end of the guide rails. Consequently, the support ring and the IRV leave the launch vehicle still attached. Being unguided, TVC must be provided by spin stabilization for the IRV. The analysis presented in the Appendix of the Phase IB report establishes the credibility of spinning up while thrusting for TVC. This procedure is followed in determining the required spin-up acceleration. The deorbit package is jettisoned before ground impact to avoid the possibility of perforating the heat source mounting plate on impact, or detonating the deorbit rocket propellant. It should be noted that the deorbit rocket itself can be disabled in case proper separation does not occur.

The sequence of events for pad or early launch abort is depicted in Figure 3-3. For the situation where this primary safety system (the abort system) malfunctions, the IRV will be subjected to the pad fire and overpressure environment. The overpressure environment is of negligible significance when compared to the basic strength capabilities of the capsules themselves. The fireball environment is, however, of greater significance. Figure 3-4 presents typical pad fire environments. A dynamic thermal model of the pad fire situation has been postulated and used in the basic analysis. This model consists of the capsule's being directly exposed to the fireball environment, followed by the capsules being exposed to the surrounding ambient environment, in a worst case situation where the IRV comes to rest upside down (nose up) on the ground.



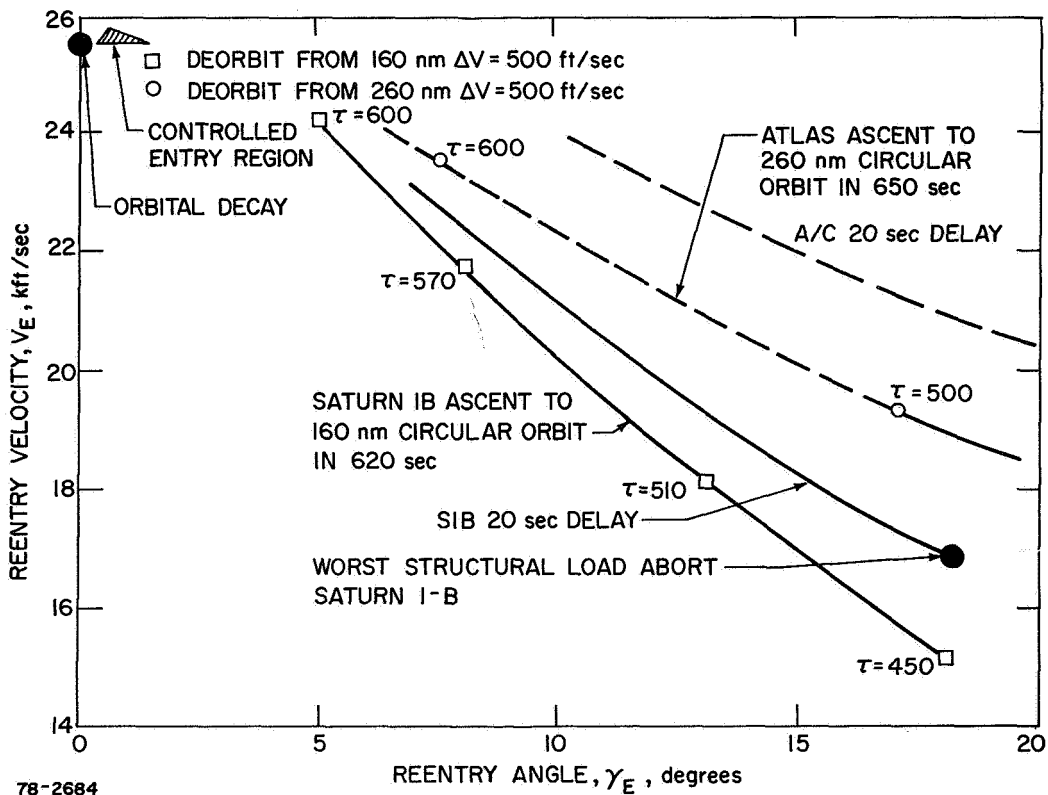
89-3335

Figure 3-3 LAUNCH PAD AND EARLY ABORT SEQUENCE



78-2683

Figure 3-4 FIREBALL THERMAL ENVIRONMENT



78-2684

Figure 3-5 DESIGN REENTRY CONDITIONS

The parameter of interest is the temperature-time history of the capsules. A thermal analysis of the pad fire situation is discussed in detail in paragraph 3.4.2. In summary, a safe situation exists for the case where the capsules are exposed to the ambient environment. For the upside down case and where the insulation surrounding the heat source plate is undamaged, the capsule temperature continues to rise. This condition requires that a recovery team get to and relieve the situation within 60 minutes after the accident.

The most critical failure mode that could occur is the release and dispersion of fuel fines in the atmosphere. The occurrence of this failure mode is most probable under the condition of an ascent system failure which results in an ascent or orbital abort situation. The principal systems which prevent the release of fines failure mode are the separation systems, the aeroshell configuration, the heat shield, heat sink and fuel capsule shell. The design and selection of the aeroshell and heat shield is predicated on the aerodynamic and reentry environments which could be achieved as a result of an abort during any phase of the mission profile. It is with this motivation that the ranges of all possible reentry conditions which lead to the most severe heating and loading environment have been determined. The resulting envelope of reentry conditions is shown in Figure 3-5. This figure summarizes the complete range of credible reentry conditions to which the IRV could be subjected during all mission phases.

These initial conditions are valid for a reentry altitude of 400 kft. When coupled with configuration, angular motion, initial attitude, and vehicle ballistic parameter, they lead to specific integrated heating loads, heating rates and structural loads. This environment provides the principal basis for aerodynamic configuration and reentry heat shield design.

Referring to the lower curves in Figure 3-5, designated as "Saturn IB Ascent" and "Atlas/Centaur Ascent", the indicated $V_e - \gamma_e$ conditions stem from any ascent system failure situation which results in engine shutdown prior to thrust application in an improper direction. The time refers to time into flight. The next upper sets of curves refer to reentry conditions which would result from engine shutdown and subsequent destruct, assuming a 20-second delay between initial malfunction and final shutdown. During this 20-second delay, thrusting is assumed to have been applied in a direction measured from the instantaneous flight path angle, ranging from 0 to 360 degrees. The curve represents the upper bound of the resulting reentry condition.

To obtain more severe reentry conditions, the following sequence and specific situations must occur:

1. A malfunction which results in a pitch-over maneuver to a specific angle (measured from the flight path angle) and (designated as "Direction of applied ΔV ") which would result in maximum reentry angle and reentry velocity.
2. A malfunction which results in fixed attitude stabilization at that pitch-over orientation.
3. An engine shutdown and destruct system failure.
4. A command guidance override system failure.

The result of these conditions and malfunctions means that the total remaining ΔV is applied in a fixed direction. These specific conditions have been computed and are shown in Figures 3.3-1 and 3.3-2 in the Phase IA Report (Ref. 3-1). Any deviation from these specific malfunctions and sequence of events will result in significantly lower reentry conditions. It is apparent that these conditions represent an incredible (i.e., essentially impossible) series of events.

The circular, "0", and square, "□", data points in the upper left hand corner of Figure 3-5 represent the resulting reentry conditions from the nominal de-orbit situation. The data point on the ordinate represents the orbital decay situation (e.g., the circular orbital velocity at 400 kft).

A summary of the system design requirements which stem from the types of environmental conditions discussed previously is presented in Table 3-6.

TABLE 3-6

SYSTEM DESIGN REQUIREMENTS

Launch Environment	Atlas/Centaur, Saturn IB, 20-second Abort Delay
Entry Initial Condition	$\alpha = 180$ degrees, Full Spin or Maximum Tumble Rate
Entry Velocity, ft/sec	17,000 to 26,000
Entry Angle, degrees	0 to -18
Spin Rate, rpm	0 to 20
Tumble Rate, rpm	0 to 6
Impact Velocity, ft/sec	<300
Pad Separation Distance, ft	200 to 250
Maximum Fuel Capsule Temperature, ° F	
• Operational	2000
• Reentry	2500
• Fireball	3000

Ascent Abort and Reentry

The IRV would be subjected to significant reentry heating and structural loads if an abort occurred during the ascent phase of the mission. Predictable reentry can only be guaranteed if the IRV has been separated cleanly from the spacecraft and IRV support structure. The support ring is an item that could possibly constitute a problem to the IRV reentry protection system if it were to reenter while still attached to the IRV. To eliminate this problem the separation system is designed to prevent the support ring from leaving the spacecraft after the early launch phase of the mission (~30 to 50 seconds) has been completed. This is accomplished by activating the "rail ring support stops" and the support ring disconnect pins. The stops physically prevent the support ring from traveling beyond the end of the rails. The disconnect pins are the only positive attachment between the IRV and the support ring. When released the ring is accelerated down the rails along with the IRV which is inertially held against the shoulder within the support ring. The acceleration is provided automatically by the separation spring and/or by the abort rockets.

Again, after separation, the deorbit package is jettisoned, if present, and (if late in the ascent phase) reentry occurs with a possible range of conditions presented previously.

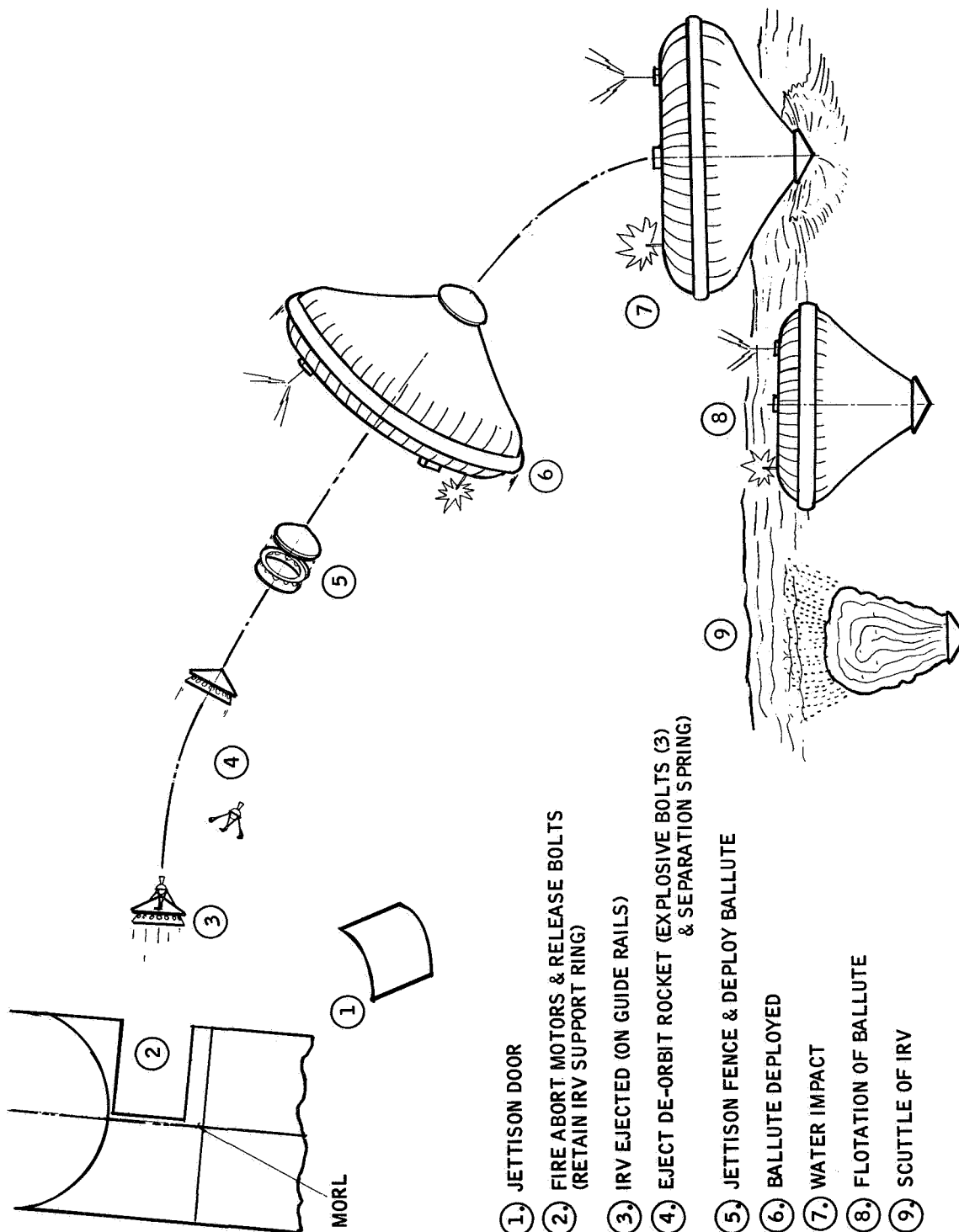
The abort sequence is depicted in Figure 3-6. For a mission, where a deorbit package is not necessary, event 4, which results in a jettison of the retro-rocket, would not be required.

Ground Impact

The events which lead to ground impact and the impact attenuation concepts are discussed in detail in the Phase IA and IB topical reports (Refs. 3-1 and 3-4, respectively). One of the following situations must develop in order to achieve ground impact: an early launch abort; ascent abort over a land mass; and a deorbit system failure which results in an improper application of the deorbit retro thrust or a random orbital decay reentry.

Possible hazards to fuel capsule during ground impact, either capsule rupture (with subsequent escape of entrapped fuel fines) or capsule burial, were items of primary concern during the study. During Phases IA and IB various methods of eliminating or alleviating these potential hazards were reviewed. In addition, it should be noted that the refractory fuel capsules in themselves are a tough safety barrier. (Tests have indicated that the individual capsules can survive impacts on an unyielding surface at velocities greater than 300 ft/sec. Vehicle terminal impact velocities are less than 300 ft/sec.) The principal objective of any impact mechanism, therefore, would be to aid in achieving a right side up (nose down), exposed and intact condition of the heat source after impact.

Two types of impact damage limiting devices were evaluated in the Phase IA and IB effort. They are structural (crushup) impact attenuation system internal to the IRV and a ballute used to retard impact velocities and ensure proper IRV attitude at impact. (In addition, the weight and volume requirements for a parachute recovery package were developed in Phase IA.) The ballute was incorporated in the reference IRV preliminary design. It is described in



1. JETTISON DOOR

2. FIRE ABORT MOTORS & RELEASE BOLTS
(RETAIN IRV SUPPORT RING)

3. IRV EJECTED (ON GUIDE RAILS)

4. EJECT DE-ORBIT ROCKET (EXPLOSIVE BOLTS (3)
& SEPARATION SPRING)

5. JETTISON FENCE & DEPLOY BALLUTE

6. BALLUTE DEPLOYED

7. WATER IMPACT

8. FLOTATION OF BALLUTE

9. SCUTTLE OF IRV

ASCENT-ABORT
MORL-CONFIGURATION

Figure 3-6 ASCENT ABORT -- MORL

78-2741

paragraph 3.1.2. (An impact attenuation system capable of ensuring retention of integrity of the heat source during impact has been studied.) The tradeoff analysis between the various impact attenuation concepts is presented in the Phase IA report. The selected concept (the rotation concept) and the associated optimization study was conducted in the Phase IB effort. The basic features of the rotation concept and its advantages over candidate systems are summarized in Table 3-7.

TABLE 3-7

ROTATION CONCEPT

<u>Purpose</u>
- Heat Source Impacts Flat
- Intact Heat Source
- Limit Damage to Capsules
<u>Advantages</u>
- Lower Weight
- Smaller Diameter
- Less Volume
- Additional Attenuation
- Less Heat Leak

The basic configuration and its expected operational characteristic are shown in Figures 3-7 and 3-8, respectively. The principle involved is discussed in detail in the Phase IA and IB reports. In operation the concept controls the direction of application of the impact loads to the heat source plate, and thus to the capsules. A flat final impact will ensure that the capsules are loaded in the most desirable manner (i.e., while supported in their retention cradles). The results of the tradeoff study between IRV gross weight and vehicle diameter for the most optimistic combinations of geometry options (see analysis in Phase IB report, Ref. 3-4) is presented in Figure 3-9. It is evident from the figure that a weight and diameter penalty must be paid in order to include impact attenuation. The minimum weight penalty is on the order of 300 pounds.

Further capsule analysis and test effort are required to determine the requirement for and/or the utility of an impact attenuation system in the IRV. The penalty is a significant cost in weight and vehicle diameter. The results of the analysis are summarized in the Phase IB report (Ref. 3-4).

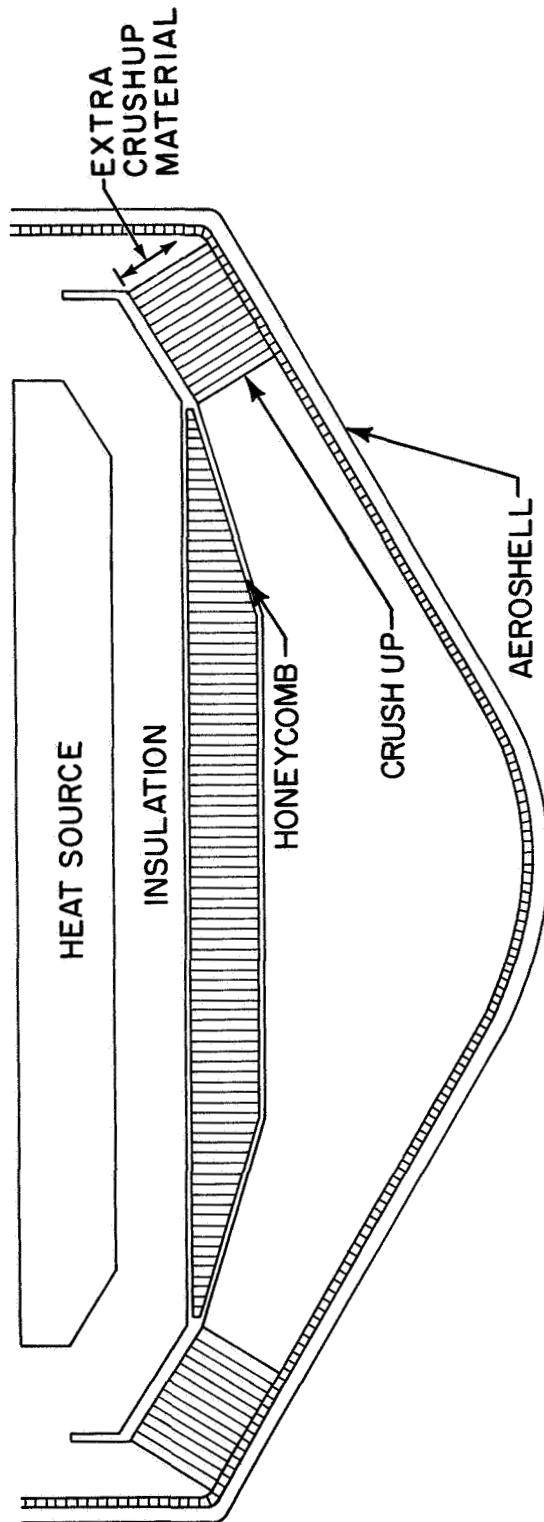
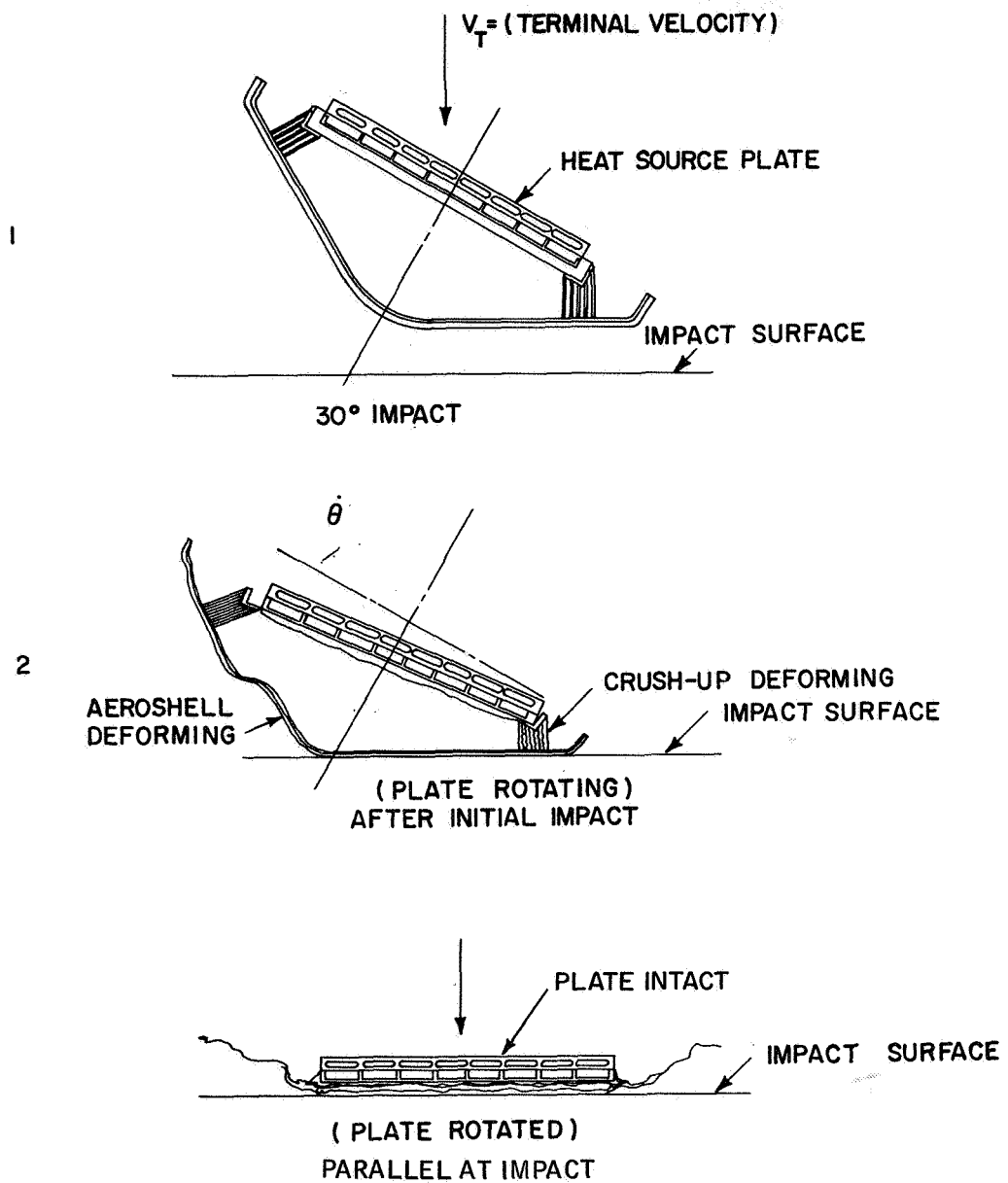


Figure 3-7 COLD PLATE CONCEPT WITH RECESSED CORNER

78-0627



776358

Figure 3-8 IRV ROTATIONAL IMPACT ATTENUATION SYSTEM CONCEPT

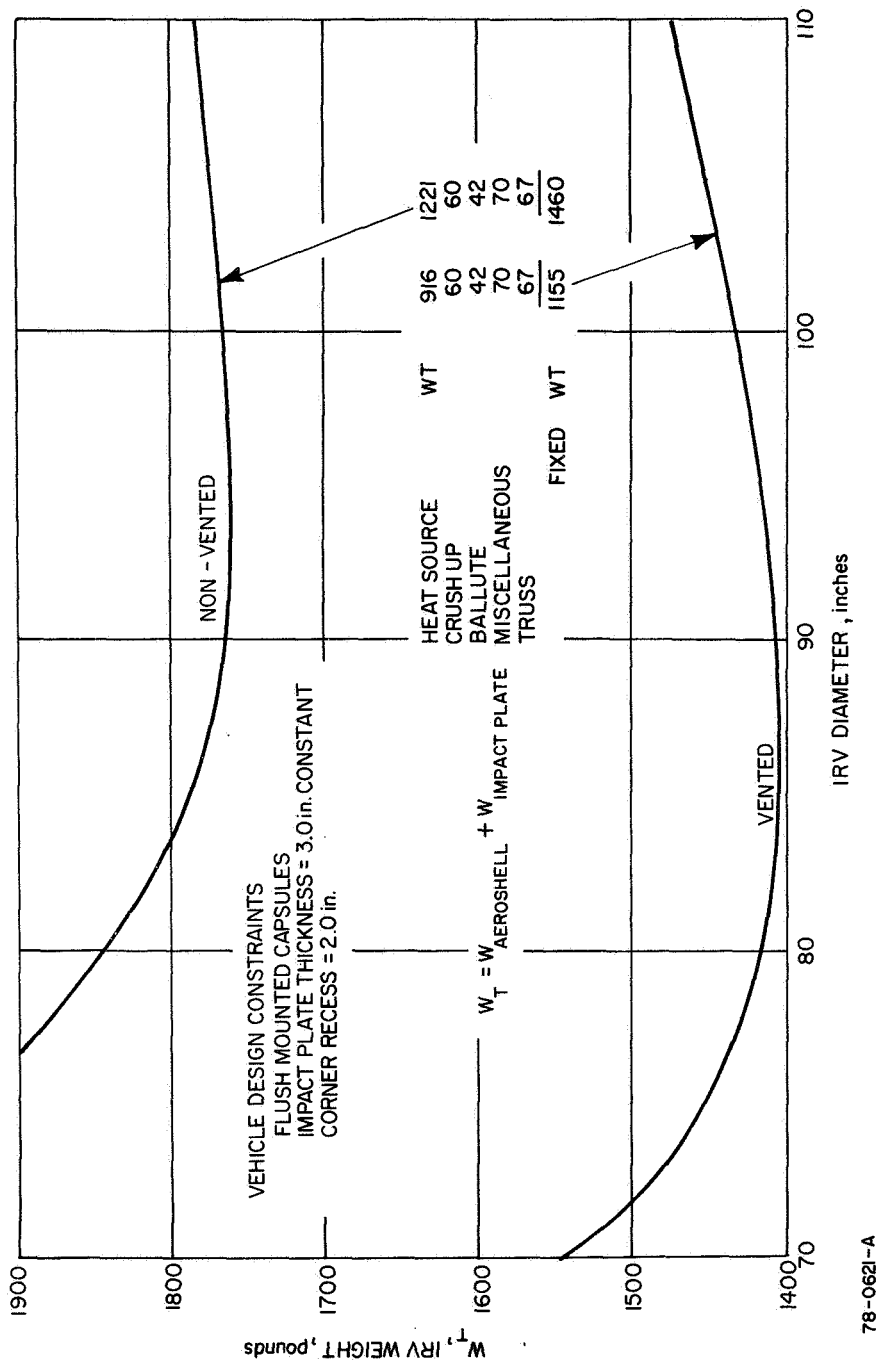


Figure 3-9 REFERENCE DESIGN FOR WEIGHT AND DIAMETER TRADEOFF STUDY -- WITH CRUSHUP

3.1.2 Drag Augmentation System

During Phase IB, the requirement for a drag augmentation system to reduce impact was reviewed. Two drag augmentation devices were examined briefly: the ring sail parachute system and the tuck-back ballute system. A tuck-back ballute was recommended for inclusion in the Phase II IRV preliminary design.

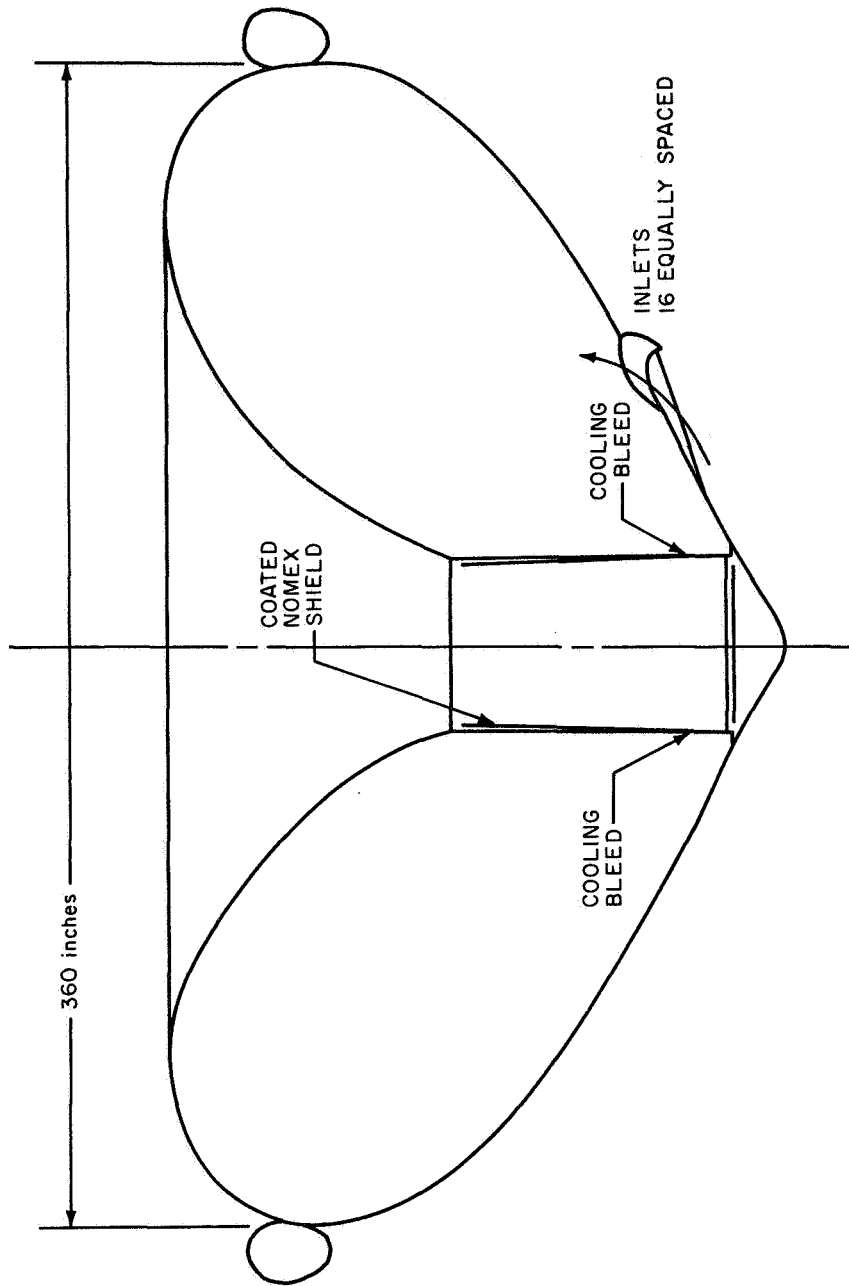
During Phase II a brief design study of the tuck-back ballute system was conducted by the Goodyear Aerospace Corporation. They developed a conceptual design of this expandable aerodynamic decelerator device. Figure 3-10 shows the basic ballute design. A maximum size attached tuck-back ballute, 30 feet in diameter, can be accommodated within the torus around the heat source (approximately 4000 in.³). With this ballute size the terminal velocity will be approximately 55 ft/sec. Sixteen inlets (each 2 feet in diameter) are provided for ram air inflation during deployment. A webbing loop located about 7 feet above the re-radiation surface is provided to establish a cylindrical hole for emitting the radiant heat. An inner reflective coated Nomex liner is used to protect the ballute structure from thermal radiation from the heat source. Cooling bleed holes are provided from the ballute envelope to the rear side of the Nomex shield. The weight of this ballute would be about 80 pounds. A packing density of 35 lb/ft³ was used to determine volume requirements. A coated Nomex sleeve is placed between the ballute storage envelope and the heat source to protect the ballute against thermal degradation during storage. Tiedown rings are normally used to clamp the inner and outer envelope surfaces to the vehicle. Nomex has been chosen as a basic construction material due to its excellent property retention characteristics under detrimental thermal and nuclear radiation environments.

Nuclear radiation effects are presented in Table 3-8 for Nomex, Dacron, and Nylon 66.

TABLE 3-8
RADIATION RESISTANCE--EFFECT OF EXPOSURE
ON YARN STRENGTH*

Dosage	Tenacity Retained (percent)		
	Nomex	Dacron	Nylon-66
β -Van de Graff			
200 mega reps	81	57	29
600 mega reps	76	29	0
X-rays (50 kv)			
50 hrs	85	22	--
100 hrs	73	0	--
250 hrs	49	0	--
Brookhaven pile (50° C)			
200 mega reps	70	45	32
1000 mega reps	55	Radioactive	Crumbled
2000 mega reps	45	Radioactive	Crumbled

*Data obtained from Goodyear Aerospace Corporation,
Akron, Ohio



89 - 3337

Figure 3-10 BALLUTE IN DEPLOYED CONDITION

In summary the ballute appears to be an attractive drag augmentation device that materially enhances the impact safety of the IRV. It can be employed in the system with comparatively small weight and diameter penalties. Therefore, it is recommended for inclusion in the reference IRV design.

3.1.3 Location Aids

Location aids have been included in the IRV to help recovery teams locate the vehicle after controlled deorbit and impact into a deep ocean recovery area. The aids are used in conjunction with the drag augmentation device and the water flotation device - both of these functions may be fulfilled by the ballute, by trapping air inside the ballute during splashdown. The location aids have been located so that they do not reduce the performance or reliability of the basic vehicle or its ballute drag augmentation system (particularly during random or non-controlled reentry).

The location aids must be capable of sustaining a 5-year life in a space environment while subjected to the thermal and nuclear environment associated with the IRV. The aids must also be small, light, and easily packaged into the IRV and, if possible, easily serviced or replaced by astronauts during the mission in earth orbit.

Several location aids were considered during the course of the study as shown in Table 3-9. The aids selected for further study are indicated by asterisks. These aids (except IR source) have been extensively used in ocean recovery work over the past decade with excellent results. The radar chaff or reflecting parachute is useful if recovery aircraft or ships are able to observe the descent; however, they require much more elaborate equipment installations on board the recovery craft. The shark repellent has been suggested to prevent the flotation system from being attacked by sharks. No effective shark repellent has yet been developed, nor has shark attack proven to be a severe problem in recovery operations. Conversely, most repellents developed to date have served to attract rather than repel sharks.

TABLE 3-9

LOCATION AID CANDIDATES

*Radio Beacon	*Luminous Colors
*Flashing Light	*IR Source
Radar Chaff	Sound Beacon
Sea Water Dye Marker	*Radar Reflecting Ballute
Shark Repellent	

The location aids selected for consideration are detailed in Table 3-10 together with volume and weight requirements. These include the use of IR sensors on the recovery craft to locate the 25 kw thermal source carried within the IRV which should create a detectable hot spot in the ocean or on land. This technique has been successfully used by forest rangers for spotting potential forest fires for about 5 years. Burned out campfires several hours old can be detected by this technique.

TABLE 3-10

LOCATION AID AND
DRAG AUGMENTATION DATA

Component	Weight (lb)	Volume (in. ³)	Limiting Storage Temperature (° F)
Radio Beacon	1.3	15.0	>220
Flashing Light	0.7	10.0	>220
Dye Marker	2.0	16.0	>220
Ballute and Flotation System	95.0	3500.0	>400
Battery (NiCad)	10.0	175.0	180 to 220
Scuttle System	2.0	20.0	>220
Junction Box, Cables	4.0	30.0	>220
Total	115.0	3764.0	

The principal problem areas which remain are:

- development of equipment which has the necessary 5-year life in the thermal and radiation environments of the heat source,
- development of a periodic replacement capability if the 5-year lifetime cannot be realized, and
- development of a power source for the location aids with the necessary lifetime and reliability. (A NiCad battery has been recommended for the reference system.)

3.1.4 Safing and Initiating System

The safing and initiating system (S&I) will provide handling, transportation and prelaunch through recovery S&I functions for the IRV. The significant requirements are that the system shall:

- be capable of functioning at approximately 225° F after 5 years storage at 225° F.
- provide launch pad abort mode.
- provide early launch abort mode.
- provide ascent abort mode.
- provide orbital abort mode and mission termination power and functions such as safing, arming and sequencing.

3.1.4.1 System Approach

The following describes the system operation (See Figure 3-11) during the various modes of operation.

Normal Mode and Orbital Abort Mode

Launch

During powered flight ascent a decrease in pressure will be used to actuate the safing switch. The switch closures will arm the sequencer and power supply circuits.

Mission Termination

Just prior to mission termination and mechanical safing switch actuation, an ejection signal will be provided through the spacecraft to the closed safing switch contacts. The signal will be utilized to start the sequencer and initiate the power supply. The sequencer will then program the signals required for the separation, deorbit and recovery functions. The power supply will then provide the required electrical energy for deorbit and recovery.

Shortly after initiation, the sequencer will provide electrical energy to initiate the release bolts and abort rockets.

Spin-up

The sequencer will then provide electrical energy to initiate the spin-up rockets.

Deorbit

After approximately one-half to three-quarter orbit delay, the sequencer will provide electrical energy to initiate the deorbit rocket.

Separation

Shortly after deorbit initiation, the sequencer will provide electrical energy to initiate the deorbit rocket support structure explosive bolts.

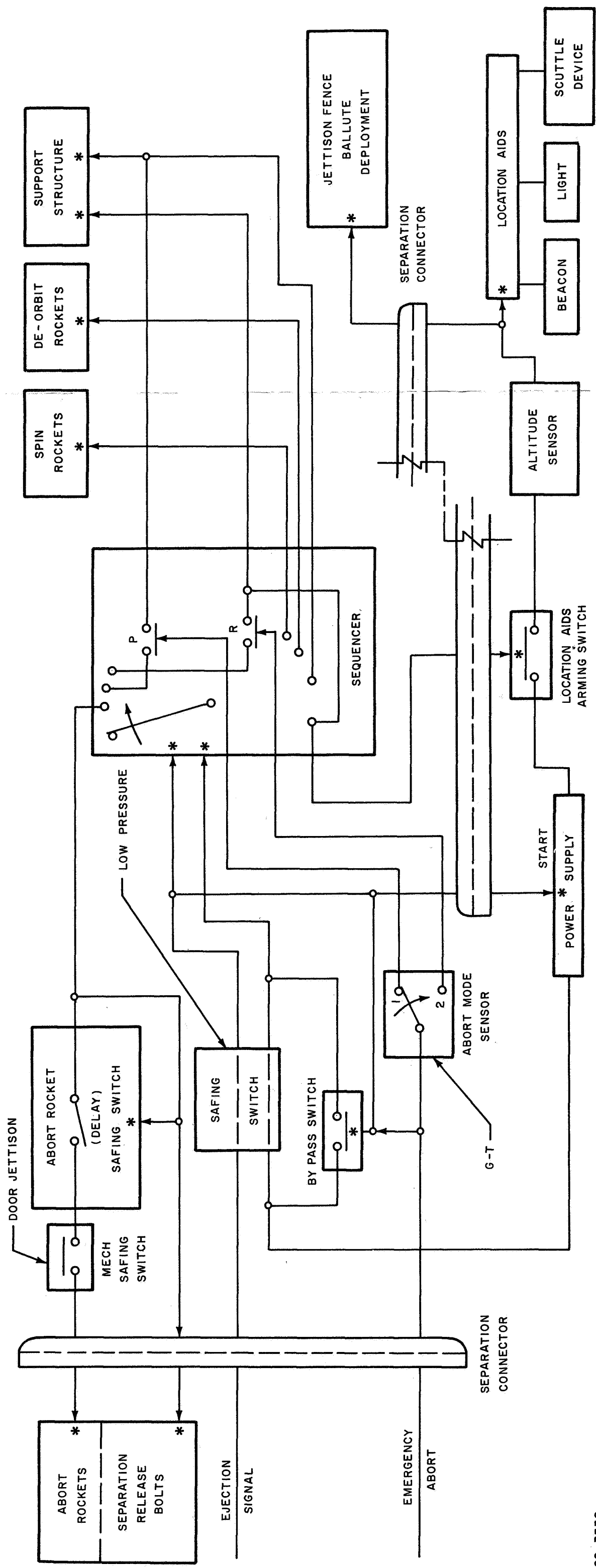


Figure 3-11 SAFING, ARMING, AND INITIATION SYSTEM SCHEMATIC

Location Aids System Arming

Shortly after separation, the sequencer will provide electrical energy to initiate the location aids system arming switch.

Location Aids System Initiation

During late reentry, the altitude sensor electrical contacts will close and provide the following functions:

- Electrical energy to initiate the jettison of the fence and thereby provide ballute deployment.
- Power to the location aids system for the radio beacon, the flashing light and scuttle device.

Launch Pad and Early Launch Abort Mode

Prior to and during early launch, the abort function will be provided as follows:

Emergency Abort Signal

Since this can occur prior to powered flight acceleration, it is necessary to provide a bypass for the launch safing switch. The emergency abort signal will be provided through the spacecraft to initiate the safing switch bypass switch, initiate the power supply, and close switch "P" of the sequencer, thereby arming the system in the abort mode.

The battery will then provide electrical power to initiate the sequencer which will then program the following functions:

- Initiate the separation release bolts and the abort rocket delay safing switch.
- Initiate the abort rockets.
- Initiate the deorbit rocket and support structure ejection.

Ascent Abort

During ascent, the abort function will be provided as follows:

Since this can occur early in powered flight prior to safing switch actuation, it is necessary to provide a bypass switch and initiate the power supply, arm the abort rocket circuit and arm switch "R" of the sequencer thereby arming the system in the abort mode. The abort mode sensor will move to position 2 during powered flight acceleration and will select the proper circuit routing for the emergency abort signal.

The battery will then provide electrical power to initiate the sequence which will then program the following functions:

- Initiate the separation release bolts and the abort rocket delay safing switch.
- Initiate the abort rockets.
- Initiate the rocket support structure ejection and provide electrical energy to initiate the location aids system arming switch.

Location Aids System Initiation

During descent, the altitude sensor electrical contacts will close and provide the following functions:

- Electrical energy to initiate the jettison of the fence and thereby provide ballute deployment.
- Power to the location aids system for the radio beacon, the flashing lights and scuttle device.

System Description

The system will be electromechanical in nature. The prime considerations for design will be system safety and reliability. Redundant components and circuitry will be utilized as required. The following describes the more important components:

Power Supply - Degradation due to the elevated storage temperature is of utmost concern. Initial investigations indicate a nickel cadmium battery with a continuous trickle-charge can possibly meet the high temperature and aging requirements.

Safing Switch - The safing switch will be a pressure sensitive device with N/O electrical contacts similar to devices utilized in previous Minuteman systems.

Launch Sensor - The launch sensor will be a damped acceleration switch which will sense peak powered flight for a minimum prescribed time.

Arming Switches - Pyrotechnic arming switches will be 1 amp-1 watt no-fire squib switches.

Altitude Sensor - The altitude sensor will be a barometric device set for the reentry altitude for proper ballute deployment.

Sequencer - The sequencer will be an electrically initiated mechanical timer driven assembly.

3.2 REENTRY PERFORMANCE ANALYSIS

The primary objectives of the aerodynamic analyses were the definition of the aeroshell and heat source heating and load environments as well as the dynamic behavior of the IRV throughout reentry. The interaction between the vehicle performance and environments as well as various system constraints dictated the evaluation of numerous design tradeoffs.

One of the most important factors influencing the capsule environment is the turnaround capability provided by the aerodynamic fence. The turnaround device is critical not only because it must ensure the proper attitude of the aeroshell early in reentry but also because it has influence on the capsule heating environment.

Definition of the heating throughout the reentry phase is necessary to define the critical or design environments for the aeroshell and heat source capsule. This definition includes the effects of vehicle orientation and dynamic behavior (spinning, tumbling). Consideration of a broad spectrum of possible reentry conditions (from ascent to in-orbit phases) was necessary to determine the worst design environment.

The aerodynamic analyses were conducted in three phases. In Phase IA system tradeoffs were made considering two blunt shapes (a 60-degree blunt cone and a modified Apollo) utilizing various heat source capsule array geometries. Selected turnaround devices were investigated to determine their effectiveness and requirements. The entry heating environment was determined for a range of parameters (i.e., capsule array geometry) to establish the critical entry conditions as well as the turnaround requirements. These studies resulted in tradeoffs that established two configurations which warranted further analyses, which were conducted in Phase IB. The two configurations differed in capsule array geometry while both utilized a blunt 60-degree half-angle cone aeroshell. In addition, during Phase IB various fence concepts were to be tested at NASA/Ames. The aerodynamic characteristics were to be determined with particular emphasis on the pitching moment coefficient. The reference turnaround device derived from the test program by NASA is a vented symmetrical fence. This fence and a flush planar heat source capsule array was selected for detailed design and performance analyses in Phase II. (See Figure 1-1.)

During Phase II, design criteria and performance were established for the aeroshell, the heat source capsules and the turnaround fence based on the Saturn IB launch vehicle ascent trajectories and orbital characteristics. The aerodynamic performance was determined throughout reentry including the terminal dynamic behavior in the presence of wind shear and gusts. The drag coefficient variation with angle of attack has a significant effect on the reentry trajectory particularly for the entry from out of orbit mode. It should be noted that the drag coefficient for the blunt cone alone at 90-degree angle of attack is decreased by an order of magnitude from the zero or 180-degree angle-of-attack value. Available aerodynamic data was modified to account for the cylindrical portion of the vehicle and the turnaround fence which contributes significantly to the drag at 90-degree angle of attack.

The fence characteristics used in the analyses were analytically determined. However, the influence of the fence effectiveness on the environment, particularly that for the capsules, was investigated parametrically for a critical entry mode (orbital decay with spin entering in a rearward attitude).

During Phase II the IRV ballistic coefficient ($W/C_D A$) increased from an original estimate of 40.2 lb/ft² to a final value of 47.7 lb/ft². In all cases where the effects of this increase could be included (e.g., heat shield thickness) appropriate changes were made. However, there are some instances, notably the capsule analysis during reentry, where both $W/C_D A$ values appear. Note that the effect

of the ballistic coefficient increase is only on the order of 10 percent on heating, but its effect on vehicle dynamics could be more significant.

Transonic and subsonic stability are important in achieving proper attitude at terminal impact. Sufficient test data is available in this regime for the blunt cone to provide bases for imposing design limitations on geometry particularly at the maximum diameter region. The data indicates a degeneration of the pitch damping derivative with effective cylindrical length. Further analysis of the data indicates that the apparent instability transonically and subsonically occurs only at small angles of attack, since a correlation of the effective pitch damping derivative with the angle-of-attack envelope for the data indicate the existence of limit cycle type motion.

The dependence of this limit cycle motion on the effective cylinder length (including the shoulder radius) results in a terminal limit cycle of ± 13 degrees, in the absence of winds, for the reference configuration.

3.2.1 Heating and Loads Summary

Generation of complete reentry trajectories was necessary to develop a comparison of the broad spectrum of possible conditions including all credible failure modes. Heating variations at various locations on the aeroshell, the turnaround fence and the heat source capsules were determined as a function of angle of attack. Table 3-11 presents a summary of the reentry conditions which resulted in significant design environments. The nominal reentry is that for controlled entry. The spinning rearward reentry from orbital decay resulted in severe heating in the base region and, in addition, resulted in the lowest turnaround altitude. Turnaround altitude is defined as that point where the angle of attack is less than 80 degrees. The tumble rate considered for design was 0.63 radian per second with spin rate of 20 rpm. The justification for the tumble rate can be found in Reference 3-1 while the criteria used to select the spin rate can be found in Subsection 3.1 of this report.

The heating environments were synthesized by determining a reference stagnation point heating. This reference heating rate is obtained for the zero angle of attack stagnation point for the aeroshell, utilizing the trajectory results from a dynamics analysis. Heating factors are applied to this reference heating to obtain the correct heating at this station, other aeroshell positions, the fence and the heat source capsules. These factors, in addition, account for the type of dynamic motion extant. Two types of motions proved to be worthy of consideration: in-plane oscillations and coning with spin, for which two limits were considered (i.e., "Lunar" type where the same reentry vehicle meridian always faces the wind vector and the high spin case where the peripheral average heating can be considered.)

The critical heating trajectories were found to be those associated with various modes for orbital decay. These reflect the combined angle-of-attack motion, heating factor and trajectory effects.

The aeroshell critical environments were established from a number of trajectories differing in entry angle of attack and rates. When reentering rearward, the influence of increased spin is favorable for the forward region of the aeroshell where the reverse is true for the heat source capsules and the aeroshell maximum diameter region. Since the worst heat source capsule environment was that associated with rearward entry with spin, further analyses were made with respect to sensitivity of the environment to the turnaround capability and spin rate.

The aerodynamic heating environments for the worst capsule are summarized in Table 3-12. The trajectories indicated are those of Table 3-11 where trajectories 5, 8, 15 and 16 are for orbital decay reentry conditions. The worst capsule environment is experienced by the outboard most capsule which is located in the base at $R/R_B = 0.72$. As mentioned previously an increase in the ballistic coefficient occurred during Phase II and is shown in Table 3-12. The values as presented in the table are consistent with the temperatures for the heat source reentry thermal analysis presented in paragraph 3.4.

The maximum heating loads (whether aeroshell or capsule) are associated with shallow reentry, while the maximum rates are associated with the steep reentry conditions which are associated with ascent abort. The critical heating condition differed not only between the capsule and aeroshell but also for the various locations on the aeroshell due to the angle of attack and oscillation variances during reentry. As is expected, the critical heating for the capsule and for aeroshell stations near the base region was associated with rearward or tumble entry modes.

The aerodynamic loads are summarized for the various entry modes for both orbital decay and ascent abort in Table 3-13. The maximum loads are those associated with the steep reentry for abort from the ascent trajectory. Comparison of the results for the Saturn IB aborts indicate maximum normal loads (N/W) and axial loads (D/W) are those obtained for the reentry conditions of trajectory 12.

TABLE 3-11

TRAJECTORY ENTRY DATA SUMMARY FOR AN ALTITUDE OF 400 kft

Trajectory No.	Entry Velocity (ft/sec)	Entry Angle, γ_e (deg)	Entry Angle of Attack, α (deg)	Rates (rad/sec)		Remarks
				Spin	Tumble	
1	25,647	- 2.15	85	2.09	0	Controlled Entry--Phase II Nominal
2	25,632	- 0.49	63	2.09	0	Controlled Entry
3	18,000	- 7.3	179	0	0.628	Orbit Injection Abort--Tumble
4	23,500	- 4.0	179	0	0.628	Orbit Injection Abort--Tumble
5	25,685	- 0.0	179	0	0.628	Orbit Decay--Tumble
6	18,000	- 7.3	179	0	0	Orbit Injection Abort--Rearward
7	23,500	- 4.0	179	0	0	Orbit Injection Abort--Rearward
8	25,685	0	179	0	0	Orbit Decay--Rearward
9	25,647	- 2.15	85	2.09	0	Controlled Entry--Nominal with Mass Assymetry
10	25,870	- 2.25	69	2.09	0	Controlled Entry--Phase IA Nominal
11	24,000	-10.0	179	0	0.628	Worst Abort--Saturn IB
12	16,970	-18.0	179	0	0.628	Controlled Entry--Deorbit Error
13	25,890	- 0.75	63	2.09	0	Controlled Entry--Deorbit Error
14	25,865	- 1.05	63	2.09	0	Orbit Decay--Rearward to Impact
15	25,685	0	179	0	0	
16	25,685	0	179	2.09	0	Orbit Decay--Failure Mode with Spin
17	26,058	- 0.73	179	2.09	0	Phase IA Two Skip
18	25,685	0	0	0	0	Orbit Decay

TABLE 3-12

DESIGN AERODYNAMIC HEATING SUMMARY

Trajectory No.	Trajectory Mode	Max. Ref. Pt. Ht. (Btu/ft ² -sec) (Ref. $\alpha = 0$)	Integrated Ref. Pt. Htg. (Btu/ft ²) (Ref. $\alpha = 0$)	Worst Capsule* Max. Htg. Rate (Btu/ft ² -sec)	Worst Capsule Integrated Htg. (Btu/ft ²)	Ballistic Coefficient W/C _D A
1	Nominal Reentry Mode	347	35,700	46	6,320	40.2
5	Tumbling-- Orbit Decay	219	76,500	46	13,010	40.2
8	Rearward-- Orbit Decay	208	68,800	10	4,262	40.2
9	Nominal Reentry (Offset c.g.)	348	36,950	75	6,800	40.2
12	Worst Abort (Structural Loads) (Saturn IB)	260	5,083	--	--	
15	Rearward Reentry to Impact-- Orbit Decay	193	55,899	77	21,010	47.7
16	Rearward Spinning Reentry-- Orbit Decay	242	106,000	36	26,900	47.7

*Located at R/R_B = 0.72

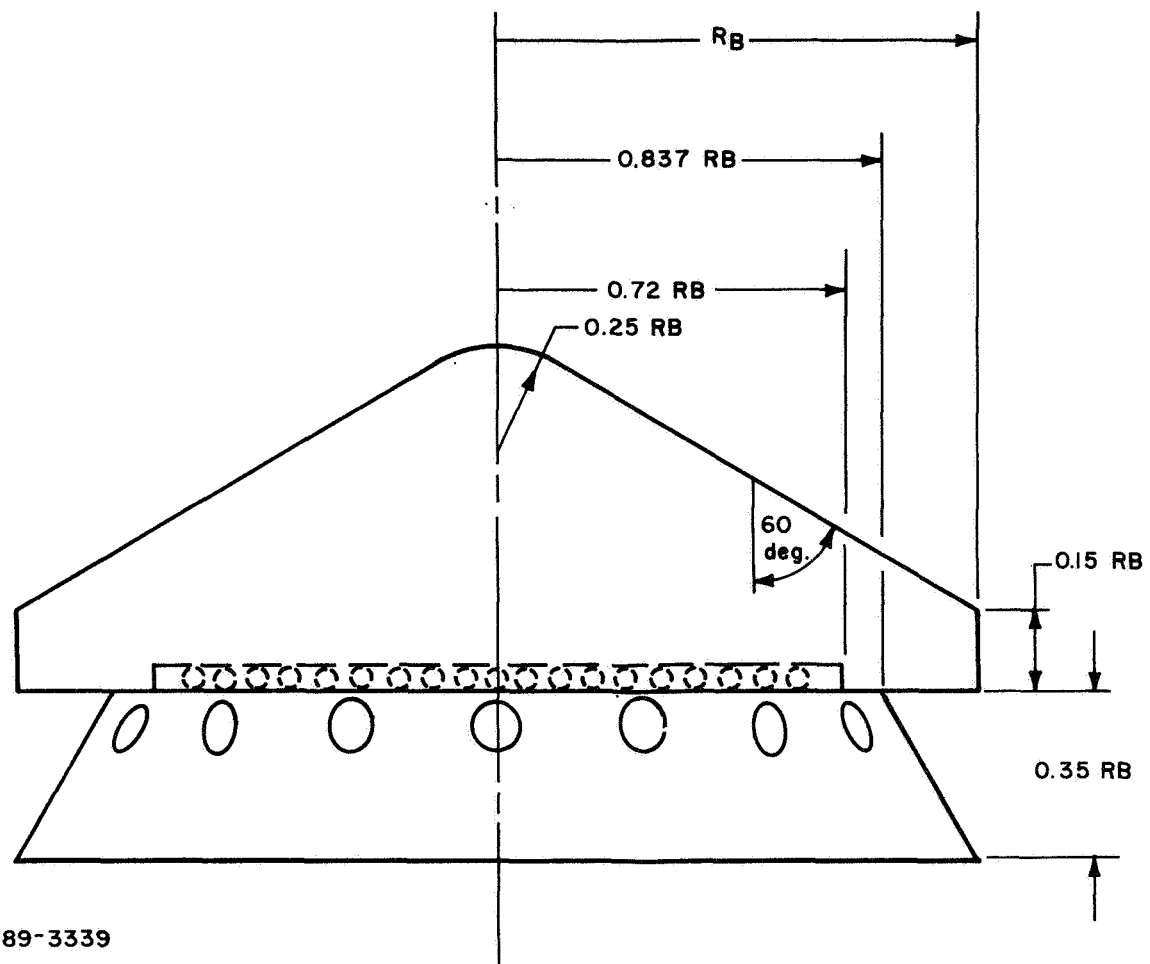
TABLE 3-13
DESIGN AIRLOADS SUMMARY

Trajectory No.	Trajectory Mode	Max. Dynamic Pressure (lb/ft ²)	Axial Loads (D/W) Maximum	Normal Loads (N/W) Maximum
1	Nominal Re-entry Mode	504	10.8	1.2
5	Tumbling -- Orbit Decay	404	8.5	0.6
8	Rearward -- Orbit Decay	389	8.2	0.2
9	Nominal Re-entry (Offset c.g.)	507	10.8	1.4
12	Worst Abort (Structural Loads) (Saturn I-B)	1430	30.4	2.4
15	Rearward Re-entry to Impact -- Orbit Decay	346	8.0	1.0
16	Rearward Spinning Reentry -- Orbit Decay	443	9.3	1.0

3.2.2 Analysis and Results

The Phase II Study is comprised of a detailed design and performance analysis of the recommended configuration developed during the Phase IB effort. The forebody, capsule and fence heating and airloads were determined during Phase II for the V-γ conditions presented in Table 3-11. The dynamic stability analysis consisted of an examination of the subsonic stability, the determination of the wind and gust effects at impact and an analysis of the reentry dynamics to define the aerodynamic heating for the aeroshell and capsules.

The configuration studied in Phase II is shown in Figure 3-12. This design consists of the 60-degree blunt cone forebody and the flush-mounted planar capsule configuration as used in the Phase IB study. The configuration for the turn-around device was recommended by NASA Ames based on shock tunnel tests. The fence consists of a vented configuration mounted outboard of the heat source capsule array.



89-3339

Figure 3-12 PHASE II AERODYNAMIC CONFIGURATION

As the shock tunnel test of turnaround devices had not yet generated sufficient data to evolve the aerodynamic coefficients, it was decided, with NASA's concurrence, that analytically determined coefficients would be used in Phase II for the recommended fence configuration. These are based on recent conservative calculations of the vented fence characteristics. The range of credible variations in the pitching moment coefficients were then examined to determine their effect on the critical heating environments.

The mission requirements and constraints imposed on the IRV and subsequently the aerodynamic analyses are reflected in the reentry conditions, i.e., velocity and angle. In addition, various subsystem failures introduce various dynamic conditions at reentry, i.e., angle of attack, tumble and spin. The reentry conditions considered were those associated with a launch of a Saturn I-B with an orbital altitude of 164 nautical miles. Aborts were considered from launch through orbital injection. Out-of-orbit reentry considered both decay and controlled modes.

The design criteria resulted from an analysis of the aerodynamic heating and loads for the above reentry conditions. Those trajectories which resulted in significant design environments were summarized in Table 3-11. The nominal reentry mode is that for controlled reentry with spin. The failure mode wherein spinup occurs with subsequent failure of the ΔV retrorocket is the spinning rearward reentry case. The credible tumble rate considered was 0.63 rad/sec, whereas the spin rate was 20 rpm. These rates are those associated with a catastrophic failure and controlled reentry retrorocket stabilization requirements, respectively. A study was made to determine whether errors in the retrorocket velocity increment and firing angle could produce a two-skip condition. For the normal reentry modes of Phase II, a two-skip condition cannot be obtained because the reentry velocities are too low.

3.2.2.1 Aerodynamic Heating

3.2.2.1.1 Forebody Heating -- The forebody heating for the Phase II IRV Study is based on the heating factor distributions presented in Reference 3-1. Figure 3-13 shows the heating factors as a function of angle of attack at significant points on the forebody with body locations identified in Figure 3-14. Heating factors for various dynamic motions, that is, oscillating, spinning and tumble were derived from this figure, and are shown in Figure 3-15. (The envelope value $\bar{\alpha}$, is the maximum angle of attack at any instant of time). The oscillating and tumble factors were obtained from considering planar motion with the average heating obtained during a cycle. The spinning factors were based on the average heating at a point during one rotation of the vehicle about its axis as a given angle of attack.

During early reentry, when the reentry vehicle is in an high angle-of-attack orientation, "lunar" motion (equal coning and spinning rates) heating factors were used. This type of motion occurred at peak rate for the heat source capsule. Subsequent to turnaround, the nominal spin factors as defined above were used for both the capsules and the aeroshell.

For the nominal reentry mode, the vehicle is spinning from reentry to impact. The heating factors for the spinning mode, as described above, are applied to these trajectories. For the tumbling reentry mode, the vehicle will experience a damped oscillation following the tumbling phase, to which the oscillation heating factors are applied. Average values are applied to the tumbling phase with the exception of the final rotation. For this, a detailed analysis at each angle

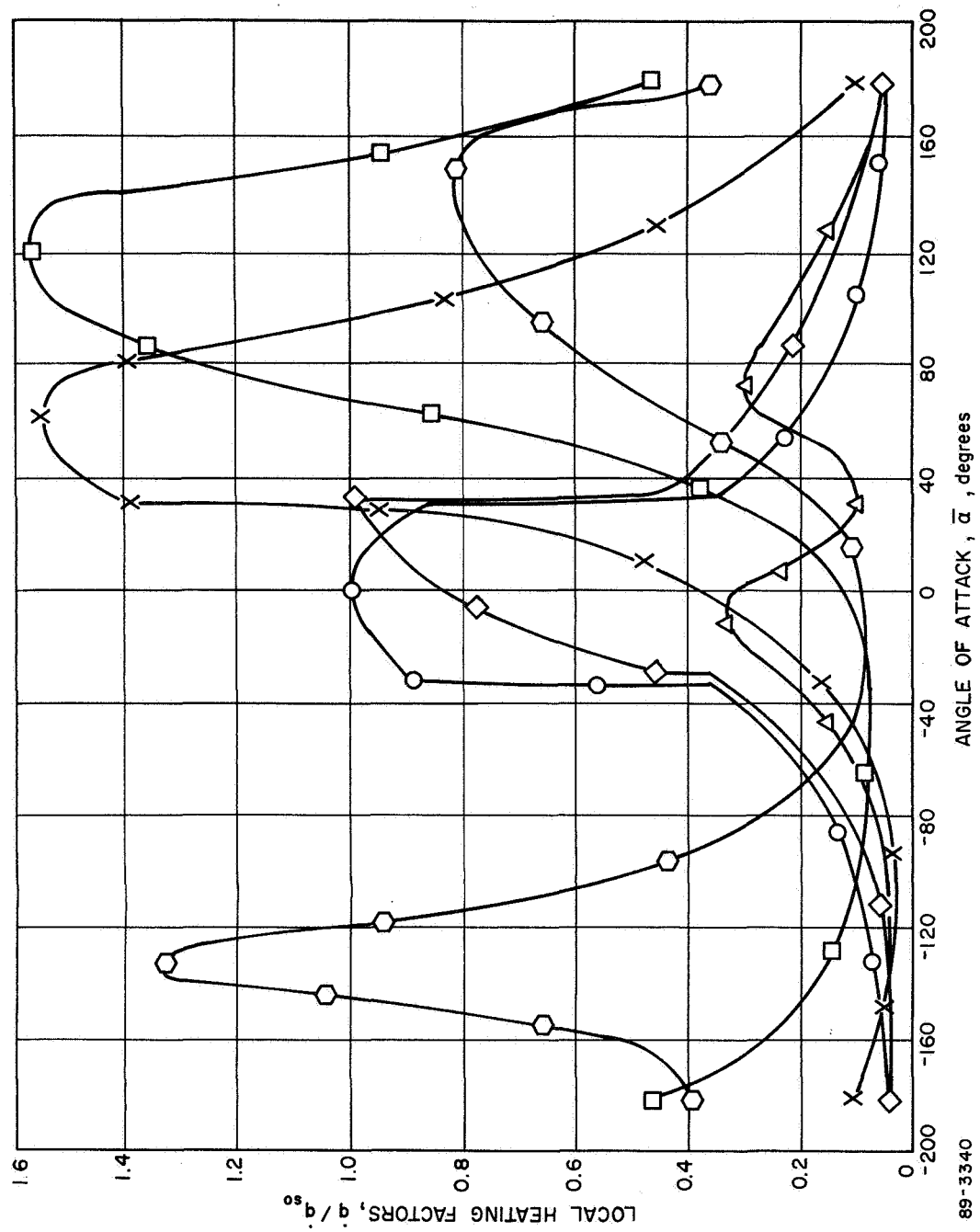
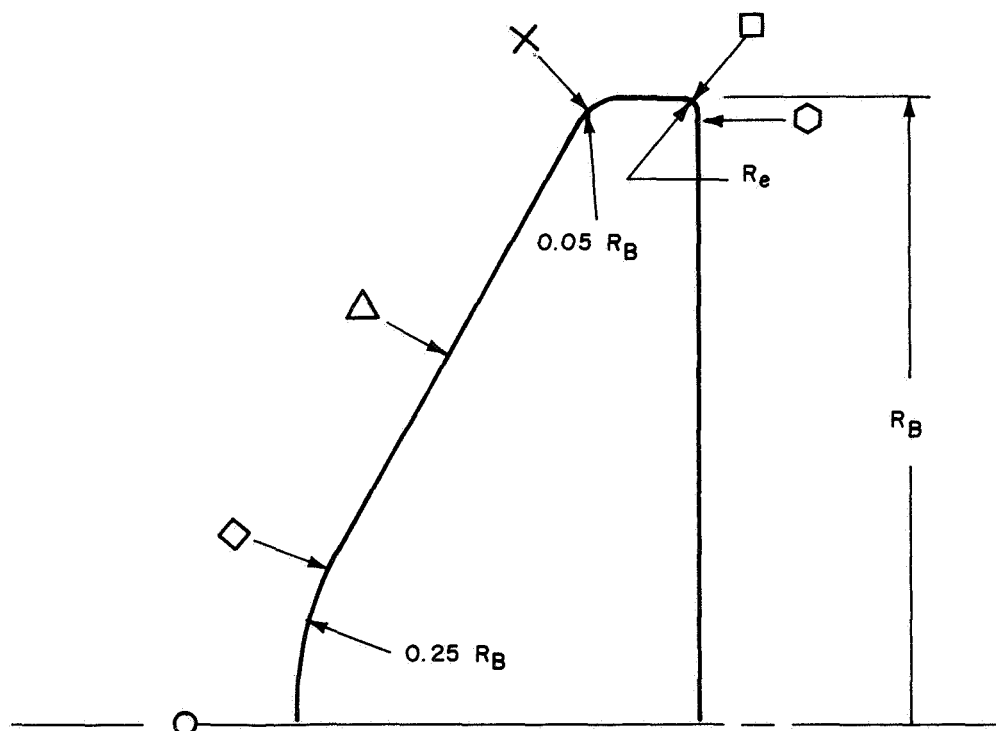


Figure 3-13 AEROSHELL HEATING FACTOR VARIATION WITH ANGLE OF ATTACK

STATION SYMBOL	R/R_B	(q/q_{so}) avg.
○	0.0	0.285
◇	0.125	0.276
△	0.550	0.154
×	0.993	0.476
□	1.000	0.56
⬡	0.970	0.47



89-3341

Figure 3-14 AEROSHELL STATION LOCATION

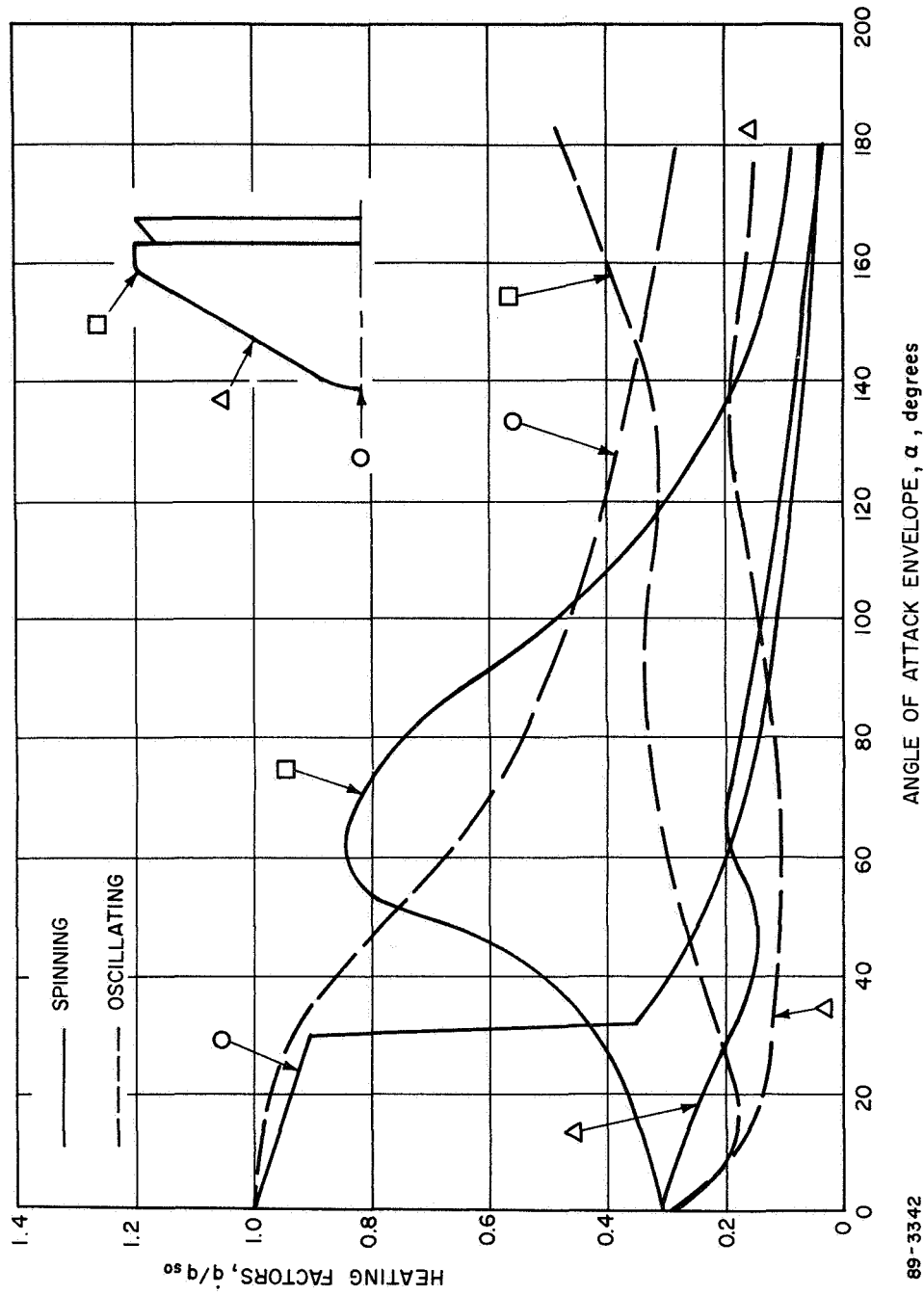


Figure 3-15 FOREBODY HEATING FACTORS

of attack was performed to determine the maximum heat rate during the tumbling phase. For the rearward reentry mode the vehicle reenters with zero rates about the three axes and at a reentry angle of attack equal to 179 degrees. No motion occurs until the dynamic pressure becomes significant enough to produce a restoring pitching moment. The vehicle will then oscillate for the remainder of the trajectory. The heating factors associated with the offset c.g. condition are the same as those for the nominal reentry condition.

The heating histories for only specific aeroshell stations for the various reentry modes are presented illustratively in Figures 3-16 through 3-20 because these trajectories gave the broadest range of reentry heating environments. The figures present both the average heating as well as that associated with the maximum angle of attack wherever appropriate. The heat pulses for the downstream locations exhibit two peaks, the earlier peak being that during turnaround for the last tumble cycle (angle-of-attack aggravations), whereas the second is that peak which is characteristic of the trajectory. The early cyclic variations of the heating cannot be drawn to the scale of the figures; in this case the average heating during a tumble cycle is used; however, peak heating for the last cycle history is as shown.

3.2.2.1.2 Capsule Heating -- Capsule heating calculations were based on the IRV fence configuration shown in Figure 3-12.

Heating distributions over the capsule array are as shown in Figure 3-21 for angles of attack of 0, 90, 158 and 180 degrees. The reference heating value \dot{q}_{so} is defined as the stagnation point heating on the nose of the IRV ($R_N \approx 8.5$ inches) at an angle of attack of zero degree. The heating levels are high due to the functioning of the holes in the fence skirt which allow flow past the capsules producing sonic conditions at the holes at angles of attack from 90 to 180 degrees. The maximum heating aggravations occur at an angle of attack of 220 degrees (138 degrees for the diametrically opposite capsule) where the flow is stagnated through a double shock system. This "system" is more efficient than the usual, single normal shock, producing a higher stagnation density at lower entropy. The double shock system also occurs at angles of attack to either side of 158 degrees, with decreased efficiency.

The variation of outboard capsule heating over a complete angle-of-attack cycle is shown in Figure 3-22. The average heating over the cycle is shown to be approximately one-half the nose stagnation point value.

Test results performed in the Avco 20-inch shock tunnel indicated that the heating with the fence is not significantly different than a flat base configuration for an angle of attack of 180 degrees for radius locations less than 0.3 of the maximum radius. For radius locations greater than 0.3 of the maximum radius, the heating with the fence is less than the flat base (Ref. 3-5) which is to be expected since the shock is swallowed. The heating factors for the spinning and oscillating dynamic modes are shown in Figure 3-23 as a function of the angle-of-attack envelope value and were determined by the methods discussed in References 3-1 and 3-4.

The tumbling motion is accounted for in detail in the following manners: a) tumbling motions prior to turnaround are treated by assuming an average heating value for the complete cycle; b) the heating for the final tumbling cycle, which produces the highest heat rates during the trajectory, is computed in detail.

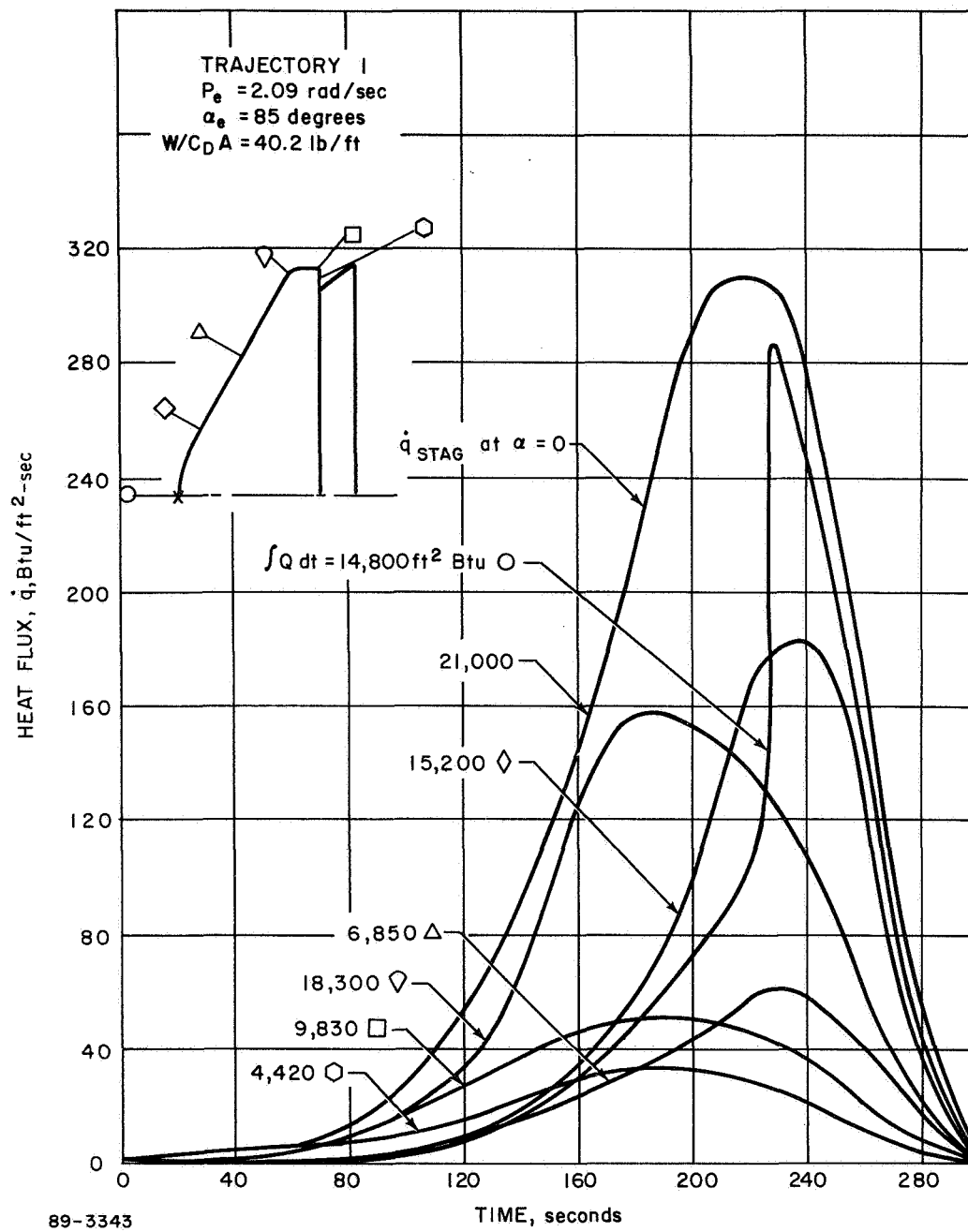


Figure 3-16 FOREBODY HEATING -- NOMINAL REENTRY MODE

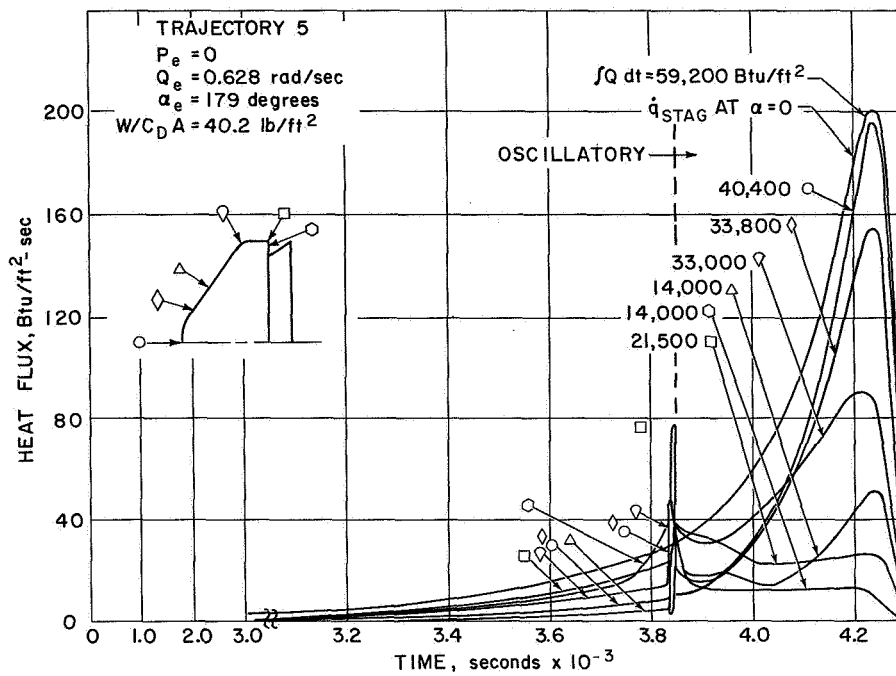


Figure 3-17 FOREBODY HEATING -- TUMBLING REENTRY MODE

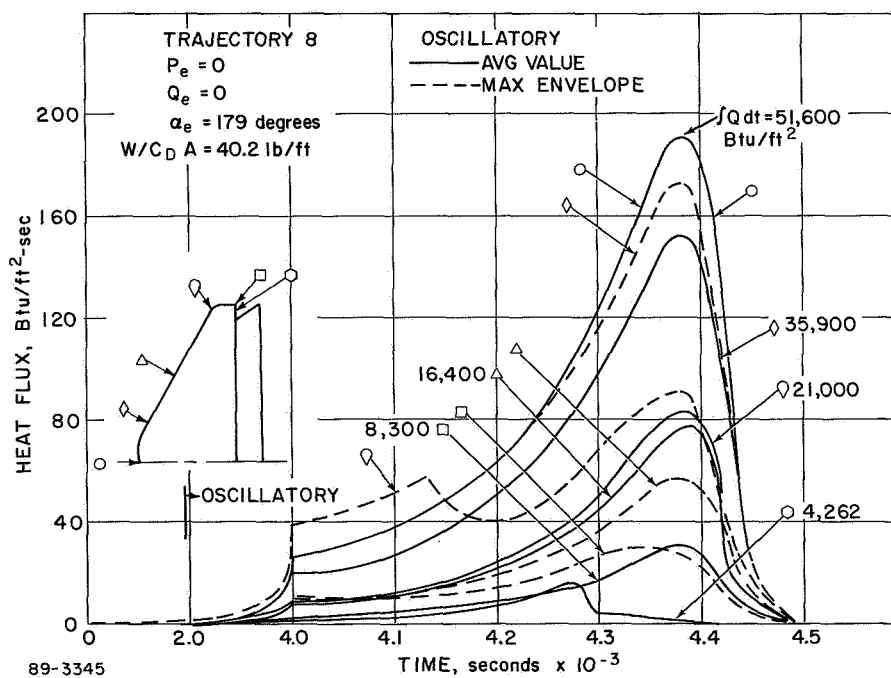


Figure 3-18 FOREBODY HEATING -- REARWARD REENTRY MODE

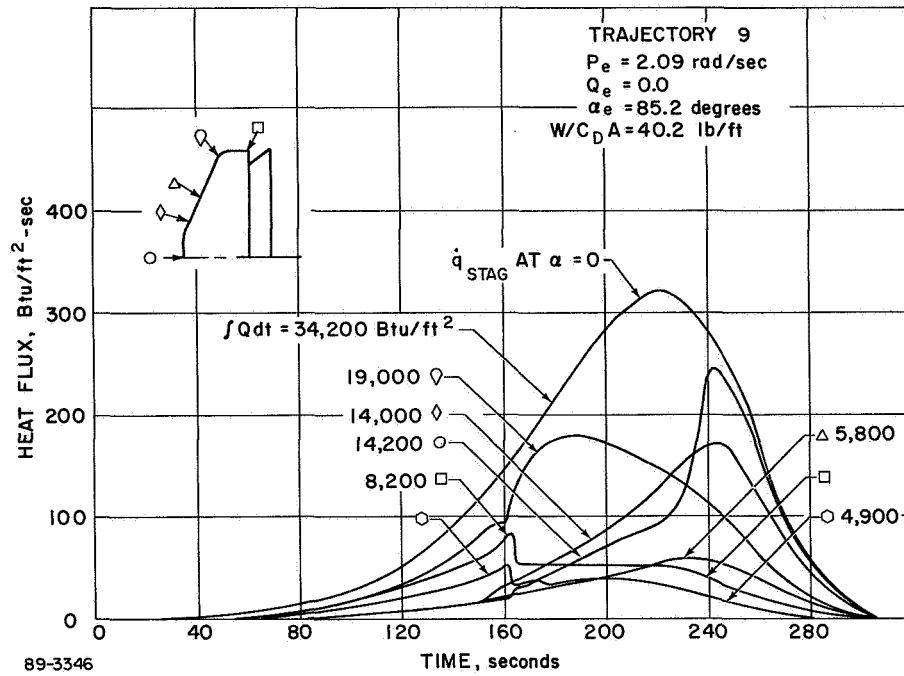


Figure 3-19 FOREBODY HEATING -- NOMINAL SPINNING REENTRY MODE

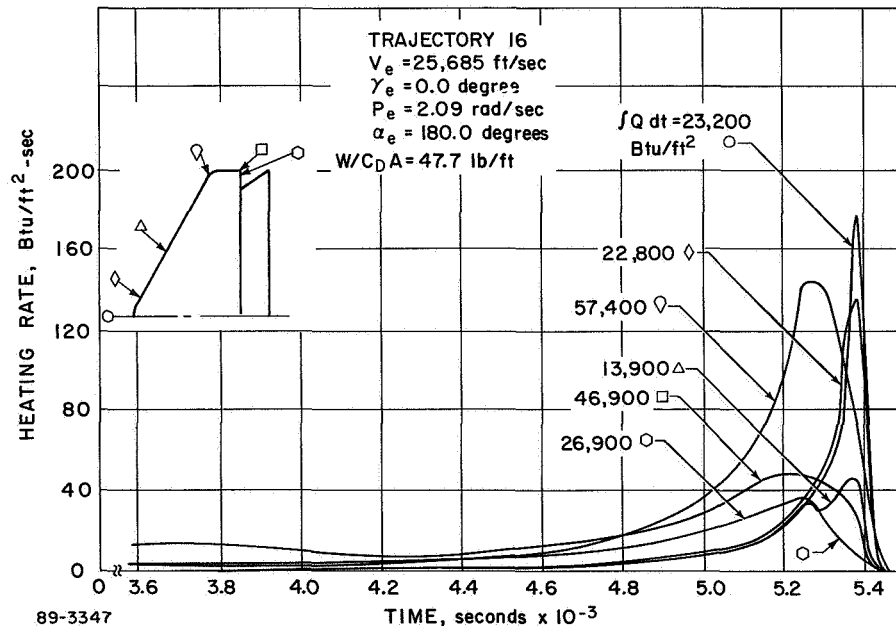


Figure 3-20 FOREBODY HEATING -- REARWARD SPINNING REENTRY MODE

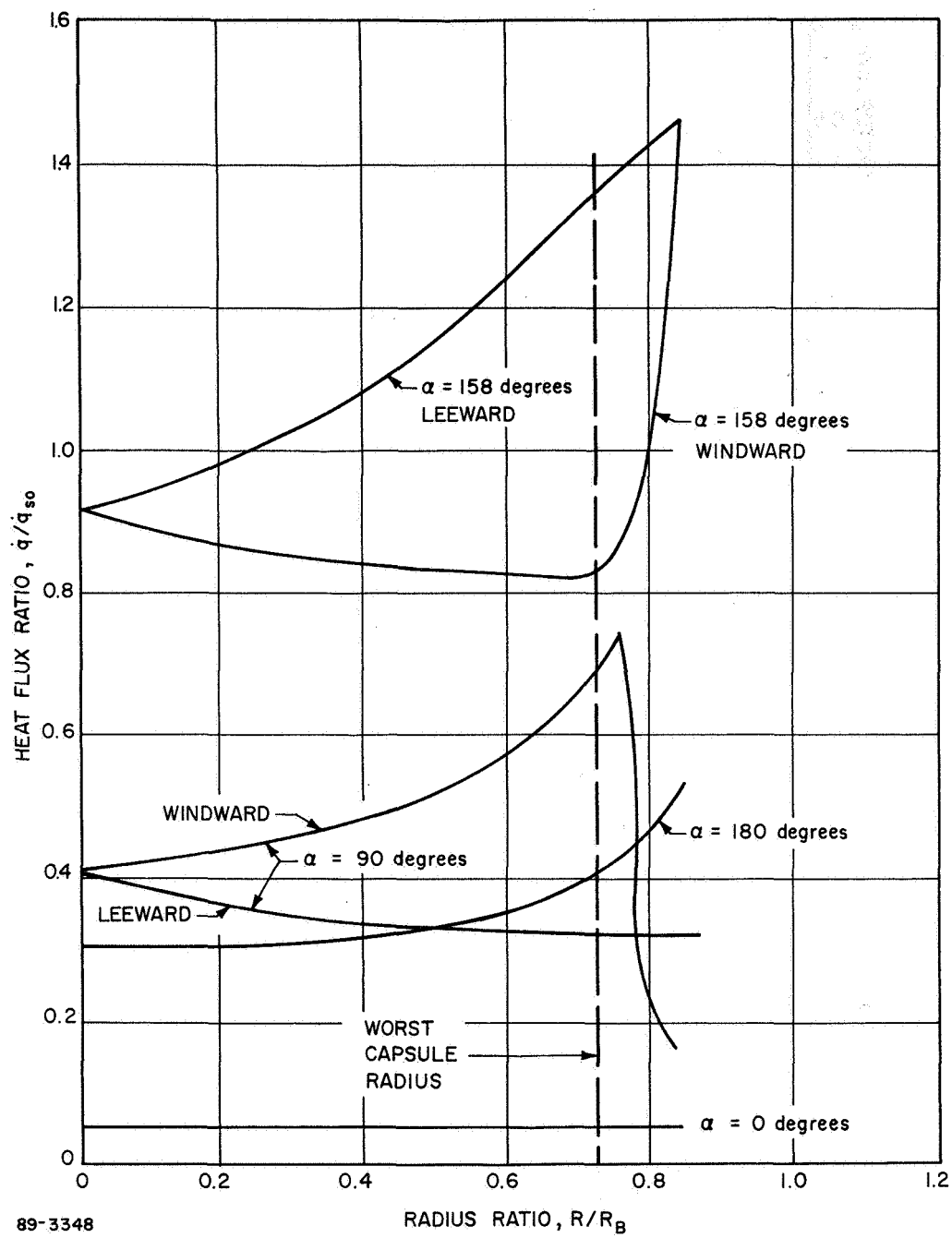


Figure 3-21 CAPSULE HEATING DISTRIBUTIONS -- PHASE II FENCES

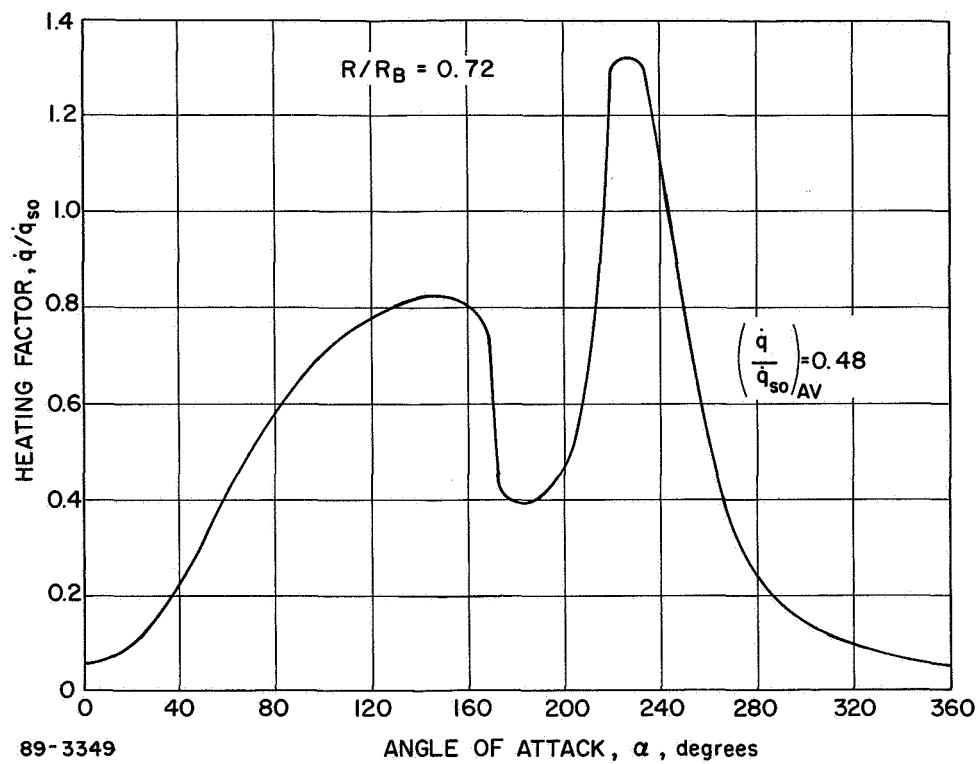


Figure 3-22 WORST CAPSULE HEATING FACTOR, ANGLE-OF-ATTACK VARIATION -- PHASE II FENCES

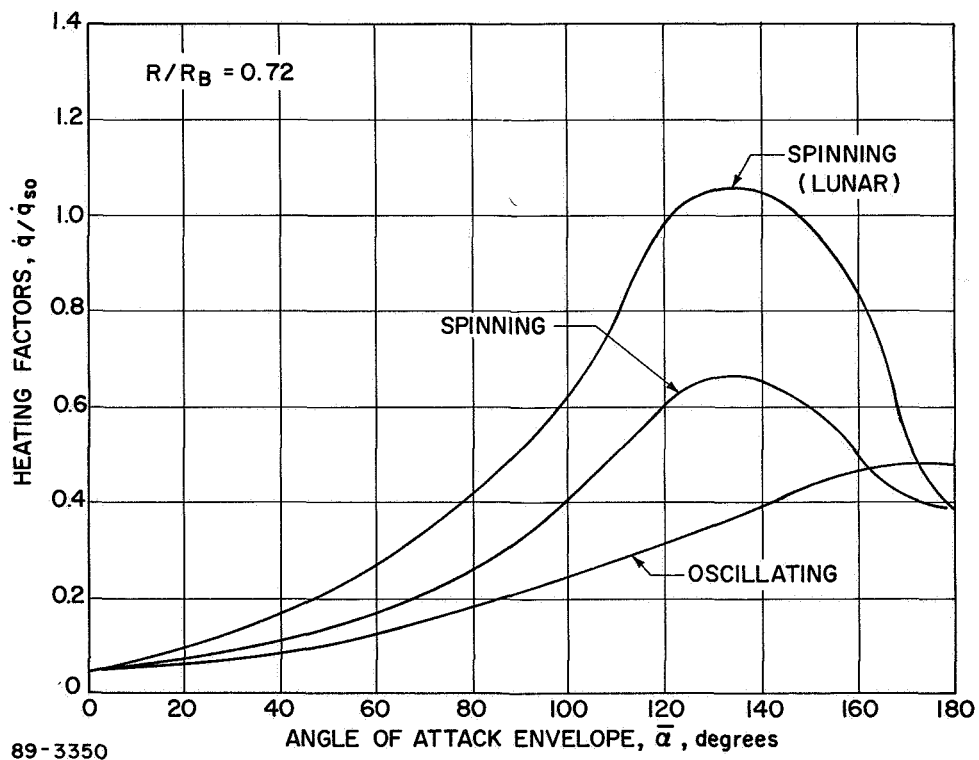


Figure 3-23 EFFECT OF DYNAMIC MOTION ON WORST CAPSULE HEATING FACTORS

The capsule heating is shown in Table 3-12 and in Figures 3-24 through 3-28 for the various reentry modes considered. In addition, the effect of turnaround capability (as reflected by the pitching moment coefficient derivative at 180 degrees angle of attack) was determined as well as the effect of spin rate. A rearward spinning mode with orbital decay was considered for this analysis. Typical results from this study are presented in Figures 3-29 through 3-31. In addition, a deorbit analysis was made to determine the effect of thrust misalignment for controlled reentry. The evaluation was performed parametrically with ΔV varied from the nominal value to a minimum value where the vehicle would not enter. The firing angles were varied from the nominal values of 180 to 90 degrees (Figure 3-32). The analysis showed that when the thrust vector control malfunctioned, severe integrated heating resulted. The effect of spin rate and pitching moment coefficient on capsule heating are summarized in Figures 3-33 and 3-34 for a spinning reentry mode with a reentry angle of attack of $\alpha_c = 179$ degrees. This range is expected to include any variations between the assumed fence effectiveness and the wind tunnel data when the tests are completed. The heating increases as the effectiveness decreases. The heating is a function of the pitching moment curve, in that it affects the turnaround capability and the angle-of-attack convergence.

The effect of spin rate is also presented (Figures 3-33 and 3-34) and illustrates the decrease in capsule heating as the spin rate decreases, since the reduced spinning stability results in earlier turnaround and improved angle-of-attack convergence.

An apparent angle-of-attack variation during orbital decay is associated with the fixed orientation of the IRV axis in inertial space (provided by spin) and the spherical atmosphere considered. A vehicle entering in a rearward attitude would be at a lower angle of attack by the time the aerodynamic moments are significant. The heating for this situation has been presented above. Additional cases were investigated for which the vehicle attitude is rearward when the atmosphere is significant. The lower heating that results for these cases (compare Figure 3-35 with Figure 3-28) is due to the high angular rate when the vehicle passes through the maximum heating aggravation attitude for the capsule. Rearward reentry case with spin (Trajectory 16) results in the maximum capsule heating through the combined effect of aggravation due to attitude as well as trajectory parameter variation.

3.2.2.1.3 Fence Heating -- The analysis for the fence heating is based on the techniques and shock patterns used to define the capsule heating in the presence of the fence configuration shown in Figure 3-12. The heating factors for locations on the midpoint of the flare section and at the hole location are shown in Figure 3-36 as a function of angle of attack. The heating factors for the dynamic modes are shown in Figure 3-37.

The heating for the flare and hole are shown in Figures 3-38 through 3-40 for Trajectories 5 and 16 with the maximum integrated heating occurring for the vehicle spinning with rearward reentry from an orbital decay. This particular trajectory (No. 16) as shown in Figure 3-44 exhibits an angle-of-attack variation which remains at values near 90 degrees for a long period of time prior to convergence. The outside surface of the fence experiences higher heating at these angles as shown in Figure 3-37, because of the stagnation conditions. At small angles of attack, the higher outside heating is caused by the flow impingement and reattachment heating, whereas the inside surface experiences base flow heating.

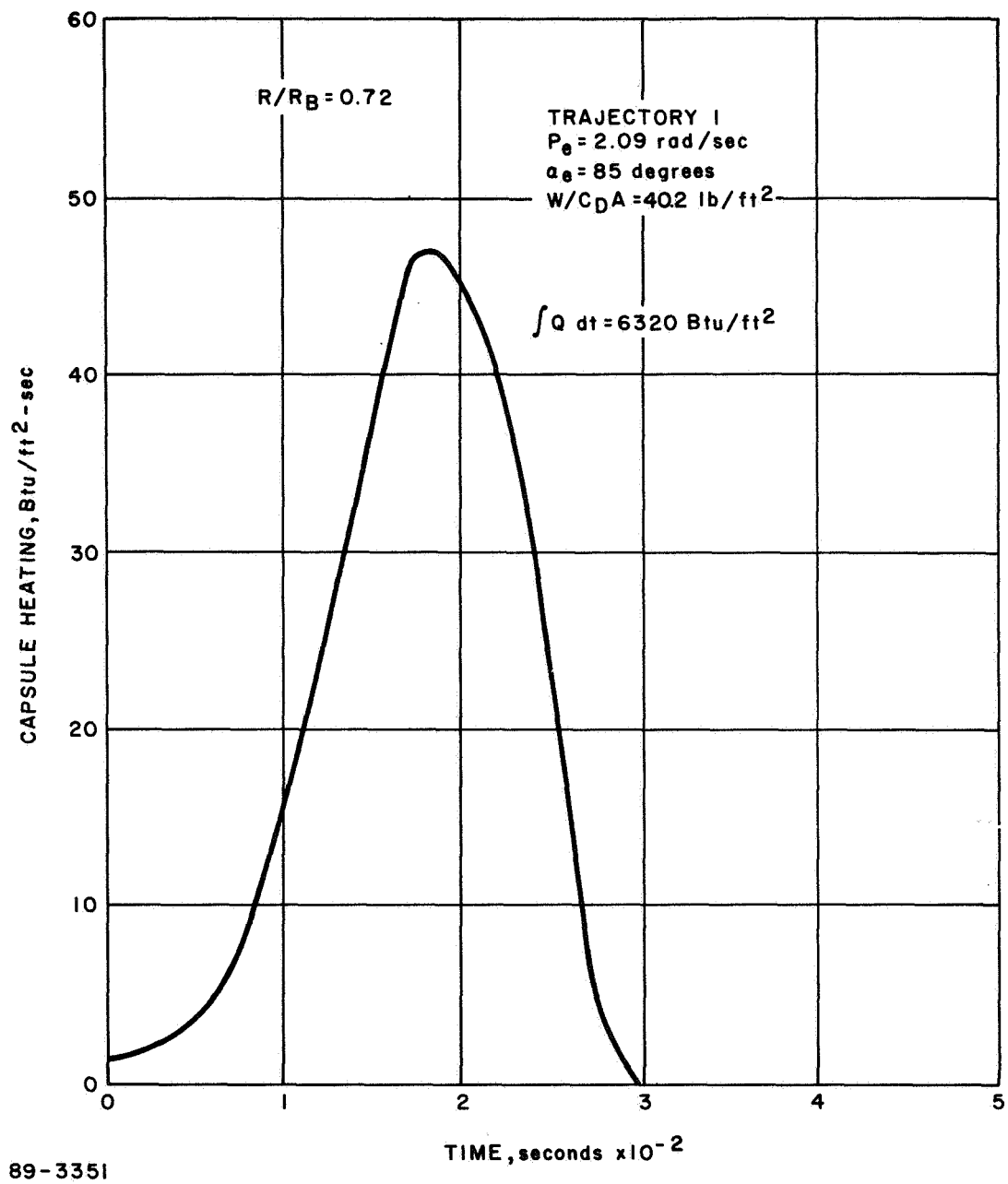


Figure 3-24 WORST CAPSULE HEATING --- NOMINAL REENTRY MODE

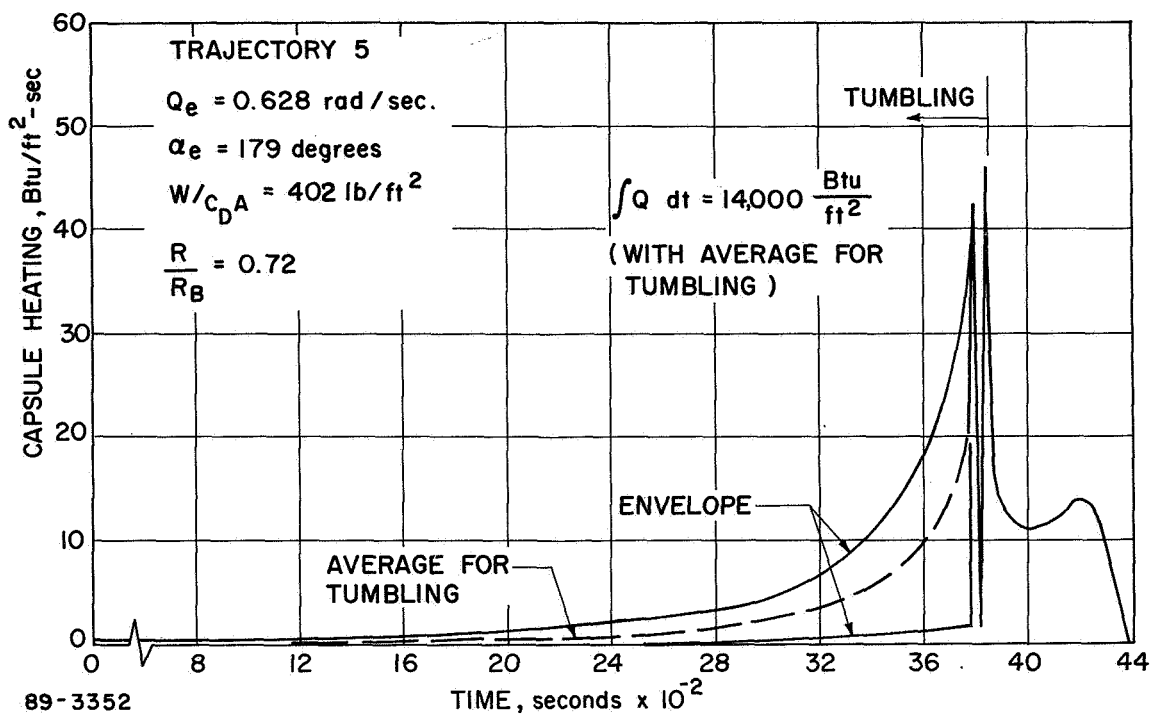


Figure 3-25 WORST CAPSULE HEATING -- TUMBLING REENTRY MODE

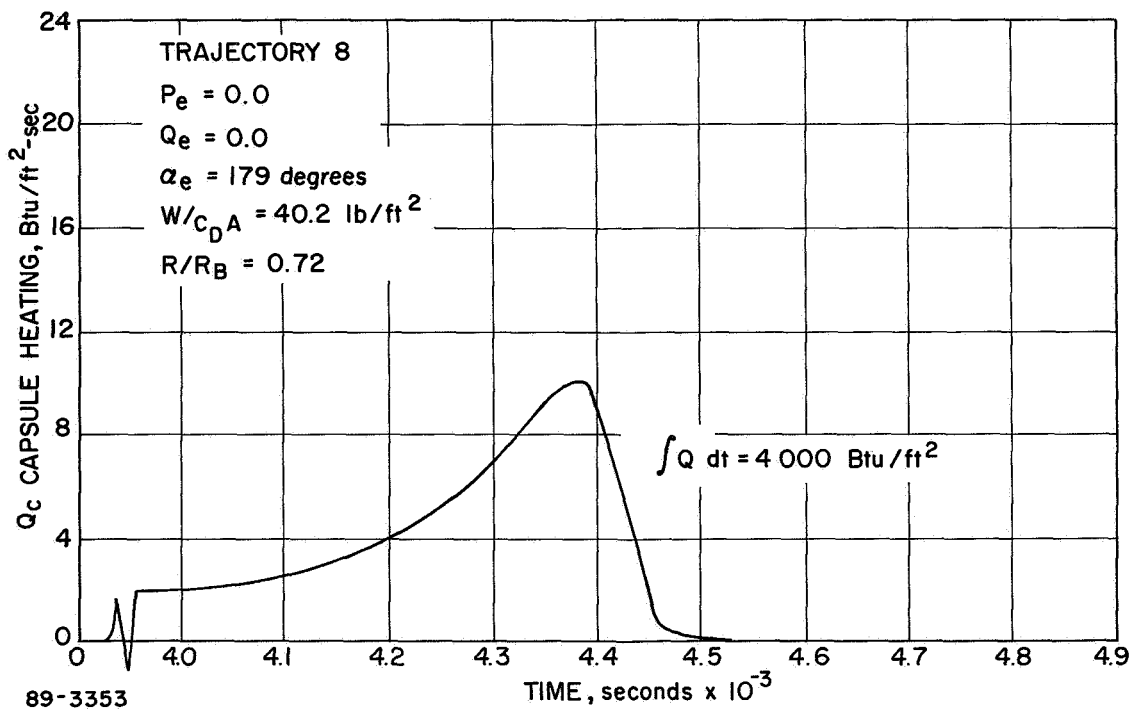


Figure 3-26 WORST CAPSULE HEATING -- REARWARD REENTRY MODE

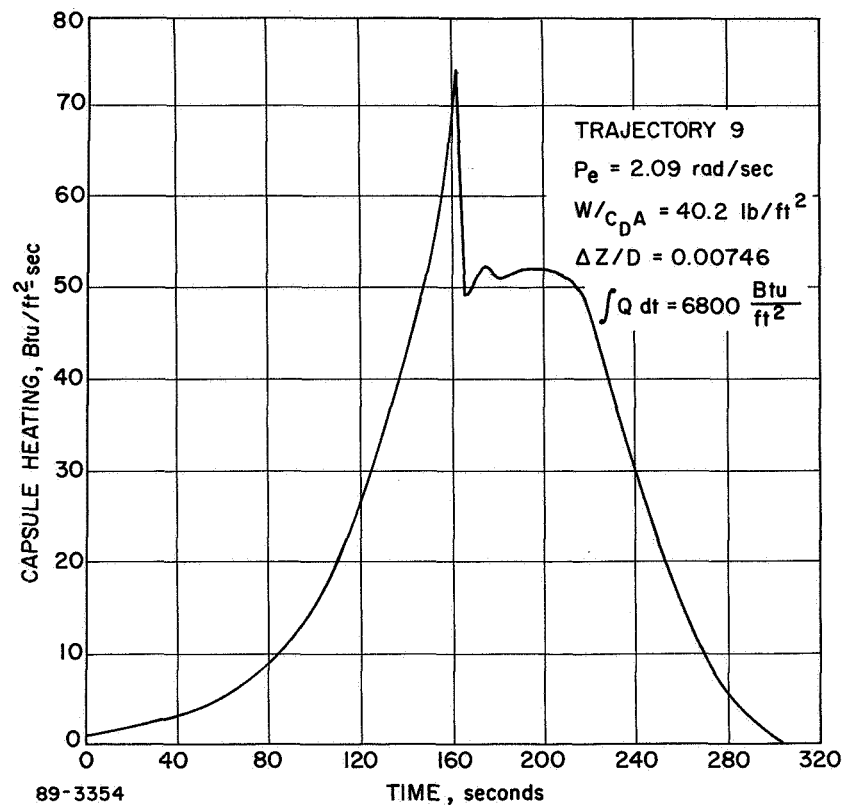


Figure 3-27 WORST CAPSULE HEATING -- NOMINAL REENTRY MODE (OFFSET C.G.)

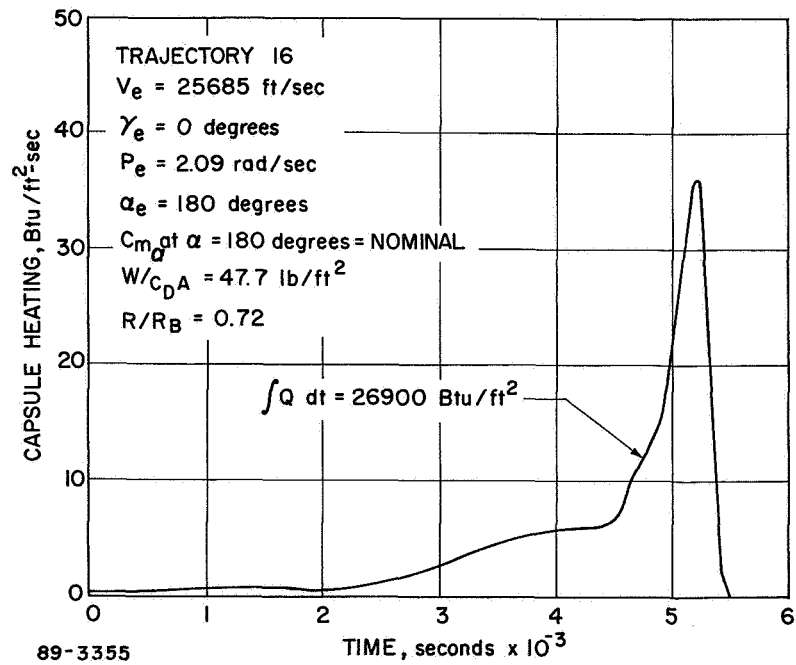


Figure 3-28 WORST CAPSULE HEATING -- REARWARD SPINNING REENTRY MODE

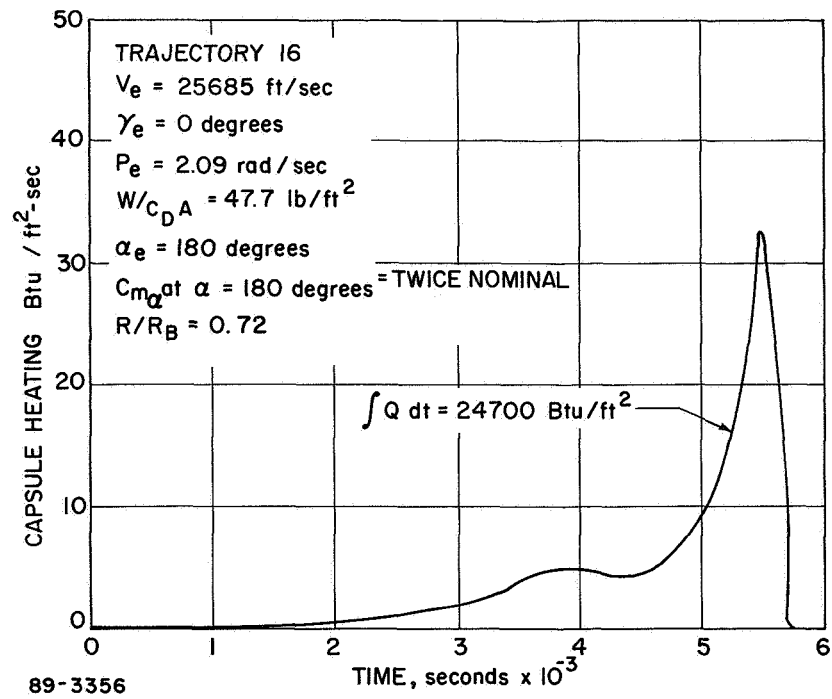


Figure 3-29 WORST CAPSULE HEATING -- REARWARD SPINNING REENTRY MODE

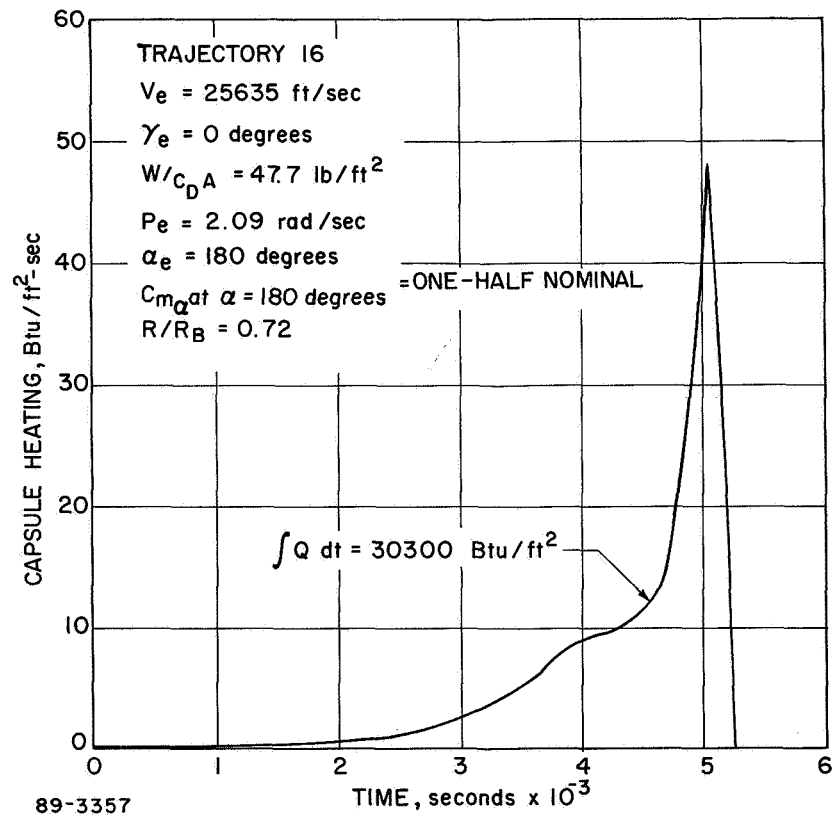


Figure 3-30 WORST CAPSULE HEATING -- REARWARD SPINNING REENTRY MODE

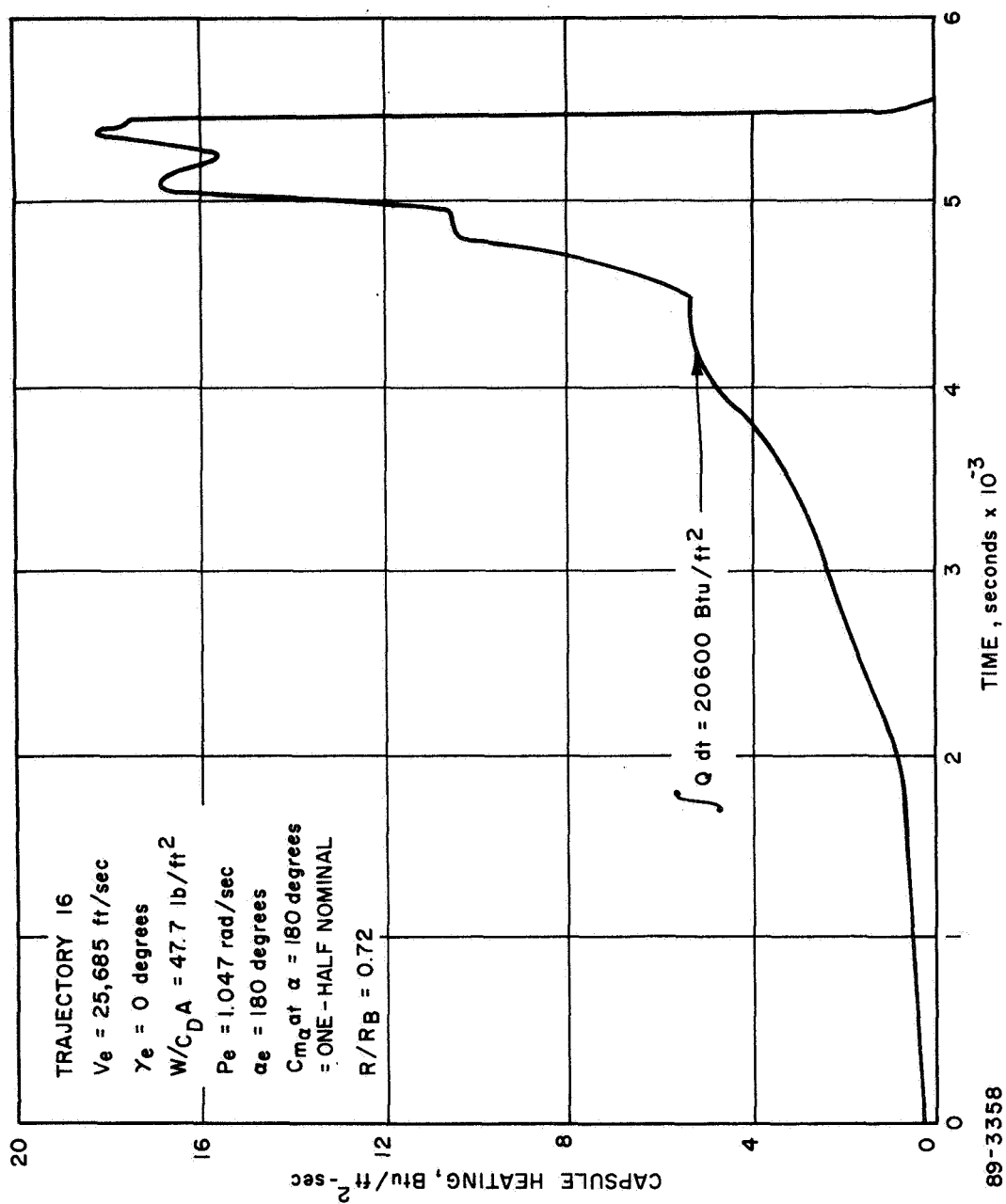


Figure 3-31 WORST CAPSULE HEATING --- REARWARD SPINNING REENTRY MODE

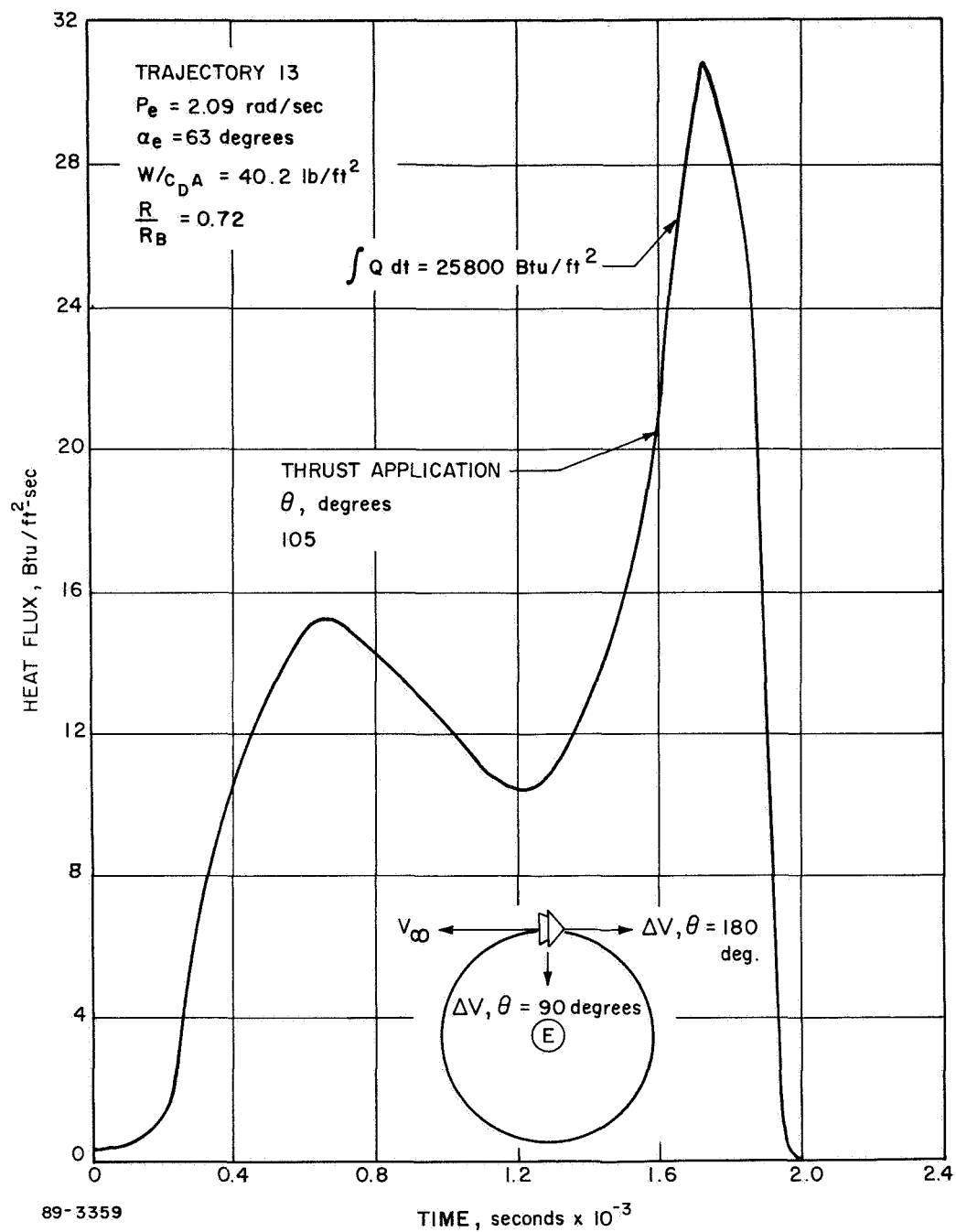


Figure 3-32 WORST CAPSULE HEATING -- DEORBIT ERROR ANALYSIS

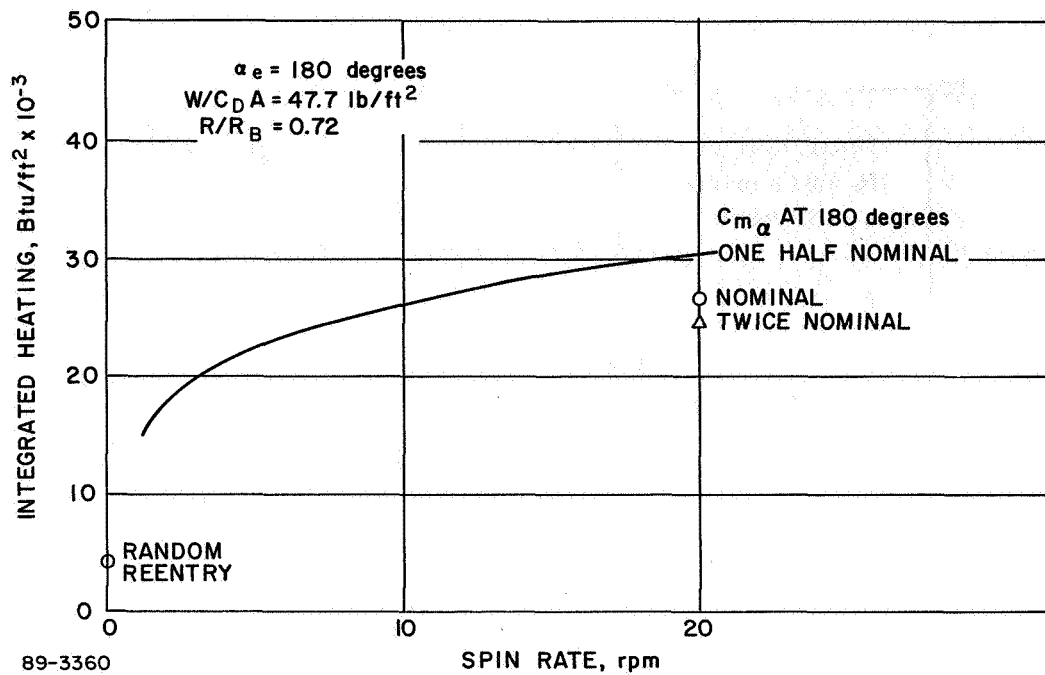


Figure 3-33 WORST CAPSULE HEATING DEPENDENCE ON FENCE TURNAROUND EFFECTIVENESS -- RETRO SYSTEM FAILURE MODE

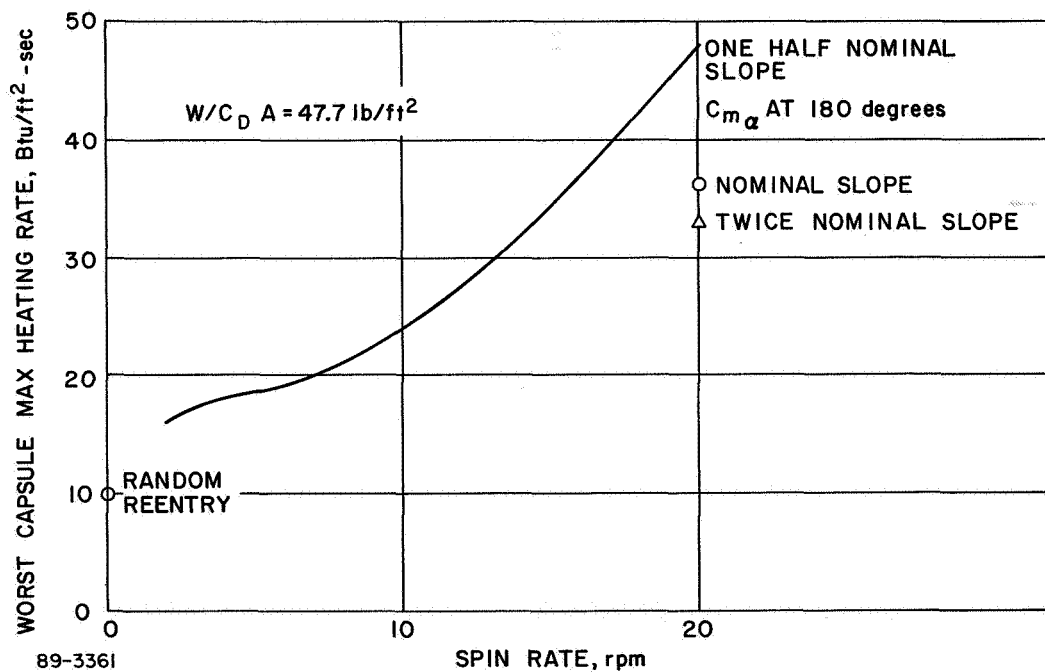


Figure 3-34 MAXIMUM WORST CAPSULE HEATING DEPENDENCE ON FENCE TURNAROUND EFFECTIVENESS -- RETRO SYSTEM FAILURE MODE

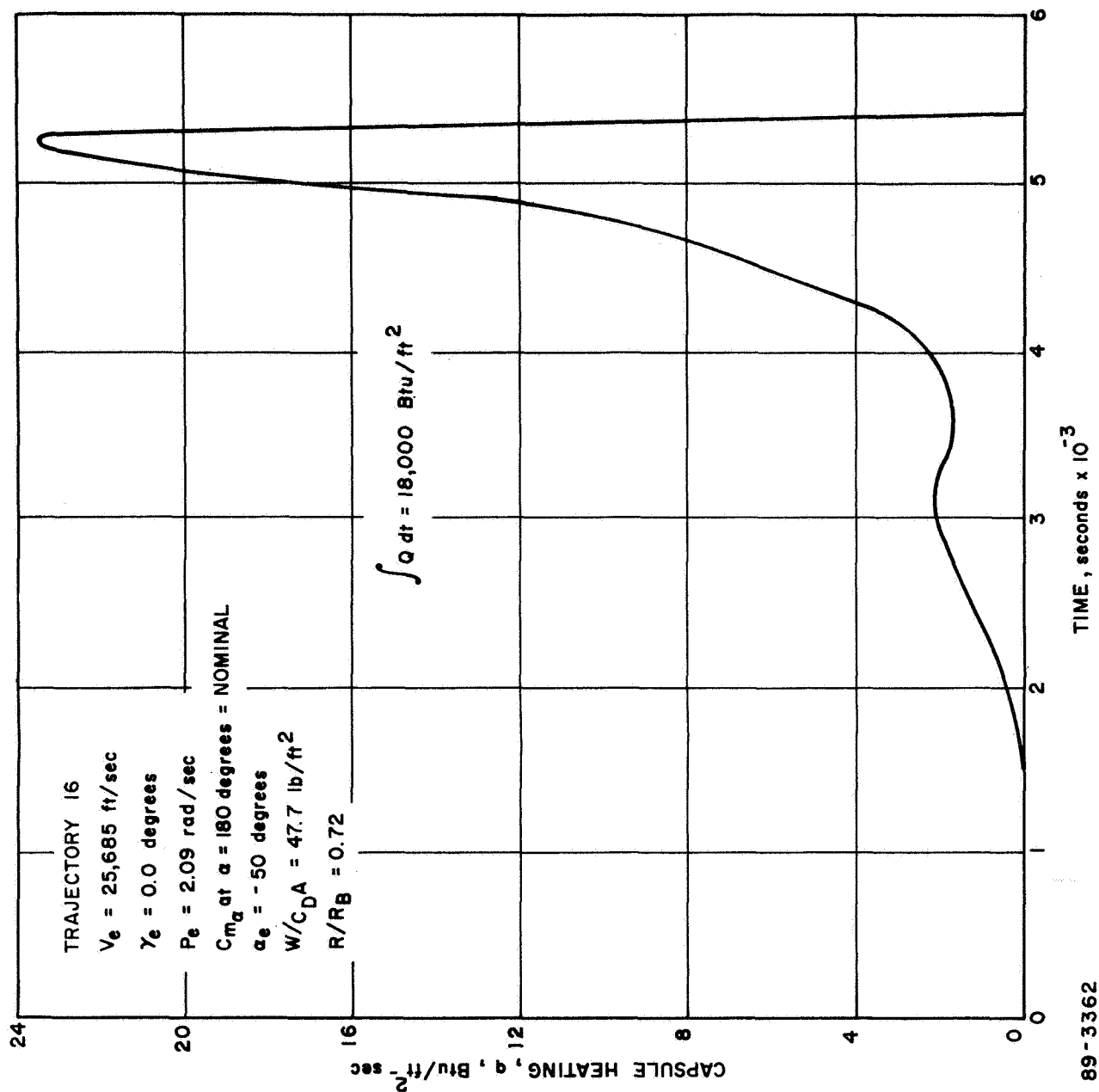
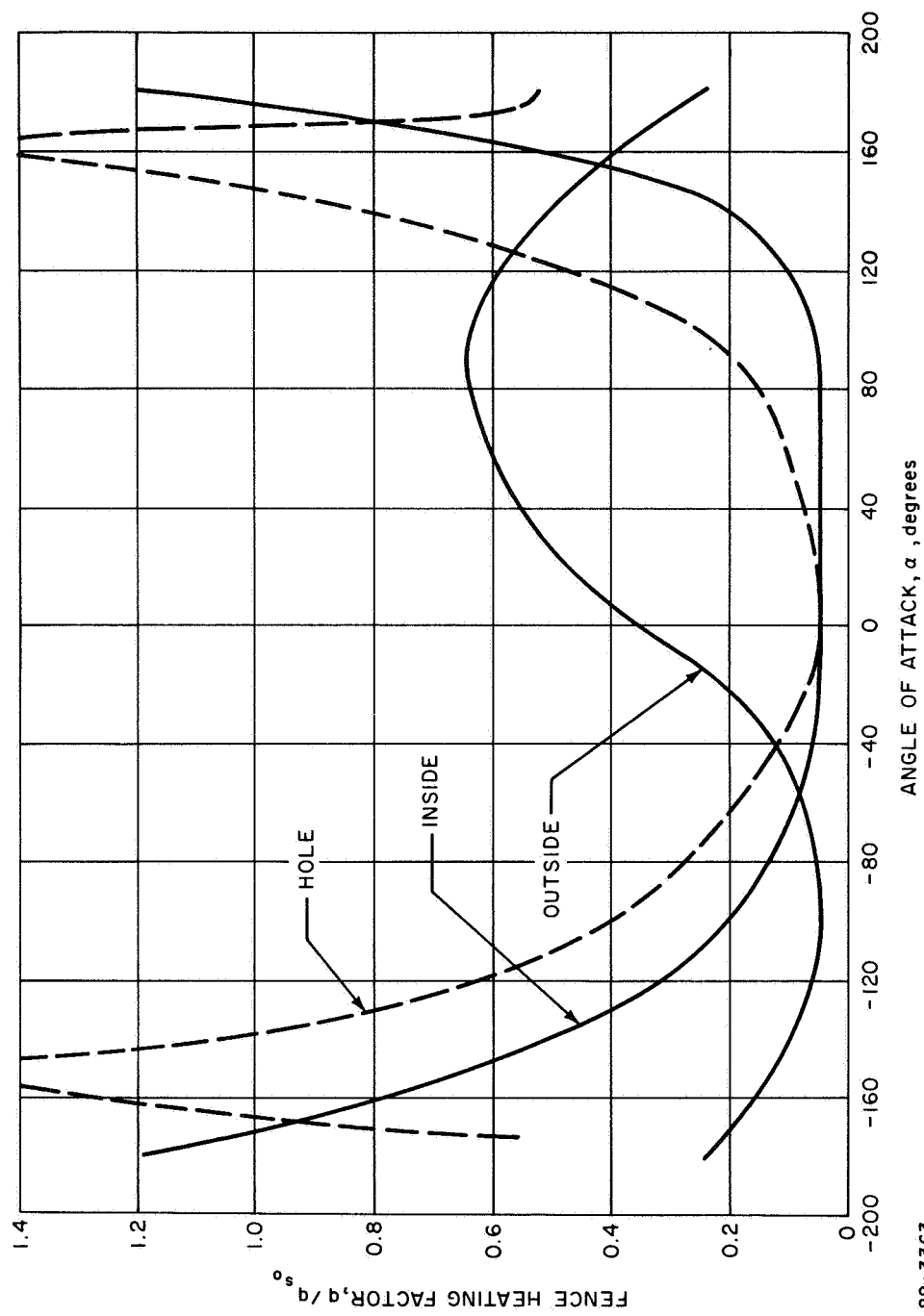


Figure 3-35 WORST CAPSULE HEATING --- REARWARD SPINNING REENTRY MODE



89-3363

Figure 3-36 FENCE HEATING FACTORS -- MIDPOINT OF THE FLARE AND AT THE HOLE

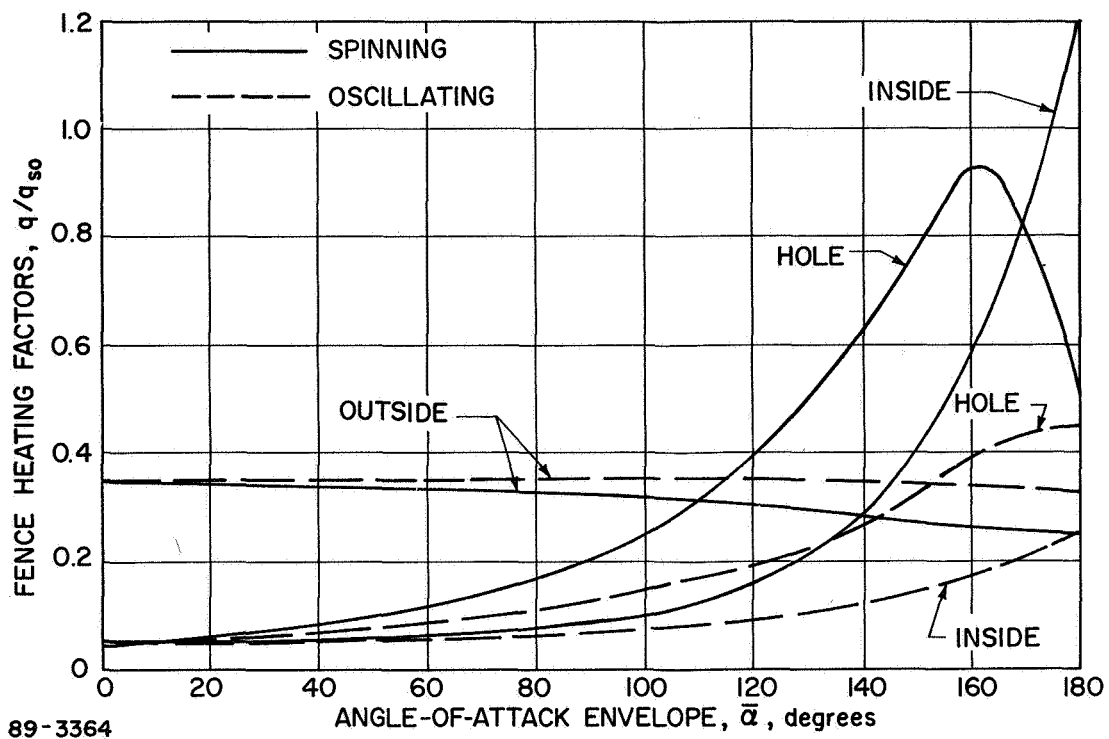


Figure 3-37 FENCE HEATING FACTORS -- DYNAMIC MODES

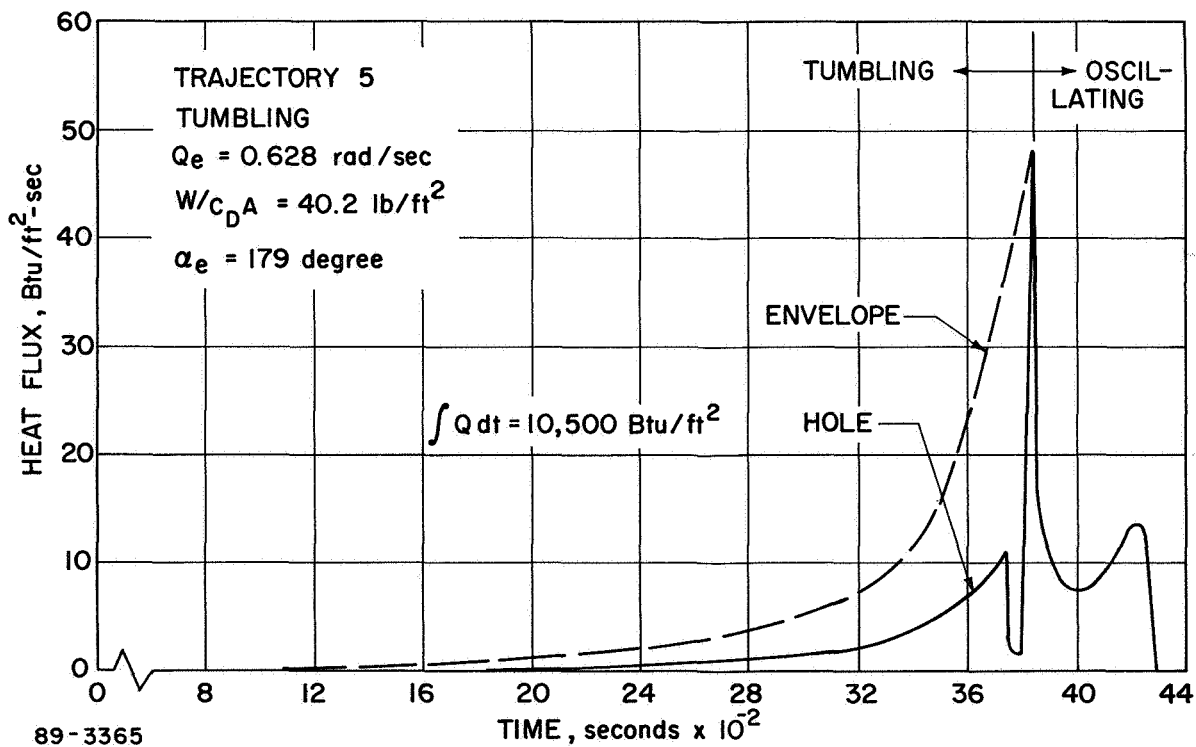


Figure 3-38 FENCE HEATING FACTORS -- HOLE

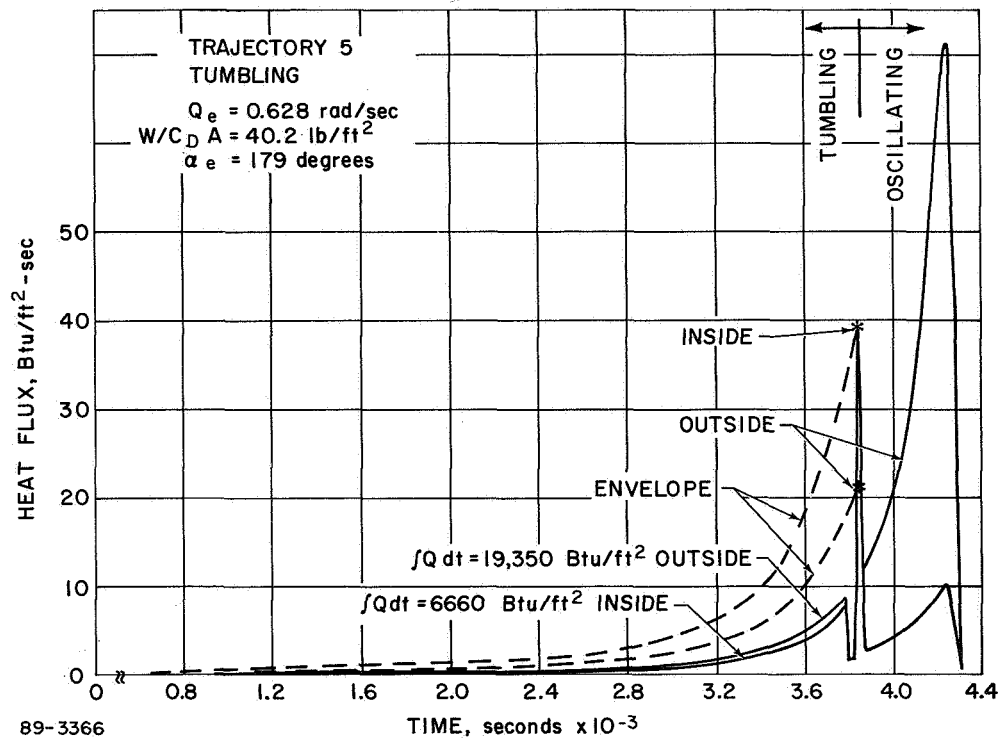


Figure 3-39 FENCE HEATING FACTORS -- FLARE

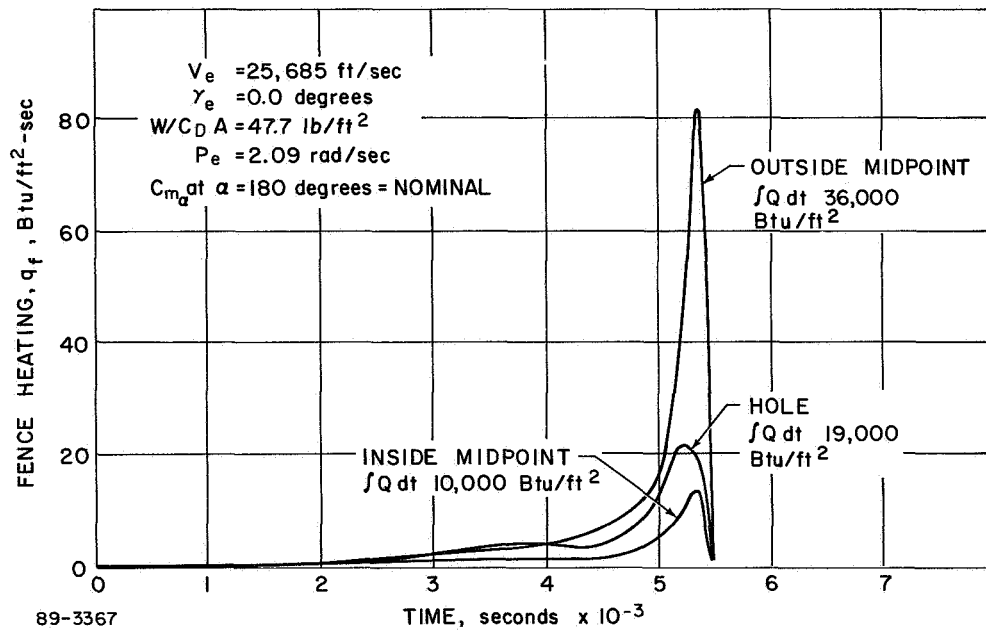


Figure 3-40 FENCE HEATING FACTORS -- REARWARD SPINNING

The edge of the fence was considered to experience two-dimensional stagnation point heating, at angles of attack greater than 90 degrees. The factor to be applied to the reference heating is equal to 1.57; at angles of attack that are less than 90 degrees the factor variation was the same as that of the aeroshell maximum diameter region.

3.2.2.2 Dynamic Stability Analysis

The dynamic stability analysis consisted of determining the vehicle angular motion during reentry, as well as the terminal dynamics including the effects of steady winds and gusts as they might affect impact angles.

3.2.2.2.1 Vehicle Entry Dynamics -- The angle-of-attack variation for the design trajectories was determined from a 6-degree-of-freedom digital program. The requirements for vehicle dynamics during the atmospheric reentry are early turnaround and angle-of-attack convergence so that the aerodynamic heating on the capsules does not cause them to exceed specified design temperatures. The angle-of-attack effects on the heating have been discussed above. The dynamics analysis investigated the effects of spin rate and fence effectiveness as well as the effects of offset c.g. and the various failure modes.

The nominal fence effectiveness (pitching moment) for the reference configuration used is shown in Figure 3-41. In addition, variations to this are shown in the figure and were obtained by varying the slope at 180 degrees to values equal to one-half and two times the nominal value as noted previously. The pitching moment coefficients at other angles of attack were also changed correspondingly. The analytically determined axial and normal force coefficients associated with the nominal pitching moment characteristics are presented in Figures 3-42 and 3-43, respectively. No variation in the force characteristics was considered. Typical variations of angle of attack envelopes, $\bar{\alpha}$, are shown in Figures 3-44 through 3-46 (the envelope values are the maximum of the angle of attack at any instant of time). In all cases the angle of attack converges when the dynamic pressure becomes significant enough to produce restoring moments.

Figure 3-44 shows the effect of an offset c.g. for a nominal reentry condition and indicates that the offset c.g. causes slightly higher angles of attack. This in turn causes slightly higher integrated heating as indicated in Table 3-12. The difference is small for the c.g. offset of 0.5 inch and presents no significant increase in heating and airloads.

Figure 3-45 compares the angle-of-attack variation for a tumbling reentry and a rearward reentry with zero rates; as would be anticipated, the tumbling mode exhibits a higher angle of attack, since the energy associated with tumble must first be overcome by the aerodynamics before convergence can occur. This is, however, not true for the case of zero rates, where convergence begins when the aerodynamic forces become large enough to rotate the vehicle. Small differences in the trajectory occur because of the differences in the effective W/C_{D_A} in the early part of the trajectory, the tumbling mode having a higher effective W/C_{D_A} than the rearward reentry mode.

Figure 3-46 presents the angle-of-attack envelope variation assuming various fence effectiveness factors for a condition with the vehicle spinning and entering the atmosphere at an angle of attack of 179 degrees. This particular combination of spin and angle of attack produces adverse characteristics in that long

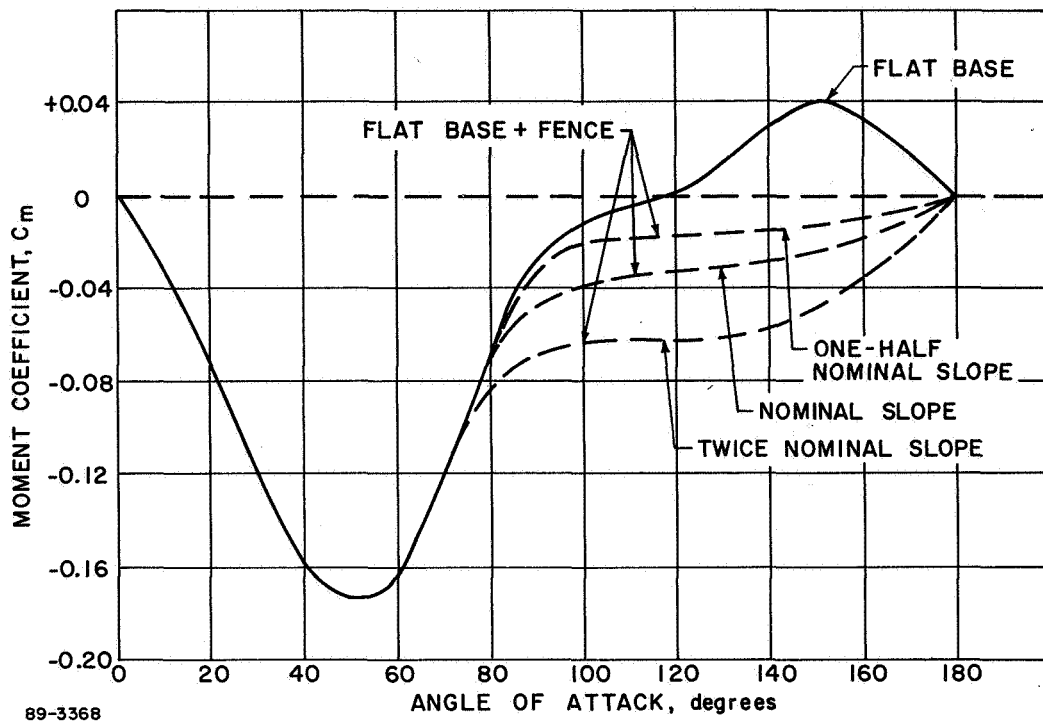


Figure 3-41 IRV AERODYNAMIC MOMENT CHARACTERISTICS

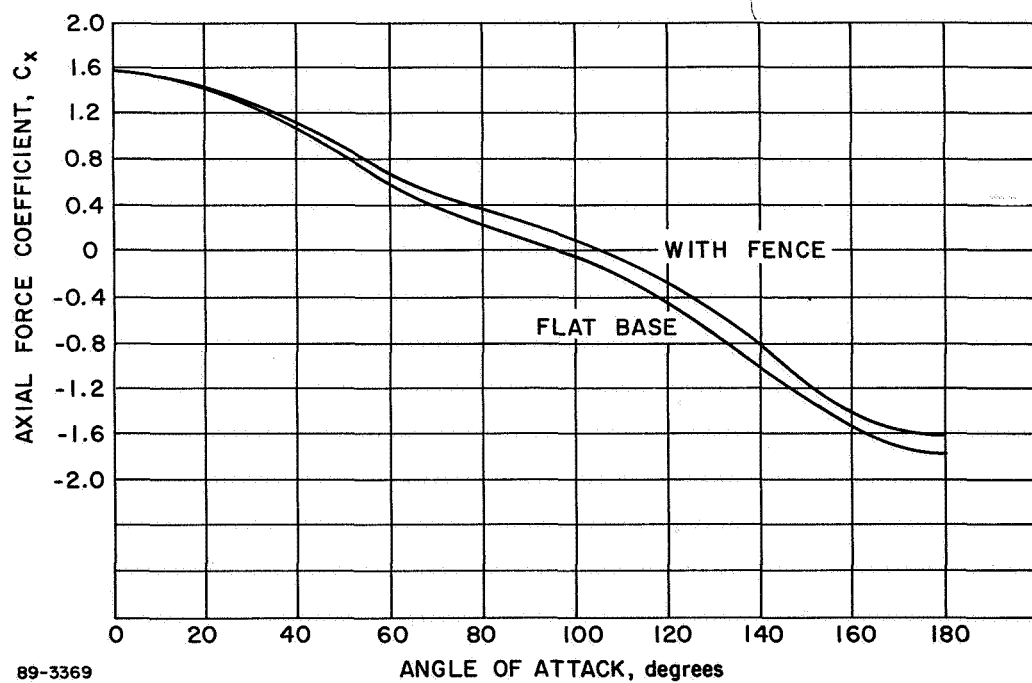


Figure 3-42 IRV HYPERSONIC AXIAL FORCE COEFFICIENT

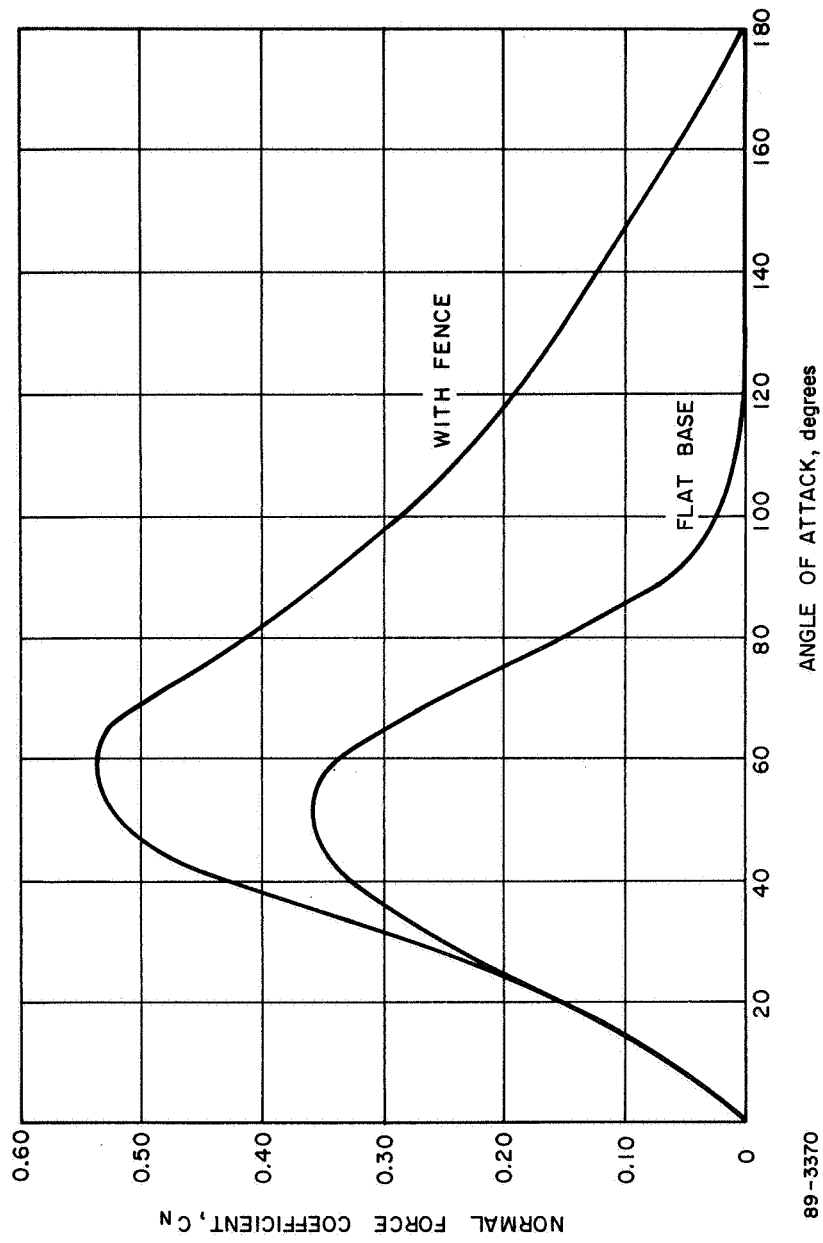
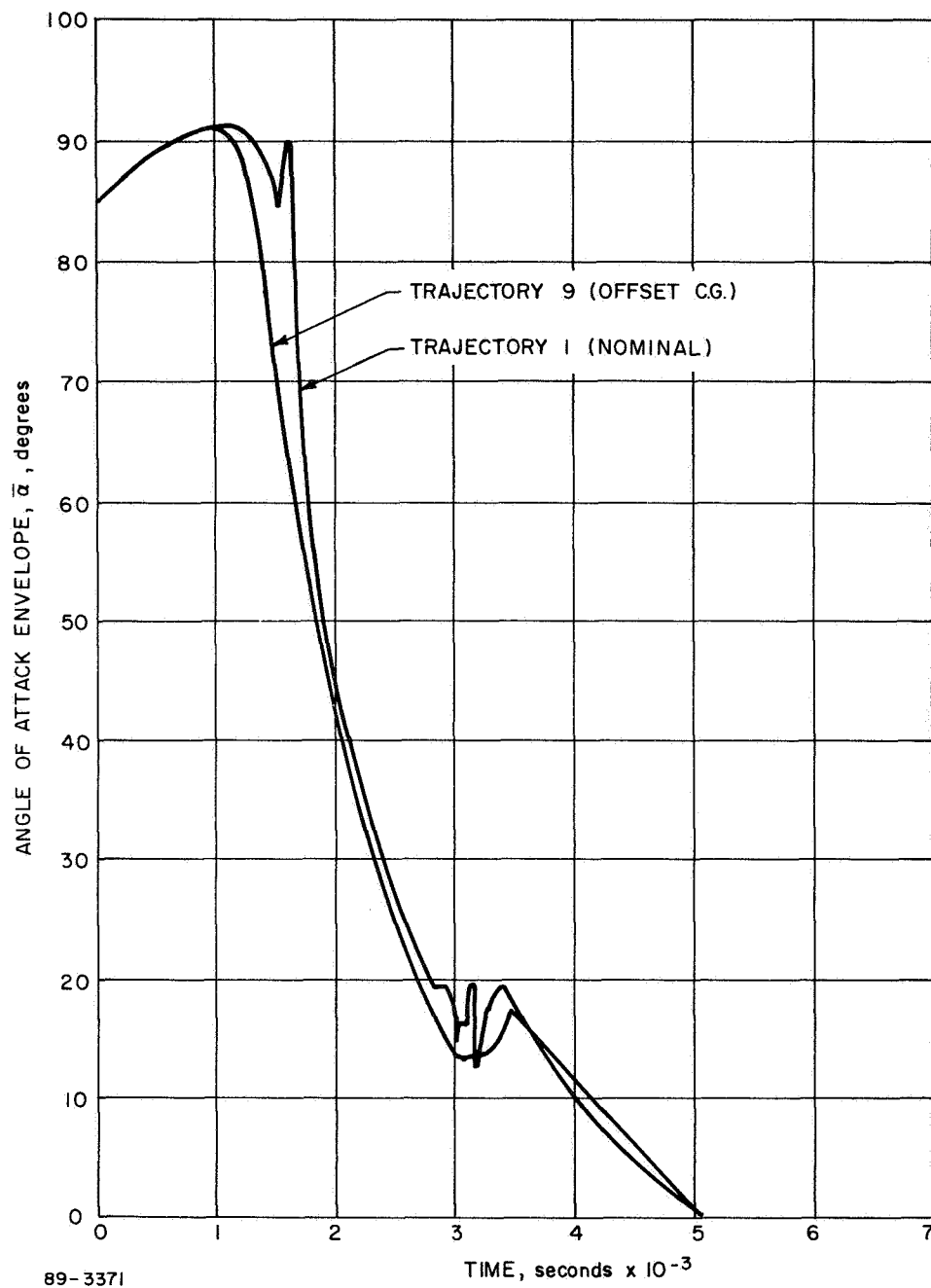


Figure 3-43 IRV HYPERSONIC NORMAL FORCE COEFFICIENT



89-3371

Figure 3-44 ANGLE-OF-ATTACK ENVELOPE HISTORIES -- CONTROLLED REENTRY

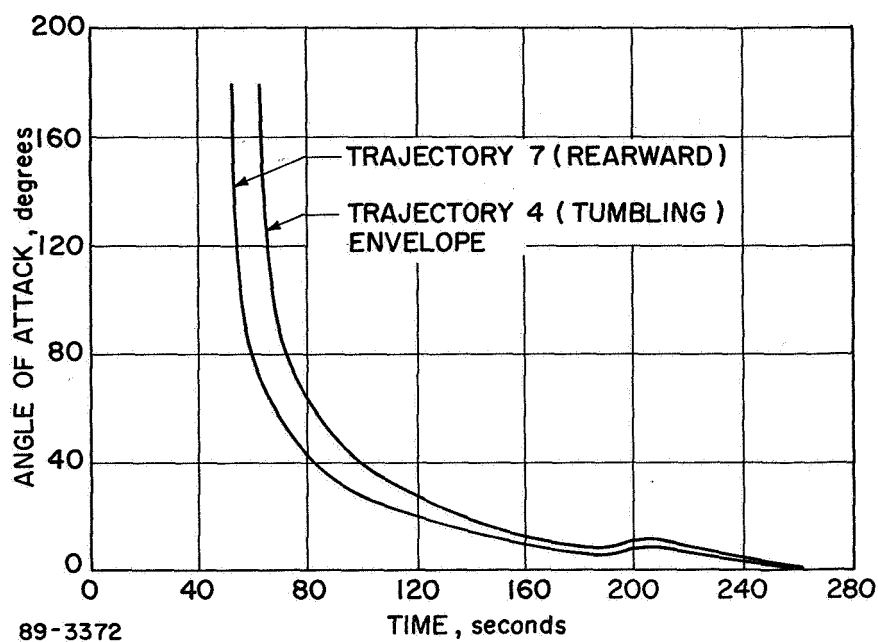


Figure 3-45 ANGLE-OF-ATTACK ENVELOPE HISTORIES -- UNCONTROLLED REENTRY

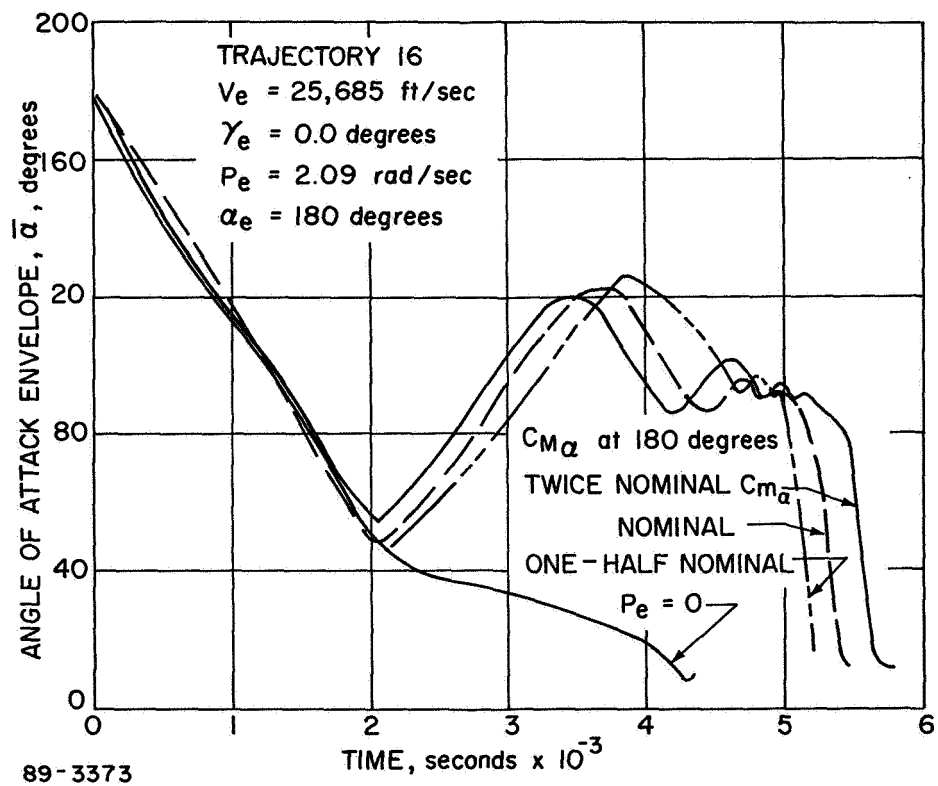


Figure 3-46 ANGLE-OF-ATTACK ENVELOPE HISTORIES -- EFFECT OF TURNAROUND MOMENT

flight times occur with the angle of attack near 90 degrees. The initial angle-of-attack variation is associated with the gyroscopic stability in conjunction with the flight path curvature. This is a low drag attitude (resulting in a high ballistic coefficient) which tends to reduce the rate of descent and therefore the angle-of-attack convergence process is delayed.

3.2.2.2.2 Wind and Gust Effects -- The wind profile and gust characteristics shown in Figures 3-47 through 3-51 were derived from References 3-6 to 3-9 and from verbal consultation with the Air Force Cambridge Research Laboratories - Environmental Consultation Service.

The literature search has shown that the average wind profile is more easily determined than the wind gusts (which are added to the average wind profile to obtain the total velocity) and is more consistent among the various sources; in addition, wind gust data are extremely scarce and more difficult to evaluate.

The wind profile shown in Figure 3-47 was obtained from References 3-6 and 3-7. The profile presented is a maximum envelope which is exceeded only 1 percent of the time and is characteristic of the windiest area of the United States (Northeastern region).

Gust velocity data were obtained from References 3-7 through 3-9, which are summarized in Figure 3-48.

The data from Reference 3-9 is a single value for design of launched missiles. Reference 3-8 presents the loading considerations for airplane design, and the data point at sea level from Reference 3-7 was derived from Figure 3-49. This latter figure shows data from four typical recorded sets of weather data, and shows the gust factor as a function of mean wind velocity. Assuming a sea level mean wind velocity of 25 ft/sec (Figure 3-47) and applying a gust factor to this value of 2.32 (Figure 3-49) yields a gust velocity of 33 ft/sec, shown in Figure 3-48. The gust velocity used for the study (i.e., 50 ft/sec) is thus conservative when compared to the other possibilities. An additional factor which must be considered is the time duration of the gusts. Figure 3-50 indicates that the gust duration increases as the gust factor decreases. Using this criterion, the gust velocity criteria used in Phase II are shown in Figure 3-51.

The dynamic analysis was performed on a 6-degree-of-freedom digital program. The wind velocities and gust altitude variations were selected as close to impact as necessary such that maximum vehicle divergence was obtained. The maximum gust velocity of 50 ft/sec was superimposed on the steady-state profile ($V_e = 25$ ft/sec) with the gusts initiated at an altitude of 110 feet, resulting in a maximum vehicle attitude, relative to the local vertical at impact.

The effect of the wind gust on the vehicle stability and impact attitude is shown in Figure 3-52. Both the spinning and non-spinning vehicles show some divergence in angle of attack with the non-spinning approximately 1.8 degrees to 14.4 degrees.

The maximum vehicle attitude at impact is 37.5 degrees and occurs for the non-spinning case. With spin the maximum angle is 31.7 degrees. These

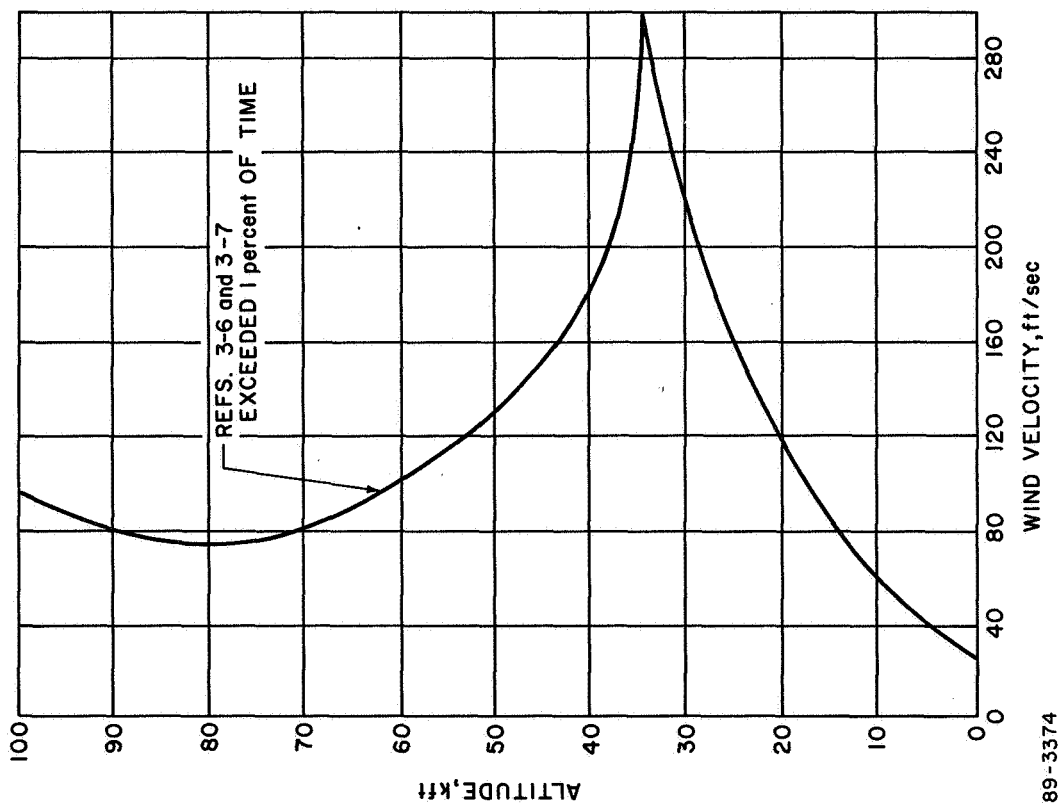


Figure 3-47 WIND PROFILE DATA

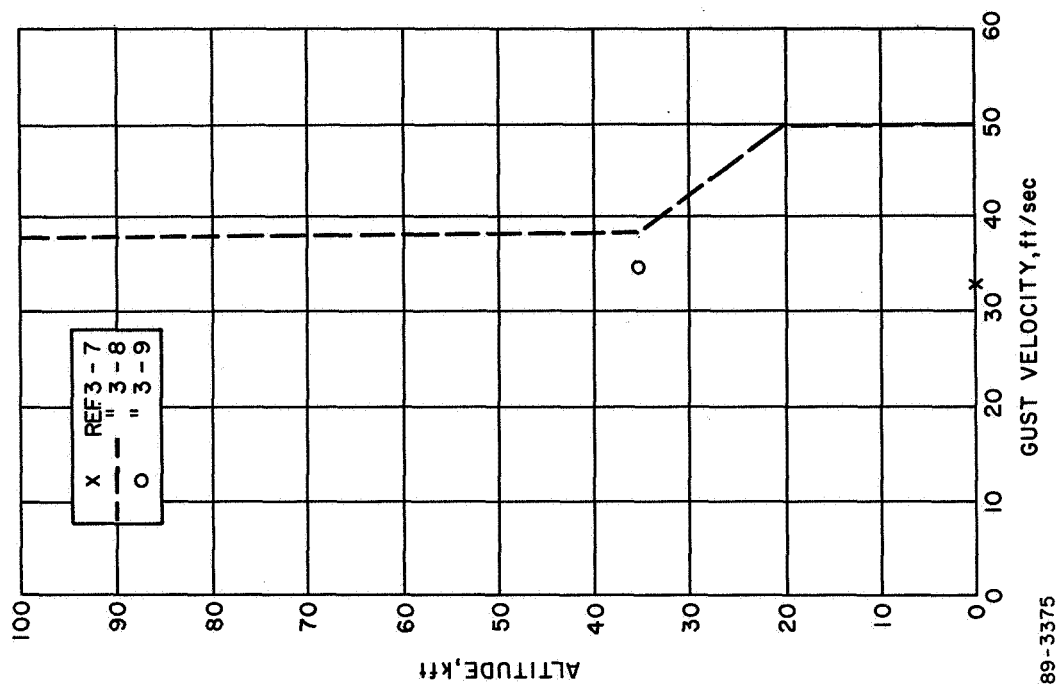


Figure 3-48 GUST VELOCITY DATA

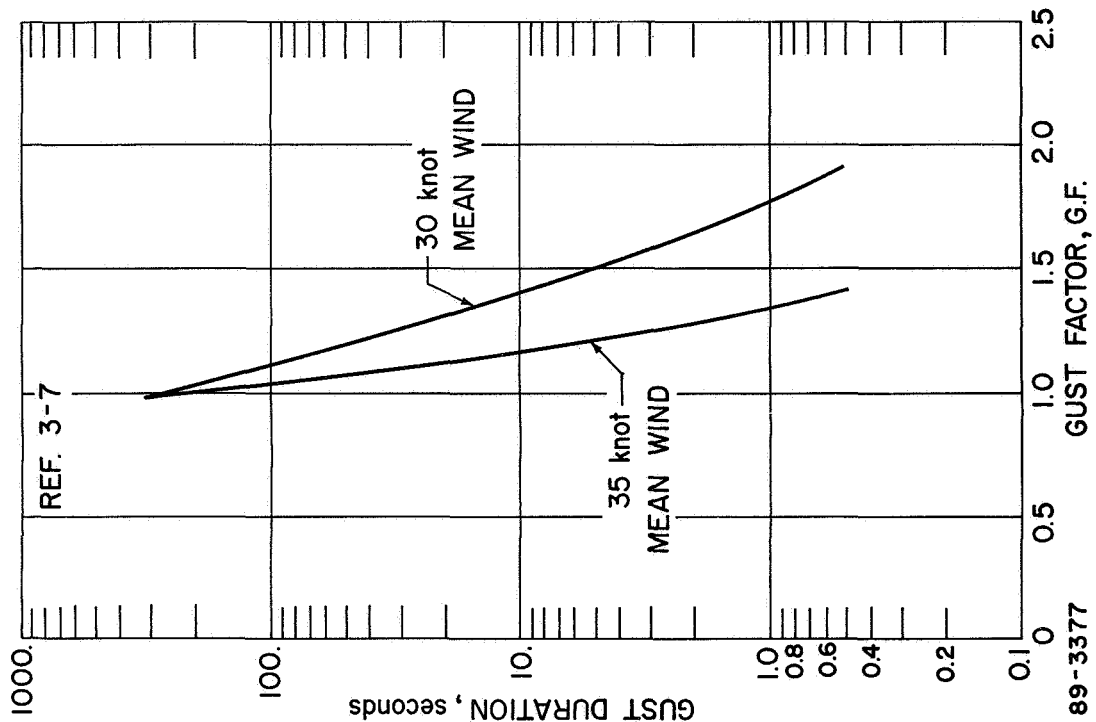


Figure 3-49 GUST FACTOR DATA

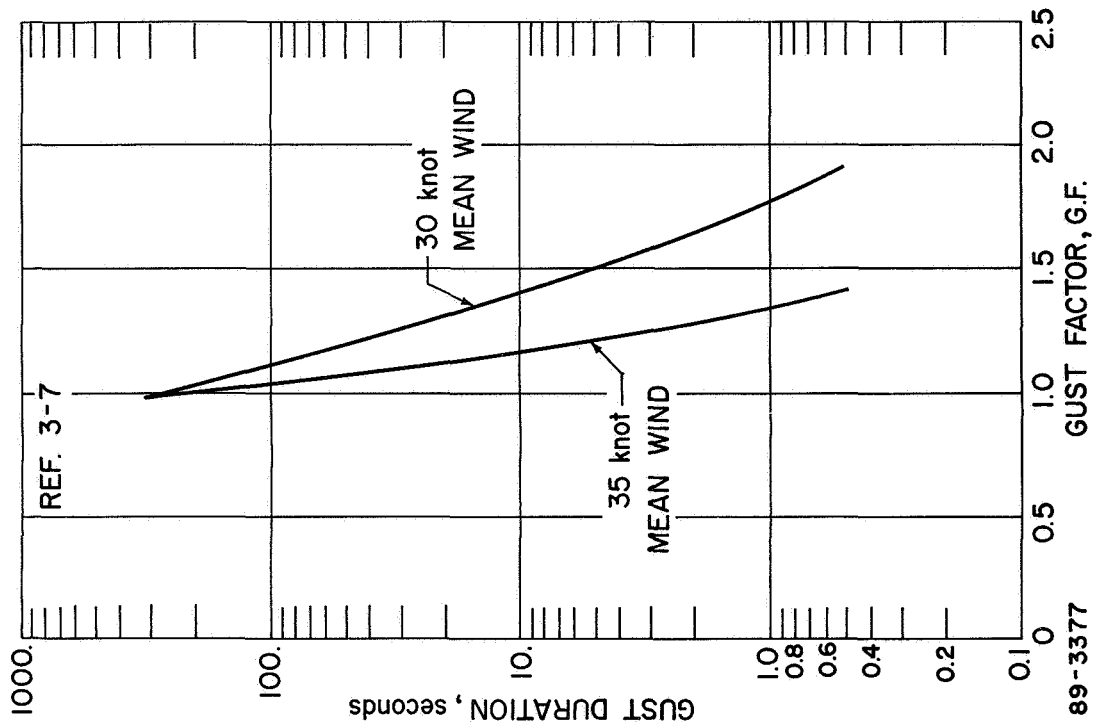


Figure 3-50 GUST DURATION DATA

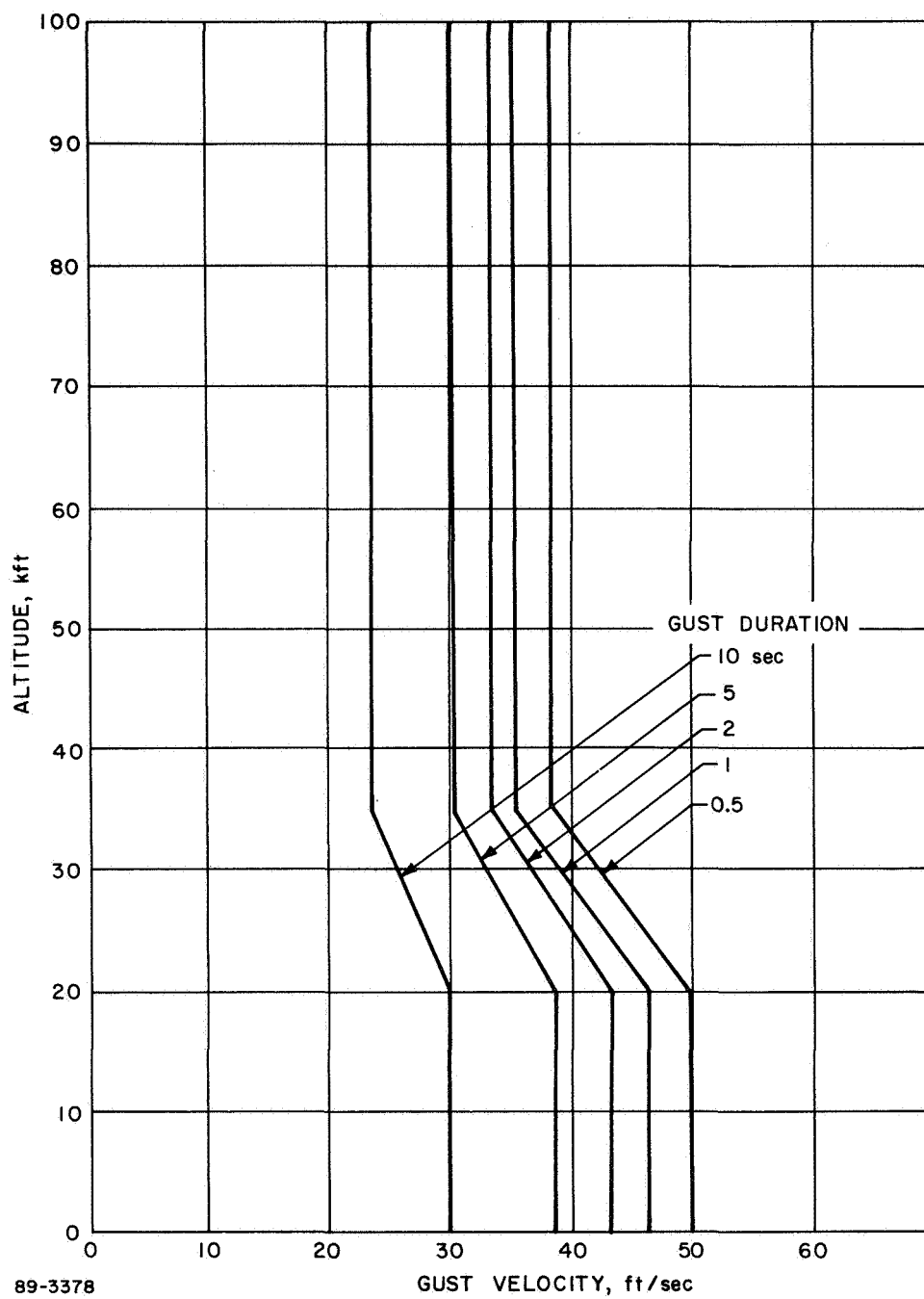


Figure 3-51 DESIGN GUST VELOCITY DATA

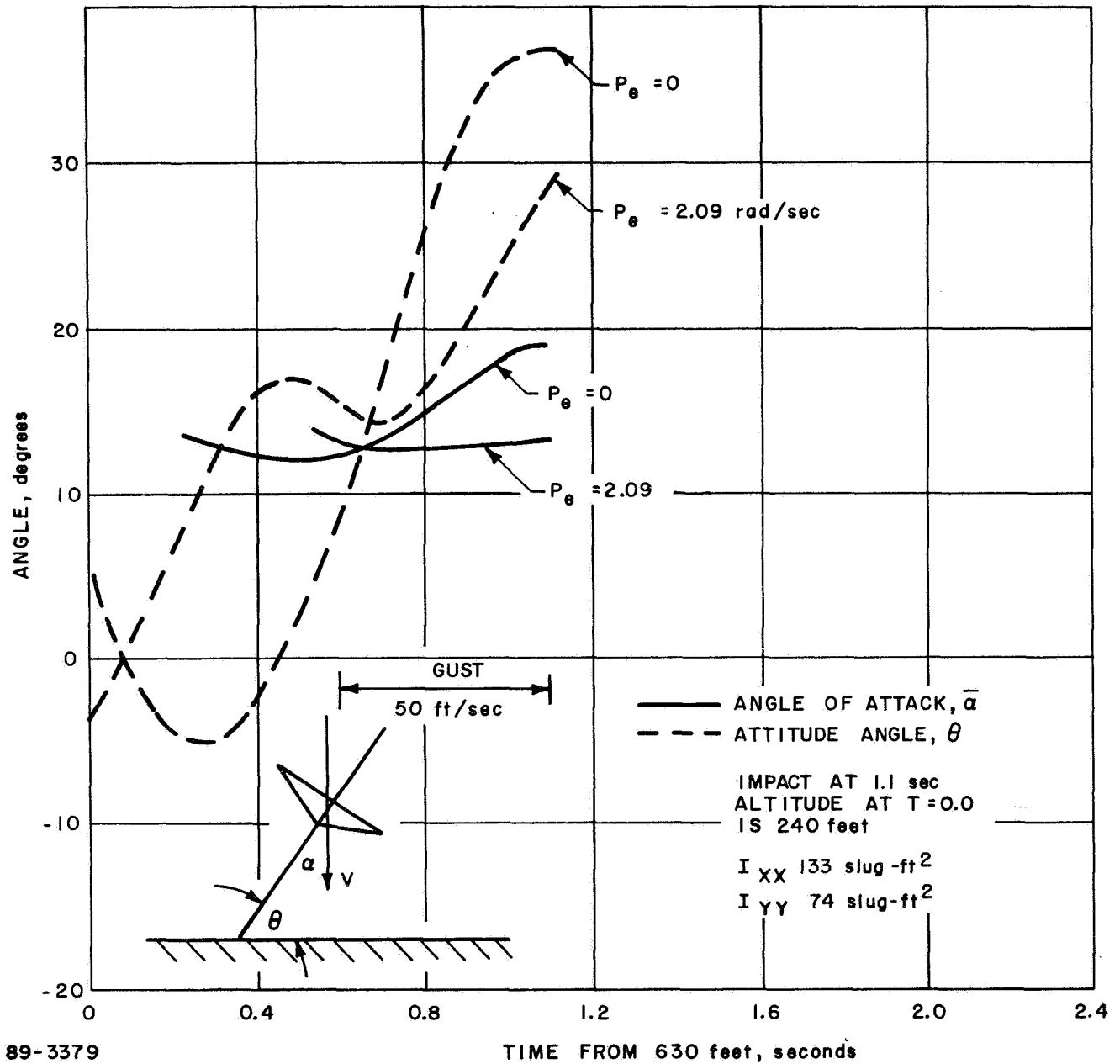


Figure 3-52 EFFECT OF WIND GUST ON VEHICLE ATTITUDE AT IMPACT

differences are caused by the fact that the non-spinning vehicle has a faster response whereas the spinning vehicle with its added spin stability will tend to stay closer into the wind. The differences, however, are small indicating little added stability due to spin.

The spin rate considered (20 rpm) is less than the critical spin rate for subsonic stability (References 3-10 and 3-11) for the mass characteristics and aerodynamic coefficients used in the Phase II study. The effect of the fence is uncertain since it is in the base flow region. The vented fence concept may be beneficial if reattachment occurs on the fence; in this case the non-steady flow phenomenon would be the predominant factor.

3.3 HEAT SOURCE DESIGN

3.3.1 Heat Source Thermal Performance

3.3.1.1 Introduction

The heat source thermal design requires that the source be maintained at safe operating temperatures during ground handling, space operation, and reentry, yet provide the capability to deliver heat to a Brayton cycle system during steady-state operation at an efficient temperature level. The thermal criteria established to ensure this capability during periods of handling and flight are shown in Table 3-14.

TABLE 3-14

HEAT SOURCE THERMAL DESIGN CRITERIA

Maximum steady-state capsule - surface temperature	2000° F
Maximum transient capsule surface temperature	2500° F
Maximum capsule temperature rise in one hour from 1800° F	700° F
Maximum transient heat source temperature while in oxygen atmosphere	600° F
Maximum steady-state heat source temperature in oxygen atmosphere	350° F
Maximum operating heat loss	1500 watts

During Phase I several heat source designs and design variations were evaluated thermally with analyses restricted in complexity to permit relative evaluation of key parameters. In these studies the following operating environments were analyzed.

a. Launch Pad

1. Steady state - ACHX cooled
2. Transient - ACHX disconnected

b. Space

1. Steady state - normal operation - primary HSHX operating
2. Steady state - normal operation - secondary HSHX operating
3. Steady state - heat source deployed in space
4. Transient - Heat source not deployed - HSHX shut down
5. Transient - reentry.

Included in these analyses were the evaluation of the temperature profile of capsule and support structure during steady-state conditions, the temperature history of mean fuel capsule temperature during transient states, thermal losses during normal operation, and the hydraulic performance of the ACHX during launch pad cooling.

During Phase II the preliminary heat source design was evaluated for the same periods as mentioned above, using more precise mathematical tools. Temperature profiles of the worst capsule were evaluated for transient and steady-state conduction by the use of a two-dimensional heat transfer model shown schematically in Figure 3-53. To facilitate this analysis, a modified digital heat transfer code (TOSS) distributed by Oak Ridge (Ref. 3-12) was used to analyze this model. The detailed description of this model and code is presented in paragraph 3.3.1.3. Results of the TOSS calculations are presented in detail in the following sections for the various periods of operation illustrating the effects of several design features.

3.3.1.2 Summary of Heat Source Thermal Analyses

The Phase II thermal analyses consisted of the evaluation of the capability of the preliminary heat source design to meet the thermal design criteria outlined in paragraph 3.3.1.1. To perform this evaluation the temperature distribution and history were calculated for key steady-state and transient periods during the lifetime of the heat source. To accomplish this a two-dimensional heat transfer model was used. Based on these results the hydraulic requirements of the ACHX were set and the thermal losses for steady-state nominal performance were evaluated.

Figure 3-54 presents the peak capsule temperature during the events in the life of the heat source that were studied. Although the sequence of events as presented in this figure follow an apparent order, this sequence is not necessarily representative of a mission but merely identifies each of the individual phases considered, and each event should be considered separately. Results and conclusions obtained from the analyses of each of these events are summarized below. Note that the temperatures indicated in Figure 3-54 are based on the active fuel length and not the total heat source area.

a. Launch Pad - Steady State

As shown in Figure 3-54 the peak exposed capsule temperature can be limited to 350° F or less with even a conservative assumption of a

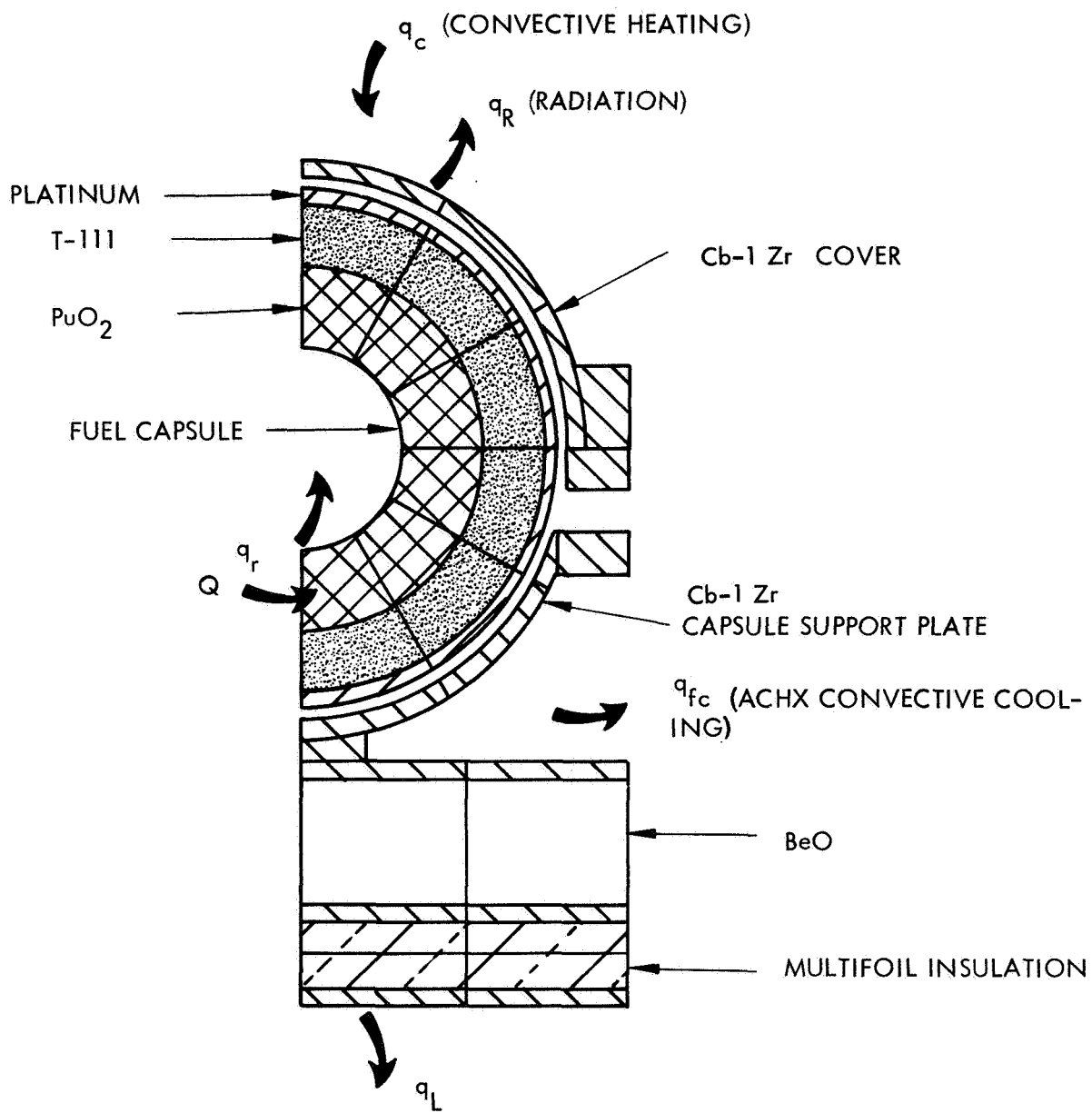
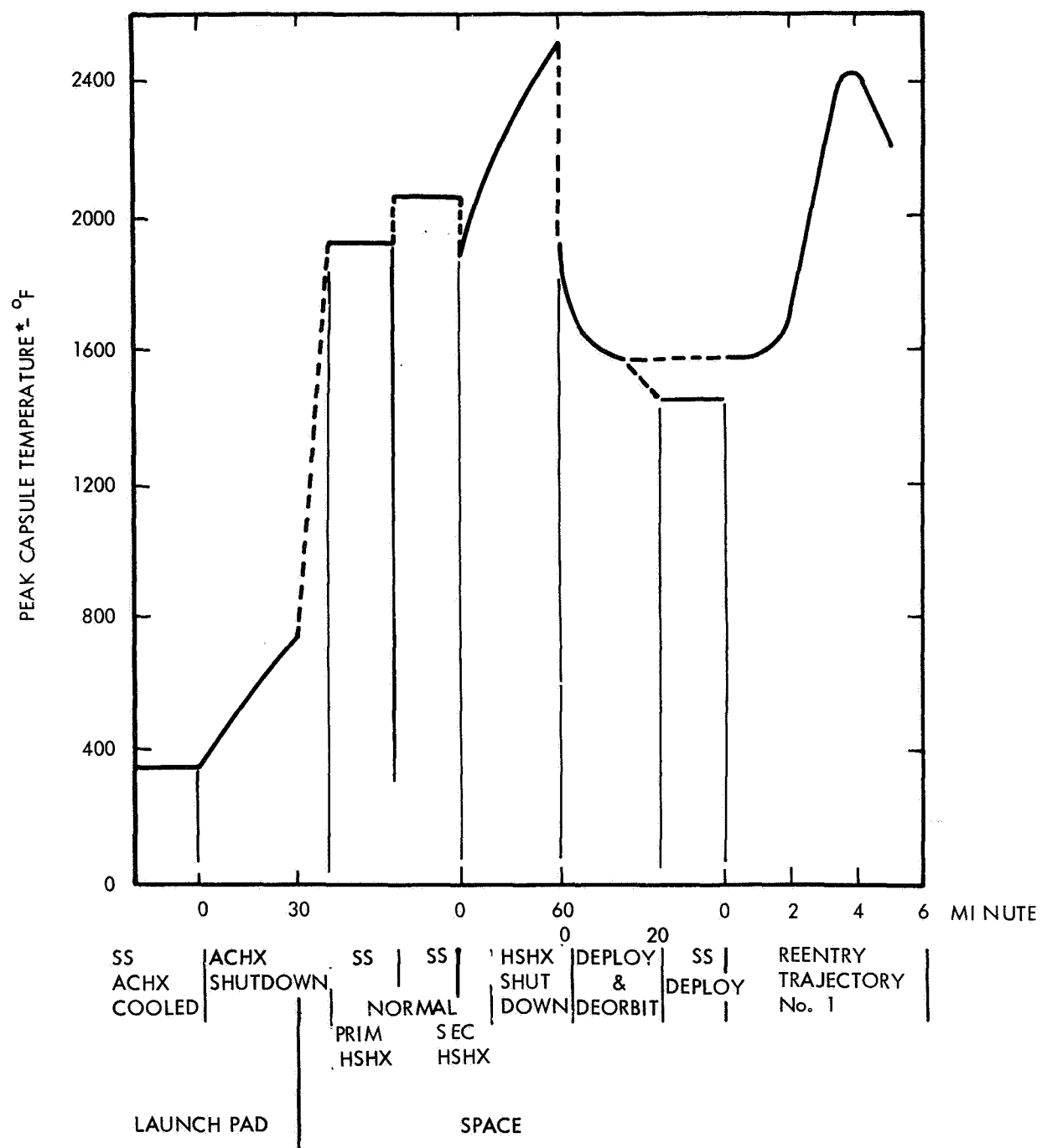


Figure 3-53 TWO-DIMENSIONAL THERMAL MODEL OF HEAT SOURCE



*Based on active fuel length of capsules and their projected radiating area.

Figure 3-54 HEAT SOURCE TEMPERATURE HISTORY

0.002-inch air gap between the capsules and the capsule support plate. Coolant requirements consist of 3.13 lb/sec of air or nitrogen entering at 70° F and 90 psi.

b. Transient Heat-Up from ACHX Cooled Steady State

The 170 pounds of BeO with a 2-mil air gap between the BeO and capsule support plate provide a 15-minute period before the capsule exposed surface reaches 600° F. This provides sufficient time for leaving the atmosphere of the earth during launch and sufficient time for transferring from a temporary to a permanent ACHX cooling system during the pre-launch ground handling period.

c. Space - Steady State

With the Brayton cycle equipment operating at full power the peak capsule temperature is 1918° F with a primary HSHX in operation and 2060° F with secondary HSHX in operation, still providing full rated Brayton cycle electrical output. The peak capsule temperature can be reduced from 2060° to 2000° F while operating with the secondary HSHX by reducing the Brayton cycle system output to 90 percent. A further reduction in power to 83 percent while operating with the secondary HSHX would reduce the peak capsule temperature to the 1918° F temperature which exists when operating at full power with the primary HSHX.

d. Heat Up From Steady-State Normal Operating Conditions, With No Heat Removal Through the HSHX

The peak capsule temperature will rise from 1918° to 2530° F in one hour with a design including 170 pounds of BeO with a contact resistance of 100 Btu/° F-ft²-hr (which represents a rather poor contact) between the BeO and the capsule support plate, thus satisfying the requirement of a temperature rise of less than 700° F in one hour. The capsule temperature rise is very sensitive to the contact resistance assumed. For an extreme case with a radiation gap, 235 pounds of BeO is required to maintain a peak capsule temperature below 2500° F one hour after starting from 1800° F.

e. Reentry

During reentry the peak capsule temperature under a cover plate is maintained below 2500° F for the credible reentry trajectories. The cover plate with a radiation gap between it and the capsules provides an effective thermal barrier, and it reduces the peak capsule temperature by 160° to 360° F compared to the case of the bare capsule during reentry heating. BeO does not provide any significant help in reducing the peak capsule temperature during the reentry trajectories.

The thermal analyses identified are based on certain assumptions which must be confirmed.

3.3.1.3 Two-Dimensional Thermal Model of Heat Source

A two-dimensional model of a typical fuel capsule was developed to analyze the thermal performance of the heat source during critical states of flight

and handling. The model was developed in sufficient detail to provide the capability to analyze the following performance states:

- Steady-state capsule temperature profile on launch pad with ACHX operating.
- Temperature time history of fuel capsule, cover plate, BeO and support structure on launch pad immediately after ACHX disconnect.
- Steady-state temperature profile of heat source in space with:
 - HS facing HSHX with primary HSHX operating
 - HS facing HSHX with secondary HSHX operating
 - HS facing space in deployed position
- Temperature-time history of heat source immediately after HSHX shutdown but prior to deployment of the HS (all heat absorbed by HS and HSHX except losses through insulation).
- Temperature-time history of the heat source during reentry while exposed to varied reentry trajectories.

To facilitate this analysis a modified version of a generalized digital heat transfer code (TOSS) was used. This code can calculate the transient and/or steady-state temperature distribution of a three-dimensional irregular body. The heat transfer mechanisms of conduction, radiation, forced convection, and free convection are considered in this code. Internal heat generation as a function of time and space is also considered. Transport properties, boundary temperatures, and forced convection film coefficients may be time dependent. This code solves the generalized heat conduction equation problem by an implicit finite difference technique employing the Gauss-Seidel convergence procedure. A nodal model of a particular physical system is analyzed with this code by specifying through input data the dimensions and properties of all nodes, connections between adjacent nodes, connections from the nodes to nodal surfaces facing boundaries, and the connections from surface nodes to boundary nodes by the appropriate heat transport mechanism.

For analysis of the heat source a two-dimensional model of the typical cross section of the heat source representing one-half of a fuel capsule was used. This model represented the smallest element over which the heat flow was symmetrical. Figure 3-55 is a sketch of the nodal model used for transient analyses. Steady-state analyses were performed with a model using twice as many nodes. Heat source components included in the model were:

KEY
LOCATIONS

COVER (1)

CAPSULE (2)
(REENTRY)

CAPSULE (2)
(S. S.)

CRADLE (3)

BeO (4)

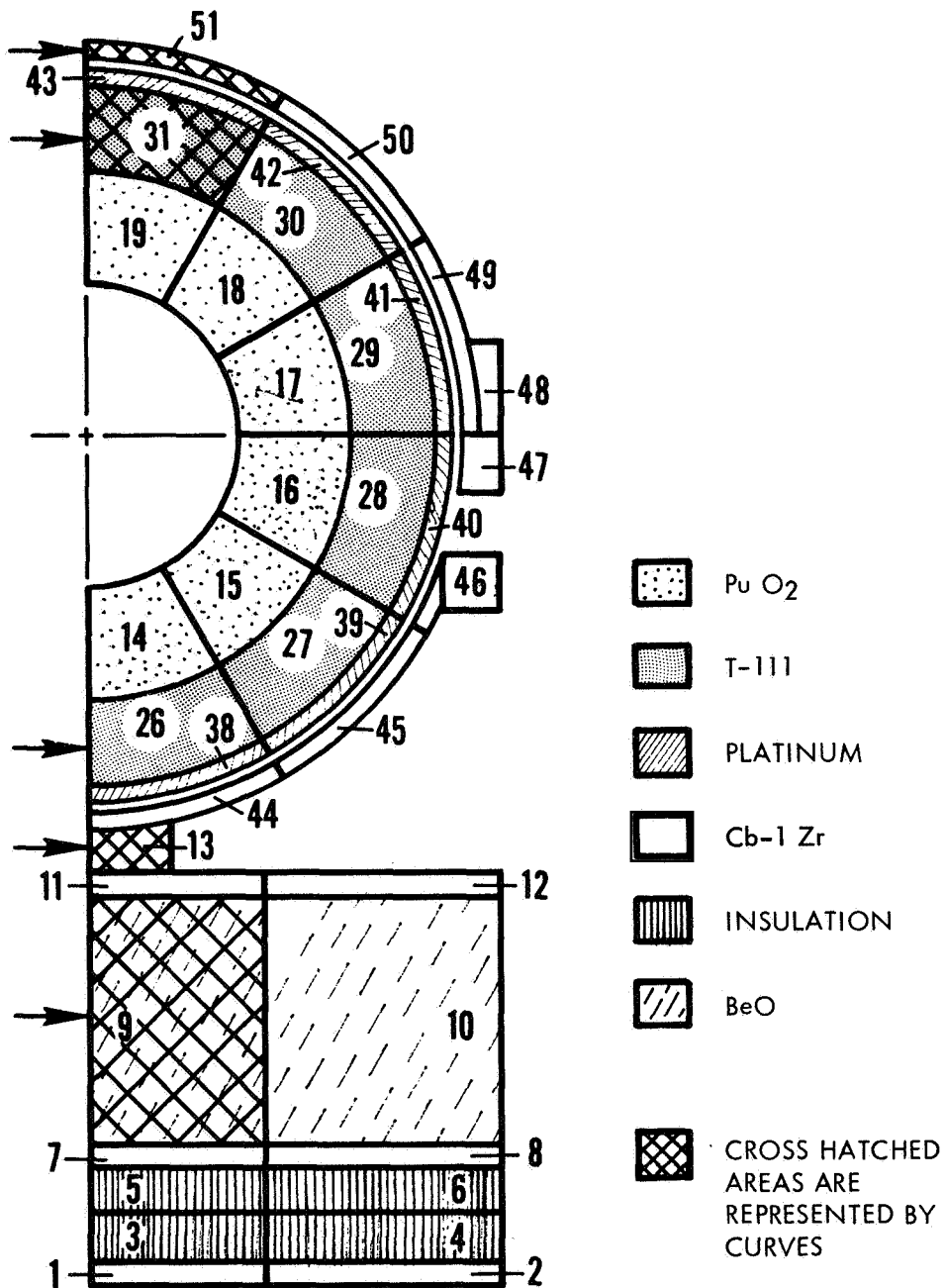


Figure 3-55 HEAT SOURCE THERMAL MODEL

- Fuel capsule
 - PuO₂ fuel
 - Helium gap
 - T-111 shell (includes capacitance of tungsten fuel liner)
 - Helium gap
 - Platinum clad
- Cover plate
- Support plate (cradle)
- BeO
- BeO support plate
- Insulation
- Insulation support plate

The general assumptions incorporated in the model included the following:

- All heat transferred two-dimensionally over the active length of fuel capsule
- All Cb-12r surfaces and fuel capsule coated with iron titanate ($\epsilon_s = 0.85$)
- BeO surface uncoated ($\epsilon = 0.25$)
- Heat flows around center of capsule and between adjacent capsule are symmetrical (adiabatic sides)
- Constant temperature insulation base
- Internal heat generation in PuO₂ nodes
- Internal radiation across inner surface of PuO₂ nodes ($\epsilon = 0.85$)
- No contact between fuel capsule and cover plate
- No contact between fuel capsule and support cradle

For each case analyzed, boundary conditions and assumptions were made such that the element represented the worst case condition.

3.3.1.4 Launch Pad Operation

While in an oxygen atmosphere the heat source is to be limited to below 350°F during steady-state periods to minimize the oxidation and deterioration of the refractory alloy structure and to prevent the possibility of ignition of the spacecraft propellant or fuel vapor fumes. During short transient periods the heat source is to be limited to less than 600°F. Maintaining these temperature limits required the use of an auxiliary cooling system.

The ACHX design presented in the preliminary design consisted of triangular shaped channels placed in the fuel capsule support plate between adjacent capsule rows to minimize the heat conduction path length. The coolants considered for this design were air and nitrogen due to their low cost and ease of handling.

TOSS calculations of the steady-state temperature distribution around the fuel capsule and support structure were performed to determine the temperature drop from the capsule to the ACHX. The effect of the contact between the capsule and capsule support plate was evaluated parametrically for three conditions; 2-mil air gap, 5-mil air gap and partial contact ($h = 300 \text{ Btu/hr-ft}^2\text{-}^\circ\text{F}$). The coolant flow rate and flow distribution requirements were calculated parametrically for ranges of inlet temperature, peak capsule temperature, and pressure (presented in paragraph 3.3.3). Based on these results, a coolant supply was defined to limit the peak fuel capsule temperature to 350°F or less.

During ground handling while switching from a temporary ACHX supply to a "launch pad" ACHX supply system, the coolant supply will be interrupted. The time in which the capsule takes to reach 600°F becomes an important factor in determining the allowed time to switch cooling systems. At launch the ACHX is disconnected also. The time to leave the earth's atmosphere coupled with the heat source heat-up rate determines the extent of oxidation damage to the refractory alloy structure, if any occurs. Transient calculations of the heat source temperature history were, therefore, performed to aid in this evaluation.

3.3.1.4-1 Steady State--ACHX Operating -- The temperature distribution of the fuel capsule and support structure was calculated with the two-dimensional model based on the following assumptions specific to the launch pad case.

- 2-mil air gap between capsule and cover plate
- Forced air cooling in the ACHX
- No heat removed by HSHX operation
- Constant temperature insulation base
- 2-mil air gap between BeO and cradle
- Air gap between the fuel capsule and the capsule support plate considered parametrically for a 2-mil air gap, 5-mil air gap, and partial contact ($h = 300 \text{ Btu/hr-ft}^2\text{-}^\circ\text{F}$)

Because of the sensible heat rise in the coolant, the hottest capsules along any cooling channel would be the capsule adjacent to the channel exit. By orificing

each of the channels, the coolant flow rates could be adjusted for each channel such that capsules at the exit of each channel would be maintained at the same peak temperature. The peak capsule surface temperature for the heat source would therefore correspond to the hot spot on the capsules adjacent to each of the channel exits.

Figure 3-56 presents the temperature distribution around the fuel capsule and support plate for the hottest capsule based on a peak capsule surface temperature of 350°F at the top of the capsule. This temperature distribution is presented for a 2-mil air gap between the capsule and capsule support plate.

Heat transfer from the ACHX channel wall to the coolant can be defined by the equation

$$Q = h A(T_w - T_b)$$

where

T_w = channel wall temperature

T_b = bulk temperature of coolant

This model calculated heat transfer from the nodes representing the channel structure to the coolant by the equation

$$Q = h \sum_i A_i (T_i - T_b)$$

where A_i , T_i are the areas and temperatures of the surface nodes. A mean wall temperature is, therefore, defined by

$$T_w = \frac{1}{A} \sum_i A_i T_i$$

A mean coolant channel wall temperature of 171°F was calculated for this case.

As shown in this figure the two large temperature drops are the coolant film drop and an interface drop across a two mil air gap. Since the capsule support plate is designed to provide a tight fit with the capsules at the low temperature level, it is reasonable to expect that good contact will be maintained between all the capsules and the capsule support plate. The assumption of a 2-mil air gap is, therefore, very conservative. Steady-state temperature distributions were defined for partial contact to obtain a more realistic estimate of the temperature drop and a 5-mil air gap as a parametric calculation to the 2-mil air gap. The resulting temperature distributions for the three interface conditions were compared for a specified mean channel surface temperature representing nominal coolant flow conditions in Table 3-15. The coolant conditions were selected to provide a 350°F peak capsule temperature with a 2-mil air gap. With partial contact between the capsule and support plate the peak capsule temperature will be 22°F lower for the same flow conditions. For a 5-mil air gap the peak capsule temperature will be 81°F greater. The coolant requirements to limit the peak capsule temperature to 350°F with a 2-mil air gap are readily obtainable and do not complicate the cooling supply system. The temperature distribution with a 2-mil air gap was, therefore, selected as the nominal case for ACHX cooling to provide conservatism to the analysis.

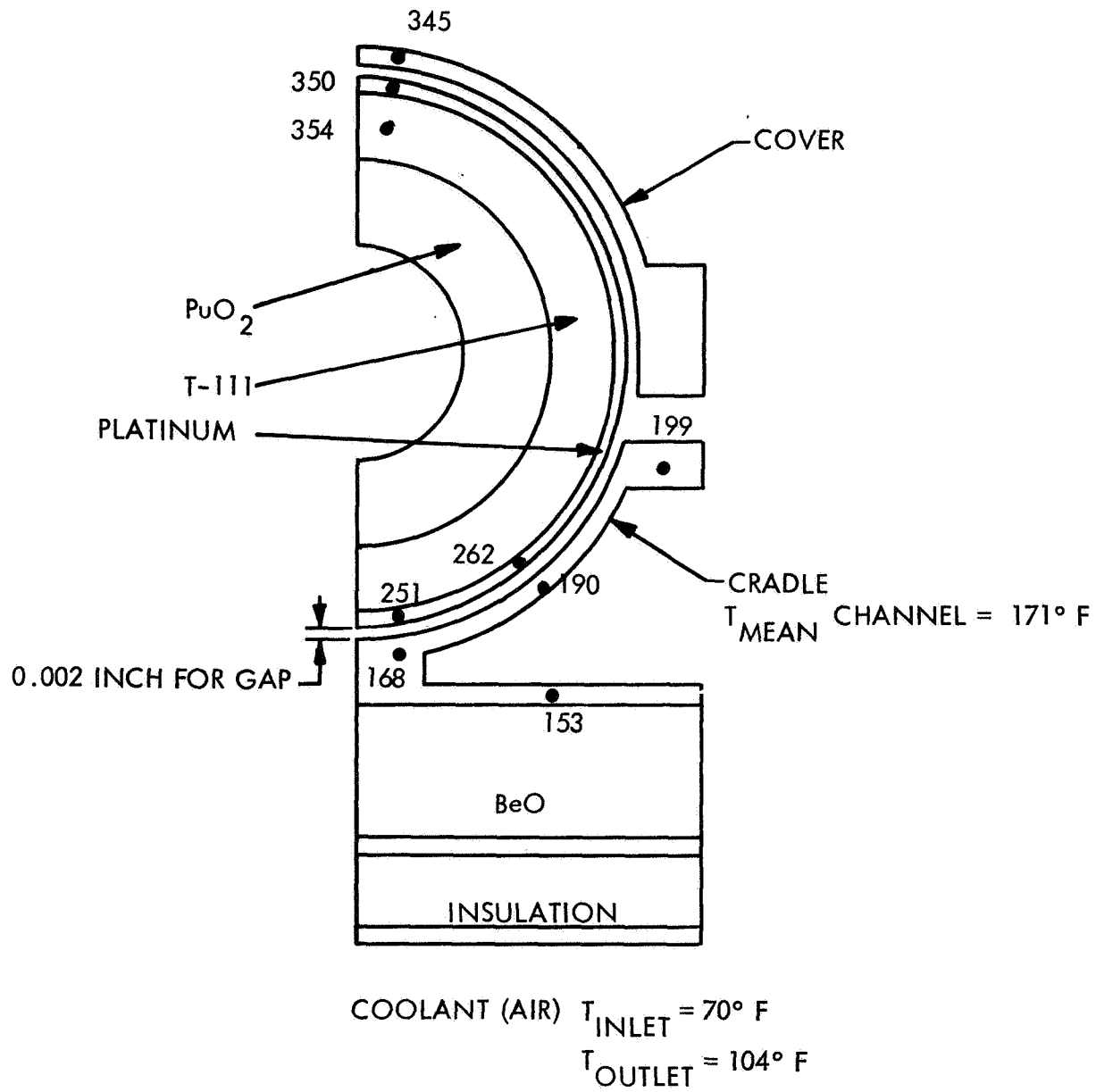


Figure 3-56 ACHX OPERATION TEMPERATURE DISTRIBUTION AT CHANNEL EXIT FOR A 2-MIL AIR GAP

TABLE 3-15

TYPICAL COOLING AIR REQUIREMENTS VERSUS GAP ASSUMPTION
FOR CONSTANT PEAK CAPSULE TEMPERATURE

	Contact (h = 300 Btu/hr-ft ²)	2-mil Air Gap	5-mil Air Gap
Coolant Inlet Temperature, °F	70	70	70
Coolant Outlet Temperature, °F	104	104	104
Mean Channel Exit Temperature, °F	171	171	171
Maximum Capsule Temperature, °F	328	350	431
Mass Flow Rate, lb /sec	3.13	3.13	3.13

As will be described in paragraph 3.3.3 the coolant can be either air or nitrogen with the hydraulic performance requirements interchangeable. The 70° F coolant inlet temperature presented in Table 3-15 corresponds to providing a coolant with no subcooling from ambient surroundings at 70°F. Although ambient temperatures may be as high as 110° F with reasonable probability, such ambient conditions are not expected to greatly hinder the ACHX since the mass flow rates can be increased to compensate. At worst, with no change in cooling flow rates, the peak temperature will increase by slightly less than the rise in ambient temperature.

3.3.1.4-2 Transient--ACHX Disconnected--The temperature history of the capsule immediately after ACHX disconnect was calculated using the following assumptions specific to this transient case:

- No heat removed by ACHX operation
- Cover radiating to HSHX with heat absorbed by the HSHX but not removed by HSHX operation
- 2-mil air gap between
 - capsule and cover
 - capsule and support plate
 - support plate and BeO
- Two-dimensional conduction over the active length of the capsule
- Capacitance of BeO and support structure corresponds to full length of capsule

Figure 3-57 presents the temperature history of the peak capsule temperature, the peak cover temperature, the peak support plate (cradle) temperature, and the BeO temperature immediately after ACHX disconnect. As shown here, the capsule will heat up from the 350° F steady-state temperature to 600° F in approximately 15 minutes. Since oxidation of Cb-1Zr accelerates considerably for temperatures in

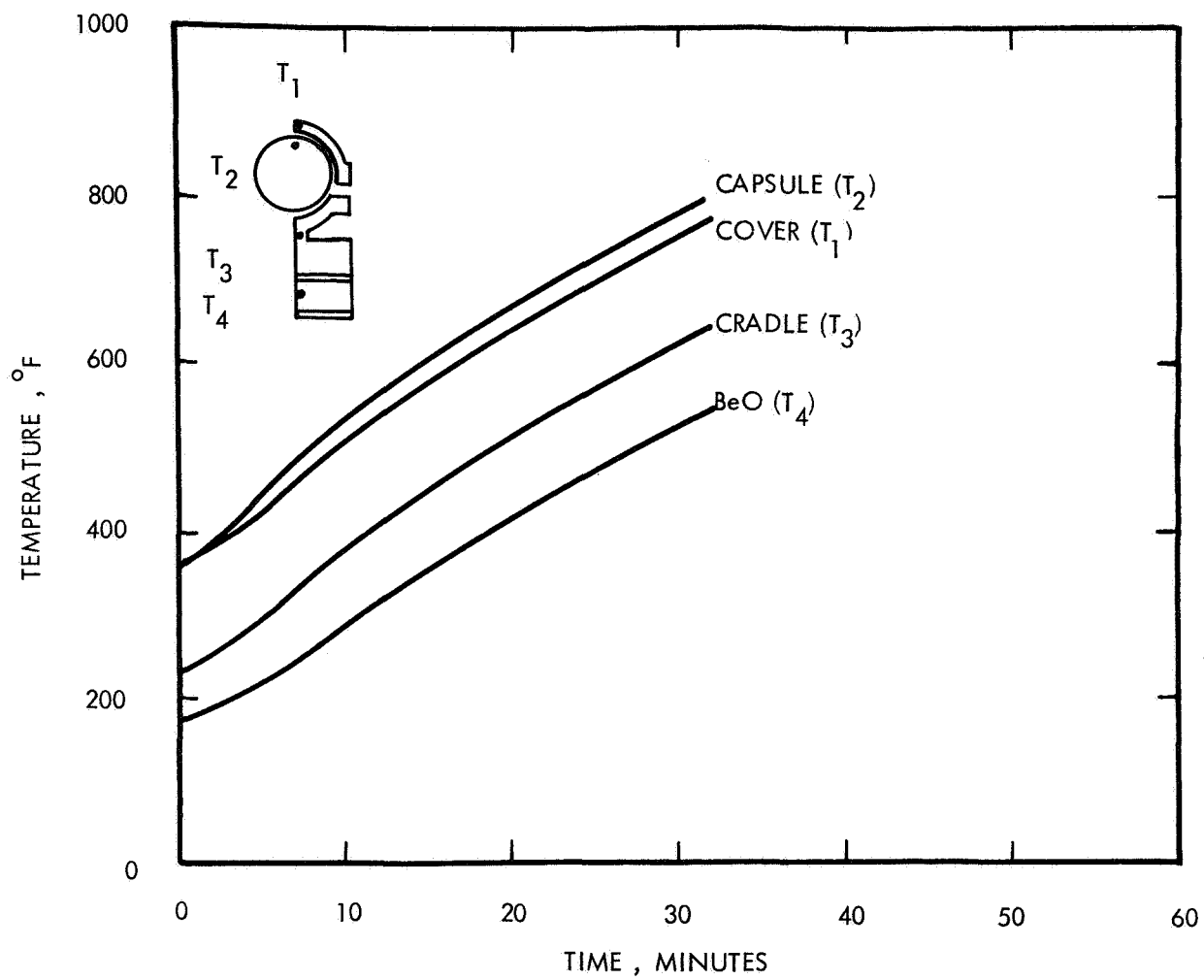


Figure 3-57 HEAT SOURCE TEMPERATURE HISTORY AFTER ACHX DISCONNECT

excess of 600° F, this 15-minute time lag is an estimate of the time that the heat source can stand while in an oxygen atmosphere with no cooling. Since the direction of heat flow was to the ACHX during steady state, conduction temperature drops across the capsule were not significantly altered, and the capsule plus the BeO are heated uniformly from the early part of the transient. This implies that the BeO is effective from the initial part of the transient in slowing the heating rate, which is not the case for the heatup in space from steady-state normal operation. The heating rate at this temperature is approximately 900° F/hr for 170 pounds of BeO, which is considerably greater than the 700° F/hr criteria for an 1800° F initial temperature. This increase in heating rate is due to a decrease in heat capacity of BeO with a decrease in temperature level.

A 2-mil air gap between the BeO and support plate was assumed for this transient analysis. Results presented later for a vacuum indicate that contact must be maintained to minimize BeO weight penalties. The 2-mil air gap case was considered to be only slightly conservative relative to the case of required contact for the heatup transient in the atmosphere since the cases have only slight differences in interface temperature drops, unlike the situation when operating in a vacuum.

The 15 minutes to reach 600° F as indicated in Figure 3-57 is the maximum allowable time for changing from the temporary to permanent cooling supply. For the case of ACHX disconnect at liftoff approximately 2.5 minutes are required for the vehicle to reach an altitude of 38 miles, which is essentially vacuum. Therefore, oxidation during normal launch is not a problem.

3.3.1.4-3 Conclusions--The preliminary design heat source can be limited to 350° F peak capsule temperature by the ACHX, and its coolant requirements are 3.13 lbs/sec of air or nitrogen entering at 70° F and 90 psi (See para. 3.3.3.).

A 15-minute time period is allowable for switching from the temporary to the launch pad coolant system. During launch the capsules will not heat up sufficiently to cause any significant oxidation problems prior to leaving the atmosphere. This is based on the requirement that the launch pad cooling system is not disconnected until the launch is fully committed, meaning that the transient heating does not start until liftoff.

3.3.1.5 Steady State--Space Operation of IRV Heat Source

The primary thermal design criterion in the mating of the heat source and HSHX designs is to maintain a peak capsule temperature below 2000° F while transferring the heat to the primary or secondary heat exchanger of the HSHX system. The HSHX system was designed as a redundant system such that heat radiated from the heat source would be absorbed and transported to Brayton cycle equipment by the primary heat exchanger, but in case of a failure, a redundant in-place heat exchanger is provided. This thermal criterion must be met with the Brayton cycle operating at full power when the primary HSHX is operating and with a minimal power reduction when the secondary HSHX is operating. During Phase II, the preliminary design of the heat source and HSHX were set. To aid in the design and to establish the operating condition, steady-state temperature profiles of the fuel capsule representing the hottest portion of the heat source were calculated. Specific assumptions for this calculation include:

- Conduction around active fueled length of capsule
- Radiation from cover plate to HSHX with view factors based on covered capsule seeing HSHX and neighboring capsule cover plate
- Radiation gaps between
 - capsule and cover plate
 - capsule and support plate
 - support plate and BeO
 - across ACHX channel.

Steady-state temperature distributions were calculated for a range of peak capsule temperatures from 1600° to 2000° F. From these results a weighted mean cover plate temperature was calculated by the equation

$$T_m = \left(\frac{\sum F_i A_i \epsilon_i T_i^4}{\sum F_i A_i \epsilon_i} \right)^{1/4}$$

to determine an effective fuel capsule radiating temperature. Figure 3-58 presents a plot of the effective radiating temperature of the fuel capsule cover versus the peak capsule temperature.

An analysis of radiation from the heat source to the HSHX was performed using a nodal model for the surfaces of both plates. The radiation model coupled with a detailed analysis of the HSHX thermal performance presented in Section 4.0 provided the basis for predicting temperature profiles over the surface of the HSHX and HS based on the cooling channel arrangement in the HSHX. Figure 3-58 was used to determine the peak capsule temperatures across the heat source based on the surface temperature profile.

With the primary HSHX receiving heat and the Brayton cycle equipment operating at full power, the maximum fuel capsule temperature was 1918° F. With the secondary HSHX receiving heat and the Brayton cycle equipment operating at full power, the maximum fuel capsule temperature was 2060° F. To limit the peak capsule temperature to 2000° F with the secondary HSHX in operation, the Brayton cycle power conversion system power level must be reduced to 90 percent of the design full power. Further reduction in the peak capsule temperature to 1918° F requires a reduction in the power level of the power conversion system to 83 percent. Figure 3-59 presents the temperature profile around a capsule at the heat source hot spot with the primary HSHX operating and the secondary HSHX operating, respectively, at full power.

As described in detail in Section 4.0 the temperature profile in the HSHX along the tubes from inlet to outlet induces a temperature profile across the HS surface by radiation. As shown in Figure 3-60 the hot spot on the HS is at the center. For the first HSHX in operation, the peak capsule temperature will vary from 1918° F for capsules located in the center to 1885° F for capsules located at the periphery

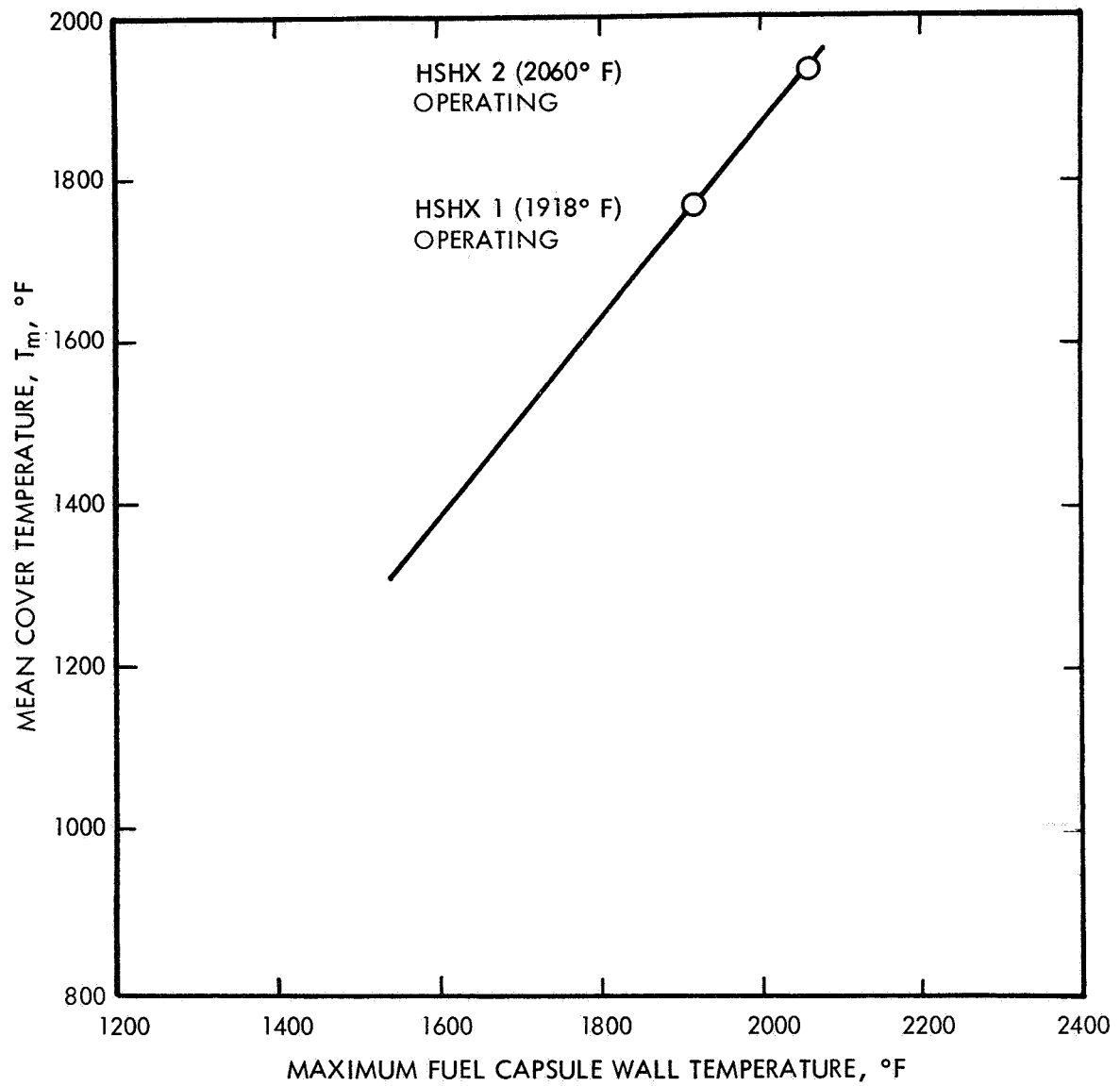


Figure 3-58 STEADY STATE HEAT SOURCE RADIATING TEMPERATURE VERSUS
MAXIMUM CAPSULE TEMPERATURE

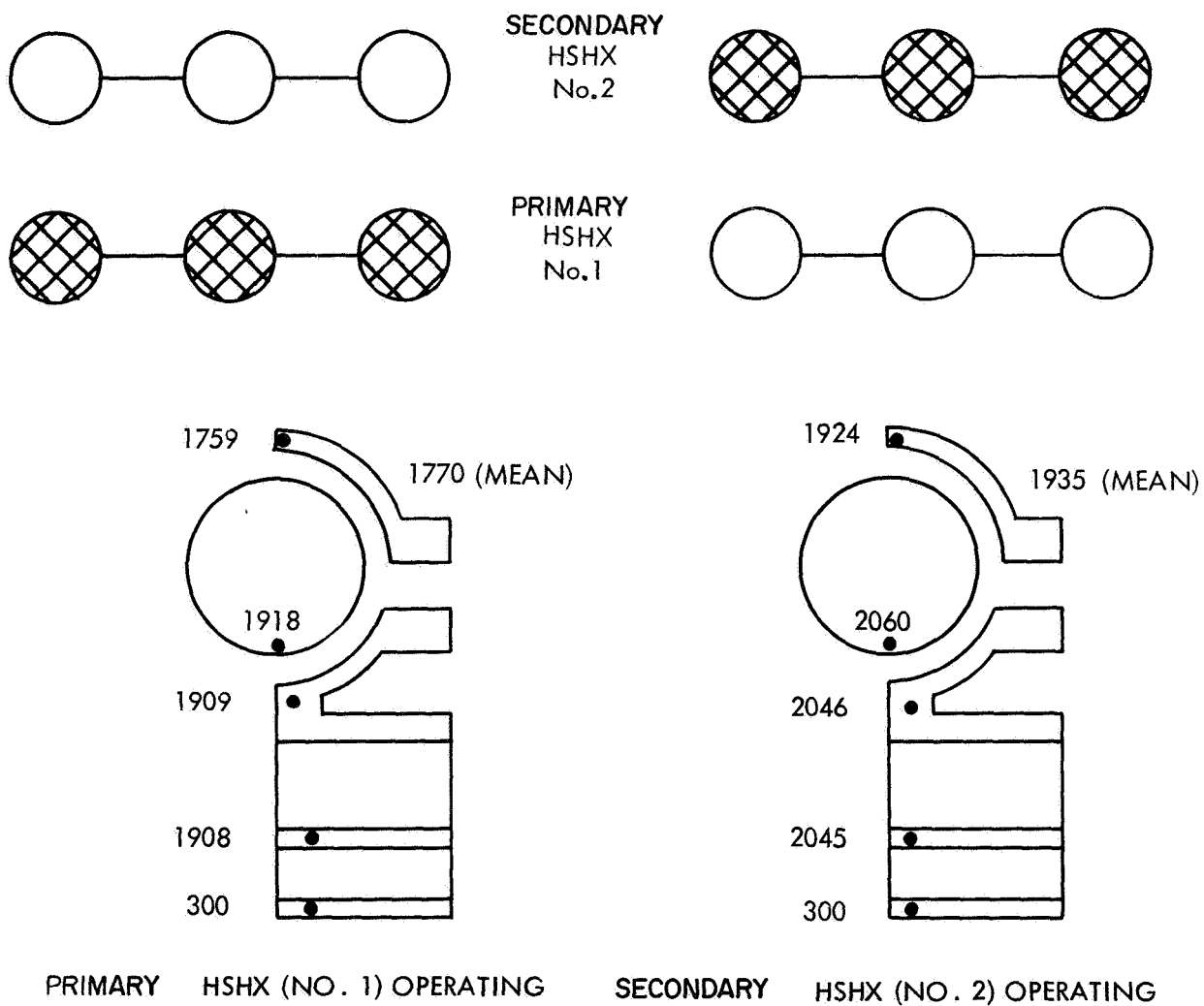


Figure 3-59 STEADY STATE TEMPERATURE PROFILE AT HEAT SOURCE HOT SPOT

of the heat source. For the second HSHX in operation at full power the peak temperatures vary from 2060° F to 2010° F for capsules located at the center and periphery respectively.

A steady-state analysis of the temperature distribution around the hottest capsule when the heat source was facing space was performed to evaluate those periods when the IRV is deployed or separated (prior to reentry). In the latter case this state provides the initial conditions for certain possible reentry trajectories. Figure 3-61 presents the temperature distribution for this state. As shown here, the effective cover plate radiation temperature is approximately 1220° F, and the peak capsule temperature is 1455° F, based on projected area of active fuel length. The large temperature differential is due to the increase in radiation temperature drops at lower temperature levels. Note that if the total heat source area is used the maximum temperature of the capsule is 1300° F.

Depending upon the orientation of the vehicle, the heat source may be facing the sun and thus receive solar energy. In these instances the heat source will be in thermal equilibrium at a higher temperature level. A worst case solar heat flux of 440 Btu/hr-ft² was used to evaluate this condition. Analysis of the heat source temperature response indicated that the mean effective radiation temperature would increase 35° F from 1220° F to 1255° F.

3.3.1.6 Transient Studies--Space

While the IRV is in space, the heat source will experience various periods during which it is transiently heated or cooled. Two thermal criteria were established for the design of a heat source that will survive these transients:

- Provide a design that maintains peak capsule temperatures less than 2500° F during transient periods
- Provide sufficient thermal capacitance that the maximum capsule temperature rise from 1800° F does not exceed 700° F in one hour

Three transient conditions were analyzed. The first is the heatup of the heat source from the nominal steady-state condition with no heat removed by HSHX operation. This transient analysis provides the design basis required to assure meeting the second criterion. This transient will occur immediately after heat removal through the HSHX has been discontinued, either through a Brayton cycle shutdown or a loss of coolant, but prior to heat source deployment. Another transient condition is the cooldown of the heat source immediately after it is projected to space either by deployment or detachment. This transient provided the initial conditions for various reentry trajectories from orbit. The third transient condition analyzed was the temperature history of the heat source during reentry. Because of the large aerodynamic heating rates that may be imposed on the heat source during reentry, a comprehensive study was made in which various trajectories were analyzed to determine worst cases. Several of the severe case trajectories were analyzed to determine the peak capsule temperature history for the preliminary design.

3.3.1.6.1 Heatup of the Heat Source Prior to Deployment--To provide sufficient thermal capacitance to absorb all the heat generated by the fuel so that the capsules heat up not more than 700° F in one hour, a heat sink material was incorporated in the heat source design. During Phase IA, BeO and graphite were considered with several packaging arrangements to provide sufficient thermal capacitance

BASED ON ACTIVE FUEL LENGTH OF CAPSULES AND
THEIR PROJECTED RADIATING AREA

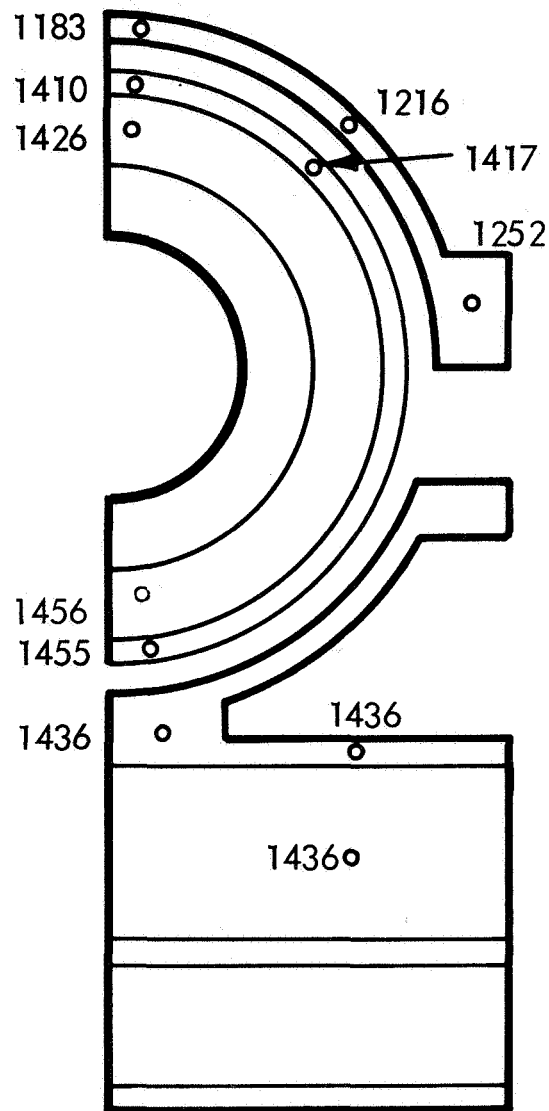


Figure 3-61 HEAT SOURCE STEADY STATE TEMPERATURE DISTRIBUTION
IN DEPLOYED STATE

with minimal conduction path penalties. The conceptual design recommended at the conclusion of Phase IB included 140 pounds of BeO in brick form placed adjacent to the fuel capsule support plate. This design provided sufficient capacitance to maintain a uniform heat source temperature rise of 630°F per hour thus allowing a 70°F margin in the heating rate. The margin was required to provide time for a reversal of the heat flow direction from the top of the capsule during steady-state operation to the bottom of the capsule during heatup. During Phase II, efforts to lighten the structure resulted in a design with reduced structural thermal capacitance. The BeO weight was, therefore, increased to 170 pounds to maintain sufficient thermal capacitance in the heat source for a heat rate of 630°F per hour. The position of the BeO was maintained the same; however, the effect of BeO contact with the heat source plate was analyzed to determine contact requirements for effective utilization of the BeO.

The temperature history of the heat source at a hot spot, where no heat conduction between adjacent capsules exists, was determined by use of the two-dimensional thermal model based on the following specific assumptions:

- Radiation from cover to HSHX with no heat removed by HSHX operation
- Initial condition is the nominal steady-state temperature profile
- Radiation gap and case of poor contact ($h = 100 \text{ Btu/hr-ft}^2\text{-}^{\circ}\text{F}$) between support cradle and BeO
- Capacitance of capsule and BeO represents the active length of the capsule for one case and the full length of the capsule for another case

Two cases were analyzed in detail. The first case, which represented the most conservative assumptions that can be made, included a radiation gap between an emissivity-coated support plate and an uncoated BeO surface. Also, the capacitance of the capsule and BeO represented only that portion over the active length of the module. For this case, the temperature history is shown in Figure 3-62. As shown, the capsule heated from 1880°F to 2750°F at the hot spot of the capsule in one hour. It should be noted that at the beginning of this transient the hot spot on the capsule was at the base of the capsule at a temperature of 1918°F . During the transient period, the heat flow direction was reversed and the hot spot on the capsule shifted to the top of the capsule which was initially at 1880°F . Furthermore, the capsule exceeded 2500°F in 35 minutes. Of this total period, approximately 27 minutes were required to redistribute the heat flow direction such that the BeO was being fully utilized. Once the BeO was heating at the same rate as the rest of the capsule, the heating rate was 660°F per hour. The primary reason for the long period required to reach a state of uniform heating was attributed to the establishing of the large temperature drop of approximately 260°F between the cradle and BeO.

A second case was analyzed for which the BeO was assumed to be in contact with the support plate. For this case, a contact coefficient of $100 \text{ Btu/hr-ft}^2\text{-}^{\circ}\text{F}$ was assumed which represents a rather poor contact. Based on data presented in the literature (Ref. 3-13), the coefficient appeared to be a conservative estimate for a moderate pressure level between two hard metals of commercial surface finish tested in a vacuum. Furthermore, the capacitance of the capsule and BeO over the full length of the capsule was used. This assumption was included without undue

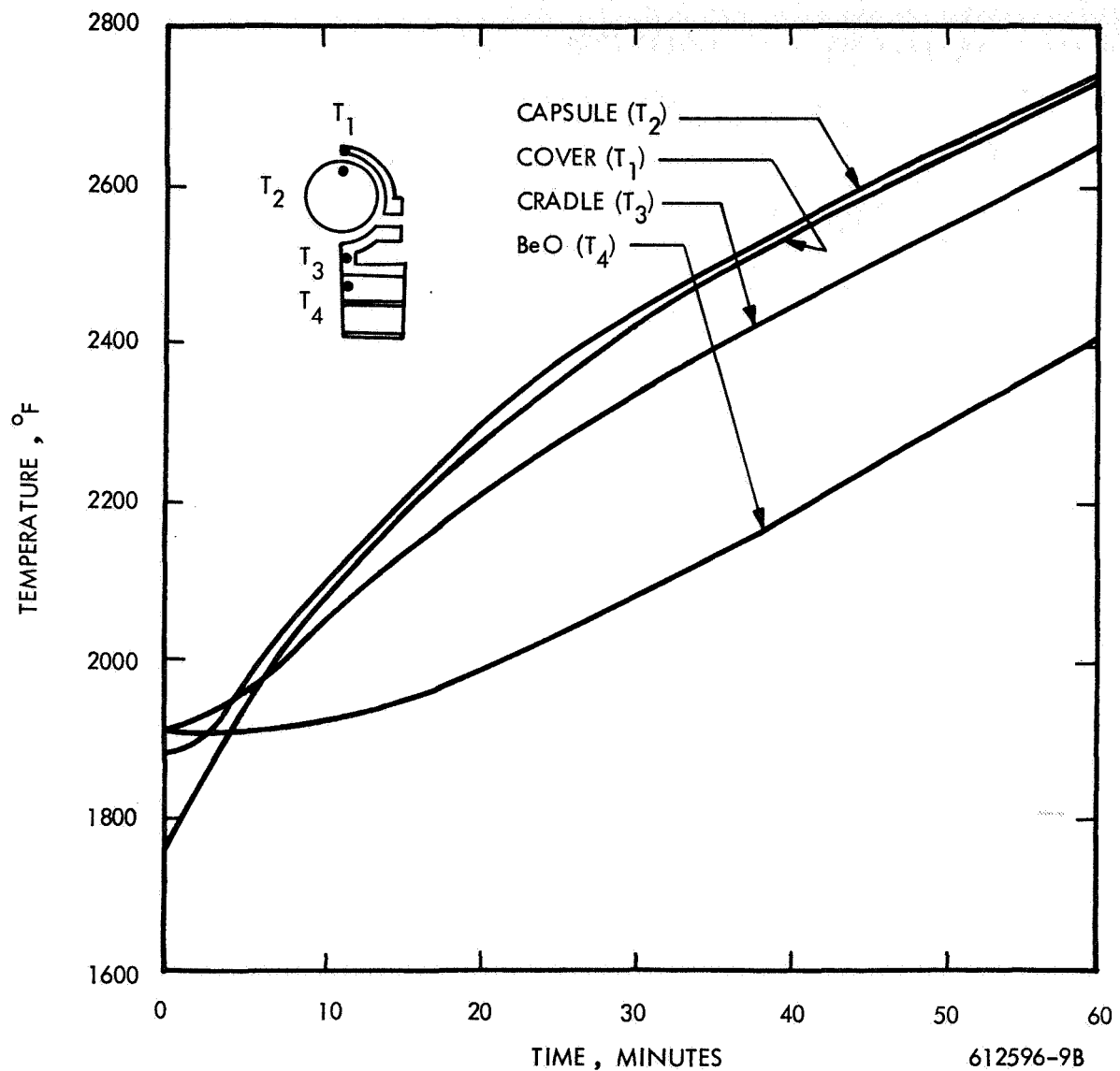


Figure 3-62 HEAT SOURCE TEMPERATURE HISTORY AFTER TERMINATION OF HSHX COOLING WITHOUT CONTACT BETWEEN BeO AND PLATE

optimism since the conduction temperature drop through the BeO is fairly small and since axial conduction to the ends of the capsule will reduce the axial conduction gradient around the capsule over its active length. Figure 3-63 presents the results of this calculation. As shown there, the capsule heats from 1880° F to 2530° F at the top of the capsule (hot spot) in one hour, a 650° F rise. The 2500° F peak capsule temperature is not exceeded until 56 minutes into the transient. If the transient had started from 1800° F per the criteria, 2500° F would not have been exceeded in one hour. The time required to develop a temperature profile across the capsule and support structure for full BeO utilization was 20 minutes (a reduction of 7 minutes). More significantly, however, the temperature lag was decreased from 260° F to 100° F between the cradle and the BeO which helped reduce the temperature rise of the capsule. For full use of the capacitance under one capsule, the heating rate was 500° F per hour. This rate was lower than the design value of 630° F per hour because of three reasons:

1. Thermal capacity of the heat source and BeO was greater at the higher temperature because of specific heat temperature dependence not accounted for in the BeO sizing calculation.
2. The HSHX capacitance which was not included for the BeO sizing provided a significant increase in capacitance and aided in the reduction of the capsule temperature rise.
3. The diameter of the BeO was less than the diameter of the heat source, therefore, heat generated by capsules at the center of the heat source was absorbed by a greater fraction of the BeO than that generated by capsules at the edge of the heat source. However, these capsules have more structure to absorb the heat.

Separation of the two effects of increased capacitance and gap temperature drop from the cradle to the BeO can be considered by comparing Figures 3-62 and 3-63. For example, adding the temperature drop from the capsule to the BeO for the first case (340° F) to the BeO temperature of the second case (2310° F) provides an approximate estimate of the peak capsule temperature of 2050° F for the case of a radiation gap between the active length of the capsule and the BeO with temperature capacitance equivalent to the full capsule length. The temperature rise in one hour for this case is 780° F which is 10 percent in excess of the rate criterion. To limit the temperature rise to less than 700° F in one hour with a radiation gap between the BeO and the cradle will require a uniform heating rate of 400° F per hr after the temperature gradient across the capsule and cradle is developed. This requires an increase in total capacitance of 25 percent, or a BeO weight increase of 65 to 235 pounds total. Since this is a significant penalty in weight, it is evident that the design must assure the maintaining of thermal contact.

3.3.1.6.2 Heat Source Cooldown After Deployment--Prior to reentry, the IRV will be deployed. During this period, the heat source will be cooled by radiation to space. This transient cooldown was analyzed to determine the initial heat source temperature for analyzing various reentry trajectories and to determine steady-state conditions for this mode of cooling. Specific assumptions incorporated into the heat transfer model for this calculation included:

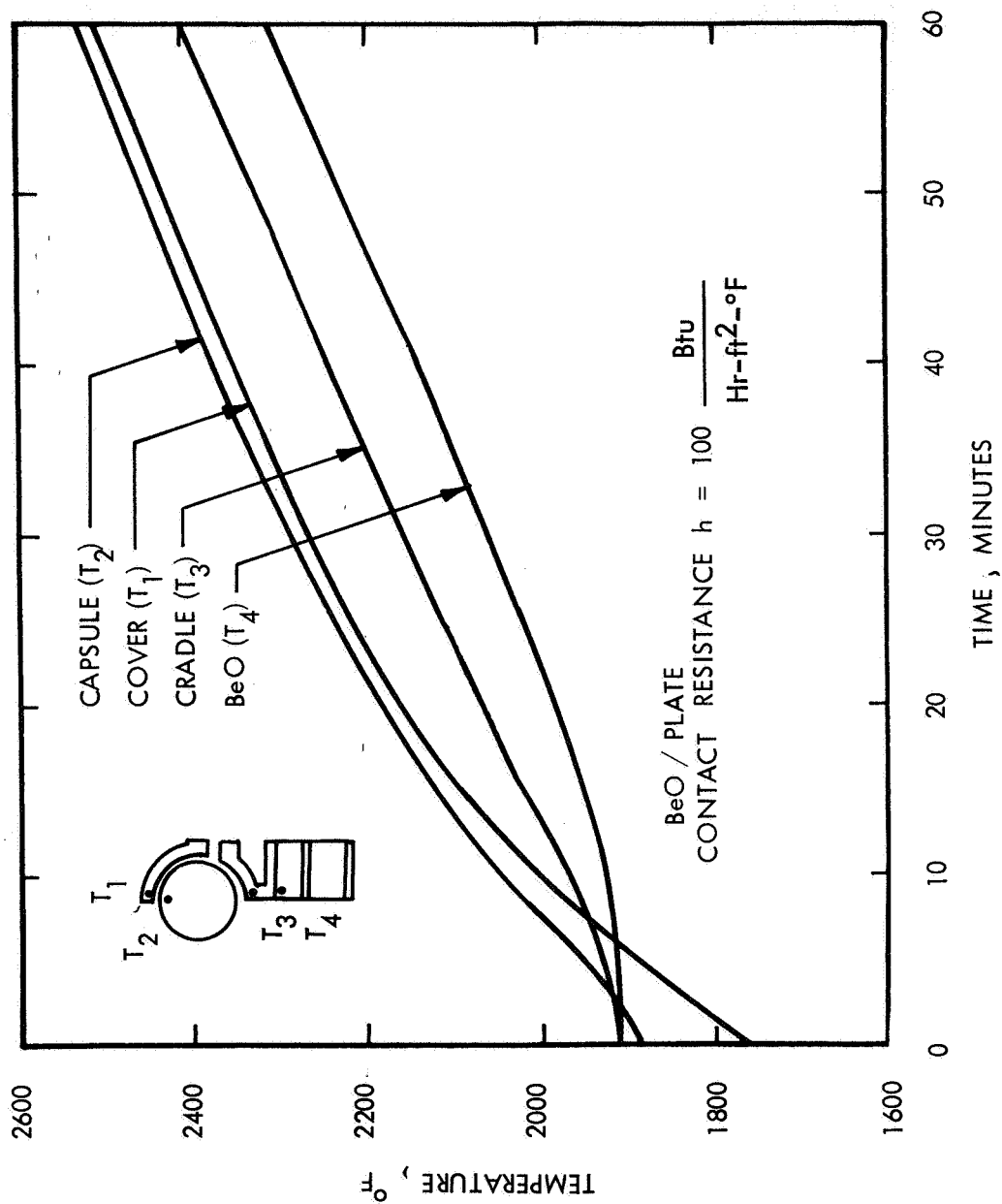


Figure 3-63 HEAT SOURCE TEMPERATURE HISTORY AFTER TERMINATION OF HSHX COOLING

- Radiation from cover to space with view factors based on capsule seeing space and neighboring capsules cover plate only
- Radiation gap between BeO and support cradle
- Radiation across ACHX channel

The temperature history of the hottest fuel capsule during the initial period of this transient is shown in Figure 3-64 starting from the nominal steady operating conditions. The capsule and cover cool very quickly initially, but later on a more gradual cooling occurs. The BeO cools much more slowly, dumping heat across the capsule to the surface of the cover. The result is a long-term transient. Critical times specified for starting the reentry trajectories were 15 minutes into deployment for nominal reentry trajectories and up to years for orbital decay trajectories. The initial conditions for the normal reentry trajectories (15-minute deployed cases) were taken from data represented by this curve while the initial condition for an orbital decay trajectory (nine-day deployments) were obtained from the steady-state conditions shown. For the latter case, the cover reaches a steady-state temperature of 1180° F.

Contact between the BeO and cradle was not analyzed. Its effect, however, would be to reduce the temperature drop between the BeO and cradle for a given heat flow. The BeO would thus initially cool more rapidly, dumping heat at a faster rate into the capsule and cover. This would tend to reduce the cooling rate of the capsule and cover. With the insulation intact, the steady-state condition would be essentially the same as shown since very little heat would be traversing the cradle-BeO interface.

3.3.1.6.3 Heat Source Temperature History During Reentry -- During the Phase I and II studies, several design features were analyzed to develop a heat source design that could maintain peak capsule temperatures below 2500° F during reentry along trajectories that provided the most severe cases of aerodynamic heating. Two design features provided significant reductions in peak capsule temperatures. One feature was the flush mounting of the fuel capsule array into the base plane of the IRV. The second design feature incorporated the use of a cover plate which completely enclosed the capsule's topside. Part of this design feature was the assurance of a radiation gap between the cover plate and capsule. Although this design feature provided a temperature penalty during steady-state performance of approximately a 30° F increase in peak capsule temperature, the reduction in peak capsule temperature during reentry was an order of magnitude greater as will be shown.

Several reentry trajectories were analyzed which included reentry angles (γ_e) ranging from zero degrees (orbital decay) to -2.15 degrees (nominal) to 18° degrees; modes of a stable, spinning or tumbling IRV, and initial angles of attack (α_e) varying from zero degree to 180 degrees. Four trajectories which exhibited combinations of the peak heating rates and the greatest integrated heating values were selected from the envelope of trajectories that were analyzed and these are summarized in Table 3-16. As mentioned in Section 3.2 the W/C_pA increased during the Phase II effort which explains the higher value for trajectory 15.

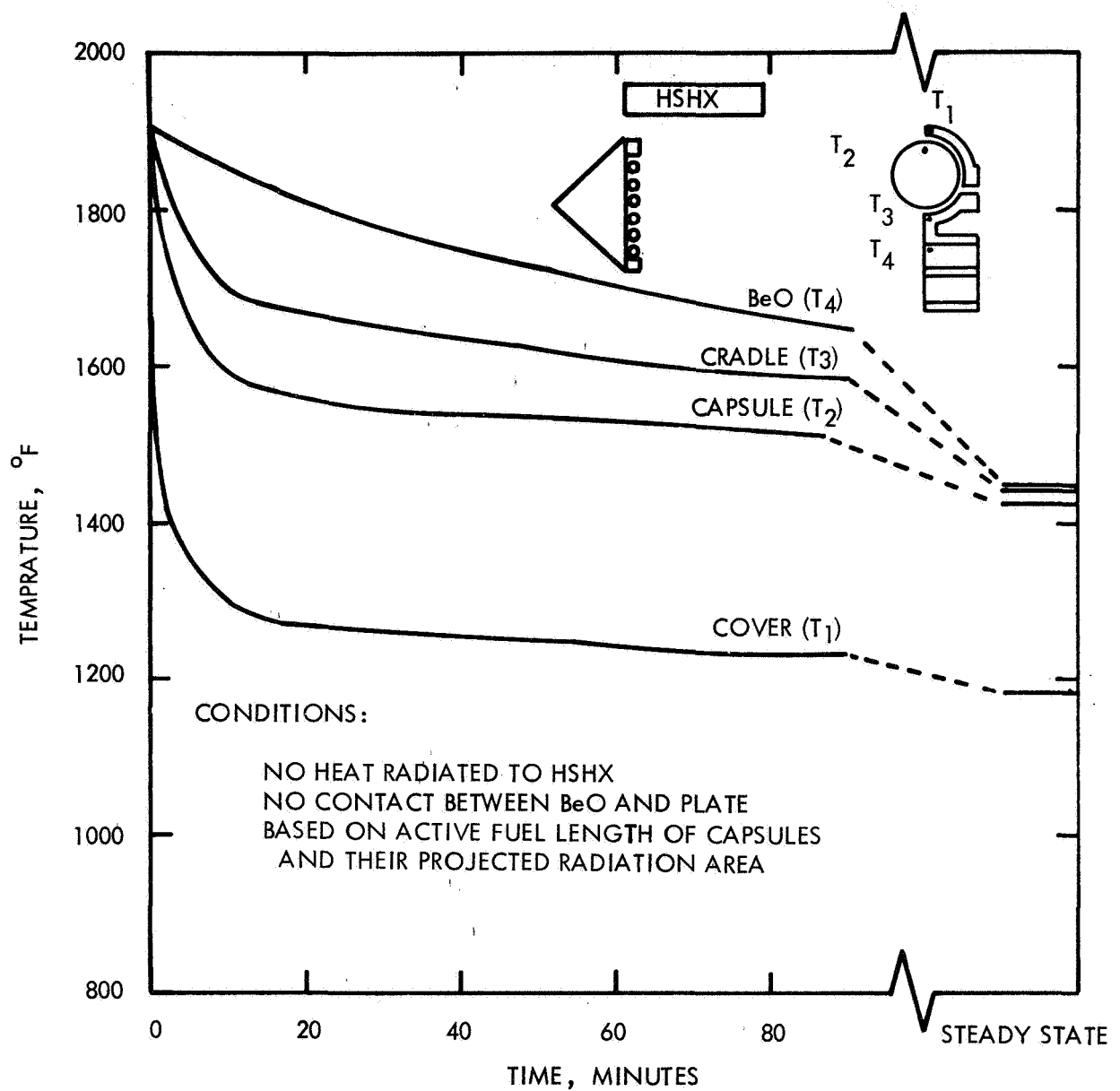


Figure 3-64 HEAT SOURCE TEMPERATURE HISTORY FOLLOWING DEPLOYMENT FROM NORMAL OPERATION

TABLE 3-16

TRAJECTORIES USED IN CAPSULE ANALYSIS

Trajectory No.	Description	Peak Heat Rate To Cover Plate (Btu/ft ² -sec)	Integrated Heating To Cover Plate (Btu/ft ²)	Ballistic Coefficient W/CpA (lb/ft ²)
1	Nominal Entry Spinning $\alpha_e = 85$ deg	46	6320	40.2
5	Orbital Decay Tumbling $\alpha_e = 179$ deg	46	13010	40.2
9	Nominal Entry Offset c.g. (-0.5 in.) Spinning	75	6800	40.2
15	Orbital Decay Rearward to Impact	77	21010	47.7

Temperature histories of the heat source were calculated for these four trajectories based on the model and assumptions listed previously. The key features of this model were that the cover plate received a time dependent heat flux corresponding to the aerodynamic heating rate and radiated heat to the capsule and to space.

Figure 3-65 presents the temperature history of the worst capsule during reentry along Trajectory 1. The temperatures shown in the figure include the cover temperature, capsule temperature at top, cradle temperature and BeO temperature corresponding to the location (nodes) indicated in Figure 3-55. The cover and capsule temperatures are the peak temperatures during reentry. This reentry which carried over a 6-minute interval started from an altitude of 400 kft 15 minutes after deployment and deorbit. The peak capsule temperature reached 2280° F, well below the 2500° F temperature limit. The cover plate heated to a peak of 2540° F. Based on earlier results, it was expected that without a cover plate the peak capsule temperature would be approximately equivalent to the peak cover plate temperature for a covered capsule. Therefore a reduction of approximately 260° F in peak capsule temperature was realized through the use of a cover plate for this trajectory. As also shown in Figure 3-65, the BeO temperature did not change significantly during this short heating pulse and therefore absorbed an insignificant portion of the total heat generated and absorbed by the heat source. The BeO, therefore, was not a major factor in reducing the peak capsule temperature for a reentry transient over the relatively short period of 6 minutes. A factor that is not shown in this curve, but which was evaluated in earlier studies, was that the peak capsule and cover temperature are primarily a function of aerodynamic heating rates and the increase of the heating rate with time during the steep heating rate part of the curve.

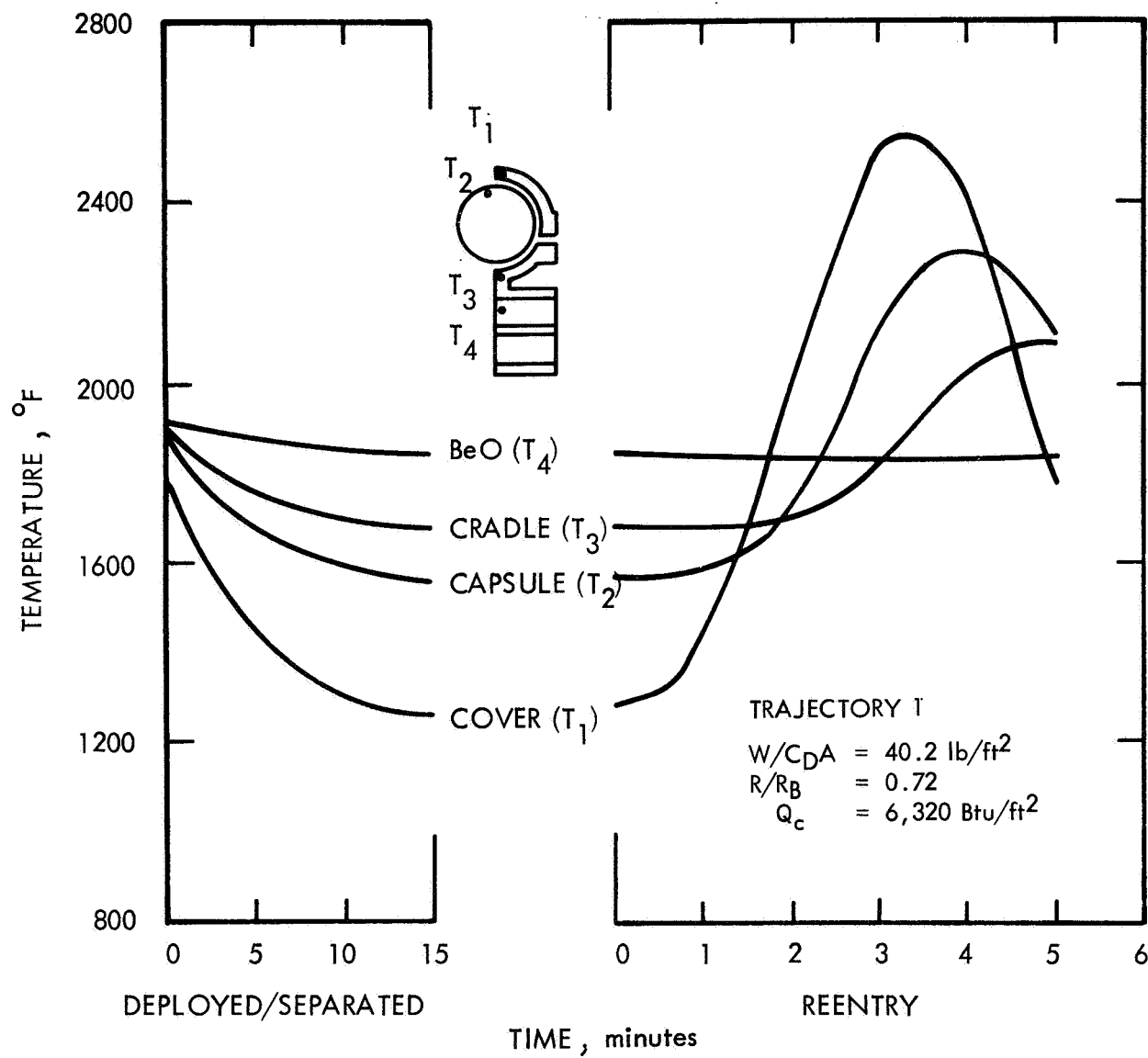


Figure 3-65 WORST CAPSULE HEAT SOURCE TEMPERATURE HISTORY -- NORMAL REENTRY MODE

The initial temperature state prior to reentry and the heat generation rates are second order effects to the aerodynamic heating rate in determining the peak temperatures during reentry. This conclusion was verified by the Phase IB results.

The cradle temperature rose significantly but peaked well past the peak of the capsule and cover temperature indicating that considerable heat was absorbed by the cradle. However, the bulk of the heat was absorbed at a time well past peak heating and did not significantly affect the peak capsule temperature.

Figure 3-66 presents the temperature history of the heat source for Trajectory 5, an orbital decay tumbling case. The heating rate calculated for this trajectory oscillates since the IRV is tumbling.

The peak cover and capsule temperatures for this case are 2560° and 2390° F, respectively, as shown in Figure 3-66. The cover for this transient provided approximately a 170° F reduction in peak temperature. This reentry spanned a total time of 70 minutes, of which the significant heating portion of the reentry spanned a period of 20 minutes. The increase in the heating rate with time was smaller than the previous trajectory analyzed, and therefore, the temperature lag between the capsule and cover was less. For longer term transients (and higher integrated heating), therefore, the cover provided less protection than for shorter transients. Trajectory 5, therefore, had a higher peak capsule temperature for orbital decay than Trajectory 1 for a nominal reentry (2390° versus 2280° F) although the peak cover temperature was approximately the same (2560° versus 2540° F). The longer reentry time of Trajectory 5 provided time for the BeO to respond to the heating pulse. Again, its effect on reducing peak temperatures was significant since its temperature rise was a gradual slope which became significant well past the capsule and cover temperature peaks. The support plate heatup, as denoted by the cradle temperature, followed the capsule heatup closely as shown by the temperature peaking of these two components at approximately the same time. However, thermal capacitance of the support plate is fairly small, and its effect in reducing the capsule peak temperatures was considered second order.

The third transient considered was the nominal reentry of an IRV with an offset center of gravity. The temperature history of the heat source for this transient is shown in Figure 3-67. This trajectory, like the first trajectory, was initiated at 15 minutes into deorbit with a 6-minute reentry span over which significant heating existed. The peak heating rate was slightly more severe than the first case as reflected in the peak cover temperature of 2780° F. Because of the steep gradient in the heating rate as was shown for Trajectory 1, the capsule temperature lagged the cover temperature significantly and therefore achieved a peak temperature of 2420° F. A potential reduction of 360° F was estimated for a covered capsule versus a bare capsule for the transient. The BeO heatup was insignificant and the cradle heatup lagged the capsule and cover such as to not affect the peak capsule temperature. The results of this transient paralleled the results obtained from the evaluation of Trajectory 1 except that the peak temperatures were higher. The cover, however, maintained the peak capsule temperature below 2500° F.

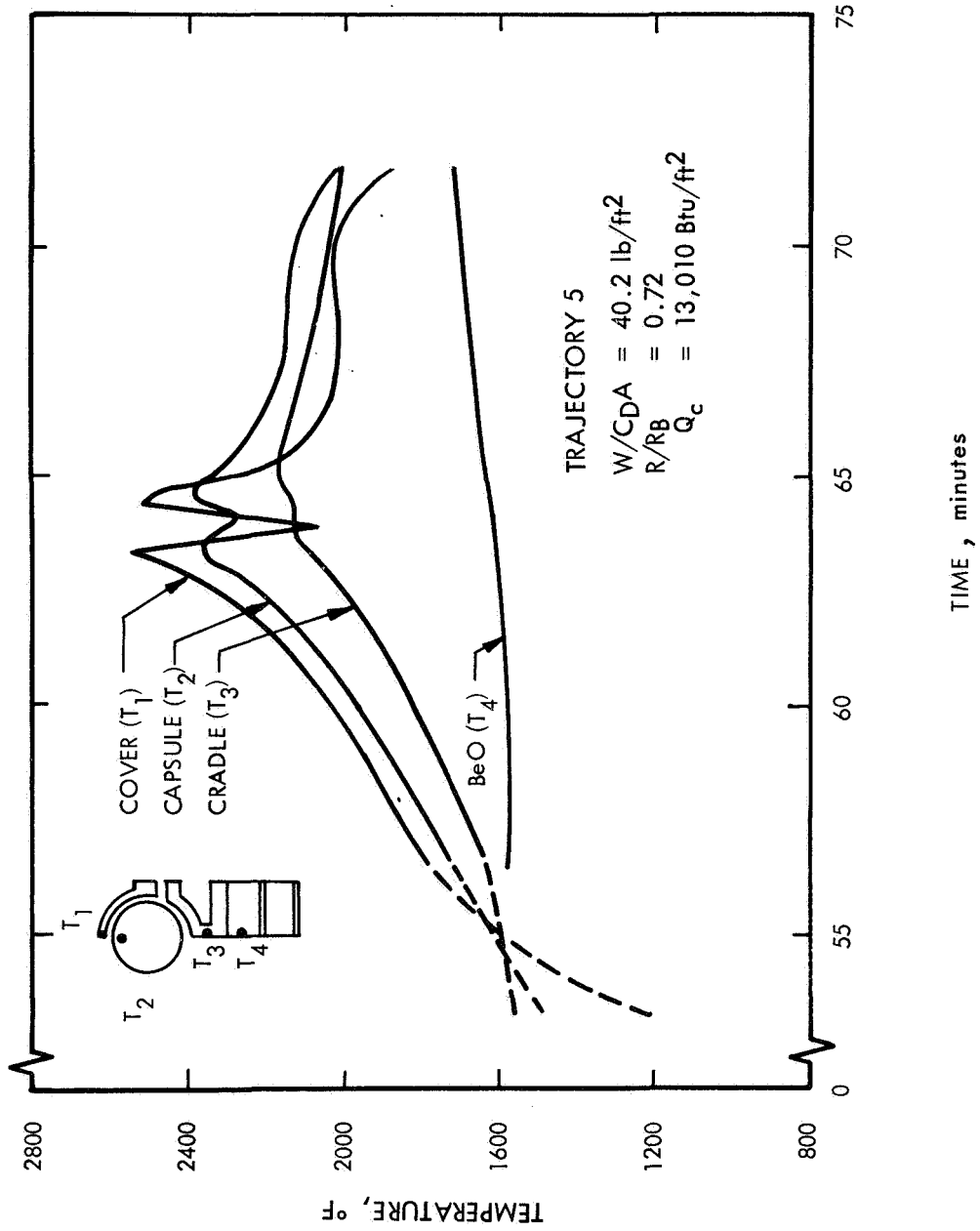


Figure 3-66 WORST CAPSULE HEAT SOURCE TEMPERATURE HISTORY --- TUMBLING REENTRY MODE

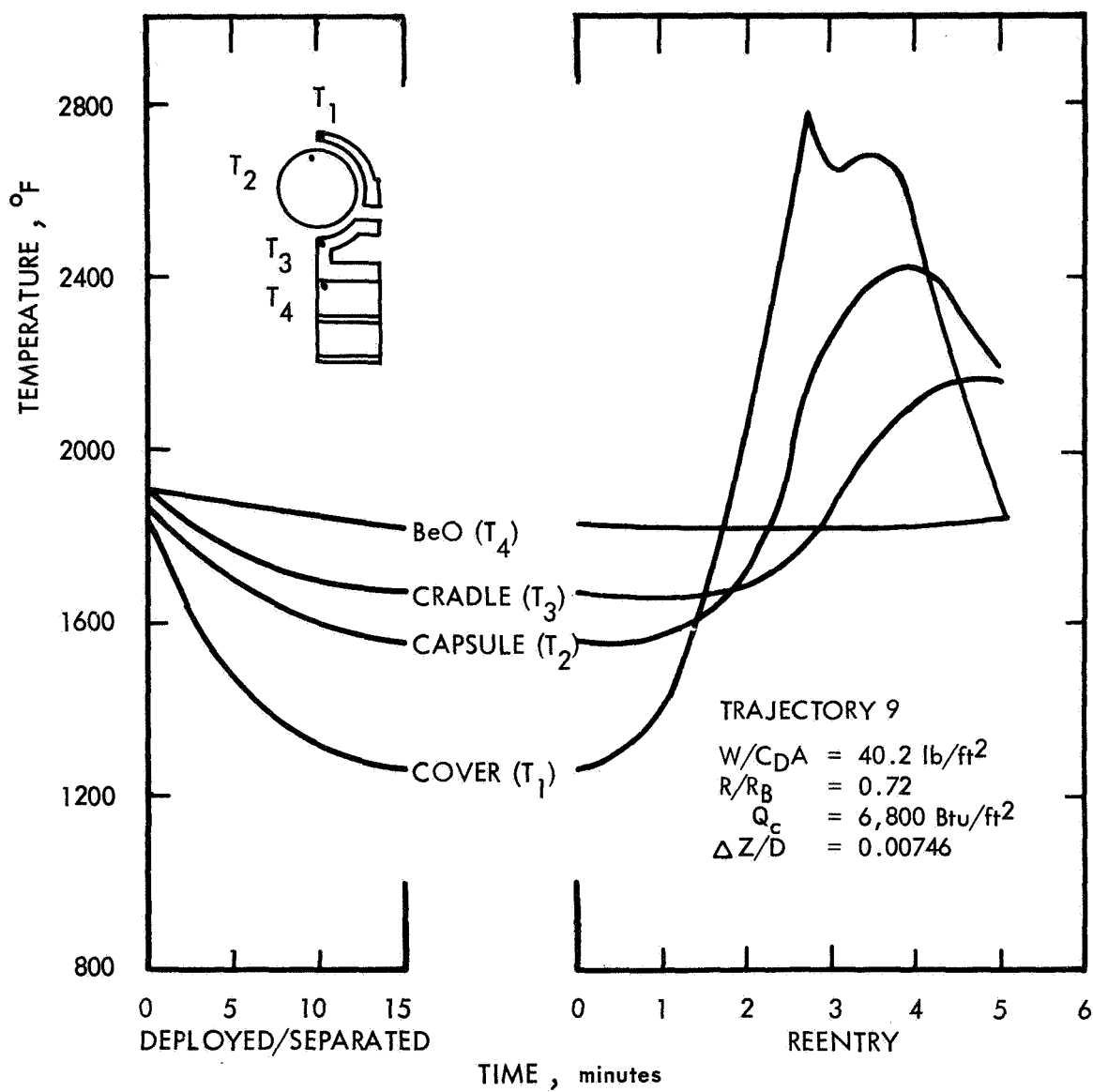


Figure 3-67 WORST CAPSULE HEAT SOURCE TEMPERATURE HISTORY -- NOMINAL REENTRY MODE (OFFSET c.g.)

To emphasize the breakdown of the heat flow and absorption during a typical reentry, the temperatures and heating rates for Trajectory 9 were integrated over the 6-minute heating pulse. The total heat generated, convected, radiated, and absorbed for each of the major components of the heat source adjacent to a typical capsule is shown in Table 3-17. As shown here, the integrated aerodynamic heating of the heat source is an order of magnitude larger than the heat generated. Furthermore, 75 percent of this heat is radiated to space. This suggests that first order approximation of the peak cover temperature can be obtained from a local steady-state analysis of the temperature level required to radiate away the aerodynamic heating pulse. This is not accurate but can very quickly provide a conservative evaluation of peak cover and capsule. For example, the peak heat pulse of Trajectory 1 was 46 Btu/sec-ft². Using Figure 3-68, which is a plot of radiation intensity versus surface emissivity and temperature, 46 Btu/sec-ft² and $\epsilon = 0.85$, indicates a steady-state radiating temperature of approximately 2800° F. The calculated value of the peak temperature was 2560° F. This is not an accurate comparison, but it indicates that a steady-state calculation provides a "ballpark" basis for evaluating pulses that may be severe.

TABLE 3-17

WORST CAPSULE REENTRY HEAT BALANCE FOR TRAJECTORY 9
($R/R_B = 0.72$) BASED ON ACTIVE FUEL LENGTH

Heat Input	Btu	
Reentry Heating	422	
Heat Generated	<u>44.3</u>	
Total	466.3	
Heat Absorbed		
PuO ₂	48	
T-111	47.8	
Cover	23.4	
BeO	8	
Platinum	12.7	
Capsule Support Plate	16.7	
BeO Support Plate	<u>0.1</u>	
Total	155.7	$\times 164 \approx 25,000$ Btu
Heat Radiated - Space	<u>319</u>	$\times 164 \approx 52,300$ Btu
Total Heat Absorbed and Radiated	474.7	77,300 Btu

Referring again to Table 3-17, the total heat absorbed by the BeO and capsule support plate was approximately 15 percent of the total heat absorbed and less than 6 percent of the heat generated and convected to the capsule.

The fourth trajectory analyzed was rearward reentry by orbital decay all the way to the ground. This was the most severe transient in terms of both peak heating and maximum integrated heating. Figure 3-69 presents the temperature history of the heat source for this transient. The peak cover temperature was 3060° F and the peak capsule temperature was 2860° F. Since this was a relatively long time

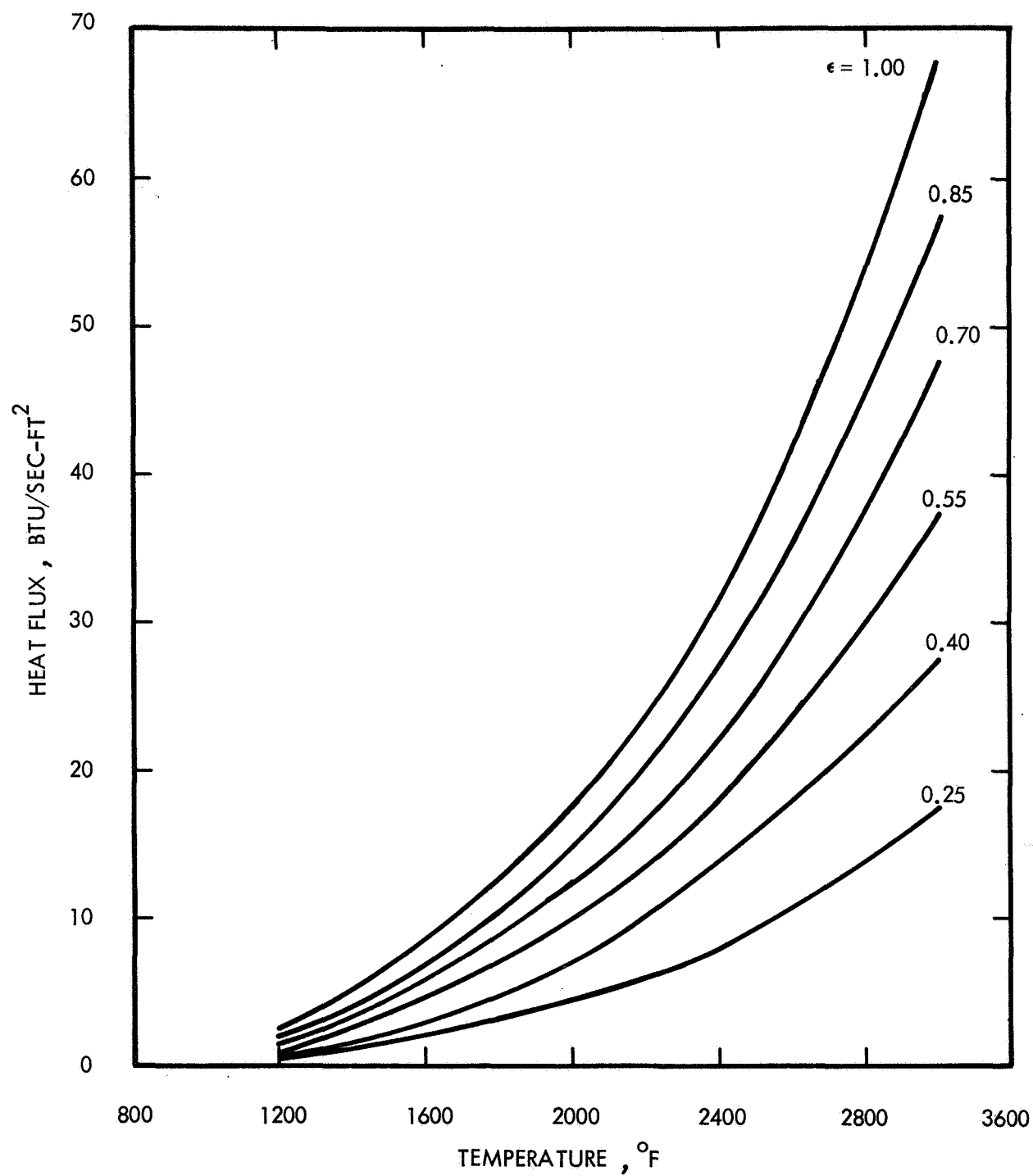


Figure 3-68 STEADY STATE RADIATION INTENSITY

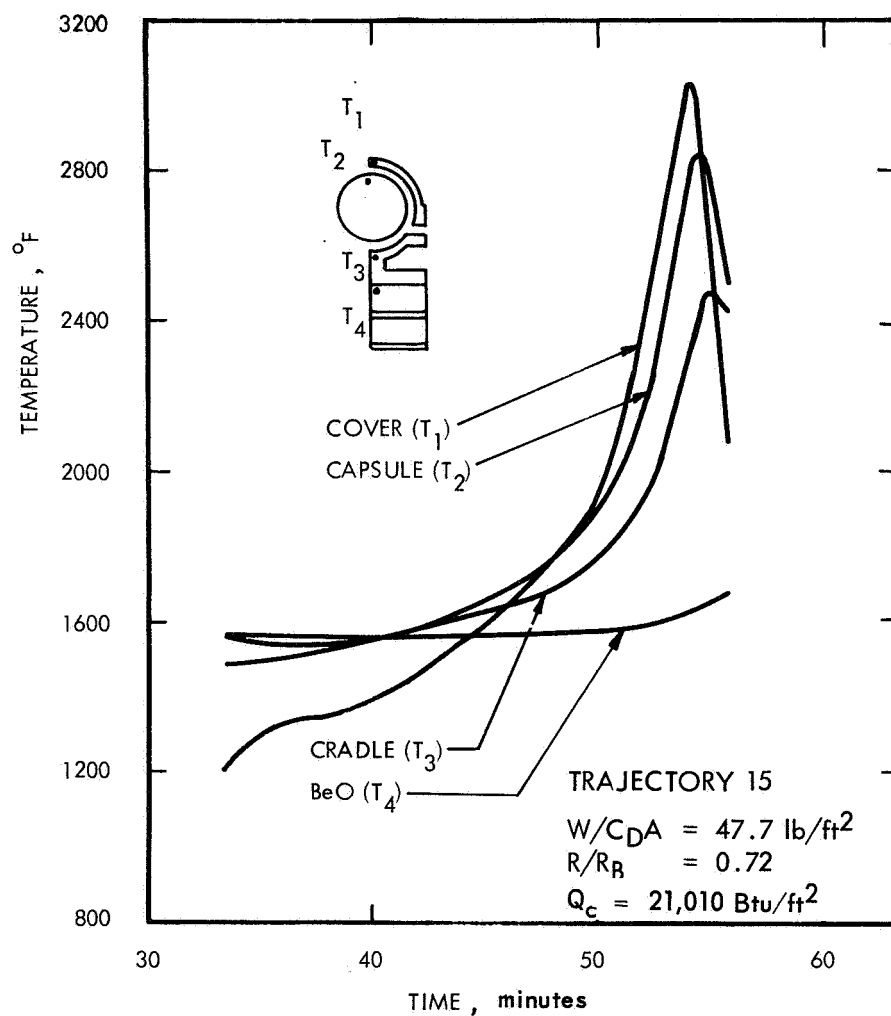


Figure 3-69 WORST CAPSULE HEAT SOURCE TEMPERATURE HISTORY -- REARWARD REENTRY TO IMPACT MODE (FROM STEADY STATE DEPLOYMENT)

reentry, the capsule did not lag the cover by much and consequently exceeded the required 2500° F temperature limit. As before, the BeO heatup was insignificant and the cradle heatup although significant was only a second order effect in reducing peak capsule temperature. Since this transient had a very low probability of occurrence, the design of the heat source was not altered to maintain a 2500° F peak capsule temperature for this reentry trajectory.

The aerodynamic heating rate for this trajectory was used to compare the results of the two-dimensional heat transfer model with the one-dimensional model employed in Phase IA and IB. This comparison is shown in Figure 3-70. The peak capsule and cover temperatures calculated with the one-dimensional model were in excess of the temperatures calculated with the two-dimensional model as expected. This difference is attributed to the heat absorbed by the support plate and BeO which is evaluated in the two-dimensional model but not in the one-dimensional model. As shown, this is a second order effect, relative to the aerodynamic heating rate.

Another fact obtained from this comparison is that the temperature drop between the capsule and cover is smaller for the one-dimensional model than for the two-dimensional model. This is a combined effect of less heat being radiated from the cover to the capsule plus the fact that at higher temperature levels the same amount of heat is radiated across a smaller temperature drop. The two results of higher temperature levels for the one-dimensional model and smaller temperature lag between cover and capsule for the one-dimensional model are conservative results. The Phase IA and IB results are therefore conservative when compared to the Phase II results using the refined analysis just discussed.

Table 3-18 summarizes the results of the reentry analysis conducted on the cover plate and capsules. With the exception of Trajectory 15 (reentry in a rearward attitude all the way to impact) peak capsule temperatures remain below 2500° F. From a practical standpoint there is no possibility of the vehicle remaining in a rearward configuration during the entire reentry period. Therefore, from an analysis of all credible reentry trajectories it appears that acceptable temperatures can be maintained on the heat source provided that the performance of the fence is adequate.

TABLE 3-18
SUMMARY OF COVER AND CAPSULE TEMPERATURES

Trajectory No.	Peak Cover Temperature (°F)	Peak Capsule Temperature (°F)
$\gamma_e = 2.15 \frac{1}{\text{deg}}$ Spinning $\alpha_e = 85 \text{ deg}$	2540	2280
$\gamma_e = 0 \text{ deg}$ $\frac{5}{\text{deg}}$ Tumbling $\alpha_e = 179 \text{ deg}$	2560	2390
$\gamma_e = 2.15 \frac{9}{\text{deg}}$ Spinning Offset c.g.	2780	2420
<u>15</u>	3060	2860
Orbital Decay Rearward to Ground		

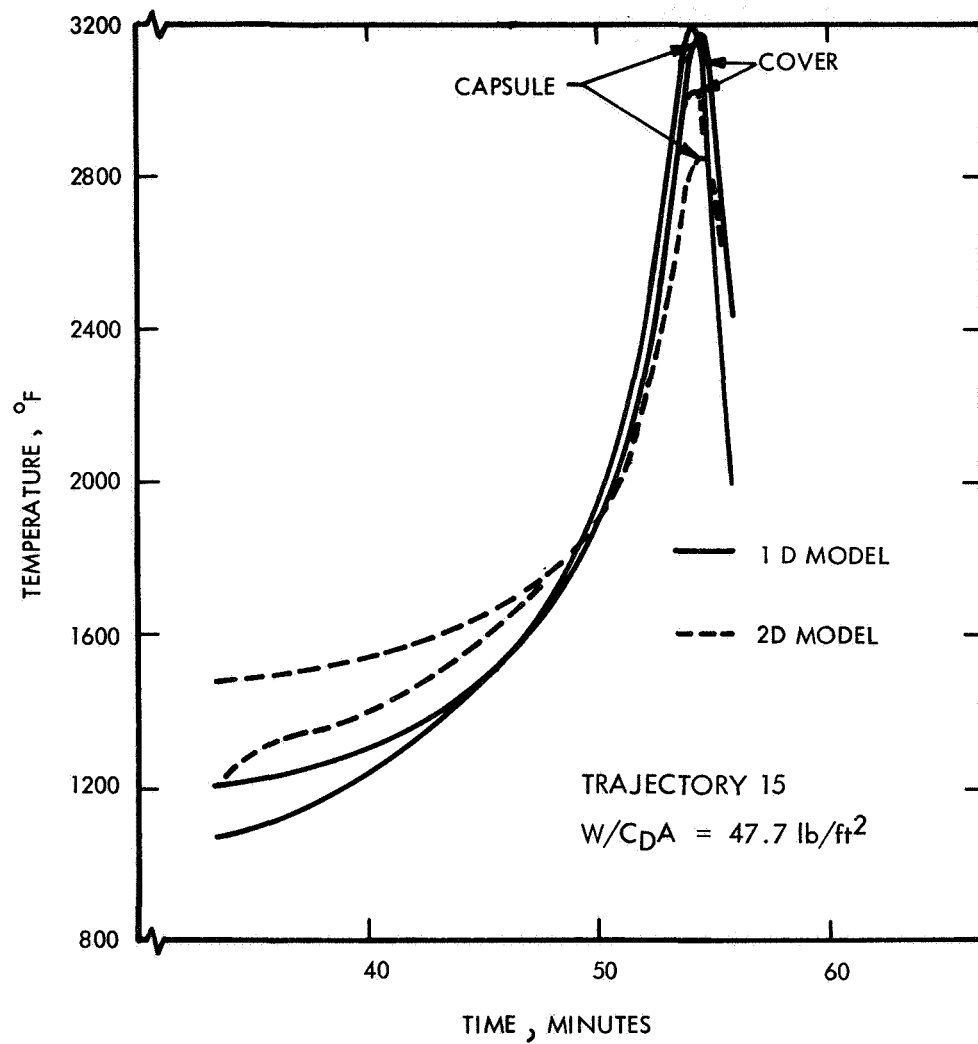


Figure 3-70 COMPARISON OF 2D MODEL TO THE 1D MODEL FOR CALCULATION OF IRV REENTRY TEMPERATURE

3.3.1.6.4 Summary of Transient Results and Conclusions -- The temperature history of the IRV was evaluated for three types of transients; namely, heat source heatup with no heat leak, heat source cooldown in deployed state, and heat source temperature excursion during reentry. Results obtained from these studies were:

- the heat source can be maintained below 2500° F for a 56-minute duration during heatup from nominal steady-state operation (1918° F peak capsule temperature with primary HSHX operating) with no heat removed by HSHX operation and with the use of 170 pounds of BeO in contact with the capsule support plate.
- the temperature rise of the heat source in one hour with no heat leak is 650° F for 170 pounds of BeO in contact with a capsule support plate and, therefore meets the "1800° to 2500° F in no less than one hour" criteria.
- the fuel capsule array mounted flush with the IRV base plane with a cover plate can maintain peak capsule temperatures below 2500° F during worst case nominal reentries and tumbling reentries from orbital decay.
- the aerodynamic heating rate and radiation to space are the dominant terms in the heat balance of the heat source.
- the initial temperature profile of the heat source does not significantly affect the peak capsule temperature.
- short-term reentries exhibit the highest cover temperatures; however, the cover plate is more effective in reducing the capsule temperature rise during reentry.
- the effect of heat absorbed by the support plate is significant but of second order importance in reducing the peak capsule temperature.
- the BeO is not an important factor in reducing the peak capsule temperature during reentry.

Conclusions of these studies are:

- 170 pounds of BeO in poor contact (100 Btu/hr-ft²-°F) with the support plate provides sufficient capacitance for the heat source to meet the thermal design criteria for transient case. No contact between the BeO and support plate results in significant BeO weight increases; therefore, design must assure thermal contact.
- peak capsule temperatures can be maintained below 2500° F during the credible reentry trajectories for a flush-mounted fuel capsule array protected with a cover plate.
- BeO is not effective in reducing the peak capsule temperatures during reentry.

3.3.2 Heat Source Mechanical Design

The IRV heat source consists of the heat source plate subassembly, the heat source support structure subassembly, and the thermal insulation subassembly. The heat source plate consists of the basic heat source elements, which are the fuel capsules; their heat source support plate which provides support for the fuel capsules and maintains them in their functional geometric array; and the cover plate and associated retention bars and bolts comprising the fuel capsule retention system. The heat source support plate is designed as a composite fabricated structure to minimize weight. It consists of a circular top plate on which are mounted the rows of fuel capsule support cradles and includes the ACHX coolant passages. A system of ribs and a bottom plate provide rigidity and incorporate the supplemental BeO heat sink. (See Figures 3- and 3- .) Other than the fuel capsules, retention bolts and BeO heat sink, the remaining heat source plate subassembly components are made of Cb-1Zr. The mechanical design of the heat source plate is discussed in this section including the design environment, material selection and structural performance.

The heat source support structure subassembly supports the heat source plate and provides the mechanical connection to the aeroshell. The thermal insulation subsystem provides an insulation boundary around the heat source plate. These subsystems and the ACHX design are discussed in the subsequent sections.

3.3.2.1 Design Environment

The IRV heat source components are designed to withstand the static and dynamic g-loads that they are subjected to during the mission lifetime. These design requirements are summarized as IRV Structural Design Parameters by Table 3-19. As noted in the table, the design loads include a 1.25 factor of safety.

The reentry loads, Item A in the table, predominate in setting the design limits since they establish higher magnitudes and generally occur at higher temperatures than the launch loads and miscellaneous loads, Items B and C. Two cases were specified for reentry loads. The one case is the worst case reentry that could occur as the result of an abort and reentry during the ascent trajectory. Since this could only occur a short time after the ACHX launch pad cooling has been terminated, the loads would be imposed while the heat source structure is relatively cool and therefore with more favorable structural properties.

The other case is the reentry from orbit during which the structure could be at or near operating temperature but where the peak axial g-loads imposed are less severe. It was determined that 500° F is a conservative limit for the maximum structural temperatures for the launch abort case and 1900° F for the reentry from orbit. These design temperatures and related structural material stress limits are given as Item D in Table 3-19. These two cases were evaluated and it was established that the worst load condition is the launch ascent abort reentry with the higher loads and lower temperatures. An indication of this condition is the comparison of the relative strength capabilities (yield strength divided by the design load) of the materials. For the abort reentry, the strength capability for the Cb-1Z and T-111 is only 870 and 1400 psi per g respectively. For the orbit reentry, these values are 1560 and 2620 psi per g respectively.

TABLE 3-19

STRUCTURAL DESIGN PARAMETERS

A. <u>REENTRY LOADS</u>		
	<u>Ascent Abort Reentry</u>	<u>Orbit Reentry</u>
IRV Maximum g-Loads		
Axial	30.4	11.3
Lateral	2.4	1.9
IRV Design Loads (F.S. = 1.25)		
Axial	38.0	14.1
Lateral	3.0	2.4
B. <u>LAUNCH LOADS</u>		
Maximum g-Loads (Saturn I-B)		
Axial	±4.0	
Lateral	±9.0	
Design Loads (F.S. = 1.25)		
Axial	±5.0	
Lateral	±11.25	
C. <u>MISCELLANEOUS LOADS (IRV)</u>		
	<u>Maximum g-Loads</u>	
	<u>Axial</u>	<u>Lateral</u>
PAD Abort	10.0	2.0
Chute Deployment/Air		
Snatch	8.0	2.0
Vibratory	0.25*	0.25*
	(*To 2000 Hz)	
D. <u>TEMPERATURE-STRESS LIMITS</u>		
	<u>Ascent Abort Reentry</u>	<u>Orbit Reentry</u>
Heat Source Temperature (Max)	500° F	1900° F
Material Yield Strength (Min)		
T-111	53 ksi	37 ksi
Cb-1Zr	33 ksi	22 ksi
E. <u>IMPACT VELOCITY</u>		
Ground Impact Velocity	150-260 ft/sec ($W/C_{D_{\text{Subsonic}}} A = 92 \text{ lb/ft}^2$)	

The structural performance was evaluated on the basis of the maximum stress failure theory since the preliminary design analysis does not provide complete evaluation of the three-dimensional stress field which is required by the other failure theories. Thermal stress due to the cold-to-hot growth of the heat source and truss system was considered, but, in general, the thermal stresses due to temperature distributions within the system are not expected to be significant for steady-state operation and were not evaluated. The structural design criteria is based on a factor of safety of 1.25 on either the yield strength of material or the critical buckling load. However, in many cases, components are sized based on other considerations such as manufacturing or thermal design requirements with resultant higher safety factors.

3.3.2.2 Heat Source Materials Selection

3.3.2.2.1 General -- The most important guideline used in the selection of materials for the IRV heat source was strength and stability at high temperature. The peak operating and transient temperatures developed in the fuel capsule are 2000° and 2500° F, respectively. Nearby structural elements see similar temperatures which generally rule out the use of conventional iron, nickel, or cobalt base superalloys and require the use of refractory metals such as columbium or tantalum.

Evaporation of high vapor pressure alloy components is a serious consideration at elevated temperatures under high vacuum conditions. At temperatures over 1600° F, the common iron and nickel base super alloys suffer significant evaporation losses. Since the evaporated components generally are scattered in line-of-sight patterns, contamination of other system components from an evaporation material may also be a serious consideration. Columbium and tantalum base alloys are free of evaporation problems at temperatures up to 2400° F, (Ref. 3-14) in high vacuum.

The heat source is designed to operate for a minimum of 40,000 hours at a maximum steady-state temperature of 2000° F. At this temperature, solid-state diffusion is rapid enough to produce contamination of different alloy systems through contact and subsequent diffusion. For this reason it is important to minimize the variety of alloys in the high temperature region of the heat source. In particular, only refractory metal alloys should be used in intimate contact at temperatures over 1400° F (Ref. 3-15).

An additional criterion was that the materials selected should be fabricable and weldable and be adaptable to the design of a sizeable complex structure. Tungsten and molybdenum base alloys were not considered for these reasons.

The materials selected are commercially available in the sizes required and the fabrication and welding techniques are within the state of the art of the aerospace industry.

3.3.2.2.2 Specific Materials Selection

Heat Source Capsule -- A non-vented, 157-watt (BOL) reference capsule, NASA/ORNL design, is considered in this design study and qualification of the capsule design or material selection is not required.

Cover Plate and Heat-Source Plate -- The purpose of the cover plate is to secure the heat source capsules during the mission life and also to protect the capsule surfaces from temperature extremes during reentry conditions. As the major radiating surface to the HSHX, the mean cover temperature will be 1770° F during normal operation. A maximum temperature of 2500° F will be encountered during credible reentry trajectories. The columbium base alloy Cb-1Zr has been selected based on its high temperature stability and fabricability. The tensile properties as a function of temperature are shown in Figure 3-71 (Ref. 3-16) and stress rupture properties are shown in Figure 3-72 (Ref. 3-17). Adequate strength for the low stress application is available up to the maximum expected temperature and its melting point of 4380° F provides a desired margin of safety for the more extreme reentry conditions. The thermal conductivity and specific heat of Cb-1Zr are presented in Figures 3-73 and 3-74 (Ref. 3-18), respectively. The heat source plate will also be exposed to steady-state operating temperatures up to 2046° F and transients slightly below the cover plate. Cb-1Zr will be used in this application and will satisfy the temperature-stress requirements.

Hold Down Bar and Locking Mechanism -- With the exception of the spring in the locking mechanism which is the molybdenum base alloy, TZM, the hold down bar and locking mechanism will be Cb-1Zr. The locking pin and nut will be subjected to steady-state operating temperatures of 1935° F and transients to 2500° F during reentry. Adequate short time and long time creep strength is provided by Cb-1Zr in this application.

Long time creep strength is the most important consideration for the spring design and Figure 3-75 (Ref. 3-19) shows the 0.5 percent creep strength for high strength heats of TZM.

Support Ring -- The steady-state operating temperature of the support ring is less than 2000° F with thermal transients slightly less than the heat source plate and cover plate. The structure will be made of Cb-1Zr for strength and stability considerations in high vacuum at 2000° F. The materials match with the heat source plate and heat sink structure is also important for thermal expansion considerations.

BeO Heat Sink and Container -- Because of its high heat capacity per unit weight and chemical stability at high temperatures, BeO will be used as the heat sink material. The BeO will be in intimate contact with Cb-1Zr at temperatures of from 1750° to 2000° F, and material compatibility is required. Although compatibility test data would be required in more definitive design efforts, the thermodynamic properties of BeO and the oxides of columbium and zirconium, shown in Figure 3-76 (Ref. 3-20), indicate chemical stability up to 2500° F (Ref. 3-20). The heat capacity and thermal conductivity of BeO are presented in Figures 3-77 and 3-78 (Ref. 3-21), respectively.

Support Truss -- The tantalum base alloy T-111 was selected for the support truss. This high strength alloy was selected to minimize the cross sectional area and consequently the heat loss through the truss structure. The thermal conductivity of T-111 is slightly higher than Cb-1Zr, but its yield strength is nearly double that of Cb-1Zr over the temperature range of interest. Therefore the strut cross-sectional area is much less with the T-111 and thus the heat loss is the lowest.

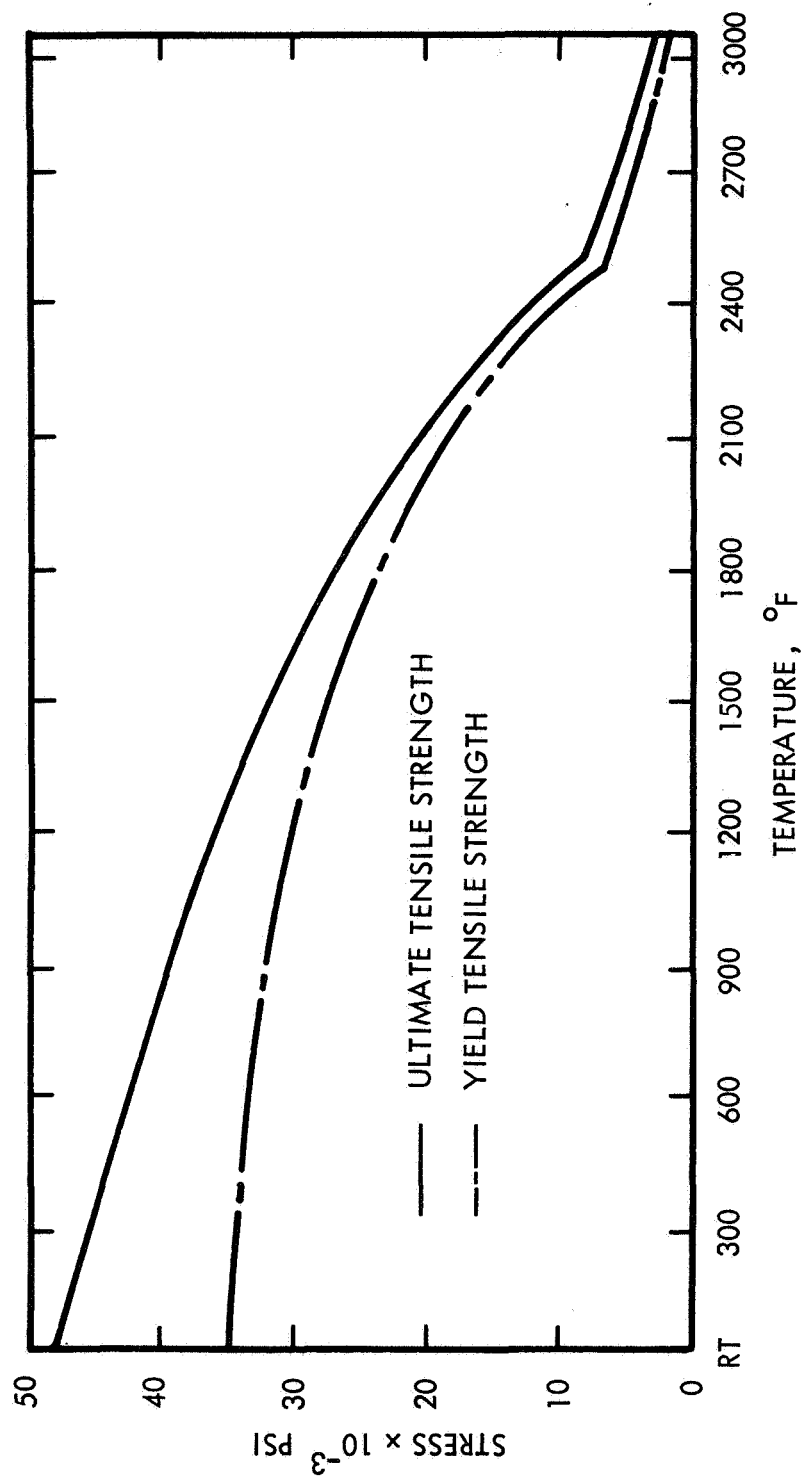


Figure 3-71 TENSILE STRENGTH VERSUS TEMPERATURE FOR Cb-12r
(RECRYSTALLIZED SHEET)

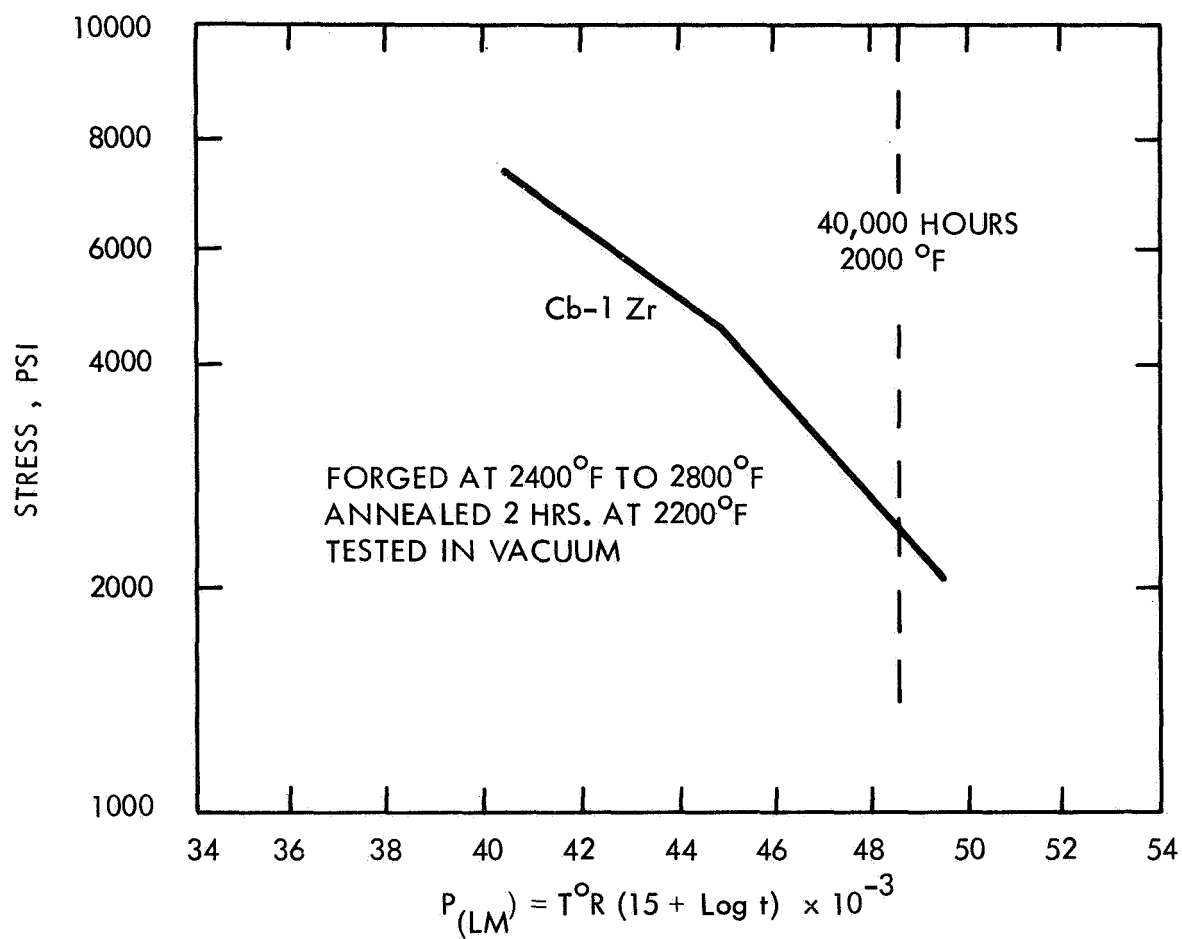


Figure 3-72 LARSON-MILLER PARAMETER PLOT OF RUPTURE STRESS IN Cb-1Zr

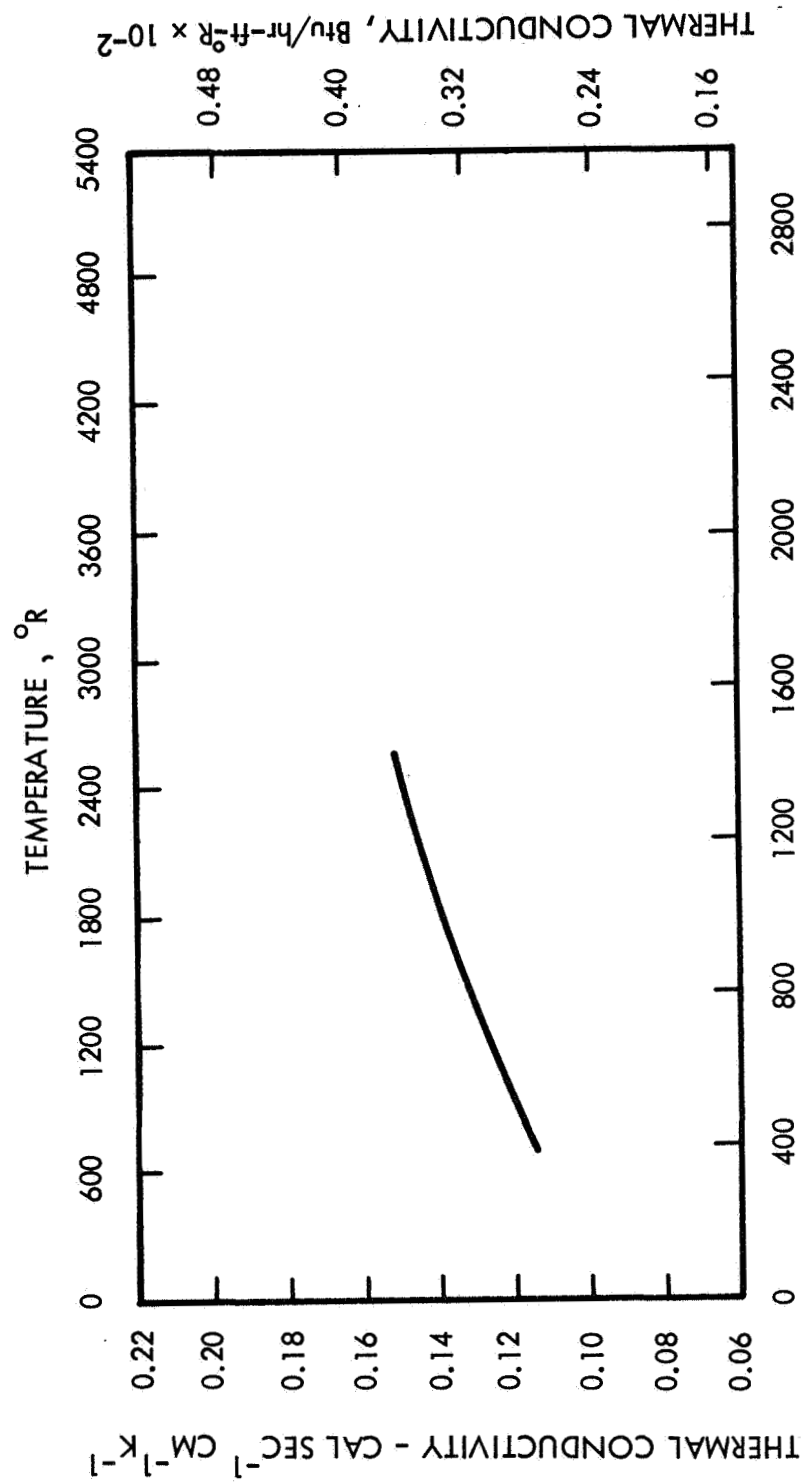


Figure 3-73 THERMAL CONDUCTIVITY -- Cb-12r

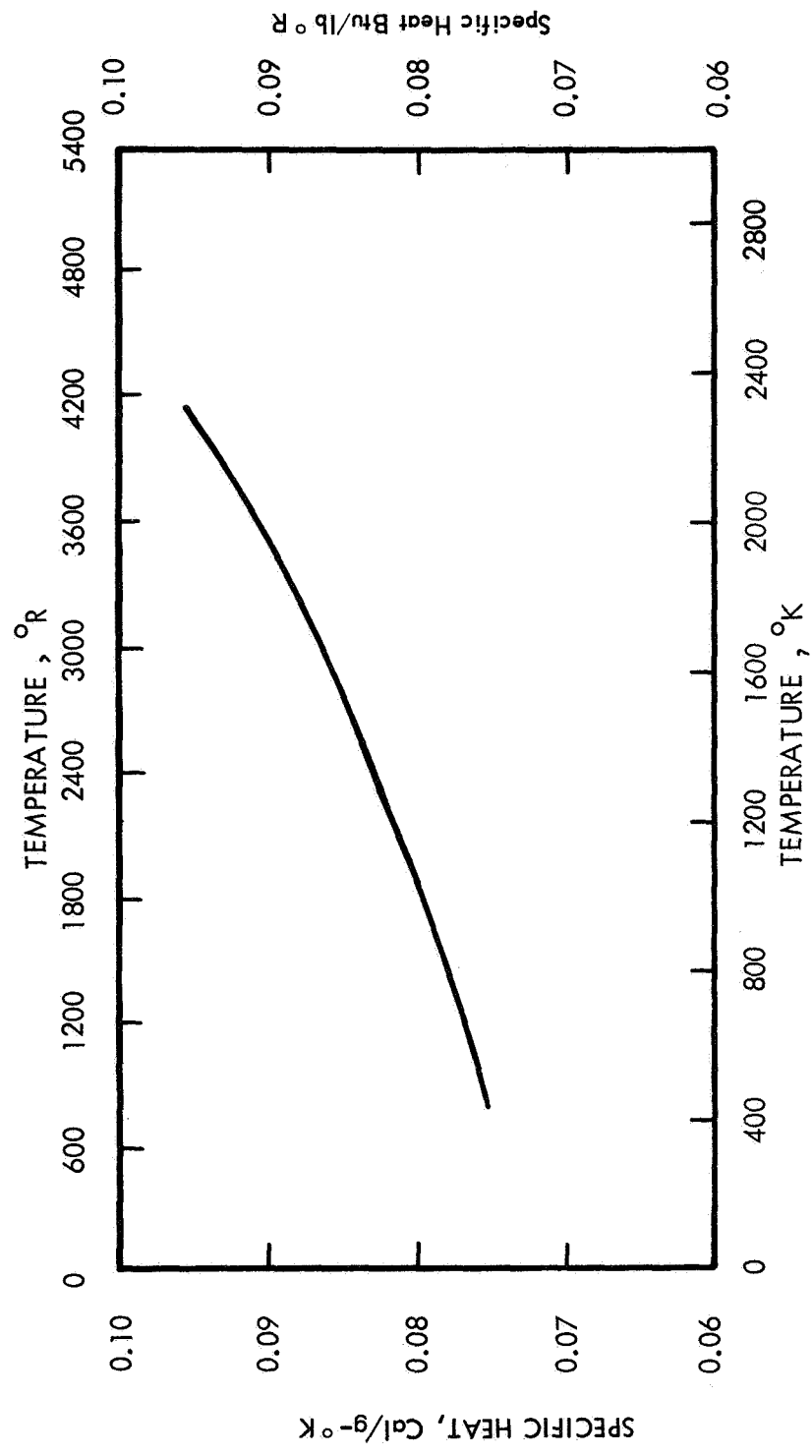


Figure 3-74 SPECIFIC HEAT -- Cb-12r

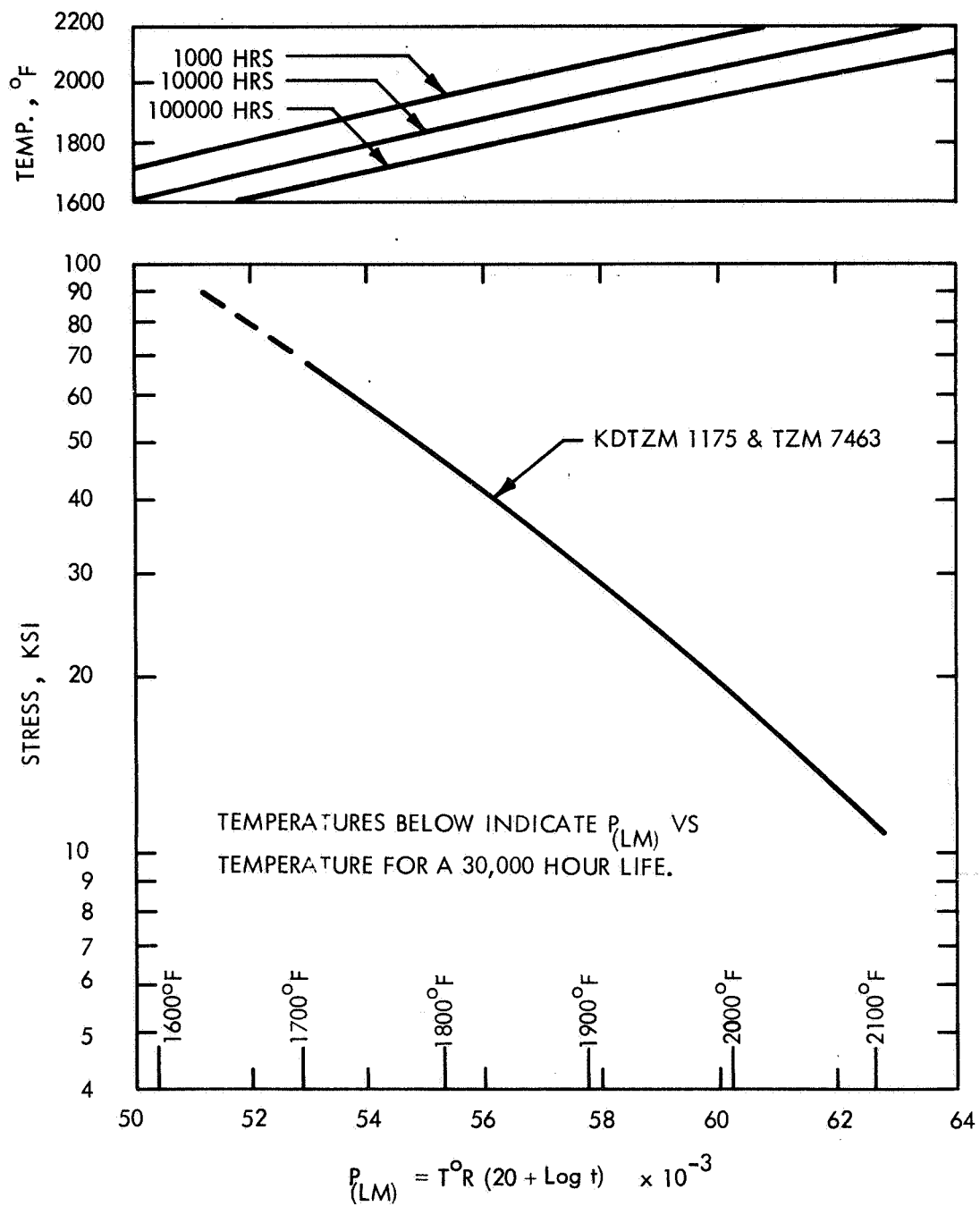


Figure 3-75 0.5 PERCENT CREEP IN TZM

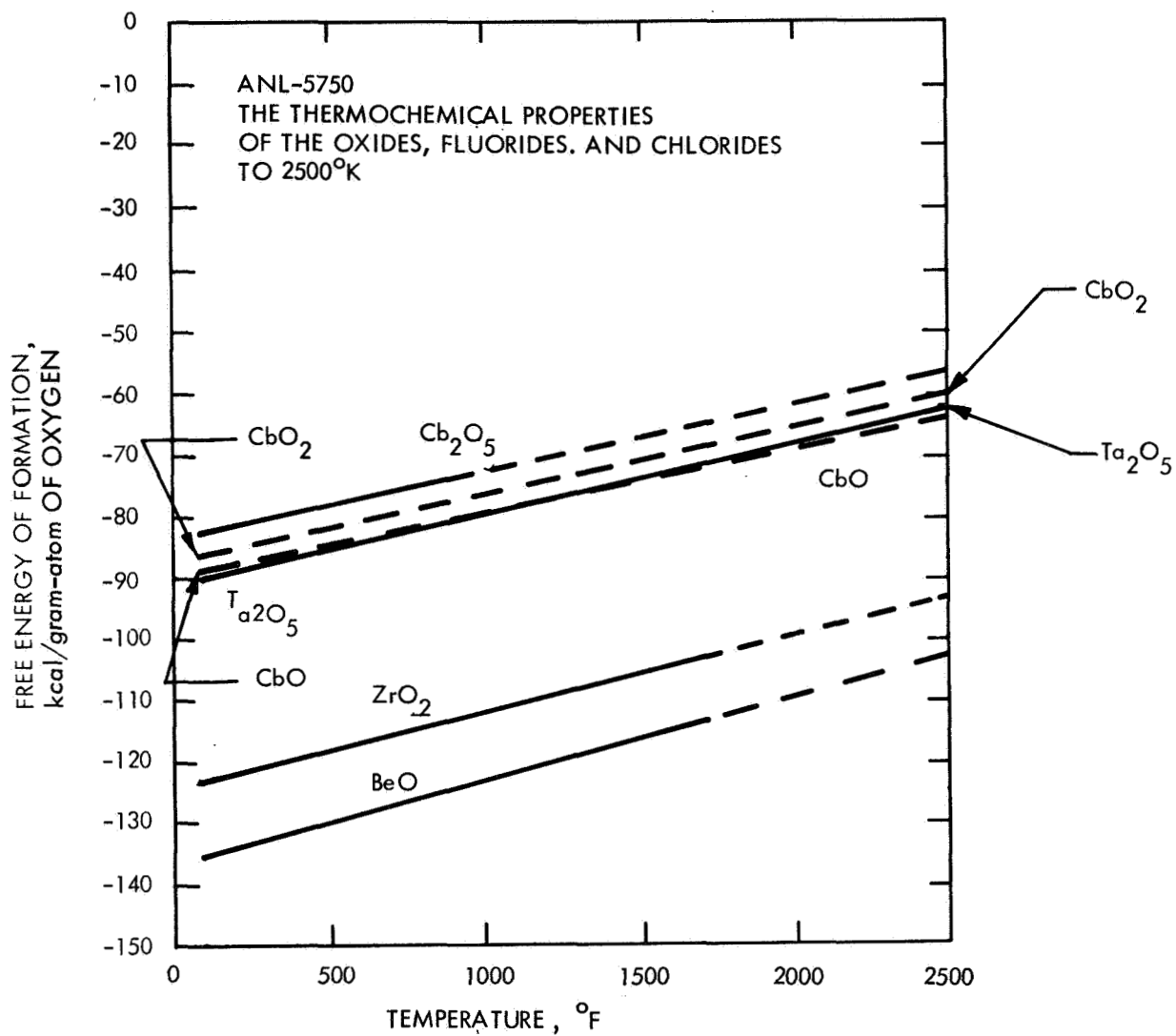


Figure 3-76 FREE ENERGY OF FORMATION OF BeO AND COLUMBIAN
AND ZIRCONIUM OXIDES

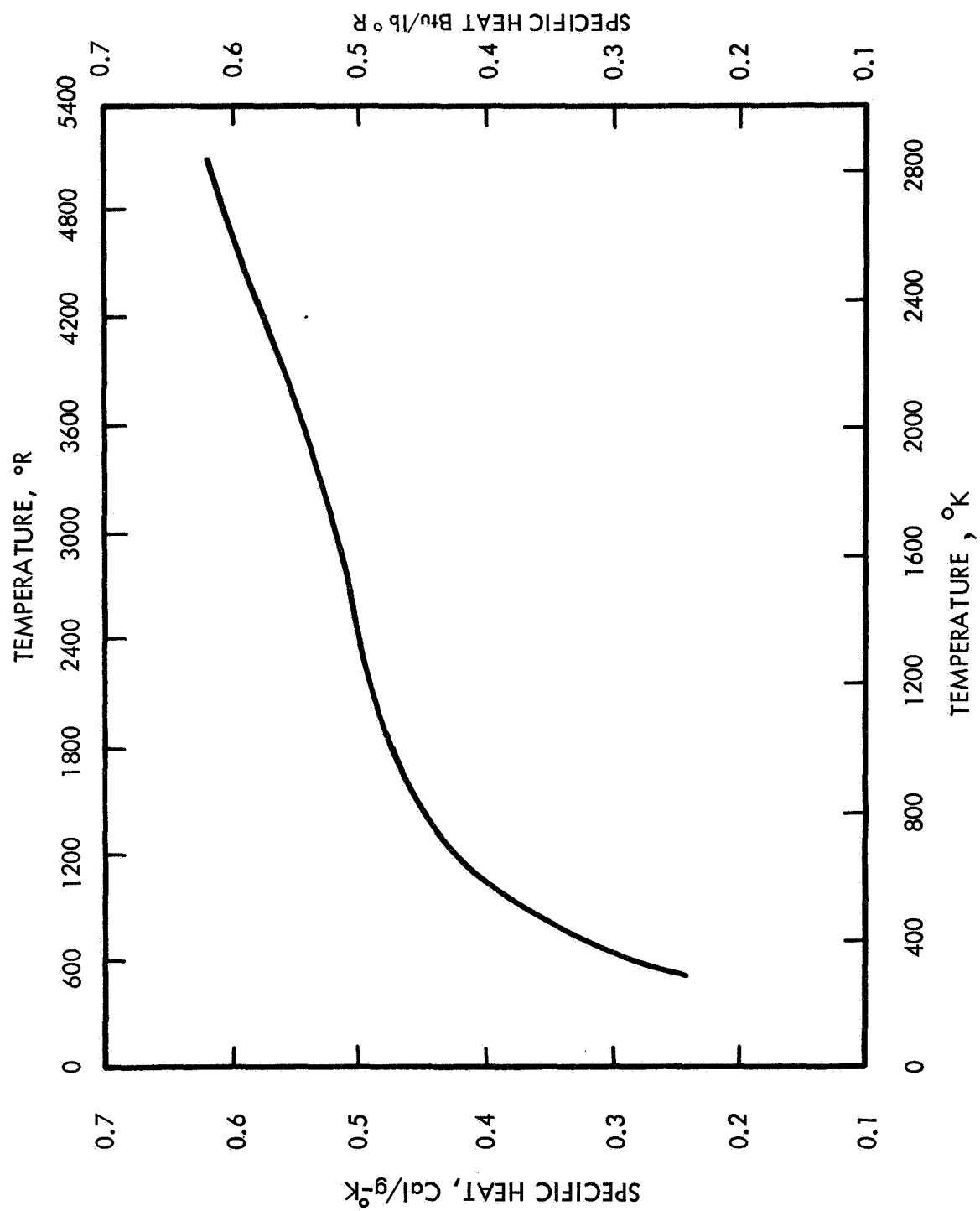


Figure 3-77 SPECIFIC HEAT -- BeO

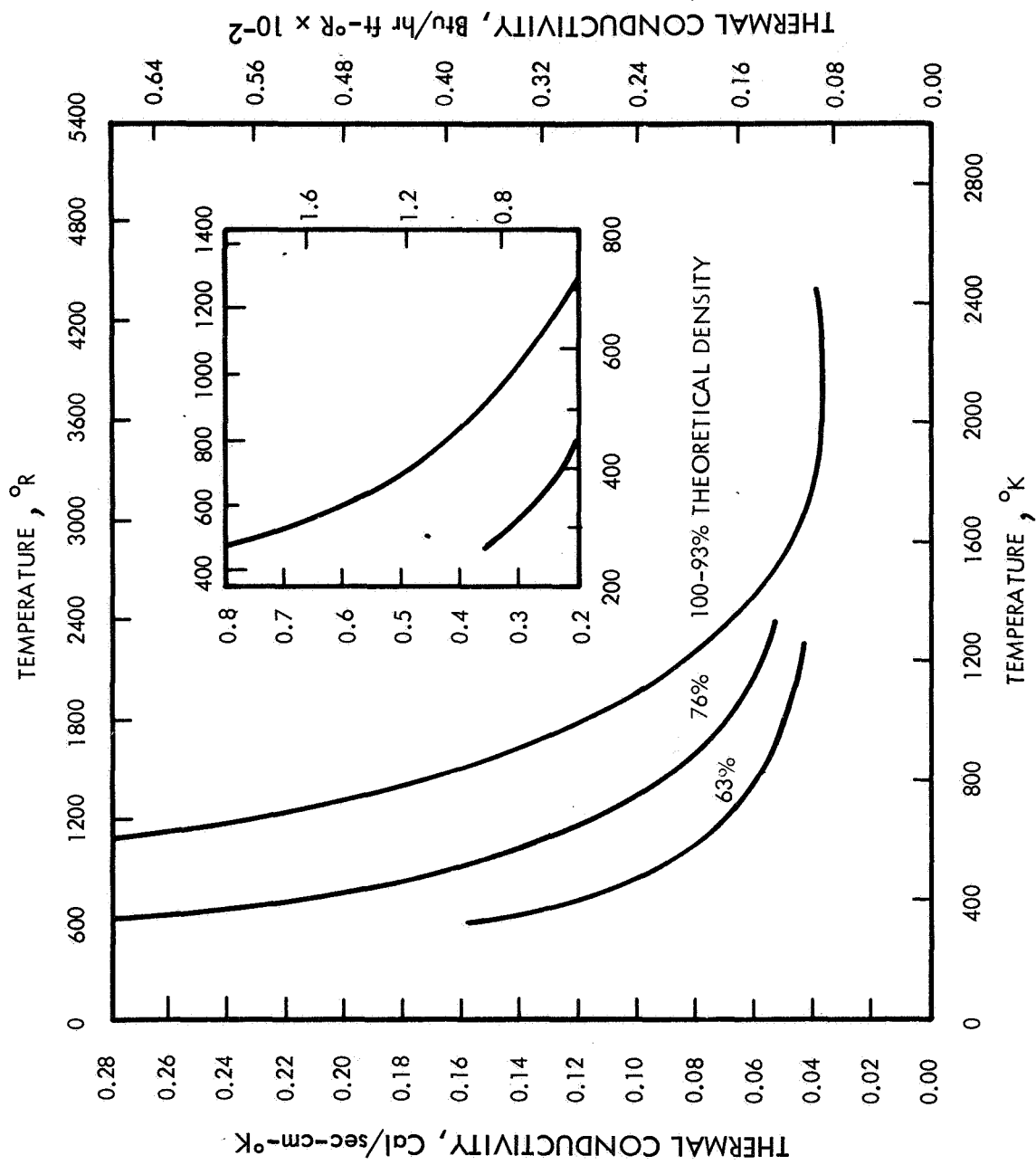


Figure 3-78 THERMAL CONDUCTIVITY -- BeO

T-111 is a fabricable, weldable refractory metal alloy, and no problems are anticipated in the manufacturing of the truss components. T-111 may be used in direct contact with Cb-1Zr at high temperatures with no problems from solid-state diffusion contamination. The alloy is also stable in high temperature, high vacuum conditions, Figure 3-79 (Ref. 3-22) shows the tensile properties of T-111 as a function of temperature and Figure 3-80 (Ref. 3-23) shows the one percent creep strength plotted as a Larson-Miller parameter. The specific heat and thermal conductivity as a function of temperature are listed in Figures 3-81 and 3-82 (Ref. 3-18), respectively.

Iron Titanate Emittance Coating -- High emittance surfaces are required on both the heat exchanger and capsule side of the cover plate and on the capsule side of the heat source plate to meet the requirements of radiation heat transfer. The reference heat source capsules are also coated with iron titanate on the exterior of the platinum alloy oxidation barrier.

The emittance and high temperature stability of iron titanate, is being studied by Pratt & Whitney Aircraft under contract NAS3-4174. Long term, high vacuum thermal cycling tests of iron titanate on Cb-1Zr indicate good adherence and stable emissivity characteristics up to 1900° F. A thermal excursion to 2800° F did not degrade the emissivity. Although there is evidence of substrate contamination from the iron titanate above 1700° F, tests are being run on intermediate barrier layers between refractory metal alloys and iron titanate.

3.3.2.2.3 Refractory Metal Oxidation Characteristics -- The tantalum and columbium base alloys designated are subject to significant oxidation at temperatures much above 350° F in a partial pressure of oxygen. Below 1000° F, for very short periods of time, the reaction is limited to the formation of a thin surface film, but if the material is subsequently heated to a higher temperature, oxygen diffusion will proceed rapidly throughout the material. Depending on the service temperature, oxygen contamination levels as low as 100 ppm may cause a significant low in ductility.

Prior to launch and service in high vacuum, the ACHX will maintain the heat source at a maximum temperature of 350° F. In the event of prelaunch interruption of cooling, the temperature of several refractory metal components may rise to produce damaging oxygen contamination. Short time (2-hours) oxidation data for pure columbium is available at temperatures of from 480° and 1000° F, and it would be helpful to list a time-temperature parameter for safe oxidation exposure. However, whether a given level of oxygen contamination will be harmful is related to the component metal thickness, since thicker sections will appreciably dilute the surface contamination, and to the subsequent service temperature since at high temperatures the oxygen contamination may not impair material ductility.

To provide a general outline of the rate of oxygen contamination at low temperatures, the following example is presented. If 100 ppm oxygen contamination is set as a limit in 0.100-inch columbium sheet, the equivalent thickness of surface oxide will be formed in 17 hours at 570° F or in 2-1/4 hours at 800° F.

In summary, 350° F is far enough below the lowest measured oxidation temperature of 480° F to be considered a safe indefinite time storage temperature. However, sufficient long time, low temperature oxidation rate data is not available to permit the prediction of a time-temperature parameter for lower temperature oxygen atmosphere exposures.

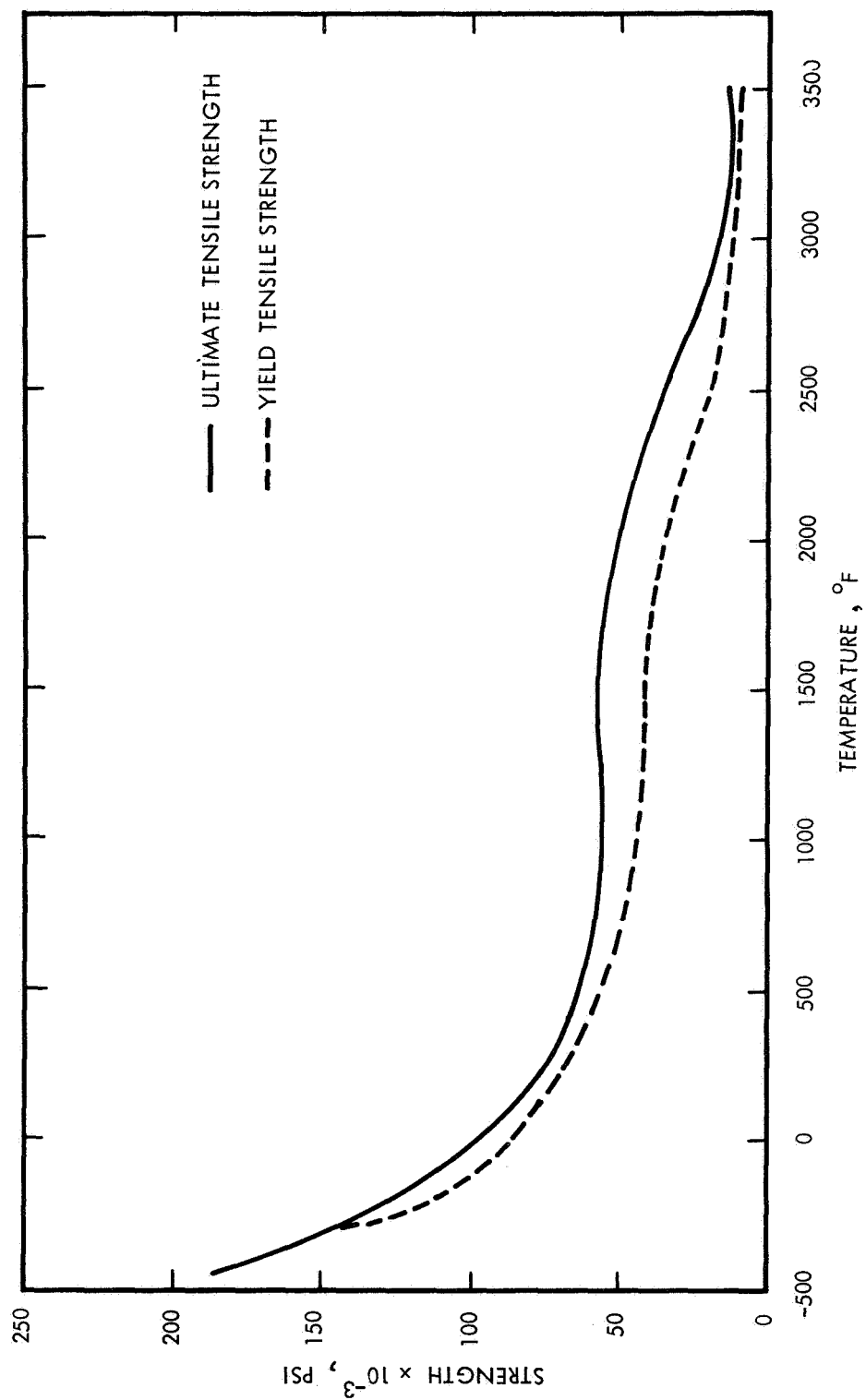
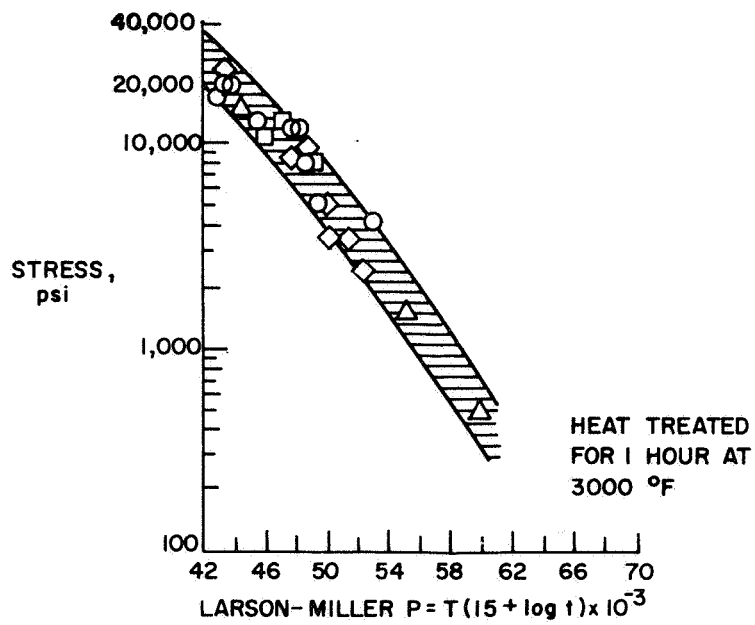


Figure 3-79 TENSILE STRENGTH VERSUS TEMPERATURE FOR RECRYSTALLIZED T-111



89-3380

Figure 3-80 LARSON-MILLER PLOT FOR T-111 -- CREEP 1 PERCENT

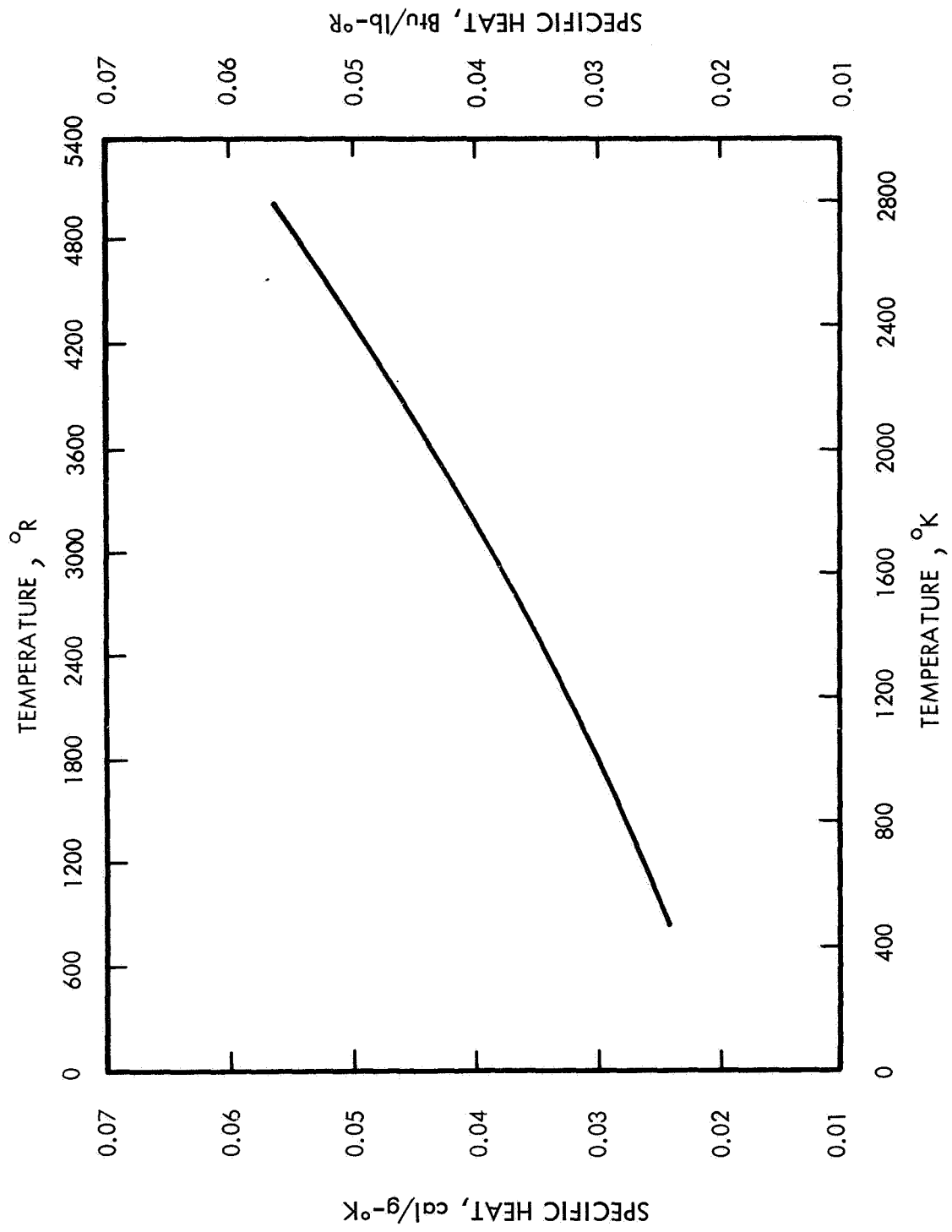


Figure 3-81 SPECIFIC HEAT -- T-111

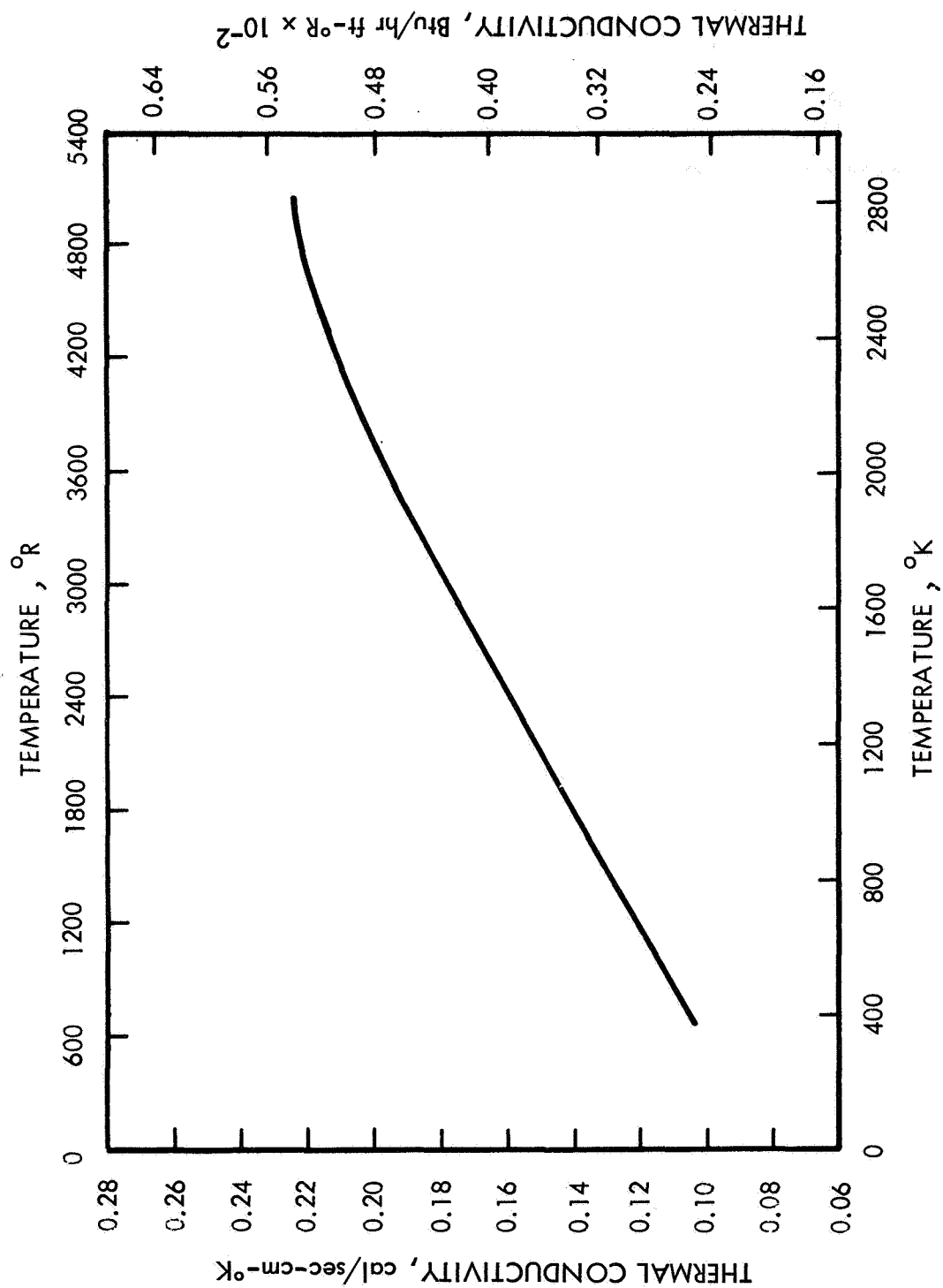


Figure 3-82 THERMAL CONDUCTIVITY -- T-111

3.3.2.2.4 Summary -- The selection criteria used for the more unconventional materials in the IRV heat source have been discussed. Table 3-20 compares selected properties of these materials. In the lower temperature regions of the IRV, such as the insulation assembly retention plate which will be exposed to maximum temperatures of 500°F, high strength-to-weight ratio conventional materials such as Ti-6AL-4V will be used.

TABLE 3-20
MATERIALS PROPERTY DATA

Material	Density (gm/cm ³)	Melting Point	
		(°C)	(°F)
Cb-1% Zr	8.57	2410	4375
Pt-10Rh	19.97	1870	3400
Al ₂ O ₃	4.00	2316	4200
T-111	16.70	2980	5400
PuO ₂ (Theoretical)	11.50	2550	4625
BeO	2.90	2570	4658

3.3.2.3 Structural Performance -- Heat Source Plate

The IRV heat source plate basically consists of a planar circular support plate upon which the fuel capsules are mounted in parallel rows of support cradles. The fuel capsules are held in place by the cover retention system. The cover plate is contoured to the rows of fuel capsules and is attached by means of bolts through retention bars between the capsule rows. The support plate and retention system are designed to retain the fuel capsules in position for the mission life-time including reentry. An exploded view of the heat source plate is shown in Figure 3-83 and further detail is shown in Figure 3-94.

The plate supports 760 pounds of fuel capsules and acts as a heat sink (with the BeO). The top support plate on which the capsule cradle rows are mounted is supported underneath by a system of parallel ribs and a bottom plate to complete the composite plate section. The support ribs are oriented perpendicular to the direction of the capsule cradles to provide more uniform rigidity at minimum weight for the support plate structure. The ACHX inlet and outlet headers make up the perimeter of the plate and are connected to the individual ACHX cooling passages which are integrated between the rows of capsule cradles. A breech lock housing inside the inner circumference of the ACHX headers provides for mechanically mounting the assembled heat source plate to the IRV truss support ring.

The sizing of the various components which comprise the total heat source plate subassembly was influenced by structural performance requirements, thermal performance requirements, manufacturing considerations and the minimum weight and diameter objectives. The components were sized on a structural basis to have a

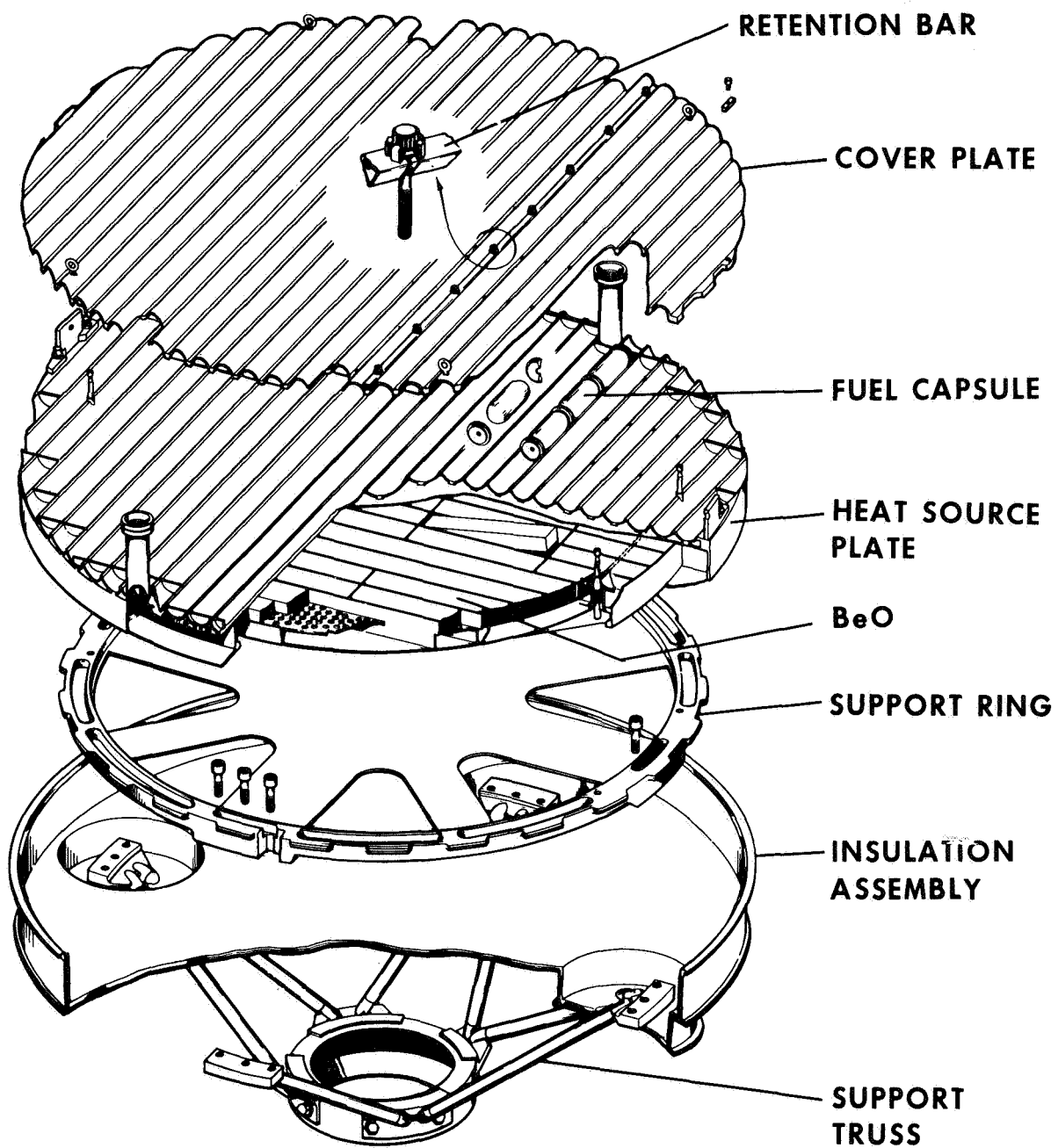


Figure 3-83 EXPLODED VIEW OF THE HEAT SOURCE PLATE

minimum factor of safety of 1.25. However, in some areas, thermal requirements or manufacturing considerations dictated sizing criteria with resultant factors of safety greater than the minimum. The structural performance of the key areas of the heat source plate are discussed in the following paragraphs and in further detail in Appendix A, Section A1.0. These areas include:

- Heat source support plate composite structure
- ACHX headers
- BeO retention panels
- Internal ribs
- Capsule retention bolts
- Heat source plate/support truss-attachment
- ACHX header pipe connections

3.3.2.3.1 Heat Source Support Plate Composite Structure -- Flexure loading under axial g-loads is the prime consideration for the structural performance of the composite plate. The section modulus for the axis parallel to the capsule rows and that parallel to the internal ribs are about equal (within 5 percent) and the flexural stiffness was evaluated using the minimum value. The flexure stiffness contribution provided by the BeO retention plates, the capsules and their retention system, and the peripheral ACHX header were conservatively neglected. The in-plane loads that may be transmitted to the plate by the truss support ring, which would tend to reduce the flexural stresses, were also neglected. Based on the axial g-loads being circumferentially reacted at the truss support ring, the composite plate has a factor of safety of 2.09 for the ascent abort reentry case (based on 33,000 psi Cb-1Zr yield stress at 500° F) and 3.75 for the orbit reentry case (22,000 psi Cb-1Zr yield stress at 1900° F).

3.3.2.3.2 ACHX Header -- The ACHX headers which form the periphery of the heat source plate are designed for the maximum possible operating pressure of 110 psig imposed by operation of launch pad cooling system. For this condition, the stress in the 0.10-inch-thick ACHX panels is 26,500 psi. The ACHX operation is terminated at launch; therefore, this load is applied independent of other loads. The maximum temperature of the heaters during this period is 200° F for which the allowable yield strength for the Cb-1Zr is 34,000 psi, providing a factor of safety of 1.28 for weld efficiency, etc.

3.3.2.3.3 BeO Retention Panels -- The BeO retention panels are provided to hold the supplemental BeO heat sink material in place within the internal rib structure. To minimize weight, the panels are perforated to remove 50 percent of the material. The 0.04-inch-thick panels, which are generally 2 x 10 inches, are held in place by intermittent welding about their periphery. The BeO load is seen mainly as a shear load to these welds. For a conservative weld strength of 20,000 psi, the required weld length is 0.24 inch. The 24-inch periphery provides for more than adequate attachment of the panels.

3.3.2.3.4 Internal Ribs -- The internal ribs which contribute to the composite plate stiffness to support the overall flexure load were also evaluated to determine their performance to the compressive loads imposed. For the heat source design load at the worst case ascent abort reentry, the load was assumed to be uniformly distributed over the ribs. Conservatively neglecting the reinforcement provided by the BeO retention panels, the resulting factor of safety based on yield strength is 37.7. Under the same loading condition, the factor of safety based on rib buckling is 1.66.

3.3.2.3.5 Capsule Retention Bolts -- Considerations for evenly locating and applying retention loads on the fuel capsules and for minimizing vibration effects to protect surface coatings from fretting influenced the selection of the number of bolts, the bolt sizes and locations. The 194 T-111 0.164-inch-diameter bolts have a root diameter of 0.129 inch. Each bolt has a load capability of 690 pounds at the 500° F ascent abort reentry design temperature and 480 pounds for the orbit reentry case (1900° F). Thus, a total load capability of 133,500 and 93,000 pounds exists respectively, which is more than the structural requirements. However, the possibility of thermal stresses, non-loaded bolts, stress-relaxation effects, and dynamic loads with their stress concentration effect requires a large safety margin. The requirement of maintaining a tight interface load on the capsule to prevent fretting under vibration is of utmost importance, since the iron titanate coating would be degraded.

3.3.2.3.6 Heat Source Plate/Support Truss-Attachment -- The heat source plate is mechanically attached to the support truss by a breech lock mechanism which permits semi-remote assembly. The plate is installed and rotated 7-1/2 percent to engage the breech lock lugs. For positive axial loads and lateral loads, the heat source plate loads are distributed over the entire truss support ring which is discussed in paragraph 3.3.5. The negative axial loads are distributed over the locking lugs. For the maximum negative axial load of 11.25g, the shear stress induced in the lugs is only 490 psi if they are uniformly loaded. Hence, the lugs are adequate even if some nonuniform loading occurs.

Four lock pin assemblies are inserted when the heat source plate is twisted into place engaging the breech locking lugs. These pins prevent relative rotation between the heat source plate and the truss support ring so that the assembly cannot become disengaged. These pins are subjected only to rotational moment between the two components since the axial and lateral loads are taken by the breech lock mechanism. These pins are capable of taking shear loads imposed by angular accelerations up to 14.2 rad/sec² when equally loaded and conservatively assuming no assistance from the friction resistance between mating lugs.

3.3.2.3.7 ACHX Header Pipe Connections -- The piping connections to the ACHX inlet and outlet headers are 5-inch-long tubes with 1.5-inch I.D. and 1.65-inch O.D. which are welded to the heat source structure. During ground handling and attachment of launch pad cooling lines to these connections, loading restrictions must be observed to ensure maintaining the integrity of the cooling gas system. Based on yielding at the built-in end, the maximum allowable radial load applied at the connection is 630 pounds. The maximum allowable axial load on the connection is 9800 pounds, based on shear of the tube-plate weld junction.

3.3.2.4 Dynamic Analysis of the Heat Source

In the preliminary design, the anticipated significant fundamental resonant frequencies of heat source assembly and components were computed. For the case of

the heat source mass axially resonating on the struts, which is considered the worst case, the dynamic stress level was computed. The following summarizes the areas considered with the corresponding results. These areas are discussed in further detail in Appendix A, Section A2.0.

a. Heat Source Plate Flexural Resonant Frequency

The heat source plate flexural resonant frequency for the umbrella mode was determined by approximating the plate as a disc with proper dimensions and uniform mass per unit area. For this condition, the fundamental frequency is 30.2 Hz.

b. Strut Lateral Resonant Frequency

The lateral resonant frequencies for the struts with builtin end conditions are $f_1 = 393$ Hz and $f_2 = 1100$ Hz. All higher resonant frequencies for this mode are greater than 2000 Hz.

c. Lateral Resonance of Truss-Heat Source

For this condition, the truss system was assumed fixed at the interface to the aeroshell. The heat source was assumed to be represented by a mass with a vibratory motion normal to the axis of the vehicle. The interconnecting struts of the truss system were approximated by a system with the same number (eight) of parallel struts. The fundamental resonating frequency for this mode is 318 Hz.

d. Axial Resonance of Truss-Heat Source

For this analysis the truss system was again assumed fixed at the interface to the aeroshell. The heat source was represented as a mass vibrating on the truss system in a direction along the vehicle axis. For this condition the fundamental frequency is 81 Hz.

e. Vibratory Stress Level in Struts

Since most components/subassemblies have resonant frequencies below 2000 Hz, resultant vibratory stresses occur. The axial resonance of the truss-heat source (case d) is considered the worst case with respect to dynamic stress and was evaluated. In accordance with Article 2.3.2 of Specification P1224-1, "Brayton Cycle Subsystem and Components Environmental Specification", an input force (F_i) of 0.25 g was used for the dynamics study. For this condition, the truss can withstand the axial resonant frequencies during launch, when the stress amplitude may get as high as 78 percent of the endurance strength.

It should be noted that the preceding cases (c, d, and e) are based on the assumption that the heat source plate represents a mass and the truss represents a spring or beam. Other components of the aeroshell were not considered in these analyses.

3.3.3 ACHX Design

As discussed in paragraph 3.3.1, the heat source is provided with an integral auxiliary cooling heat exchanger (ACHX) sized to maintain the heat source temperature below 350° F while in an oxygen atmosphere to minimize the probability of structure oxidation and to prevent the possibility of a combustion hazard due to propellant vapor fumes.

The ACHX design consists of triangular shaped channels placed in the fuel capsule support plate between adjacent capsule rows, semicircular inlet and outlet headers at the heat source periphery, and two inlet and outlet connectors. Minor changes in the header design were made to accommodate changes in the insulation system design and redesign of the cooling system connections. Orifices were provided and sized to maintain the proper distribution of coolant to each of the channels.

Two-dimensional heat transfer calculations of the steady-state temperature distribution around the fuel capsule and support structure were performed to determine the temperature drop from the capsule to the ACHX. The effect of the contact between the capsule and capsule support plate was evaluated for three conditions; the 2-mil air gap, the 5-mil air gap, and the partial contact ($h = 300 \text{ Btu/hr-ft-}^{\circ}\text{F}$). The results of these calculations, presented in paragraph 3.3.1, indicated that a peak capsule temperature could be readily limited to 350° F or less with a moderate temperature drop from the peak capsule temperature to the cooling channel mean wall temperature. In particular, a temperature drop of 157° F was predicted for a capsule in partial contact with the support plate. Even with no contact between the capsule and cradle, a 179° F temperature drop was estimated (2-mil air gap). This case was considered very conservative since the heat source design readily assures at least partial contact to all capsules. To be conservative, the temperature profile for the second case was used for predicting cooling requirements.

Both air and nitrogen were considered for this design due to their low cost and ease of handling. The coolant flow rates and flow distribution requirements were calculated parametrically for ranges of inlet temperature, peak capsule temperature, and pressure. Only slight differences in coolant requirements were predicted for air versus nitrogen. These differences are well within the accuracy of the calculation. The parametric results presented in this section were therefore considered equally applicable to air or nitrogen. Based on the results, a cooling state was defined to limit peak capsule temperature to below 350° F. Cooling channel sizes and orifice sizes were developed to meet performance requirements.

3.3.3.1 Mechanical Description

The ACHX system consists of coolant headers, inlet and outlet connectors, and coolant channels in the heat source plate as shown in Figure 3-84. Headers which have approximately 4 square inches of cross-sectional area are arranged around the periphery of the heat source plate. The flow channels which are approximately 0.37 in², run parallel between and below the rows of fuel capsules connecting the inlet and outlet headers. Each flow channel is orificed at the return header to maintain a constant channel exit wall temperature across the heat source plate.

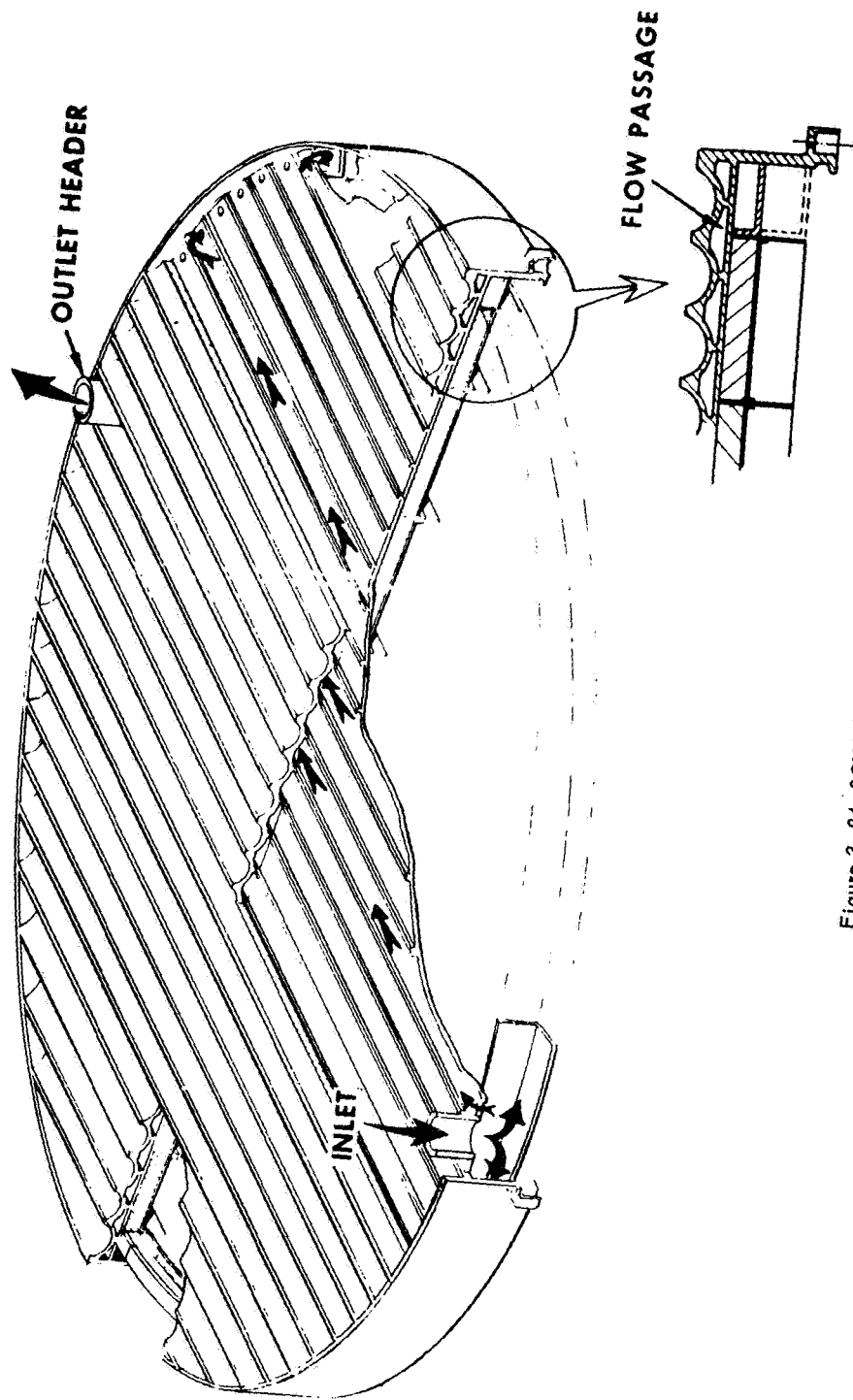


Figure 3-84 SCHEMATIC OF ACHX

The ACHX header which surrounds the heat source plate is baffled to separate the inlet and outlet headers. There are two 1.5-inch-diameter connections to each of the inlet and outlet headers for connection of the cooling air used during fuel capsule loading, transportation, and launch pad operation. The inlet and outlet connections are provided with quick disconnect devices to allow easy and expeditious hookup with either a portable or launch tower coolant supply and circulation system. This device also allows an easy separation of cooling lines when the system is committed to launch. This is described in further detail in Subsection 5.3.

3.3.3.1.1 Hydraulic Performance -- The auxiliary cooling system requirements were established based on flowing air (or nitrogen) in parallel through the ACHX channels. Variation in flow rates from channel to channel was required because of the variation of the number of capsules in each row across the diameter of the circular heat source. Control of the channel flow was achieved through the equalization of pressure drop by orificing the channel exits. Because of the sensible temperature rise of the coolant fluid, the exit wall temperature at the coolant exit would be the hottest temperature along the channel. The temperature drop around the capsule from the capsule hot spot to the channel wall is fairly constant along a channel since very little heat is transferred axially along a channel. The hottest capsules would, therefore, be those capsules located adjacent to the channel exits. If a peak capsule temperature is specified for the heat source array, then the two-dimensional steady-state temperature distributions determine the maximum allowable wall temperature at any exit. The exit wall temperature is the sum of the sensible temperature rise of the coolant, the wall to fluid film temperature drop, and the inlet temperature. For a given heat load to any channel, the mass flow rate, therefore, uniquely determines the peak capsule temperature for a specified coolant inlet temperature.

A model was established to calculate the channel mass flow rates to cool the heat source for a particular heat load distribution corresponding to the preliminary design. The model was based on the assumption that coolant through each channel picked up one-half of the heat generated from each capsule adjacent to the channel. Flow parameters upon which parametric calculations were based include the coolant inlet pressure and temperature, the coolant properties, and the exit wall temperature.

The model calculated the mass flow rates required for each channel having the same exit wall temperature based on the following heat transfer equation:

$$T_{\text{exit wall}} - T_{\text{coolant in}} = \frac{Q}{m c_p} + \frac{Q}{h A}$$

where the heat transfer coefficient is determined by the relation:

$$Nu = 0.021 Re^{0.8} Pr^{0.4} \left(\frac{T_w}{T_b} \right)^{-0.5} \left(1 + \left(\frac{D}{L} \right)^{0.7} \right)$$

The pressure drop and orifice equations used to determine the required orifice size to provide the proper mass flow rate distribution across the array of channels were the following:

$$\Delta P = \frac{G^2}{2 g_c P_1} \left\{ (K_c + 1 - \sigma^2) + 2 \left(\frac{P_1}{P_2} - 1 \right) + f \left(\frac{A}{A_x} \frac{P_1}{P_m} + \frac{4Le}{D} \right) + Cl - (1 - \sigma^2 - K_e) \frac{P_1}{P_2} \right\} \quad (\text{Ref. 3-25})$$

$$f = \left(0.0014 + \frac{0.125}{Re_w^{0.32}} \right) \left(\frac{T_b}{T_w} \right)^{0.5}$$

$$Cl = (1 - \beta^2)(1 - \beta^4) \frac{1}{\beta^4} - \left(\frac{1}{c} \right)^2 \frac{1}{Y^2} \quad (\text{Ref. 3-26})$$

$$Y = 1 - \frac{1-r}{K} (0.41 - 0.35 \beta^4) \quad (\text{Ref. 3-26})$$

$$\beta^2 = \frac{A_{\text{orifice}}}{A_{\text{channel}}} \quad (\text{Ref. 3-26})$$

$$r = P_{\text{orifice}} / P_{\text{upstream}} \quad (\text{Ref. 3-26})$$

$$C = 0.6$$

For the preliminary design, the orifice sizes were based on standard orifice data for circular plates in cylinders as presented in Perry (Ref. 3-26). By specifying a percent of the total pressure drop in the largest channel to be across the orifice for that channel, the orifice size and total pressure drop was specified for a known channel mass flow determined by the heat balance. Orifice sizes for other channels were determined for the same total pressure drop and the channel mass flow rate.

Channel mass flow rates, channel velocities, total mass flow rate, and total channel head losses were determined parametrically for various inlet temperatures and pressures, percent orifice pressure drops, and exit wall temperatures.

Figure 3-85 shows the effect of the percent orifice pressure drop and pressure level on the total head loss for a particular inlet temperature and exit wall temperature. As shown, the obvious trends are to increase pressure and decrease the percent orifice pressure drop to minimize the channel velocities and thus channel head loss. Since larger percent orifice pressure drop tends to stabilize flow conditions, a tradeoff occurs between pumping power requirements and stability. Such a tradeoff cannot be easily defined and depends upon factors outside the scope of this project such as the launch pad cooling system power supply system. Therefore, as pressure drop of 30 percent was selected for this analysis for preliminary sizing of the orifices.

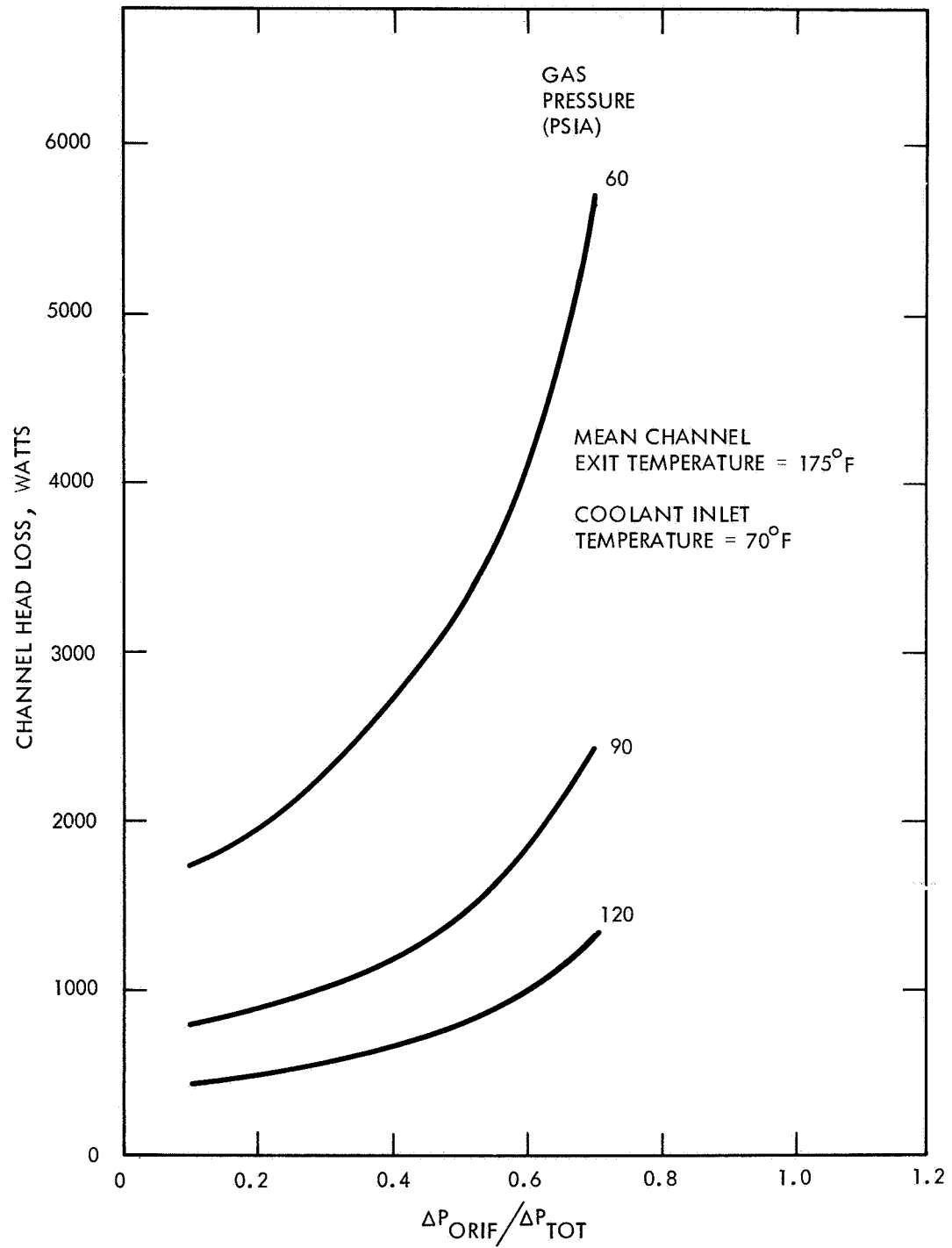


Figure 3-85 WALL EFFECT OF ORIFICE PRESSURE DROP ON CHANNEL HEAT LOSS

The analysis of the ACHX showed that one of the critical design limitations on the ACHX was the size of the inlet tube headers. Because of the large total mass flow rates required and the available space for routing the inlet ducts, Mach numbers of 0.3 or greater were necessary in the inlet tubes and influenced the determination of the pressure level. Figure 3-86 presents a performance map of peak capsule temperature versus total mass flow rate for lines of inlet constant temperatures. This data is presented for a steady-state temperature drop across a 2-mil air gap from the capsule to the cradle. Cross-plotted are the inlet tube Mach numbers corresponding to an inlet pressure of 90 psi. As shown here for a coolant inlet temperature of 70° F, corresponding to standard day conditions, a mass flow rate of 3.13 lbm/sec is required to limit the peak capsule temperature to 350° F.

Variation of inlet pressure results in the variation of inlet tube Mach number as shown in Figure 3-87 for a 350° F peak capsule temperature and several inlet temperatures. As shown here, pressures below 60 psi are not desirable because of the excessive inlet tube velocities required. The selection of 90 psi was made somewhat arbitrarily over a reasonable range of pressure levels from the standpoint that the inlet tube velocities were of a manageable level and increased pressure levels did not significantly reduce the velocities.

The coolant flow requirements selected based on the above results are summarized in Table 3-21 for the nominal steady capsule temperature distribution. The design point requirement is 3.13 lb/sec of air at 90 psi and 70° F inlet temperature to maintain a peak capsule temperature of 350° F. The orifice sizes for the cooling channels are presented in Figure 3-88 for this design point.

TABLE 3-21

ACHX PERFORMANCE SUMMARY

Fluid	Air or Nitrogen
Coolant inlet pressure	90 psi
Coolant inlet temperature	70° F
Maximum capsule temperature	350° F
Mean channel wall exit temperature	171° F
Mean coolant outlet temperature	104° F
Outlet pressure	88.4 psi
Mass flow rate	3.13 lbm/sec
Peak channel velocity	102 ft/sec
Inlet tube velocity	425 ft/sec

The 70° F inlet temperature is readily obtainable without provision for precooling the coolant supply unless the ambient conditions exceed this temperature. Although ambient temperatures may be as high as 110° F with reasonable probability, such ambient conditions are not expected to greatly hinder the ACHX since the mass flow

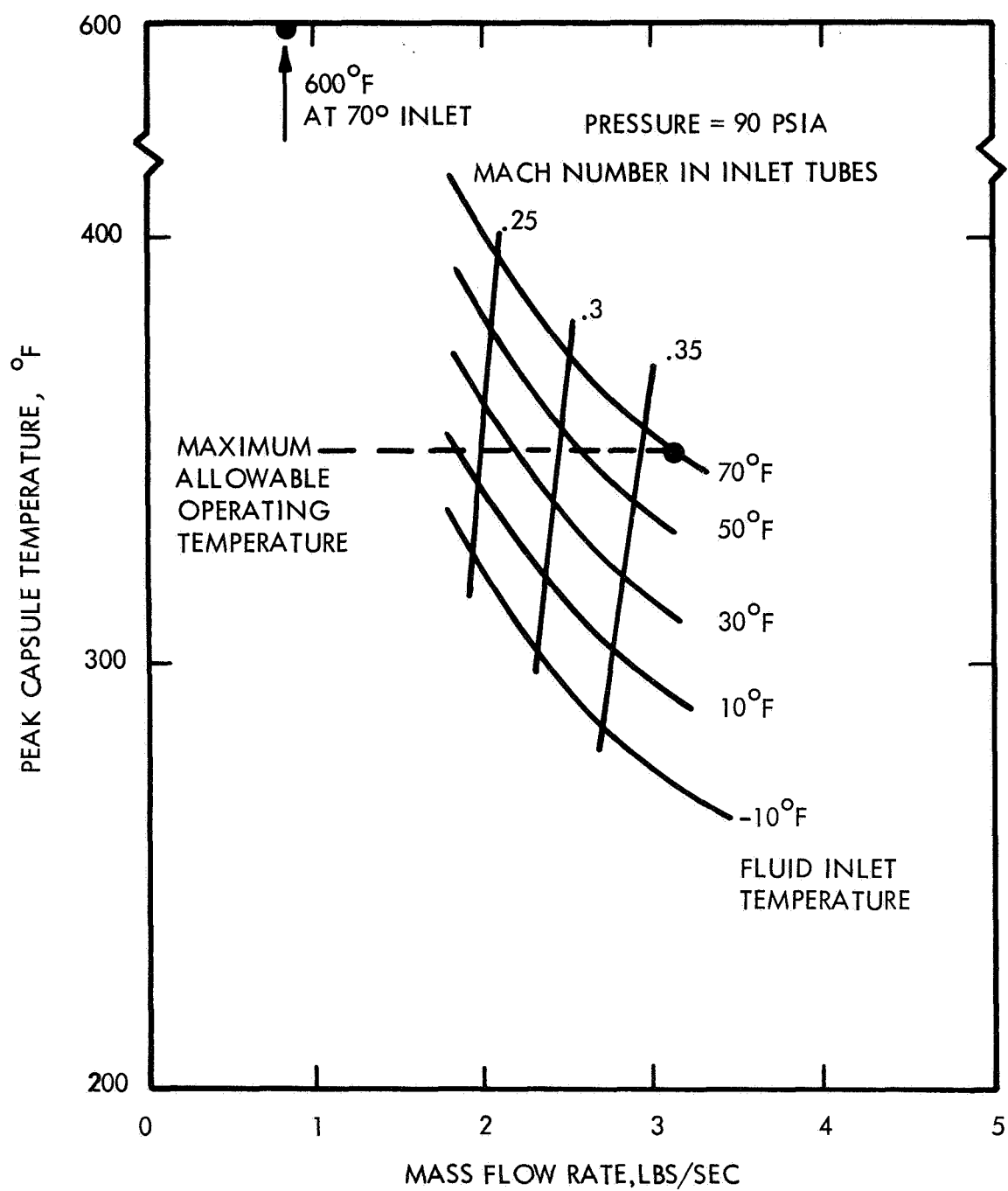


Figure 3-86 PERFORMANCE MAP OF PEAK CAPSULE TEMPERATURE VERSUS TOTAL MASS FLOW RATE

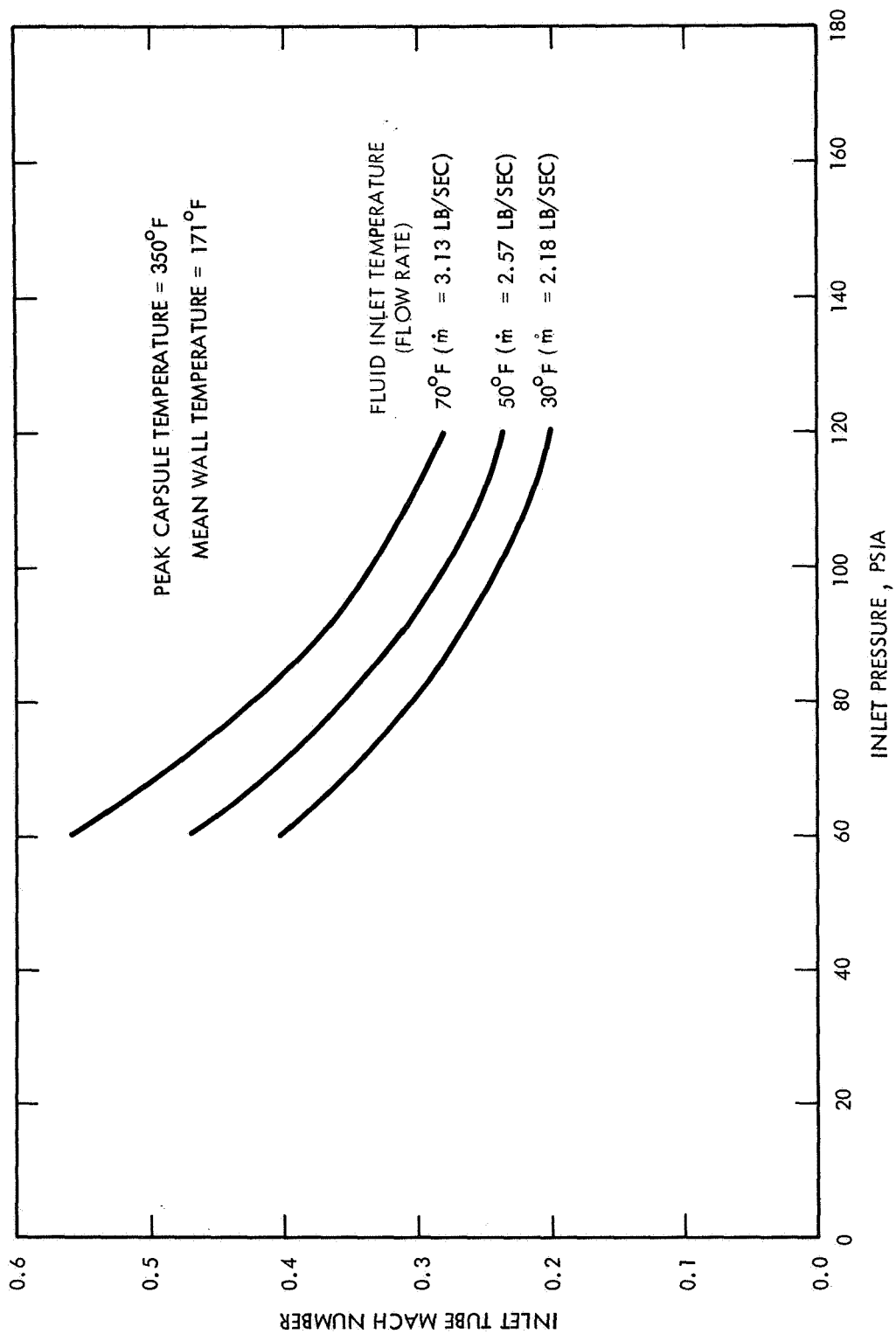


Figure 3-87 ACHX HYDRAULIC PERFORMANCE FOR A PEAK CAPSULE TEMPERATURE OF 171°F

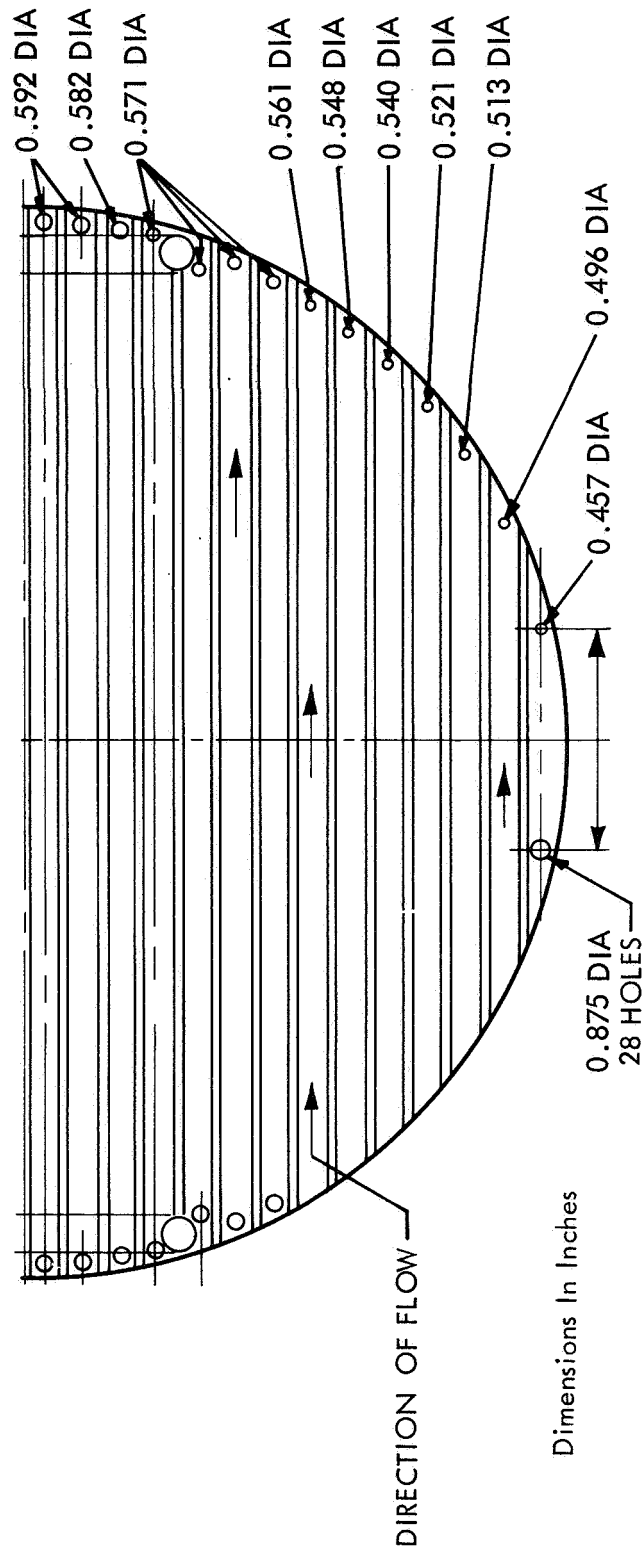


Figure 3-88 ACHX ORIFICE HOLES THROUGH TOP PLATE

rates can be increased to compensate. Furthermore, a margin of safety is built into the calculations due to the use of a conduction temperature drop across a 2-mil air gap between the capsule and capsule support plate considered to be very conservative.

3.3.4 Insulation Subsystem

One of the major design objectives was to limit the total heat loss from the IRV and Brayton cycle equipment to 1500 watts during normal operating conditions. Of this total, approximately 50 percent loss from the heat source side was established as a design goal. Several design features were used to minimize the heat loss, the most obvious being the inclusion of multifoil insulation around the heat source. During Phases IA and IB, a 2-inch layer of superinsulation was used.

Close scrutiny of superinsulation indicated that it was designed and optimized for a lower temperature range than is of interest for the IRV and that, furthermore, very little performance data is available at higher temperatures. In addition, no fabrication assembly information was available. Consequently, in the early stage of the Phase II effort, the superinsulation system was replaced by a Thermo Electron Corporation (TECO) multifoil insulation that is better characterized for use at the IRV temperature levels. The multifoil insulation system described in the following paragraphs has been designed with the assistance and cooperation of TECO.

Other design features employed to minimize heat losses were the provision of a strut design with a minimum ratio of cross section area to strut length and the provision of a Min-K 2020 material insulation ring at the joint between the heat source insulation system and the HSHX insulation system to avoid a "shine-through" (direct path) heat loss.

3.3.4.1 Thermal Insulation Design

The multifoil insulation system recommended by TECO consists of 100 layers of zirconia-coated molybdenum foil insulation. The 0.5-mil molybdenum foil is sprayed with particles of zirconia and stacked together to form the thermal barrier. Insulation layers are held together by several ZrO₂ pins which are located approximately one pin to each square foot of insulation to prevent the layers from sliding with respect to one another.

The weight of the multifoil insulation has been calculated to be 59 pounds, based on 0.5-mil foils. Although the TECO experience to date has been primarily with foils equal to or thicker than 1 mil, it appears a reasonable extension of the current technology and appears feasible to consider 0.5-mil foils in the preliminary design. If necessary a 1-mil foil system can be considered at the expense of an increased weight of 59 pounds. The added volume can be readily incorporated into the preliminary design.

The multifoil insulation is supported by the insulation support plate. This member is a titanium plate with eight radial stiffening ribs, a side skirt, and a flange which interfaces with the aeroshell as shown in Figure 3-89. Three positioning pins, spaced 120 degrees apart, position the insulation relative to the heat source plate.

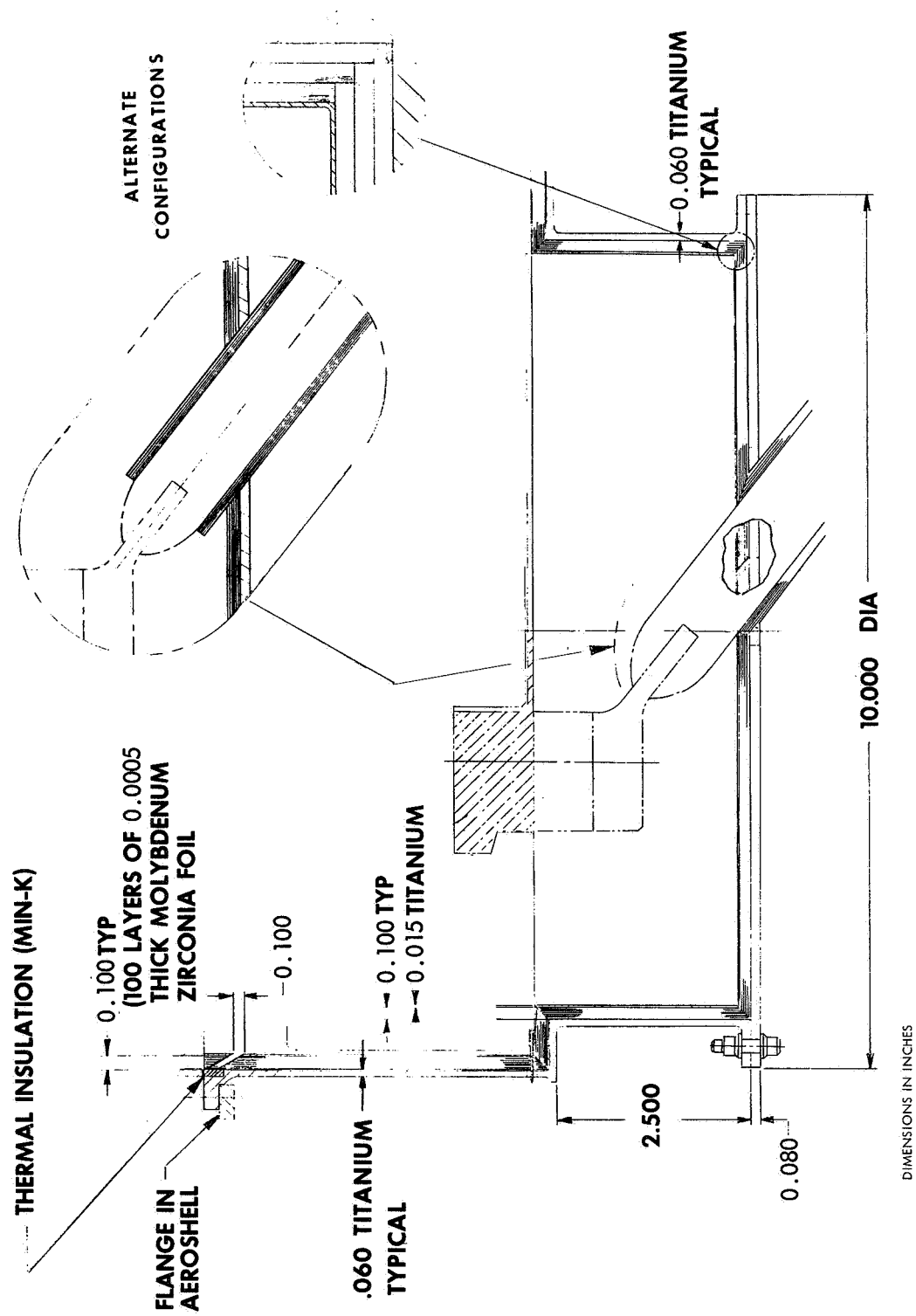


Figure 3-89 HEAT SOURCE INSULATION DETAIL

Penetrations in the insulation for the truss connections which support the heat source plate are located 90 degrees apart. These are in the form of cups, 10.5 inches in diameter and 2.58 inches deep, with a bottom plate which splits around the struts. The interface joint which mates with the Brayton cycle insulation shows the insulation joined on a 30-degree angle with an axial gap of 0.100 mil to eliminate the possibility of any long-term bonding between the two insulation systems. A Min-K 2020 type insulation ring is then located outside of the insulation barrier to minimize the effects of direct "shine-through" to the aeroshell.

Although the thermal performance data currently available from TECO are promising, it should be noted that there are a number of areas of further technology development work which need to be investigated. The thermal performance of a multifoil insulation system, after it has been subjected to a vibration environment similar to a missile launch condition, must be evaluated. Various joint designs and heat losses associated with each joint type should be determined. Since the TECO experience has been with 1-mil or thicker metal foils at a modest size of about 6-inch diameter to date, the fabrication and assembly of a large insulation system using 0.5-mil foils requires further development effort.

3.3.4.2 Insulation Support Plate Structure

The insulation plate is 0.06-inch thick with a radius of 26.87 inches. The insulation system must survive launch only (9g). It must support insulation weight and its own weight (59 + 12.5 lb).

$$\text{Load} = (W_i + W_p) g$$

$$W = 644 \text{ lb}$$

Now for simply supported edges, the maximum stress is given by

$$\sigma_{\max} = \frac{3W}{8\pi m t^2} (3m + 1)$$

where

$$m = (\text{Poisson's ratio})^{-1}$$

$$\sigma_m = 70,500 \text{ psi}$$

And for built-in edges

$$\sigma_{\max} = \frac{3W}{4\pi T} 2$$

$$\sigma_m = 42700 \text{ psi}$$

For titanium with $\sigma_y = 85 \text{ ksi}$ at 500° F (at launch)

$$\text{f.s.} = \frac{85}{78.5} = 1.21 \text{ (minimum)}$$

3.3.4.3 Insulation System Heat Loss

3.3.4.3.1 Insulation Specification and Data Base -- The heat loss calculations were based on the following performance data, supplied by TECO.

- Mo-ZrO₂ planar heat flux curve (Figure 3-90)
- Corner and joint losses based on overlap corner data (Figure 3-91)

Nominal temperatures used for the heat loss evaluation were 1900° F hot side and cold side.

3.3.4.3.2 Component Evaluation -- Estimates were made of the four heat loss components through the heat source insulation. For the heat losses through the planar insulation sections, the heat flux data in Figure 3-90 was suggested by TECO as being most probable. A very conservative heat flux was also recommended by TECO for development of the pessimistic estimate of the insulation performance.

For evaluation of the total heat losses through the insulation, the following components were analyzed:

- Insulation Plane

$$\begin{aligned} \text{Area} &= (\pi) (50) (4) = (\pi) (50)^2/4 = (\pi) (10) (2) (4) \\ &= 2833 \text{ in.}^2 = 18250 \text{ cm}^2 \end{aligned}$$

Based on Figure 3-90 (corrected to 100 foils)

$$(q/A) \text{ most probable} = (0.012 \text{ watt/cm}^2) (40/100) = 0.0048 \text{ watt/cm}^2$$

$$(a/A) \text{ pessimistic} = 0.015 \text{ watt/cm}^2$$

$$Q_{\text{most probable}} = (0.0048) (18250) = 87.6 \text{ watts}$$

$$Q_{\text{pessimistic}} = (0.015) (18250) = 274 \text{ watts}$$

- Positioning Penetrations

Assume: 15 penetrations (1-ft²)

ceramic (ZrO₂)

O.D. = 0.1 inch

Poor contact between ZrO₂ and Cb-1-Zr ($h = 100 \text{ Btu/hr-ft-}^\circ\text{F}$)

$$\frac{1}{U} = \frac{X}{K} + \frac{1}{h} = 0.0236 = 0.01$$

$$U = 29.8 \text{ Btu/hr-ft}^2\text{-}^\circ\text{F}$$

$$Q = (15) (29.8) (\pi) (0.1)^2 (1600)/4/144/3.413 = 1.4 \text{ watt}$$

For the effect of penetrations on insulation

$$\frac{Q'}{Q} = 1.9$$

$$Q' = (1.9) (11.4) = 22 \text{ watts}$$

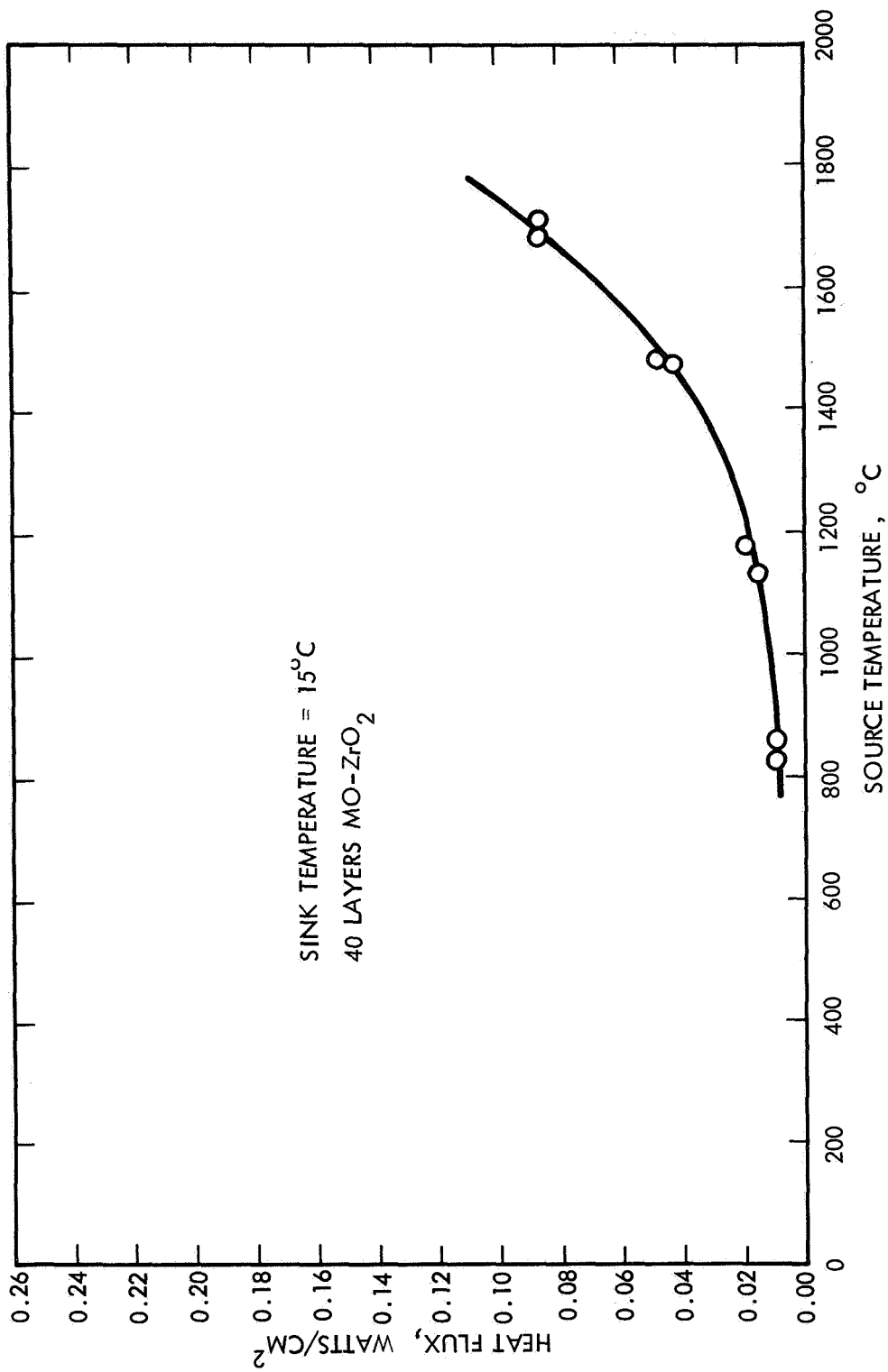


Figure 3-90 PLANAR HEAT SOURCE FOR MULTI-FOIL INSULATION

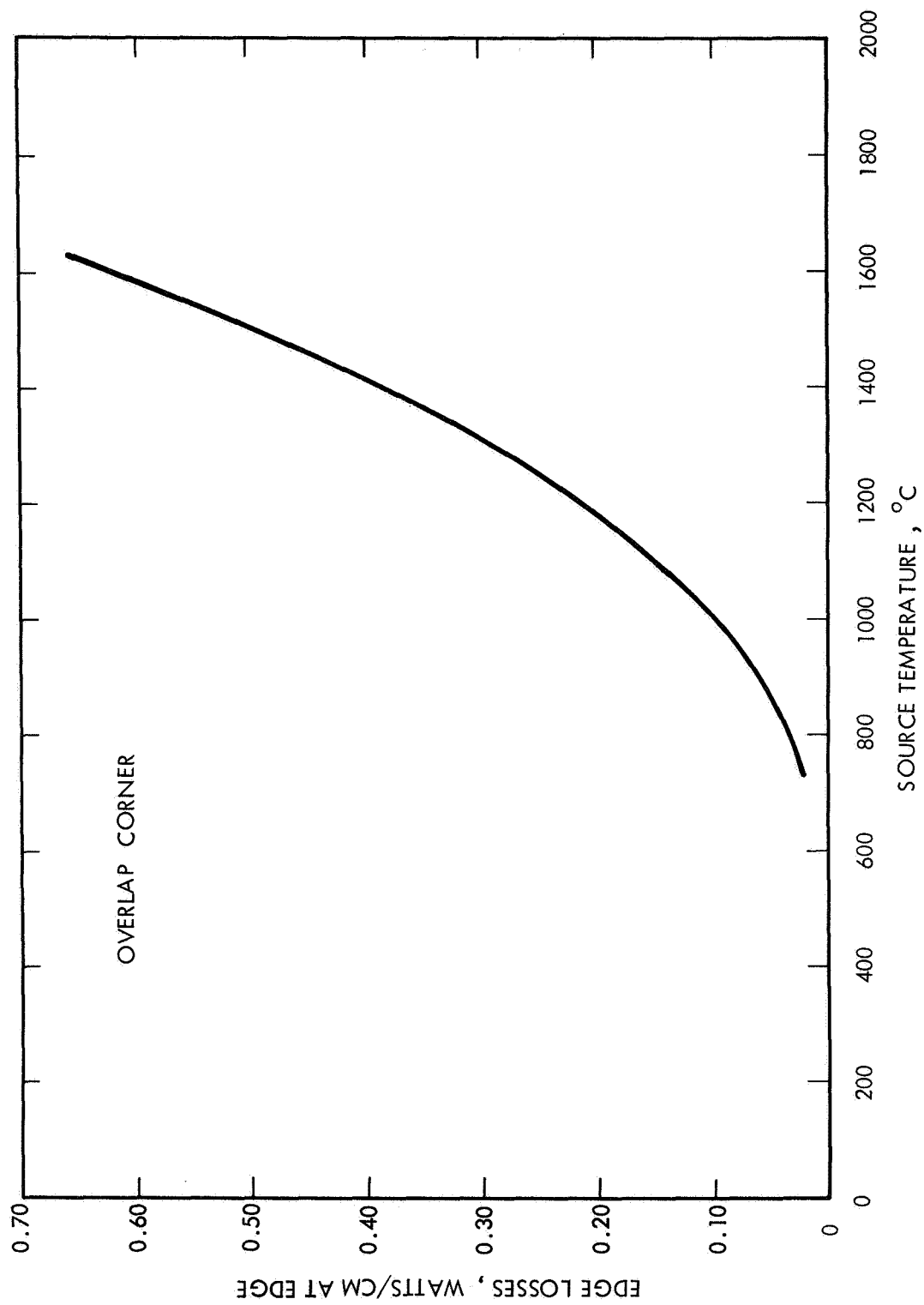


Figure 3--91 EDGE THERMAL LOSSES FOR MULTI-FOIL INSULATION

- Insulation Edge Losses

From Figure 3-91

$$(q/L)_{\text{most probable}} = 0.125 \text{ watt/cm}$$

Total edge length

$$L = (\pi) (50) + (\pi) (10) (2) (4) + (4) (10) + (8) (\pi) (1) \\ = 475 \text{ in.} = 1200 \text{ cm}$$

$$Q_{\text{most probable}} = (0.125 \text{ watt/cm}) (1200 \text{ cm})$$

$$Q_{\text{most probable}} = 150 \text{ watts}$$

$$Q_{\text{pessimistic}} = 150 \text{ watts}$$

- HS-HSHX Joint Loss

$$L = (\pi) (50) = 157.5 \text{ in.} = 400 \text{ cm}$$

By treating this joint as a right angle corner loss as recommended by TECO, use same q/L as above.

$$Q = (0.125) (400) = 50 \text{ watts}$$

3.3.4.3 Heat Loss Summary

Based on the heat loss components evaluated above, the summary of heat losses is presented in Table 3-22 for a nominal hot side temperature of 1900° F and a nominal cold side temperature of 300° F. Strut heat loss components are taken from paragraph 3.3.5. The most probable heat loss was estimated to be 498 watts and the pessimistic estimate was 684 watts. These heat loss estimates represent the losses from the heat source only (HSHX heat losses are evaluated elsewhere) and meet the design objectives noted earlier.

3.3.5 Truss Subsystem

3.3.5.1 Mechanical Design

The basic heat source support system consists of a support ring with a scalloped circular tie plate (Cb-1Zr) and eight hollow struts (T-111) which are connected to four pads at the top and the bottom ends of the struts. The top four pads are bolted to the support ring. Bottom pads are bolted to a ring located on the reentry vehicle aeroshell. The struts penetrate the insulation plane at eight locations. Insulation is wrapped around the strut and tapered toward the strut bottom. Design details are shown in Figures 3-92 and 3-93.

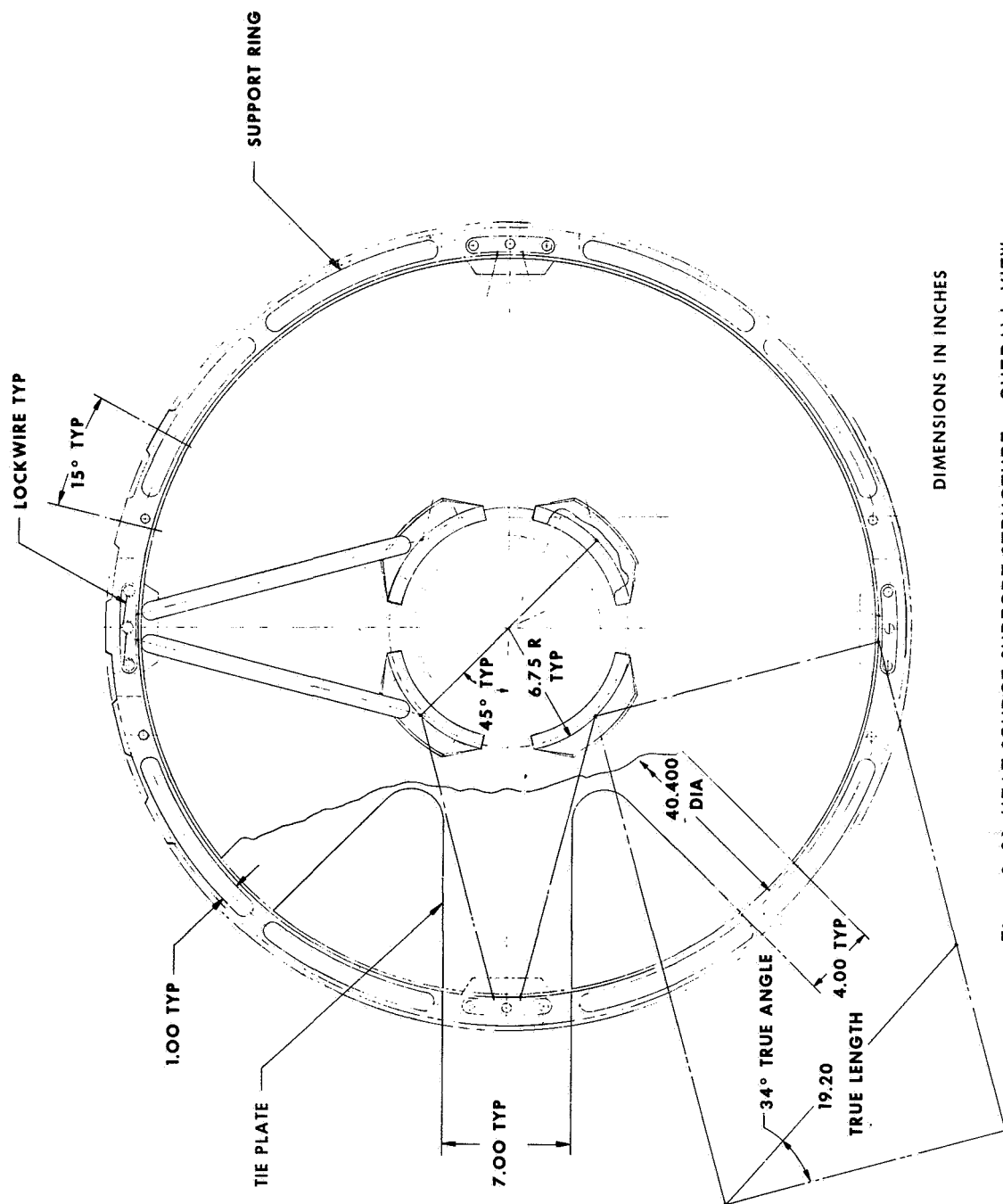


Figure 3-92 HEAT SOURCE SUPPORT STRUCTURE -- OVERALL VIEW

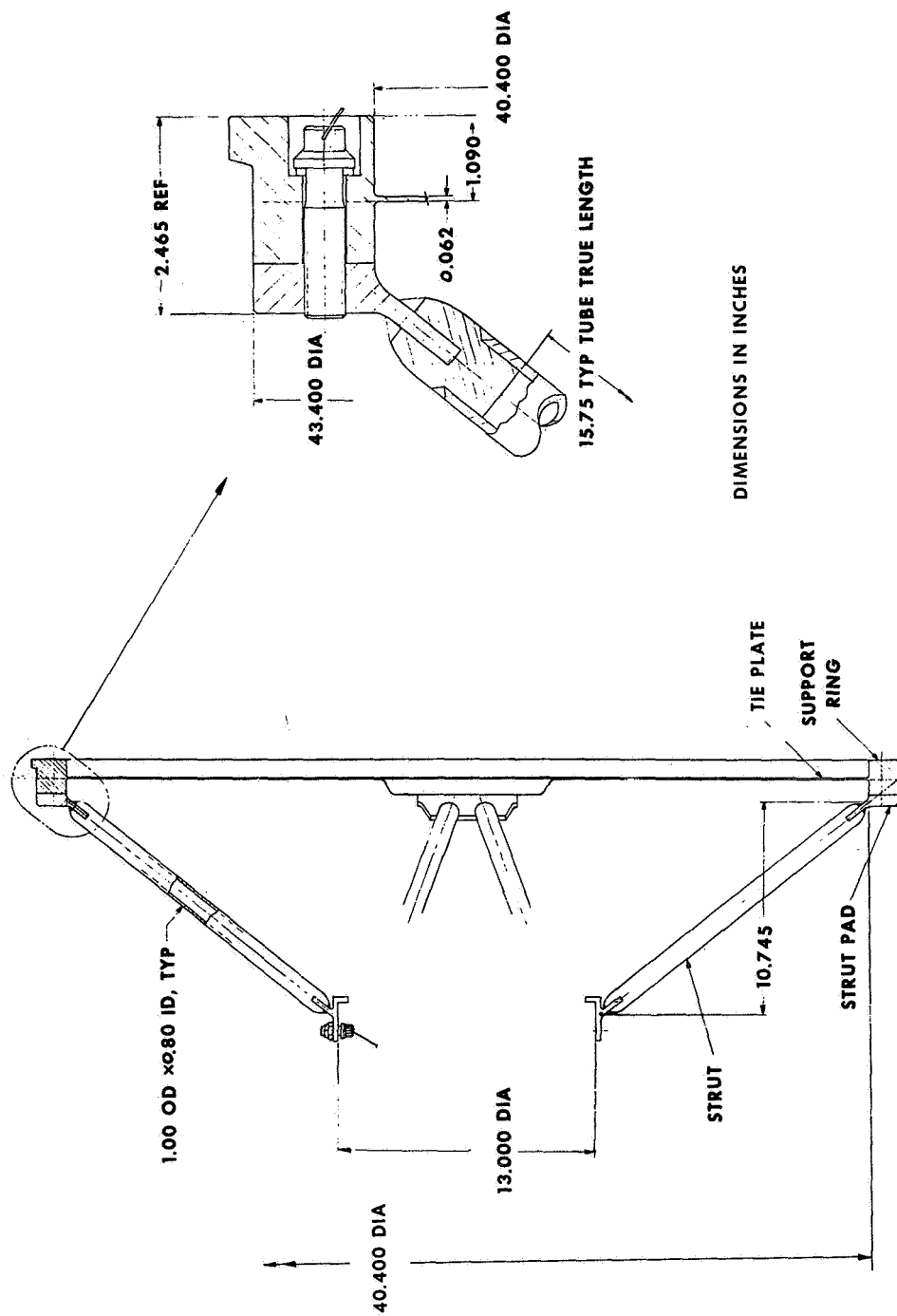


Figure 3-93 HEAT SOURCE SUPPORT STRUCTURE -- DETAIL VIEW

TABLE 3-22

HEAT SOURCE HEAT LOSS SUMMARY

	Heat Losses (watts)	
	Most Probable	Pessimistic
Insulation Plane	88	274
Insulation Positioning Penetrations (15)	22	22
Insulation Corners	150	150
HS-HSHX Joint	<u>50</u>	<u>50</u>
Total Insulation	310	496
Strut	175	175
Strut Insulation	<u>13</u>	<u>13</u>
Total Strut	188	188
Heat Source Heat Loss	498	684
Hot Side Temperature = 1900° F		
Cold Side Temperature = 300° F		

During Phase II, in an effort aimed at achievement of a minimum diameter reentry vehicle, the heat source was positioned as close to the aeroshell nose as feasible. This resulted in a shortened truss system with 19.2-inch struts (22-inch struts were used in Phase IB) and a shallower strut angle, 34 degrees, with respect to the heat source plane (reduced from 45 degrees in Phase IB). During the Phase IB effort, bi-metal struts with T-111 refractory alloy at the hot end (top) and Rene 41 super-alloy at the cold end (bottom) were considered for the truss system design to reduce the heat loss. However, it was a complex structure to design and fabricate. As a result the simpler single material strut design is recommended, on the assumption that the resultant heat leaks are acceptable.

The load environments of paragraph 3.3.2.1 apply with the worst-load condition associated with the early launch abort reentry.

3.3.5.2 Structural Analysis

The major components of the truss support system and corresponding areas of predominating structural requirements are:

- Struts -- Combined lateral and axial g-loads for the worst case ascent abort reentry applied in least favorable vehicle orientation; and truss bending stress due to thermal expansion/contraction of the heat source plate.

- Support Ring and Tie Plate -- Same worst load condition as struts.
- Truss Attachment Bolts -- Designed to withstand worst case reentry loads but to shear on impact.

The structural performance of these components is summarized in the following paragraphs and presented in detail in Appendix A, Section A3.0.

3.3.5.1.1 Struts -- The struts are designed to survive the axial compressive stresses and buckling imposed during the worst case reentry. These reentry loads, which are discussed in paragraph 3.3.2.1, are 38.0 g axial and 3.0 g lateral including a design 1.25 factor of safety and are assumed to occur simultaneously. Because of symmetry only a 45 degree segment of truss system need be considered for defining the worst vehicle orientation for the application of the lateral load. Referring to Figure 3-92, this segment is bounded by planes through the centers of adjacent upper and lower attachment points and intersecting along the vehicle axis. It was determined that orientations resulting in the application of the lateral g-load being centered at either end of this arc were more severe than intermediate positions along the arc. The worst case orientation, and hence design condition, is with the center of application of the lateral load being in a plane through one of the lower truss/aeroshell ring attachment points and the vehicle axis. For this condition the combined axial and lateral reentry loads result in a maximum axial strut load of 14,650 pounds. The required cross-sectional area is 0.278 in.² to limit the stress in the T-111 strut to the yield stress of 53,000 psi at the 500° F design temperature. For the 1.0-inch O.D. struts, this results in a 0.8-inch I.D.

The load capability of the strut based on buckling criteria is over 200 g. Thus, while the cross-sectional area must remain as established for the yield stress requirement, it would be possible to use a smaller O.D. and I.D. strut. However, since built-in ends, which cannot be achieved in reality, were assumed in determining the buckling capability and making additional allowance for the fact that the struts may also see some deflection-dependent end moments, the excess capability is conservatively retained. Optimizing the strut diameters to minimize weight is unnecessary since the cross-sectional area is fixed by yield stress requirements.

The strut stress resulting from bending due to relative thermal growth of the heat source plate during heatup to operating temperature was also considered. During launch pad operation, the system is held in equilibrium at about 350° F. Upon launch, the ACHX cooling is terminated and the heat source begins to heat up. Assuming that the truss does not thermally adjust, the struts will experience bending to accommodate the radial expansion of the heat source. For a heat up to 2000° F, the bending stress in the strut pads is 13,700 psi. This would present no problem and is quite conservative since the truss is in good thermal contact with the heat source and would therefore thermally adjust better than assumed. Furthermore, any thermally induced bending stresses are expected to relax with time at the elevated temperature.

3.3.5.1.2 Support Ring and Tie Plate -- The truss system support ring provides an attachment retainment for remote assembly of the heat source to the IRV. The ring is attached to the truss at four positions 90 degrees apart and transposes the four point truss support into a distributed peripheral support of the heat source plate near its perimeter. The ring and its tie plate also contain the radial loads induced by the angular configuration of the truss design. The

structural design of the support ring is determined by the ascent abort reentry loads (worst condition).

Since the struts are at an angle to the support ring, it is subjected to both vertical (axial) and radial loads. To minimize the structural weight a 0.060-inch tie plate is incorporated within the support ring to help sustain the radial loads and limit the radial deflection rather than impose additional loads on the mating housing of the heat source support plate. The tie plate, scalloped to further minimize weight, is welded to the support ring in the region of each of the four truss attachment points. The radial load at each quadrant is 17,700 pounds requiring a 7-inch tie width weld for weld stress of 30,000 psi. The resultant radial deflection for this design under the worst load condition is 0.121 inch with an accompanying bending stress in the ring of 13,000 psi and a hoop tension stress of 1,330 psi. If the heat source support plate mating housing acts to assist in limiting the radial deflection, these stresses would be reduced and they, therefore, represent the upper limit.

The vertical (axial) component of the truss-support reactive load is circumferentially distributed. As a consequence, the support ring also experiences flexure about an axis parallel to the plane of the ring. These bending stresses due to plate loading were determined by assuming that the ring-plate interface loading could be approximated by beam-on-elastic foundation theory. The heat source plate was assumed to have a constant foundation modulus while in actuality the plate would deform to have its entire periphery supported. A truss support ring width of 1.50 inches was selected, and the ring thickness determined to allow the truss to adequately support the heat source support plate during the worst design condition while not overstressing the ring. The circumferentially varying load is a maximum at the locations of the truss attachments where the maximum bending stresses occur. The interface pressure decreases with distance from this peak to one-half the peak value at about 5 inches and it approaches zero at about 12 inches. Hence, the ring thickness is similarly reduced to minimize weight and as shown in Figure 3-92 further weight reduction is accomplished by slots machined in the ring cross section in the lightly loaded region. These reductions are based on limiting maximum stress in the Cb-1Zr ring to the 33,000 psi allowable yield stress at 500° F for the worst case ascent abort reentry design condition. This structural performance is dependent upon attaining the proper range of foundation modulus ($K_p \approx 69,000 \text{ lb/in.}^2$) for final design of the heat source plate. If the modulus is very high the interface pressure on the heat source plate could be excessive and if the modulus is very low the support ring could be overstressed.

3.3.5.1.3 Truss Attachment Bolts -- The bolts which attach the support truss to the aeroshell interface ring at the lower end and to the support ring at the upper end were sized to withstand the reentry loads but to shear on impact before the struts fail. This further minimizes the potential for the struts to be an impalement hazard to the fuel capsules on impact by permitting them to fold in rather than bend or buckle. For an aeroshell bolt temperature of 350° F, the allowable bolt shear stress is 60,000 psi resulting in a total bolt shear area requirement of 0.274 in.² This requirement is met by the two 0.438 inch UNF bolts in each of the four lower attachments. For the upper attachment bolts a higher temperature, 1500° F, was used and for the corresponding allowable shear stress, 40,000 psi, the required bolt shear area is 0.45 in.² The three 0.5-inch diameter UNF bolts in each of four upper attachments satisfy this requirement.

Under a vertical impact the bolts will fail at 45.5 g load while the struts can survive up to 50.8 g vertical load. Under non-vertical impact, the bolts will still shear first but at lower g-loads.

3.3.6 Heat Source Preliminary Design

The IRV heat source preliminary design is shown on Figure 3-94. The heat source consists of three basic assemblies: the heat source support plate assembly, a thermal insulation barrier, and the structural support system. The heat source support plate assembly contains: the radioisotope fuel capsules; a beryllium oxide heat sink; and the auxiliary cooling heat exchanger (ACHX), which is required to maintain the temperature of the heat source below the oxidation level of refractory metals, during fuel capsule loading, transportation, and launch pad operation.

A thermal insulation battier which is a self-supporting assembly has been designed to minimize the heat loss from heat source and to facilitate assembly and deployment of the heat source in space. It consists of 100 layers of zirconia-coated molybdenum insulation stacked together to form a thermal barrier. The insulation assembly also includes the insulation support system which supports and sandwiches the insulation between the heat source plate and the support structure.

The structural support system which physically attaches the heat source to the reentry vehicle is a basic eight-leg truss design, capable of withstanding all launch, abort, and reentry conditions. It has been designed on a reasonable compromise between minimum weight and minimum thermal conduction loss through individual struts.

Attachment of the heat source plate assembly to the support system is accomplished by a simple breech lock mechanism which eases assembly or disassembly during launch pad operation. Two lifting lugs have been incorporated into the heat source plate, for lifting and handling the assembly during launch pad operation. They are removed prior to launch.

Due to the differential thermal expansion anticipated, all dimensions have been calculated as hot dimensions at operating temperature. The diameter of the heat source plate assembly at operating temperature is 49.0 inches. This dimension includes a 0.4-inch increase in diameter from room temperature. Support structure and thermal insulation barrier have also been dimensioned in the hot condition. The total weight of the heat source assembly is 1476 pounds. Table 3-23 shows a breakdown of component parts and mass moments of inertia.

3.3.6.1 Heat Source Plate Assembly

The heat source plate assembly shown in Figure 3-95 has been designed as a minimum weight, minimum diameter structure. It is fabricated from Cb-1Zr refractory material capable of withstanding the high temperature requirements in space environment. The circular planar configuration, 49.0 inches in diameter, supports and contains the 164 PuO₂ fuel capsules which are arranged in 27 rows with 1.73-inch centerline spacing. The capsule spacing and overall heat source plate diameter were optimized from thermal and mechanical analysis considerations. Included in the heat source plate assembly are the auxiliary cooling heat exchanger (ACHX), a beryllium heat sink and the capsule retention cover plate.

The fuel capsule cradles are fabricated sections welded together to form the heat source plate. Incorporated into the section are the ACHX cooling channels which run parallel between capsule rows. Designed into the support plate, Figure 3-96,

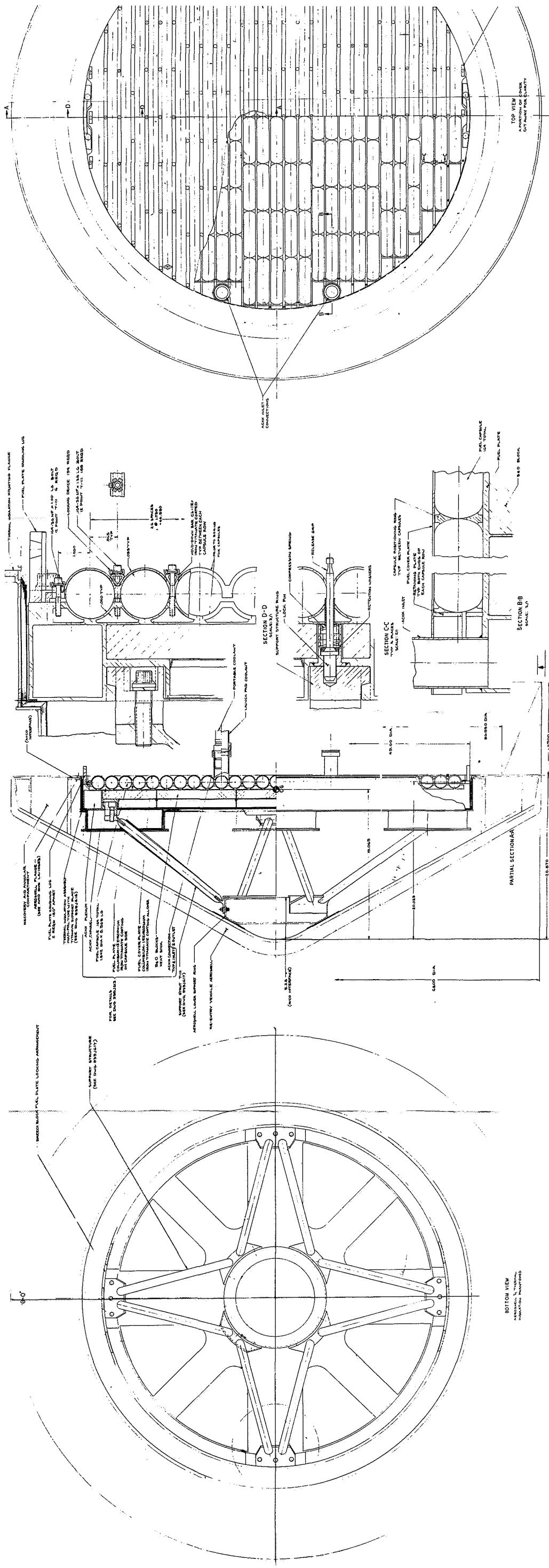
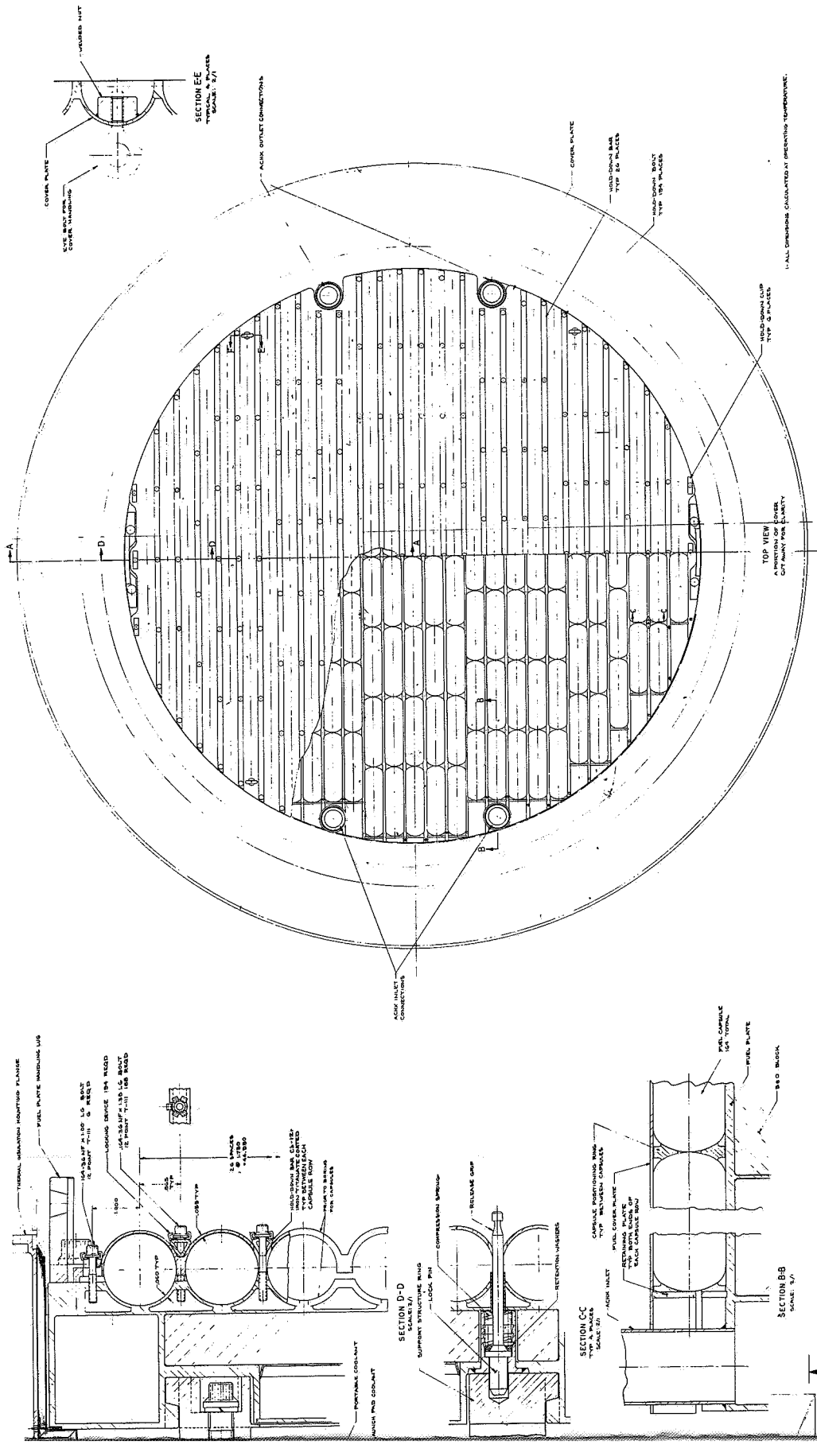
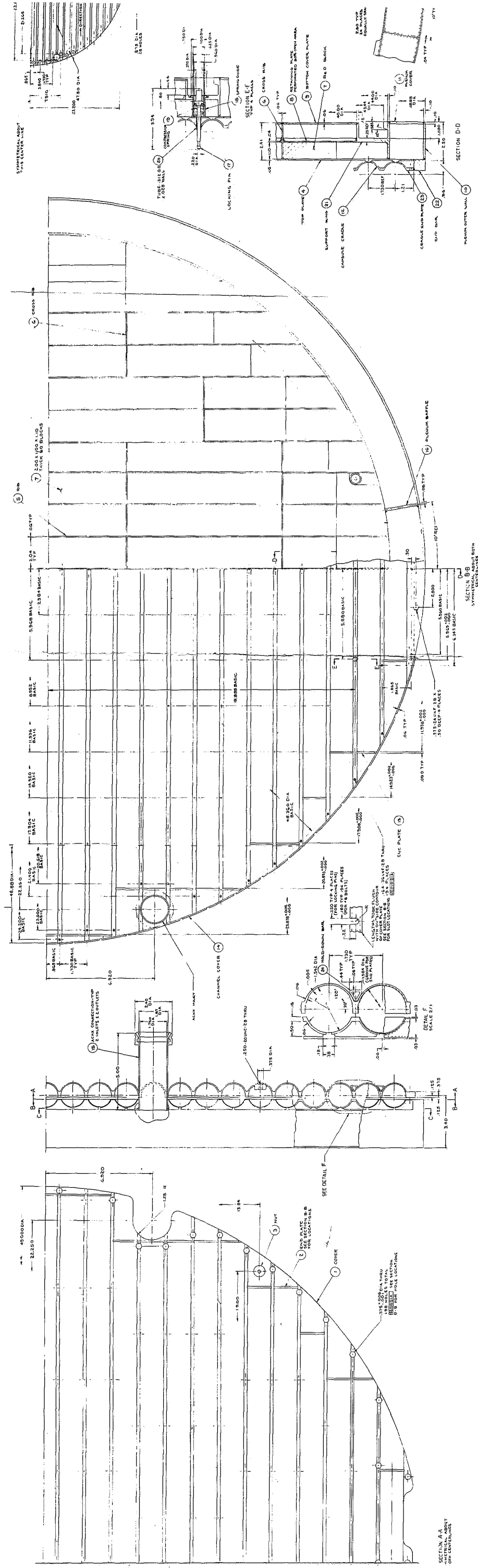


Figure 3-94 IRV ASSEMBLY

2



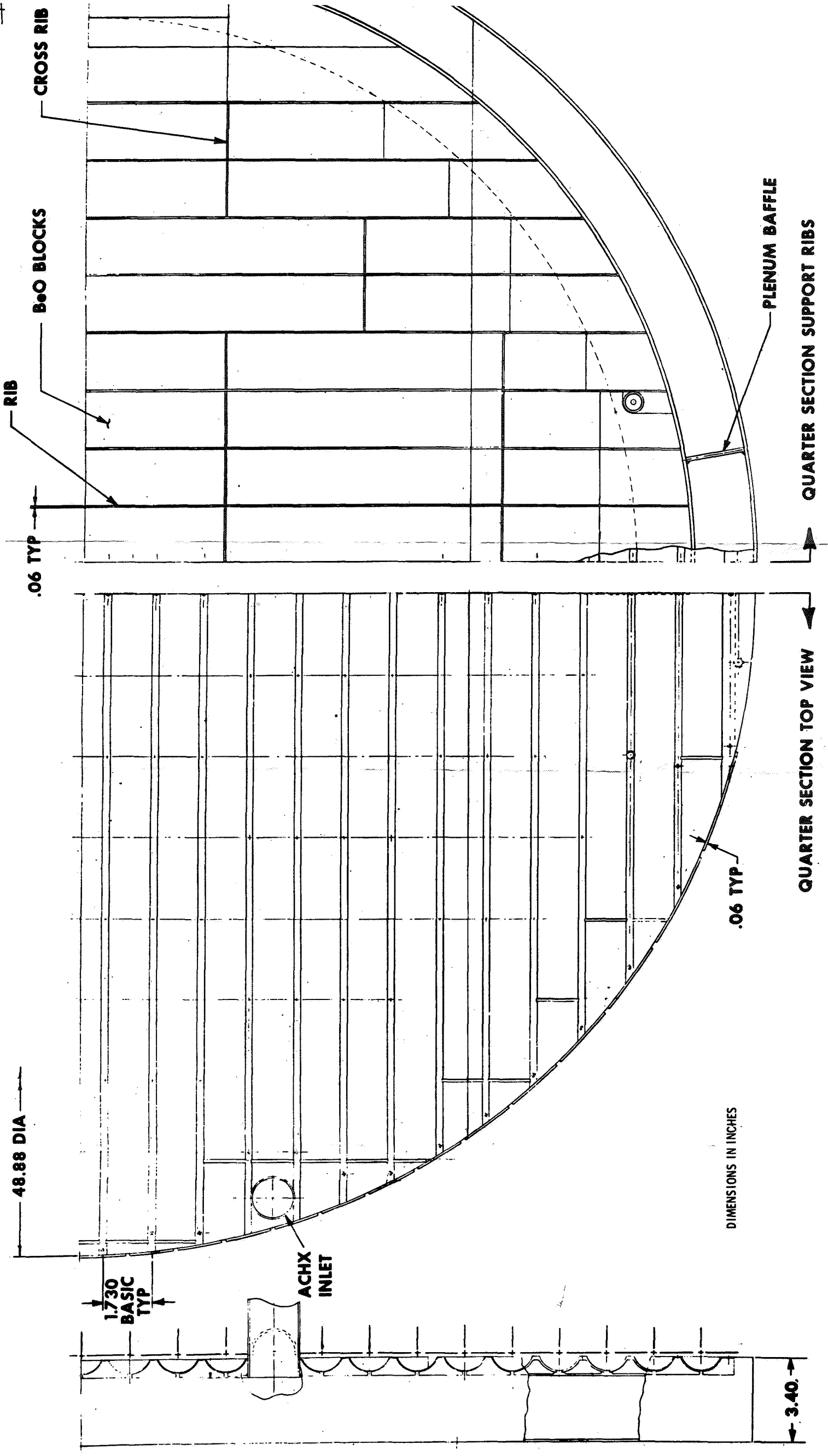


[illegible]

-199-

-199-

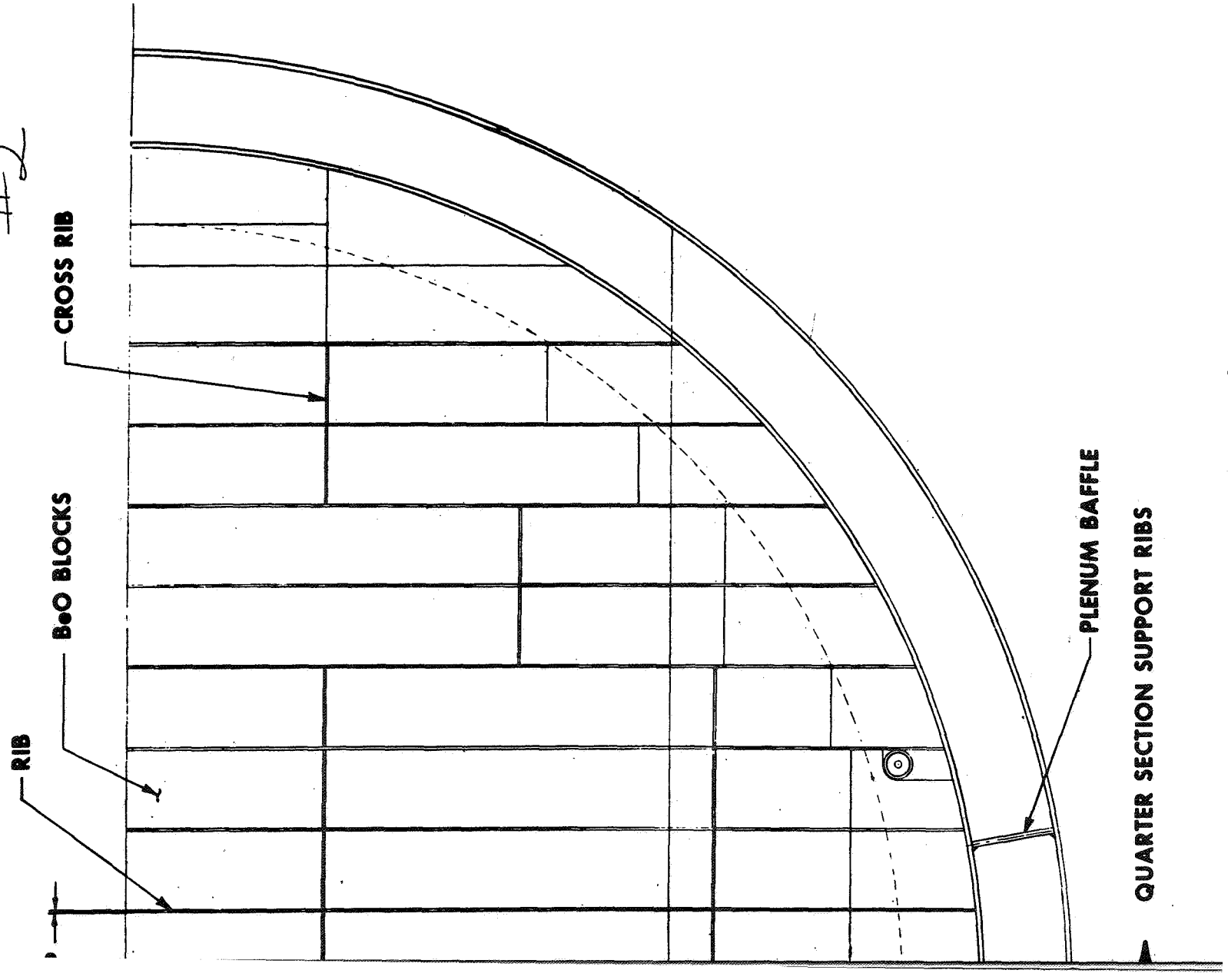
#1



612596-49 D

Figure 3-95 HEAT SOURCE PLATE ASSEMBLY

#2



QUARTER SECTION SUPPORT RIBS

612596-49 D

is the ACHX header which forms the periphery of the circular plate. The circular header is baffled at the center to form both inlet and outlet headers, both of which have two 1.5-inch-diameter connections. The cooling channels which are located between the rows of capsules connect to the inlet and outlet heads. Structural ribs are located below the top plate and at right angles to the capsule cradles for maximum rigidity. These ribs serve the dual purpose of structural members and as individual housings for a beryllium oxide heat sink.

TABLE 3-23

HEAT SOURCE WEIGHT AND
MOMENT SUMMARY

		Weight (lb)
<u>Fuel Capsules</u>		755
164 at 4.6 pounds per Capsule		
<u>Heat Source Plate Assembly</u>		402
Heat Source Plate	232	
BeO	170	
<u>Heat Source Cover Plate Assembly</u>		87
Cover Plate	57	
Retention Bars and Bolts	30	
<u>Heat Source Support Structure</u>		153
Support Ring and Plate	83	
Truss and Hardware	70	
<u>Insulation Assembly</u>		79
Insulation Foils	59	
Insulation Support	20	
Heat Source Total Weight		1476
Mass Moments of Inertia:		
$I_p = 94 \text{ slug-ft}^2$		
$I_T = 50.5 \text{ slug-ft}^2$		

A breech lock mechanism is also designed into the heat source plate assembly, Figure 3-97. It mates with the support structure mechanism and, with four lock pins, completes the locking mechanism. The locking pins are spring loaded. These springs are made of a refractory alloy (e.g., T.Z.M.) to reduce the possibility of relaxation due to creep at operating temperature. However, a backup system has been included to ensure reliability. It consists of a series of washers, which engage into steps which are machined into the spring guide tube. This occurs only if and when the spring relaxes. This design allows quick assembly or disassembly as required on the launch pad. A bottom plate which is welded to the structural ribs, forming a box beam structure, completes the heat source plate.

Fuel capsule retention is accomplished by the cover plate, Figure 3-98, which is contoured to mate with the fuel capsules. To ensure complete capsule containment and to avoid point contact load between adjacent capsule ends a beryllium oxide positioning ring, Figure 3-99, is installed between capsule ends prior to positioning the cover plate.

The total weight of the heat source support plate assembly has been calculated as 1244 pounds.

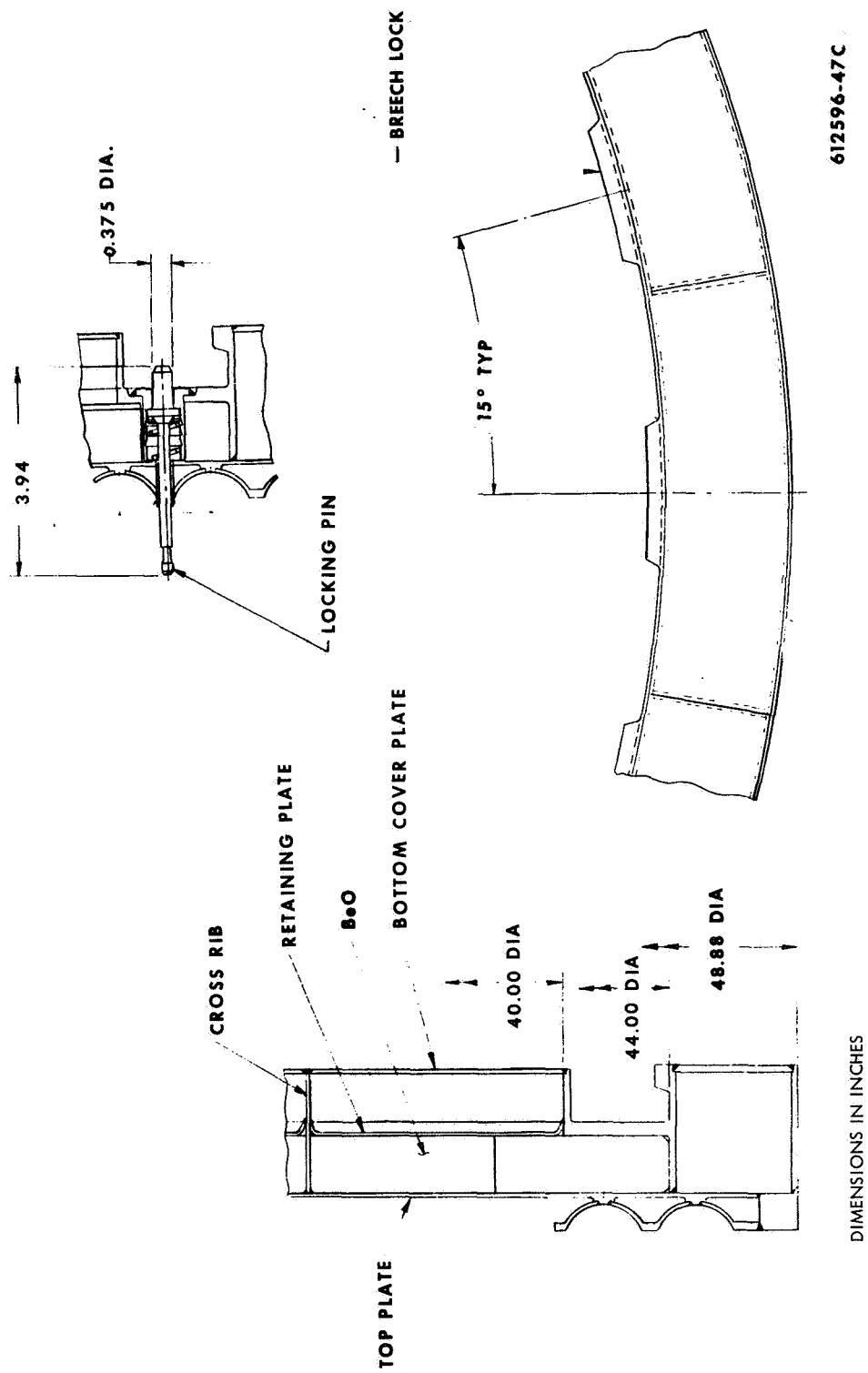
3.3.6.1.1 Fuel Capsule--PuO₂ microsphere was specified as the fuel for this application. A prior safety consideration that the fuel capsule be designed for absolute containment of the fuel for 10 half-lives (890 years) under all operating or abort conditions, including ground impact, ground burial, and ocean immersion, led to the reference capsule design supplied by NASA as shown on Figure 3-100.

The basic capsule design shown employs a multilayer capsule construction where each layer of material is optimized for specific functions, such as:

- fuel liner material is selected for chemical compatibility with the fuel fuel. (W)
- container structure material is selected for creep rupture properties and strength at high temperature with impact survival (T-111, T-222, ASTAR 811C).
- noble metal clad to protect the container structure from oxidation. (Pt or Pt - Rh)

The container structure is coated with a diffusion barrier (such as Al₂O₃ or ThO₂) to prevent embrittlement of the container structure, while the outside surface of the oxidation resistant cladding is coated with a high emissivity material to enhance the radiative heat transfer.

3.3.6.1.2 Heat Sink--The beryllium oxide (BeO) heat sink material was selected for its high heat capacitance and light weight. The heat sink provides thermal inertia for a) loss of HSHX cooling b) launch pad fire and c) ACHX transfer. Upon loss of HSHX cooling an increase in capsule temperature dictates that the heat source must be deployed to radiate to space. The heat sink provides the time for this operation to be completed, without excessive capsule temperature increase.



612596-47C

Figure 3-97 CROSS-SECTION OF HEAT SOURCE PLATE

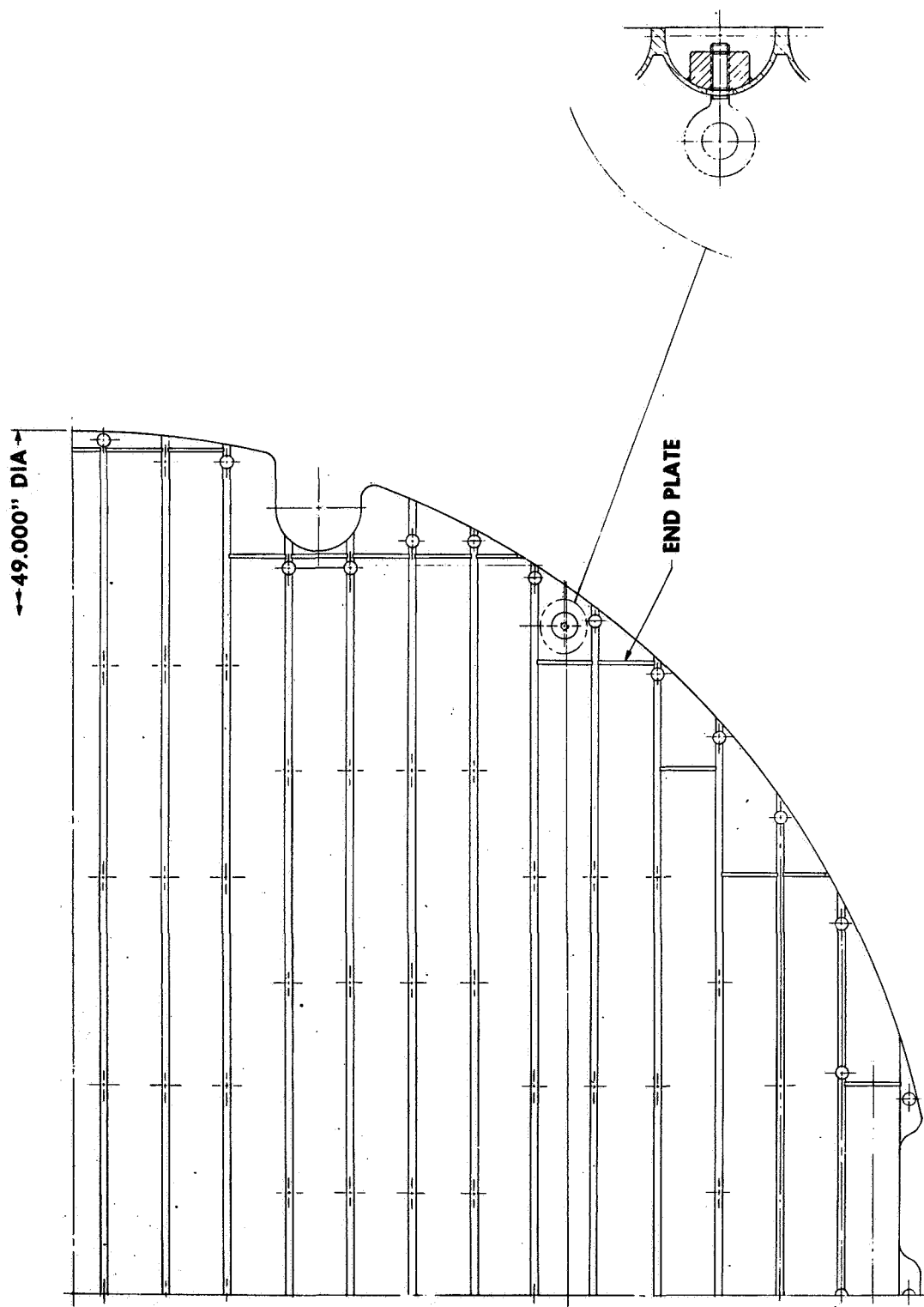
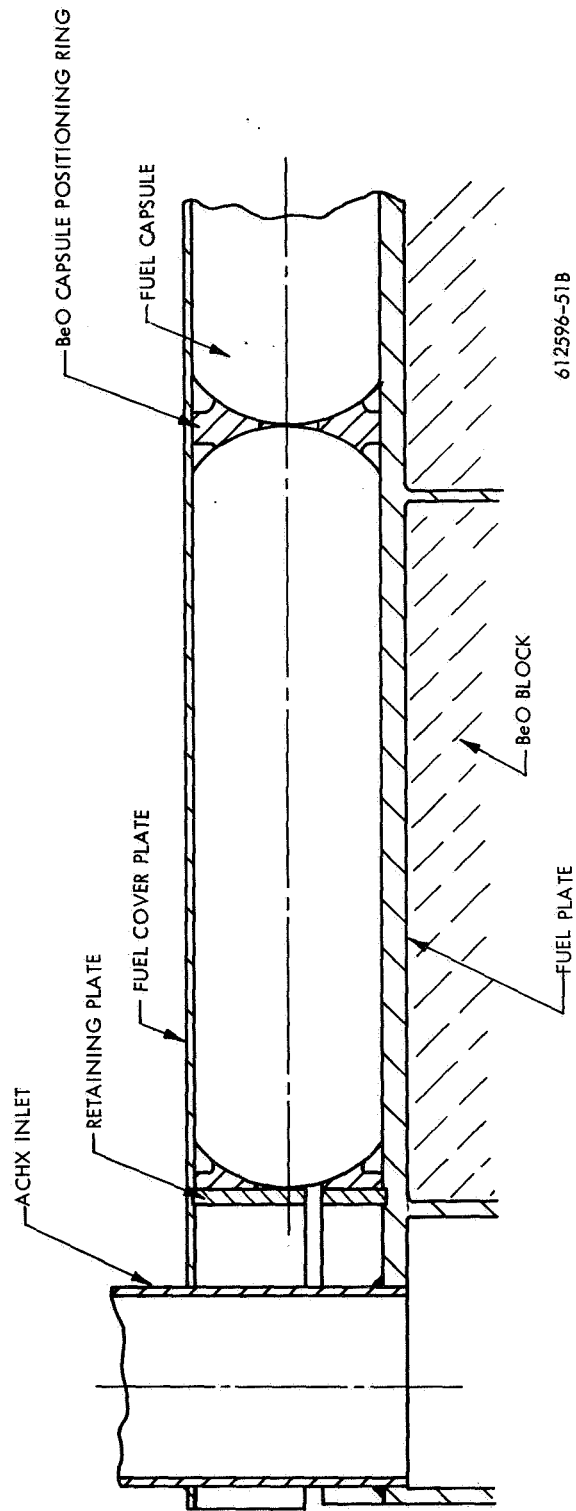


Figure 3-98 COVER PLATE



612596-51B

Figure 3-99 LONGITUDINAL SECTION DETAIL OF HEAT SOURCE FUEL PLATE ASSEMBLY

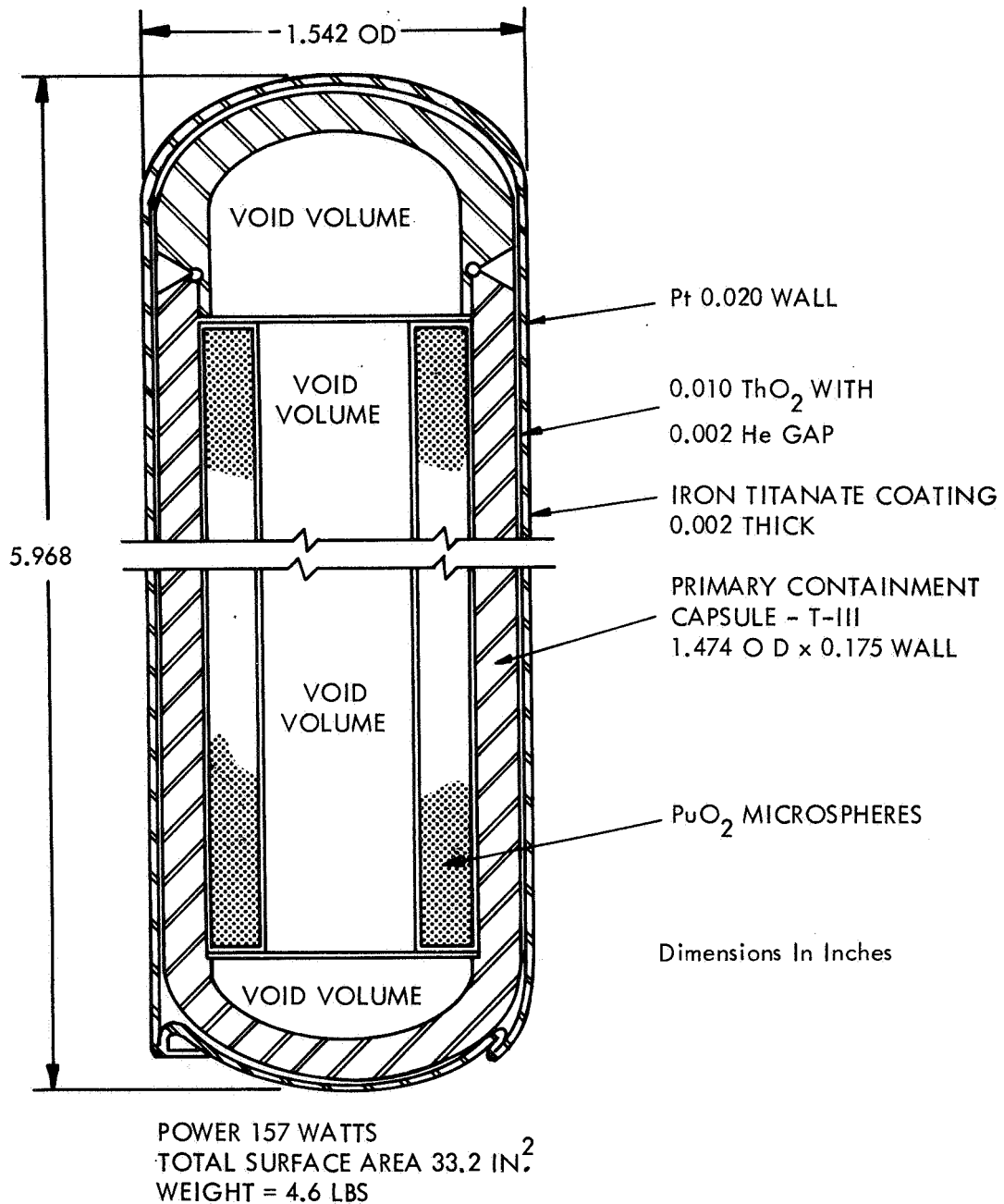


Figure 3-100 LEWIS RESEARCH CENTER REFERENCE FUEL CAPSULE

Since the heat sink augments the heat source thermal capacity it also reduces thermal transients on the launch pad. The heat sink which is located in the heat source plate is manufactured in blocks approximately 10 inches by 2 inches by 1.1 inch thick. It weighs 170 pounds. The beryllium oxide sections are supported between the structural ribs by a 40-mil perforated Cb-1Zr plate designed to retain the heat sink against the underside of the capsule cradles and cooling channels. Figure 3-101 shows a typical BeO heat sink section and retaining plate welded in position during the heat source plate assembly.

3.3.6.1.3 ACHX Headers and Flow Channels -- The functional requirement of the ACHX system is to maintain the temperature of the heat source below 350° F during capsule loading, transportation, and launch pad operation. This has been accomplished by building the necessary headers and channels into the heat source plate. The headers which have approximately 4 inches of cross sectional area are arranged around the periphery of the heat source plate. The flow channels which are approximately 0.37 in.² run parallel between and below the rows of fuel capsules connecting the inlet and outlet headers. Each flow channel is orificed at the return header, to balance the coolant flow between the channels. The ACHX header is baffled at the center pin to provide both inlet and outlet headers. Each header has two 1.5-inch-diameter connections to the cooling air supply used during fuel capsule loading, transportation, and launch pad operation. This supply is disconnected during the launch.

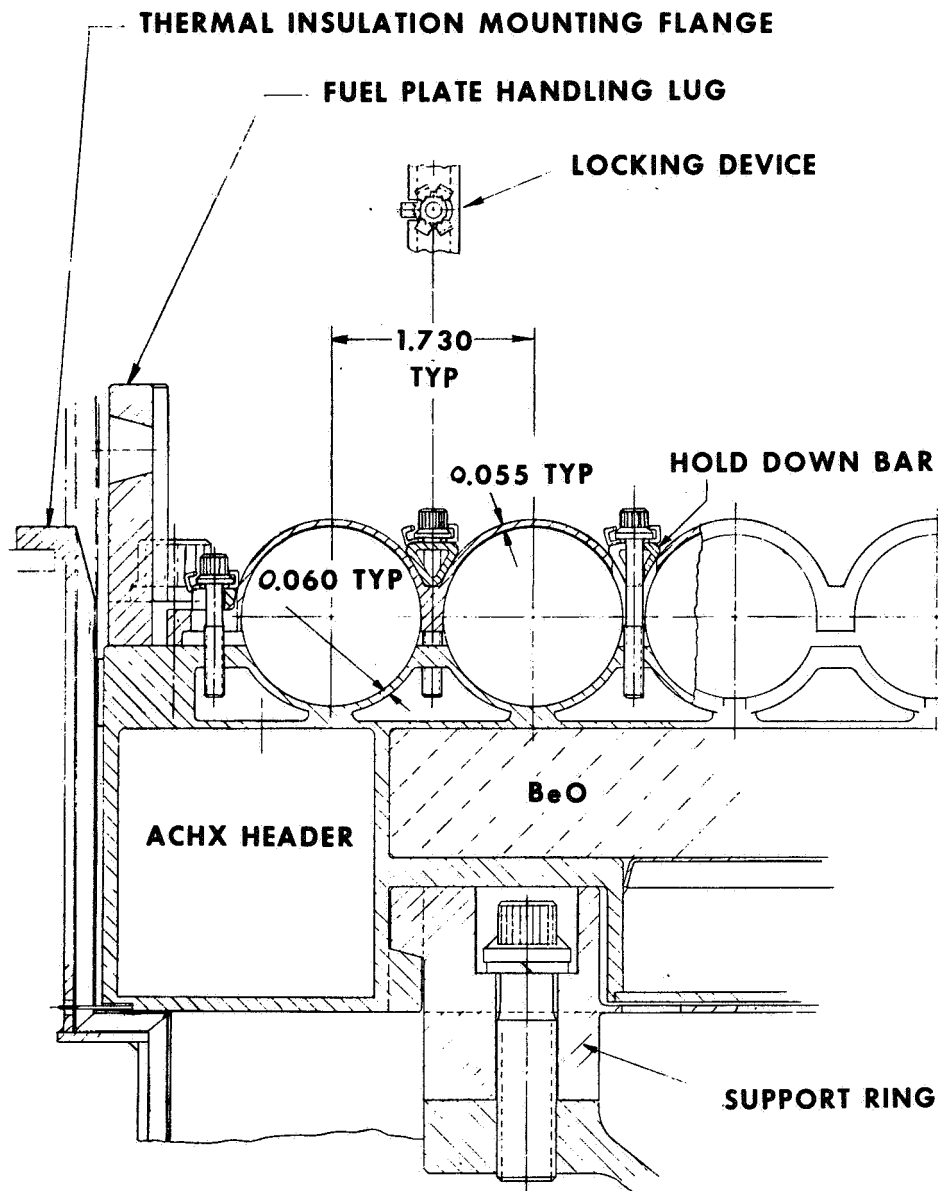
3.3.6.1.4 Retention Cover Plate -- The retention cover plate is manufactured from Cb-1Zr. It is designed to mate with and retain the 164 radioisotope fuel capsules cradled in the heat source plate. The basic requirement of the cover plate is to ensure that the capsules are retained during the entire five years of mission with a minimum of movement, and to protect them during any reentry sequence. During the reentry phase, it is essential that a radiation gap exist between the cover plate and capsule. A 5-mil gap, 120 degrees wide has been machined into each capsule row of the cover plate to accomplish this spacing. (Figure 3-102).

The cover plate is fastened to the support plate by 194 T-111 screws, 0.164 inch in diameter. These are located between the capsule rows and threaded into the cooling channels prior to the capsule installation. The cover plate is drilled to pass over the heads of the screws and their lock washers. A triangular retaining bar is then slipped under the screw heads. The screws are tightened and locked by the pre-installed lockwashers. These lockwashers serve two functions: first, to prevent loosening of hold down screws under potential vibration load environment during launch and space operation, and second, to provide a physical barrier between T-111 screws and emissivity coating on the cover plate and the retention bars. T-111 is not compatible with certain emissivity coatings such as iron titanate or calcium titanate.

3.3.6.2 Thermal Insulation Assembly

The thermal insulation barrier assembly, shown in Figure 3-103, consists of 100 layers of zirconia-coated molybdenum foil insulation. The 0.5-mil molybdenum foil is sprayed with particles of zirconia approximately 0.5-mil thick and stacked together to form the thermal barrier.

The penetrations in the insulation for the truss connections which support the heat source plate are located at 90 degrees apart. These are in the form of cups 10.0 inches in diameter, with a bottom plate which split around the struts.



DIMENSIONS IN INCHES

Figure 3-101 TYPICAL BeO HEAT SINK SECTION AND RETAINING PLATE

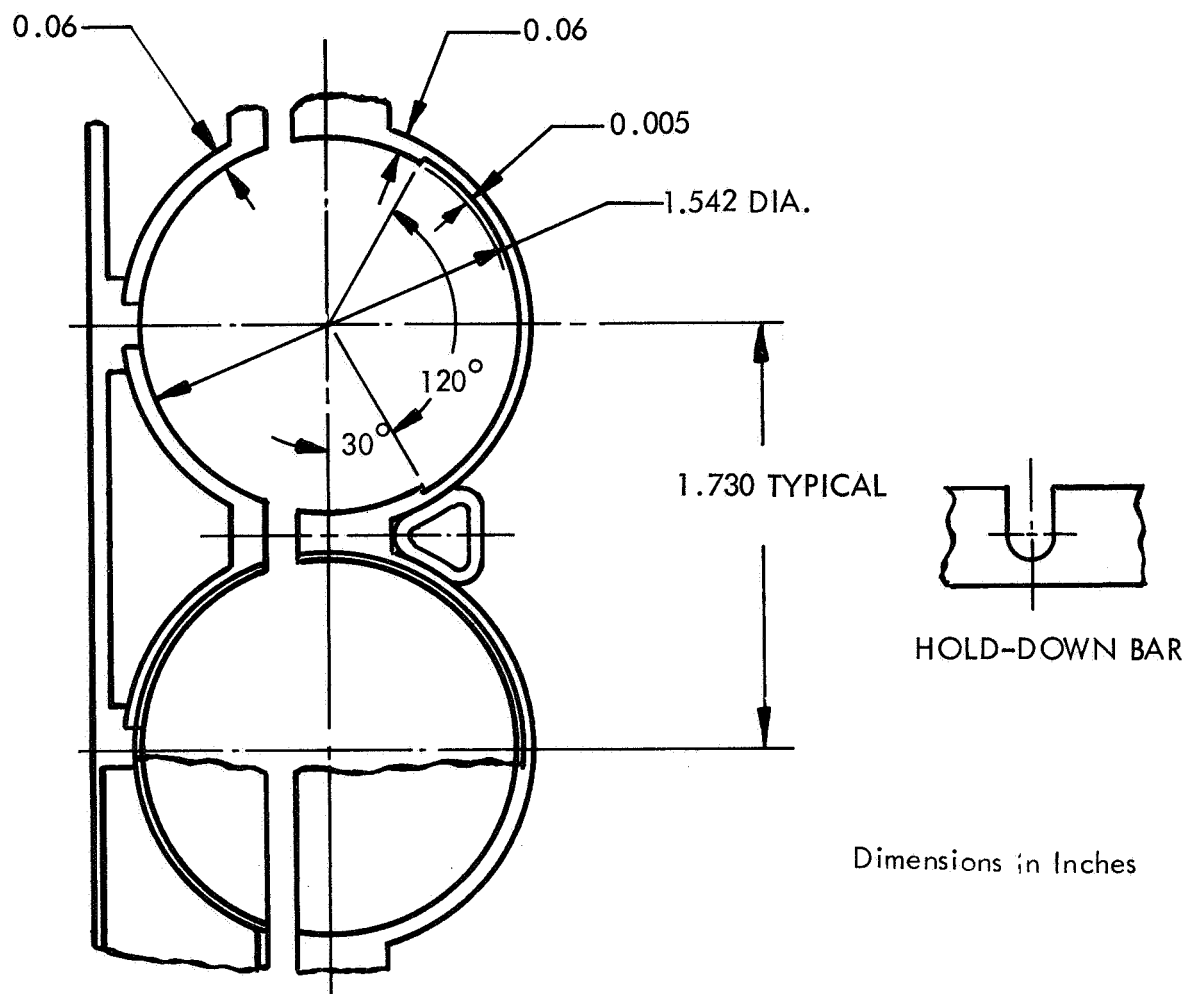
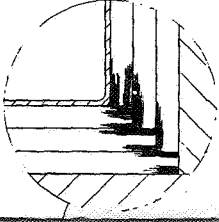


Figure 3-102 CROSS-SECTION DETAIL OF HEAT SOURCE FUEL PLATE ASSEMBLY



RIER

Figure 3-104 shows the interface joint which has been suggested, the insulation is joined on a 30-degree angle with an axial gap of 0.100 mil between the heat exchanger insulation. A ring of Min K2020 or equivalent insulation is then installed outside of the insulation barrier to minimize the effect of direct "shine through" to the aeroshell. The gap also gives assurance that two insulation shells will not weld together, after operating for long time periods in the space environment.

The insulation weighs 59 pounds. This weight is based on the use of 0.5-mil Mo foil. An alternate approach would be to use 1-mil foil, which has been demonstrated on smaller components. Although an increase in weight would be incurred, possible use of 1-mil foils should remain under consideration pending insulation fabrication and testing effort. The insulation assembly also contains the insulation support plate, a titanium ribbed plate with a side skirt and flange which mates with the aeroshell.

During the final detailed design of the insulation assembly close attention will be required to ensure that joint and fabrication details are optimized and that provision is made for the effects of thermal expansion.

3.3.6.3 Heat Source Structural Support System

The heat source structural support system shown on Figure 3-105 has been designed to meet all launch, abort, and reentry loads. The worst loading condition occurs under a launch abort reentry condition with g-loads of 30.4 and 2.4 for axial and lateral directions respectively. The heat source temperature at this time is 500° F or less. A nominal safety factor of 1.25 has been applied to the support system structural components.

The support system consists of a basic eight leg truss system, attached at top to a Cb-1Zr support ring plate 43.40 inches in diameter and at the aeroshell to a 13.0-inch-diameter base ring. The top support ring plate has been provided to minimize bending of the support ring during reentry and is scalloped to reduce weight.

The truss connections are located at 90 degrees around the support ring. They are attached at four raised sections, 7.0 inches long by 0.75 inch deep. To these are bolted the four upper truss connections as shown on Figure 3-106.

The individual truss connections are fabricated from T-111 and are welded to the individual struts which form the truss system. The lower strut connection has been designed to meet the same conditions as the upper connections but due to lower temperature conditions, only two 0.5-inch-diameter Cb-1Zr bolts are required where three were required on the top connection.

The struts are fabricated from T-111 material with an outside diameter of 1.0 inch and an inside diameter of 0.8 inch. They have a cross-sectional area of approximately 0.283 in.².

3.3.6.4 Insulation and Support Structure Assembly

Prior to installation into the aeroshell, the insulation assembly and support structure are assembled as a unit.

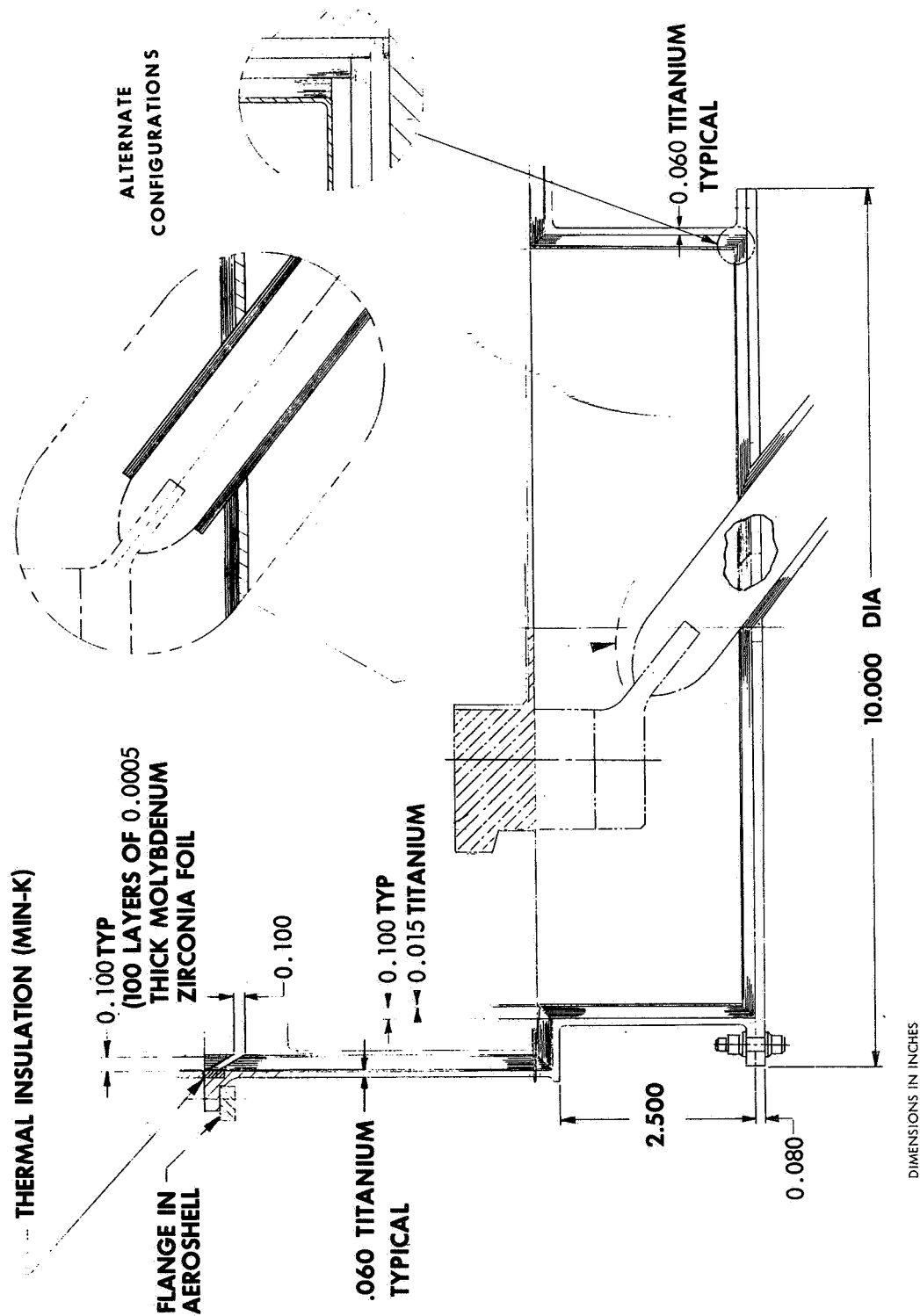
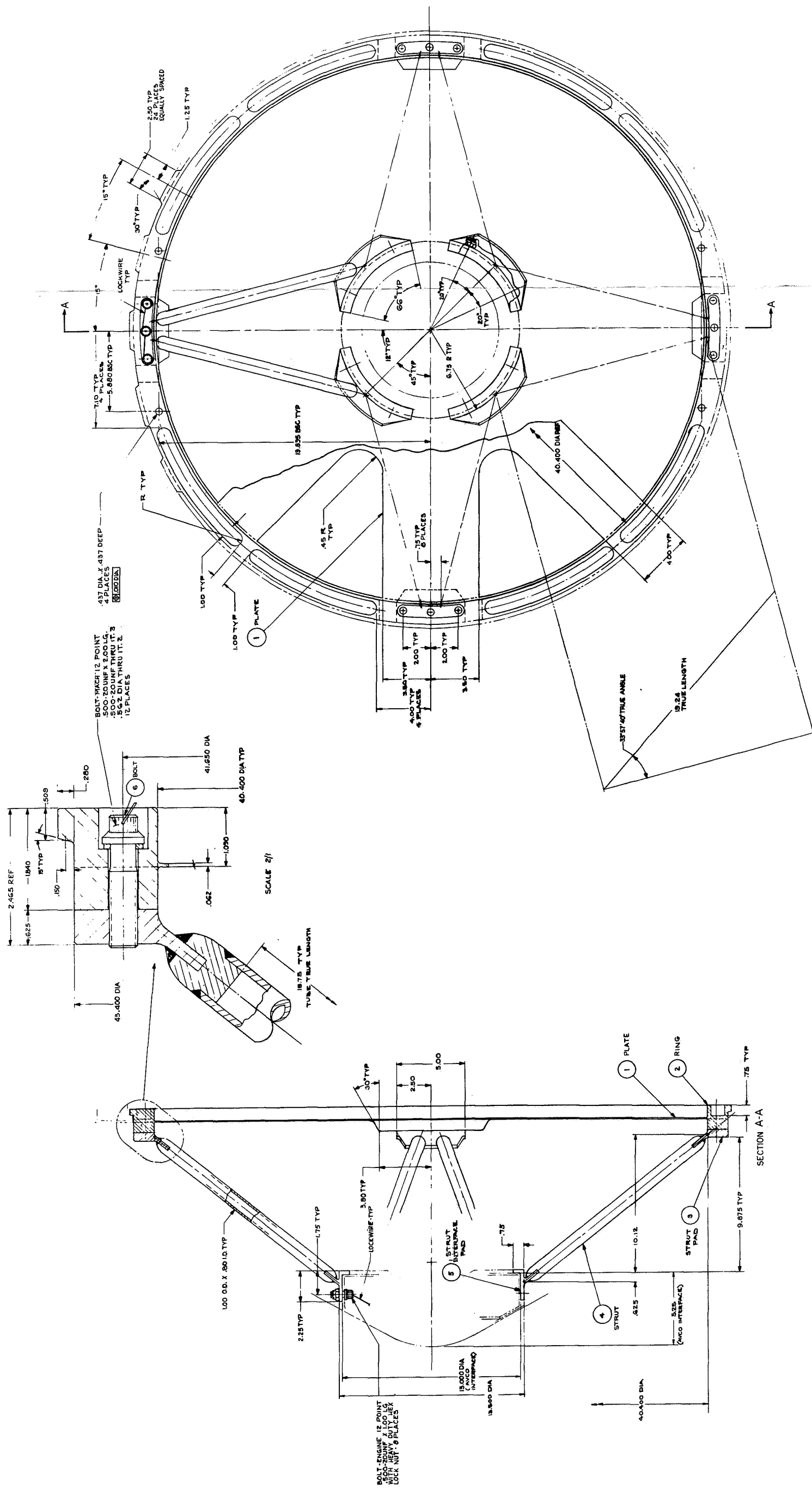


Figure 3-104 HEAT SOURCE INSULATION DETAIL



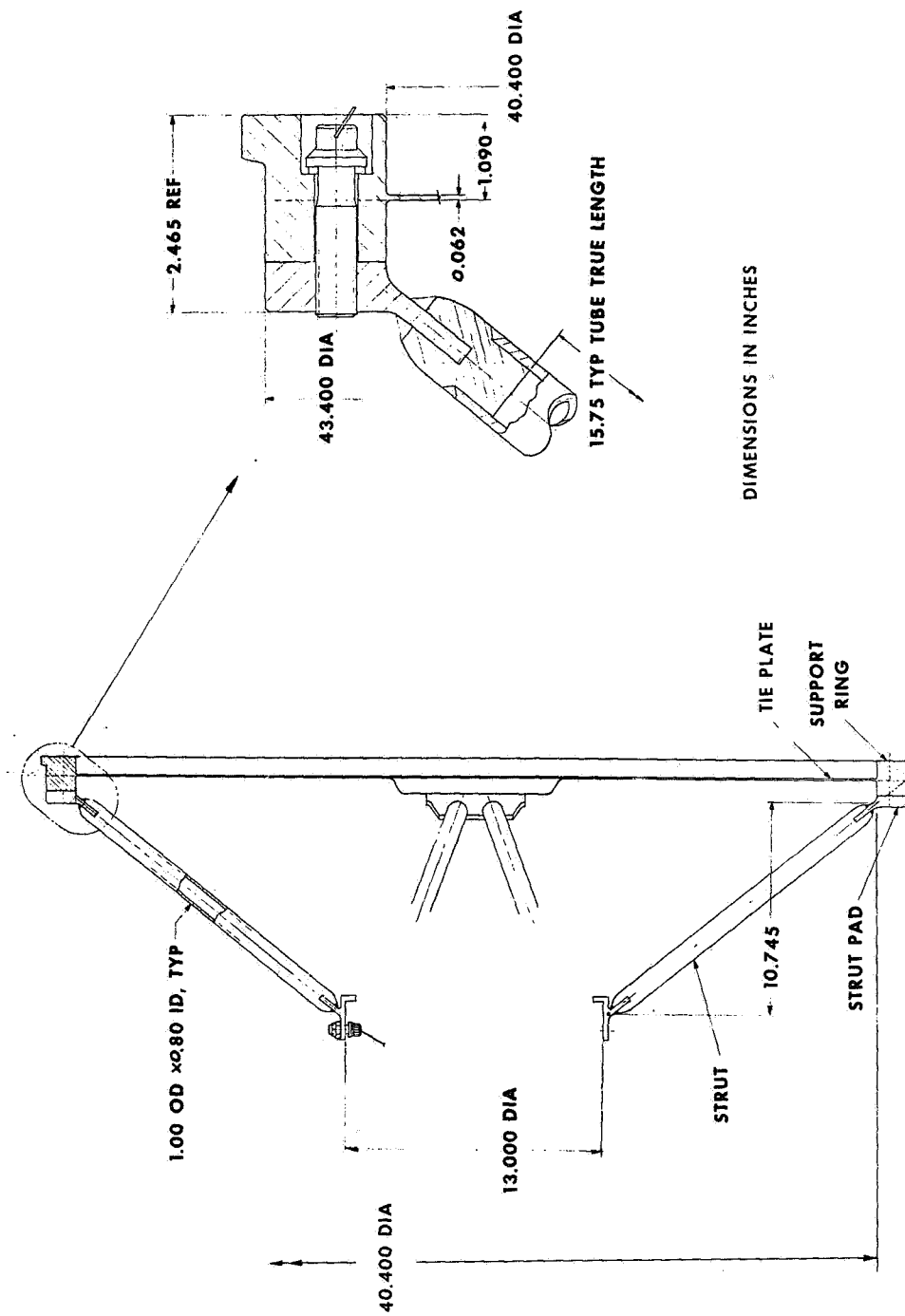


Figure 3-106 HEAT SOURCE SUPPORT STRUCTURE -- DETAIL VIEW

This is accomplished as shown in Figure 3-107. The individual struts of the truss are insulated and the main insulation package with the support plate is positioned over the top of the truss connections. The top support ring is then bolted to the truss support which captivates the insulation between the support ring plate and insulation support plate. Finally, the split bottom plates of the penetration cups are bolted on.

The complete assembly is then installed into the aeroshell with the insulation support plate bolting to the recovery aid housing and the lower truss connection bolting to a support ring at the aeroshell. This operation is accomplished through the removable section of the nose cone.

The assembly of the heat source plate to the support structure is accomplished during the launch pad operation. This operation is described in Subsection 5.3, Ground Handling Requirements.

3.4 ISOTOPE REENTRY VEHICLE (IRV)

The primary function of the IRV is to deliver the isotope heat source safely to earth for a wide-spectrum of failure modes ranging from abort during the launch to in-orbit malfunctions.

In addition, the IRV design must be such that a booster explosion or an inverted landing (i.e., capsules adjacent to ground) can occur without causing a catastrophic failure of the capsules.

The main constituent in the IRV is the aeroshell (or structure and heat shield) which must be lightweight and in addition withstand the axial, normal and vibration loads associated with launch and reentry. This structure must also be compatible with the truss network used to support the heat source within the IRV. The heat shield material which protects the structure during reentry should be low in weight, reliable and at a stage of development where it is known to be adequate in the aerodynamic shear and pressure environment anticipated for the IRV.

Since the aerodynamic shape used in the preliminary design of the IRV is stable rearward, a fence is required to ensure vehicle turnaround before excessive capsule temperatures are reached. The IRV also contains a ballute (to reduce impact velocity) and location aids in an annulus between the heat source and cylindrical portion of the vehicle.

The IRV must also provide pads (for loads) and support rings for the deorbit and abort rocket systems together with explosive bolts and other necessary hardware. In addition, access to the vehicle interior must be available to allow assembly of the heat source, insulation, etc. to the aeroshell.

The overall design and integration with the Brayton Cycle PCS during operation must be such as to limit the heat leak to 1500 watts and, therefore, adequate insulation must be provided, especially at interfaces.

The purpose of this subsection will be to describe in detail the IRV preliminary design together with the thermal and structural analysis used to define thicknesses and other details. Methods of analysis, tradeoffs and final structural and heat

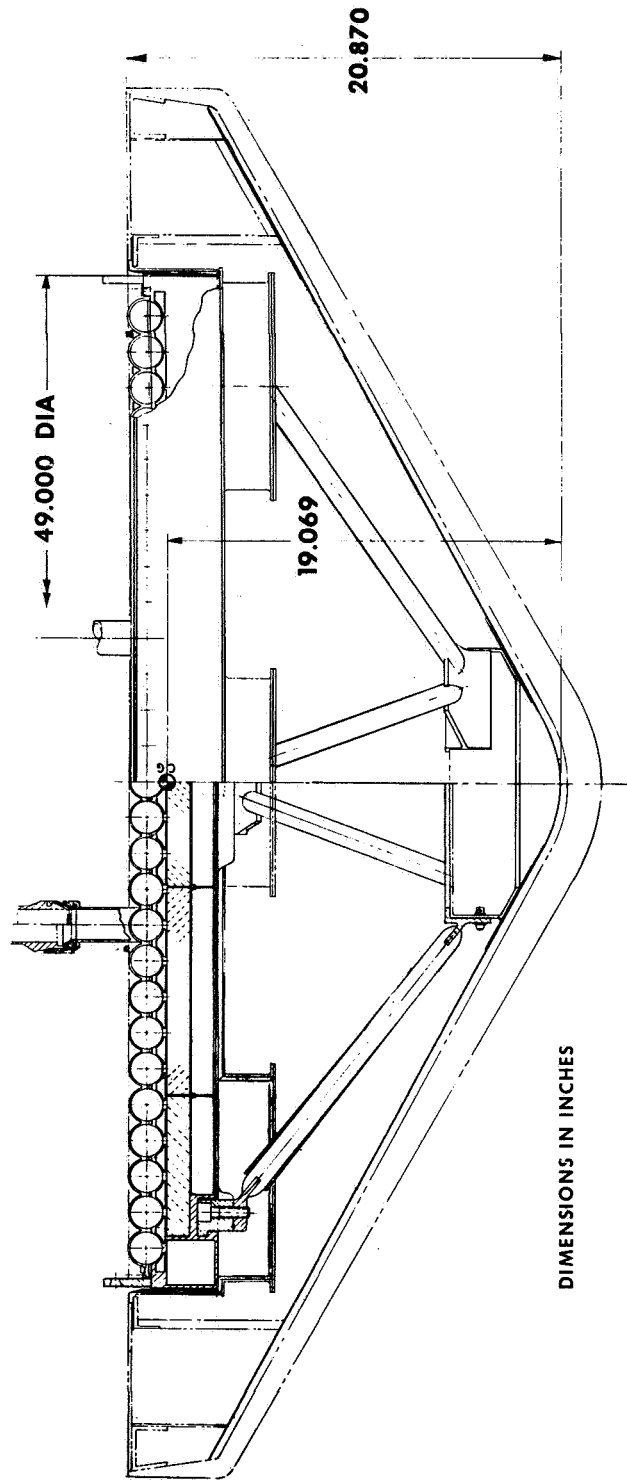


Figure 3-107 CROSS SECTION OF HEAT SOURCE ASSEMBLY

shield thicknesses are provided together with the assessment of the booster explosion and inverted landing problems.

3.4.1 Reentry Vehicle

3.4.1.1 Heat Shield

As mentioned in the Phase IB report the heat shield material used on Apollo (Avcoat 5026-39 HC-G) was selected as the thermal protection system for the IRV. During the preliminary design phase the thermal effort was oriented towards the definition of heat shield requirements using Avcoat 5026-39. This definition was complicated by the multiplicity of possible reentry conditions and a tradeoff between the allowable operational and reentry aeroshell temperatures. This subsection describes in detail the procedures used to develop an adequate heat shield design for the IRV.

3.4.1.1.1 Design Considerations -- To ensure that no problems developed with respect to utilizing Avcoat 5026-39 as the heat shield, a review of significant environmental parameters was conducted during the preliminary design phase. Table 3-24 shows the maximum levels of significant parameters as predicted for the IRV heat shield. None of the levels shown in Table 3-24 should cause any degradation or unpredictable failure (e.g., severe erosion) of the material in view of all the test data available from the Apollo program. The maximum pressure and shear predicted for the Apollo vehicle is 1.2 atmosphere and 17 lb/ft², respectively.

To define the heat shield thicknesses for the IRV, it is necessary to evaluate the influence of several factors. The items most significant in the heat shield design include the aerodynamic heating environment, and initial entry temperature together with the allowable maximum reentry structural temperature. This latter temperature has been defined as 450° F from structural considerations.

TABLE 3-24

AEROSHELL HEAT SHIELD ENVIRONMENT*

$$W/C_D A = 47.7 \text{ lb/ft}^2$$

Maximum Integrated Heating	57,400 btu/ft ²
Maximum Heating Rate	312 btu/ft ² -sec
Maximum Stagnation Pressure	1.35 atmospheres
Maximum Aerodynamic Shear	8.3 lb/ft ²
Maximum Flight Time	10,600 seconds

* Considering all trajectories and locations on aeroshell.

The selection of the design trajectory is reasonably complex due to the multitude of reentry environments possible. Not only do the reentry velocities and angles vary because of different abort modes, but even for a given set of reentry conditions (V_e, γ_e) a wide range of environments is possible due to vehicle dynamics (tumbling, spinning and reentry angle of attack). Therefore, it is possible that the heat shield requirement at each location on the aeroshell can be designed by a different trajectory. Table 3-25 shows the integrated heating at several vehicle locations for the trajectories (certain trajectories have been omitted since the heating is negligible and does not control the heat shield design). The asterisk denotes the reentry condition selected for design of the heat shield at a particular location and it will be discussed later. Of particular interest is the fact that the rearward spinning case from out of orbit can cause severe heating problems at the maximum diameter and base regions of the vehicle.

Another factor which influences the heat shield design is the initial reentry temperature. For the IRV study it was assumed that the initial condition was identical to the structural operational temperature in space. This is somewhat conservative since a temperature drop will be realized due to separation of the IRV from the Brayton Cycle Unit prior to reaching the altitude of reentry (400 kft).

A significant tradeoff exists between the operational and reentry temperature since increasing the heat shield thickness increases the operational temperature but decreases the reentry temperature rise. Since the reverse is also true, it therefore becomes necessary to determine the thickness which not only limits the operational temperature to adequate levels but also maintains acceptable reentry temperatures.

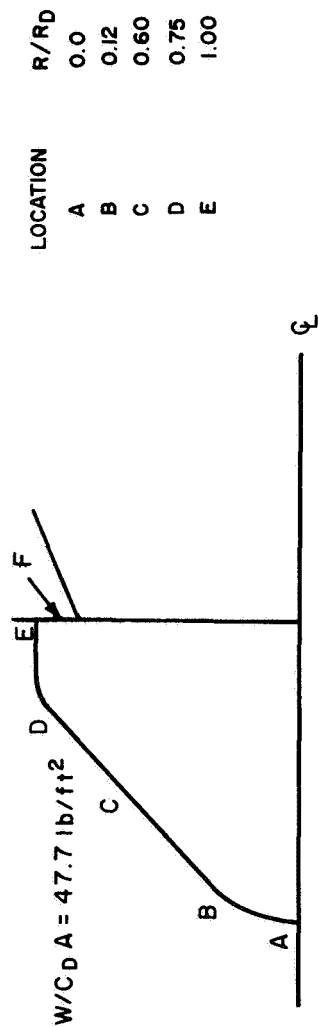
Figure 3-108 shows the tradeoff and for the design point shown a thickness of 1.60 inches of Avcoat 5026-39 provides a maximum bond line entry temperature of 450° F while maintaining an operational temperature of 220° F. Both of these conditions are acceptable from a long term heat shield and bond standpoint as well as reentry structural considerations.

3.4.1.1.2 Reference Design -- The design of the reference heat shield was based on the use of parametric studies. Figure 3-109 shows the reentry temperature rise for various thicknesses with the integrated heating level as a parameter. From this plot and Figure 3-108 it was possible to generate the curve indicated in Figure 3-110 showing the variation of required heat shield with integrated heating. From these data and the heating definition presented in Figure 3-108 it was possible to develop a summary table shown in Table 3-26. The data presented in the latter table includes a safety factor of 1.10 on the heat shield thickness. This factor is lower than that used in previous IRV reports since the design procedure used which assumes the worst trajectory at each location is in itself conservative. Table 3-26 also indicates the reentry condition (i.e., trajectory controlling the design at the various locations and the associated integrated aerodynamic heating.

It is interesting to note that the heat shield requirements in the area of the aerodynamic fence were based on a titanium structure while the remaining data is presented for an aluminum honeycomb aeroshell. The implication of this change is, of course, that the use of a titanium structure allows the reentry temperature to reach 600° F (bond limit) compared to 450° F for aluminum. A typical temperature history of the heat shield bond line and aeroshell are shown in Figure 3-111.

TABLE 3-25

SUMMARY OF HEATING DATA USED IN HEAT SHIELD DESIGN



Trajectory No.	Trajectory Mode	V _e (ft/sec)	γ _e (deg)	α _e (deg)	Location					
					A	B	C	D	E	F
1	Nominal Spinning	25,647	-2.15	85	16100	16570	7500	19950	10700	4260
2		25,447	-0.49	63	17200	22100	11550	34700	14200	7380
4	Tumbling	23,500	-4.0	180	16100	13950	4900	9700	4580	1700
5		25,685	-0.0	180	44000	36800	15300	36000	23400	12500
7		23,500	-4.0	180	16200	14900	5300	8400	3600	1200
8	Rearward	25,685	-0.0	180	56200*	39100	17900*	22900	9000	4260
9	Offset c.g. Spinning Nominal	25,647	-2.15	85	15500	15300	6300	20700	8900	4850
16	Required Spinning	25,685	0	180	23230	22800	13900	57400*	46900*	26900*
18	Out of Orbit Reentry	25,685	-0.0	0	51400	44000*	15400	12900	6200	5400

*Design Condition

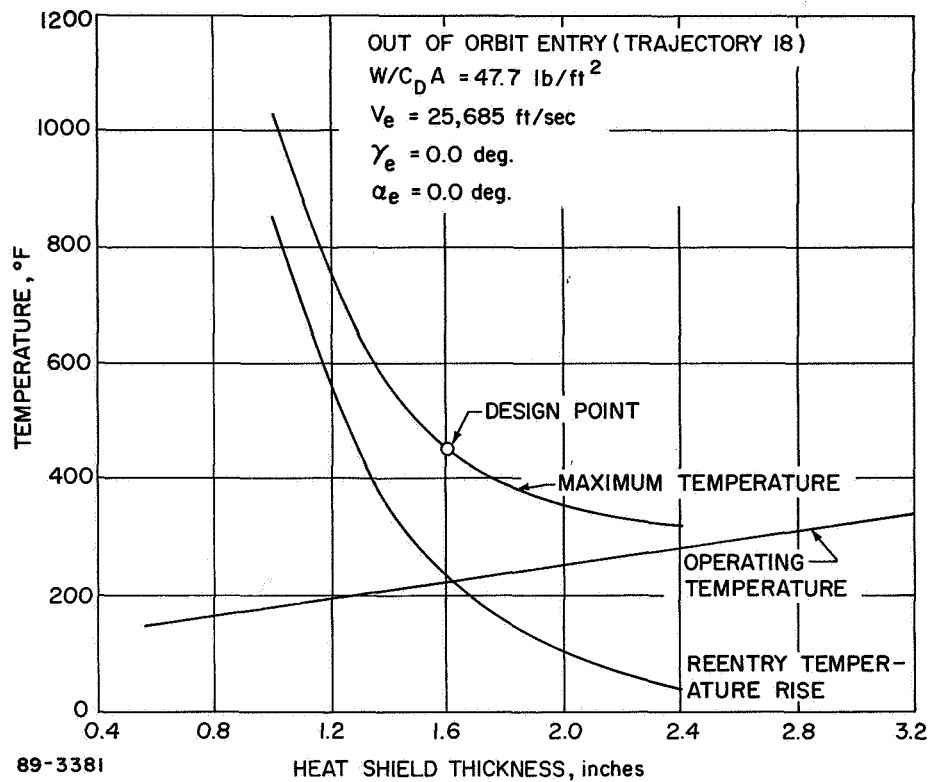


Figure 3-108 TYPICAL AEROSHELL BONDLINE TEMPERATURE, AVCOAT 5026-39 HC-G, STAGNATION POINT

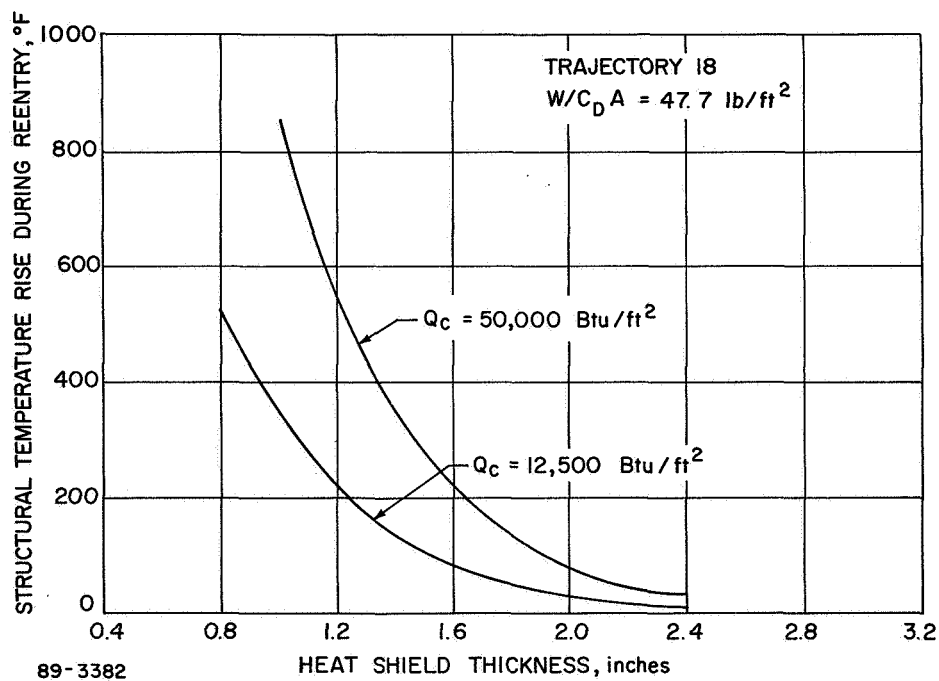


Figure 3-109 IRV HEAT SHIELD REQUIREMENTS, AVCOAT 5026-39 HC-G, OUT OF ORBIT REENTRY

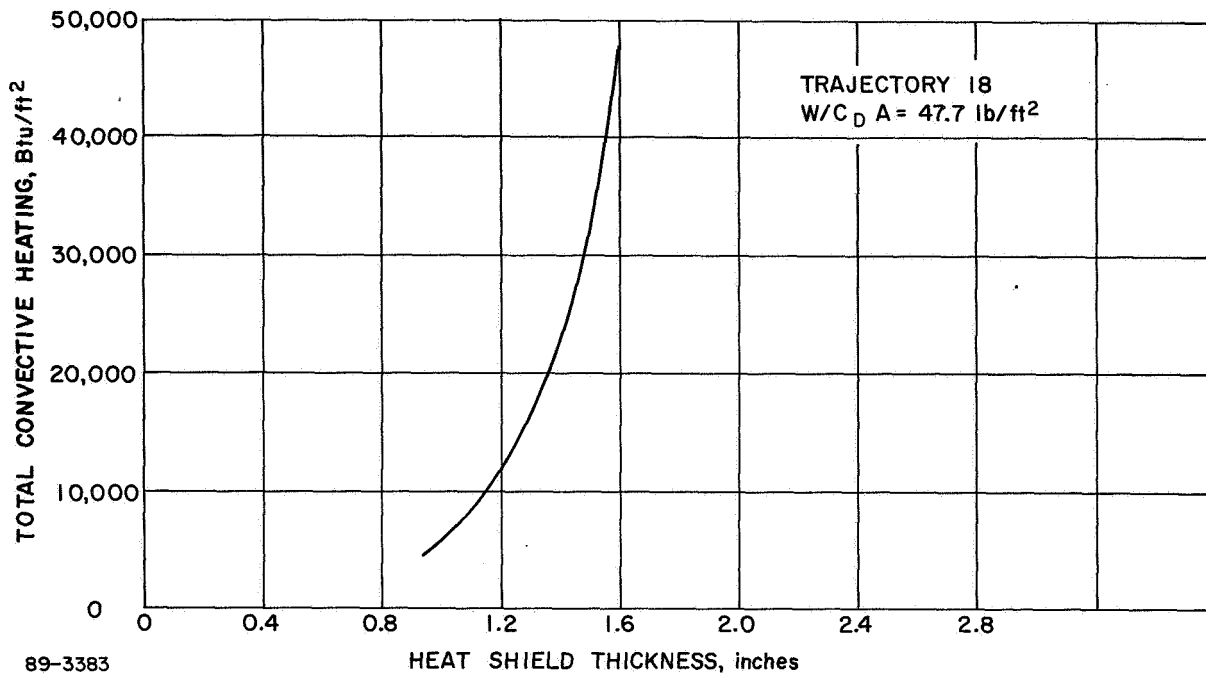


Figure 3-110 IRV HEAT SHIELD REQUIREMENTS, AVCOAT 5026-39 HC-G, OUT OF ORBIT REENTRY

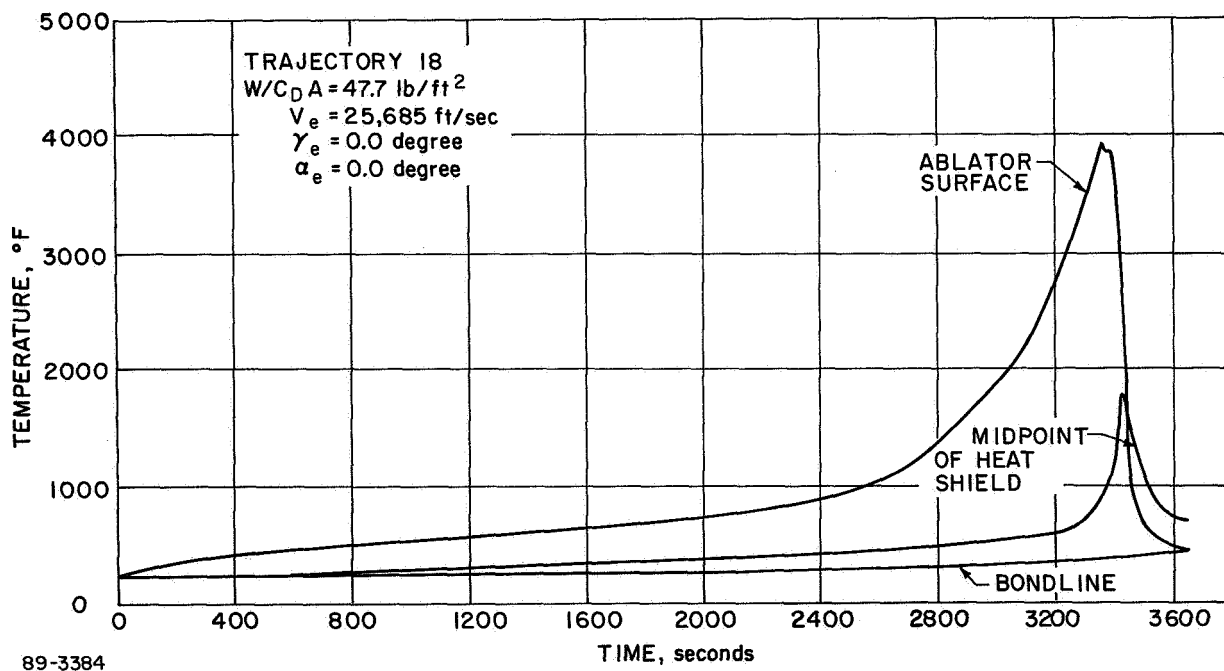
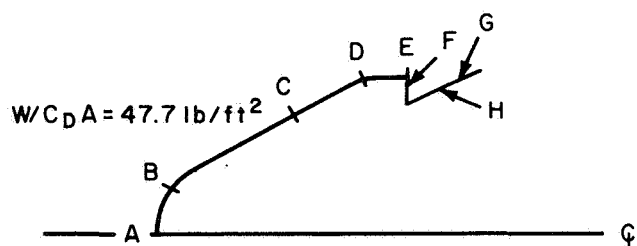


Figure 3-111 TYPICAL TEMPERATURE HISTORY, AVCOAT 5026-39 HC-G, STAGNATION POINT, OUT OF ORBIT REENTRY

Since the Avcoat 5026-39 thicknesses on the fence area are comparatively large, the use of a 3-D graphite material for the fence was investigated. Figure 3-112 shows the maximum fence temperature as a function of graphite thickness. The relative insensitivity to thickness is due to the fact that the heat shield is primarily performing as a radiator. A temperature history of the graphite fence is shown in Figure 3-113. This temperature data does not indicate that any structural problem should be encountered on the 3-D fence considering the available structural properties.

TABLE 3-26

IRV HEAT SHIELD REQUIREMENTS
AVCOAT 5026-39 HC-G



Location	Heat Shield Thickness (inches)	Design Trajectory	Trajectory No.	Integrated Heating (btu/ft ²)
A	1.87	Orbital Decay ($\alpha_e = 180$ deg)	8	56,200
B	1.72	Orbital Decay ($\alpha_e = 0$ deg)	18	44,000
C	1.45	Orbital Decay ($\alpha_e = 0$ deg)	18	17,900
D	1.87	Spinning Rearward	16	57,400
E	1.76	Spinning Rearward	16	46,900
F	1.50	Spinning Rearward	16	26,900
G	1.22	Spinning Rearward	16	23,000
H	1.12	Spinning Rearward	16	15,000

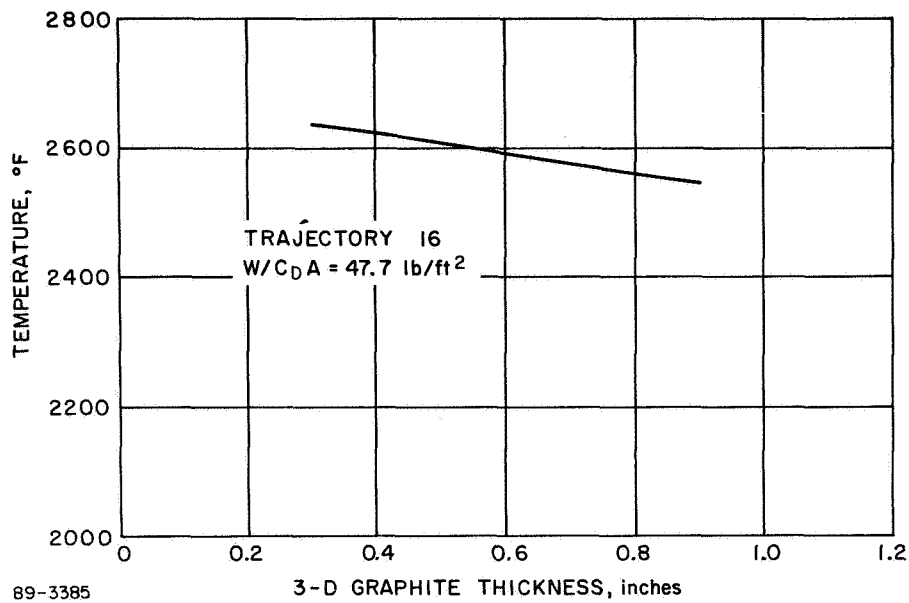


Figure 3-112 3D GRAPHITE FENCE TEMPERATURES MIDPOINT OF FENCE -- REARWARD SPINNING REENTRY MODE

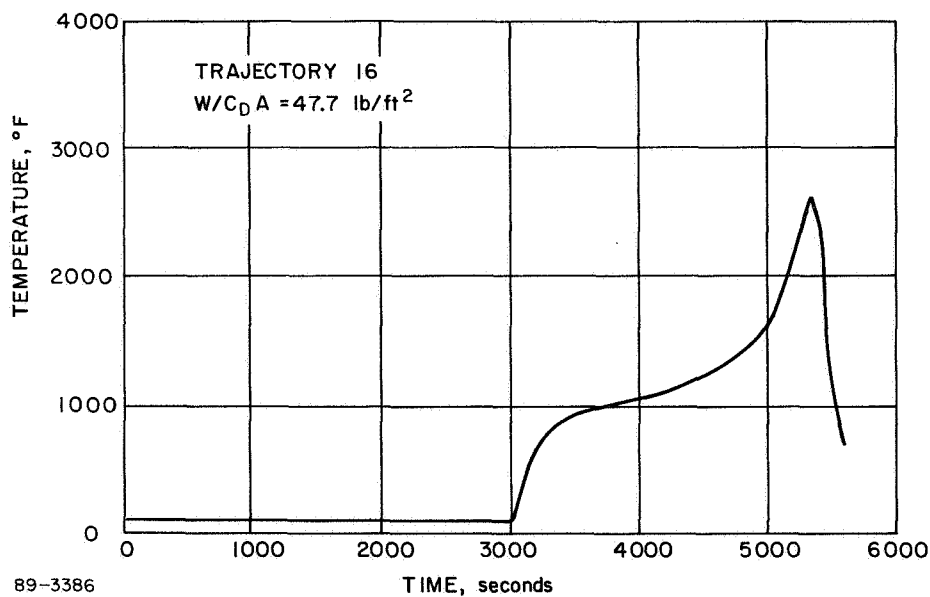


Figure 3-113 IRV FENCE HEATING MIDPOINT OF THE FENCE FOR 0.30-INCH THICK THORNEL 3D GRAPHITE -- REARWARD SPINNING REENTRY MODE

3.4.1.2 Aeroshell Structure

3.4.1.2.1 Structural Load Requirements -- The significant structural load environments considered for the Phase II IRV design study include launch, abort, reentry and ballute deployment. The load factors which represent the maximum expected load conditions are summarized in Table 3-27 for each of these environments. The levels in the table represent limits for the purpose of design and are multiplied by a safety factor of 1.25 except for the pad abort condition where an adequate safety factor is already inherent in the values. Launch acceleration factors for both the Atlas/Centaur and Saturn I-B launch vehicles are given in terms of the launch vehicle axis. For the Atlas/Centaur launch configuration, the IRV and launch vehicle axes are parallel and the given load factors can be applied directly to the IRV. For the Saturn I-B configuration, the IRV vehicle axis is normal to the launch vehicle axis and hence the longitudinal, A_x , and lateral, A_n , load factors of 9 and 4 g, respectively, are transposed into longitudinal and lateral load factors of 4 and 9 g, respectively, for the IRV. The load factors for reentry are the most severe. In addition to these reentry inertia loads, the aeroshell will experience maximum aerodynamic pressure forces of 24.8 psia at the stagnation point and 18.6 psia on the cone (including a factor of safety of 1.25).

TABLE 3-27

IRV STRUCTURAL LOAD ENVIRONMENT

1.0	Booster Launch Loads with Respect to Booster Axes (Including Vibration Component)	g (Limits)	
1.1	Atlas/Centaur	A_x	A_n
	(a) Maximum Axial Load Condition	6.4	0.5
	(b) Maximum Lateral Load Condition	2.3	2.0
1.2	Saturn I-B Design Loads	9.0	4.0
2.0	Pad Abort (Separation with Respect to IRV Axis)	10.0	2.0
3.0	Reentry (Worst Abort Saturn I-B) ($\gamma_e = 18^\circ$) ($V_e = 16,970$ fps)	30.4	2.4
4.0	Ballute Deployment	8.0	2.0

In addition to structural loads, the aeroshell will experience thermal loading, both during long-term operation in orbit as well as during earth reentry. The aeroshell must withstand the severe reentry load and heating environment after long-time space operation at elevated temperatures.

It is anticipated that the aeroshell, in general, will experience a nominal in-orbit operating temperature of 230° F while exposed to earth radiation associated with the reference orbit (see paragraph 3.4.2). At this temperature, aluminum will not experience appreciable strength degradation and can therefore

be considered the prime aeroshell material. In addition, 2024-T81 aluminum alloy was specified for the aeroshell since it appears to retain better strength capabilities after long exposure at elevated temperatures than other aluminum alloys. The normal long-term operating temperature of the strut support ring, however, is 460° F, which is too excessive for aluminum under long-term exposure conditions. Therefore, titanium was used as the strut support ring material since it can withstand long-term exposure at 460° F without major loss of strength.

During the peak-load phase of reentry, the aeroshell temperature was assumed to be 350° F and the strut-support ring temperature, 500° F. These levels are considered to be conservative for design purposes. Both the aeroshell and ring temperatures will increase gradually until, at impact, the maximum temperature of the aeroshell and strut-support ring could reach 450° and 600° F respectively. The reentry load profile, however, takes a sharp drop after the peak-load point, and hence the significance of any strength degradation of these structural materials at these higher temperatures is nullified by a much greater reduction in loads.

3.4.1.2.2 Aeroshell Structural Design -- The major design modifications in the Phase II reference aeroshell design from Phase IB include a reduced vehicle diameter, change in the strut support ring location, and attachment and support of the IRV vehicle. As a result, a structural reevaluation of the major aeroshell components was performed.

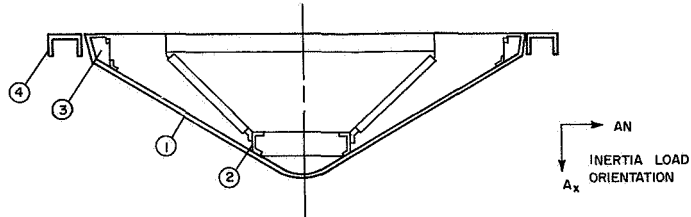
The nominal honeycomb face sheet and core requirements were reevaluated for the reduced vehicle diameter of 68 inches and the current aerodynamic design loads. The maximum design cone pressure is 18.6 psi compared to 15.6 psi used in the Phase IB study. Based on membrane stress only, it was determined that the existing 0.017-inch aluminum face-sheets were adequate for the current design configuration and loads. Local bending effects, particularly at the strut support ring and base ring, were not considered; but as previously investigated in a detailed stress analysis in Phase IB, the facesheets can be beefed up either by tapering or by attaching doublers to control stress concentrations due to local bending and shear forces.

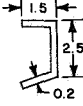
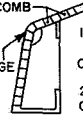
The honeycomb core thickness requirement, which is based on resistance to general buckling instability, was found to be 0.42 inch as compared to 0.52 inch for the 85-inch-diameter design of Phase IB. The reduction in diameter more than offsets the increased cone pressure in affecting this core thickness reduction.

The strut support ring was also reevaluated because of changes in radial location, material, and loads. Specifically, these changes consisted of 1) moving the radial location of the strut support ring from the previous 13.5 inches to 6.5 inches to increase strut length and 2) substituting titanium for aluminum because of the high long-term operating temperature of 460° to 500° F. Because of the position change of the strut-support ring, the strut angle is reduced and consequently in-plane kick loads to the ring are greater. The ring was reanalyzed for combined in-plane and out-of-plane bending due to the concentrated strut loads; and it was found that reentry still provided the critical design load environment for the ring.

A summary of the structural evaluation of the conical shell, strut support ring, and other major aeroshell components is presented in Table 3-28. Also shown in the latter table are the critical design load environments and governing failure modes which were used to establish the structural requirements of these components.

TABLE 3-28

SUMMARY OF STRUCTURAL REQUIREMENTS FOR
MAJOR COMPONENTS

No.	Structural Component	Material and Construction	Design Load Environment	Failure Mode	Structural Requirements (inches)
1	Conical Shell	Honeycomb 2027 - T81 Al	Entry ($A_x = 37.8g$) $A_n = 3.1g$ $P_c = 18.6 \text{ psi}$ $T = 350^\circ \text{ F}$	Facesheet - Yield Core - General Buckling Instability	Facesheet, $t_f = 0.017$ Core, $t_c = 0.42$
2	Truss Support Ring	T ₁ - 6Al -4V Channel	Entry: $A_x = 37.8g$ $A_N = 3.1$ $T = 500^\circ \text{ F}$	Combined Out-of-Plane and In-Plane Bending	
3	IRV Base Ring	202A - T81 Al Built-up Box Section	Saturn I-B Launch: $A_x = 5.0g$ $A_N = 11.3g$	Combined Out-of-Plane and In-Plane Bending	HONEYCOMB $t_f = 0.017$ $t_c = 0.42$ JOINT AND EDGE M5M3 0.1 in. THICKNESS, FLANGES 
4	IRV Support Ring	7075 - T6 Al Channel Ring	Saturn I-B Launch: $A_x = 5.0g$ $A_N = 11.3g$	Combined Out-of-Plane and In-Plane Bending	4.0 x 4.0 x 0.25 Channel

3.4.1.2.3 Dynamic Analysis of IRV Aeroshell -- A vibration analysis was performed for the IRV blunted-cone aeroshell in its reentry mode. The analytical model used to represent the aeroshell is shown in Figure 3-114 and includes the blunted-cone shell and spherical nose cap, the heat source strut support ring, local stiffening in the region of the strut support ring, and the base ring. In the analysis, neither the struts nor the heat source plate were included, but the masses of these components were accounted for and uniformly distributed into the strut support ring. The effect of this simplification on the dynamic behavior of the aeroshell is not considered to be very significant since the strut support ring is very stiff as is the local shell at the attachment point; hence, the selected model should furnish satisfactory data on shell vibrational characteristics.

Both the base ring and heat source strut support ring have been idealized in the model as equivalent homogeneous shell segments having similar bending and extensional properties as the rings.

The aeroshell honeycomb structure has also been modeled by an equivalent homogeneous material with the same bending and extensional properties. The aeroshell heat shield was assumed to contribute little to the stiffness characteristics of the composite aeroshell and hence was ignored; however, the mass of the heat shield is significant and was included in the inertia calculations.

The complete aeroshell structure was first subdivided into a series of conical elements, connected to each other at nodal circles. As shown in Figure 3-114, the aeroshell configuration was represented by 17 nodal circles. The motion of each element is described by the displacements of the nodal circles. Four nodal degrees of freedom are considered (net axial, radial, and tangential translation as well as rotation in the meridian plane) and hence the system had 68 degrees of freedom. The mass and stiffness matrices were computed for the system utilizing the Sabor III computer program, (Ref. 3-27). The stiffness matrix for each element is found by determining the strain energy which is related to the stresses and strains present in the elements. This is achieved by assuming a displacement function for the nodal coordinates and introducing them into the stress-strain and strain-displacement relationships for the shell elements. The total shell stiffness matrices are input to Avco Computer Program 1384, Reference 3-28, which then solves for the frequencies and mode shapes of the system.

The displacement function for radial displacement is taken as:

$$W(\theta) = A \cos n\theta$$

where

A = the peak magnitude of W

n = the harmonic number

θ = the circumferential position

$W(\theta)$ = the radial displacement at the circumferential location θ

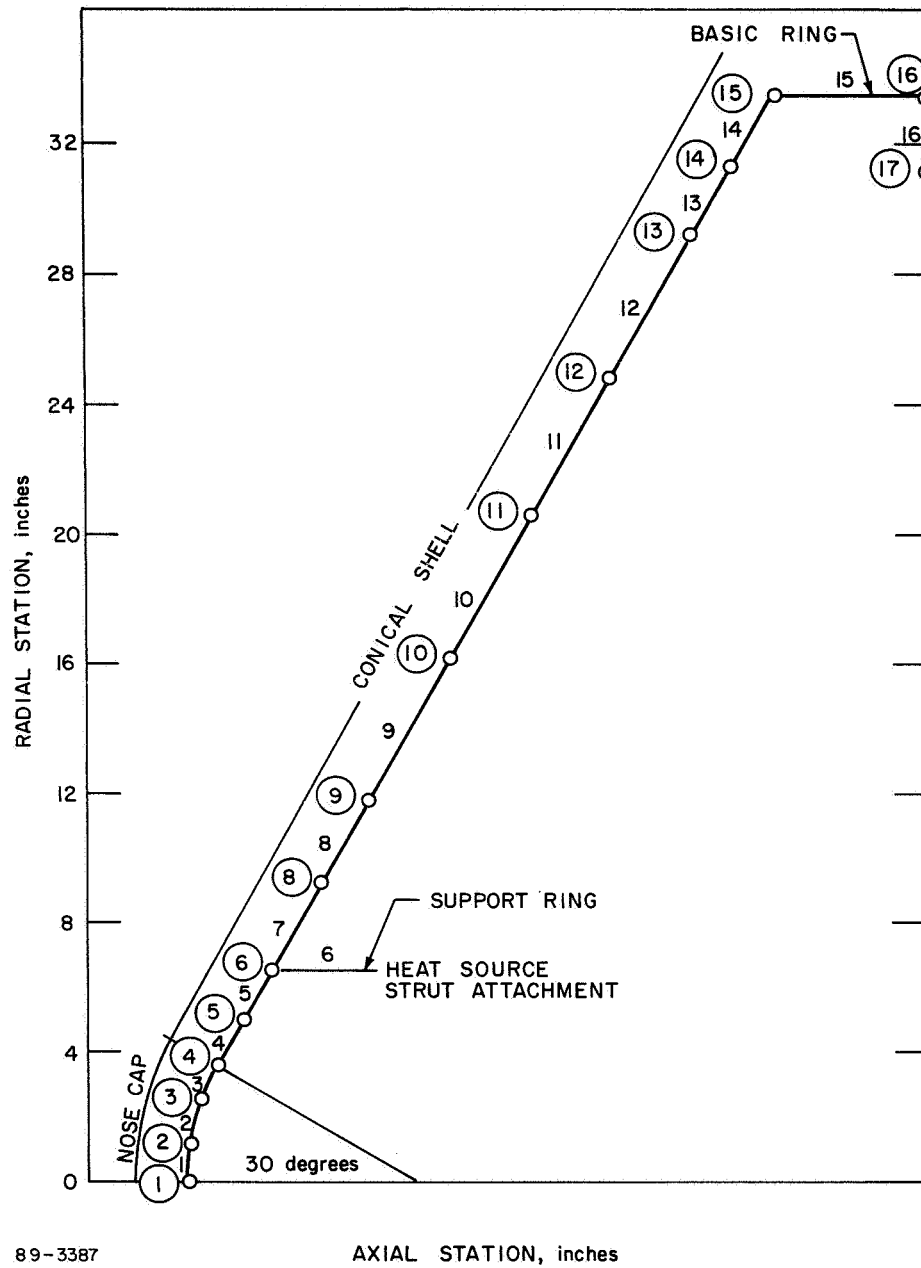


Figure 3-114 IRV AEROSHELL MODEL FOR VIBRATION ANALYSIS

A different set of modal data was computed for each harmonic number n up to $n = 4$. The $n = 0$ case actually corresponds to an axial mode of vibration since axial displacement is constant around the circumference. The $n = 1$ case is similar to a lateral or beam-type vibration mode since each modal section moves but retains its original circular shape. For $n = 2$ and higher, each nodal circle oscillates about its undeformed shape but experiences no net motion as a whole. A vibration mode description for each harmonic is shown in figure 3-115. Since there are as many natural modes of vibration as there are degrees of freedom in the system, the modal data for each harmonic n consisted of a set of 68 natural mode shapes and frequencies. The lowest natural frequency for each harmonic number n is by far the most important and hence is the only one considered in the analysis. The lowest natural frequency for each harmonic number is plotted in Figure 3-116. As shown, the minimum natural frequency of the system occurs at the second harmonic and is approximately 32 Hz. The axial (U) and radial (w) modal displacements for $n = 0, 1, 2$, and 3 are shown in Figures 3-117 and 3-118. These plots correspond to the natural frequencies given in Figure 3-116.

Aerodynamic studies indicate that the oscillatory frequencies of the IRV during reentry from either orbit or abort are lower than one Hz which is far below the lowest natural shell frequency of 32 Hz and hence no appreciable dynamic load magnification is expected.

3.4.2 Thermal Control

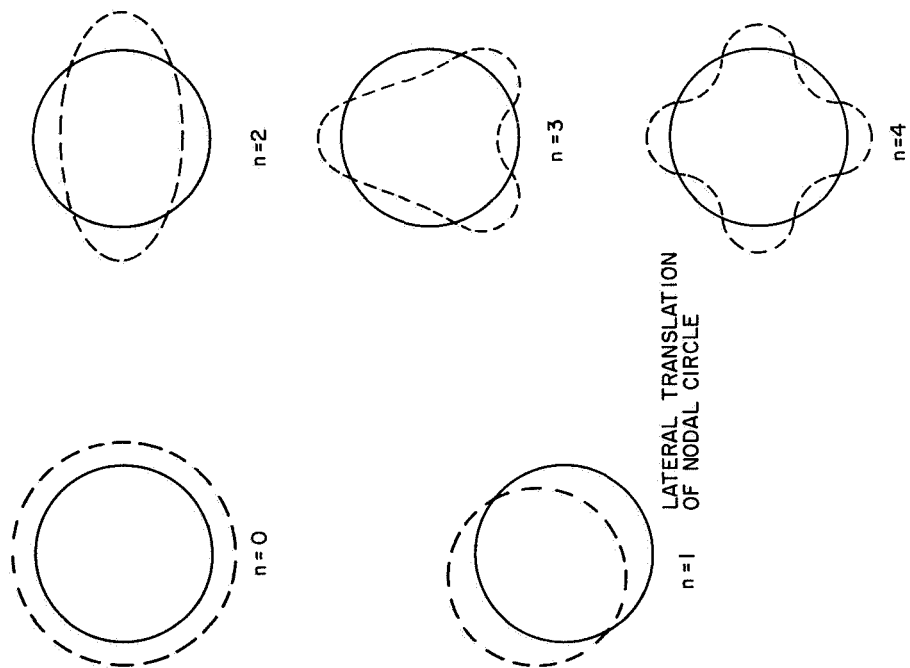
The maintenance of acceptable temperatures within the IRV for the range of environments considered is quite complex. During normal operation, of course, temperatures at critical locations (heat shield, location aid area) must be held to specified limits consistent with the 5-year lifetime. In addition it is required that during normal operation the heat leak not exceed 1.5 kw. The reentry period requires special attention since the location aid compartment will be subject to increased levels of heating especially if a rearward attitude is maintained for a significant length of time.

Two possible accident conditions also must be investigated. The first is a booster failure at launch which could subject the IRV to a fireball environment. Secondly, the IRV could land in an upright orientation (capsule against the ground) after impact which could cause excessive heat source temperatures due to the poor conduction capabilities of the soil.

All of the above phases or conditions must be investigated so that the adequacy of the design can be demonstrated. A discussion of these analyses and the assumptions used are discussed in the following paragraphs.

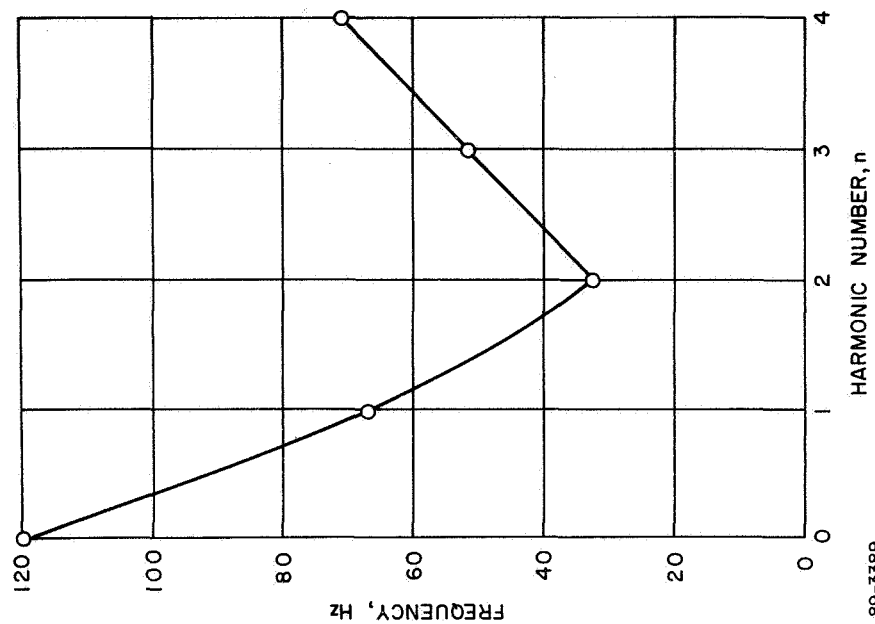
3.4.2.1 Normal Operation

A major concern of the truss support system is the hot-spot temperature that exists at the aeroshell end of the truss members. Considerations for limiting temperatures include degradation in mechanical properties of both the ablator adhesive and substructure material and outgassing of the ablator itself under the long-time exposure to elevated temperatures and the hard vacuum of space. Although, in general, it is felt that 300° F is a feasible design



89-3388

Figure 3-115 VIBRATION MODE DESCRIPTION FOR EACH
HARMONIC NUMBER, n



89-3389

Figure 3-116 IRV FIRST NATURAL FREQUENCY AS A FUNCTION
OF HARMONIC NUMBER

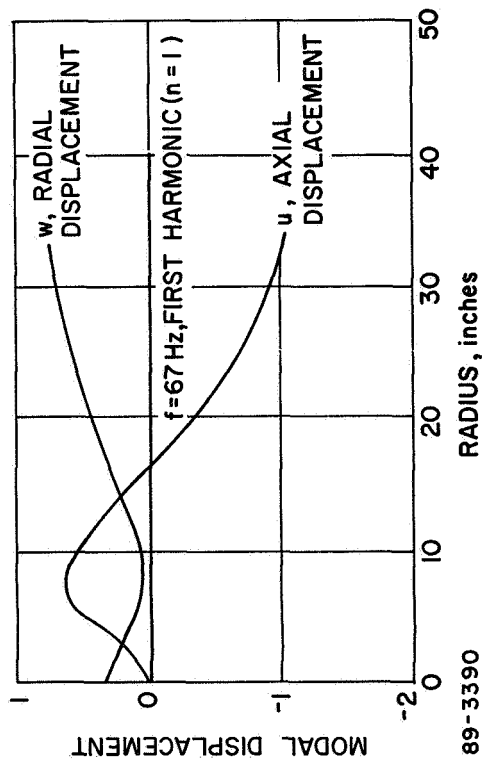
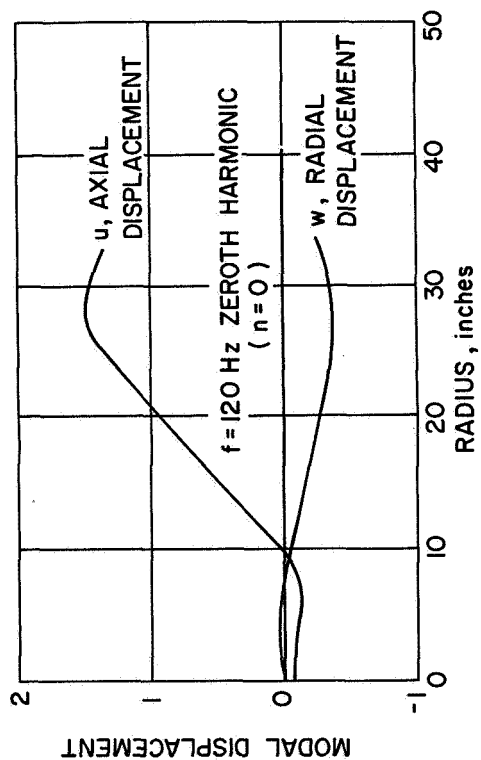


Figure 3-117 IRV AEROSHELL MODAL DISPLACEMENTS ZEROth AND FIRST HARMONICS

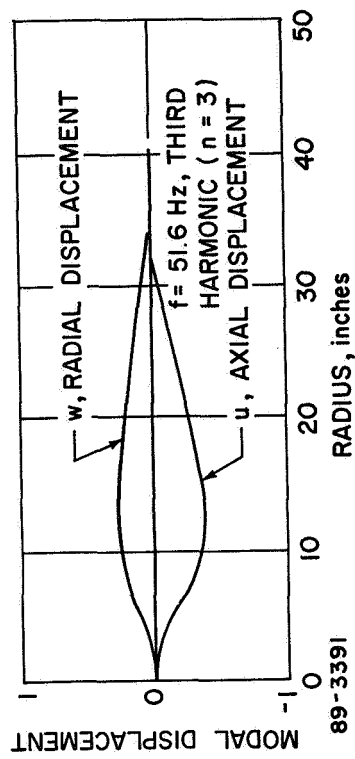
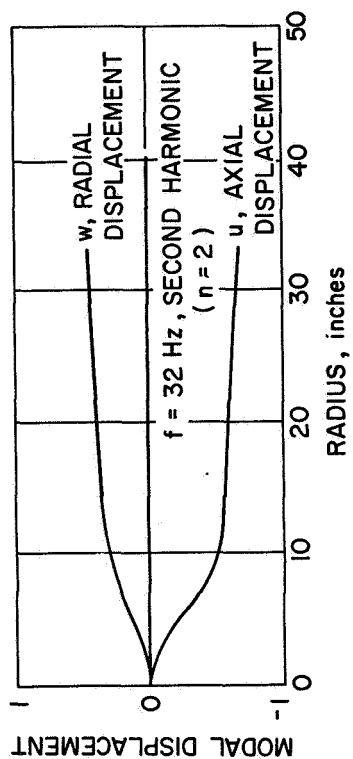


Figure 3-118 IRV AEROSHELL MODAL DISPLACEMENTS SECOND AND THIRD HARMONICS

temperature limitation for the candidate low-temperature ablator (Avcoat 5026-39/HC-G), ablator adhesives, and substructure construction, it would be prudent to design for substantially lower temperatures (2000° F) if the truss design would permit it.

3.4.2.1.1 Summary of Ground Rules and Assumptions -- The study for the normal operating mode is based on the following assumptions and constraints:

- Aluminum honeycomb aeroshell
- Thermal control coating of zinc oxide/potassium silicate
- 100 nm circular, polar orbit, 90-degree inclination
- Heat shield permanently earth-oriented
- Heat source temperature 1900° F

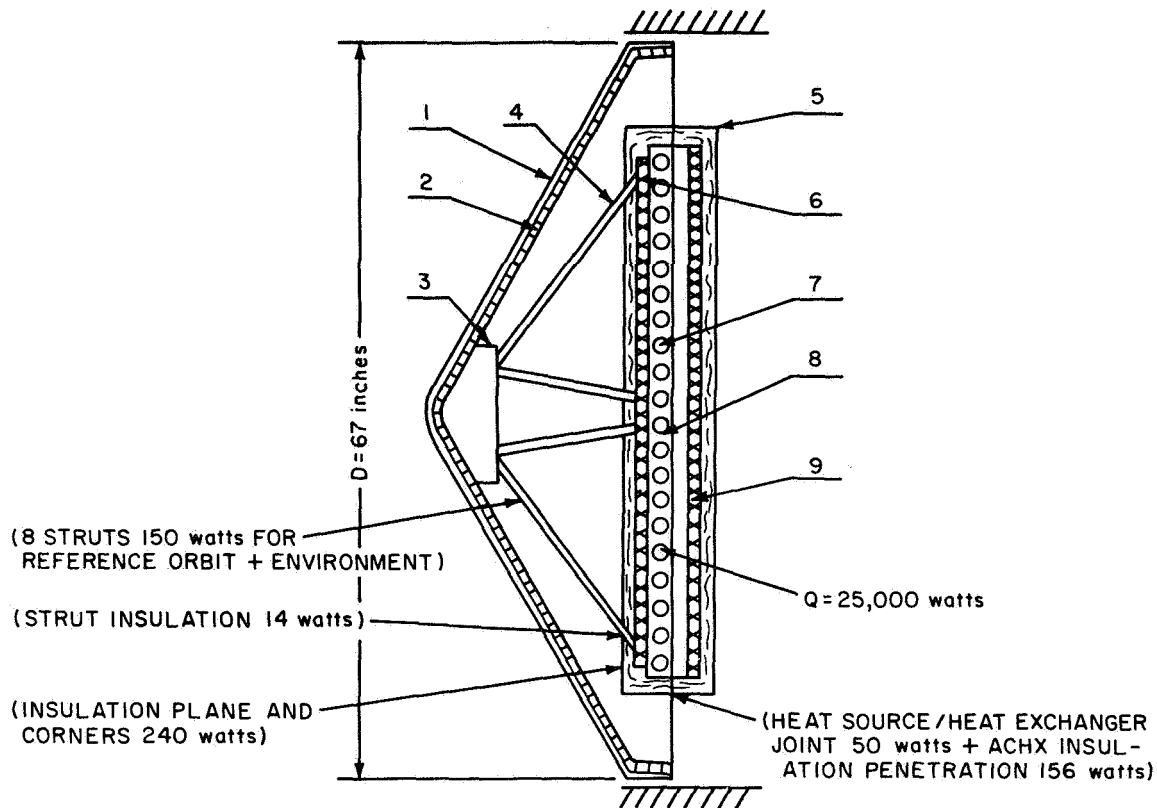
The temperature of the system in space is determined by the balance between entering and leaving thermal energy. In the case of the IRV aeroshell orbiting around the earth, the following energy sources and sinks have to be taken into consideration:

- External Energy: Direct sun impingement, earth thermal radiation and earth-reflected solar energy (albedo) where applicable.
- Internal Energy: Heat leakage from the radioisotope heat source through the IRV structure (strut, strut insulation, insulation plane and corners, heat source/heat exchanger joint).
- Dissipated Energy: Heat radiated away from the total area of the aeroshell.

Temperature bounds can be expected for the two extreme environmental conditions of permanent exposure to either sun or space. As noted earlier, the following study is based on a 100 nm, circular, polar orbit with the sun vector in the orbit plane and a permanently earth-oriented aeroshell which receives maximum albedo radiation when the IRV passes the subsolar point (worst case assumption). In this case, the external energy level is determined by the magnitude of impinging earth thermal radiation and earth albedo only and is within the boundaries of the two extreme cases. All three cases have been analyzed and are compared to show the interrelations between the external environment and internal heat dissipation and its effect on the aeroshell temperature distribution.

The reference design is shown in Figure 3-119. For orbital geometry and incident heat loads see Figures 3-120 and 3-121. A thermal environment averaged around the orbit has been used in all calculations and steady-state conditions are assumed. Note that the incident heat loads are not negligible relative to the allowable heat leak for 1.5 kw (180 Btu/ft²-hr-° F).

3.4.2.1.2 Analytical Model and Expressions -- The thermal model, properties and dimensions are shown in Table 3-29. A steady-state energy balance for the earth-oriented IRV takes on the following form:

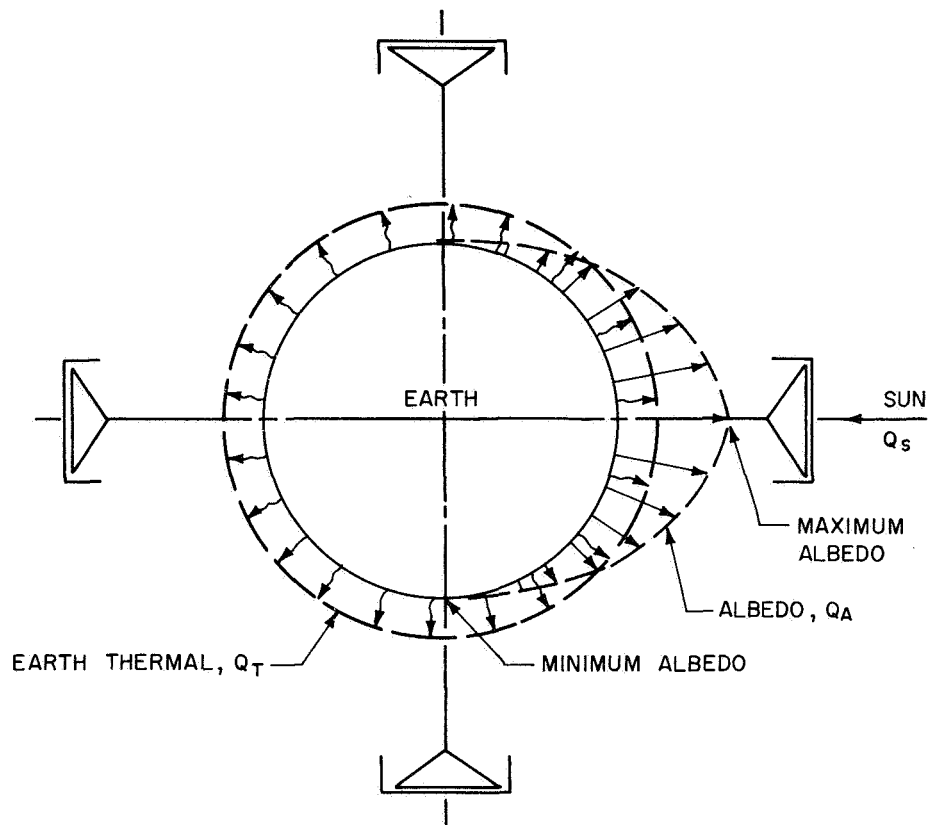


COMPONENT	MATERIAL	DIMENSIONS
1 HEAT SHIELD	5026-39 HC-G	THICKNESS: 1.34 TO 2.23 inches
2 AEROSHELL STRUCTURE	Al-HONEYCOMB	FACESHEET THICKNESS: 0.05 TO 0.017 inch
3 ATTACHMENT RING	Ti	CORE HEIGHT: 0.42 inch
4 STRUT (8 TOTAL)	TiII	THICKNESS: 0.2 inch LENGTH: 19.5 inches
5 INSULATION ASSEMBLY	VARIOUS	CROSS SECTION: 0.286 inch ²
6 HEAT SINK	BeO	
7 FUEL CAPSULES	VARIOUS	
8 SUPPORT STRUCTURE	Cb IZr	
9 HEAT EXCHANGER	Cb IZr	

NOTE: DATA IN PARENTHESES ARE MOST PROBABLE THERMAL LOSSES. TOTAL LOSS
460 watts + STRUT LOSS 150 watts = 610 watts

89-3392

Figure 3-119 REFERENCE DESIGN -- NORMAL OPERATION



REFERENCE ORBIT: 100 nm, CIRCULAR POLAR, 90 degree INCLINATION, SUN IN ORBIT PLANE
 IRV ORIENTATION: PERMANENTLY TOWARDS EARTH
 SOLAR RADIATION: $Q_s = 0$
 EARTH THERMAL: $Q_T = 63 \text{ Btu/hr-ft}^2$
 EARTH ALBEDO: $Q_{A \text{ max.}} = 169 \text{ Btu/hr-ft}^2$
 $Q_{A \text{ min.}} = 2 \text{ Btu/hr-ft}^2$
 ORBITAL AVERAGE = 53 Btu/hr-ft^2

89-3393

Figure 3-120 ORBITAL GEOMETRY AND INCIDENT HEAT LOADS -- NORMAL OPERATION

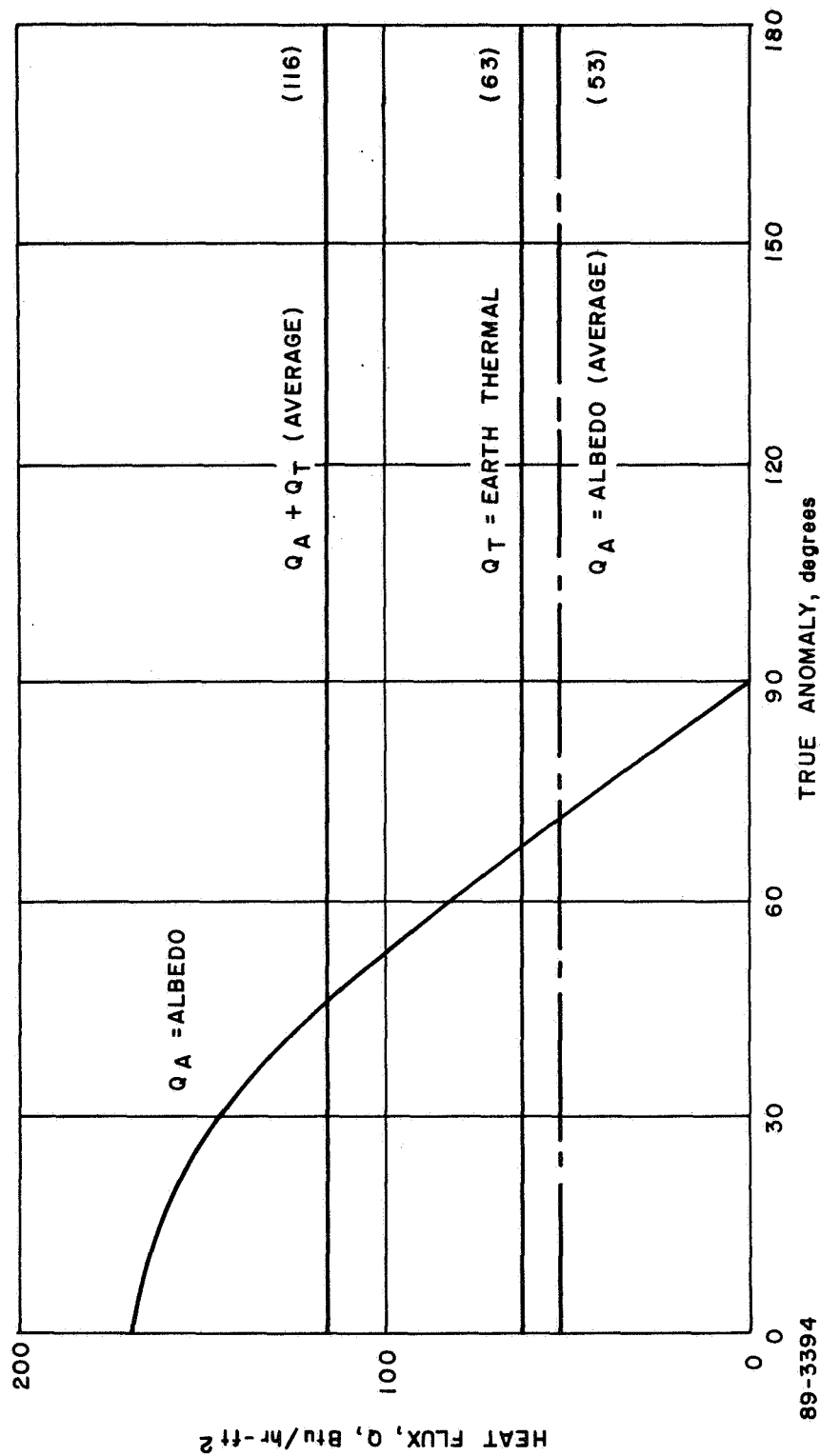


Figure 3-121 INCIDENT RADIATION VERSUS TRUE ANOMALY FOR REFERENCE ORBIT --- NORMAL OPERATION

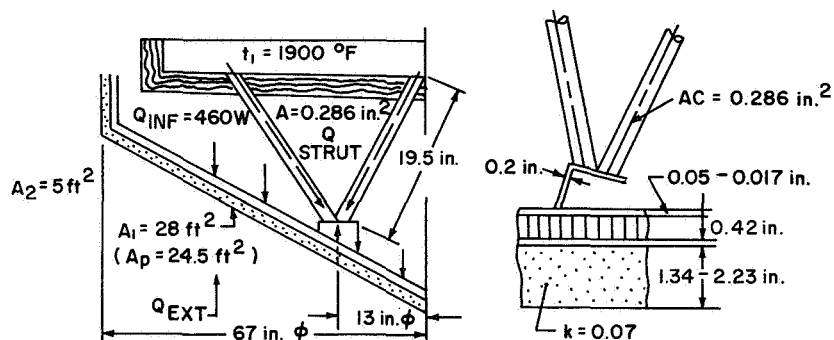
TABLE 3-29

THERMAL MODEL, PROPERTIES AND DIMENSIONS NORMAL OPERATION

ASSUMPTIONS

Thermal Model

Multi-dimensional conduction through struts, attachment ring, aeroshell structure and heat shield.



External Thermal Environment

- a. Permanent space exposure*
- b. Earth thermal radiation and albedo, no direct sun, for reference orbit (100 nm, circular, polar orbit, 90 degree inclination, permanent earth orientation).
- c. Permanent sun exposure*

Aeroshell Coating

Degraded "stable" white coating (zinc oxide/potassium silicate):
 $\alpha = 0.4^{**}$
 $\epsilon = 0.9$

Thermal Conductivities

Component	Material	k***
Heat shield	5026-39/HC-G	0.07
Aeroshell structure	Al [†]	100.
Attachment ring	Ti	10.
Struts	Ti11	38.

*Analyzed for comparison only.

**Value assumed for analysis only.

***Btu/hr-ft-°F

†Honeycomb, $\rho = 0.03$ of Al

$$Q_{IN} = Q_{OUT} \quad (1)$$

$$a_s q_A A_P + a_I q_T A_P + q_{INT} = \epsilon \sigma A_T T^4 \quad (2)$$

Albedo + Earth Thermal + Internal = Reradiated

$$T = \left[\frac{1}{\sigma} \left(\frac{a_s}{\epsilon} \frac{A_P}{A_T} q_A + \frac{a_I}{\epsilon} \frac{A_P}{A_T} q_T + \frac{q_{INT}}{\epsilon A_T} \right) \right]^{1/4} \quad (3)$$

where

q_A = incident albedo (Btu/hr-ft²)*

q_T = incident earth thermal radiation (Btu/hr-ft²)*

q_{INT} = internal energy (Btu/hr)

a_s = solar absorptance

a_I = infrared absorptance

ϵ = infrared emittance

A_P = projected area, relative to the sun (ft²)

A_T = total radiating area (ft²)

σ = Stefan-Boltzmann constant (0.1714×10^{-8} Btu/ft²-hr-° R⁴)

T = absolute temperature (° R)

Examination of Equation 3 leads to the following conclusion:

In the case of no or low internal heat dissipation, the temperature decreases with higher ϵ and is largely controlled by the a/ϵ ratio. The higher the internal heat dissipation, the less effective a/ϵ , i.e., internal heating dominates over external heating. If internal heat dissipation is a problem, the ratio should be minimized and ϵ should be maximized. Equation 3 also shows that the effect of incident earth radiation on temperature is independent of a or ϵ (assuming $a = \epsilon$).

*Incident heat fluxes include the geometric form factor for the appropriate radiation.

The bulk of this analysis has been performed by use of a digital computer thermal network analyzer.

3.4.2.1.3 Thermal Control Coating Selection -- Table 3-30 indicates the optical properties of potential thermal control coatings. It should be noted that before any coating can be selected a test program should be conducted to ascertain any problems with respect to degradation and compatability with the heat shield.

TABLE 3-30

ABLATOR COATING SYSTEM SUMMARY

Type	α	ϵ	α/ϵ	Remarks
No coating (Avcoat 5026-39/ HC-G)	0.6	0.9	0.666	High α highly undesirable
Zinc oxide/ potassium silicate; undegraded	~ 0.2	~ 0.9	~ 0.222	
Degraded coating	0.4	0.9	0.444	Selected for analysis
Silver/ silica	0.05	0.8	0.063	"Second generation" coating

The zinc oxide/potassium silicate coating ("stable" white coating), (Refs. 3-29 and 3-30) appears to be the most preferable coating available at the present time. The coating selection may have to be revised as initial research is continuing with silver/silica ("second generation") thermal control coatings. These coatings consist of a silver deposit overcoated with silica in a vapor deposition process (Ref. 3-31). The very low α/ϵ ratio of these coatings would make them preferable to other coating systems.

As indicated in Table 3-30, the undegraded value of α for the zinc oxide/potassium coating is 0.20. For practical purposes, the 5-year design life-time in orbit, a nuclear environment and undetermined heat shield compatibility problems should be considered. A coating value ($\alpha = 0.4$, $\epsilon = 0.9$) has, therefore, been selected which falls between the uncoated ablator ($\alpha = 0.6$) and the undegraded zinc oxide/potassium silicate coating ($\alpha \approx 0.2$). Recent laboratory data indicate that the zinc oxide potassium silicate paint-type

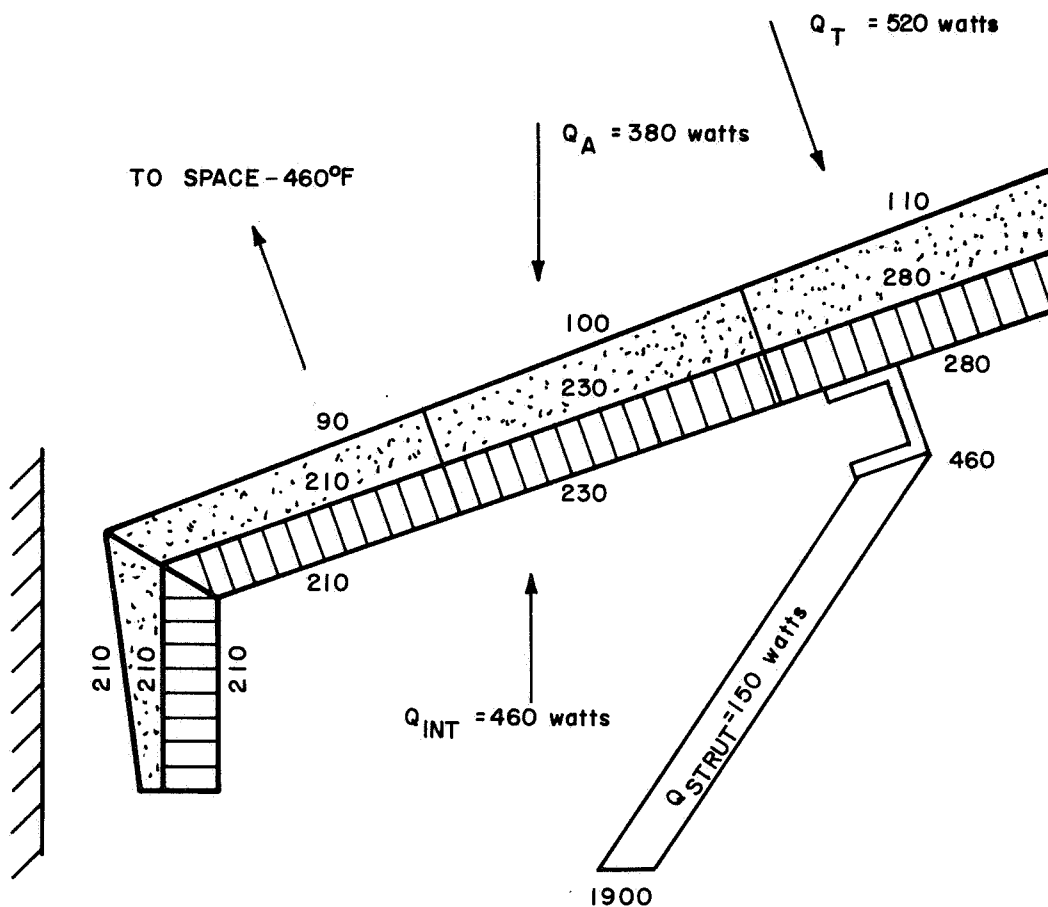
coating IITRI No. Z-93 showed reasonable stability of solar absorptance at 300° F for a testing duration of approximately 5000 hours (Ref. 3-32). The increase in solar absorptance observed was 0.06 with initial and final values of 0.14 and 0.20, respectively. If this lower value of degraded absorptivity ($\alpha = 0.20$) is valid for a 5-year lifetime a reduction in temperatures of approximately 10° and 75° F would be realized for the reference orbit and sun-exposed cases respectively.

3.4.2.1.4 Summary of Results -- Steady-state temperature distributions are shown in Figure 3-122 for the reference case (normal operation, reference orbit, aluminum aeroshell). Aeroshell hot-spot temperatures of 280° F can be expected, which is higher than the desirable limit of 200° F but tolerable. Temperature distributions in an aluminum and titanium aeroshell are compared in Figure 3-123 for exposure to sun and space (no earth or albedo radiation). The most favorable situation is an aluminum aeroshell permanently exposed to space with a resulting hot-spot temperature of 200° F. A change from aluminum to titanium will cause a hot-spot temperature increase by 120° F under the most favorable environmental condition (i.e., radiation to space).

Study results are summarized as follows:

- An aluminum aeroshell (in contrast to titanium) (Figure 3-123) tends to distribute internal heat loads quite well and thus to reduce hot-spot temperatures significantly. Aluminum has therefore been selected for reference design aeroshell material.
- Temperatures are marginal but within limits in the realistic case of no direct solar exposure but full exposure to earth and albedo radiation.
- Temperatures are well within limits in the case of space exposure only, and out of limits in the case of full sun exposure.

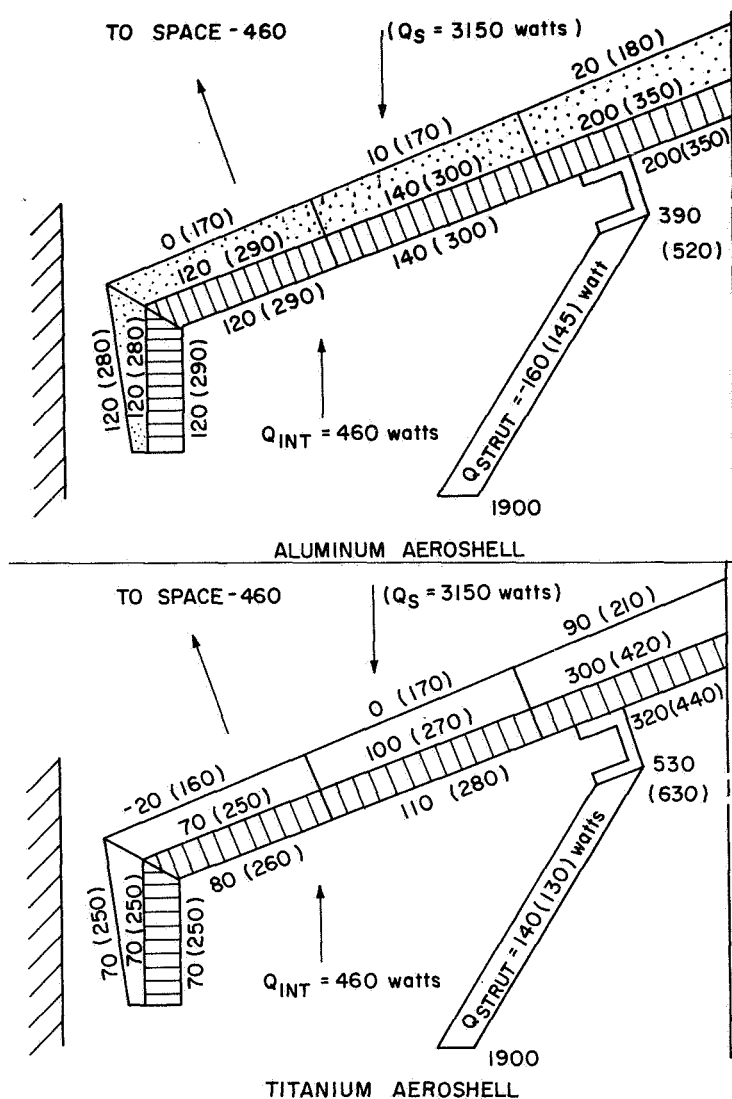
3.4.2.1.5 Conclusions -- It is concluded that, since temperatures in the actual case of interest are marginal, and the temperature distribution within the aeroshell is largely affected by the interaction of many parameters, careful thermal design supported by further analysis and testing is mandatory to ensure adequate IRV performance.



Q_T = EARTH THERMAL RADIATION
 Q_A = EARTH ALBEDO (ORBITAL AVERAGE)
 Q_{INT} INTERNAL HEAT LOSSES (EXCEPT STRUT LOSSES)
 ALL TEMPERATURES IN °F

89-3395

Figure 3-122 STEADY STATE TEMPERATURE DISTRIBUTION FOR ALUMINUM AEROSHELL, REFERENCE ORBIT -- NORMAL OPERATION



Q_S = SOLAR RADIATION

Q_{INT} = INTERNAL HEAT LOSSES (EXCEPT STRUT LOSSES)

ALL TEMPERATURES IN °F

TEMPERATURES IN PARENTHESES REFER TO THE CASE OF SOLAR EXPOSURE

89-3396

Figure 3-123: COMPARISON OF ALUMINUM AND TITANIUM AEROSHELL, SUN AND SPACE EXPOSURE -- NORMAL OPERATION

3.4.2.2 Pad Fire Analysis

One of the environments that could be experienced by the IRV is a fireball caused by the catastrophic failure of a booster at launch. For the situation investigated here two boosters were considered, i.e., Titan III and Saturn V. The Saturn V environment is conservative relative to that of the Saturn I-B booster considered in the IRV program. The analysis must also consider the possibility of two vehicle orientations one of which would consist of the vehicle sitting with the capsules adjacent to the ground (Case A). The other situation would consist of the capsules facing upward and directly exposed to the fireball (Case B).

In the following analysis, it is assumed that the initial temperature of the heat source when first exposed to the fireball is 350° F. This temperature is consistent with the ACHX-cooled heat source when on the pad. In addition, heat shield properties were used which reflect the degree of degradation anticipated in this fireball environment.

The thermal models for these two cases are shown in Tables 3-31 and 3-32. The assumption is made that in either case the external node assumes immediately the temperature of the fireball. This assumption is, of course, conservative since some temperature drop will be experienced between the fireball and IRV. The internal conduction path in Case A between the heat source and ablator takes into account intact insulation, exposed to the atmosphere ($k = 0.0324 \text{ Btu/hr-ft-}^{\circ}\text{F}$) and an intact truss support system. In Case B, radiation through the air gap between the fireball exposed cover plate and the capsules is considered.

Results of this study are shown in a heat source temperature history, Figure 3-124, together with the two environments under consideration. Results are summarized as follows:

The heat source temperature rise in the upside-down configuration (Case A) is governed by the internal heat generation and amounts to approximately 600° F/hour. The superinsulation temperature limit (2500° F) is reached in less than 4 hours. It is felt that, before any critical heat source temperature would develop, a rescue team would be able to alleviate the problem. The heat source temperature in the heat source up configuration never exceeds 1500° F during initial exposure to any environment. The maximum temperatures are 1450° (Titan III). After the fireball has burned out, the capsule cover plate will approach a steady-state temperature of approximately 1000° F.

From the above results, it is concluded that heat source temperatures reached during a pad fire under the assumption of worst-case environmental conditions are below allowable transient and steady-state temperatures. Therefore, the fireball environment, due to its transient nature, does not appear to represent a limiting thermal case for this analysis.

3.4.2.3 Upside-down Landing

A finite possibility exists for the vehicle to eventually land in a position with the base plane (and heat source) flat against the ground. This could be caused most probably by a flip over or tumbling of the vehicle after impact with the ground.

TABLE 3-31

PAD FIRE THERMAL ANALYSIS AND DESIGN DATA -- CASE A, HEAT SOURCE DOWN

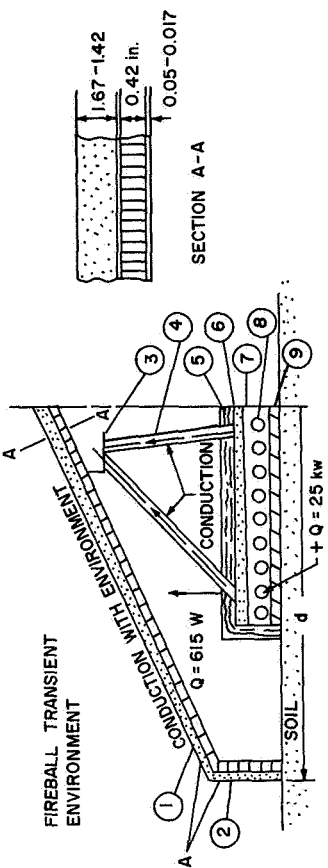
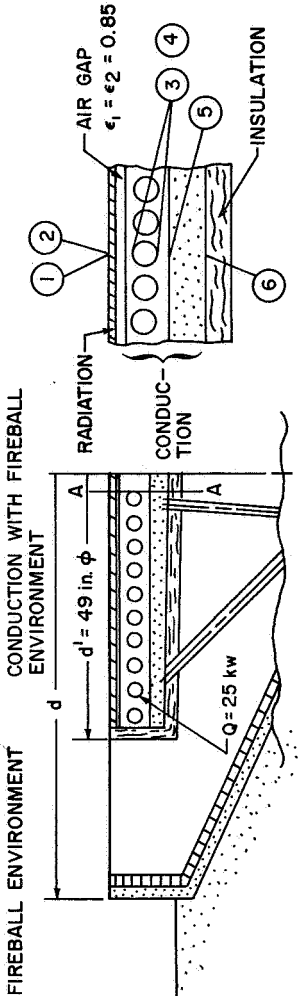
<p>REENTRY VEHICLE DATA:</p> <p>Diameter $d = 68$ inches</p> <p>Surface Area $A = 33\text{ft}^2$</p> <p>Materials:</p>			 <p>Diagram labels: FIREBALL TRANSIENT ENVIRONMENT, CONDUCTION WITH ENVIRONMENT, CONDUCTION, SOIL, $Q = 615 \text{ W}$, $Q = 25 \text{ kW}$, SECTION A-A</p>		
Node	Material	Thickness (in.)	Weight (lb/node)	$C_p \rho \Delta T$ (Btu/lb-°F)	k (Btu/hr-°F-ft)
① Heat Shield	5026-39/HC-G	1.67 to 1.43	110.	0.35	0.40
② Aeroshell Structure	Al-Honeycomb	0.42	30.	0.21	100.
③ Attachment Ring	Ti	0.2	7.3	0.13	10.
④ Strut (8 total)	T-111	(x)	--	0.035	40.
⑤ Insulation Assembly	--	--	193.	--	0.0324
⑥ Heat Sink	BeO	1.2	170.	0.50	10.
⑦ Structure	Cb-Izr	0.055	232.	0.083	38.
⑧ Capsules (164)	PuO ₂ T-111 Pt	-- -- --	150. 455. 150.	0.056 0.034 0.044	38.
⑨ Cover Plate	Cb-Izr T-111	0.055	67. 20.	0.083 0.034	(38.) 38.
THERMAL ENVIRONMENT					
<p>External: Fireball transient</p> <p>Internal: Heat load 25 kw, total heat loss 615 watts (insulation exposed to air) + strut loss</p> <p>Initial Temperatures: 350° F (entire vehicle)</p> <p>(x) Length: 19.5 inches, cross section: 0.286 in.²</p>					

TABLE 3-32

PAD FIRE THERMAL ANALYSIS AND DESIGN DATA -- CASE B, HEAT SOURCE UP

REENTRY VEHICLE DATA					
 <p> FIREBALL ENVIRONMENT CONDUCTION WITH FIREBALL ENVIRONMENT RADIATION CONDUCTION AIR GAP $\epsilon_1 = \epsilon_2 = 0.85$ INSULATION d = 67 inches Surface Area A = 33 ft² Q = 25 kw d' = 49 in. ϕ A </p>					
Materials:					
Node	Material	Thickness (inch)	Weight (lb/node)	C_p (Btu/lb-°F)	k (Btu/hr-°F-ft)
(1) (2) Cover Plate	Cb-1Zr T-111	0.055	67. { 87. 20.	0.083 0.034	(38.) 38.
(3) (4) Capsules (156)	PuO ₂ T-111 Pt	-- -- --	150. { 755. 455. { 150.	0.056 0.034 0.044	38.
(5) Structure	Cb-1Zr	0.055	232.	0.083	38.
(6) Heat Sink	BeO	1.2	170.	0.50	10.
THERMAL ENVIRONMENT					
External: Fireball transient Internal: Heat load 25 kw Initial Temperatures: 350° F (entire vehicle)					

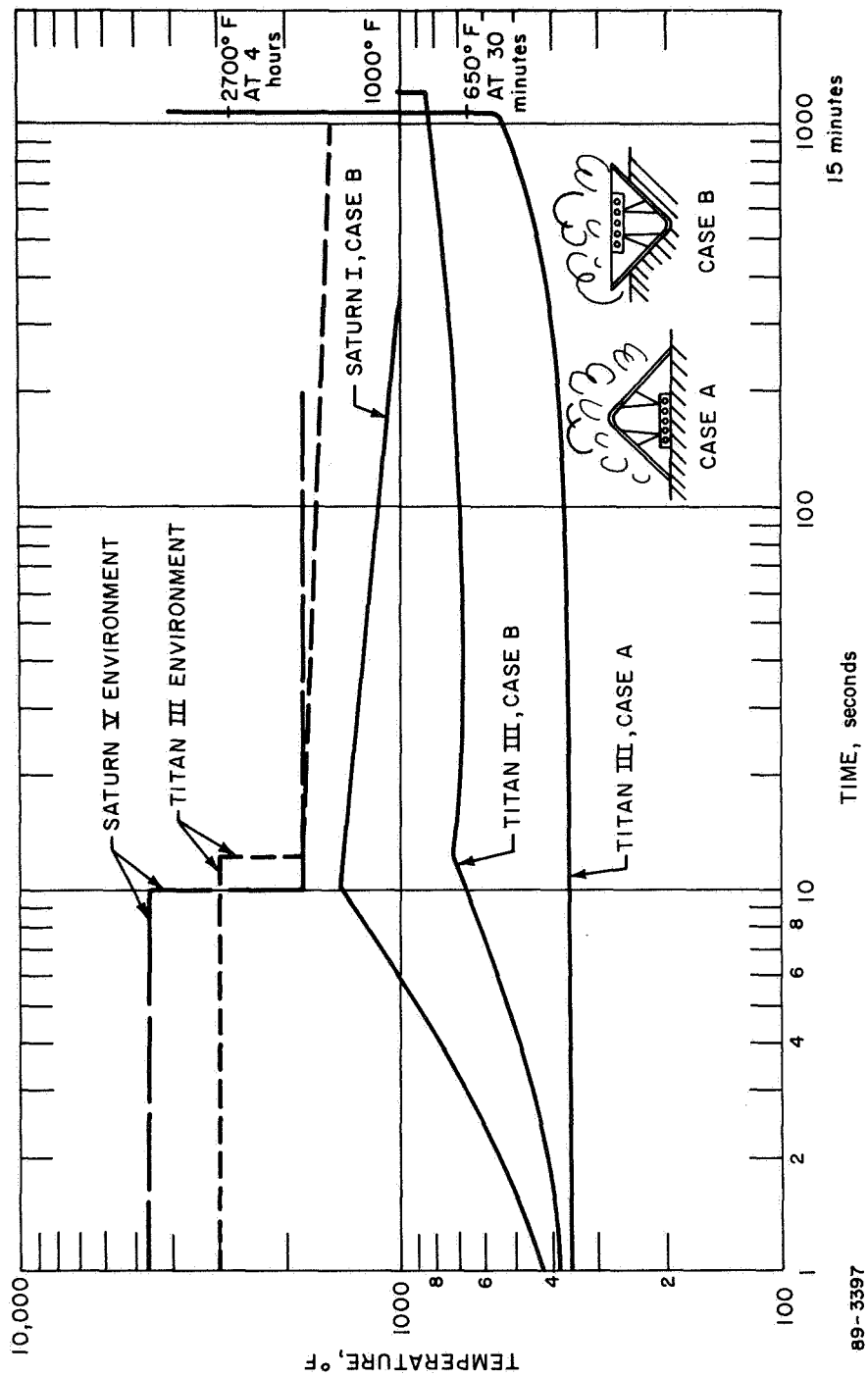


Figure 3-124 HEAT SOURCE TEMPERATURE HISTORY -- FIREBALL

To evaluate the problems associated with such a condition, a thermal analysis was performed. The assumptions used in the study include:

- 1) a heat source impact temperature of 1900° F.
- 2) an initial aeroshell temperature of 80° F with both radiation and convection to atmosphere.
- 3) aluminum honeycomb aeroshell structure is oxidized.
- 4) struts are destroyed at impact.
- 5) heat source insulation is destroyed either by impact or oxidation.
- 6) low density ablator is partially degraded consistent with reentry analysis.

The most critical assumption above is 5) since elimination of the insulation is required to make the heat source temperatures acceptable. While some question might exist concerning this assumption, it should be noted that, if necessary, some design alteration could be made to automatically destroy the insulation at impact. The necessity of this latter approach, however, would depend on results of tests conducted on the insulation material to see if it would be destroyed by the higher temperatures experienced after impact.

The thermal network analyzed consists of ten nodes with dimensions, properties, and a thermal environment as shown in Table 3-33. Radiative interchange has been considered internally between the lumped masses of the heat source assembly (Nodes 5 to 7) and the opposite oxidized honeycomb facesheet (Node 4) as well as between the honeycomb facesheet and the ablator backface (Nodes 2 and 3). In all cases, an emittance of 0.9 was used. Externally, the analysis considers radiation and natural convection from the charred ablator surface ($\epsilon = 0.9$) to the atmosphere as well as soil conduction. A conservative external convective heat transfer coefficient of $h = 1.0 \text{ Btu/hr-ft}^2\text{-}^{\circ}\text{F}$ has been assumed. A more realistic coefficient ($h = 1.8 \text{ Btu/hr-ft}^2\text{-}^{\circ}\text{F}$, Ref. 3-33) would result in a decrease in temperature of approximately 50° F relative to those temperatures indicated in Figures 3-125 and 3-126. Significant temperature histories and distribution summaries are shown in Figures 3-125 and 3-126. Results are summarized as follows:

Ablator and honeycomb structure steady-state temperatures are approached very rapidly during the first hour. From there on, temperatures increase slowly to achieve virtual steady-state conditions after more than 10 hours.

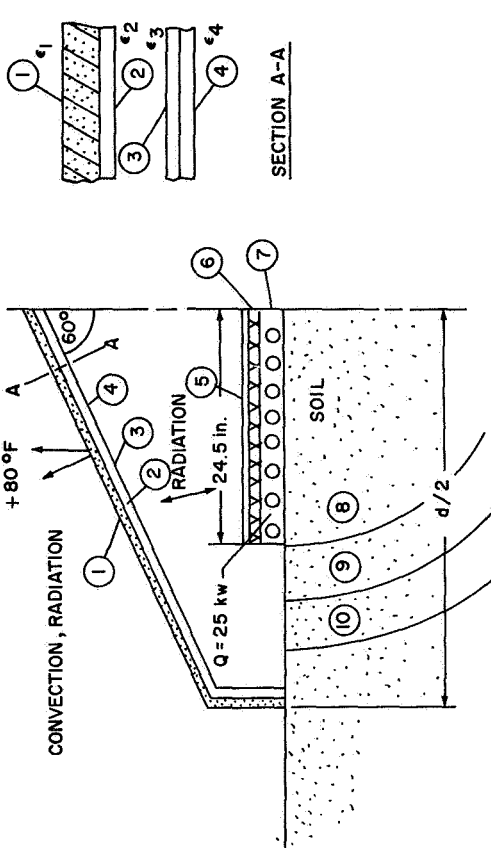
The heat source temperature decreases slightly during the first hour, depending on initial assumptions, but increases afterwards at a rate of between 88° F/hour (between 0.5 and 1.5 hours) and 12° F/hr (between 5 and 6 hours) in the case of no soil conduction. If soil conduction is considered, the equivalent rate is 67° F/hour and 9° F/hour.

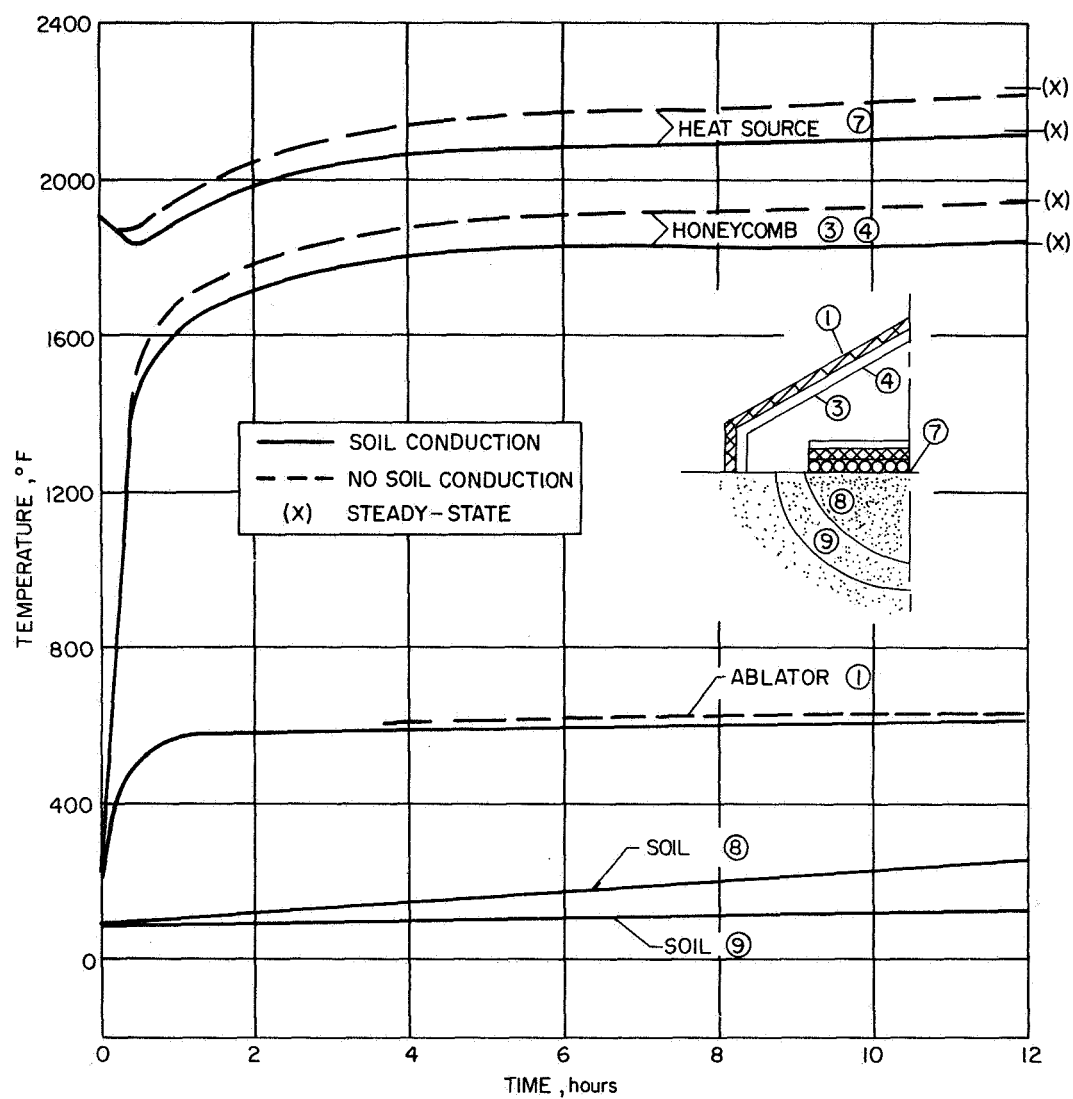
Heat source steady-state temperatures are expected after more than 10 hours and have been estimated to be 2220° F (no soil conduction) and 2120° F (soil conduction) for the two cases under consideration.

Assuming the validity of the thermal model analyzed, the IRV can survive for a limited time only until the maximum continuous heat source temperature of 2000° F

TABLE 3-33

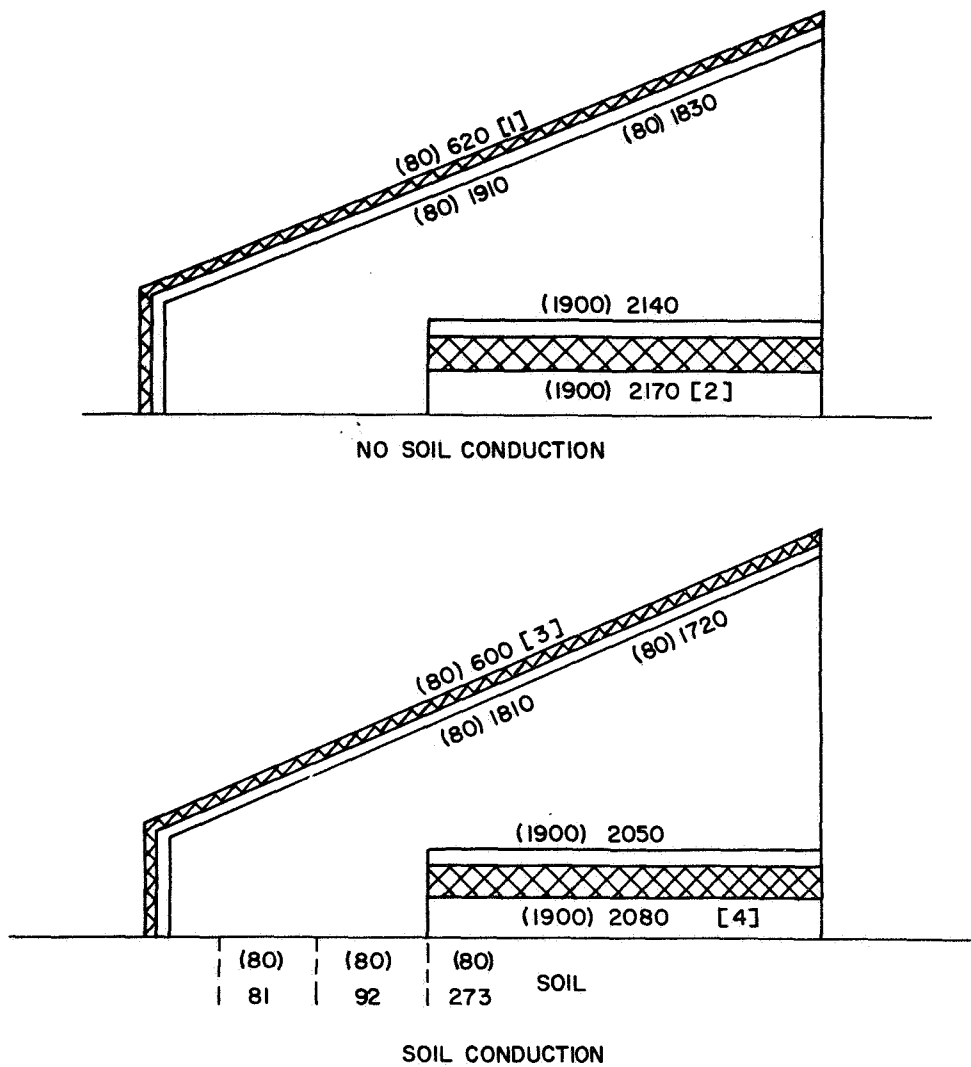
UPSIDE-DOWN AND POST IMPACT THERMAL ANALYSIS AND DESIGN DATA

<p>REENTRY VEHICLE DATA</p> <p>Diameter d - 68 inches</p> <p>Surface area A - 33ft²</p> <p>Materials:</p>						
						
Node	Material	Thickness (inch)	Weight (lb/node)	C_p (Btu/lb-°F)	k (Btu/hr-°F-ft)	ϵ
(1) Ablator	Charred ablator	1.2	117.	0.5	0.21	0.9
(2) (3) (4) Honeycomb	Al ₂ O ₃	0.016 (ea.)	12.	0.26	3.0	0.5
(5) Support	Cb-lZr	--	320.	0.07	40.	0.5
(6) Heat Sink	BeO	--	185.	0.5	10.	--
(7) Fuel Capsules	(T-111)	--	755.	0.035	40.	--
(8) (9) (10) Soil	Sand	--	various	0.20	0.20	--
<p>THERMAL ENVIRONMENT</p> <p>External: Atmosphere and initial soil temperature 80° F</p> <p>Internal: Heat load 25 kw</p> <p>Initial Temperatures: Ablator, honeycomb 80° F</p> <p>Heat sink, fuel capsules 1900° F</p>						



89-3398

Figure 3-125 UPSIDE-DOWN LANDING AND POST IMPACT TEMPERATURE HISTORY



ALL TEMPERATURES IN °F
 NUMBERS IN PARENTHESES ARE INITIAL TEMPERATURES
 [1] STEADY STATE TEMPERATURE, 630°F
 [2] STEADY STATE TEMPERATURE, 2220°F
 [3] STEADY STATE TEMPERATURE, 610°F
 [4] STEADY STATE TEMPERATURE, 2120°F

89-3399

Figure 3-126 UPSIDE-DOWN LANDING AND POST IMPACT TEMPERATURE HISTORY -- 6-HOUR EXPOSURE

is reached. The capsule transient behavior can only be approximately determined in a lumped-mass analysis while an exact prediction would require much more detailed analytical effort supported by test results.

3.4.3 Isotope Reentry Vehicle Preliminary Design

During the Phase II effort an IRV preliminary design was evolved and consisted of a 60 degree half-angle blunt cone with an outside diameter of 68.0 inches. The reference heat source within the vehicle was 49.0 inches in diameter and the top of the capsules are flush with the aft plane of the IRV. A view of the entire system can be found in Figure 3-127.

The main constituent in the IRV is the heat source since this item controls the vehicle size and weight. The unit is composed of 164 isotope capsules, support plate, truss and capsule retention systems and BeO for heat sink capabilities. (See Subsection 3.3 for details.) In addition, insulation surrounds the heat source to minimize losses to 1.5 kWt. This insulation must be designed to provide for acceptable temperatures of the location aids etc. which are located in the annulus adjacent to the heat source.

The basic structure of the vehicle consists of aluminum honeycomb sandwich with 0.017-inch face sheets and a 0.42-inch core. At regions where support is required (e.g., attachment ring) local thickening is provided to adequately handle the loads. This attachment ring (Figure 3-127a,) carries the reentry load from the heat source and distributes it around the aeroshell through a truss system. The struts comprising the truss system are insulated to reduce heat leaks. This ring approach is superior to point attachment since local areas are not subject to the relatively high loads, and also the hot-spot temperature problem due to the heat flow down the truss is reduced. The transition from cone-to-cylinder is accomplished at the aft end of the IRV. The cylinder is limited in length to 15 percent of the base radius due to subsonic stability considerations. This short cylinder section is the same sandwich material as the cone, locally reinforced to resist launch load conditions. The aft end of this section is terminated in a "C" shaped channel as a primary structural member. This channel is used to support the aerodynamic fence and rear cover which is covered with heat shield material. The aft cover also acts as a device for deploying the ballute.

To facilitate assembly of the aeroshell with the heat source, a removable nose cap is utilized. The nose cap is bolted around its periphery by a series of structural bolts protected by removable ablator plugs, Figure 3-127. A flexible RTV gasket is used to allow thermal expansion and to reduce loads to the ablator. A ballute is packaged in an annular cavity in the back surface of the IRV surrounding the heat source and insulation. This ballute is deployed late in reentry at low supersonic Mach number to augment drag and ensure survival at impact. The location aids have also been placed in this same cavity.

The reference heat shield material is the Apollo thermal protection system (Avcoat 5026-39 HC-G) which consists of an epoxy resin gunned into a fiberglass honeycomb matrix. The honeycomb is attached to the substructure with HT424 tape to ensure an adequate bond, and once this has been determined, the resin is gunned into the cores. Fiberglass edge members are required at joints and interfaces to eliminate the existence of open cells. The molded version of the Avcoat 5026-39 material would be used in the cylinder region of the vehicle to reduce attachment difficulties introduced at the cone-cylinder junction. Also, in the region of the

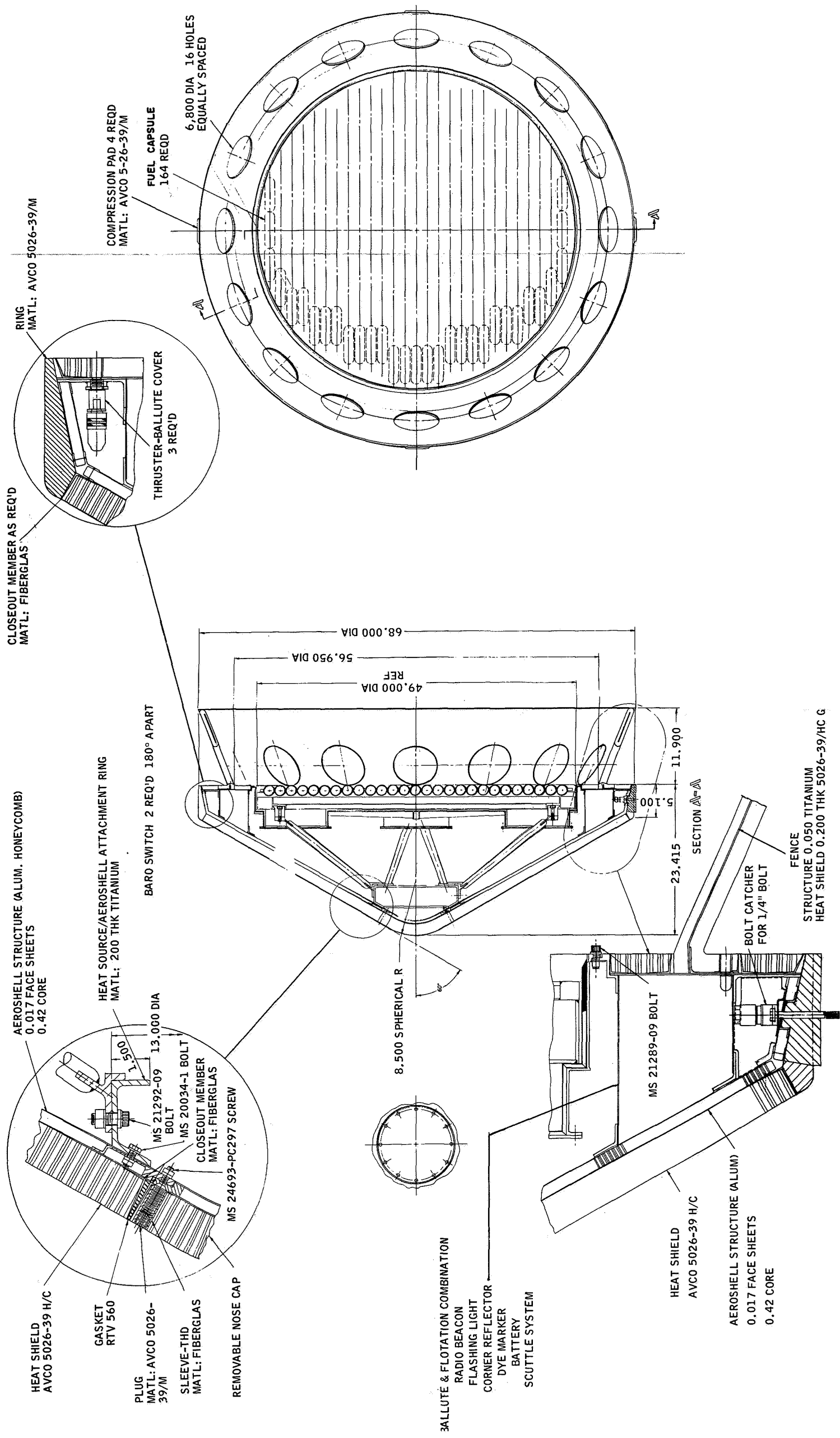


Figure 3-127 IRV WITH BALLUTE AND LOCATION AIDS -- 68-INCH DIAMETER REFERENCE DESIGN

rear door, either gunned or molded Avcoat 5026-39 could be used. Test data indicates that the thermal performance of the gunned and molded Avcoat 5026-39 is practically identical and, therefore, similar thicknesses would be adequate.

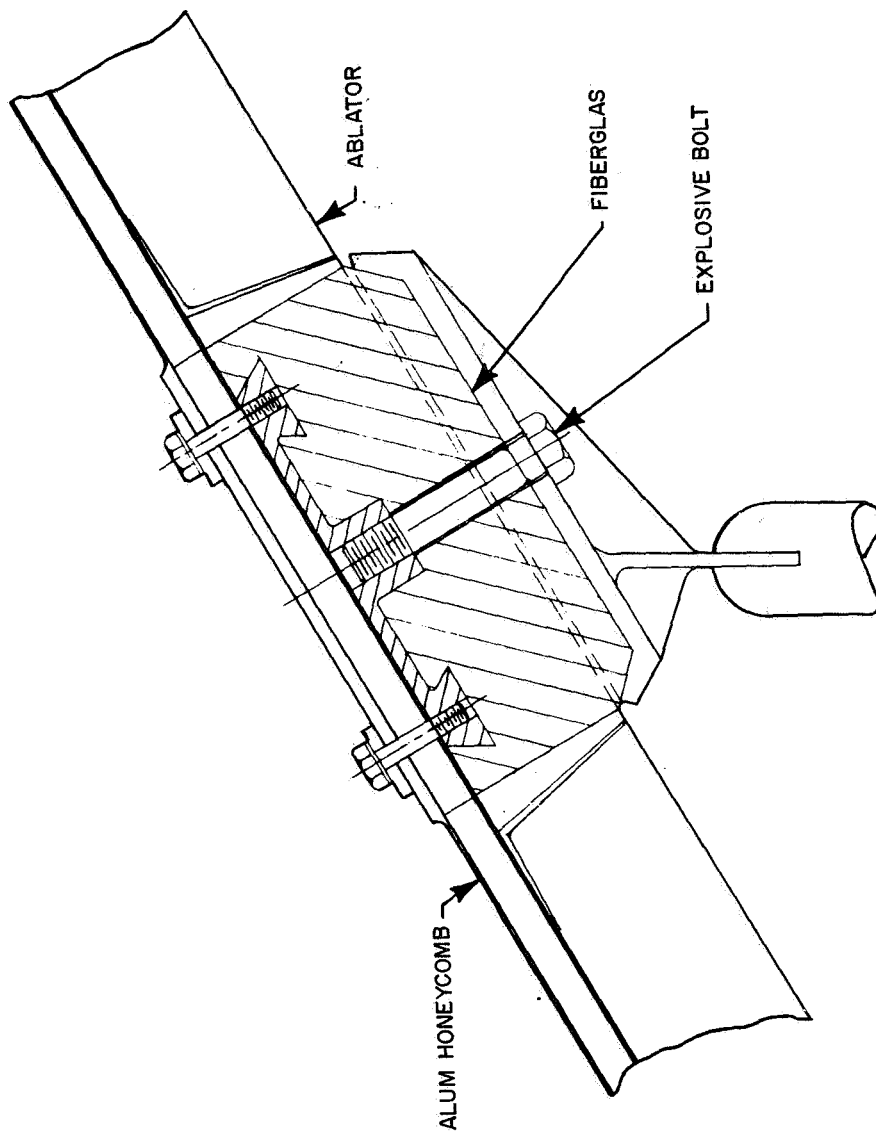
At four locations on the cylindrical section of the IRV Avcoat 5026-39 molded pads are provided which interface with the support ring attached to the spacecraft (Figure 3-127b). These pads are tapered (20-degree included angle) so that when separation is required, no locking will occur. At separation, an explosive bolt is fired which allows the release of the IRV from the support ring. The pads protrude about 0.6 inch above the adjacent heat shield which could cause some local erosion effects. However, a review of test data indicates that the environmental level of heating and shear is not above the material threshold level. In the configuration illustrated four fiberglass pads are located on the conical section of the aeroshell (see Figure 3-128) and are used to support the deorbit rocket assembly. Similar pad designs are used in Apollo and have performed adequately and therefore no problem is anticipated in these regions of dissimilar materials.

The turnaround device is made of titanium with ablator on the inside and outside because of the high heating possible in this area during various failure modes. The fence is defined as 35 percent of the vehicle base radius in length. There are also 16 holes equally spaced around the fence. The fence is attached to the rear door with plate nuts as shown in Figure 3-127b. Three squib actuated thrusters hold the cover/fence combination over the ballute cavity (Figure 3-127c). These are used to jettison the cover and deploy the ballute. These thrusters are triggered by a baroswitch which ejects the rear door and fence at the desired altitude, thus allowing operation of the ballute and other aids.

A summary of the weights of the IRV subsystems is shown in Table 3-34. The heat source is seen to represent 75 percent of the weight and, therefore, to reduce total weight significantly would require other approaches to the heat source design (e.g., vented capsules). The ballute and location aids weight 115 pounds together but do not increase the aeroshell weight significantly since aeroshell size is defined by the heat source diameter and allowable cylinder length. The reference fence design weighs 99 pounds (including heat shield) but this could be reduced to about 32 pounds if a three-dimensional graphite fence is used as a heat shield/structure combination. Table 3-35 summarizes the significant items as obtained from the IRV preliminary design study. Included are the mass properties (pitch and roll moments of inertia) center of gravity location and impact velocity for various vehicle attitudes.

3.5 REFERENCES

- 3-1 Isotope Reentry Vehicle Design Study, Conceptual Design, Phase IA, Topical Report, AVSSD-0071-68-CR, NASA CR 72366 (May 1968).
- 3-2 Golub, Cyril N., Environmental Parameters of an Aborted Launch, Pawa Inc.
- 3-3 Snap 27, Quarterly Progress Report (Fall 1967).
- 3-4 Isotope Reentry Vehicle Design Study, Conceptual Design, Phase IB, Topical Report, AVSSD-0193-68-CR, NASA CR 72463 (October 1968).



89-3400

Figure 3-128 DETAIL OF TRUSS AEROSHELL ATTACHMENT POINT

TABLE 3-34

MASS PROPERTIES SUMMARY
FOR REFERENCE DESIGN
(Vehicle Diameter 68 inches)

	Weight (pounds)
A. Heat Source	(1476)
Fuel Capsules	755
Heat Source Plate	402
Cover Plate Assembly	87
Support Structure	153
Insulation Assembly	79
B. Aeroshell	(386)
Heat Shield	215
Bond	4
Structure	68
Honeycomb	24
Truss Support	5
Brackets and Stiffeners	29
Hardware	10
Fence	99
Structure	15
Heat Shield	84
C. Ballute and Flotation Systems	(95)
D. Location Aids	(20)
E. IRV Entry Weight	(1977)

TABLE 3-35

ISOTOPE REENTRY VEHICLE (IRV)
PERFORMANCE SUMMARY

Configuration	60 degree Half-angle blunt cone
Diameter (in.)	68
X_{cg}/D	0.31
$W/C_D A$ (lb/ft ²) (hypersonic)	48
Terminal velocity (ft/sec)	
- $\alpha = 0$ degree	266
- $\alpha = 180$ degrees	232
Entry wt (lb)	
Moments of inertia:	
I_{xx} (roll, slug-ft ²)	186
I_{yy} (pitch, slug-ft ²)	102
Materials	
- Aeroshell	Aluminum honeycomb
- Fence	Titanium honeycomb
- Heat shield	Avco 5026-39 (Apollo heat shield material)

- 3-5 Burke, A.F., Shock Tunnel Tests of the Effect of Various Base Attachments on the Heat Transfer Distribution on the IRV Body at 180°, Interoffice Memo R500-68-35 (25 June 1968).
- 3-6 Climatic Extremes for Military Equipment, MIL-STD-210A.
- 3-7 Handbook of Geophysics, United States Air Force Geophysics Research Directorate (1961).
- 3-8 Airplane Strength and Rigidity - Flight Loads, MIL-A-8861 (ASG) (18 May 1960).
- 3-9 Conversation with N. Sissenwine, Air Force Cambridge Research Laboratories.
- 3-10 Coakley, T. J., Dynamic Stability of Symmetric Spinning Missiles, J. Spacecraft (October 1968), pp. 1231-1332.
- 3-11 Shirley, D. L. and J. E. Misselhorn, Instability of High-Drag Planetary Entry Vehicles at Subsonic Speeds, J. Spacecraft (October 1968), pp. 1165-1169.
- 3-12 Modified Transient and/or Steady-State (TOSS) Digital Heat Transfer Code, WANL-TME-1108 (13 February 1965).
- 3-13 Hargadon, J. M., Jr., Thermal Interface Conductance of Thermoelectric Generator Hardware, ASME, 66WA/NE-2.
- 3-14 Bourgette, D. T., High Temperature Stability of Refractor Base Alloys in Vacuum, Trans. Vac. Met. Conf. (1965).
- 3-15 Goodspeed, R. C., and R. W. Buckman, Evaluation of Refractory/Austenitic Bimetal Combinations, WANL-PR-EE-004, Final Tech. Report, NAS3-7634.
- 3-16 The Engineering Properties of Cb and Cb Alloys, DMIC Report 188 (6 September 1963).
- 3-17 Wah Chang Product Data, Columbium, Tantalum, and Tungsten Alloys Technical Incorporation, 3 (January 1968).
- 3-18 Thermophysical Properties of High Temperature Solid Materials, 2, Part 1, Purdue University (1967).
- 3-19 TRW Inc. Contract NAS3-2545, Eighteenth Quarterly Progress Report, CR-72524.
- 3-20 Glassner, A., The Thermodynamical Properties of the Oxides, Fluorides, and Chlorides to 2500° K, ANL-5750.
- 3-21 Thermophysical Properties of High Temperature Solid Materials, 4, Part 1, Purdue University (1967).
- 3-22 Ammon, R. L., and R. T. Begley, Pilot Production and Evaluation of Tantalum Alloy Sheet, Summary Phase Report, WANL-PR-M-004 (15 June 1963).
- 3-23 Davies, Robert Lee and Paul E. Moorhead, Properties and Fabrication of Refractory Alloys for Isotope Containment, NASA Lewis Research Center, Cleveland, Ohio (4 February 1969).

- 3-24 Kays, W. M., Convective Heat and Mass Transfer (New York, McGraw-Hill, 1966).
- 3-25 Kays, W. M., and A. L. London, Compact Heat Exchangers (New York, McGraw-Hill, 1964).
- 3-26 Perry, Chemical Engineering Handbook.
- 3-27 Percy, J. H., et al, SABOR III: A Fortran Program for Linear Elastic Analysis of Shells of Revolution by the Matrix Displacement Method, M.I.T. Aeroelastic and Structures Laboratory, TR 121-6, NASA STAR N 65-36654 (September 1965).
- 3-28 Parker, P. S. and P. B. Moulton, Avco Report TR-S10-T-195, Model Analysis of a Linear Dynamic System Computer Programs 1384 AM, AY, AW, B & M,
- 3-29 Pearson, B. D., Preliminary Results from the Ames Emissivity Experiment on OSO-II, Progress in Astronautics and Aeronautics, Vol. 18, Academic Press (1966), p. 459-472.
- 3-30 Streed, E. R., and J. C. Arvesen, A Review of the Status of Spacecraft Thermal Control Materials, SAMPE Volume II (Society of Aerospace Material and Process Engineers), Western Periodicals Co., 1967, p. 181-192.
- 3-31 Greenberg, S. A., D. A. Vance, and E. R. Streed, Low Solar Absorptance Surfaces with Controlled Emittance: A Second Generation of Thermal Control Coatings, AIAA Thermophysics Specialist Conference, New Orleans, Paper No. 67-343 (April 1967).
- 3-32 Aerospace Sciences Laboratory Lockheed Missiles and Space Company Sunnyvale Calif., Emissivity Coatings for Low Temperature Space Radiators, Interim Progress Report for Period Ending 1 June 1968, prepared for NASA/Lewis contract NAS-3-7630.
- 3-33 McAdams, Heat Transmission, 3rd Edition, McGraw-Hill.

4.0 HEAT SOURCE HEAT EXCHANGER (HSHX)

On the basis of the Phase IB studies, the 49-inch-diameter circular planar heat source was selected for Phase II, the detailed preliminary design effort. In addition, the 53.5-inch-diameter, 2-pass involute HSHX was selected as the basic approach for the HSHX.

The final heat source heat exchanger design configuration is illustrated in Figure 4-1. The core of the heat exchanger is composed of eighteen 1.44-inch-diameter tubes, each 68-inches long. Each tube describes an involute spiral from the outer circular ring manifolds to a central reversing header. The Brayton cycle working fluid is introduced into the top circular ring manifold where it is distributed to nine of the involute tubes, which conduct the gas across the core of the heat exchanger where it enters a central reversing header. From the central reversing header, the gas enters the nine return involute tubes where the gas is conducted back across the heat exchanger core and enters the bottom circular ring exit manifold. Thus, the major portion of the core consists of an array of tubes in which the flow in alternate tubes is in the opposite direction and the Brayton cycle working fluid makes two passes across the heat exchanger, one in and one out.

4.1 HSHX DESIGN

4.1.1 Description

The detailed involute HSHX design is shown in Figure 4-2. The basic heat transfer portion of the HSHX occupies a 48-inch-diameter circle corresponding to the size of the heat source. The Brayton fluid both enters and exits from the heat exchanger at the periphery and flows around the circumference in annular manifolds. The inlet manifold has a constant diameter of 2.40 inches and a wall thickness of 0.045 inch; it is located above the outlet manifold, in which has a diameter of 3 inches and a wall thickness of 0.045 inch. The 48-inch-diameter active portion of the heat exchanger is composed of 18 tubes, each with an O.D. of 1.44 inch and a wall thickness of 0.045 inch.

The Brayton fluid in the inlet manifold enters alternate tubes and follows an involute path toward the center of the HSHX where it enters a header box, is turned, and then reenters adjacent tubes, flowing back out to the periphery and exiting through the outlet manifold. Since the central header box is 4.0 inches in diameter, the tubes must be staggered around the circumference, with the inlet legs located above the outlet legs. Staggering is begun 4 inches from the center of the header box with the outlet legs undergoing a downward bend and the inlet legs joining the header box above the outlet legs. The weight of the heat exchanger is 130 pounds.

Although the actual physical layout of the tubes for the involute HSHX is not easy to visualize, it can be described by an algebraic equation. If ϕ , as shown in Figure 4-3, is the angle (with respect to a reference axis) that a radial line makes when drawn to intersect the tube centerline at radius r , then the angle ϕ in radians is

$$\phi = \sqrt{\left(\frac{r}{r_1}\right)^2 - 1} - \arccos \frac{r_i}{r}$$

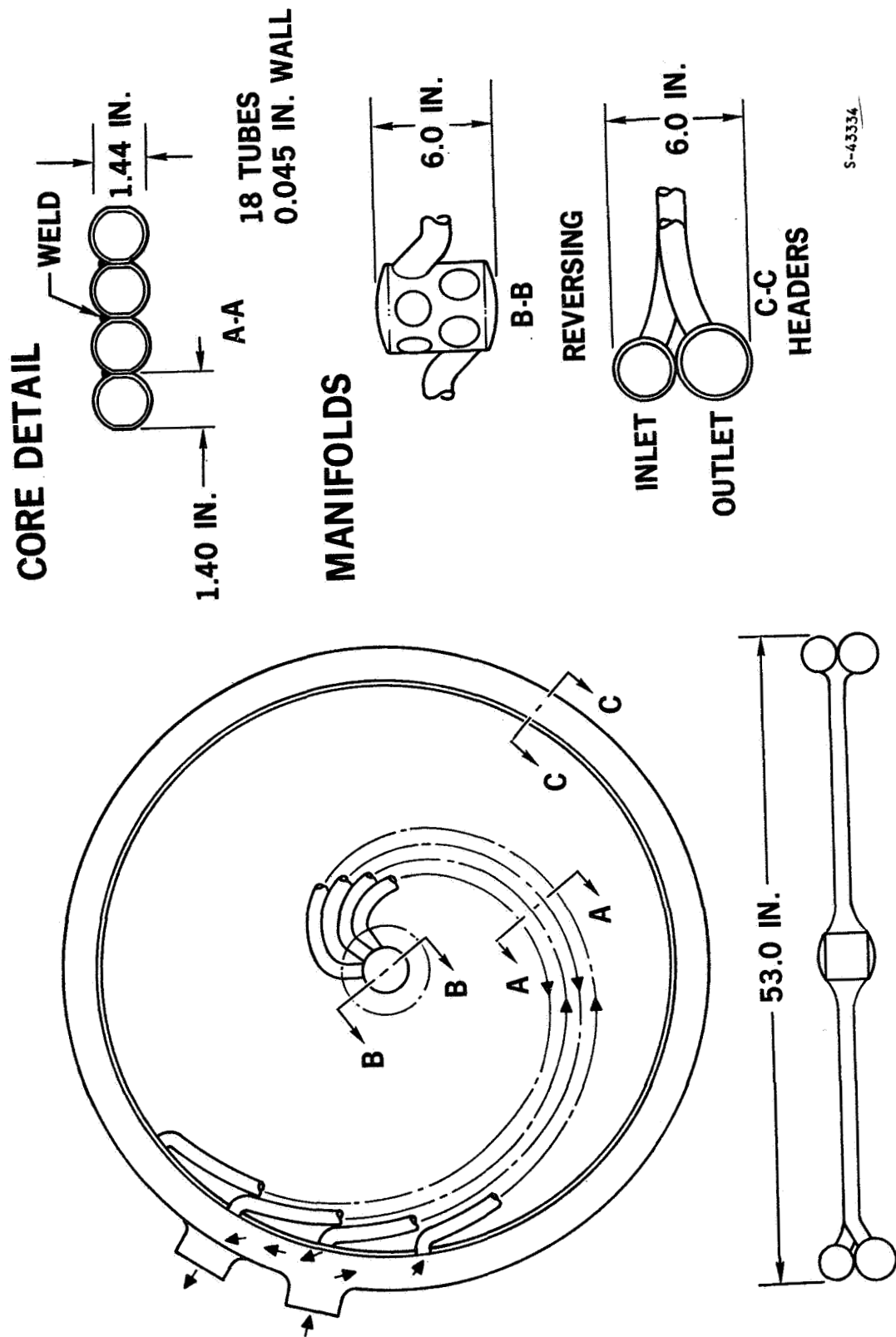


Figure 4-1 TWO-PASS TUBULAR HSHX -- FINAL CONFIGURATION

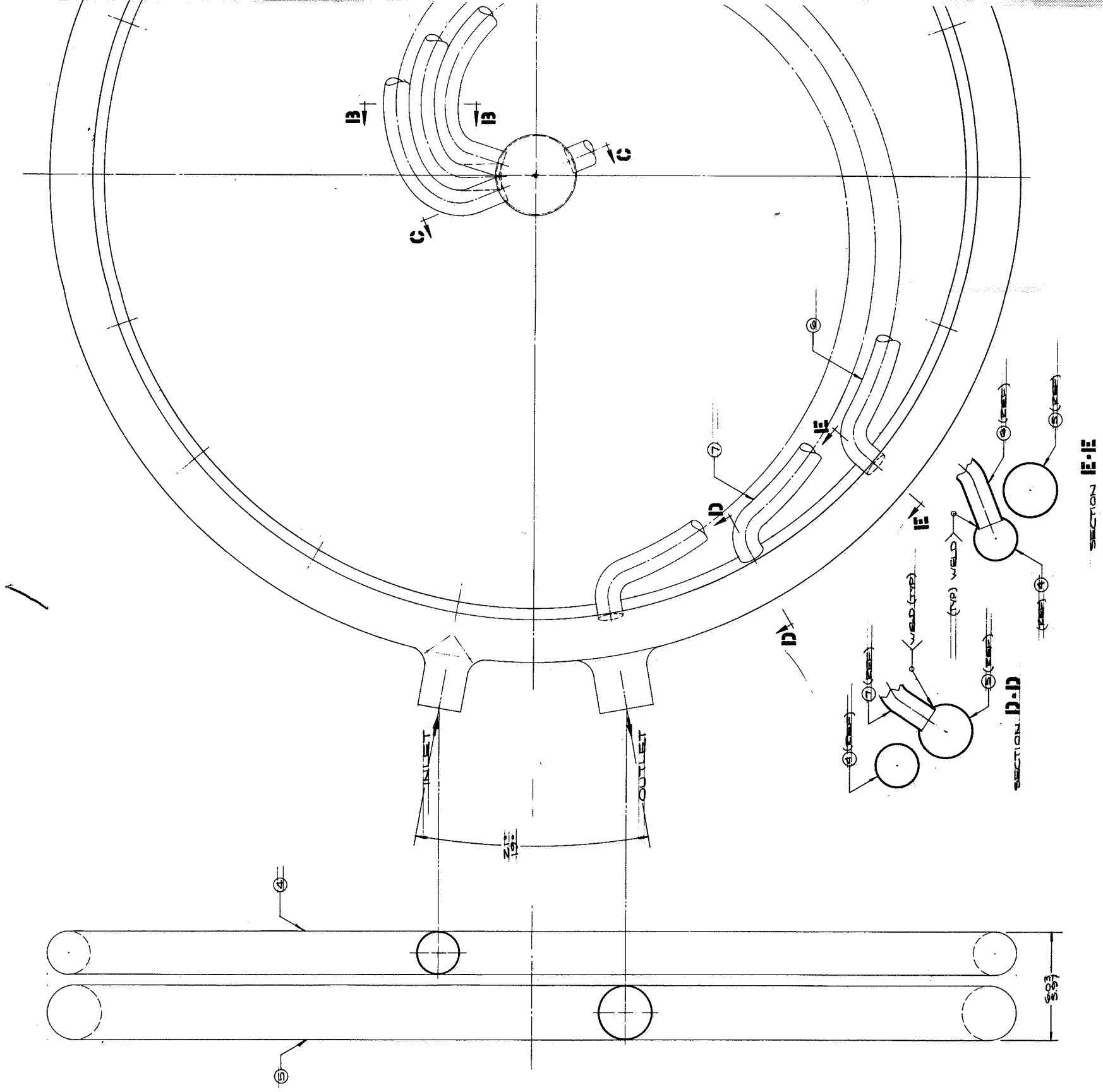


Figure 4-2 HSHX ASSEMBL

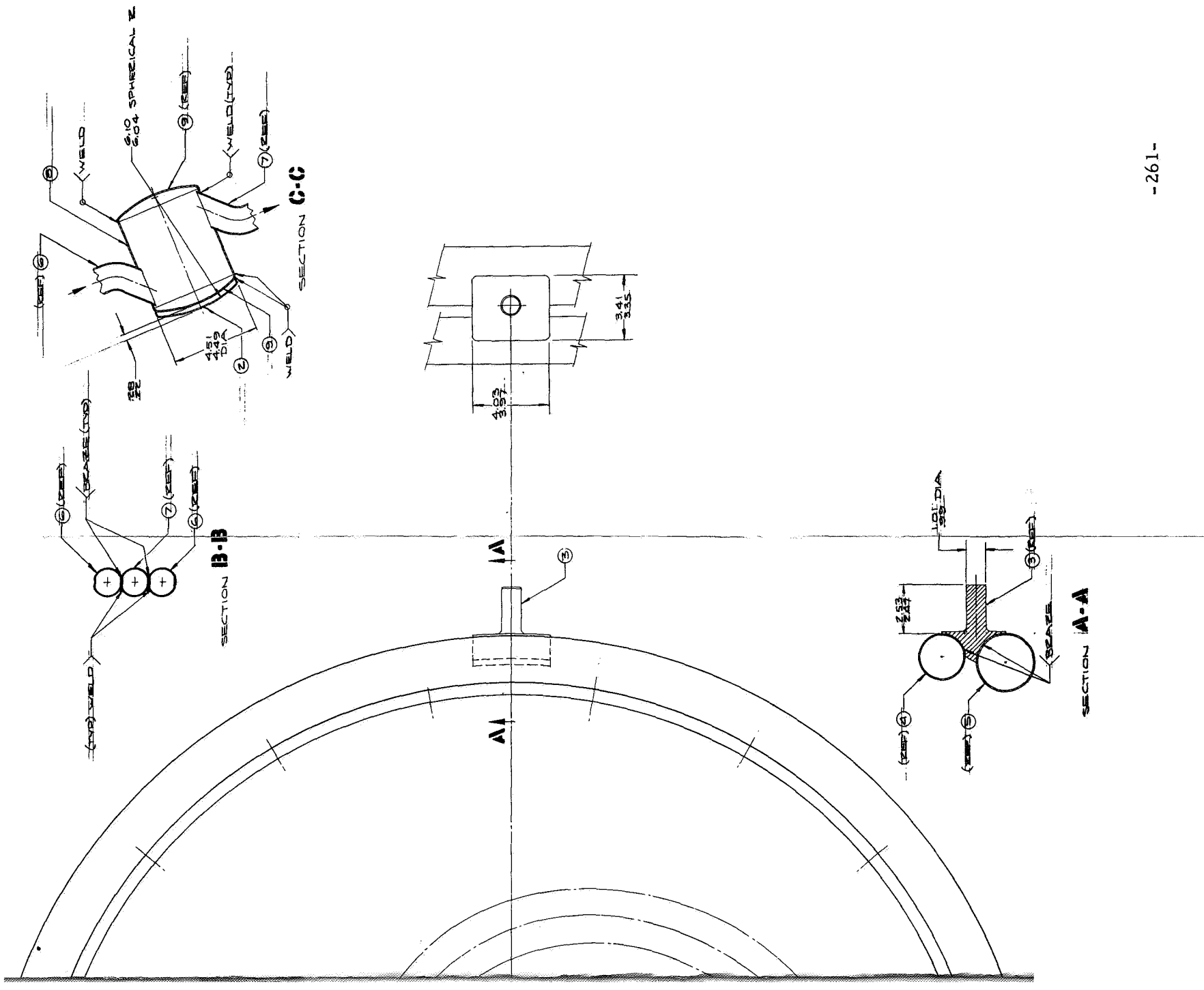
)). This equates tubes.

at the inter-
and outlet
ger must be
ie manifolds.
the heat ex-
d to join the
turn upward,
manifolds and

E AXIS

The flattened
on is also
g a sound
ermits ther-
ion of the

roaching
ere deter--



where r_i is the inner radius of the involute (in this case, 4 inches). This equation completely describes the involute pattern of the heat exchanger tubes.

The circular tubes are slightly flattened to provide enough surface at the interface between tubes to braze the tubes together. To join the inlet and outlet manifolds, the ends of the tubes at the periphery of the heat exchanger must be bent. The tubes are bent at almost right angles perpendicular to the manifolds. Superimposed on this, the inlet legs bend upward from the plane of the heat exchanger to join the inlet manifold, and the outlet legs turn downward to join the outlet manifold. Near the central header box, the inlet legs again turn upward, and the outlet legs turn downward. The tube ends are welded to the manifolds and the central header box.

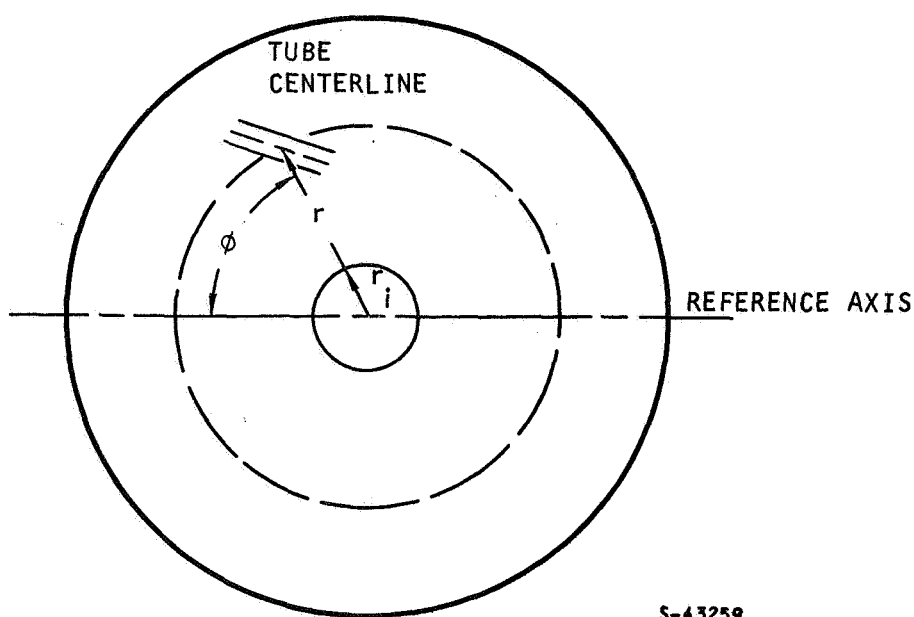


Figure 4-3 INVOLUTE TUBE GEOMETRY

The inlet and outlet legs are in close contact along their length. The flattened surfaces of the tubes form an interface that is brazed; this junction is also welded from one side of the heat exchanger. In addition to offering a sound structural approach to the HSHX design, this type of construction permits thermal conduction between the hot and cold legs, resulting in a reduction of the maximum temperature on the heat source.

4.1.2 Materials Selection

On the basis of a 5-year life in a vacuum at metal temperatures approaching 1800° F, the most important requirements for structural materials were determined to be the following:

- Resistance to evaporation effects

- Compatibility with emissive coatings
- Metallurgical stability
- Suitable mechanical and physical properties (creep resistance, short-time mechanical properties, thermal expansion, and elastic modulus)
- Fabricability
- Compatibility with brazing filler metals.

Emissive coatings will be required to achieve an acceptable temperature level. The requirements for emissive coatings are:

- Total normal emittance of at least 0.8
- Stability and adherence in vacuum at high temperatures for 5 years
- Compatibility with substrate material
- Adequate ductility
- Ease of application.

4.1.2.1 Structural Materials

The two basic alternatives for high-temperature structural materials are refractory metals and superalloys. The pertinent characteristics of candidate materials are treated in the following discussion.

4.1.2.1.1 Evaporation -- The evaporation of metallic constituents can lead to three major detrimental effects:

- Weakening of multicomponent alloys by internal void formation
- Degradation of emissive properties of coatings
- Possible loss of emissive coatings due to substrate evaporation.

Figure 4-4 shows evaporation rates in a vacuum as a function of temperature for various metals. The evaporation rates were calculated from vapor pressure data, using the following modification of the Langmuir equation:

$$S = 1.85 \times 10^6 \frac{Kp}{s} \frac{\sqrt{M}}{T}$$

where S = rate of sublimation, cm/yr

p = vapor pressure, torr

s = density of the solid material, gm/cm³

M = molecular weight of metal in the gas phase

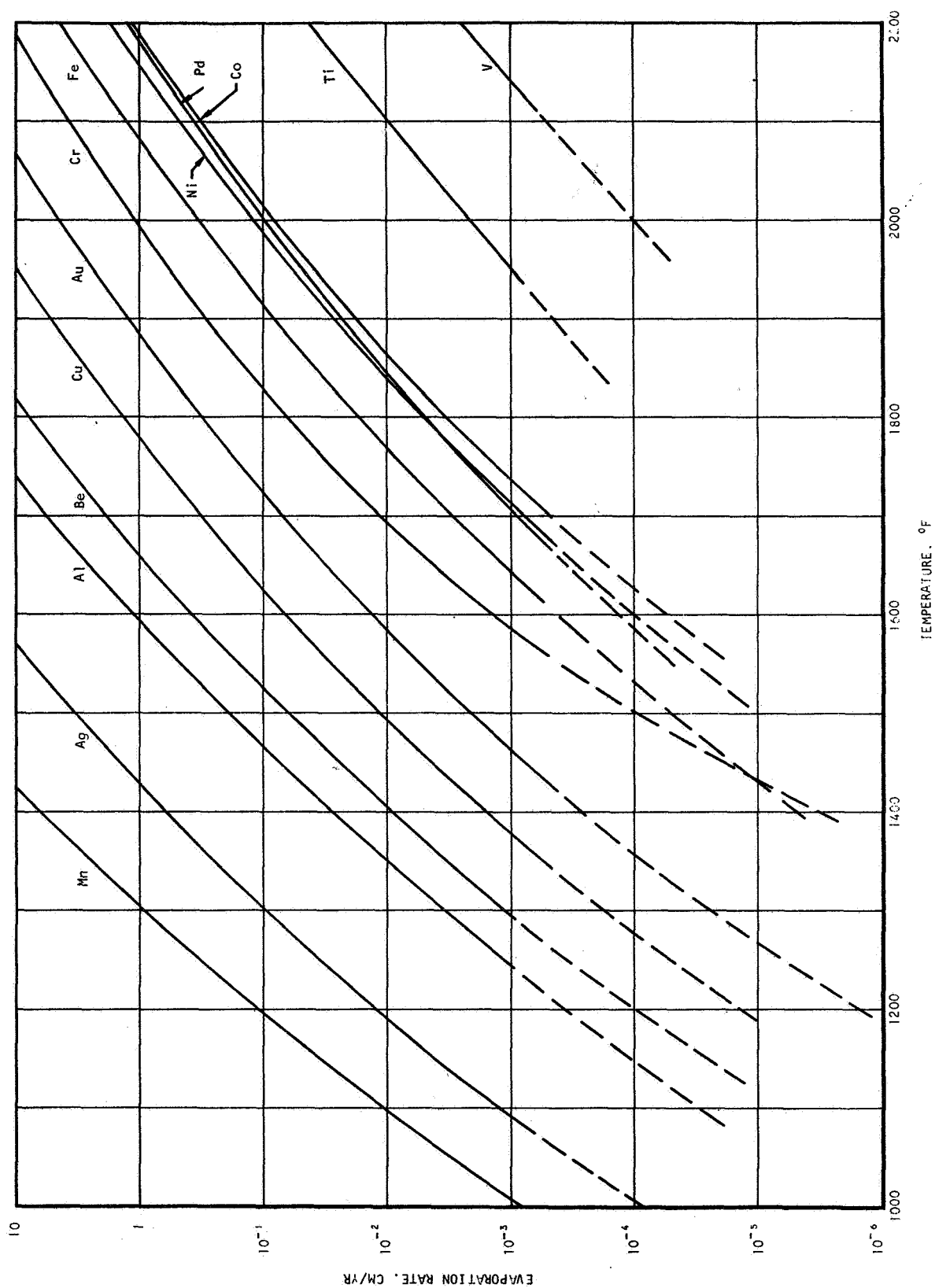


Figure 4-4 MATERIAL EVAPORATION RATES IN VACUUM

A-7095

T = temperature, °K

K = evaporation coefficient

The evaporation coefficient, K, must be experimentally determined. To provide a rough comparison, all curves shown in Figure 4-4 were calculated assuming an evaporation coefficient of unity.

Multicomponent alloys will be affected in a different manner than pure metals. The evaporation of alloy constituents is nonlinear with time and results in concentration gradients of the more volatile elements throughout the thickness of the member. Further, the changes in composition and microstructure may result in important changes in physical and mechanical properties.

D. T. Bourgette of the Oak Ridge National Laboratory has reported the results of long-time exposure of 316 stainless steel in a vacuum at high temperatures (1475° to 1835° F). The major effects noted were:

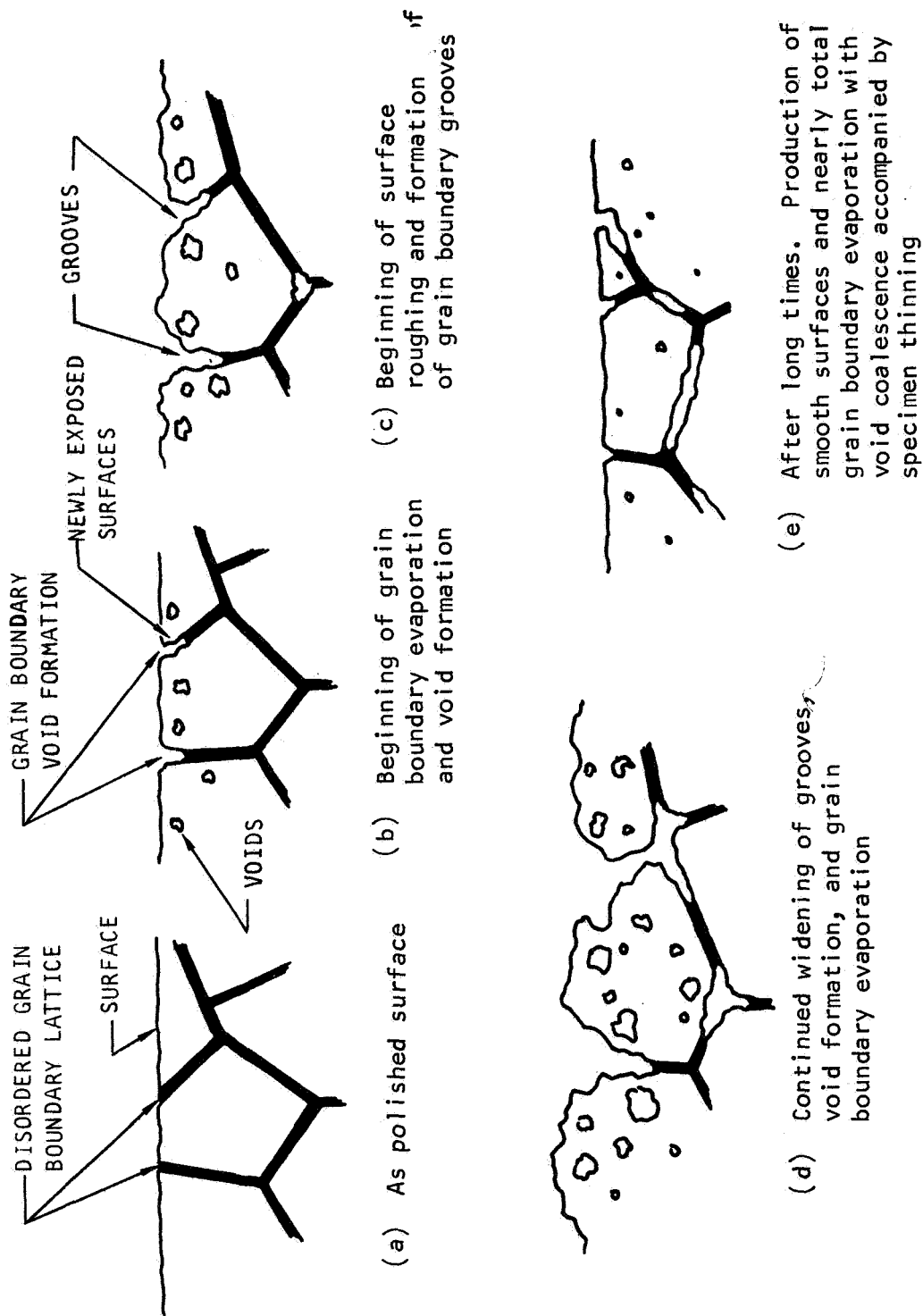
- subsurface void formation
- grain growth at surfaces
- excessive void formation in grain boundaries
- disappearance of precipitated phases
- material loss from edges of surface grains.

These effects are depicted graphically in Figure 4-5. Further work by Bourgette with L-605 and by Charlot and Westerman (Ref. 4-1) with Hastelloy X-280 and L-605 show that, during a 5-year exposure in a vacuum at temperatures of 1700° F and above, multicomponent superalloys would undergo serious degradation in properties.

Although several superalloys such as Hastelloy B and Hastelloy N (Inor-8) have low chromium content and would not suffer from evaporation as severely as the higher chromium alloys, they still would require protection against evaporation and would have only marginal creep strength. It is unknown, at present, whether or not coatings can alleviate the problem of evaporation. Such a coating would have to be resistant to diffusion of metal atoms through it, and should be crack- and pore-free. The presence of occasional cracks or pores in the coating might not be detrimental since conductance of a gas through a small crack or pore is relatively low, and therefore evaporative losses may be minimal.

Since the only metallic component of TD nickel is pure nickel, it is the only superalloy that would be resistant to internal void formation. There should be only a uniform recession rate from the surface, unless the higher interatomic energies at grain boundaries result in an accelerated evaporation rate at grain boundaries. To our knowledge, however, there is no data regarding evaporation effects on TD nickel. In addition, the low ductility of TD nickel does not recommend it as a good heat exchanger material.

Refractory metals must be used, therefore, if evaporation loss in superalloys can not be prevented, or if in the absence of test work on coated alloys, positive assurance against substrate evaporation is necessary.



A-17237

Figure 4-5 EVAPORATION PROBLEM OF MATERIALS IN VACUUM USING AN EVAPORATION SEQUENCE FOR THIN SPECIMENS OF TYPE 316 STAINLESS STEEL EXPOSED TO HIGH VACUUM BETWEEN 1475° AND 1835° F AS AN EXAMPLE

4.1.2.1.2 Mechanical and Physical Properties -- Mechanical and physical properties of major importance are creep and rupture strength, short-time tensile yield, ultimate strength, elongation, coefficient of thermal expansion, and elastic modulus.

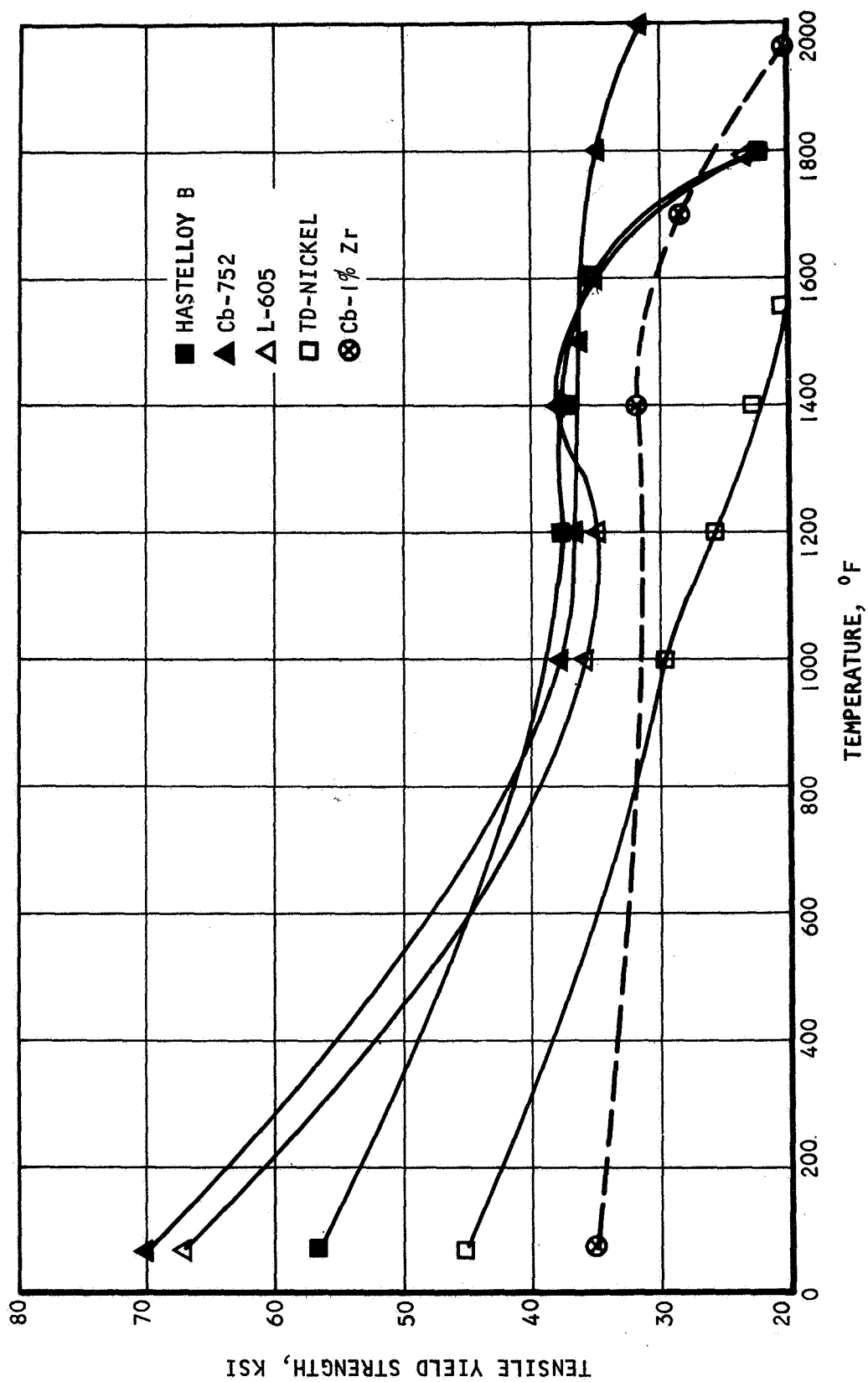
Short-time tensile properties are of importance because of the severe loads imposed during launch, and because of rapid temperature transients imposed during system startup.

For 5-year service in a vacuum, creep and rupture strengths must be known as accurately as possible. Long extrapolations are necessary, and serious error can occur for two reasons:

- Metallurgical reactions can cause breaks or changes in slope of the log rupture stress versus log time curves. These reactions may be internal microstructural changes, such as grain growth, recrystallization, precipitate formation, etc., or surface changes caused by diffusion, evaporation, or interaction between the metal and emissive coating.
- Where a limited amount of data is available and a spread in the points exists, there is a statistical uncertainty in curve fitting and in the extrapolation made. A common method of improving this situation is the use of time-temperature parameters, such as the Larson-Miller and Manson-Haferd parameters. When stress is plotted against these parameters, a greater number of experimental points can be fitted to a master rupture curve. Even when using these parameters, however, uncertainty exists in such extrapolations.

Figures 4-6 through 4-9 show the important physical and mechanical properties of several representative candidate materials. Two columbium alloys are shown, Cb-1Zr and Haynes Alloy Cb-752. With the Cb-1Zr alloy, considerable experience has been gained in fabricating this alloy for liquid metal systems; and there is a large amount of property data available. Alloy Cb-752 is included because of its good workability and fabricability, improved rupture and creep strength, and because its contamination resistance is slightly better than for Cb-1Zr. TD nickel is included because of its good creep strength and because it should not be susceptible to internal void formation due to evaporation effects. It is not a strong candidate, however, because of its low ductility. Hastelloy B is an example of a commercial superalloy that has low chromium content. It also has fair creep strength at 1700° F. L-605 has relatively good creep strength, and is probably the strongest of the commercially available solid-solution-hardened superalloy sheet materials.

Cobalt-tungsten alloys have been under development at NASA specifically for hot structures and ducting in space applications. Since these materials are composed of relatively nonvolatile elements, they have a good potential. Several of these alloys have exhibited excellent creep and rupture strengths, based upon limited data. Small quantities of sheet have been rolled that exhibit good ductility at room temperature. More complete short-time properties data would be desirable, however, especially elevated-temperature ductility. The formability has not been established and machinability is not expected to be especially good because of rapid work hardening. These alloys have not been developed to the point where they can be considered for any immediate applications as complex as the HSHX.



A-28317

Figure 4-6 TENSILE YIELD STRENGTH VERSUS TEMPERATURE OF CANDIDATE ALLOYS

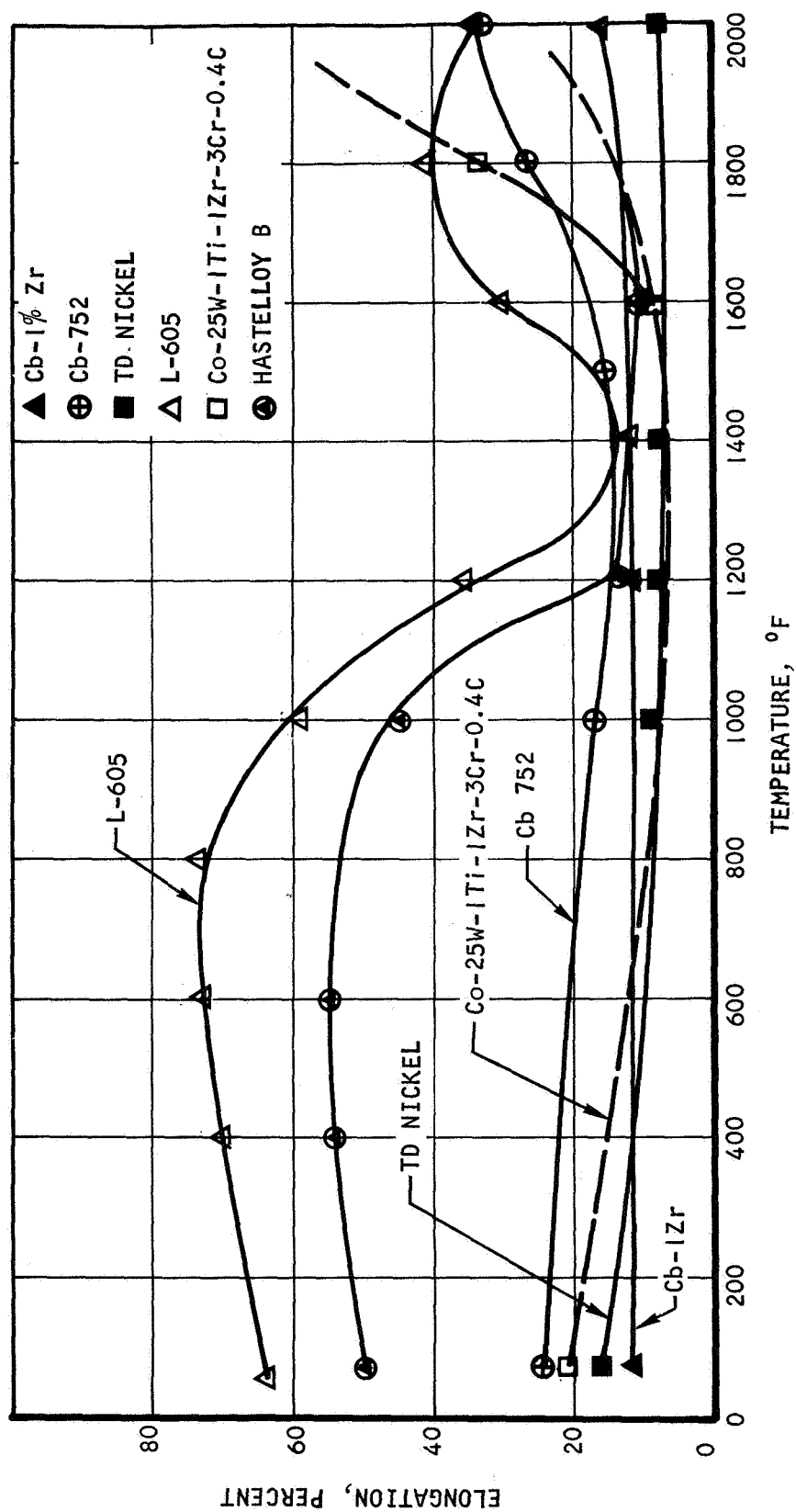


Figure 4-7 ELONGATION VERSUS TEMPERATURE FOR CANDIDATE ALLOYS

A-28311

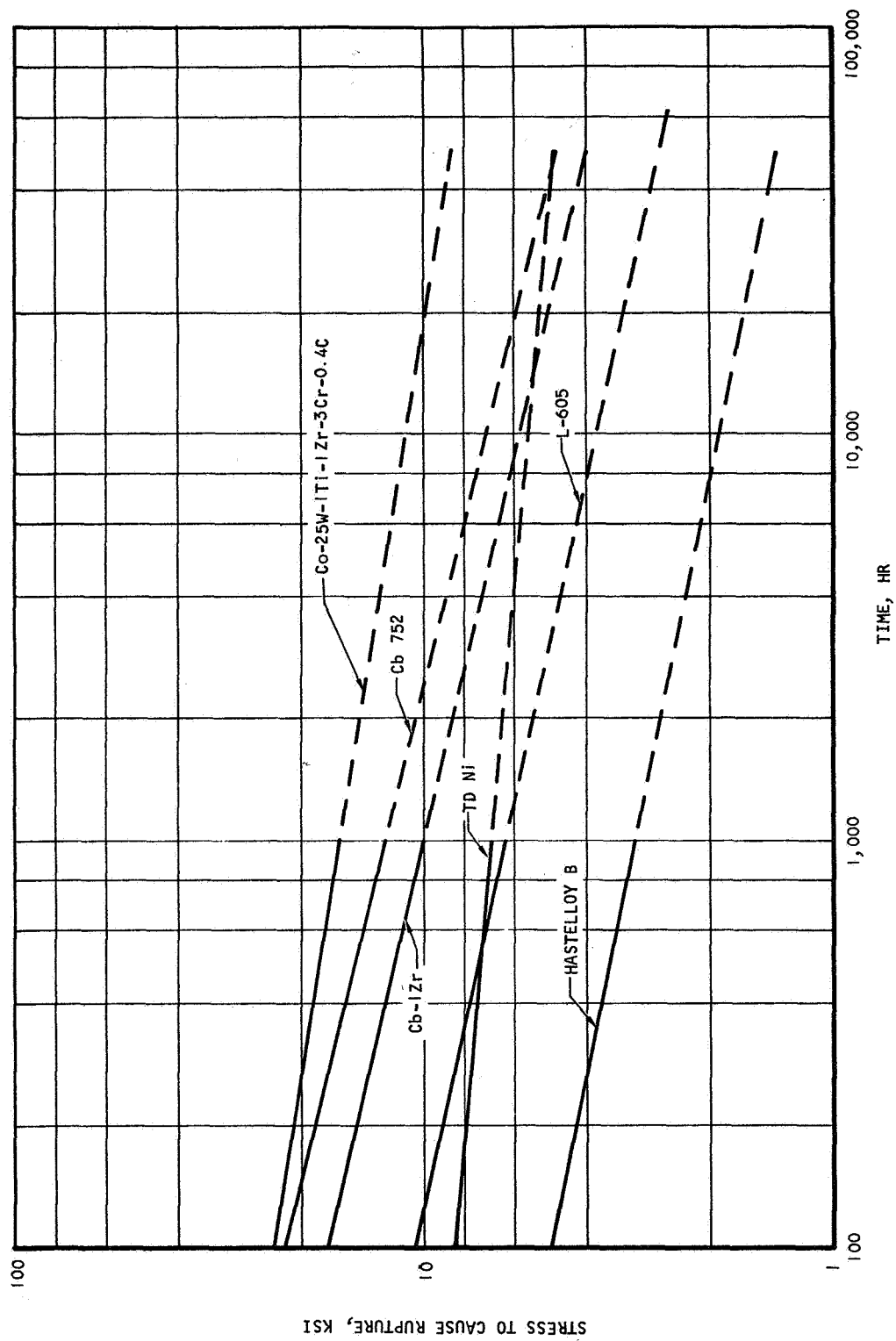


Figure 4-8 RUPTURE STRENGTH FOR CANDIDATE MATERIALS AT 1700° F

B-13020

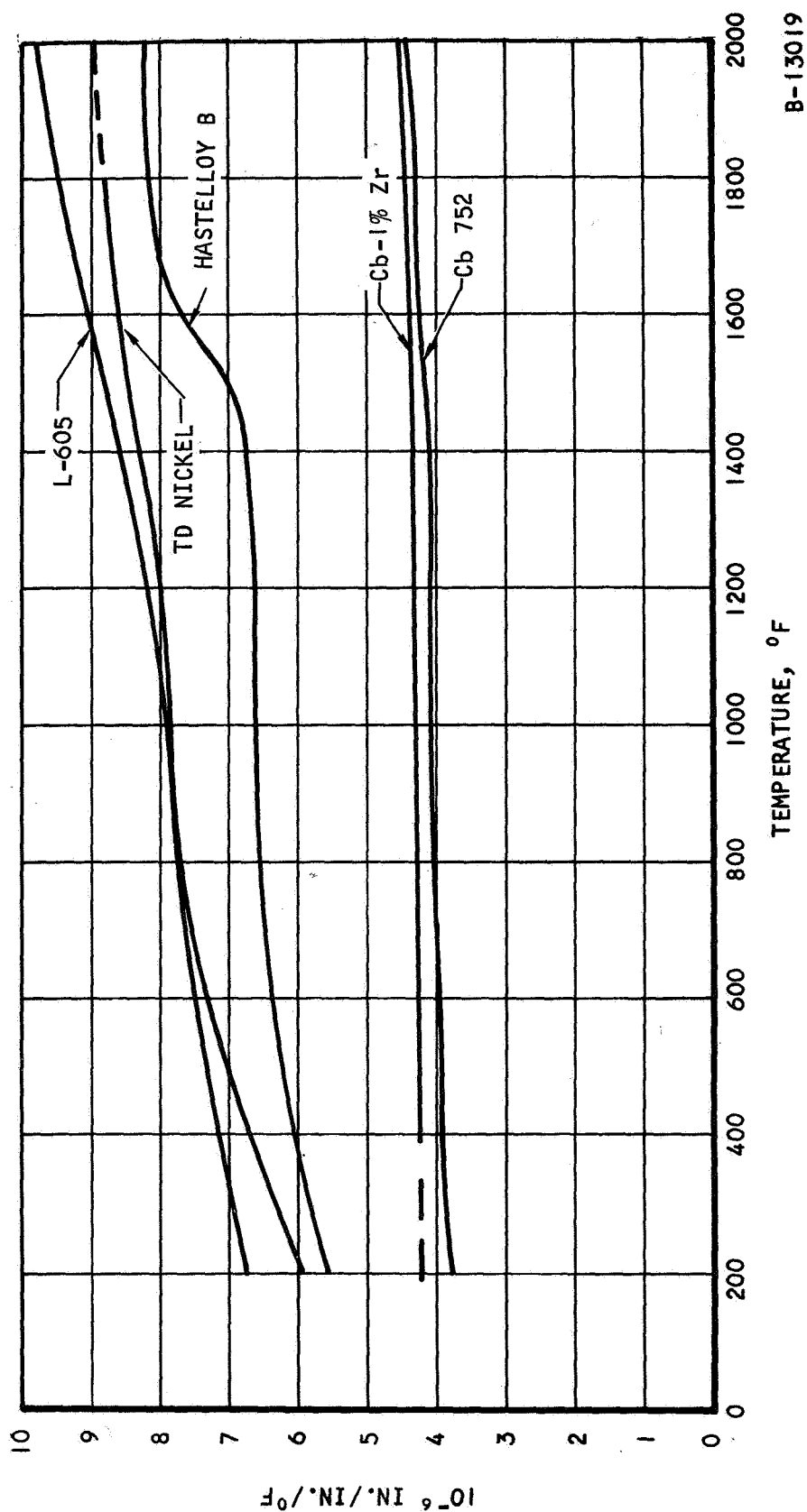


Figure 4-9 MEAN COEFFICIENT OF THERMAL EXPANSION

B-13019

4.1.2.1.3 Summary of Structural Materials Selection -- Since the HSHX is to operate for 5 years in a vacuum at temperatures around 1800° F, the materials preferred for all portions of the HSHX are the refractory metals: columbium, molybdenum, tantalum, and tungsten. The superalloys are considered unsuitable because they are susceptible to degradation through evaporation of their volatile components. TD nickel is the only superalloy with satisfactory evaporation characteristics, but it was rejected because its low ductility at elevated temperatures would present a low-cycle fatigue (thermal fatigue) problem.

Of the refractory metals, columbium has a density of 0.310 lb/in.³, molybdenum 0.369 lb/in.³, tantalum 0.600 lb/in.³, and tungsten 0.697 lb/in.³. Since the fabricability of columbium is much better than molybdenum, and the columbium alloys are comparable in strength to the other refractory alloys at the temperatures expected in the HSHX, a columbium alloy seems the most appropriate choice. Cb-1Zr was selected because of its:

- low evaporation rate
- satisfactory materials properties
- commercial availability (which also results in having the most test data available, including studies with emissive coatings)
- good fabricability
- some usage in other heat exchanger applications.

4.1.2.2 Emissive Coatings

A coating having a total normal emittance of 0.8 or greater will be required for the HSHX. This coating will have to survive several thermal cycles in a vacuum or argon during ground testing, and 5 years in a vacuum at about 1700° F during operation. Loss of the emissive coating during operation would result in over-temperature of the fuel capsules and possible failure of the system.

The best choice for an emissive coating appears to be iron titanate. In a NASA-funded program (Contract NAS3-4174), a Cb-1Zr tube, plasma-arc sprayed with a 4-mil coating of iron titanate, completed 10,000 hours of testing at 1700° F in a vacuum of 10⁻⁷ torr or better. During the test, the specimen was cycled between 1700° F and room temperature 51 times. During the test, the emittance decreased from 0.88 to 0.84. Results of a 5000-hour cycling test between 1500° and 1800° F (3125 cycles) indicates the iron-titanate coating on Cb-1Zr was suitable for space radiator applications at temperatures up to 1800° F. The coating had a stable emittance of 0.88, and adherence between the coating and substrate was excellent throughout the test. Coating stability was also good. Limited diffusion of iron and titanium into the Cb-1Zr occurred to a maximum depth of 4 mil as determined by microprobe analysis. Diffusion of oxygen into the Cb-1Zr increased overall hardness throughout the 10-mil tubing wall. Based on tests conducted with uncoated tubing, the major source of oxygen was from residual gases in the test chamber and not from the iron-titanate coating. Oxygen may be a problem more in long-term vacuum tests than in the harder vacuum of space for which the HSHX is being designed. The longer exposure time anticipated for the HSHX (approximately 5 years or 44,000 hours), however may intensify

the diffusion problem and require the use of a diffusion barrier between the iron titanate and the Cb-1Zr material. Another problem area may be the possible incompatibility between the iron titanate and the braze alloy selected for brazing.

The basic reasons for selecting iron titanate as the HSHX emissive coating are its:

- high emissivity
- good thermal stability in a vacuum at high temperature, with no appreciable loss of material or emissivity
- small reactivity in connection with Cb-1Zr
- available test data for up to 10,000 hours of exposure at high temperature (1700° F)
- ease of application (plasma-arc sprayed).

4.1.2.3 Braze Material

Brazing is to be employed only as a means of obtaining maximum contact between the inlet and outlet tubes that make up the heat exchanger core. Welding will provide structural support between the tubes. Because a gap between the tubes and the bottom of the weld fillet is likely to occur due to sluggishness of the weld metal, back brazing is employed to fill this gap and also provide a positive heat transfer path at the flat area of the tubes. Although the braze alloy function is a simple one, its selection is extremely important. The brazing alloy selected should have the following characteristics:

- does not degrade the properties of the tubing during brazing or in long-term exposure at operating temperature (5 years, 1700° F temperature, vacuum)
- can be brazed at a temperature compatible with Cb-1Zr. It is desired to select the alloy with the lowest brazing temperature possible that will still provide adequate strength and meet the other requirements listed
- thermally stable; that is, will not evaporate or become brittle during service
- forms a ductile joint
- good wetting and filleting characteristics.

Considerable effort has been expended to develop brazing alloys with high-temperature strength for brazing columbium alloys. The main alloy systems meeting the requirements are those of titanium (Ti), zirconium (Zr), and vanadium (V). Varying the compositions of these systems will result in alloys suitable for brazing from about 3000° down to about 2100° F.

Based on the results of the latest investigations, the two alloys that combine the best brazing characteristics and meet the requirements of the heat source

heat exchanger are: 1) Zr-28V-16Ti-0.1Be and 2) Zr-28V-16Ti. The only difference between these alloys is in the beryllium content. A small addition of beryllium is advantageous in that it decreases the brazing temperature (from 2250° to about 2150° F) and increases fluidity and filleting characteristics. A larger amount of beryllium would be detrimental because it would result in an increase in the formation of beryllides and therefore a brittle joint. Both of these alloys appear to combine the features desired for back brazing the heat exchanger. These features are:

- They are thermally stable for an extended exposure time at 1700° F. In a recent NASA-sponsored study on brazing alloys for columbium, neither zirconium, titanium, nor vanadium diffused from the Zr-28V-16Ti or Zr-28V-16Ti-0.1Be brazing alloy into the Cb-1Zr material after a T-joint specimen was exposed at 1750° F for 1000 hours in a vacuum. No void formation was noted either by metallography or microprobe analysis.
- The brazing temperature is compatible with the stress-relief and annealing temperature of Cb-1Zr and is within a temperature range compatible with the existing furnace capabilities of 2150° to 2250° F.
- They have good brazing characteristics.
- They formed a ductile T-joint in the as-brazed condition that remained ductile after 143 hours at 1750° F in a vacuum.
- There is negligible erosion of Cb-1Zr by either brazing alloy during the brazing cycle.
- They have good shear strength at 1750° F (see Table 4-1).

TABLE 4-1

SHEAR STRENGTH OF CANDIDATE BRAZE ALLOYS

Condition	Zr-28V-10Ti (ksi)		Zr-28V-10Ti-0.1Be (ksi)	
	RT	1750° F	RT	1750° F
As brazed	38.5	17.7	37.6	12.0
1750° F (143 hr of exposure in a vacuum)	--	16.3	--	16.3

While these two alloys appear promising, they will have to be evaluated further to better determine their long-term stability and reaction with Cb-1Zr and the iron-titanate emissive coating.

4.1.2.4 Potential Materials Problems

The most prominent materials problems or materials unknowns at this time are related to long-term exposure. These problem areas, which require further study, are:

- the interaction of an iron-titanate coating with Cb-1Zr and with the brazing alloy. As a result of the interaction, iron titanate becomes less ductile. It may be necessary to apply a diffusion barrier between the iron titanate and the structural metal.
- the stability characteristics of the coating, that is, emissivity and adherence
- the stability and properties of brazed Cb-1Zr joints after long-term exposure
- the accurate prediction of long-term creep and rupture of Cb-1Zr.

4.1.3 Fabrication

4.1.3.1 Techniques

4.1.3.1.1 Formability -- Formability is good for the Cb-1Zr alloy at room temperature. None of the forming operations planned would normally be considered difficult, but the tendency for columbium to gall could present a problem in forming tubular components to the required shapes.

Roll forming a 0.045-inch sheet into cylindrical shapes to weld into manifold and ducting components, cupping the sheet to form the return manifold and caps, rolling flats on the heat exchanger tubing to provide greater contact area between the inlet and outlet tubing in the core, and bending the heat exchanger tubes to required shapes are the basic forming operations planned. One of the most severe forming operations involved in fabricating the heat exchanger is the cupping and drawing operations to form a seamless return manifold. If an intermediate anneal is required to complete forming, however, the recrystallized material resulting from the anneal should provide good ductility and formability. If expedient, an alternate approach, which consists of roll forming and welding sheet into the cylindrical shape required for the return manifold, could be used to bypass the capping and drawing operation.

4.1.3.1.2 Welding -- Welding will be used for fabricating components and also in the assembly operations. All anticipated welding is of a conventional nature and does not appear to be difficult. Tungsten-arc welding in an inert-gas atmosphere (TIG welding) is recommended. The primary area of concern in welding columbium, or in exposing it to elevated temperatures during a stress-relieving or annealing operation, is absorption of oxygen, nitrogen, or hydrogen gases. It is similar to titanium, another reactive metal, in that it can be easily welded, but if contamination occurs due to pickup of these gases, the weld can be embrittled. Although it is possible to weld in air by using an argon or helium gas shielding at the torch, this is not recommended for the HSHX because the affinity of columbium for oxygen and nitrogen and the problems imposed by shielding would make this method unreliable. One method is to weld in an enclosed chamber capable of being evacuated to less than 10^{-4} torr, and having a leak rate no greater than $15 \mu/\text{hr}$.

Another method is to evacuate the chamber and fill with inert gas. The inert gases used for welding should be at least 99.99 percent pure, have a maximum dew point of -80°F , and a combined oxygen and water content no higher than 50 ppm.

High purity argon gas can be purchased to 99.996 percent purity with a guaranteed oxygen and water vapor content less than 22 ppm. Liquid argon of 99.998 percent purity and 11 ppm combined oxygen and water can also be purchased.

Fixturing will be necessary to prevent distortion during welding. To avoid contamination, columbium, tantalum, molybdenum, or tungsten should be used in fixture components that contact the columbium parts at areas near the weld. Fixturing will be necessary for welding sheet into components and for weld-assembling of components into the heat exchanger.

Welding of heat exchanger tubes to the return manifold is an area where distortion may be a problem due to extensive welding in a small area. The use of flats on the tube will help increase the distance between tube welds (land area) if holes in the return manifold are Eloxed with flats. Fitting the tubes into the return manifold and into the inlet and outlet manifolds will help hold the tubes in place during welding. Tack-welding of the tubes and fixturing will be required.

Welding of the heat exchanger tubes together to form the heat exchanger core is another area where distortion will have to be controlled. Welding the tubes into the manifolds and tack-welding of tubes prior to final welding will aid in the fixturing.

Because of the high melting temperature of columbium, considerable heat is generated during its welding. Intermittent welding may therefore be necessary to allow heat dissipation. The use of a water-cooled chamber would also be helpful.

4.1.3.1.3 Stress Relieving -- Stress relieving will be necessary after certain stages of forming and welding have been completed. The minimum number of interstage anneals is indicated in a later discussion on fabrication of components and the assembly sequence. Stress relieving, postweld annealing, and interstage annealing will all be performed at 2200° F in a good vacuum furnace (less than 1- μ pressure).

Contamination is almost as serious a problem during heat treatment as during welding. All fixtures and the furnace must be cleaned. Wrapping in tantalum foil is recommended as a getter to reduce contamination. To further ensure freedom from contamination, it is recommended that tantalum-wrapped parts be immersed in clean columbium chips and placed in a suitable basket or container. An alternate to vacuum annealing is retort annealing using argon gas with 10 ppm H₂O and 2.5 ppm O₂ maximum.

4.1.3.1.4 Brazing -- In the same manner as the annealing process, brazing is carried out in a vacuum environment of 10⁻⁵ torr or better to prevent contamination of the materials. A hold time of about 5 minutes at brazing temperature is required.

4.1.3.1.5 Applying Emissive Coating -- All surface areas of the heat exchanger must be plasma-sprayed with about a 4-mil coating of iron titanate. Since spraying will be done after final assembly, some areas may be difficult to coat. The important surfaces that receive direct radiation from the heat source and require a high-emissivity coating, however, can be satisfactorily coated (line of sight from heat source and plasma torch will be about the same).

4.1.3.2 Component Fabrication

The steps and sequence developed for the fabrication of the components of the HSHX are illustrated in Figures 4-10 through 4-13. For some of the operations, an alternate approach is also given.

4.1.3.3 Assembly Sequence

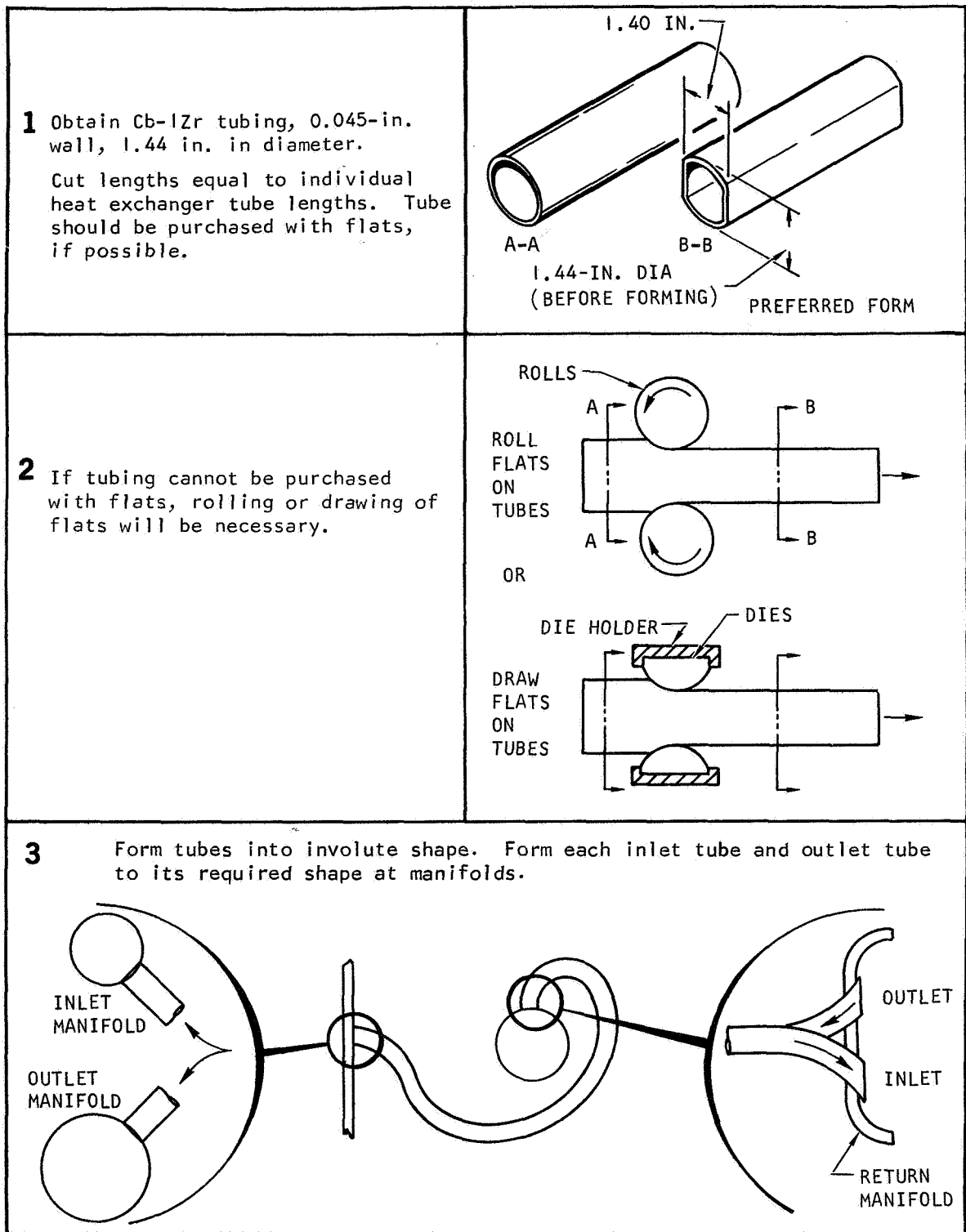
- a Insert and tack weld all 18 heat exchanger tubes into return manifold and into inlet and outlet manifolds. This should help ensure a more rigid setup for welding and eliminate assembly problems due to distortion that would occur if assembly were done after welding. Tack weld tubes together.
- b Weld tubes to return manifold. Weld from inside of manifolds (see Figure 4-14).
- c Weld tubes to inlet and outlet manifolds from inside of manifold through access port or area (see Figure 4-15).
- d Stress relieve assembly at 2200° F for 1 hour.
- e Leak-check tube to manifold joints. Repair weld if necessary.
- f Weld circular patches to manifolds to seal access port (Approach 1). If Approach 2 is used, weld manifold outer sections to inner sections. Weld cap(s) to return manifold.
- g Weld heat exchanger tubes together on one side (see Figure 4-16).
- h Add brazing alloy (Zr-28V-16Ti-0.1Be) to the opposite side of weld and braze to fill in any voids or gaps left from welding and to obtain the maximum contact area possible between inlet and outlet tubes. Apply stopoff to all areas, except the immediate braze area. Braze in vacuum (10^{-5} torr or better) at 2130° F with a hold time of 5 minutes.
- i Braze support boss (welded to outlet manifold) to inlet manifold (combined with above brazing cycle).
- j Remove all stopoff coating after brazing; then flame-spray the iron-titanate emissive coating to all exposed heat exchanger surfaces so as to obtain a coating thickness of about 4 mils. The preferred surface for applying the iron titanate is Cb-1Zr because of known results; hence, it is desirable to limit the area covered by the braze alloy.

Figure 4-17 shows a typical assembly sequence.

4.2 ANALYSIS AND SYSTEM PERFORMANCE

4.2.1 Pressure Drop and Flow Distribution

Pressure drop and flow distribution should be considered simultaneously when discussing design requirements for the heat source heat exchanger. Since the turbulent flow exists essentially throughout the present design, the analysis is simplified.



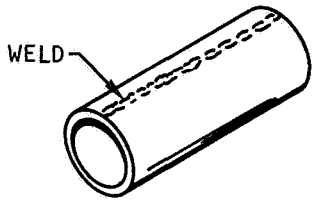
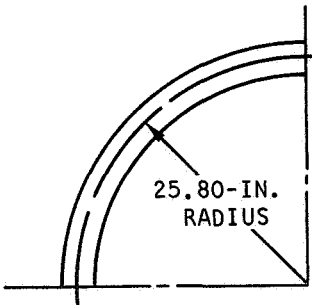
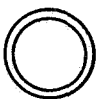

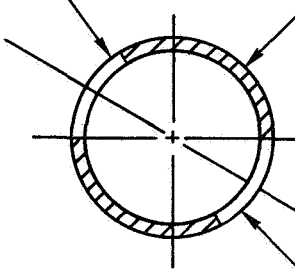
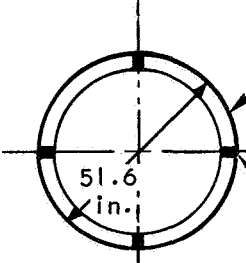
S-43257

Figure 4-10 FABRICATION OF CORE

APPROACH 1	
1 Cup and draw to required shape (0.20-in.-thick sheet).	<p>CUP AND DRAW</p>
2 Stress relieve.	
3 Elox holes at required 45-deg angles to accept 9 inlet and 9 outlet heat exchanger tubes. Elox holes to have same flats as tubes to provide sufficient land between holes for welding.	<p>ELOX HOLES AT 45-DEG ANGLES</p>
4 Form end cap (0.080-in.-thick sheet).	
APPROACH 2	
1 Roll form sheet into cylinder (4.50 in. in diameter and 4.76 in. long). Weld and planish.	<p>ROLL FORM WELD AND PLANISH</p> <p>ELOX HOLES AS ABOVE</p>
2 Stress relieve.	
3 Elox holes as in Approach 1, above.	
4 Form end caps.	

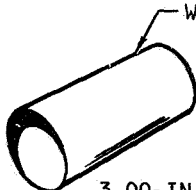
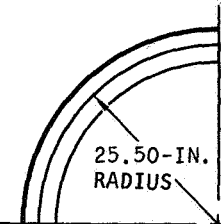
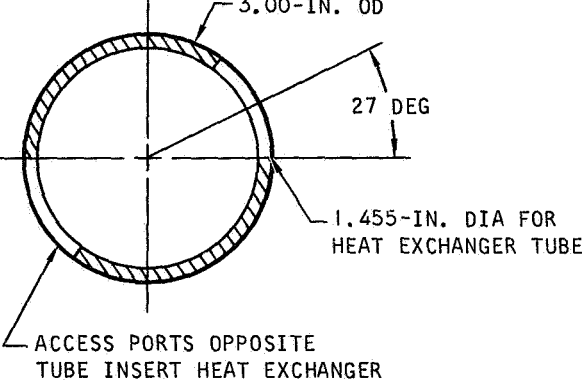
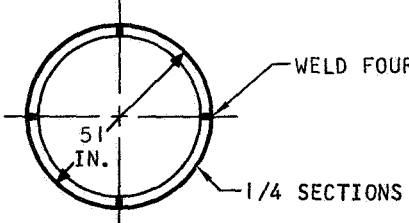
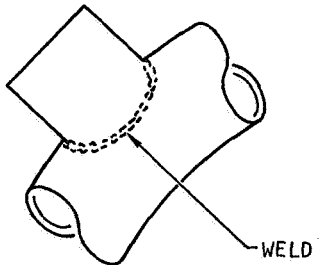
S-43258

Figure 4-11 FABRICATION OF RETURN MANIFOLD

<p style="text-align: center;">APPROACH 1</p>	
<p>1 Roll form 0.045-in. sheet into four 42.5-in.-long cylinders each and weld.</p>	 <p style="text-align: center;">2.40-IN. OD X 42.5-IN. LENGTH</p>
<p>2 Stress relieve.</p>	
<p>3 Bend tubing lengths 90 deg to form quarter-sections of circular manifold with mean diameter of 51.60 in. (weld should fall on mean diameter).</p>	 <p style="text-align: center;">25.80-IN. RADIUS</p>
<p>4 Stress relieve and finish form.</p>	
<p>5 Elox 9 holes in inlet manifold to accept 9 inlet heat exchanger tubes. Holes may be circular to accommodate round tube or have flats to accommodate tube with flats.</p> <div style="display: flex; justify-content: space-around; align-items: center;">   </div> <p style="margin-top: 10px;">Elox access port opposite heat exchanger tubing inlet.</p>	<p style="text-align: center;">ACCESS PORTS OPPOSITE HEAT EXCHANGER TUBE INSERT</p>  <p style="text-align: right;">2.40-IN. OD</p> <p style="text-align: right;">28.5 DEG</p> <p style="text-align: right;">1.455-IN.-DIA HOLE FOR HEAT EXCHANGER TUBES</p>
<p>6 Weld quarter-section together to form circular manifold of 51.60 in. mean diameter</p>	 <p style="text-align: right;">1/4 SECTIONS</p> <p style="text-align: center;">51.6 in.</p> <p style="text-align: right;">WELD FOUR PLACES</p>

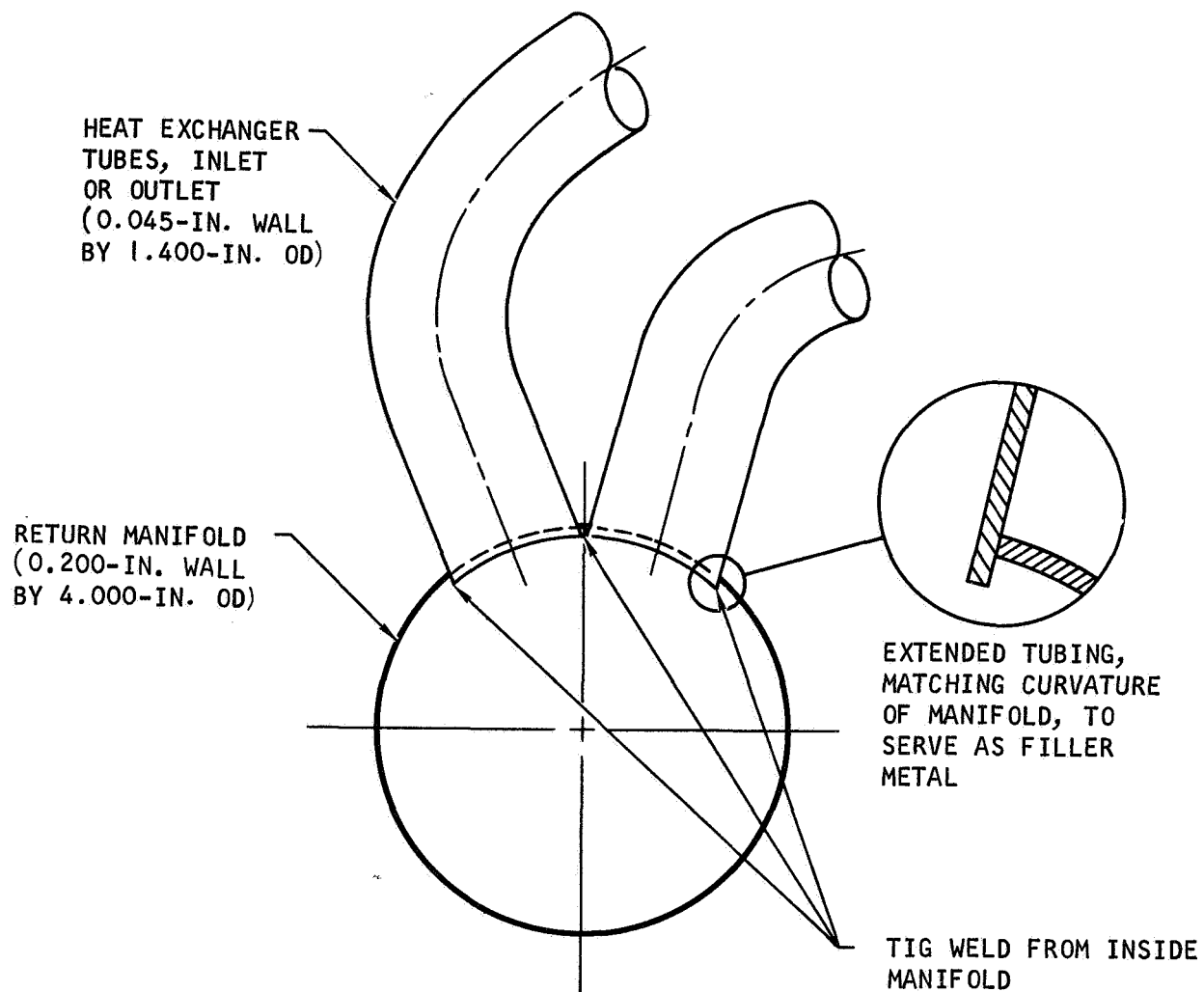
S-43253

Figure 4-12 FABRICATION OF INLET MANIFOLD

<p>1 Roll form 0.045-in. sheet into four cylinders of 40.6-in. length each and weld.</p>	 <p>WELD</p> <p>3.00-IN. OD X 40.6 IN. LENGTH</p>
<p>2 Stress relieve.</p>	
<p>3 Bend tubing lengths 90 deg to form quarter sections of circular manifold with mean diameter of 51.00 in. (weld should fall on mean diameter).</p>	 <p>25.50-IN. RADIUS</p>
<p>4 Stress relieve.</p>	
<p>5 Elox 9 holes in outlet manifold to accept 9 outlet heat exchanger tubes. Holes may be circular to accommodate round tubes or have flats to accommodate tubes with flats. Elox access ports opposite heat exchanger tubing outlet for welding.</p>	 <p>3.00-IN. OD</p> <p>27 DEG</p> <p>1.455-IN. DIA FOR HEAT EXCHANGER TUBE</p> <p>ACCESS PORTS OPPOSITE TUBE INSERT HEAT EXCHANGER</p>
<p>6 Weld quarter-sections together to form circular manifold of 51.00 in. mean diameter.</p>	 <p>WELD FOUR PLACES</p> <p>51 IN.</p> <p>1/4 SECTIONS</p>
<p>7 Cut section out of outlet manifold to accommodate outlet flange (3.00 in. dia) 20 deg from outlet tube hole. (Fabricate flange by roll forming sheet pattern into cylindrical shape, welding, and stress relieving.) Weld flange to manifold.</p>	 <p>WELD</p>
<p>8 Stress relieve.</p>	

S-43255

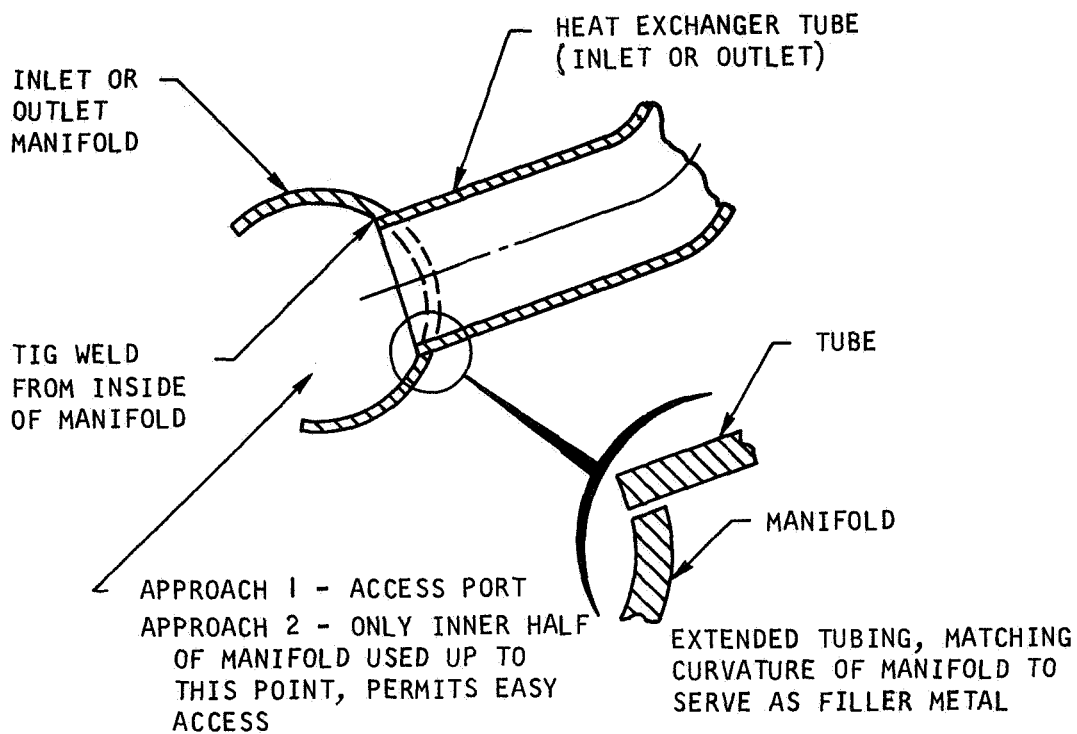
Figure 4-13 FABRICATION OF OUTLET MANIFOLD



- a. INSERT AND TACK WELD ALL 18 FORMED TUBES INTO RETURN MANIFOLD AND INTO OUTLET AND INLET MANIFOLDS TO MINIMIZE DISTORTION DURING WELDING
- b. TIG WELD TUBES TO RETURN MANIFOLD

S-43261

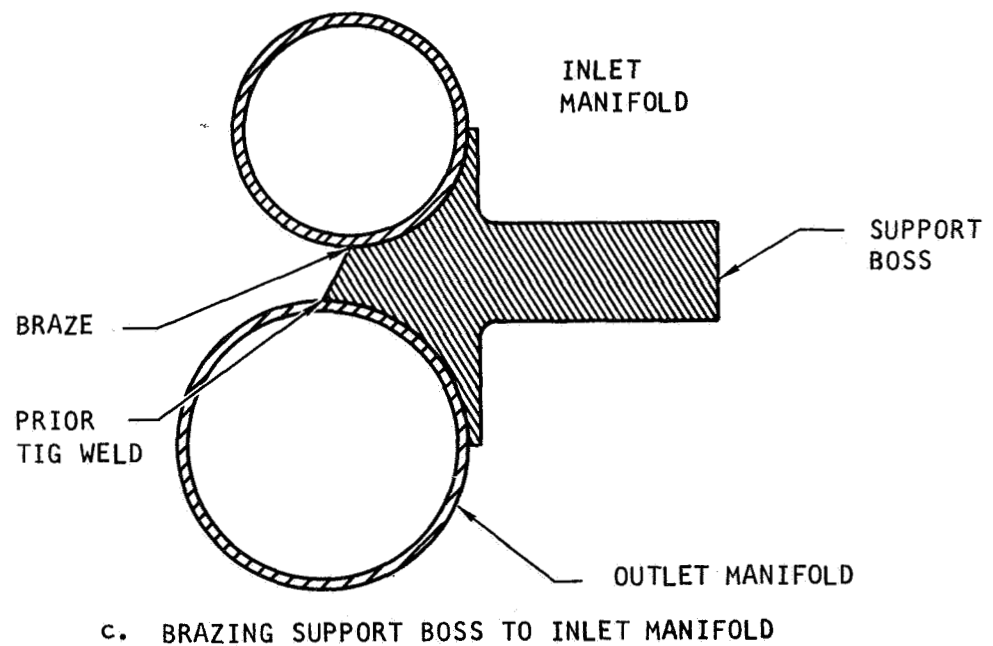
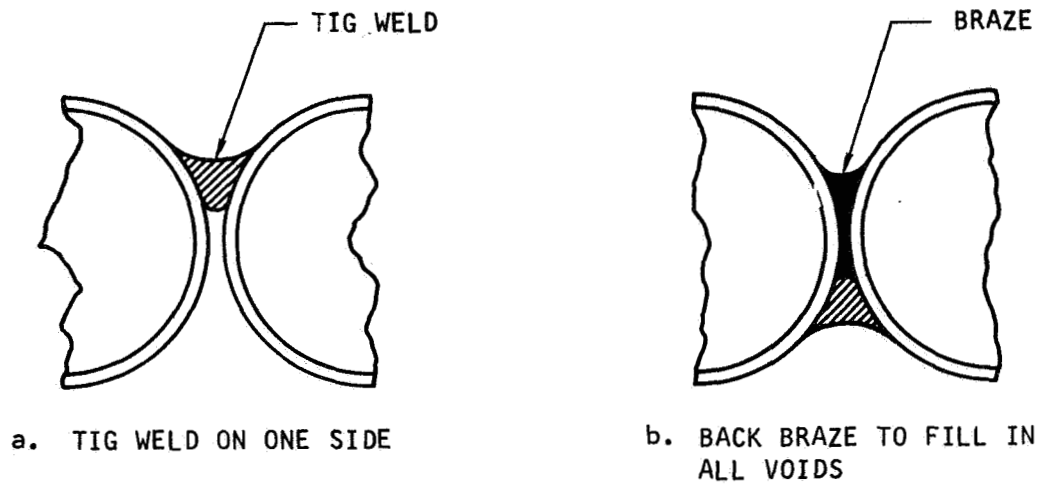
Figure 4-14 WELDING HEAT EXCHANGER TUBES TO RETURN MANIFOLD



- a. TIG WELD TUBES INTO INLET AND OUTLET MANIFOLDS
- b. STRESS RELIEVE AT 2200°F FOR 1 HR
- c. LEAK CHECK TUBE-TO-MANIFOLD JOINTS. REPAIR WELD IF NECESSARY.
- d. TIG WELD ACCESS PORTS CLOSED (APPROACH 1) OR WELD INNER AND OUTER MANIFOLD SECTIONS TOGETHER (APPROACH 2)

5-43262

Figure 4-15 WELDING HEAT EXCHANGER TUBES TO INLET AND OUTLET MANIFOLDS

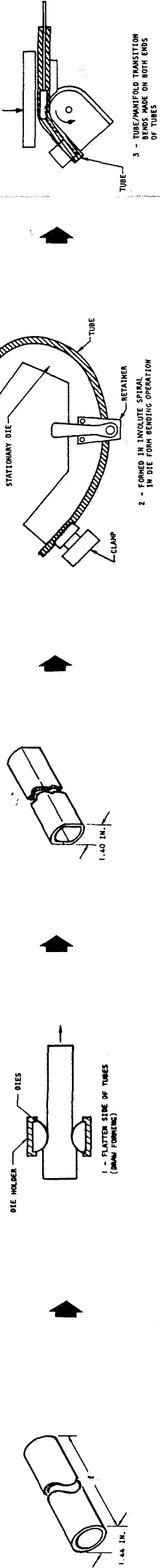


S-43263

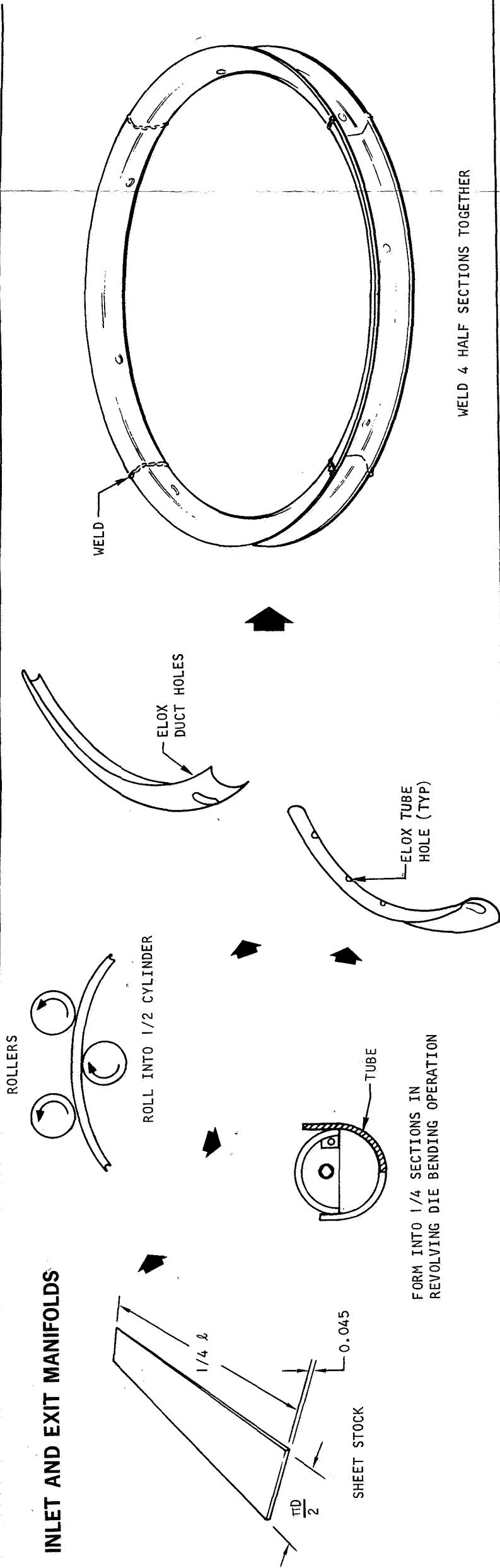
Figure 4-16 JOINING OF HEAT EXCHANGER TUBES TO FORM CORE BRAZING OF BOSS TO INLET MANIFOLD

FABRICATION

TUBES



INLET AND EXIT MANIFOLDS



CENTER MANIFOLD

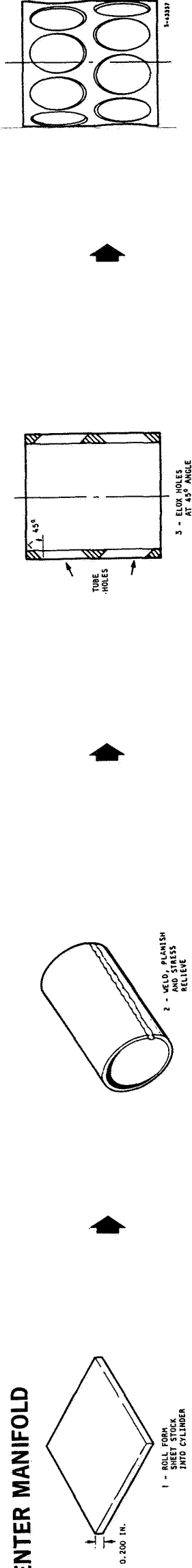


Figure 4-17 TYPICAL FABRICATION AND ASSEMBLY SEQUENCE

ASSEMBLY

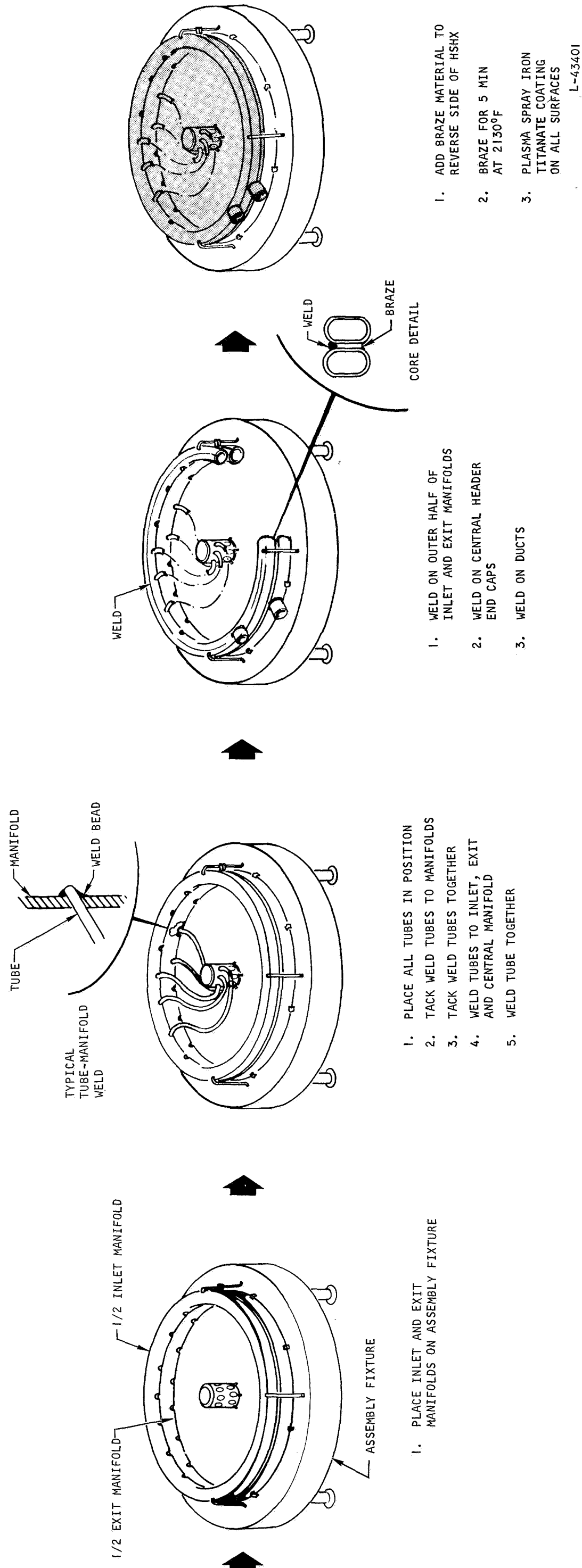


Figure 4-17 (Concl'd)

Because the tubes and manifolds making up the heat exchanger are circular, friction factors for the flow are minimized, and within the range of Reynolds numbers existing in the heat exchanger, can be represented by the expression

$$f = 0.046 \text{ Re}^{-0.2}$$

The pressure losses between the inlet and outlet of the heat exchanger are due to friction, momentum changes, turning, and entrance and exit losses. These have been analyzed separately and are summarized in Table 4-2.

Friction pressure drop was calculated using the standard equation

$$\Delta P_f = \frac{2G^2 fL}{g\rho D}$$

Entrance, exit, and turning losses were calculated on the basis of the equation

$$\Delta P = K \frac{G^2}{2g\rho}$$

where K is a loss coefficient based on the flow geometry, and $G^2/2g\rho$ is the velocity head downstream of the transition.

When considering momentum effects and flow distribution, and the requirements they impose on the manifold design, it is concluded that several approaches can be used to establish the configuration for a manifold to obtain the desired characteristic. Due mainly to structural and fabrication considerations, the manifolds were specified to be circular in cross section and of a constant diameter.

Because the arrangement of the Brayton cycle system components makes U-flow ducting necessary, the inlet and outlet manifold diameters must be carefully selected to obtain an acceptably small amount of flow maldistribution among the heat exchanger tubes. Basically, a pressure rise can result along the inlet manifold due to momentum decrease in the flow. If the diameter of the inlet manifold is made sufficiently smaller than that of the outlet manifold, the momentum recovery rate in the inlet manifold can just offset losses incurred in the outlet manifold.

The design procedure is to assume theoretically uniform flow to the various tubes of the heat exchanger and then size the inlet and outlet manifolds so that the pressure drop from the inlet to the outlet flange of the heat exchanger is the same for the flow paths that go through the first and last tubes. The pressure drop through the path that includes the middle tube can then be evaluated, and the fractional maldistribution approximated as:

$$\text{flow maldistribution} \approx \frac{2 \left(\sqrt{\Delta P_{\max}} - \sqrt{\Delta P_{\min}} \right)}{\sqrt{\Delta P_{\max}} + \sqrt{\Delta P_{\min}}}$$

The heat-source heat exchanger component pressure drops and subsequent calculated flow maldistribution are summarized in Table 4-2

TABLE 4-2

PRESSURE DROP SUMMARY

Component	Pressure Change, psi		
	First Loop*	Middle Loop	Last Loop**
Inlet manifold momentum	0	+0.172	+0.230
Inlet manifold friction	0	-0.045	-0.067
Inlet manifold to tube	-0.091	-0.105	-0.113
Tube friction momentum and turning losses	-0.292	-0.292	-0.292
Turning plenum losses	-0.136	-0.136	-0.136
Tube to outlet manifold	-0.063	-0.035	-0.023
Outlet manifold friction	0	-0.009	-0.014
Outlet manifold momentum	0	-0.125	-0.167
Net change in pressure	-0.582	-0.575	-0.582
Flow maldistribution \approx 1 percent			

* Nearest from entrance

** Furthest from entrance

4.2.2 Heat Source

4.2.2.1 Source Description

The heat source consists of a 49-inch-diameter planar array of 164 fuel capsules. A scalloped metal plate covers the fuel capsules as a part of the fuel capsule retention scheme. The design of the heat source heat exchangers (HSHX) is based on an effective source temperature which is defined as:

$$T_{\text{eff}} = \left[\frac{1}{A_c} \int_{A_c} T_s^4 dA_c \right]^{1/4}$$

where T_{eff} = effective source temperature

A_c = source surface area

T_s = source surface temperature

The relationship between the effective source temperature and the temperature drop in the fuel capsules was determined by Westinghouse. Figure 4-18 shows the effective source temperature (mean cover temperature) as a function of the maximum T-111 fuel capsule temperature at steady-state conditions.

4.2.2.2 Source-HSHX Thermal Model

An analysis of the heat transfer between the heat source and the HSHX should consider the radiant heat interchange between the heat source and HSHX 1 as well as between HSHX 1 and HSHX 2, the conduction across the heat exchangers, and the convection between the Brayton fluid and the walls of the HSHX in operation. The interaction between radiation, conduction, and convection results in a very complex heat transfer process. Therefore, an accurate determination of the temperature distribution over the heat source and the HSHX's requires the use of computer techniques.

A thermal analysis was carried out for the present case (planar circular heat source array and an involute tubular heat exchanger). The diameter of the heat source was taken as 48 inches. It was assumed that full output power from PCS 2 is required when HSHX 1 is inoperative, that is, outlet gas temperature from HSHX 2 is 1600° F.

The physical model treated in this analysis is sketched in Figure 4-19. The heat flow in the system is simulated by a thermal-resistance thermal-capacitance network. Each element in the system is represented by a node in this electrical analog.

The surface of the heat source facing HSHX 1 is divided into five elements of equal size. It is assumed that all the heat generated in the fuel capsules is radiating from this surface and is distributed uniformly over the surface. The heat-source temperatures in this analysis should be considered as effective source temperatures. Therefore, any temperature drop in the fuel capsules must be added to these temperatures to get the maximum source temperature.

When HSHX 1 is not in operation, heat is transferred primarily by conduction between the various portions of the heat exchanger. Each of the upper and lower surface areas of HSHX 1 and its inlet and outlet manifolds is divided into circular elements as shown in Figure 4-19. Heat is transferred between these two halves by conduction and radiation.

The Brayton fluid flows in and out of the tubes of HSHX 2 as shown in Figure 4-19. Both the fluid and the wall temperature as well as the wall heat flux vary along the tube. Since an accurate determination of these variations is necessary for the proper design of the HSHX, the upper and lower halves of each tube are divided into several elements along the tube. Each of these elements is thermally connected, through convection, to the Brayton fluid. Heat is transferred between the upper and lower elements of the tube by conduction. Heat transfer between inlet and outlet tubes is important and is taken into consideration in the thermal network.

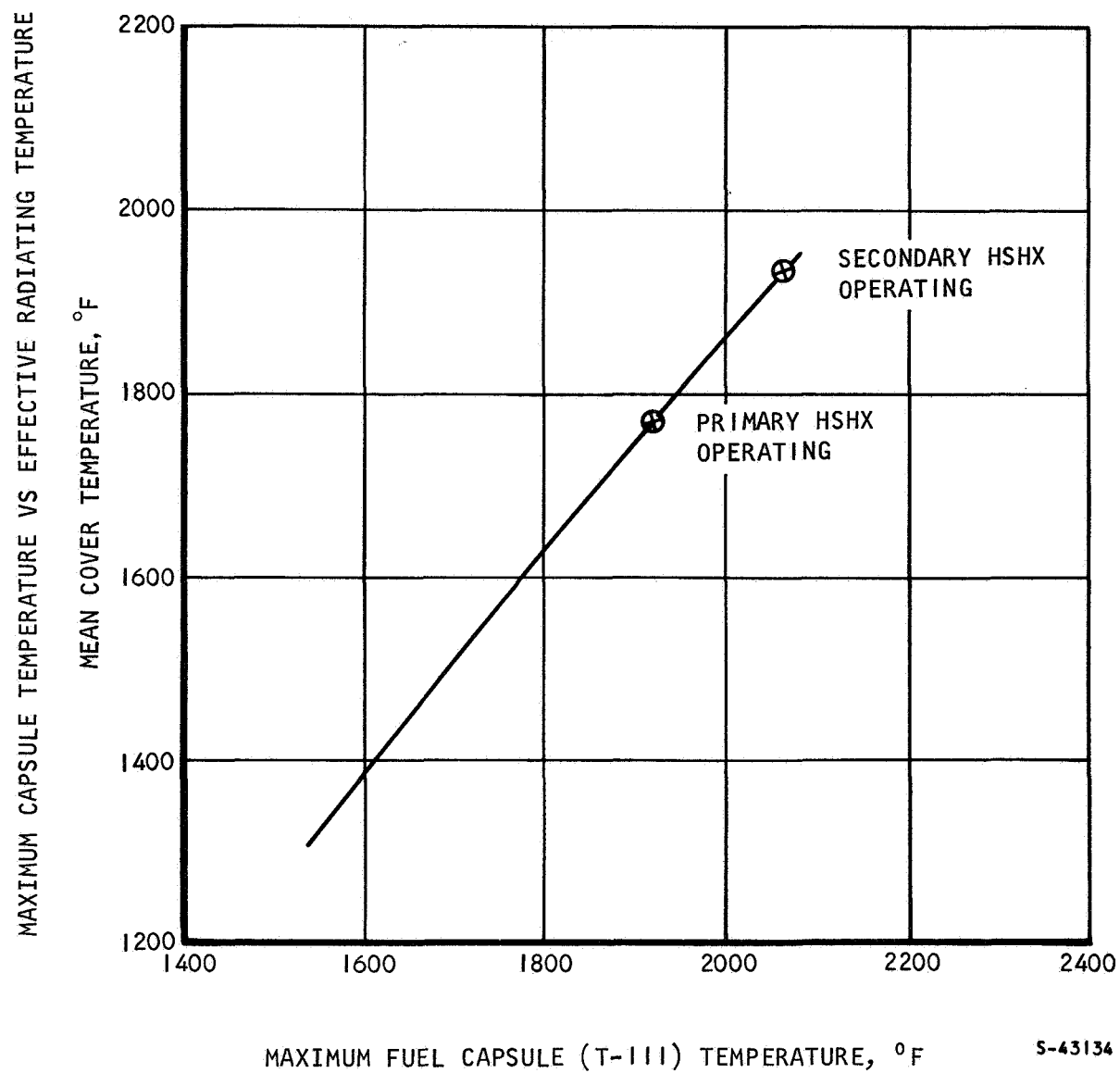


Figure 4-18 STEADY-STATE PERFORMANCE CIRCULAR PLANAR HEAT SOURCE

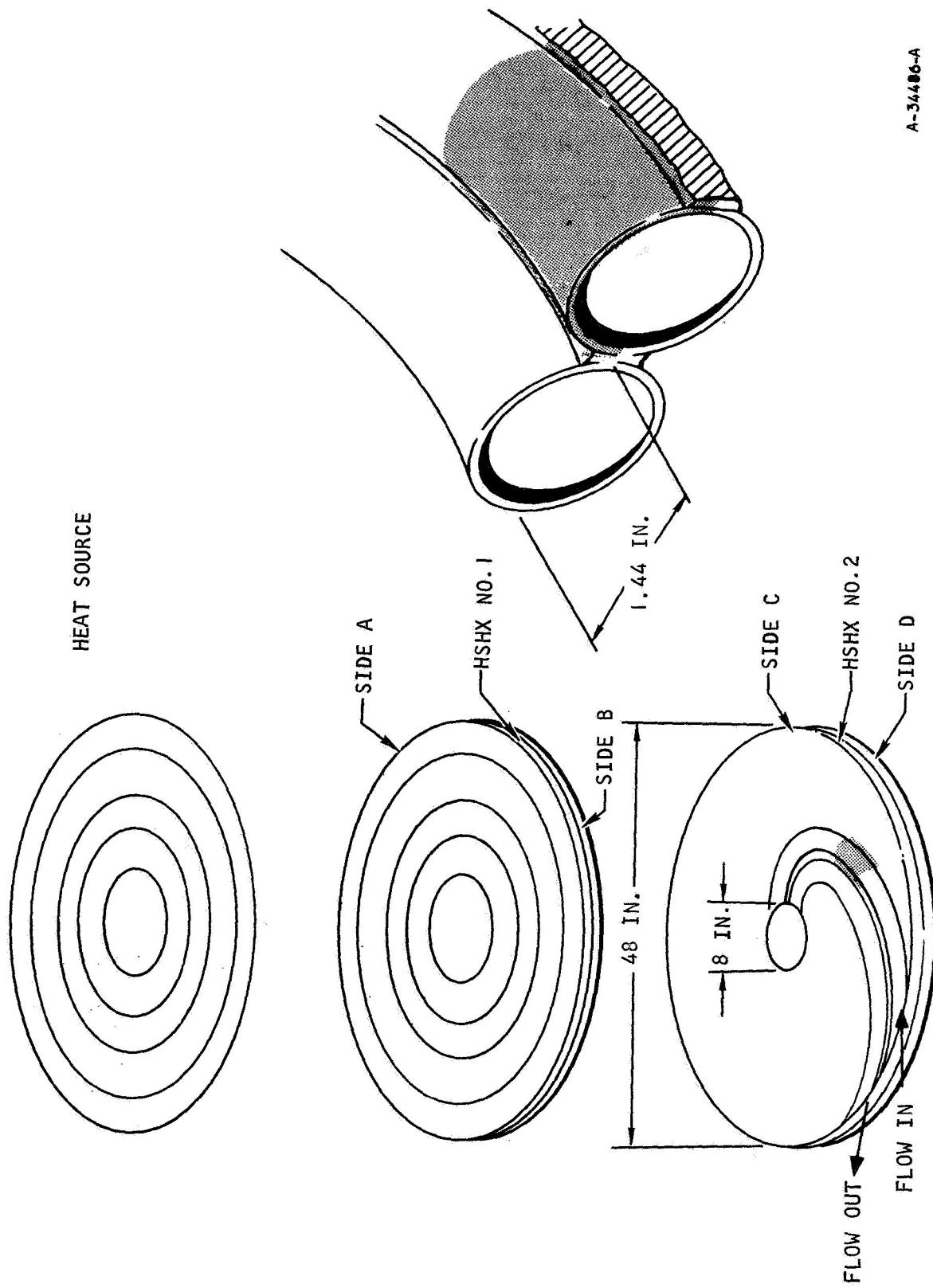


Figure 4-19 THERMAL MODEL FOR INVOLUTE HEAT-SOURCE HEAT EXCHANGER

The assumptions used in the analysis are summarized below:

- a. Each element is isothermal and assumes one discrete temperature.
- b. Each surface is gray.
- c. The radiation reflected and emitted from each element is distributed diffusely.
- d. The top surfaces of the heat source, the side walls, and the lower surface of HSHX 2 are perfectly insulated.
- e. A prescribed and uniform heat flux exists at the elements of the heat source.
- f. Heat is transferred between the two halves of the heat exchanger by conduction and radiation. A suitable value of the thermal resistance between the two halves was determined by separately analyzing the tube and fin combination.
- g. The Brayton fluid in HSHX 2 is also divided into elements. Heat is transferred between each element and the two halves of the HSHX by convection.
- h. The heat transfer coefficient inside the tubes of the HSHX is constant and is predicted by fully developed turbulent-flow correlations for moderate temperature differences such as the Dittus-Boelter correlation.

With assumptions (a) to (c), the radiation view factors between various elements in Figure 4-19 are computed with the CONFAC-II computer program. Knowing these view factors and using the remainder of the above assumptions, the various elements are represented as discrete nodes in an electric network simulating the heat transfer processes. This, in turn, is analyzed using a second computer program, MLFTHAN-MARK-1, to obtain the temperature distribution for the physical system shown in Figure 4-19.

4.2.2.3 Transient and Steady-State Temperature Distribution

During startup of the system, the Brayton fluid inlet temperature to the HSHX is related to the transient performance of the heat-source heat exchanger as well as the transient performance of other components in the system (see Figure 4-20). A computer program (supplied by NASA) was used to simulate the thermal performance of the various components in the system during startup conditions. The transient profile of the gas inlet temperature to the HSHX was found to be approximately the same for either HSHX 1 or HSHX 2 operation. Figure 4-21 shows the inlet temperature as a function of time during startup. These values were used in the thermal model described previously, and the computer program MLFTHAN-MARK-1 was utilized to obtain the transient temperature at various points in the HSHX cavity.

4.2.2.3.1 HSHX 2 -- Figure 4-22 presents the gas temperature response at the outlet of the HSHX during startup of the system using HSHX 2. This figure

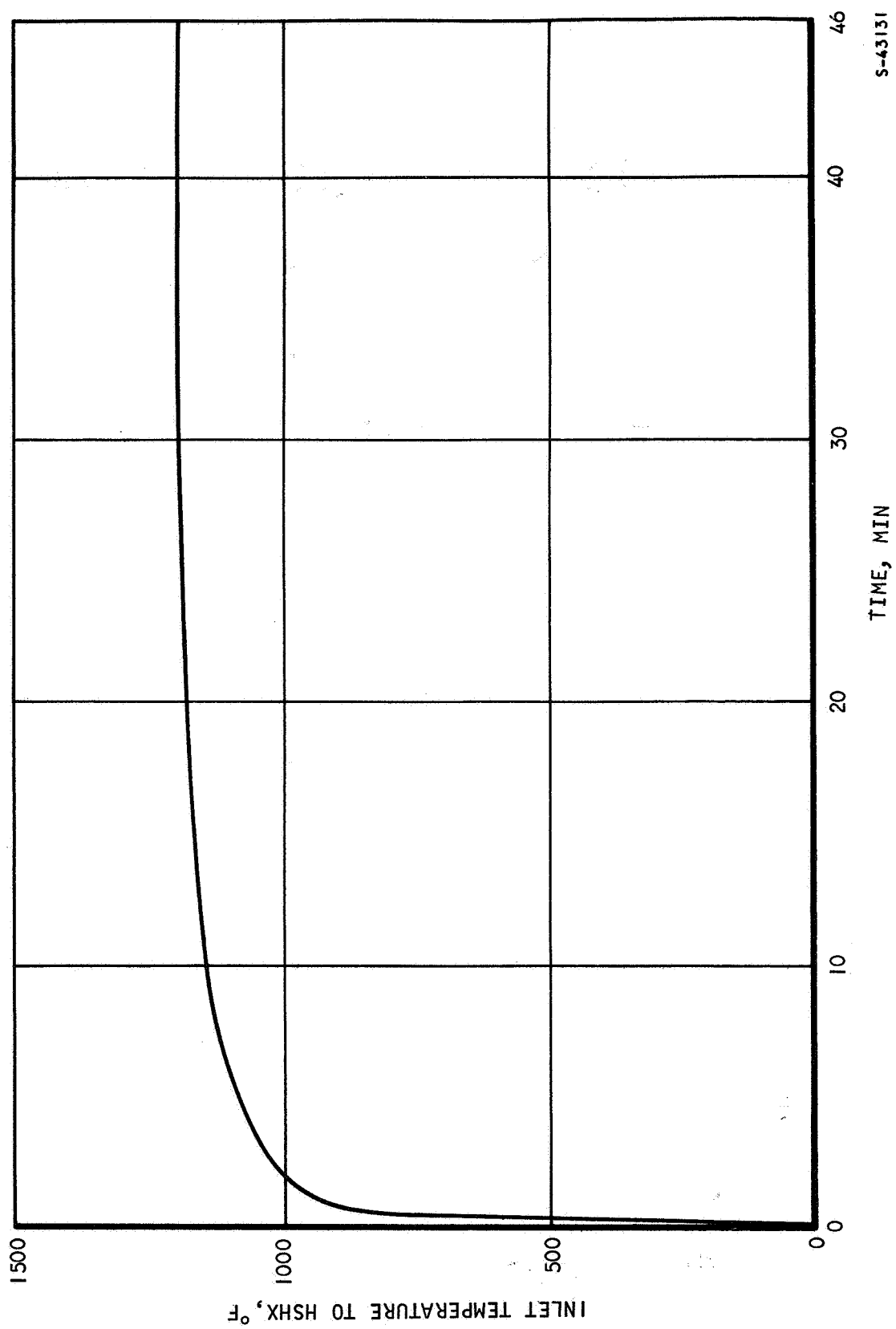
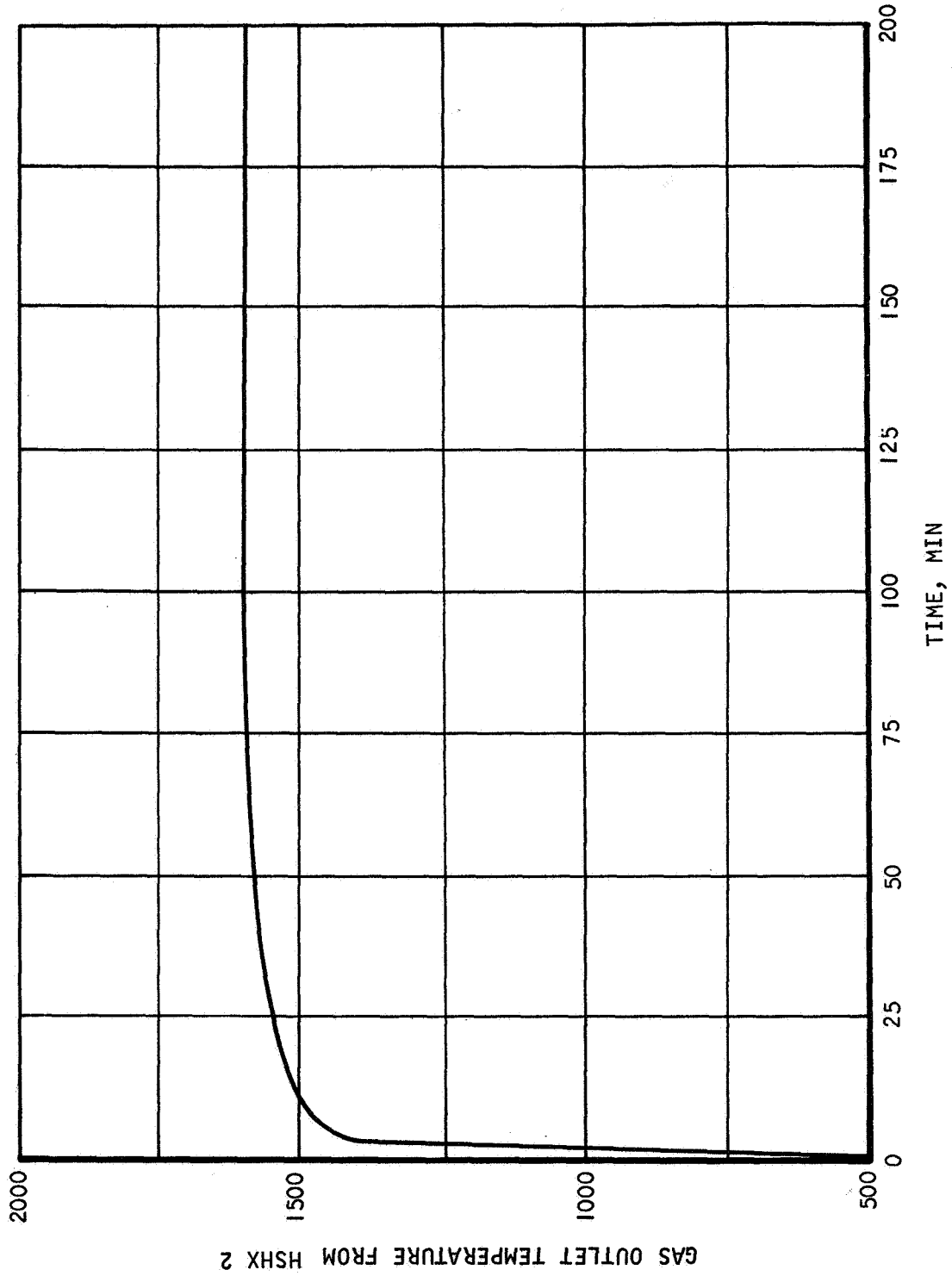


Figure 4-21 GAS INLET TEMPERATURE TO HSHX DURING STARTUP



S-43135

Figure 4-22 TIME HISTORY OF THE GAS OUTLET TEMPERATURE DURING THE STARTUP OF HXHX 2

reveals that the gas outlet temperature reaches about 1400° F in less than 3 minutes. It continues to rise in a more gradual manner to the desired value of 1600° F. The fast initial rise may be attributed, in part, to the small flow rates of the Brayton fluid immediately after startup.

The response of the maximum effective source temperature during startup of the system using HSHX 2 is shown in Figure 4-23.

The initial system temperatures during startup were taken to be those corresponding to a source steady-state temperature of 1800° F. Figure 4-24 shows that the maximum effective source temperature rises slowly to its steady-state value of 1935° F. The computer results show that the steady-state conditions are approached in a very gradual manner and that they are reached after a long time. However, the steady-state value of the maximum effective source temperature is reached within 100° F after a period of 30 minutes.

The steady-state temperature distribution when HSHX 2 is in operation is shown in Figure 4-25. A typical temperature distribution along one of the tubes in HSHX 2 is depicted in this figure. The Brayton fluid temperature rise is also shown. The fluid enters the tube at 1200° F; the temperature gradient along the tube is large in the first pass due to the high heat flux in this pass. The temperature gradient decreases gradually in the second pass. The fluid outlet temperature is 1600° F, which corresponds to full output power from PCS 2.

The computer results for the effective and maximum heat-source temperature distribution, and the temperature distribution for HSHX 1 on the side facing the heat source, are also shown in Figure 4-24. The ΔT from the effective radiating temperature to the fuel capsule hot spot is taken from the Westinghouse work shown in Figure 4-18. From Figure 4-24 it can be seen that the design temperature limitation of 2000° F is exceeded by approximately 60° F.

4.2.2.3.2 HSHX-1 -- The response of the gas outlet temperature during startup of the system using HSHX 1 is depicted in Figure 4-25. The temperature demonstrates the same fast rise in the first few minutes followed by a gradual increase to its desired steady-state level of 1600° F.

The response of the maximum effective source temperature during startup of PCS 1 is shown in Figure 4-26. The temperature in this case decreases gradually from an initial assumed temperature of 1800° F to its steady-state value of 1770° F. This is because the initial source temperature is higher than that required to obtain full power output from PCS-1.

Finally, the steady-state temperature distributions in HSHX 1 and the heat source are shown in Figure 4-27. It is obvious in this case that the maximum source temperature is considerably lower than 2000° F.

4.2.2.3.3 Central Return Header -- During this phase of the analysis, it was discovered that the cap of the central header represented a hot spot due to the poorer heat transfer to the gas at this point. The actual computer results predicted a cap surface temperature of 1725° F for the HSHX 1 during operation and 1760° F for HSHX 2 under full power conditions. For structural reasons, it is desirable to reduce the cap temperatures to the lowest values possible. This was done by placing a piece of sheet metal (Cb-1Zr) over the cap facing

the direction of heat flow to insulate this surface as illustrated in Figure 4-28. Also shown in this figure are the temperatures at different critical structural regions for the case of HSHX 1 in operation. The effect of the radiation barrier over the cap is seen to reduce the pressure-containing cap surface from 1725° to 1672° F. The source temperatures shown in Figures 4-24 and 4-27 reflect the higher radiation shield surface temperatures (1725° F for HSHX 1 in operation).

4.2.2.4 Off Design Performance

Where it is desirable to operate the Brayton cycle power system at less than design temperature levels a loss in power output is incurred. Figure 4-29 presents the variation in power output as the turbine inlet temperature is decreased and the thermal power is held constant. This is done by changing the gas loop inventory (that is, pressure) as indicated in this same figure.

4.3 INSULATION SYSTEM

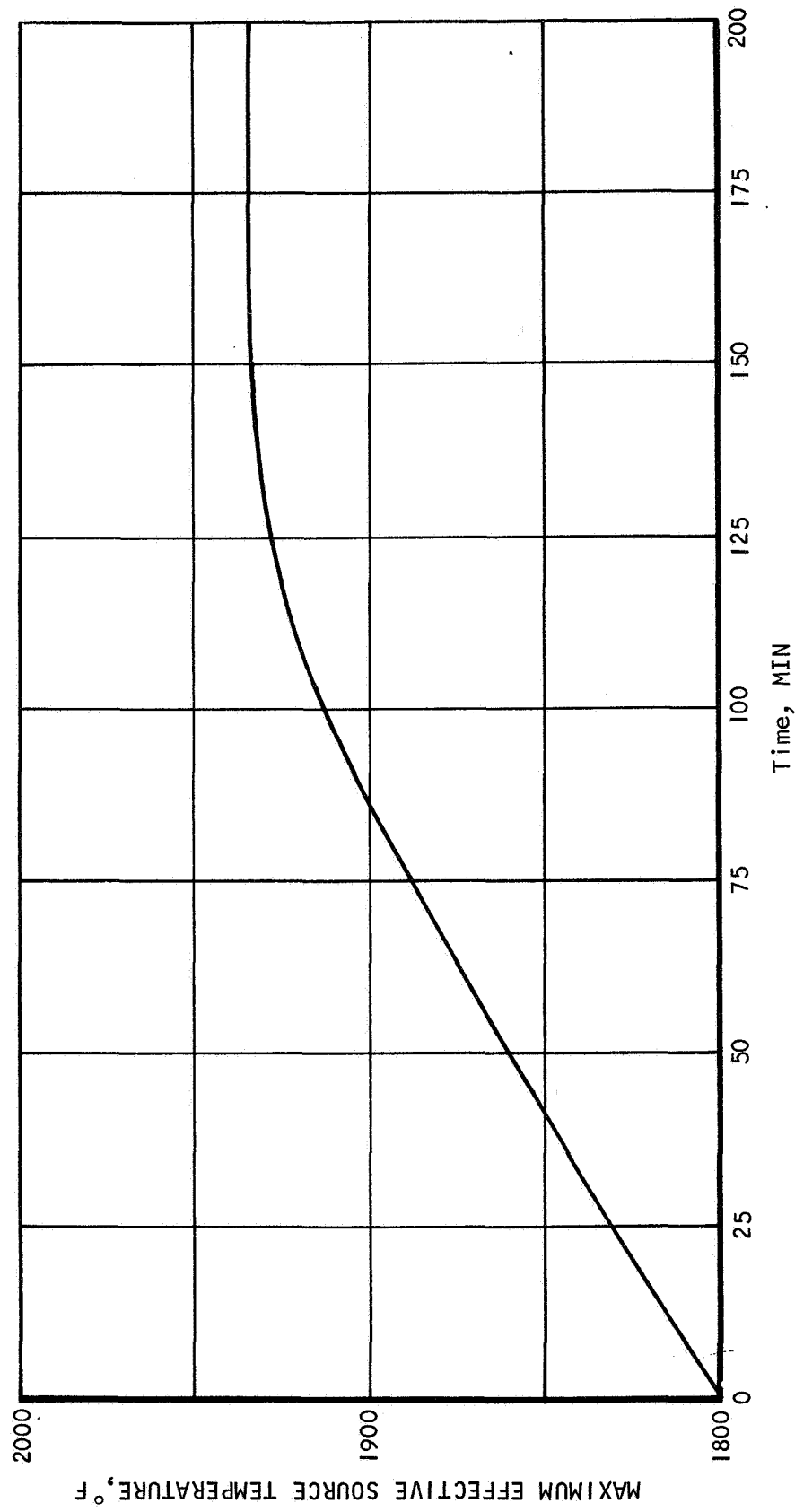
4.3.1 Description

The main areas of the HSHX to be insulated are the heat exchanger cavity, the inlet and outlet ducts to both heat exchangers, and the structural supports to the heat exchangers.

Figure 4-30 shows the various areas of heat leaks and the recommended insulating materials at these locations. A minimum thickness of 0.25 inch of Multi-foil is used to cover the cavity boundaries. This thickness was selected to keep the total heat losses below 1 kw. Figure 4-30, which shows a conception of aft support, illustrates the type of penetrations through the insulations that are necessary for installation purposes. Therefore, the thickness of the Multi-foil is increased to about 0.375 inch to limit the heat leak at these locations. A thickness of 2-1/2 inches of flexible MIN-K 2020 (a product of Johns-Manville) was estimated to be satisfactory for the insulation of the ducts and to cover the flange and the duct outer mounting brackets. The MIN-K will have stainless steel with gold coating as a facing material. This will decrease the heat lost by radiation from the ducts to the environment. A thickness of 1 inch of asbestos is used between the flanges of the inlet and outlet ducts to reduce the heat conducted along the tube walls. While the HSHX is not in operation, the asbestos minimizes the heat conducted to the PCM. The supports of the PCM act as heat leaks, dissipating the small amount of heat conducted to the PCM through the ducts.

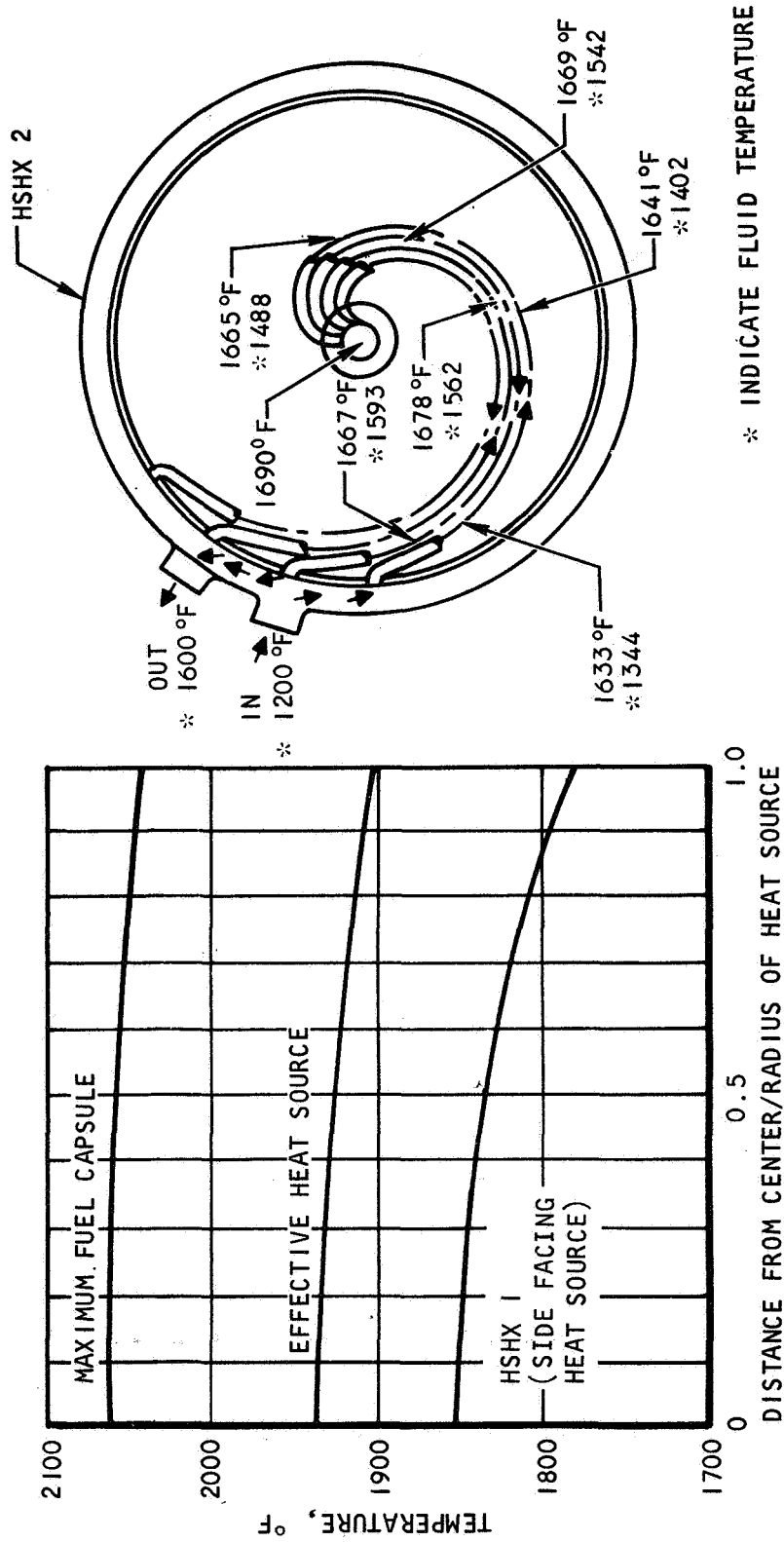
4.3.2 Material Performance and Selection

Multi-foil insulation may consist of many parallel layers of thin metal foil separated from one another by high-purity refractory oxide particles. The layers of foil act as thermal radiation barriers and as few as 10 to 20 layers constitute an effective insulation barrier. Since the spacing between foil layers can be reduced to only 1 μ , a very large number of radiation shields may be placed in a given thickness of insulation. The oxide particles prevent adjacent layers of metal foil from coming in contact with one another. The low thermal conductivities of the oxides plus the high contact resistances that exist between particles and foil in a vacuum combine to minimize the conduction component of the total heat transfer through the insulation.



S-43137

Figure 4-23 RESPONSE OF THE MAXIMUM EFFECTIVE SOURCE TEMPERATURE
DURING THE STARTUP OF HSHX 2



S-43141

Figure 4-24 INVOLUTE HEAT-SOURCE HEAT EXCHANGER PERFORMANCE
(HEAT EXCHANGER 2 IN OPERATION)

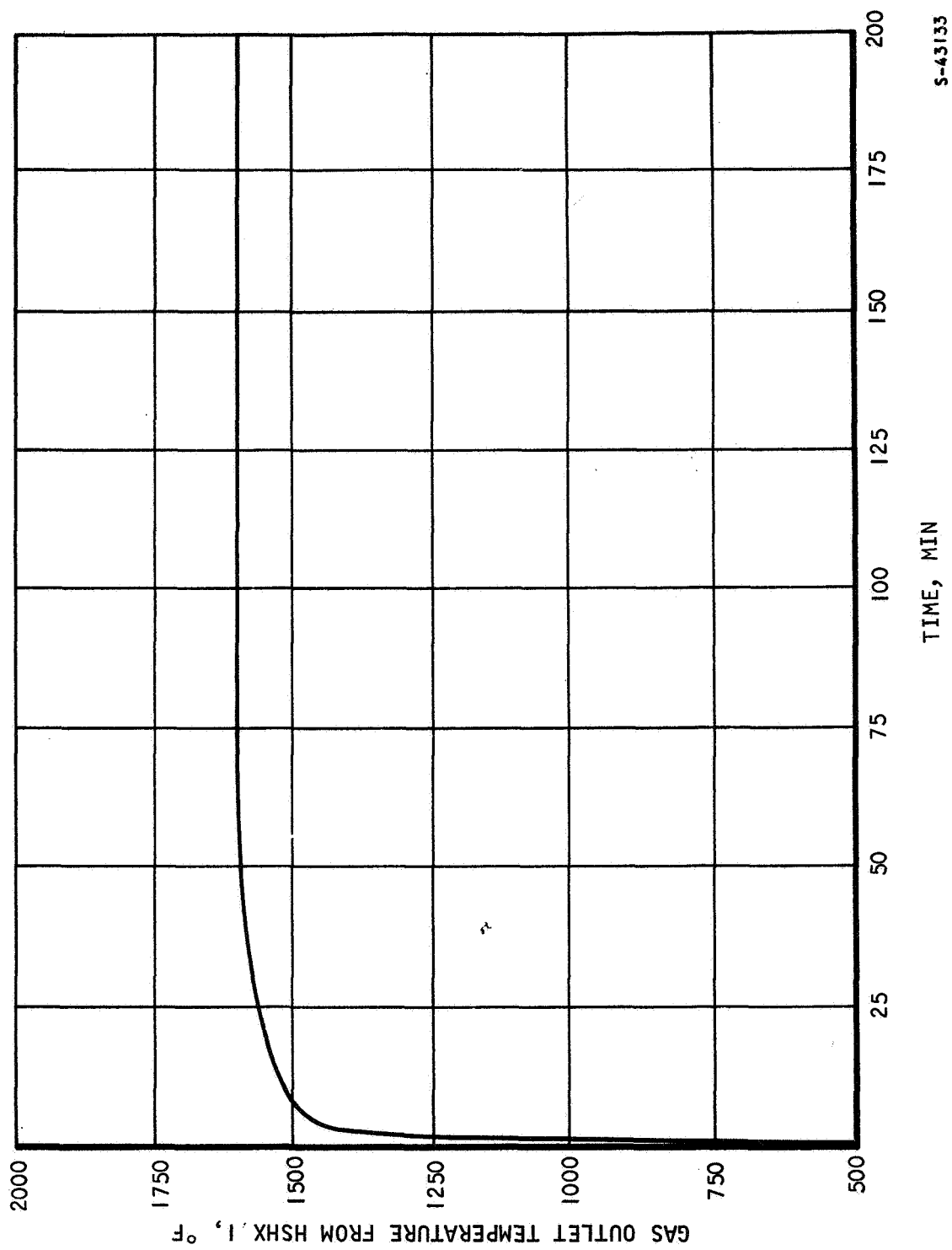
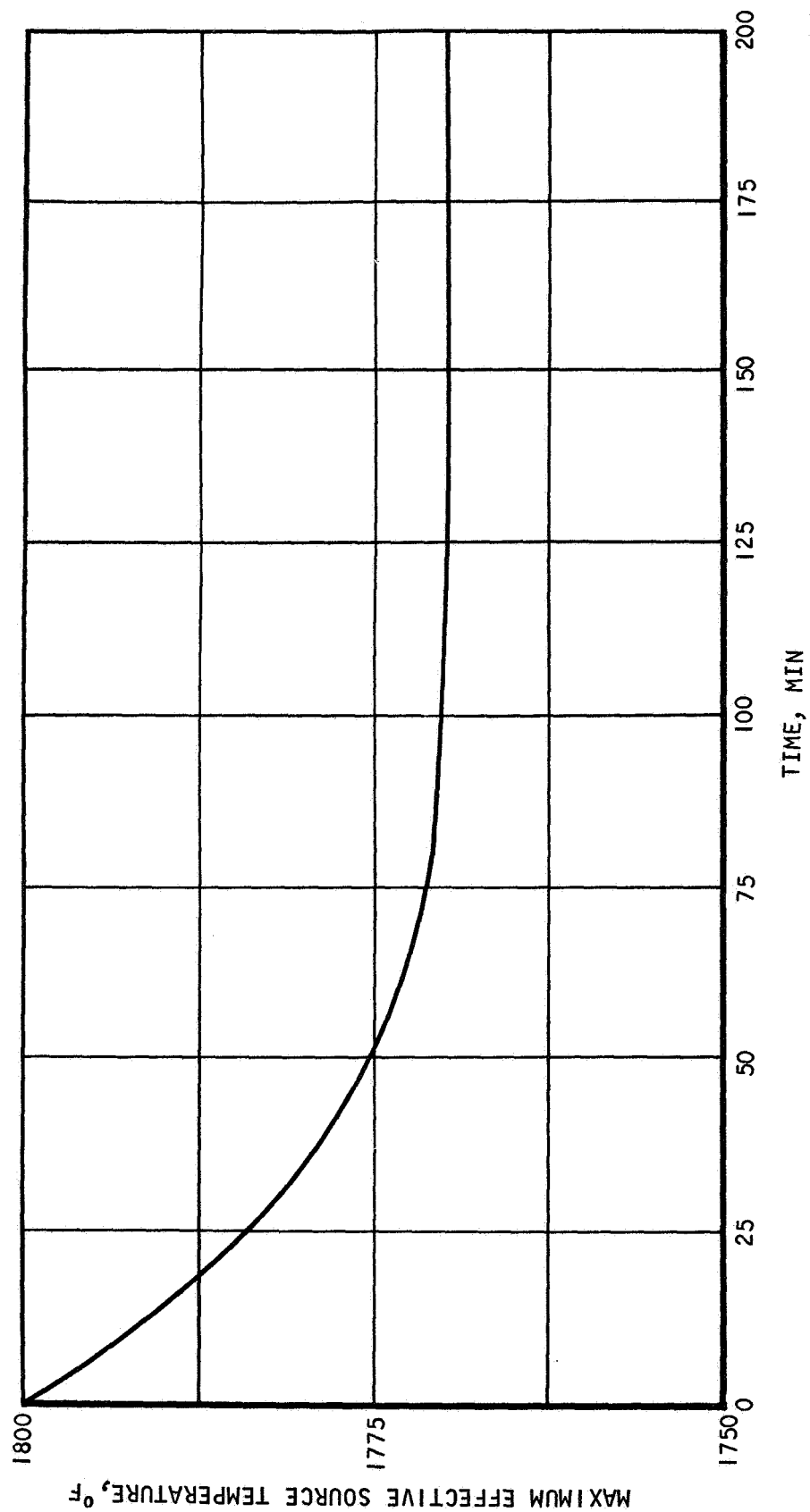


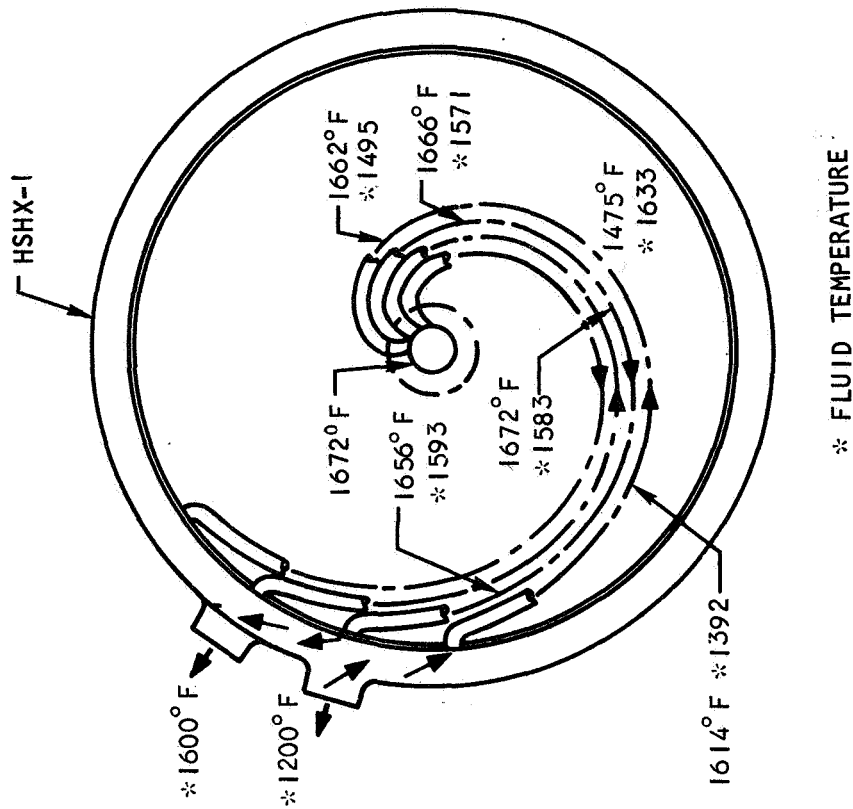
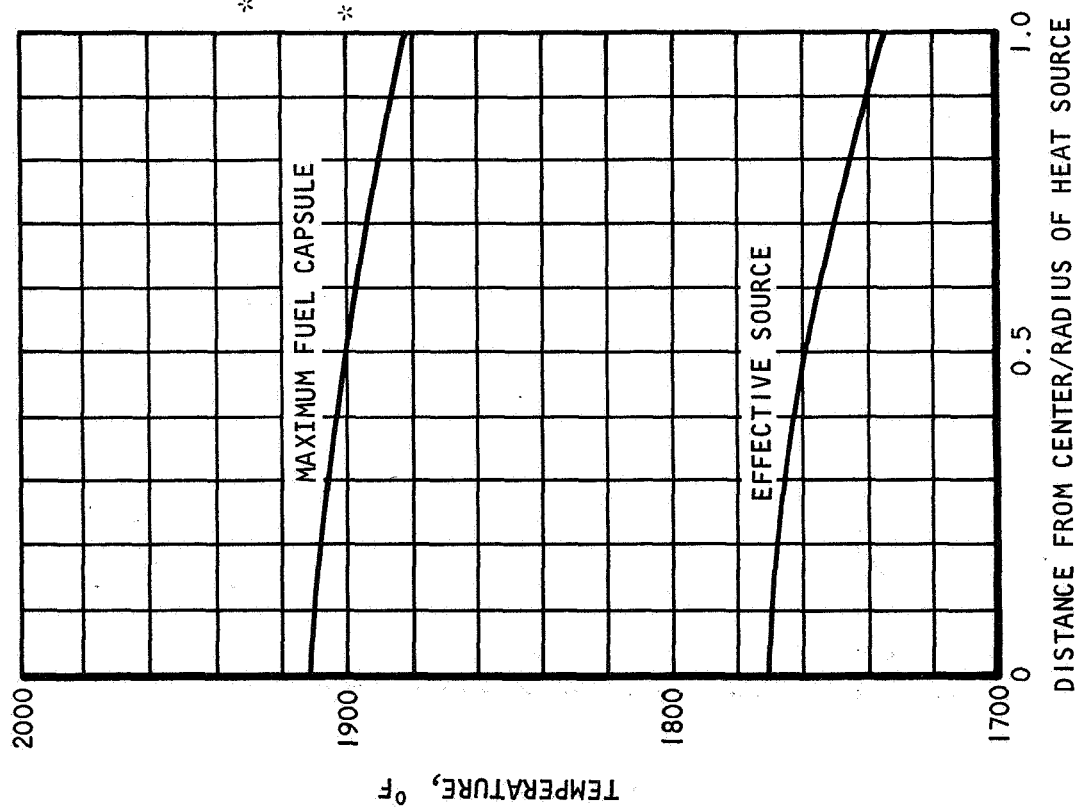
Figure 4-25 GAS OUTLET TEMPERATURE DURING STARTUP OF HXHX 1

S-43133



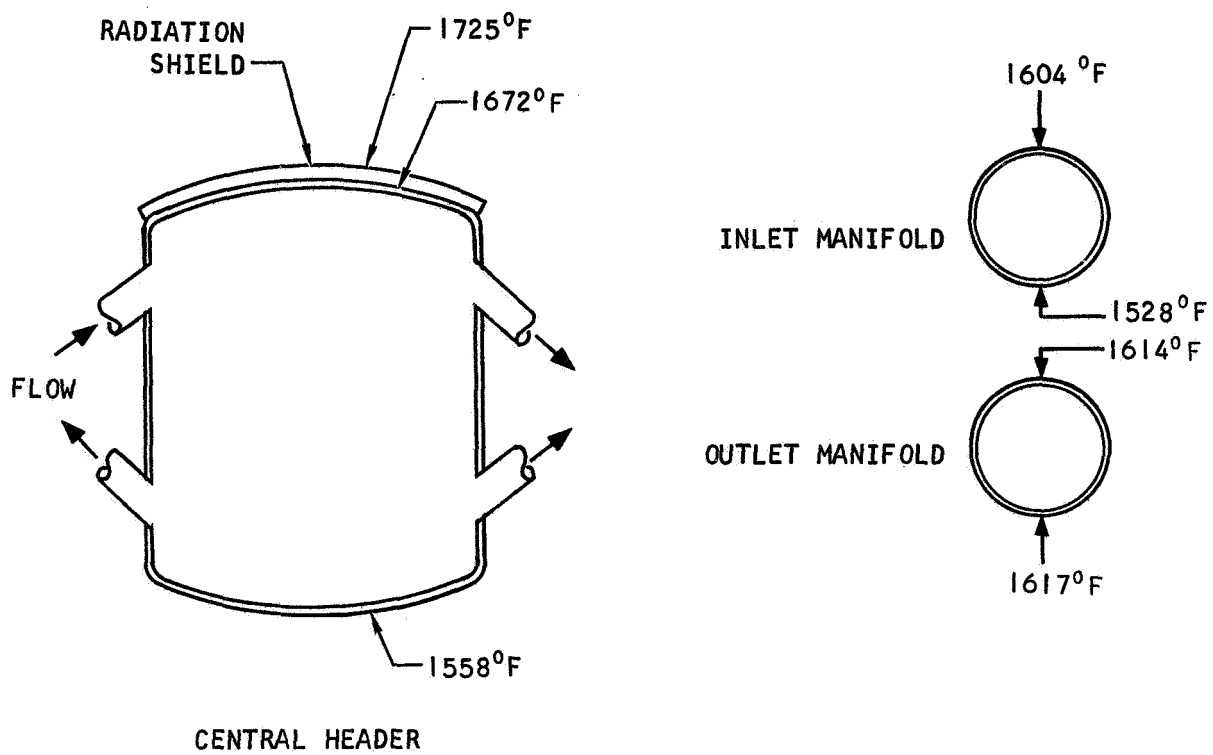
S-43138

Figure 4-26 RESPONSE OF THE MAXIMUM EFFECTIVE SOURCE TEMPERATURE DURING STARTUP OF HSHX 1



S-43140

Figure 4-27 HEAT-SOURCE HEAT EXCHANGER STEADY-STATE PERFORMANCE
(HEAT EXCHANGER 1 IN OPERATION) (48-IN. DIA.)



S-43404

Figure 4-28 HSHX COMPONENT TEMPERATURE DISTRIBUTIONS

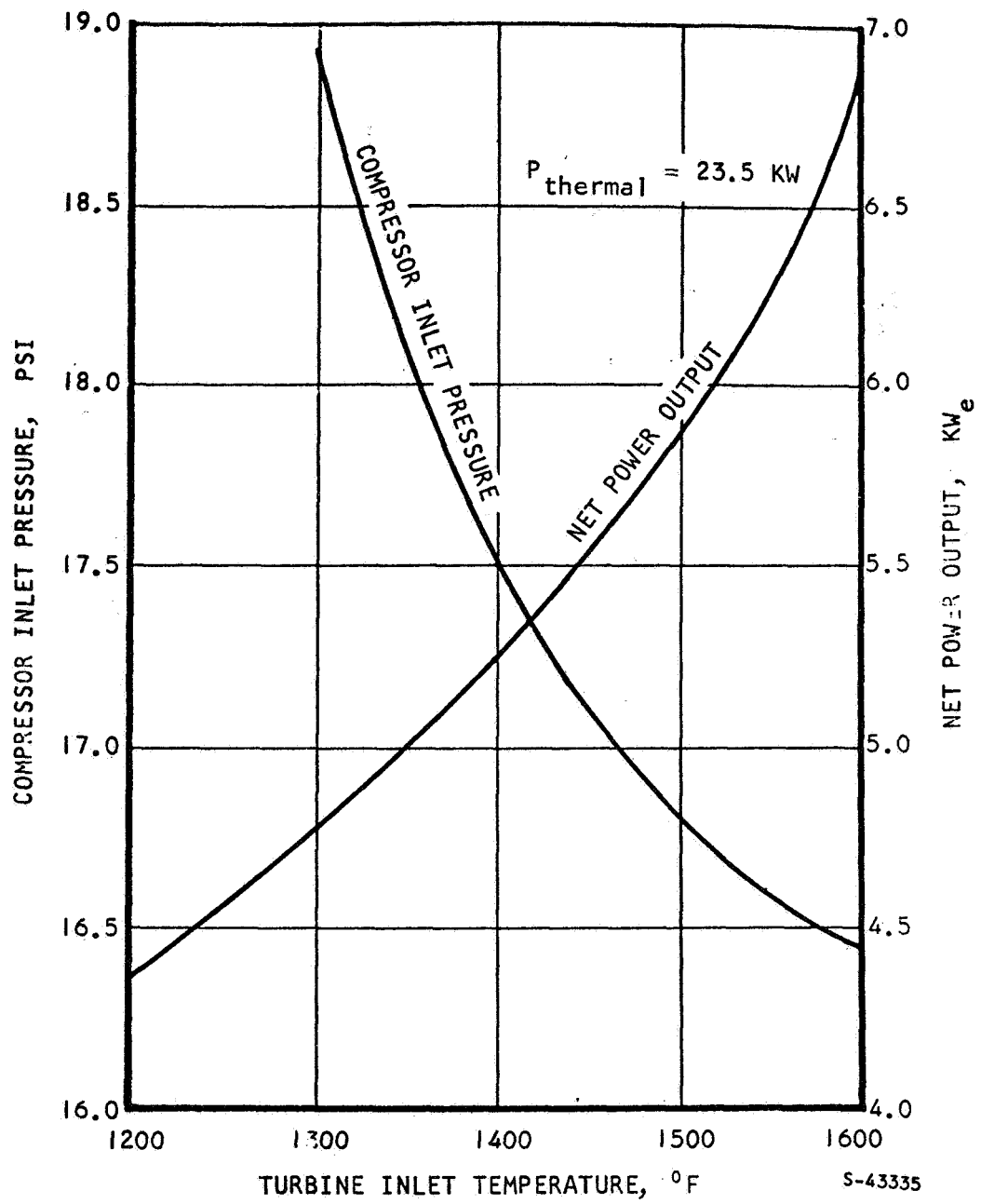
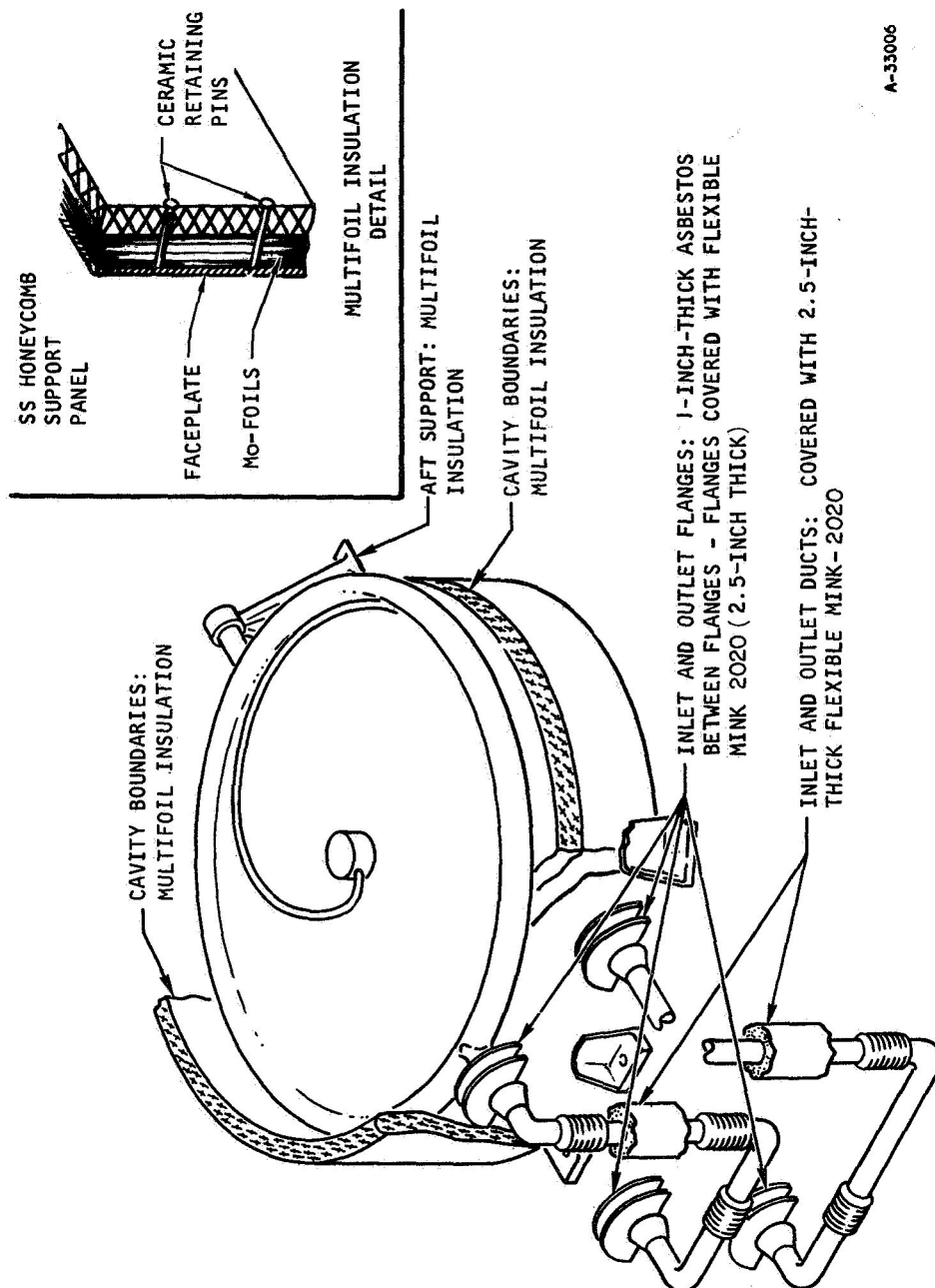


Figure 4-29 TURBINE INLET TEMPERATURE VERSUS POWER OUTPUT



A-33006

Figure 4-30 ASSUMPTIONS FOR HEAT LEAK ESTIMATES

Examples of the performance of Multi-foil insulation are shown in Figures 4-31 and 4-33. A molybdenum-thoria combination was selected since it out performed other insulation material combinations. Heat flux data for planar Mo-ThO₂ insulation samples are shown in Figure 4-31. The data points show the measured heat fluxes through the various samples resulting from the temperature difference established across the insulation by the indicated source temperature and a sink temperature of 40° C. The average effective thermal conductivity for the samples is shown in Figure 4-32. The effect of the geometry on the insulation capability of Multi-foil can be seen by comparing Figures 4-31 and 4-33. (The effect of geometry seems to be small.)

Load-bearing insulation has a higher thermal conductivity due to increased solid conduction. Figure 4-34 plots the heat flux through a 40-layer sample and a 100-layer sample of tungsten-thoria combination, each subject to pressures changed from 2.58 psi to 1.21 psi (a 47-percent decrease), the measured heat flux through both the 40- and the 100-layer samples decreased by 43 percent.

Flexible MIN-K 2020 has been selected to insulate the inlet and outlet ducts and flanges. MIN-K is a fibrous material that contains appreciable quantities of exceedingly fine particulate matter. The pore structure of MIN-K is so minute that it has a thermal conductivity lower than the molecular conductivity of still air. The thermal conductivity decreases appreciably at higher altitudes. For example, Figure 4-35 shows that at an altitude of 10 miles, the conductivity decreases by as much as 50 percent. This characteristic is directly attributable to the outgassing of the MIN-K.

4.3.3 Heat Leaks

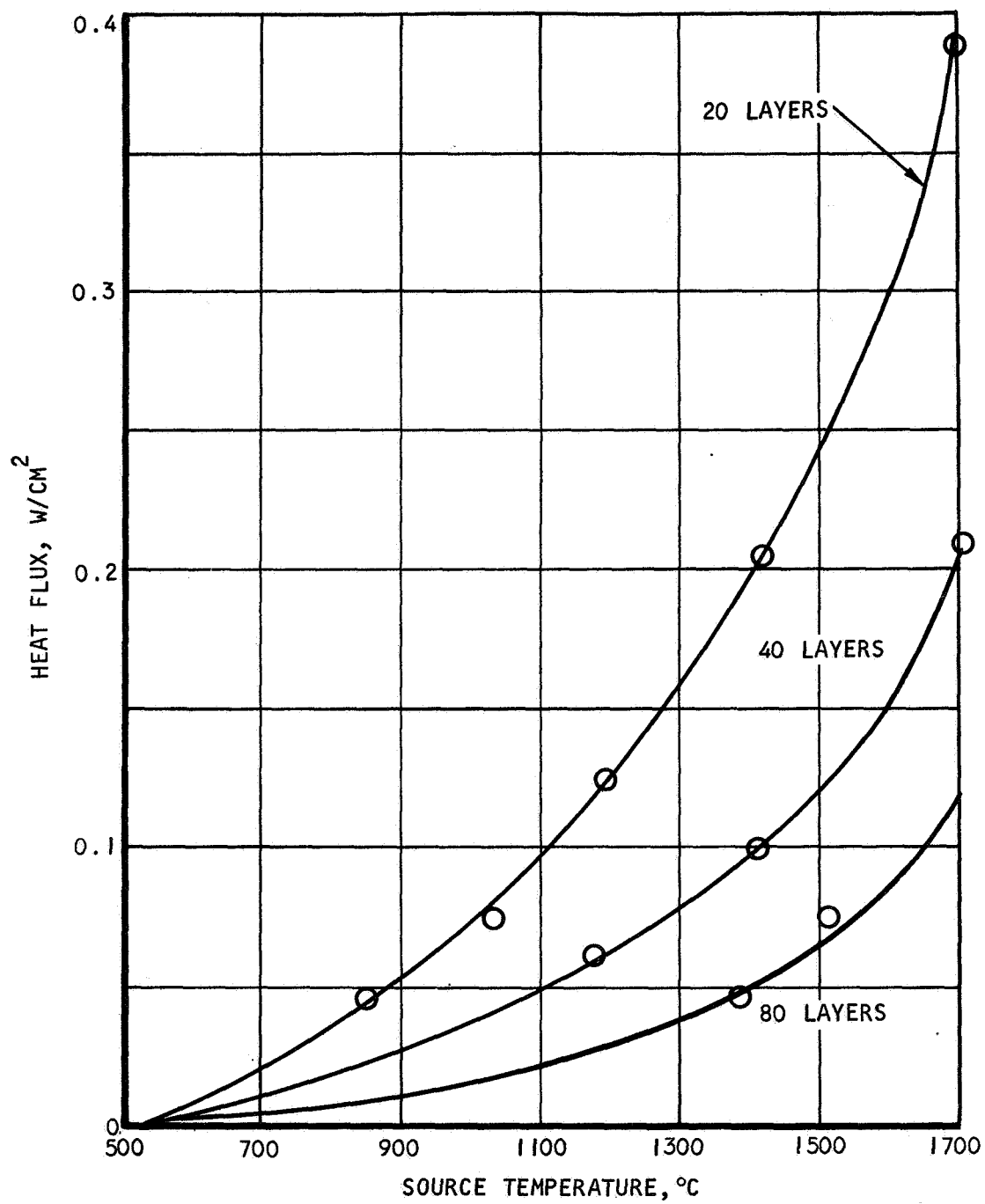
The magnitude of the heat leaks at various locations in the system are listed in Figure 4-36. These values were determined at steady-state conditions during the operation of PCS 2. If PCS 1 is in operation, the heat losses are lower than those listed in Figure 4-36; the differences, however, are small. The heat leaks are based on the thicknesses of the insulating materials shown in Figure 4-30. The thickness of the Multi-foil corresponds to about 125 layers of Mo-ThO₂ combination while 200 layers are used at the aft support.

The Multi-foil is supported by titanium honeycomb panels. The weight of the insulation and its supporting frame is about 13 lb/ft².

4.4 STRUCTURAL CONSIDERATIONS

4.4.1 Introduction

The structural analysis of the heat-source heat exchanger configuration with respect to pressure containment and thermal loads is summarized below. Heat exchanger installation considerations are discussed in Subsection 5.2 of this report. The unit as designed is shown to be satisfactory for the expected 50,000-hour design life and 100 start/shutdown cycles. Pressure containment stresses are shown to be within those allowable for Cb-1Zr in all cases. The critical transient thermal stress condition resulting from tube and inlet manifold differential expansion is shown to give a minimum estimated life of 357 cycles. The analysis shows that a finite fatigue life for this unit cannot be avoided.



S-43132

Figure 4-31 PLANAR HEAT FLUX TEST RESULTS (Mo-THO₂ INSULATION, BRUSH COATED, ZERO LOADING)

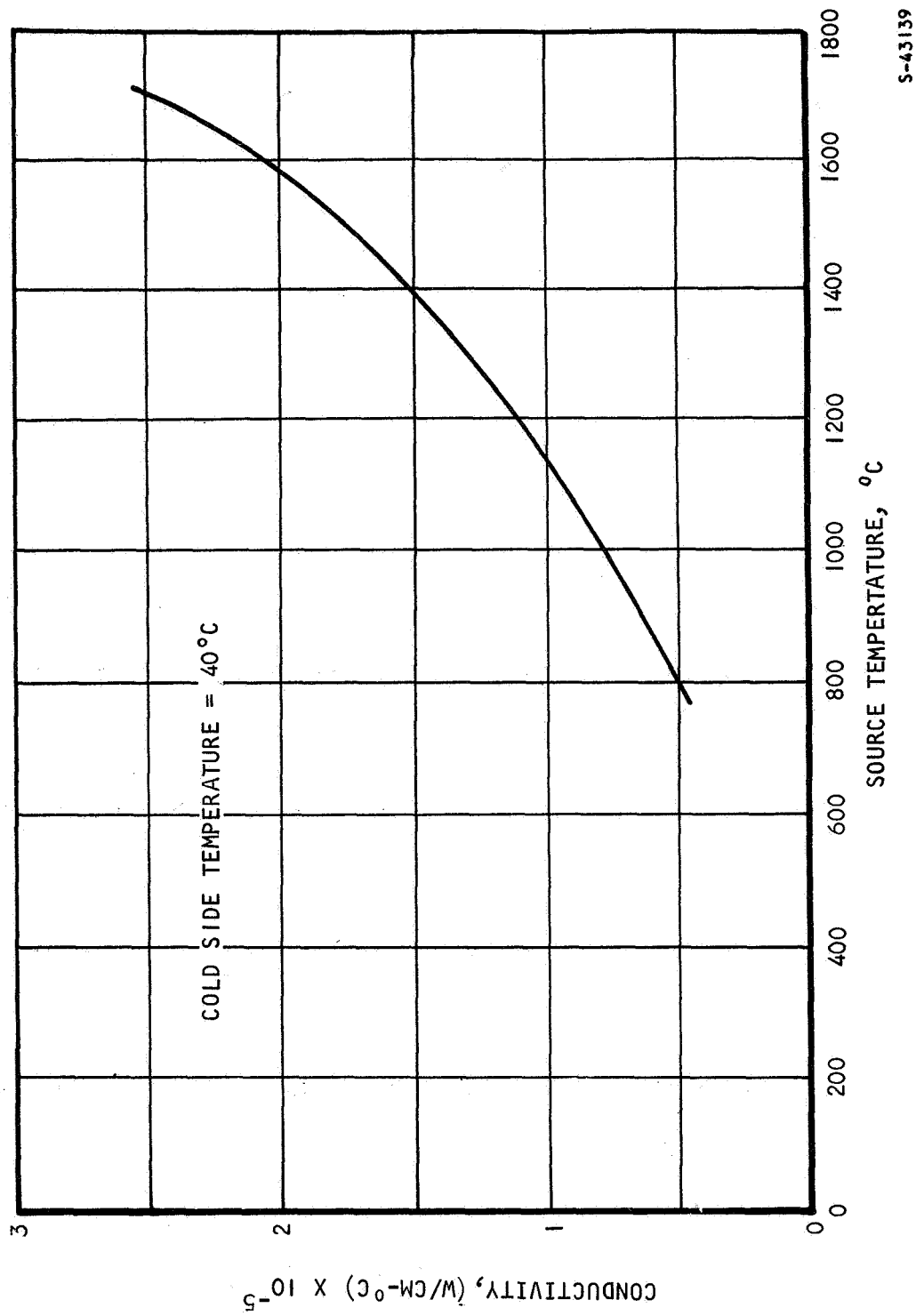
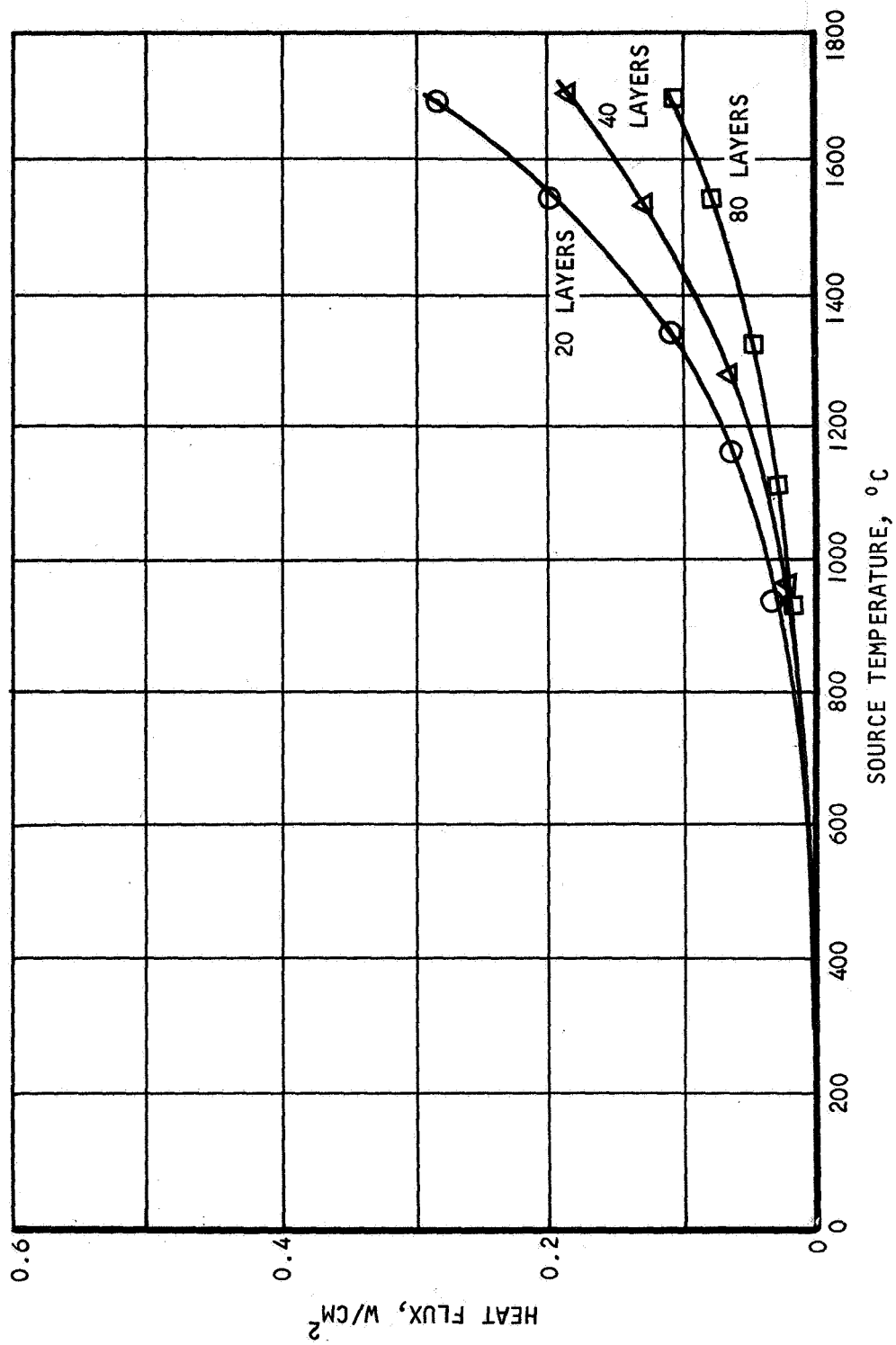


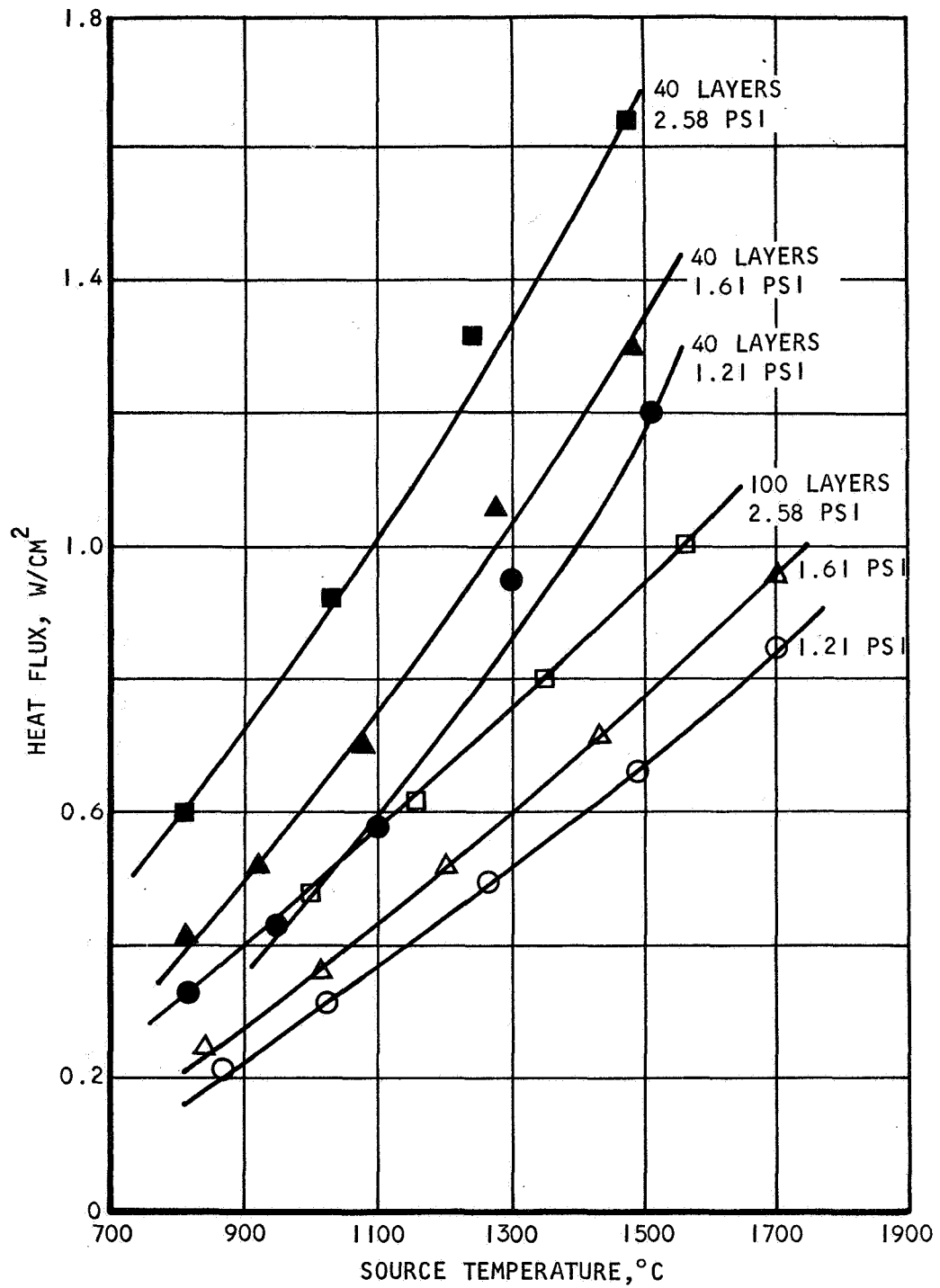
Figure 4-32 AVERAGE EFFECTIVE THERMAL CONDUCTIVITY BETWEEN SOURCE AND SINK TEMPERATURES (PLANAR Mo-THO₂ INSULATION)

S-43139



S-43129

Figure 4-33 CYLINDRICAL HEAT FLUX TEST RESULTS (Mo-THO₂ INSULATION, SPRAY COATED, ZERO LOADING)



S-43136

Figure 4-34 PLANAR HEAT FLUX TEST RESULTS (W-THO₂ INSULATION, SPRAY COATED, PRESSURE LOADING, 40- AND 100-LAYER SAMPLES)

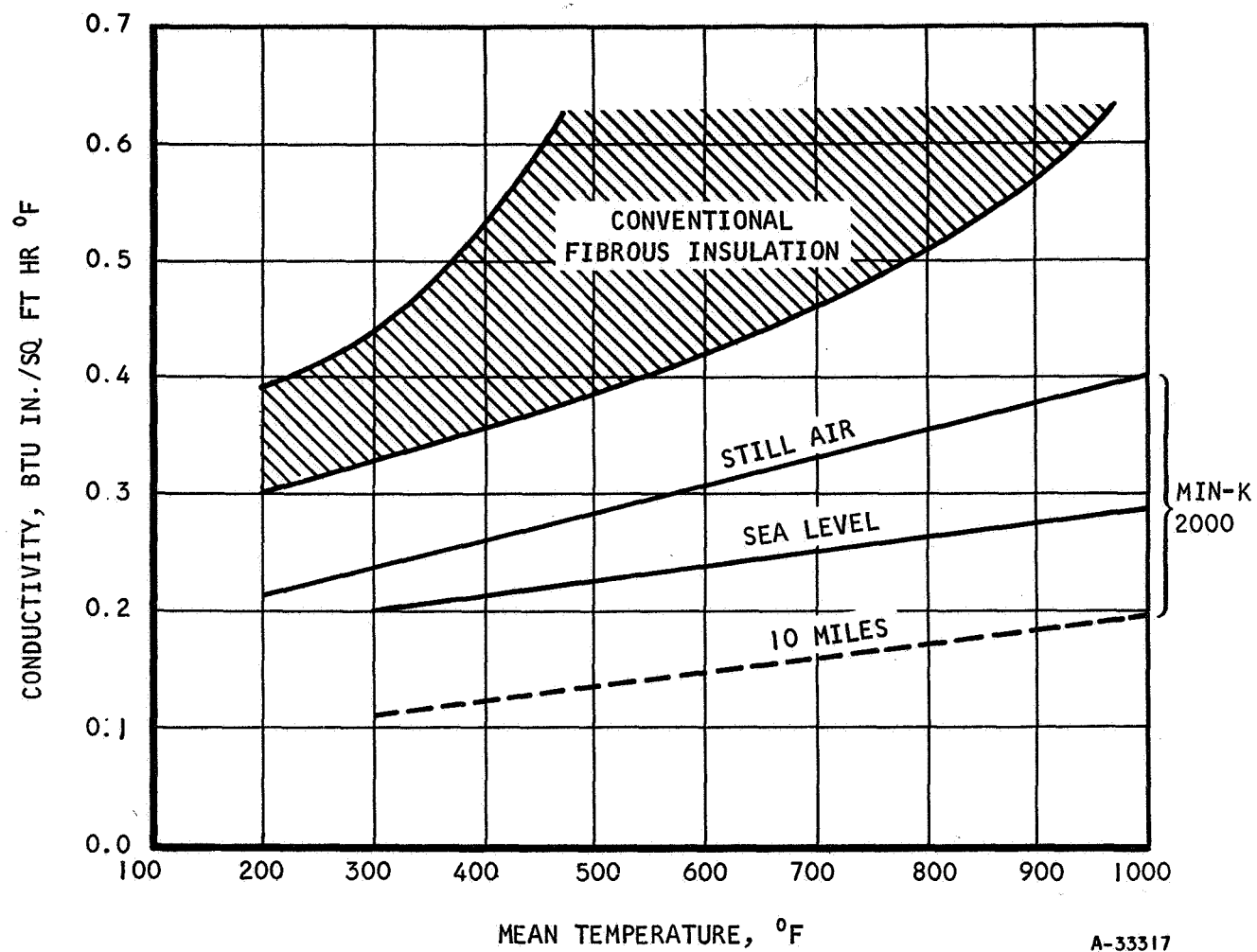
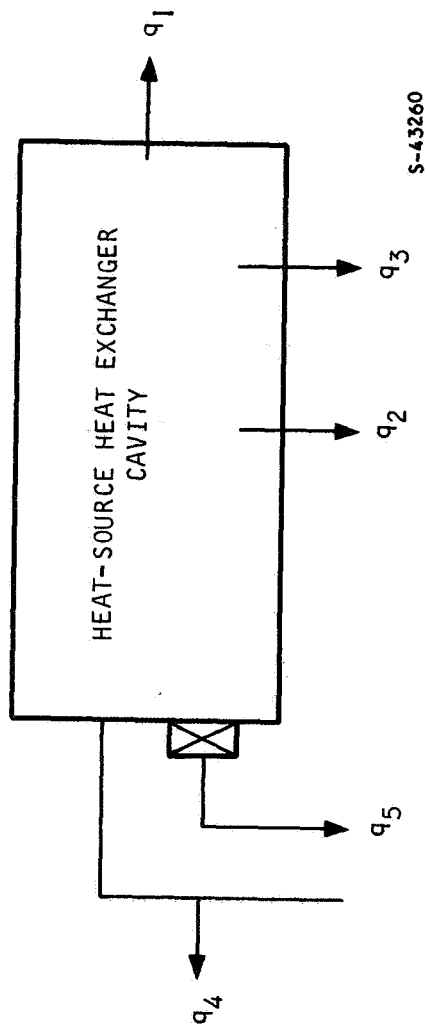


Figure 4-35 THERMAL CONDUCTIVITY COMPARISON



HEAT LEAK SOURCE	Thickness, Number of Foils	Heat Leak, w
q_1 = heat loss from sidewalls of HSHX cavity in watts	125	305
q_2 = heat loss from base of HSHX cavity in watts		
q_3 = heat loss from aft support in watts	200	61
q_4 = heat loss from inlet and outlet ducts in watts	2-1/2 in. MINK-2020	404
q_5 = heat loss from mounting brackets in watts	200	202
Total		972

Figure 4-36 HEAT LEAK ESTIMATES

4.4.1.1 Pressure Containment Analysis

Heat exchanger maximum operating stresses have been computed for the headers and tubes to verify that the local allowable stresses at maximum operating temperature are not exceeded. Table 4-3 gives the Cb-1Zr allowable stresses versus maximum metal temperature as presented in a discussion of structural design criteria in Reference 4-2. The operating pressure is 56 psi. The maximum operating temperatures are taken from Figure 4-27. Table 4-4 summarizes the results of these calculations for the various heat exchanger components and shows that all components are satisfactory. The assumptions used in computing the stresses are included in each case. Joint design has not been finalized at this time and local reinforcements may be required between the tubes and manifolds. The maximum stresses, however, are not expected to increase and possible local joint geometry changes will not change the basic thicknesses shown in the table.

Additional components not included in the above are the main ducts to the BHXU-BRU package and the bellows sections in the ducts. These components will require additional pressure containment analysis. In particular, the bellows design requires a computer program to determine pressure stresses. The work completed on ducting arrangement is reported in Subsection 5.2 of this report.

4.4.1.2 Thermal Stress Analysis

A preliminary stress analysis reported in Reference 4-2 indicated that substantial thermal loads are developed in the transition region from the welded tube area to the inlet and outlet headers due to temperature differences between the tube array and the headers. It was previously assumed that unwelded lengths of tubing would be required at the edge of the welded area to avoid excessive thermal loads. The unwelded lengths of tubing, however, reduce the heat transfer capability of the heat exchanger and may be objectionable from a vibration standpoint. Additional analysis was performed for the tube geometry shown in the heat exchanger layout drawing assuming that the tube section connecting the header to the welded is a straight tension or compression member. The first tube adjacent to this tube was examined to determine its flexibility and load capability when loaded in diametral compression as shown in Figure 4-37.

The operating condition that produces the most severe thermal loading condition is a transient occurring during the initiation of gas flow as depicted in Figure 4-38. At the beginning of gas flow, the inlet header is in contact with coolant at a temperature of about 0° F. The entering cold fluid is heated as it passes through the heat exchanger, and the tube array and outlet manifold are cooled to a lesser degree than the inlet header. The resulting temperature difference between the inlet header and tubes produced during this transient is assumed to be 500° F, compared to an operating difference of about 100° F. The transient case is, therefore, about five times as severe as the operating condition under this assumption.

The difference in thermal expansion between the inlet header and the tube array is given by the following expression:

$$\delta = R \left[\begin{array}{cc} (\alpha \Delta T)_{\text{TUBE}} & - (\alpha \Delta T)_{\text{INLET}} \\ \text{ARRAY} & \text{HEADER} \end{array} \right]$$

TABLE 4-3

Cb-1Zr ALLOWABLE STRESSES

Temperature (°F)	Tensile -- Compressive Allowable (psi)	Bending Allowable (psi)	Inertia Load Allowable (psi)
70	23,300	35,000	35,000
400	23,100	34,700	34,700
1000	22,600	34,000	34,000
1200	22,300	33,500	33,500
1300	22,000	33,000	33,000
1400	12,050	18,100	32,000
1500	6,750	10,100	31,000
1600	3,650	5,320	30,000
1650	2,750	4,120	29,500
1700	2,000	3,000	29,000
1750	1,400	2,100	28,500
1800	1,100	1,650	28,000

TABLE 4-4

HEAT EXCHANGER PRESSURE CONTAINMENT SUMMARY

Component	Maximum Operating Temperature (°F)	Maximum Operating Stress (psi)	Allowable Stress for Cb-12r (psi)	Comments
Inlet manifold $t = 0.045$ in. (minimum) OD = 2.40 in.	1604	1480	3580	Tube joint reinforcement assumed; stress computed by $\sigma = PR/t$ for cylinder
Outlet manifold $t = 0.045$ in. (minimum) OD = 3.00 in.	1617	1870	3340	Same as above
Return manifold cylinder $t = 0.200$ in. OD = 4.50 in.	1640	2800	2930	Tension area between tubes supports cap load; stress = load/area
Return manifold cap $t = 0.080$ in. (spherical) $R = 5.82$ in.	1672	2040	2520	Stress computed for spherical portion by $\sigma = PR/2t$
Tubes $t = 0.045$ in. OD = 1.44 in.	1672	1340	2420	Stress computed for cylinder with a 1.50-in. bend radius which gives a 1.5-stress concentration factor; $\sigma = 1.5 PR/t$

Notes: 1. t = thickness, in.2. P = pressure, psi3. R = radius, in.

4. OD = outside diameter, in.

5. σ = stress, psi (tension in all cases)

6. Maximum operating temperatures taken from Figure 4-27

7. Allowable stresses taken from Table 4-3

8. Maximum operating pressure = 56 psi

Assuming that the tube array is at an average temperature of 1400° F and the outer tube radius is 23 inches, the deflection is:

$$\delta = 23 [(4.32 \times 10^{-6})(1400 - 70) - (4.23 \times 10^{-6})(900 - 70)]$$

$$\delta = 0.051 \text{ in.}$$

An approximate estimate of the effect of this differential thermal movement has been determined assuming that one tube, loaded as shown in Fig. 4-37, absorbs the entire 0.051-inch deflection. Calculations of the flexibility of the annular header, straight tube segment, and the tube in diametral compression indicated that the latter element has by far the lowest stiffness and therefore absorbs most of the differential expansion. Tubes interior to the first tube will also effectively contribute to the overall flexibility. Since the load distribution is not known, a conservative estimate was obtained by considering only the first tube in diametral compression. The compressive load required to deflect the tube 0.051 inch is 190 pounds. This load causes a maximum elastic bending stress of 131,000 psi. The tube yield stress at 1400° F is 32,000 psi, so plastic deformation will occur and the elastic bending stress of 131,000 psi will not be realized in actual operation. This stress calculation indicates that considerable plastic deformation will occur during each of the operating cycles associated with this loading, and the fatigue life of the tube must be considered. As discussed in Reference 4-2, the design criterion adopted for this structure is that a desired life of 100 cycles be achieved by designing for a theoretical life of 400 cycles.

The fatigue life of the tube under the above thermal loading was estimated using the accumulated plastic strain per cycle to compute fatigue life as discussed in Reference 4-2. An assumed ideal elastic-plastic stress-strain curve has been estimated for each loading cycle assuming that the tube is loaded to a known strain during the cycle shown in Figure 4-38 and that unloading consists of forcing the tube to its original undeflected shape. Figure 4-39 shows this typical cycle with the first cycle from 0-1-2-3-4 and subsequent cycles following the loop from 4-1'-2-3-4. The total strain per cycle, ϵ_{TOTAL} , was estimated from the maximum elastic bending stress as shown in the figure, assuming uniform straining of the tube. The estimated value for ϵ_{TOTAL} is 0.0089 in./in. and since the elastic strain at the 32,000 psi yield stress is 0.0022 in./in., the plastic strain per cycle, ϵ_p , is:

$$\epsilon_p = \epsilon_{\text{TOTAL}} - 2\sigma_y/E$$

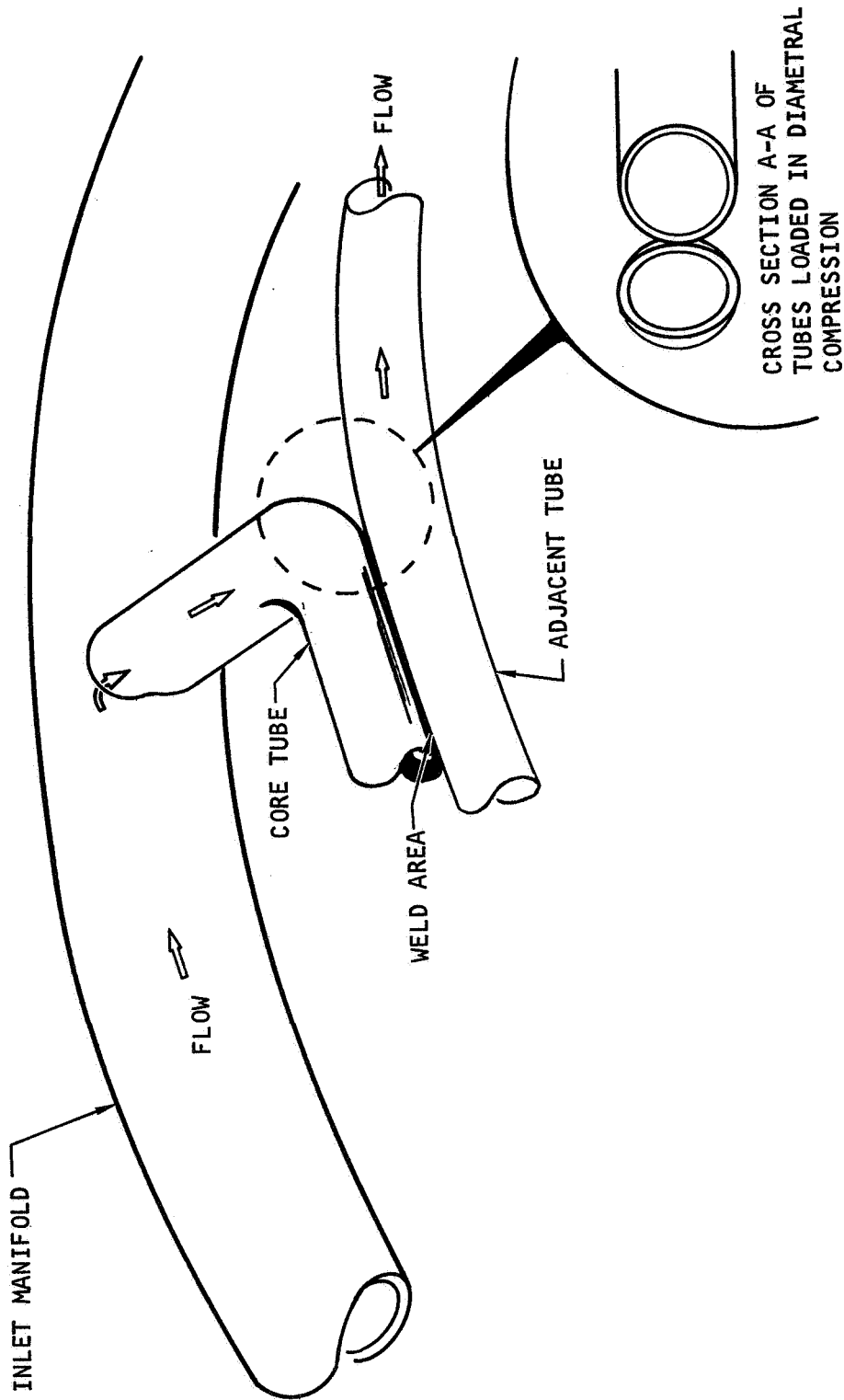
$$\epsilon_p = 0.0089 - 2(0.0022) = 0.0045 \text{ in./in.}$$

The equation for cycle life N is:

$$N = (C/\epsilon_p)^2$$

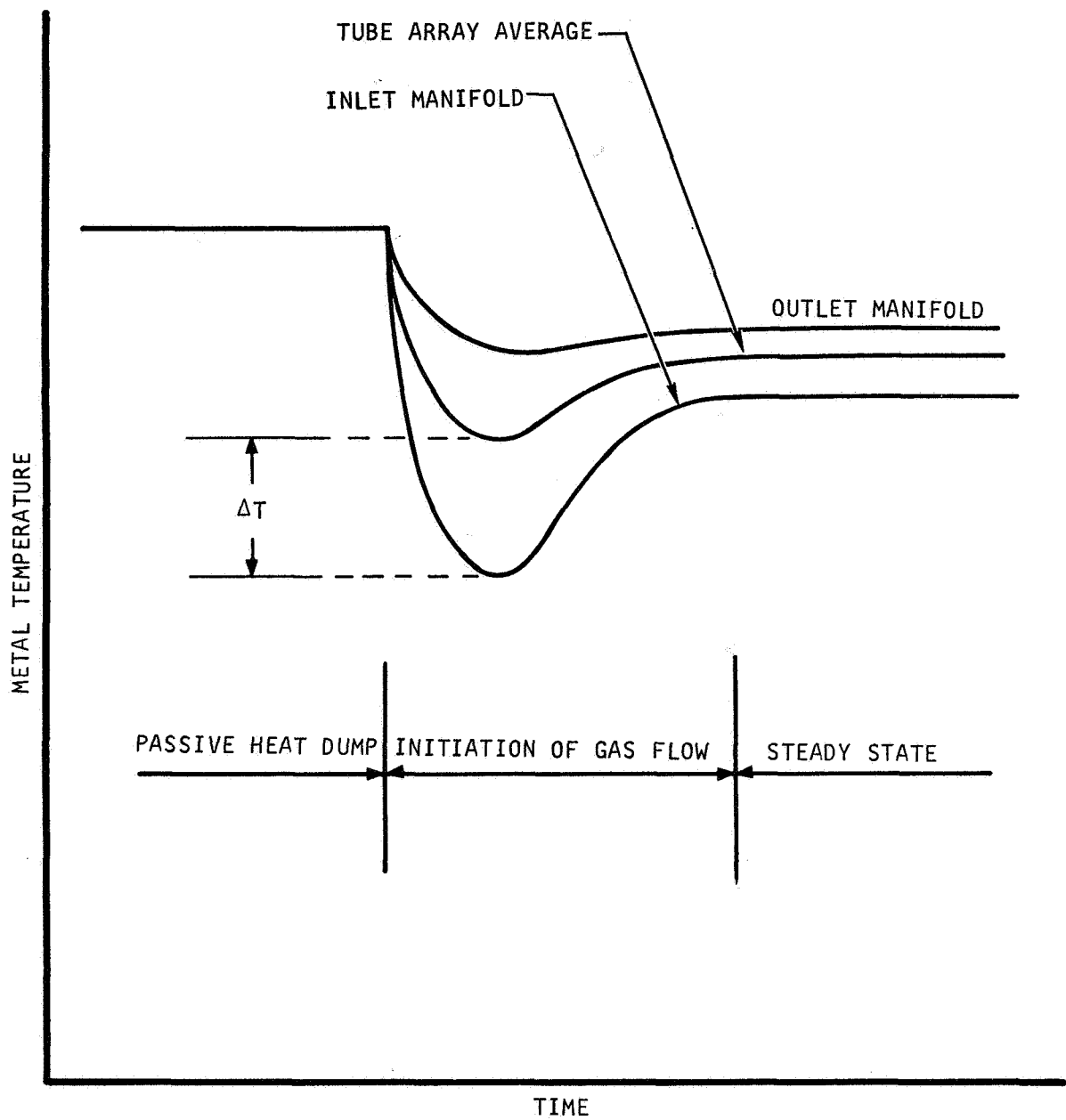
where, C, for a ductility for Cb-1Zr of 12 percent is 0.17. Including a strain-concentration factor of 2 to account for local geometry changes and nonuniform strains, the adjusted value for plastic strain per cycle is 0.009 in./in. The estimated life of the tube is:

$$N = (0.170/0.009)^2 = 357 \text{ cycles}$$



S-43374

Figure 4-37 TUBE-TO-HEADER TRANSITION REGION



S-43373

Figure 4-38 SCHEMATIC OF TIME-TEMPERATURE TRANSIENT OCCURRING WHEN GAS FLOW IS INITIATED

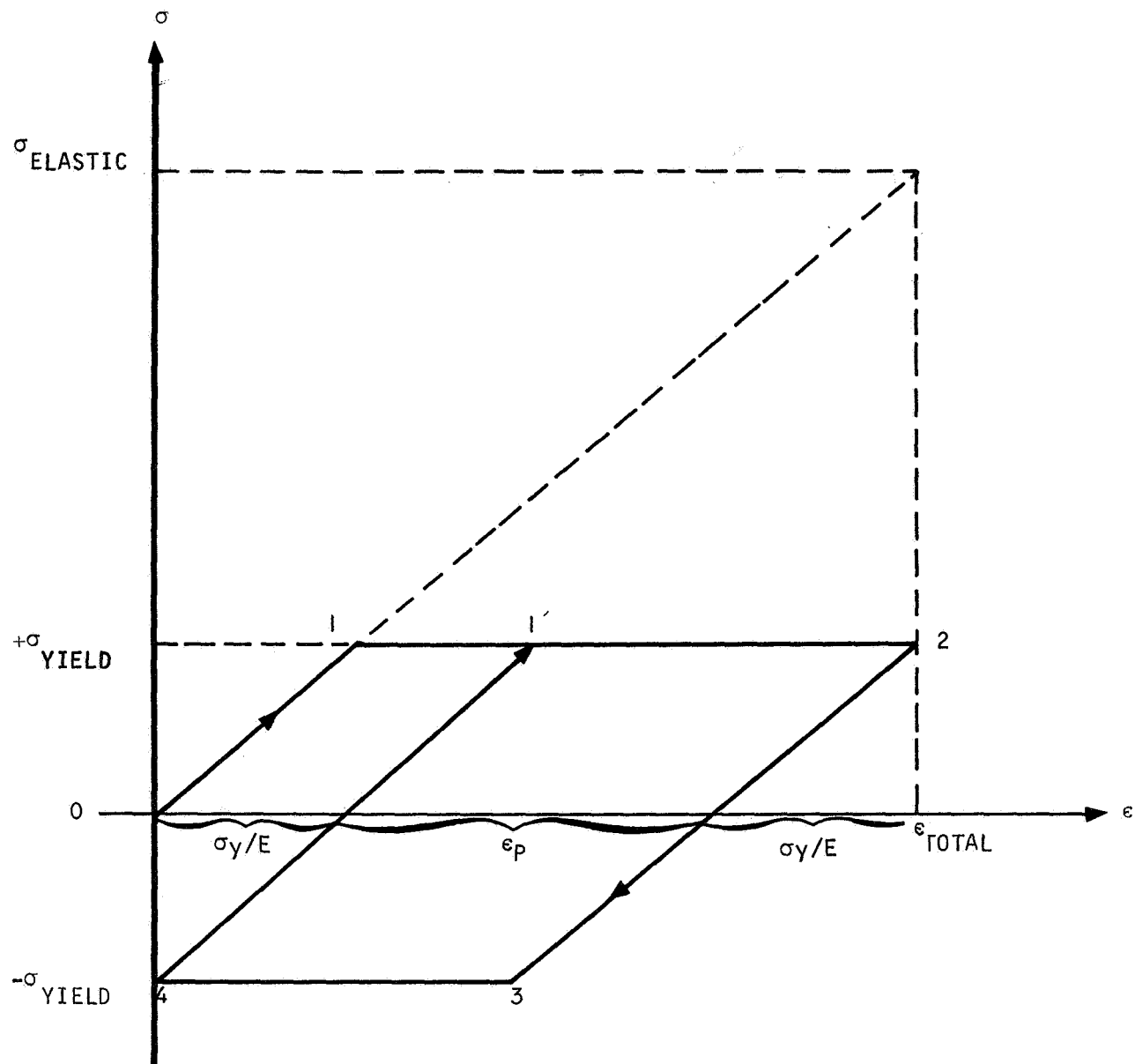


Figure 4-39 ASSUMED TUBE ELASTIC-PLASTIC CYCLE FOR 500° F TEMPERATURE DIFFERENCE BETWEEN THE INLET HEADER AND THE TUBE ARRAY

This result shows that, for the estimated 500° F temperature difference during the assumed transient condition, a cycle life near the required 400 cycles is estimated. Since relatively severe conditions have been assumed and imposed on the one tube, it is expected that the design is satisfactory. One of the important results illustrated by this calculation is that a finite fatigue life is expected for this unit.

4.4.1.3 Heat Exchanger Mounting and Assembly

A discussion of the heat exchanger mounting, piping, and assembly considerations is contained in Section 5.0 including relative locations of the BRU-BHXU and HSHX, and piping arrangements between the BHXU package and the HSHX.

4.5 ENGINEERING DRAWINGS

The following engineering drawings are contained in this section.

<u>Title</u>	<u>Figure No.</u>
HSHX Assembly	Fig. 4-40 (Dwg. No. 184244)
HSHX Tube	Fig. 4-41 (Dwg. No. 184245)
HSHX Manifold, Inlet	Fig. 4-42 (Dwg. No. 184246)
HSHX Manifold, Outlet	Fig. 4-43 (Dwg. No. 184247)
HSHX Manifold, Return	Fig. 4-44 (Dwg. No. 184248)
HSHX Cap, Manifold, Return	Fig. 4-45 (Dwg. No. 184249)

4.6 REFERENCES

4-1 Charlot, L. A. and R. E. Westerman, High Temperature Corrosion and Evaporation of Haynes 25 and Hastelloy X-280, Corrosion, Vol 23, No. 2, (February 1967) pp. 50-56.

4-2 Isotope Reentry Vehicle Design Study Conceptual Design -- Phase IB--Topical Report, NASA CR-72463, AVSSD-0193-68-CR (October 1968).

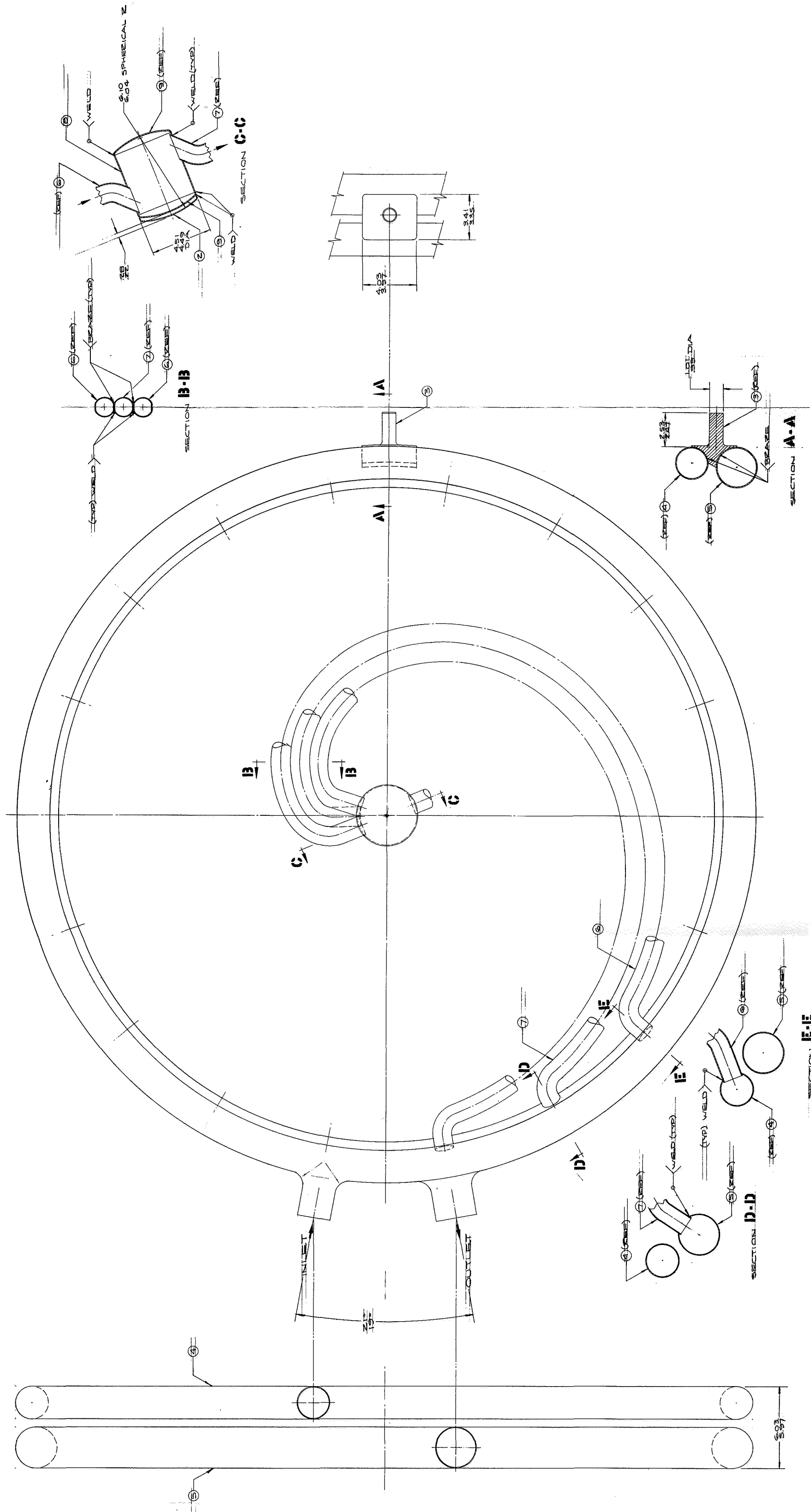
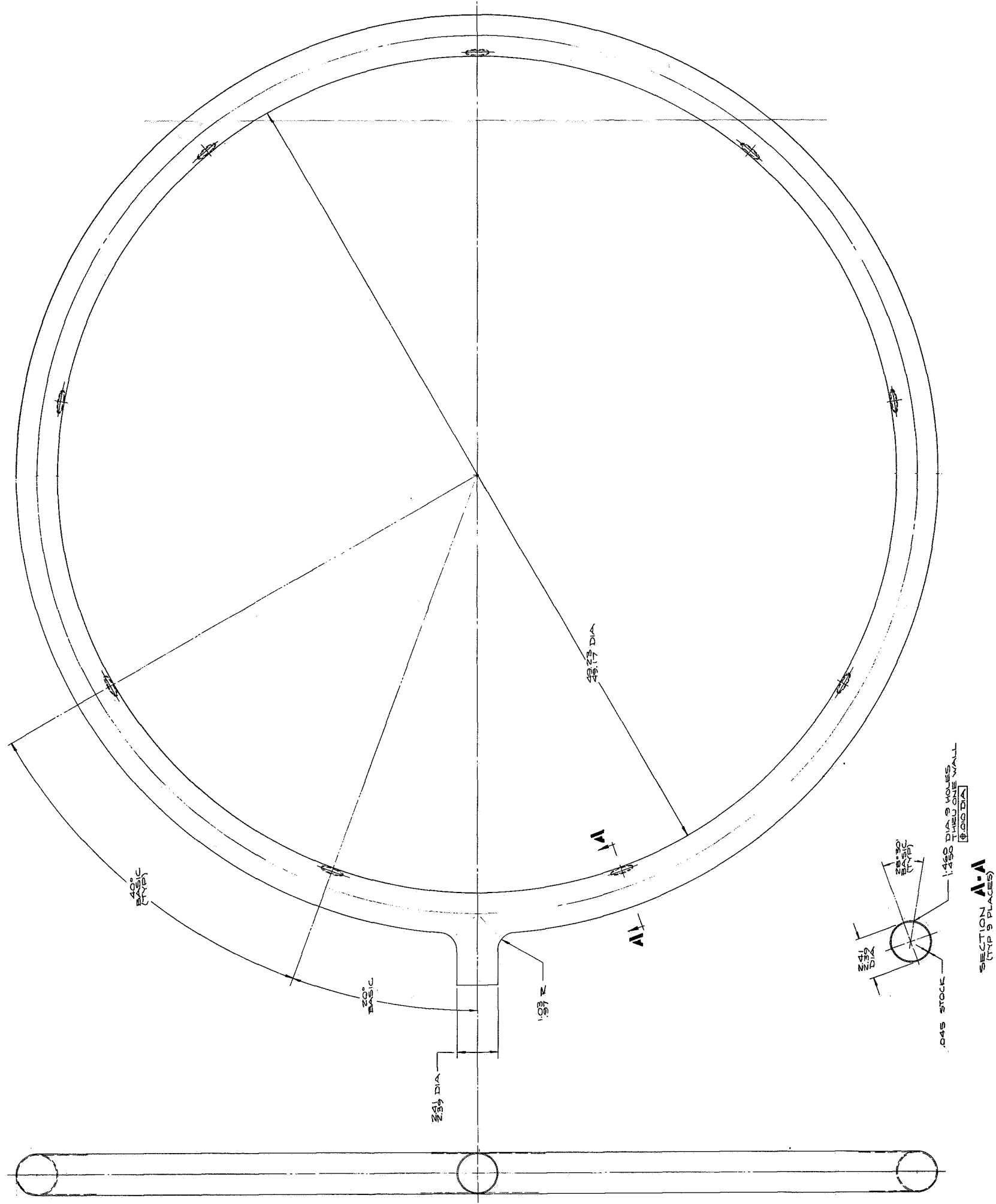
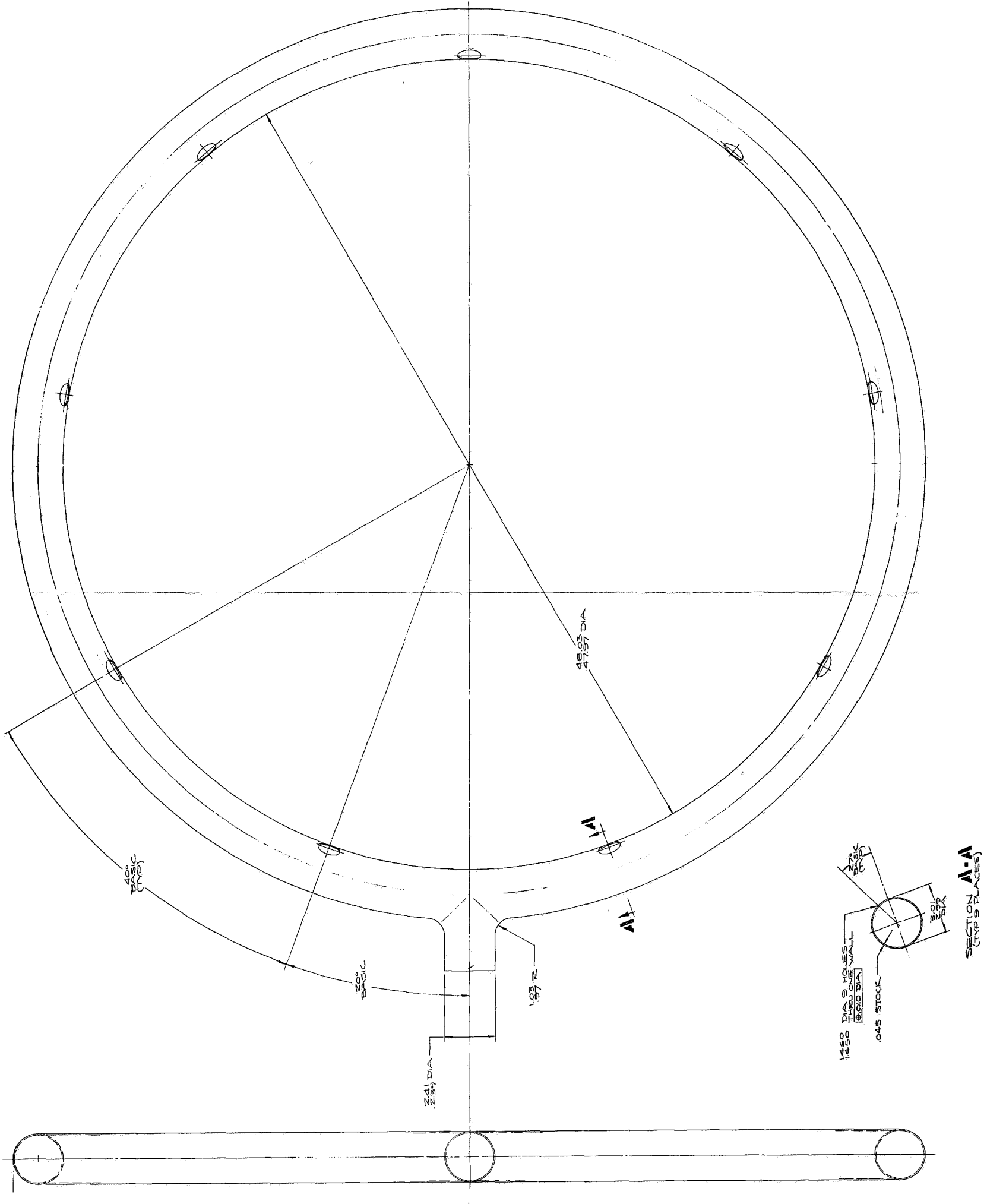


Figure 4-40 HSHX ASSEMBLY



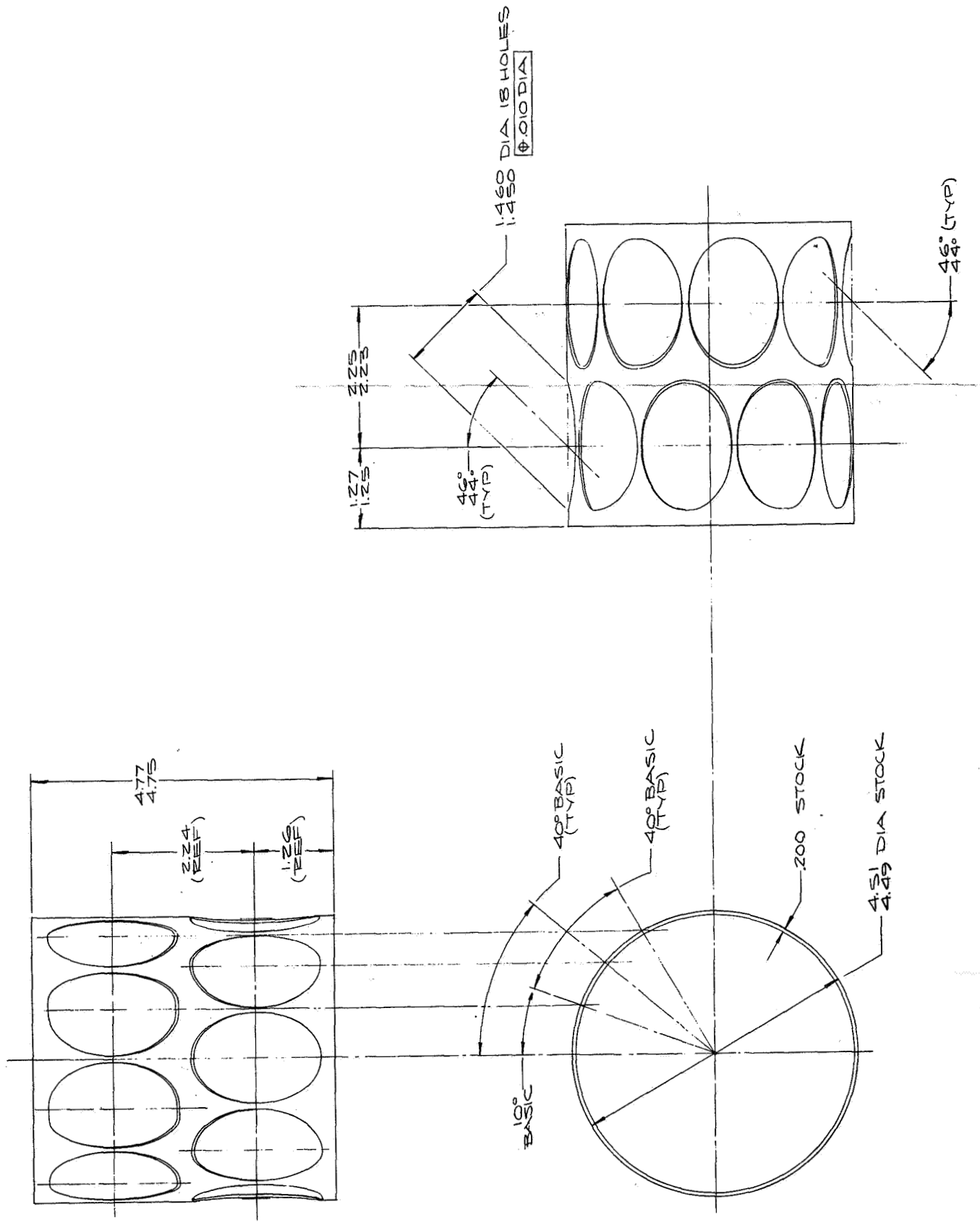
NOTES: UNLESS OTHERWISE SPECIFIED

Figure 4-42 HSHX MANIFOLD, INLET



NOTES: UNLESS OTHERWISE SPECIFIED

Figure 4-43 HSHX MANIFOLD, OUTLET



1. MACHINED SURFACES 125/
NOTES: UNLESS OTHERWISE SPECIFIED

Figure 4-44 HSHX MANIFOLD, RETURN

NOTES: UNLESS OTHERWISE SPECIFIED

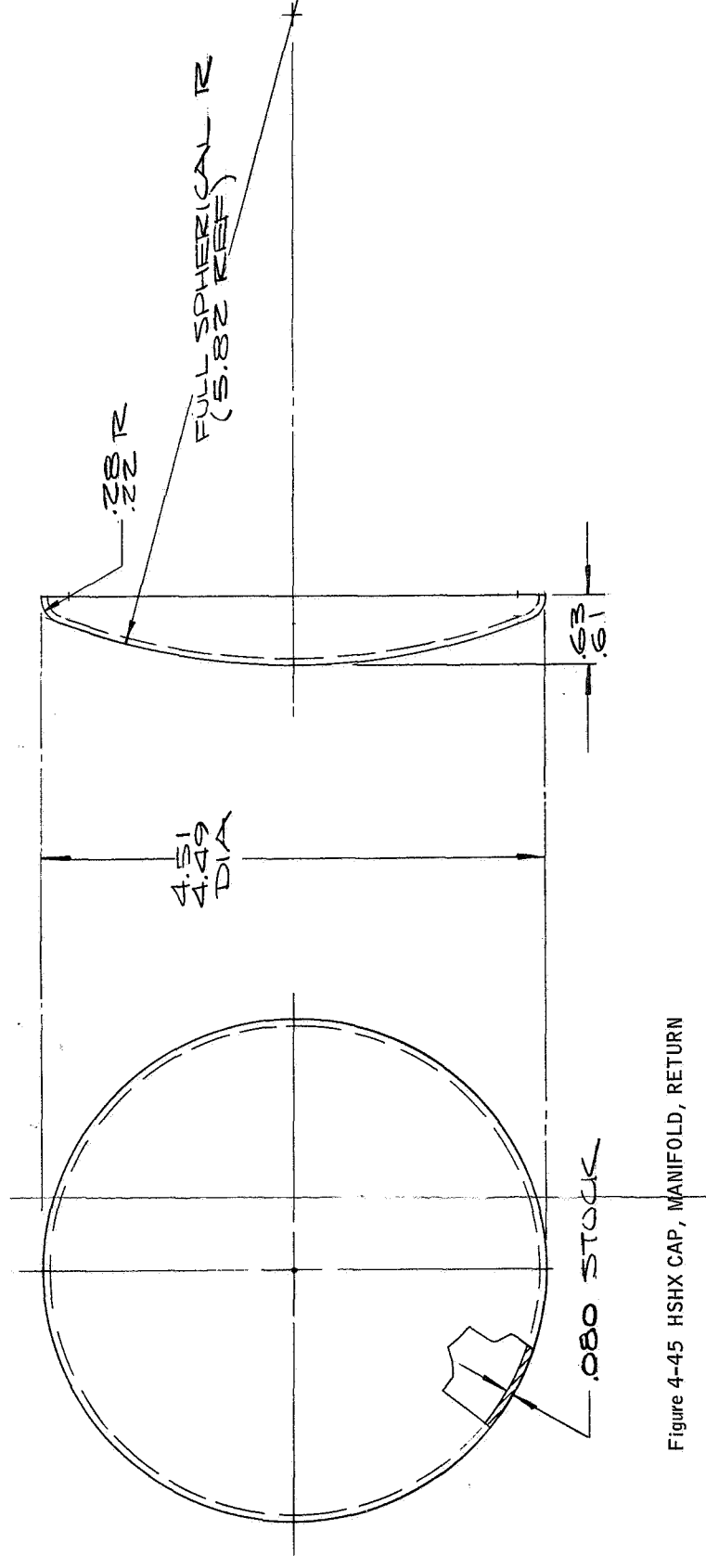


Figure 4-45 HSHX CAP, MANIFOLD, RETURN

5.0 IRV SYSTEM INTEGRATION

This section contains a description of the systems integration related tasks completed during Phase II of the IRV preliminary design study. The basic areas treated in this study are:

- Brayton cycle power system description
- IRV/Brayton cycle spacecraft installation concepts
- Ground handling requirements

The cycle description is based on the Brayton cycle power system being investigated by the NASA Lewis Research Center. It also includes the description of a typical spacecraft integration concept and finally describes the general details of ground handling requirements for this class of isotopic power system.

5.1 BRAYTON CYCLE POWER SYSTEM

The Brayton cycle power system described in this section is based on the system being developed by the NASA Lewis Research Center as part of their space power program.

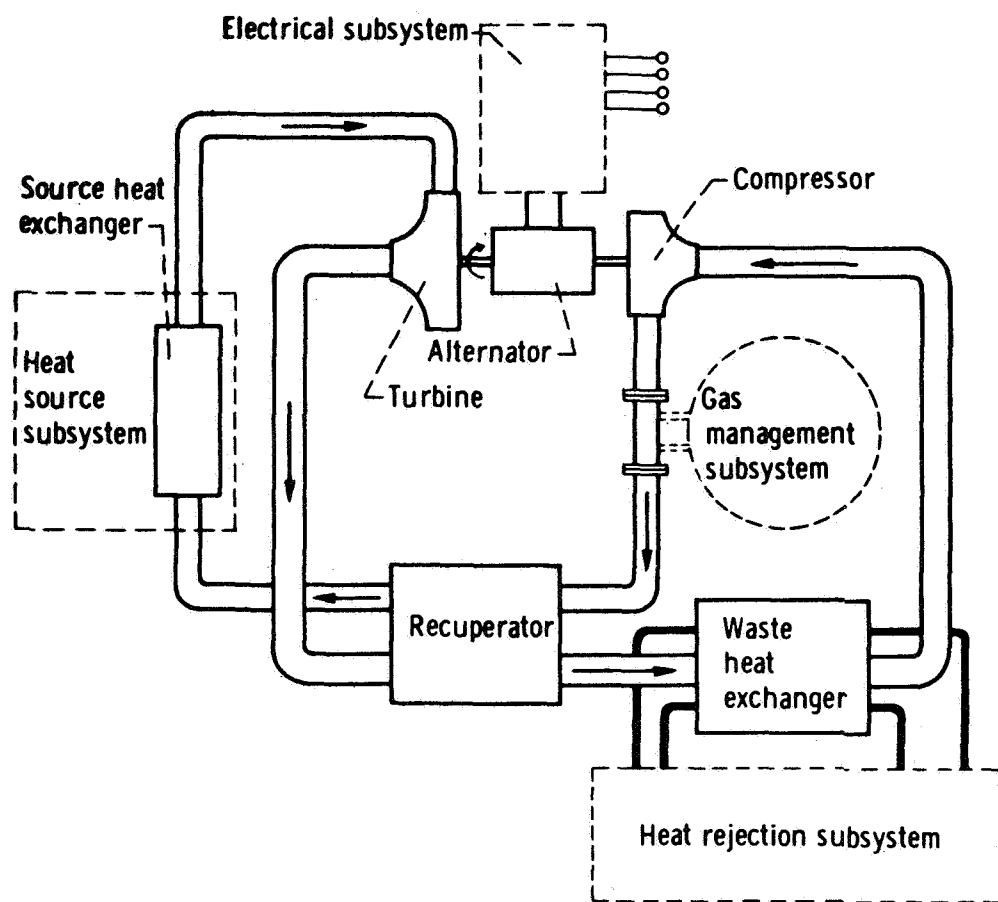
The NASA program is directed to the development of a flexible (2 to 10 kw_e) ground test research system and consequently the components, configuration, power level, etc. are not necessarily optimum for any specific vehicle/mission application. Reference 5-1 presents a summary of the NASA Lewis Brayton cycle research program. Some of the material presented in Reference 5-1 is restated here to provide an overall picture of a complete Brayton cycle space power system utilizing the NASA ground test engine components.

5.1.1 Cycle Description

Figure 5-1 shows a schematic of the Brayton gas loop with the four major subsystems shown in phantom. The heat source subsystem adds heat to an inert working gas in its heat exchanger. The hot gas flows to a single-stage, radial-inflow turbine. Expansion of the gas through the turbine spins the machinery shaft and produces useful work. Part of this work is absorbed by driving a single-stage, radial-outflow compressor. Most of the remaining shaft work is available to a four-pole, brushless alternator. The rotating shaft is supported by journal and thrust bearings that are lubricated by the working gas itself.

After expansion in the turbine, the gas flows through a recuperator. This heat exchanger transfers the majority (approximately 70 percent) of the energy that is potential waste heat back to the cooler gas flow leaving the compressor. Then a gas-to-liquid heat exchanger removes the unusable heat. The cooled gas is compressed, ducted back through the recuperator, and returned to the source heat exchanger.

The electrical subsystem regulates and distributes the output power and controls the power system. Output frequency is regulated, and hence, the rotating shaft operates at a constant speed. The gas management subsystem is used mainly to



S-43443

Figure 5-1 POWER SYSTEM SCHEMATIC DIAGRAM

start and stop the power system; however, it is also used to adjust the working gas inventory.

The heat rejection subsystem liquid coolant is also used to cool the alternator and electrical subsystem components. For added reliability, two identical coolant loops are available for use. During normal power system operation, one loop is active while the other is passive. The liquid loop couples the Brayton cycle power system to the space radiator where the waste cycle heat is rejected to space.

The Brayton cycle power system operating conditions selected for the 7-kw_e isotope power system is shown in Figure 5-2. This set of operating conditions was the reference design for the isotope heat source system used in this study.

5.1.2 System Components

The Brayton cycle power conversion system consists of the following major components:

- Recuperator
- Waste-heat heat exchanger
- Turbine-compressor-alternator assembly (BRU)
- Heat-source heat exchanger
- Electrical subsystem
- Gas management subsystem
- Heat rejection subsystem.

A brief description of the above components is presented in the following paragraphs.

Recuperator

The recuperator is shown in Figure 5-3a, and is a counterflow type heat exchanger. Plate-and-fin surfaces or sandwiches are used for both gas flows. The core is formed by alternate stacking of hot- and cold-gas-flow sandwiches. The overall core dimensions are 8.5 by 20 by 20 inches.

Waste-Heat Heat Exchanger

The waste-heat heat exchanger illustrated in Figure 5-3b has a cross-counterflow arrangement. There are eight liquid passes back and forth across a single gas flow pass. This core also uses plate-and-fin sandwiches for both the liquid and gas flows. Each liquid sandwich has eight separate passages, each about 20 inches long, perpendicular to the gas flow direction. The gas flow length is about 16 inches. The core is formed by alternate stacking of liquid- and gas-flow sandwiches, and the overall core stack height is about 6 inches. Since there are dual liquid passages, the order of sandwich stacking is active-liquid, gas, inactive-liquid, gas and so on.

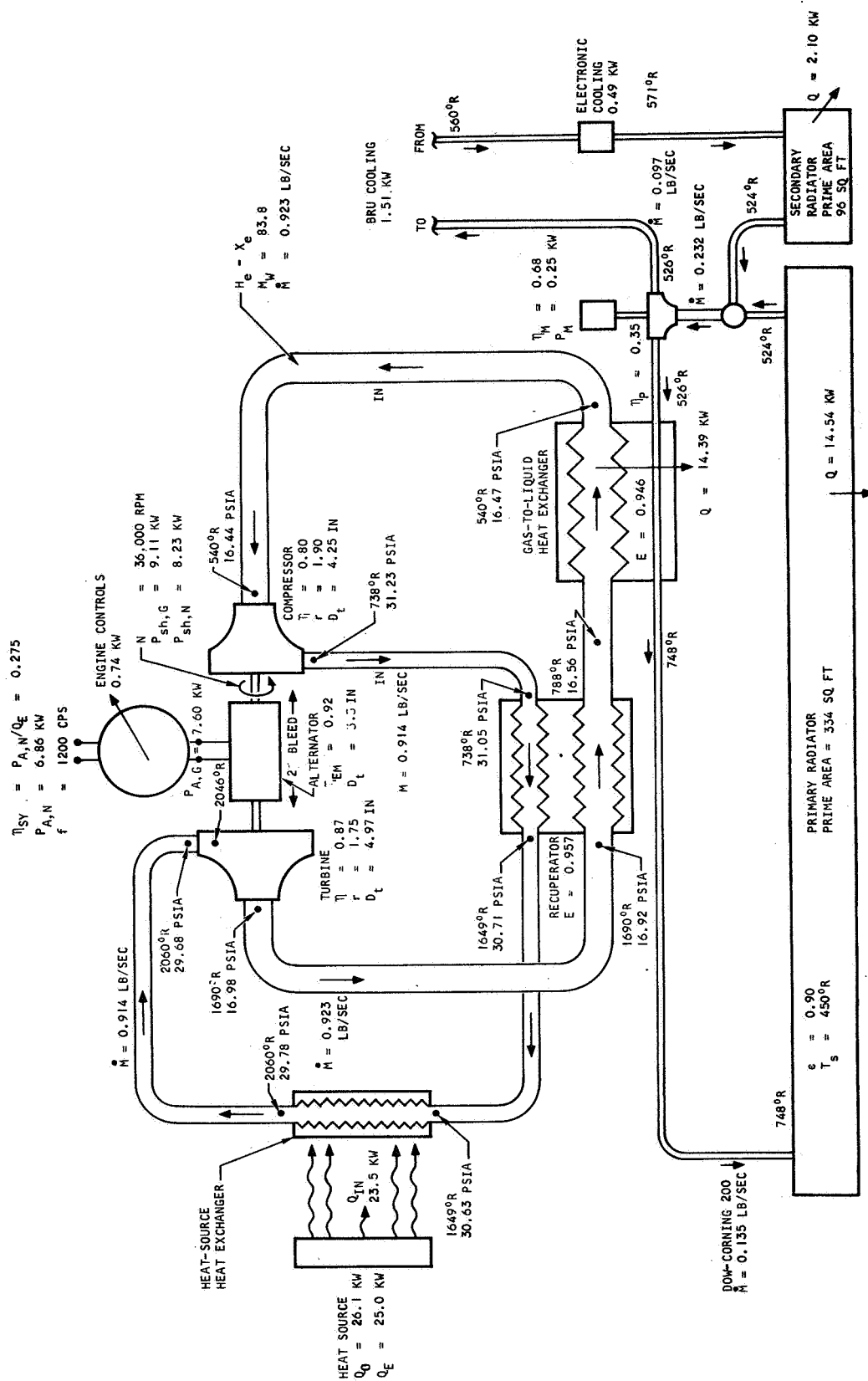
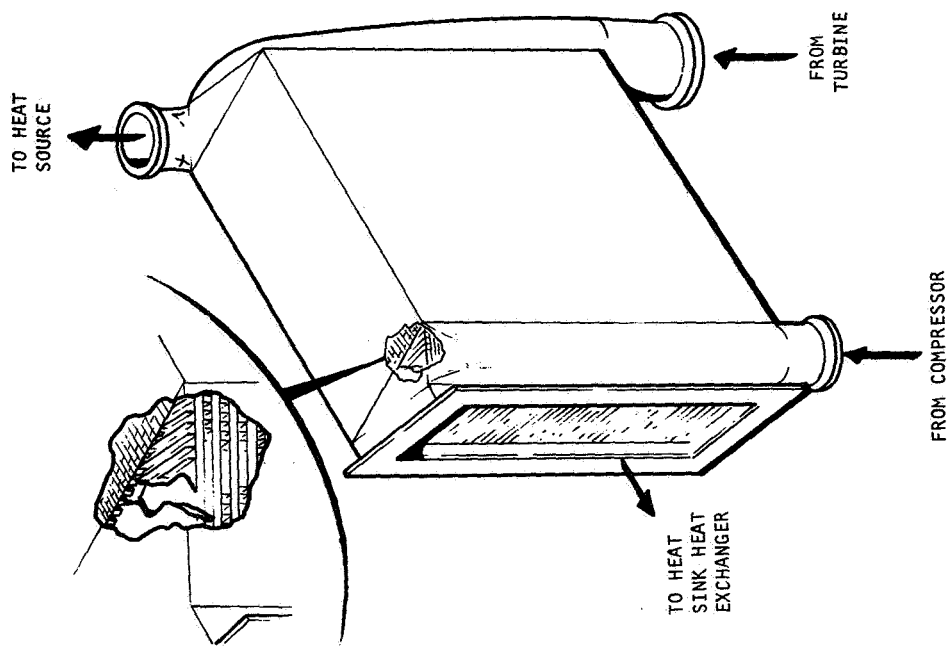
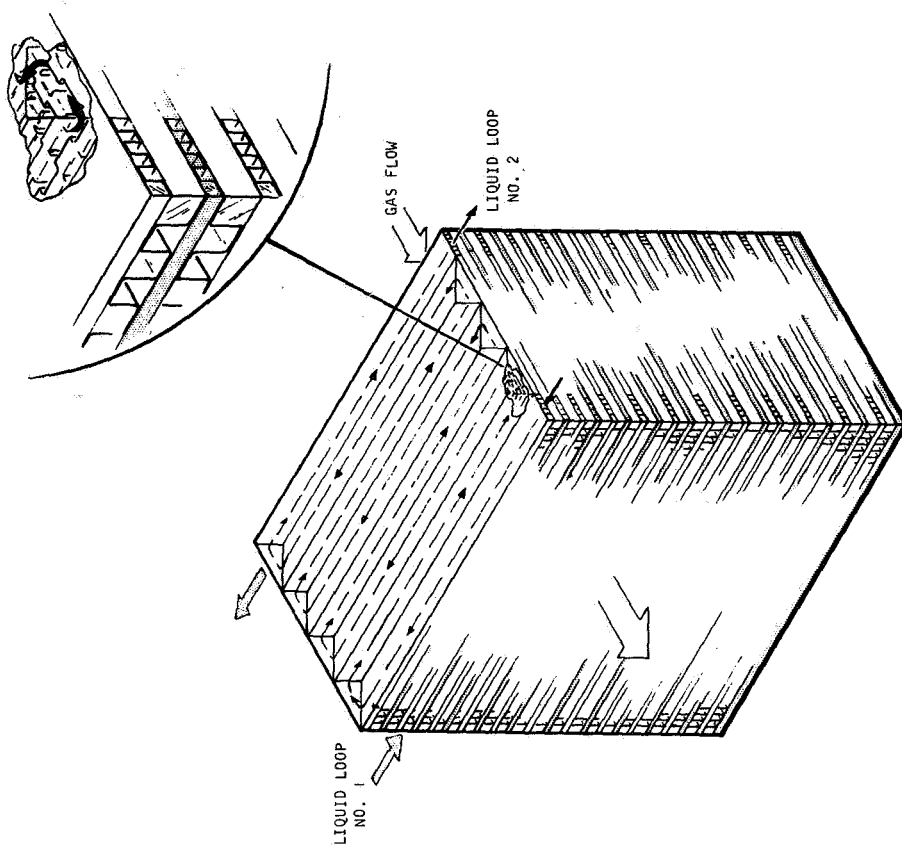


Figure 5-2 SCHEMATIC DIAGRAM OF Pu238 BRAYTON POWER PLANT
(REFERENCE 25 kw_t SOURCE; NOMINAL 7 kw RATING)



A-32026

a. REGULATOR



A-12463

b. WASTE-HEAT HEAT EXCHANGER
(8-PASS-CROSS-COUNTERFLOW
PLATE FIN) (TWO LIQUID LOOPS)

S-43445

Figure 5-3 BRAYTON POWER SYSTEM COMPONENTS (NASA ENGINE B)

The recuperator, waste-heat heat exchanger, and the associated ducting and support system is referred to as the Brayton cycle heat exchanger unit (BHXU).

The BHXU is designed for the nominal 10-kw output conditions. Overall design system pressure loss is 8 percent (which is consistent with the design ratio of turbine-to-compressor pressure ratios). The BHXU itself is designed not to exceed 4-1/2 percent pressure loss.

Since these heat exchangers are designed for 0.95 effectiveness at the 10-kw conditions, they have increased effectivenesses at the lower power levels. The lower system power levels have smaller gas mass flow rates. With reduced flow, the heat transfer coefficient drops. The amount of heat to be transferred over the fixed core area, however, also drops. The net effect is the increase in heat transfer effectiveness for both exchangers at the lower power levels. A photograph of BHXU 1 is shown in Figure 5-4.

Brayton Rotating Unit (BRU)

The BRU consists of the turbine, compressor, and alternator all mounted on a common shaft. The BRU is illustrated in Figure 5-5.

Design choices resulted in a turbine impeller tip diameter of 4.97 inches, an alternator rotor diameter of 3.3 inches, and a compressor impeller tip diameter of 4.25 inches. These small machines were designed for relatively high efficiencies. At the 10-kw power level, these efficiencies were 0.87 for the turbine, 0.92 (electromagnetic) for the alternator, and 0.80 for the compressor.

Initial component testing of the turbine and compressor has shown that the design efficiencies were met or exceeded. Preliminary test results indicate a design-point efficiency of 0.90 for the BRU turbine, and a peak efficiency of 0.83 for the BRU compressor. The alternator efficiency was measured at 0.92 which was the design goal.

The BRU has a design temperature difference of about 1500° F from the hot to the cold end. The design alternator stator, hot-spot temperature limit is 356° F. Dual liquid passages containing the heat rejection system coolant are looped around the alternator housing. Either liquid passage can provide the needed cooling.

One journal bearing is located between the turbine wheel and the alternator rotor; a second bearing is located between the alternator rotor and the compressor wheel. Each journal bearing includes three pivoted pads; two are fixed, and the third is spring loaded. A Rayleigh-step thrust bearing is located between the compressor wheel and the compressor-end journal bearing. The thrust bearing includes stepped-stator plates on both sides of a flat-plate rotor.

During normal BRU operation, about 2 percent of the compressor discharge gas is ducted into the bearing and alternator cavity. This high-pressure gas provides the means for hydrodynamic (self-acting) bearing operations. Labyrinth shaft seals located just inboard of both the turbine and compressor wheel enclose the bearing and alternator cavity. The compressor bleed flow, however, leaks through these seals (approximately 1 percent each) and reenters the turbine and compressor flow passages.

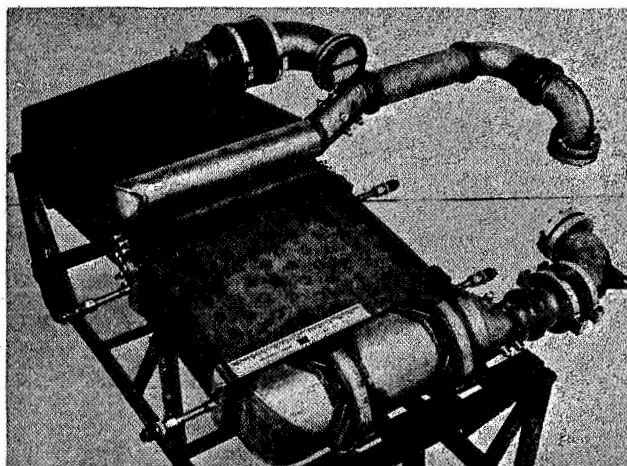
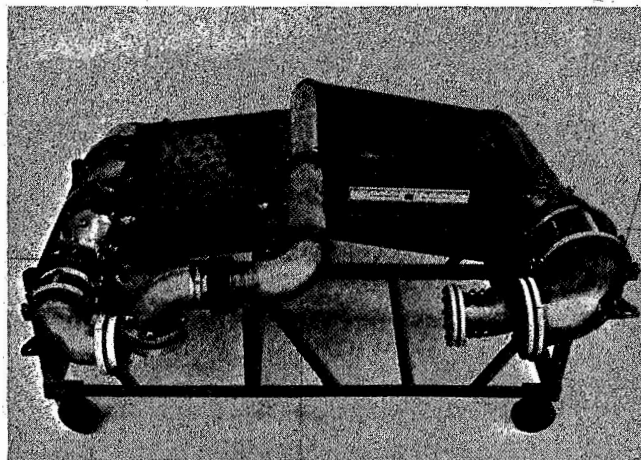
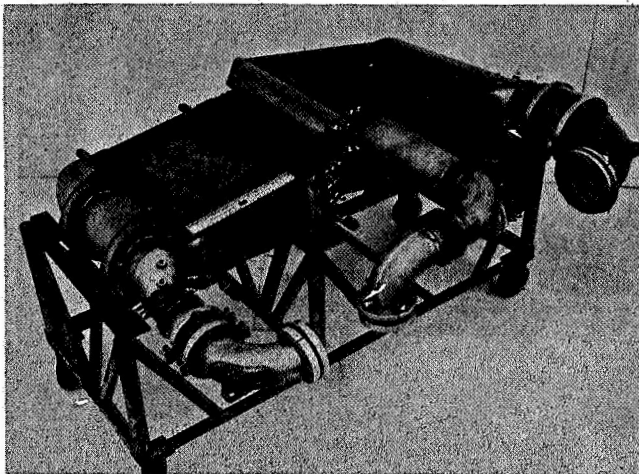


Figure 5-4 BRAYTON CYCLE HEAT EXCHANGER UNIT NO. 1 --
COMPLETE ASSEMBLY

F-9668

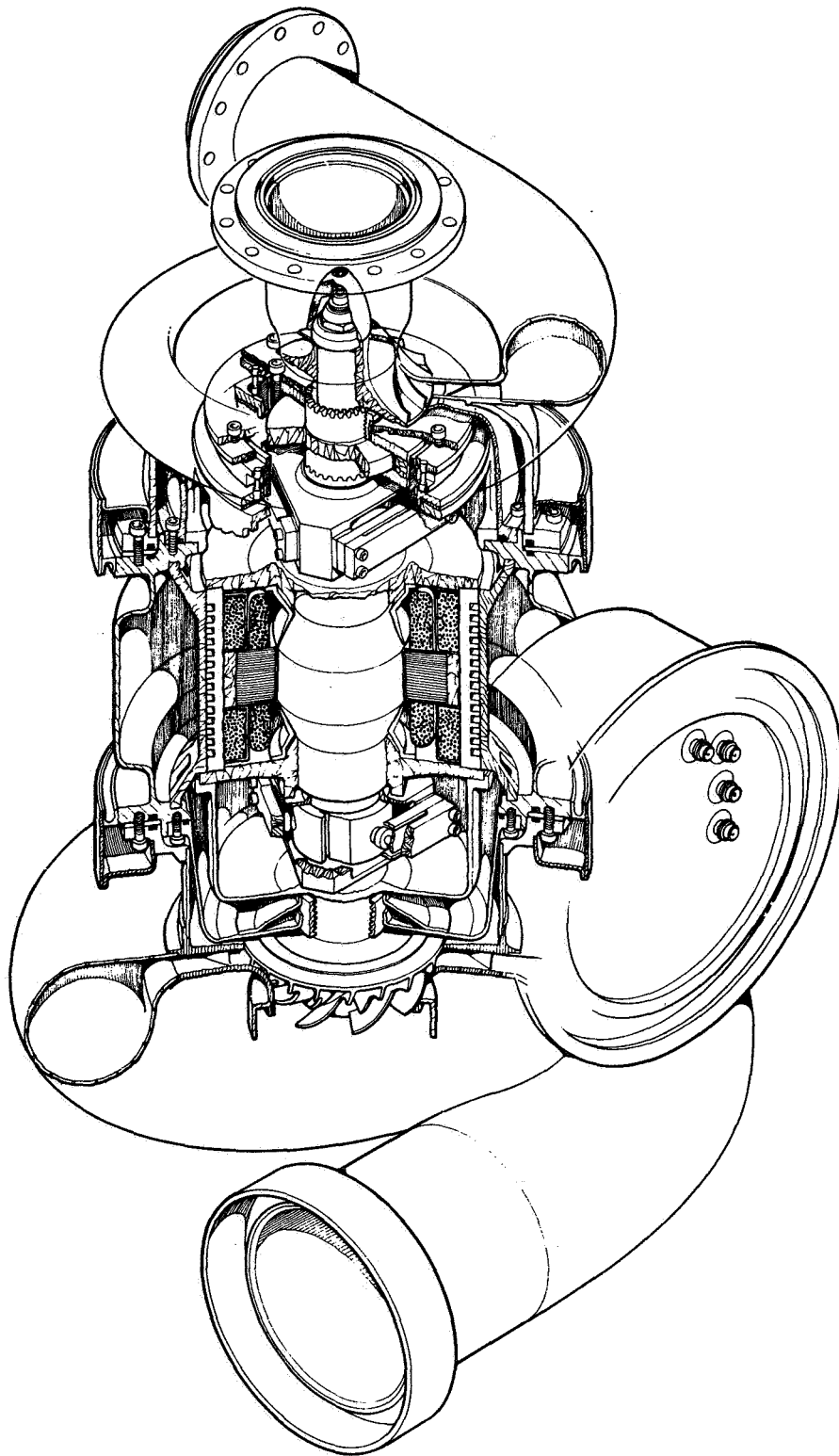


Figure 5-5 BRAYTON ROTATING UNIT (BRU)

During BRU starts and stops, the bearings are designed for hydrostatic (pressurized) operation. The gas management subsystem provides the high-pressure jacking gas to each bearing pad.

The BRU is designed to perform efficiently over the net system power output range from 2 to 10 kw. The compressor discharge pressure will vary from about 13 psia at 2 kw to about 44 psia at 10 kw. At the low power level, the pressure is high enough to provide satisfactory bearing operation. At the high power level, the pressure is not so high as to result in large alternator windage losses.

Heat Source Heat Exchanger

A typical Brayton cycle heat source heat exchanger (HSHX) for an isotope heat source is shown in Figure 5-6. This particular design was evolved from the studies performed and reported in Section 4.0 of this report.

Figure 5-7 shows a packaging arrangement of the BHXU-BRU in a mounting frame and Figure 5-8 illustrates the addition of the HSHX to this package.

Electrical Subsystem

Figure 5-9 shows a schematic of the electrical subsystem. It contains an electrical control package, the user's load bus, a parasitic load, a dc power supply, a signal conditioner, and two inverters.

The control package regulates alternator output voltage, provides alternator excitation, and controls the BRU speed. It also distributes the power output among the user load bus, the parasitic load and the dc power supply.

The user load bus supplies alternating current at 208 v, line-to-line, or 120 v, line-to-neutral.

The parasitic load contains three banks of resistive elements. It is used with the speed control to regulate output frequency (and hence, BRU speed).

During normal power system operation, the dc power supply rectifies part of the ac output to provide internal direct current needs at ± 28 v. During starts and stops, silver-cadmium batteries supply the dc needs. Direct current is used in the signal conditioner, the control package, and the inverter.

Power Conversion System (PCS) control modules are located remotely from the engine system. Functional controls are provided for starting by gas injection, stopping, bearing jacking gas flow, valve operation, gas-loop inventory regulation, and coolant-loop operation. Also, protective control modules are provided for emergency stops, gas-loop overpressures, and electrical subsystem overloads, undervoltage, or overvoltage. The signal conditioner forms an interface between the PCS instrumentation and its control and monitoring panels. Signals from and commands to the PCS pass through this component.

Static inverters provide 400-Hz power to the pump-motor assemblies (PMA) in the heat rejection subsystem.

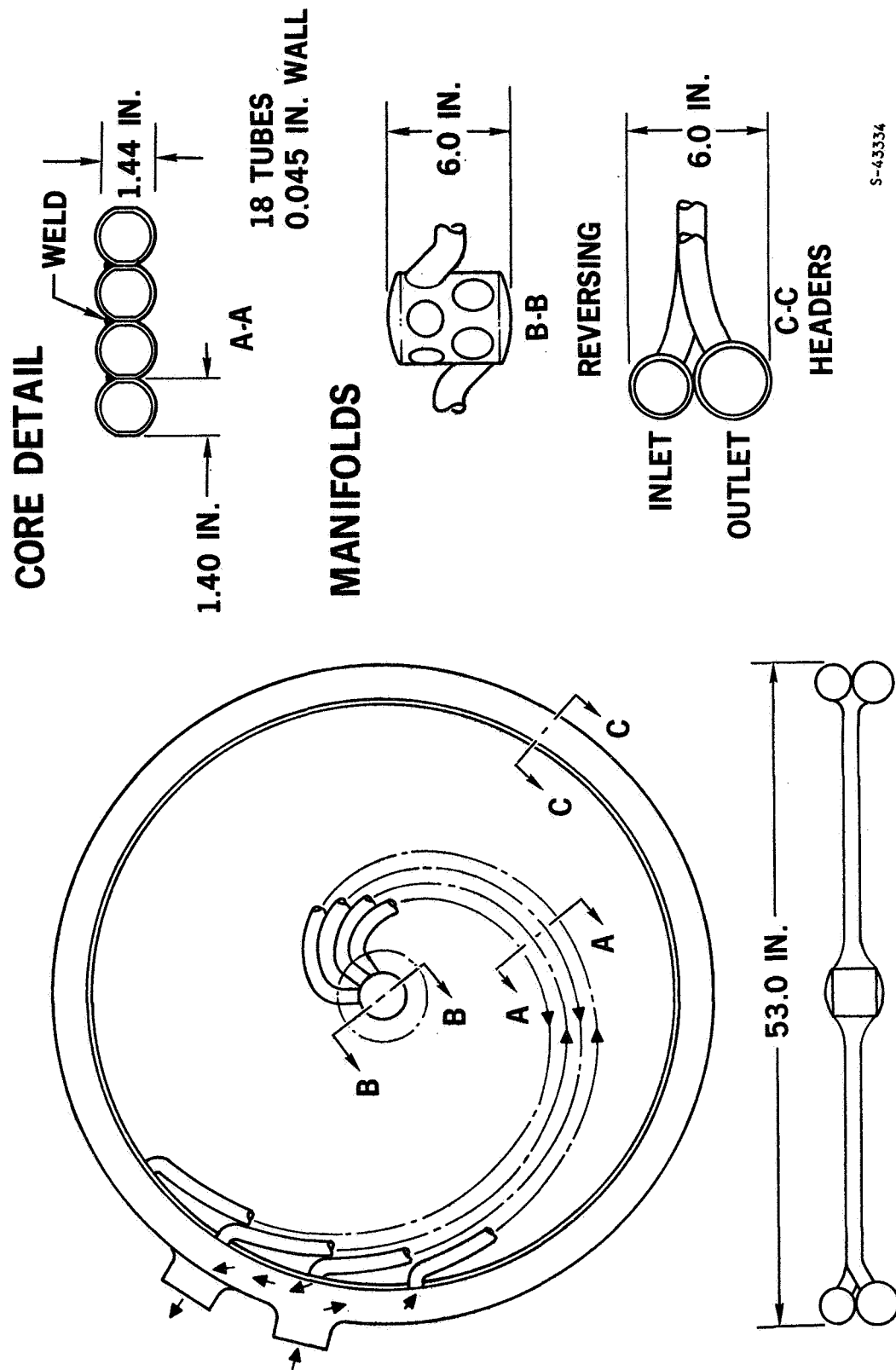


Figure 5-6 TYPICAL HSHX FOR ISOTOPE HEAT SOURCE (25 kw_{th})

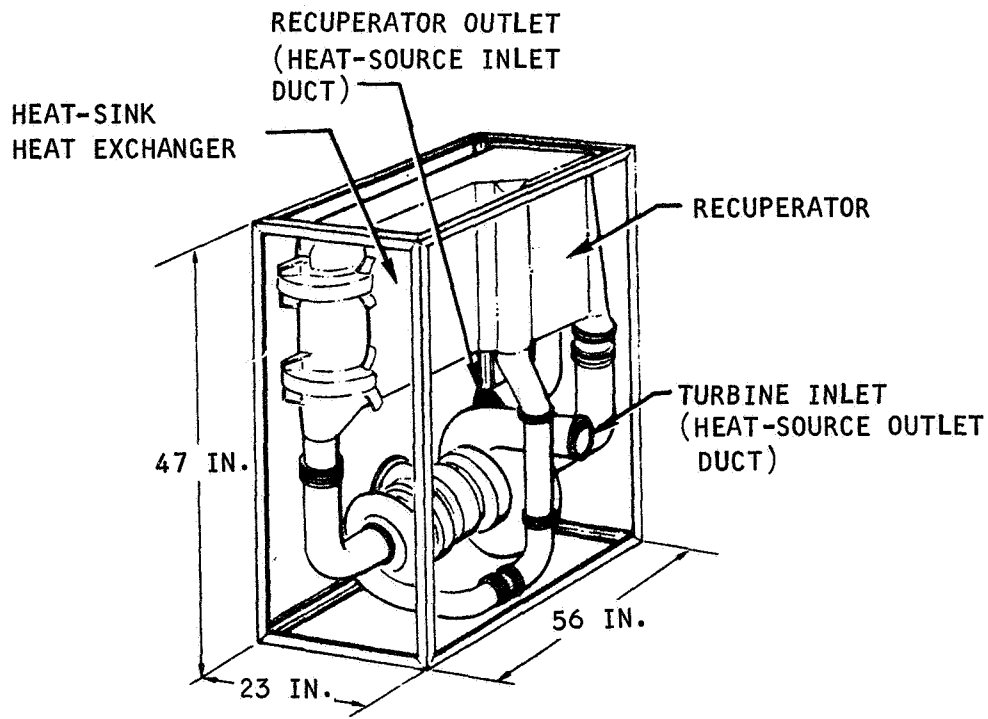
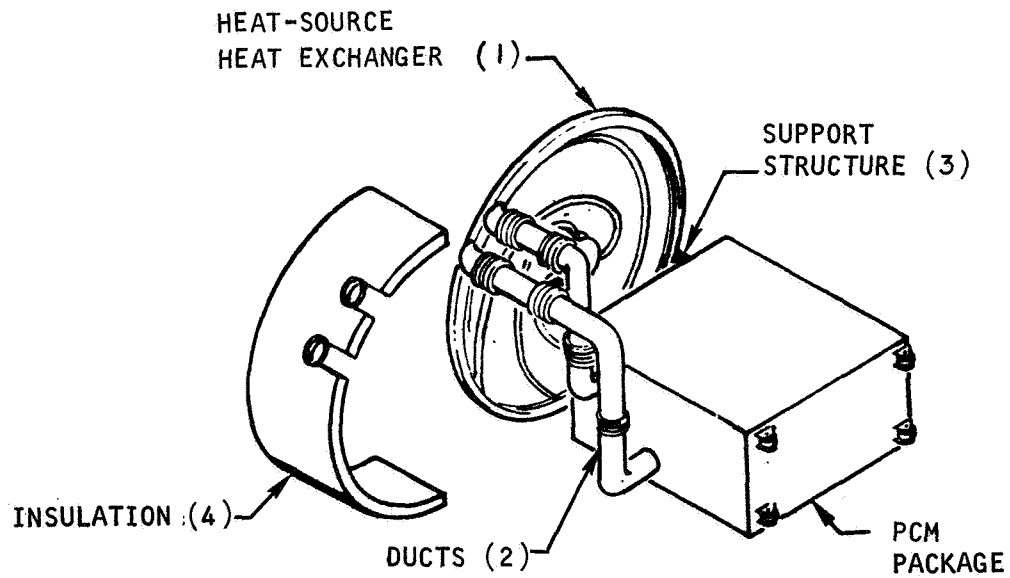


Figure 5-7 BRAYTON CYCLE CONVERSION MODULE



A-33454

Figure 5-8 BRAYTON CYCLE POWER CONVERSION MODULE WITH TYPICAL
HSHX INSTALLATION

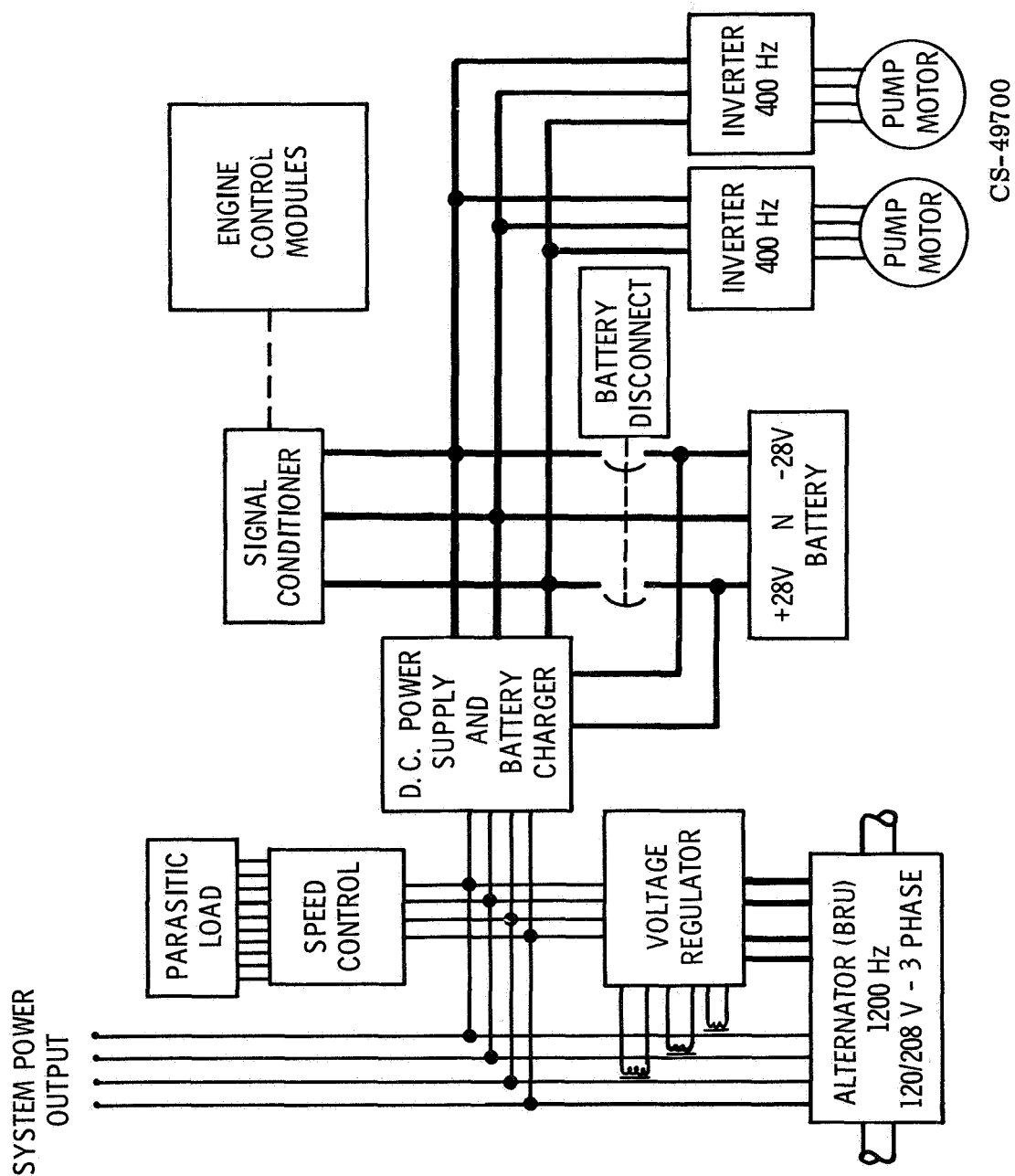


Figure 5-9 ELECTRICAL SUBSYSTEM SCHEMATIC DIAGRAM

Gas Management Subsystem

The gas management subsystem consists of a gas supply tank and fill-and-vent lines that connect to the Brayton gas loop. Supply lines are also connected to the BRU housing for pressurizing the bearing cavities. The fill-and-vent lines are filtered and fitted with valves. An actuated butterfly valve in the main gas loop prevents reverse gas flow during power system starts.

The gas management subsystem functions to:

- supply bearing jacking gas
- inject gas for power system starts
- control gas inventory (to control power level)
- vent gas for power system stops.

Initial power system starts will be made by gas injection. In the start sequence, both the heat-source and heat-rejection subsystems are prepared and functioning. The gas management subsystem then supplies jacking gas to each bearing pad and injects gas downstream of the closed check valve into the recuperator. The gas flows through the loop and is vented upstream of the butterfly valve at the exit of the compressor. This flow rotates the BRU shaft and brings the BRU above self-sustaining speed. At this point, the vent valve is closed, the butterfly valve is opened, and the main injection is stopped. The BRU accelerates to design speed, and the bearing jacking gas flow is stopped.

During power system operation after a start, the gas management subsystem provides a means for gas inventory control. Gas may be added or removed by valve sequencing. Design power system stop sequence includes stopping the heat-source subsystem input, supplying bearing jacking gas, loading the alternator, and venting the gas loop. The gas management subsystem provides jacking gas until the BRU shaft reaches essentially zero speed. A control subsystem also provides an automatic sequence of these events for emergency power system stops.

The electrical control package, signal conditioner, dc power supply, battery packs, and inverters all mount on cold plates. These cold plates are cooled with fluid from the heat rejection subsystem.

Heat Rejection Subsystem

The heat rejection subsystem is shown schematically in Figure 5-10. In the ground test system, the radiators are replaced by a heat exchanger in which heat rejection will be to a facility heat sink. The three parallel, dual coolant flows pass through the waste heat exchanger, the alternator housing of the BRU, and a series of four cold plates on which the electrical subsystem components are mounted. The three coolant flows then pass through the radiators and are then merged. The flow is then filtered and sent to a pump for recirculation. Each loop has its own separate and independent pump. Although not shown in Figure 5-10, an accumulator is planned to be used upstream of each pump inlet to maintain pump suction pressure. The PMA's are supplied with 400-Hz power from inverters in the electrical subsystem.

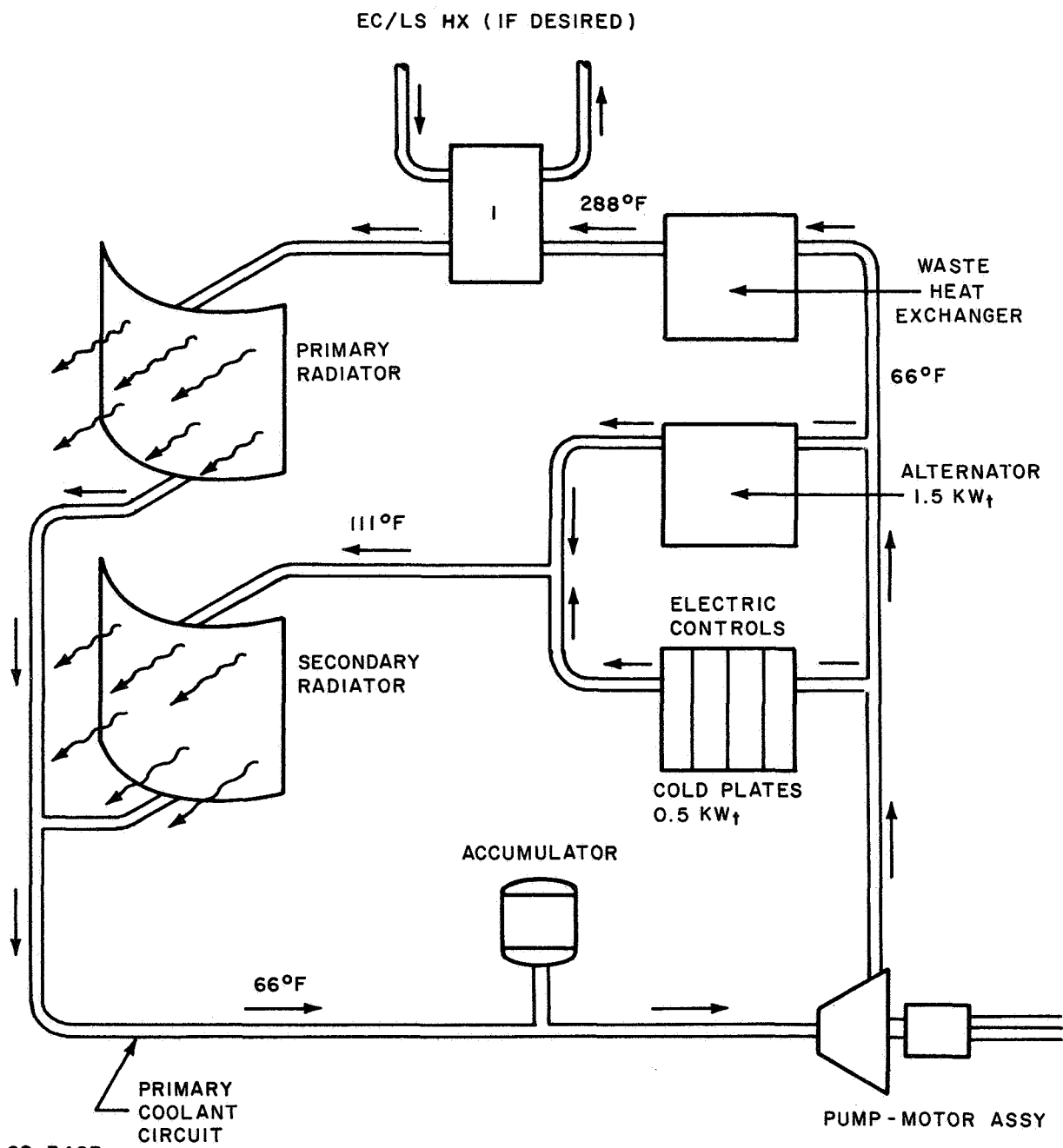


Figure 5-10 HEAT REJECTION SUBSYSTEM SCHEMATIC DIAGRAM

The heat rejection subsystem coolant is a Dow Corning 200 silicone liquid.

The temperatures and heat loads shown in Figure 5-10 are for 10 kw of net system output. The temperature rise on the liquid side of the waste heat exchanger is about 220° F; while the temperature rise across both the BRU and the cold plates is about 30° F. The waste heat exchanger load is 20.5 kw, while the BRU heat load is 1.8 kw and the electric component heat load is about 1 kw. At less than 10 kw of system output, each of these heat loads decreases. Over the entire power range from 2 to 10 kw, more than 85 percent of the total heat rejection subsystem heat load is from waste Brayton cycle heat.

The radiator area required (Figure 5-2) for the 7-kw system is seen to be 430 ft². Figure 5-11 shows a typical liquid-cooled, dual-loop, space radiator design developed for a Brayton cycle power system (Reference 5-1). The two parallel liquid loops share the same radiator area by having alternate tubes of liquid circuits 1 and 2. This is possible since only one of the coolant circuits is active at a given time. In the design shown in Figure 5-11, the heat from the liquid coolant is transferred to the surface of the vehicle skin by conduction through the internal stiffening corrugations. The effectiveness of this radiator design is 0.81; thus a physical area of $430/0.81 = 530$ ft² is required for the 7-kw system.

5.1.3 System Performance

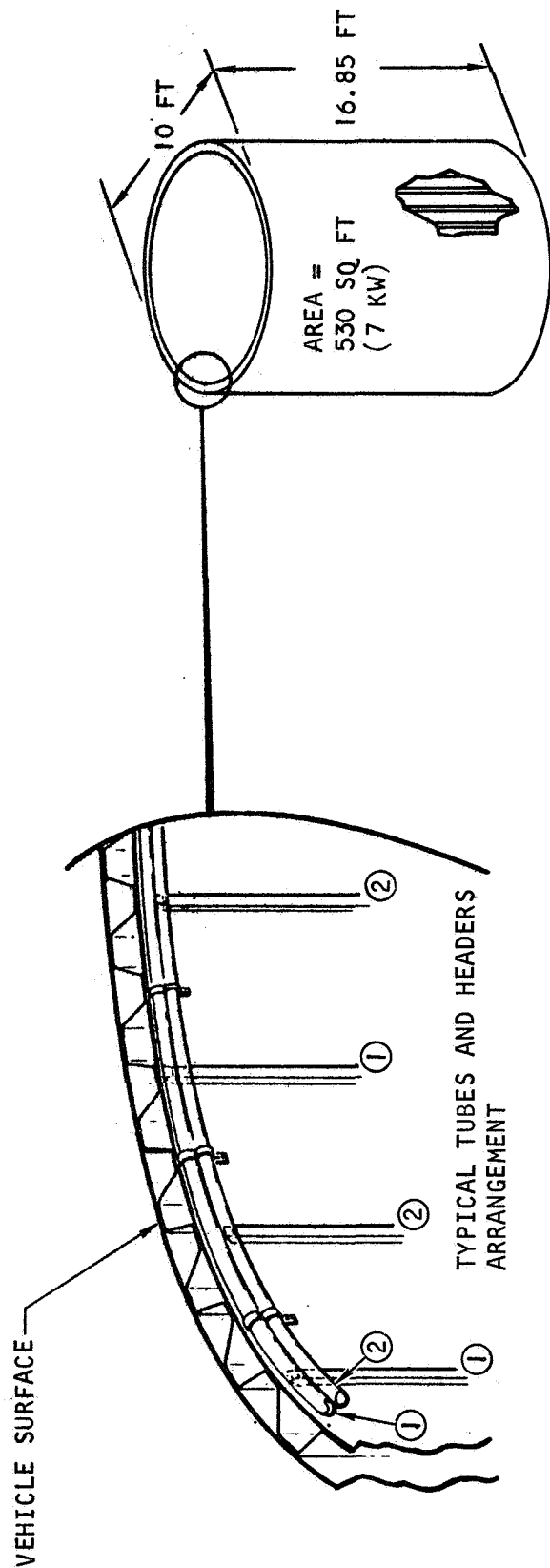
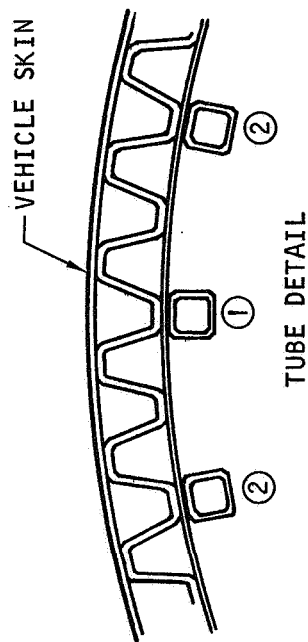
At the operating conditions specified on Figure 5-2, the net electrical power delivered to the user bus is 7 kw_e nominal, 3-phase, 400-cycle, 208-v (line-to-line) power. This yields a net overall efficiency of 28.0 percent including a 1.5-kw_t heat leak from the isotope heat source. In some cases, it may be desirable to reduce the isotope heat-source temperatures, and hence turbine inlet temperature, at the expense of overall cycle efficiency. Figure 5-12 shows the drop in cycle efficiency as the turbine inlet temperature is reduced. Also shown is the corresponding system pressure level (compressor inlet pressure) required as the turbine inlet temperature is reduced.

Figure 5-13 indicates the variation in Brayton cycle system power output as a function of radiator area, thermal power, and turbine inlet temperature. The data in this figure are typical only since they were scaled from the parametric studies conducted in Reference 5-1.

5.2 IRV/BRAYTON CYCLE/SPACECRAFT INTEGRATION

Preliminary consideration has been given to system integration in the previous Phases IA and IB efforts into the Atlas/Centaur and Saturn I-B/MORL launch vehicles. Figure 5-14 depicts the IRV/Brayton Cycle/Atlas-Centaur integration concept developed in Phases IA and IB. This approach is considered conceptually feasible for the current IRV/Brayton Cycle system design with only minor modification.

However, as the study has proceeded through Phase II, a further review of safety requirements has led to a detailed study of IRV attachment, cooling, spinning, jettison techniques, and action sequencing.



- ① COOLANT CIRCUIT 1
- ② COOLANT CIRCUIT 2

Figure 5-11 TYPICAL RADIATOR CONFIGURATION

S-43353

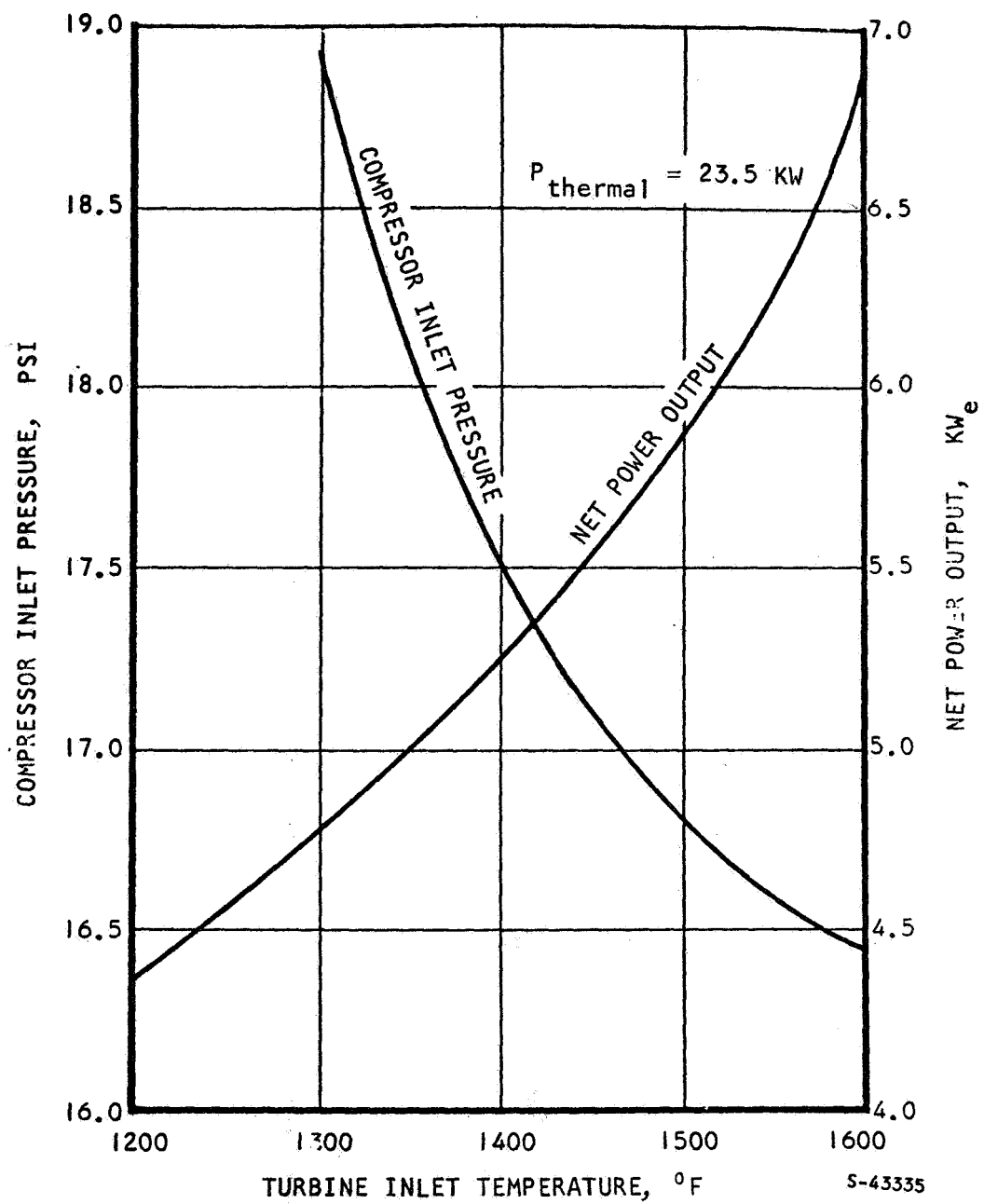
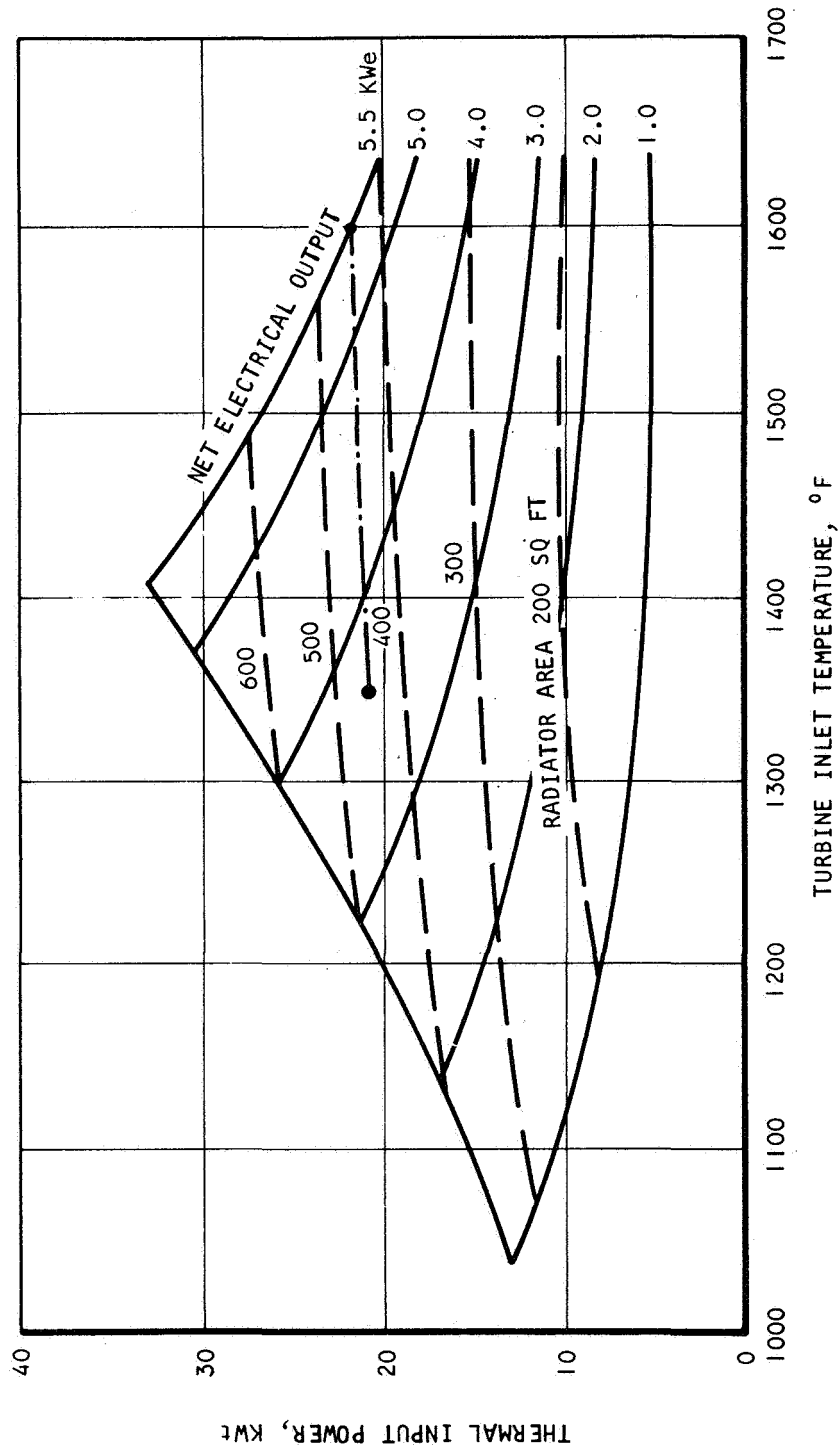


Figure 5-12 TURBINE INLET TEMPERATURE VERSUS POWER OUTPUT



A-33449-A

Figure 5-13 TURBINE INLET TEMPERATURE VERSUS POWER OUTPUT
(TYPICAL ONLY)

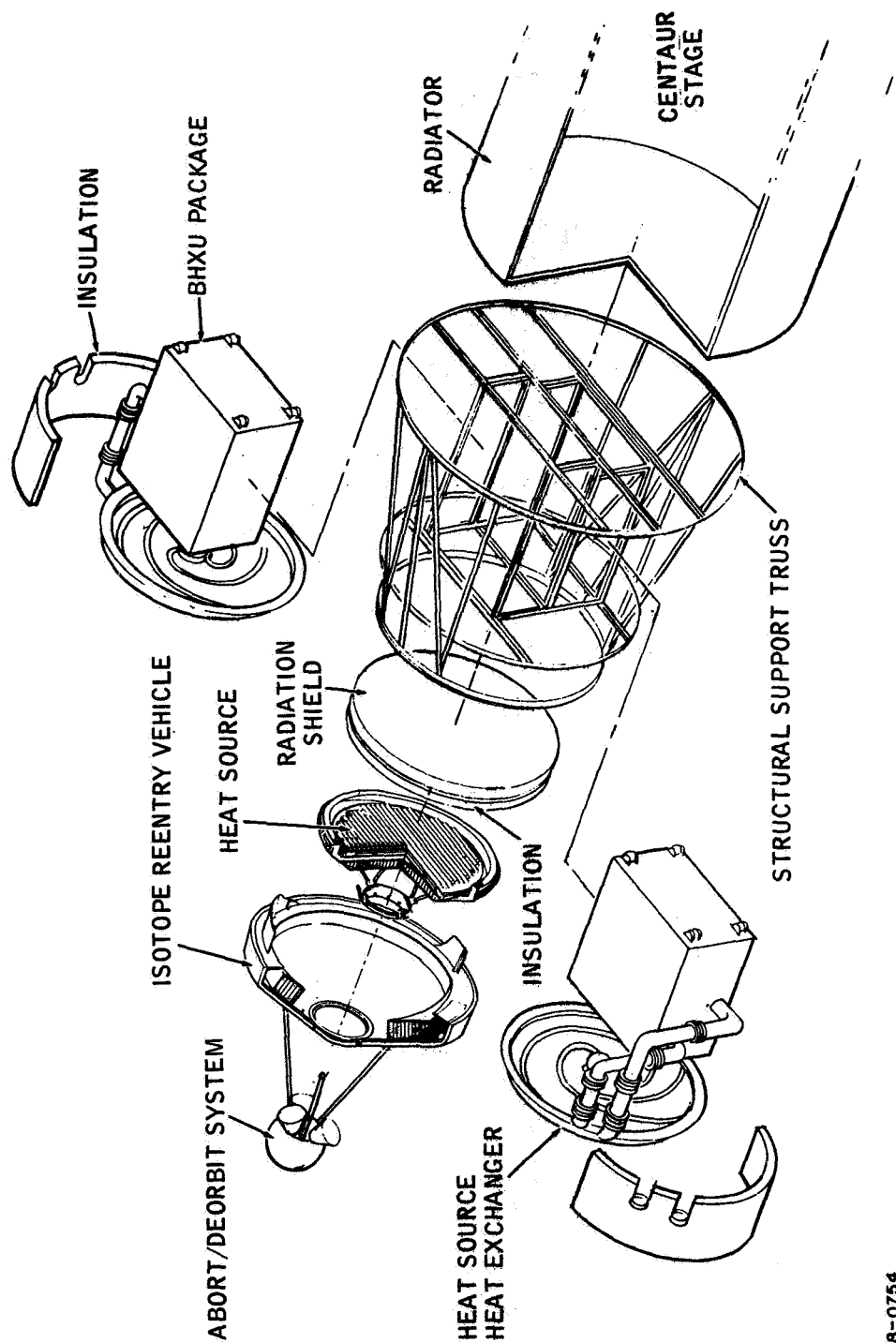


Figure 5-14 IRV/BRAYTON CYCLE/ATLAS-CENTAUR INTEGRATION

78-0754

To develop a "universal" integration concept, the artifice of postulating a typical spacecraft (S/C) mounting volume has been employed, rather than developing detailed specific mounting concepts for the Atlas/Centaur and the Saturn I-B/MORL. By installation of the total system in a small diameter and volume S/C, the applicability of this class of power supply to any currently postulated manned orbital vehicle has been demonstrated. To illustrate the general approach a typical installation in MORL is shown in paragraph 5.2.2. It should be noted that the general installation concept developed can also be mounted in an Atlas/Centaur - OAO shroud with only minor modification.

5.2.1 General Installation Requirements

In order of priority, the installation depicted in Figure 5-15 is governed by safety, minimum system weight, and minimum system volume requirements.

Crew safety (shielding) has been considered only briefly in the study as the location and magnitude of biological shielding is so dependent on undefined factors (e.g., sleep restraint locations, area residence times) that a valid shield design is not possible without a detailed mission and spacecraft study. Preliminary shielding calculations indicate that the assumption of a shield weight of 500 pounds is credible for manned missions with reasonable separation distances (> 10 feet) between crew compartments and the heat source. The typical S/C layout developed in this study has ample volume available for location of crew and equipment shielding as required.

In developing the typical integration concept, emphasis has been placed on:

- component attachment and support
- abort and deorbit mechanization
- emergency cooling methods.

The major consideration and alternatives in these areas are treated in the ensuing discussion.

5.2.1.1 Component Attachment and Support

Figure 5-15 illustrates the location and relationship between the basic IRV/Brayton cycle system components in a typical S/C volume where dense packaging is a definite requirement. The Brayton cycle equipments used in this layout are identical in configuration and weight to the units described in Subsection 5.1. IRV and HSHX configuration and weights are identical to those designs described in paragraph 3.4.3 and Section 4.0. The perspective view (Figure 5-16) includes three-dimensional views of the PCM's, the IRV and the HSHX insulation plenum chamber (with its cooling doors open). It also shows the dual usage of the heat rejection radiator as both a container and a structural member. Basic equipment groupings can also be observed in Figure 5-16.

The rationale followed in establishing the groupings and component locations is to minimize the layout-imposed penalties for support structure, wiring harness, piping runs, and thermal control. Particular attention was given to minimizing or eliminating the valves in gas or liquid system and to logical placement of electrical components to make most efficient usage of the supporting and cooling "cold plate" thermal control system.

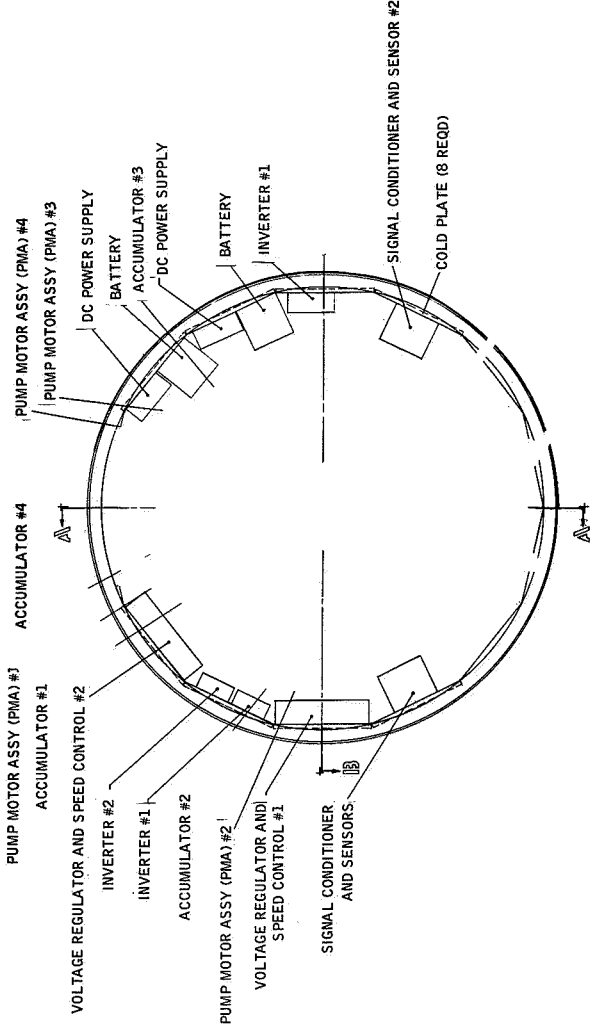


Figure 5-15a

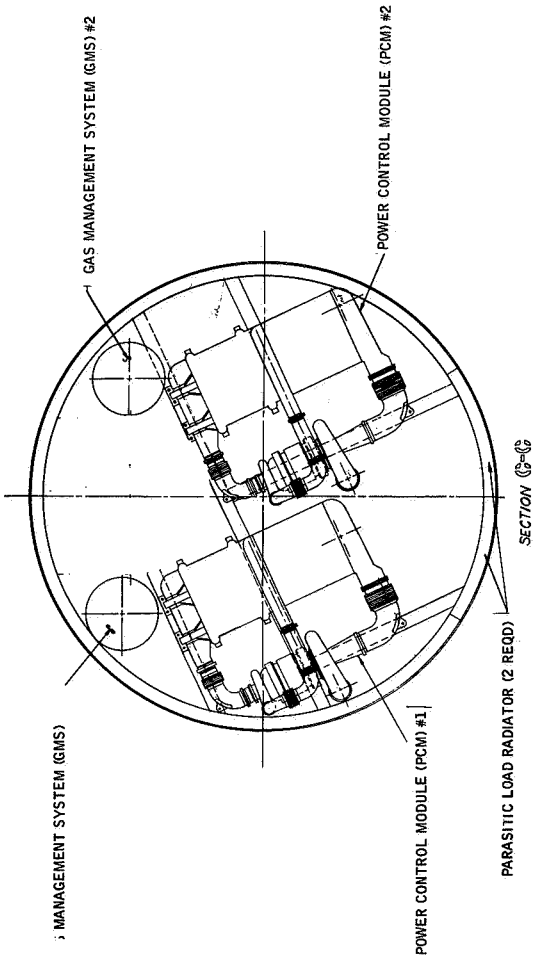


Figure 5-15d

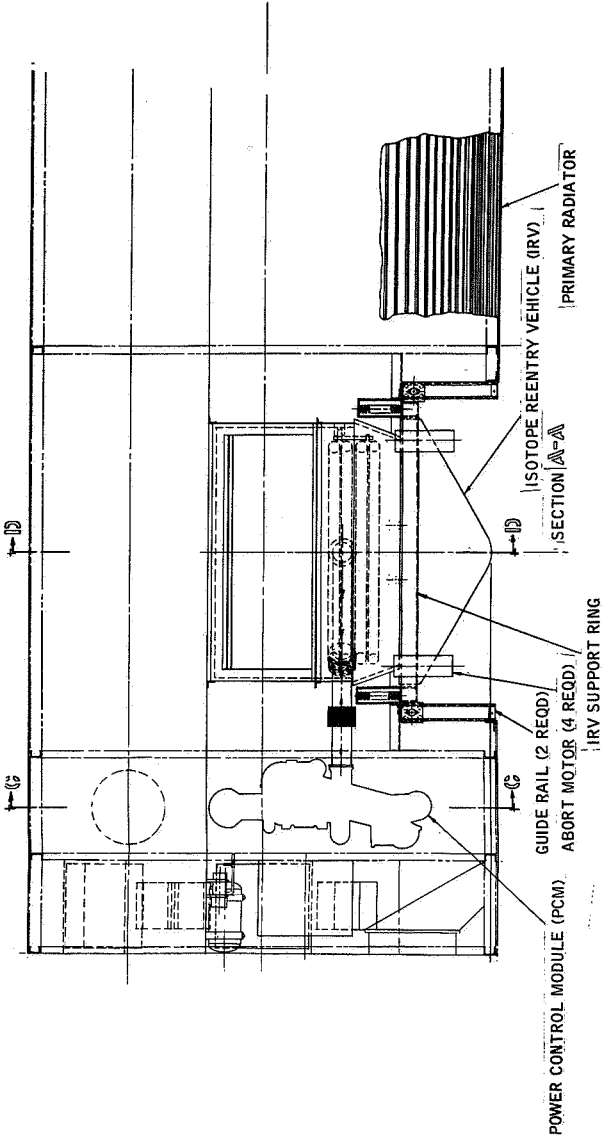


Figure 5-15b

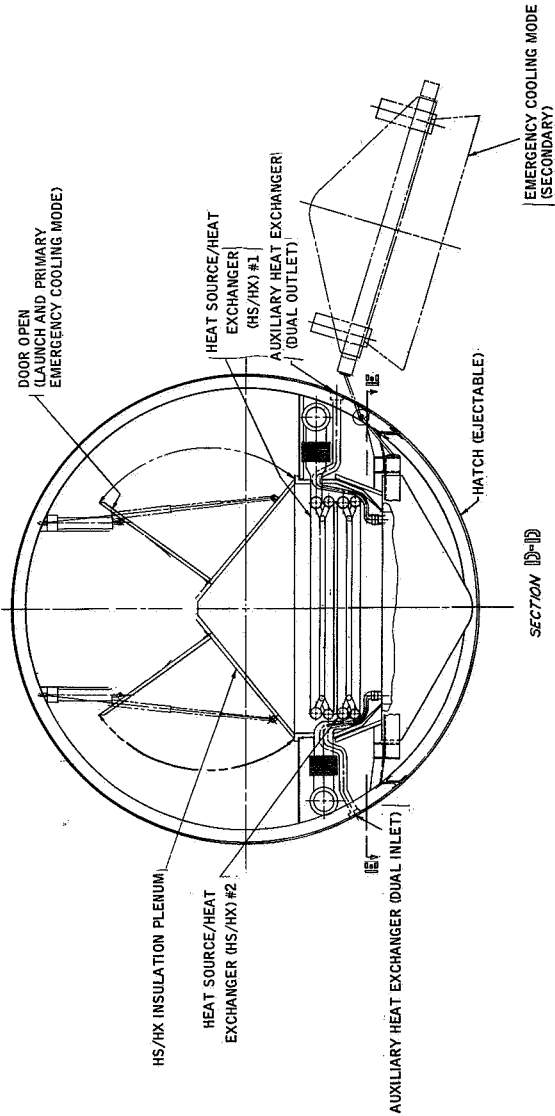


Figure 5-15e

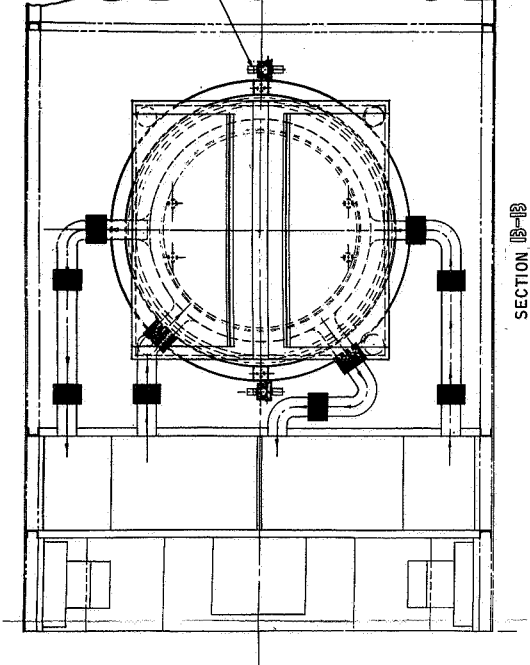


Figure 5-15c

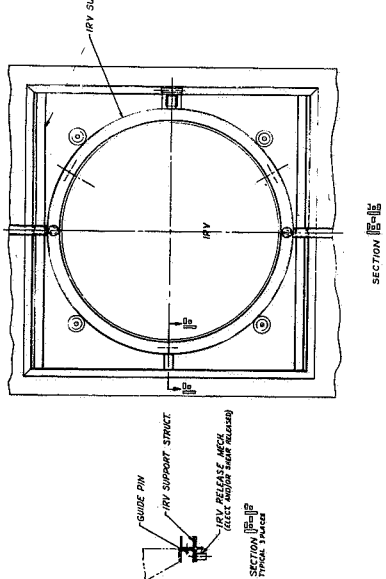


Figure 5-15f

Figure 5-15 TYPICAL IRV/BRAYTON CYCLE/SPACECRAFT INTEGRATION

2

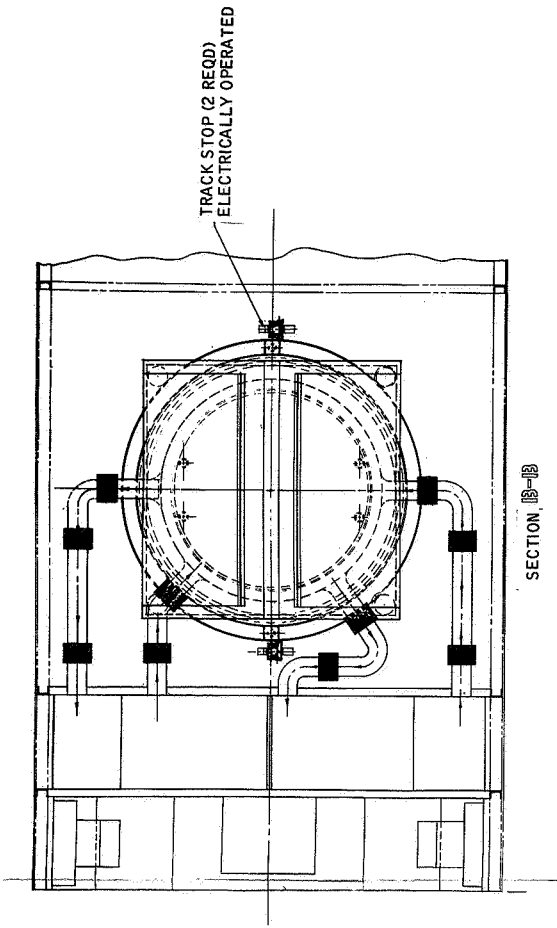
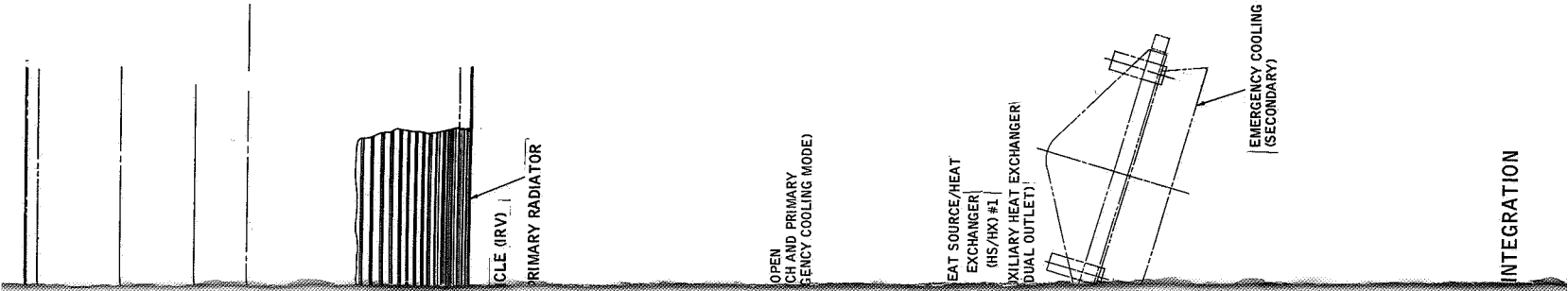


Figure 5-15c

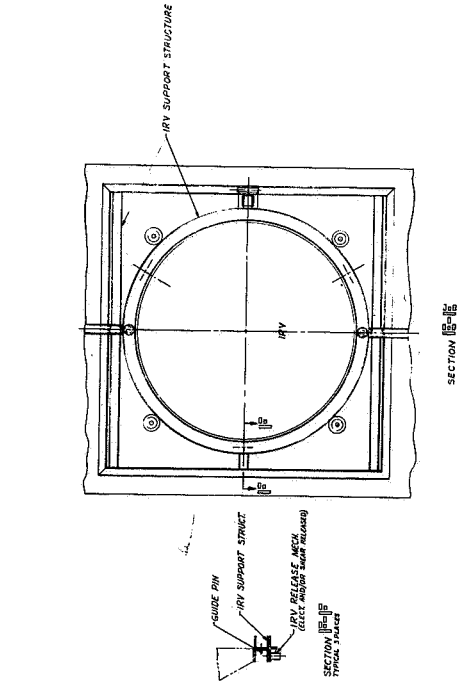


Figure 5-15f

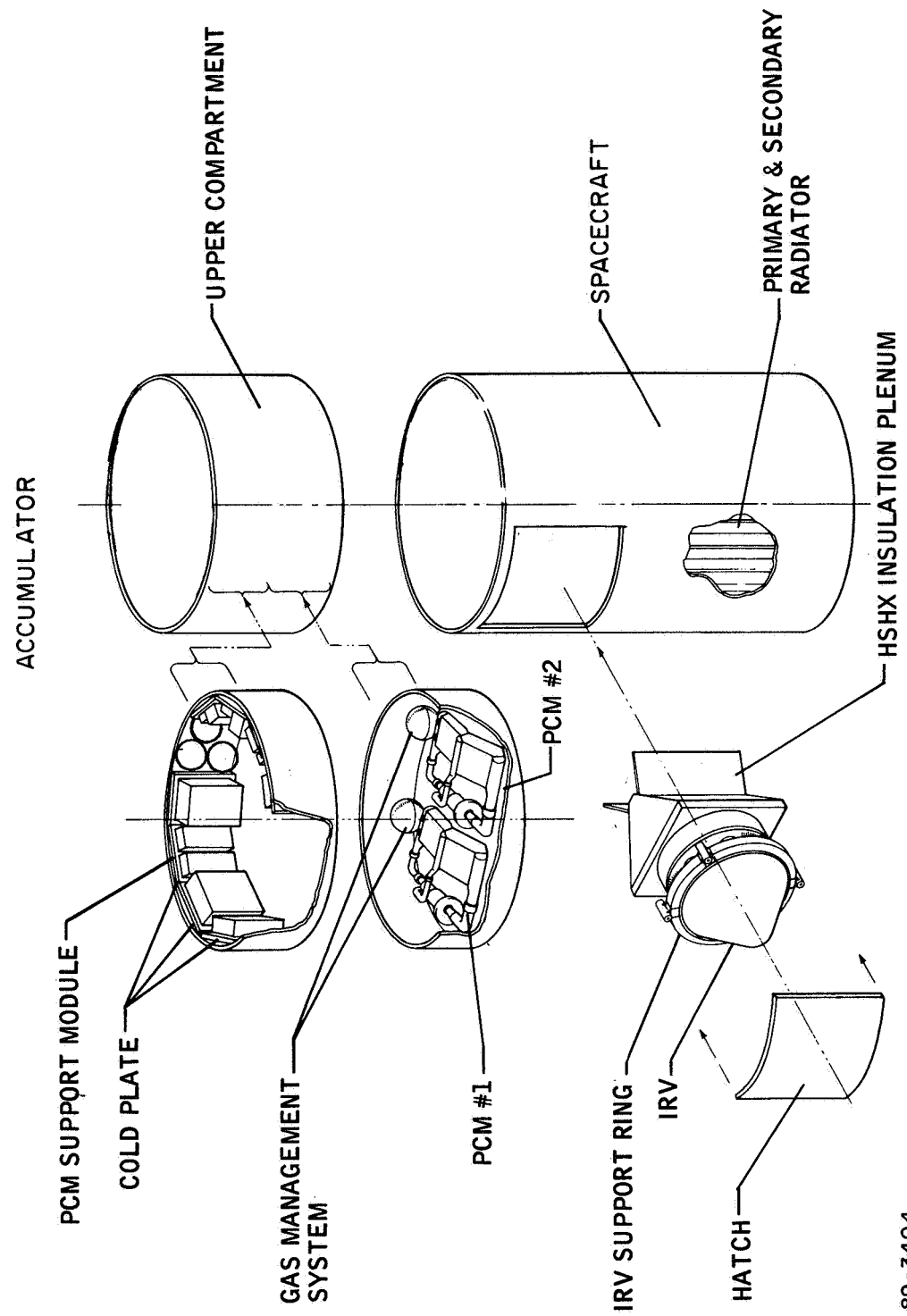


Figure 5-16 PERSPECTIVE VIEW OF THE IRV AND HSHX CONFIGURATION

89-3404

A top section view of the overall installation compartment is shown in Figure 5-15a. This section, taken through the top wafer, shows the distribution of electrical and fluid control components around the periphery of the S/C. To eliminate the necessity for valves in the vital liquid heat rejection systems, two separate coolant loops are provided for each of the PCM's, resulting in a requirement for four PMA's and accumulators. The primary and secondary radiators contain four separate coolant passage systems, reflecting this conservatism. Resultant weight penalties are minor, approximately 400 pounds. The cold plates, used both for removal of heat and support for the electrical components, are also shown in Figure 5-15a. Figures 5-15b and 5-15c are respectively an elevation and a top view of the spacecraft's IRV/Brayton cycle compartment. Figures 5-15b and 5-15c show the basic size spacing between the various components. As seen in Figure 5-15b the radiator tubes run parallel with the long (or roll) axis of the compartment. The radiator is designed as a structural member. With the exception of the IRV access door and two parasitic load resistor panels, the entire compartment outer shell is composed of either primary or secondary radiator sections.

Individual component loads are transmitted to the external structure through a system of internal aluminum stringers. The loads are in turn distributed over the external shell (radiator) by a series of aluminum stiffening rings. These rings are box sections to maximize resistance to torsional loads. The support structure design loads used are consistent with the launch environments summarized in paragraph 3.4.1.2. All support structure is 7075-T6 aluminum.

Figure 5-15c shows a good view of the interconnecting ducts between the HSHX and the PCM's. The ducting consists of four pipe runs, each with three bellows forming a universal space mechanism. This design feature is required to isolate the two units during inertia loading and to accommodate relative thermal expansions during operation. The three bellows in each pipe are required to allow for relatively large expansions in all directions, with deflection up to 0.25 inch for thermal expansion alone. The elevation view (Figure 5-15e) only shows one pipe run, a unit with two 2-degree-of-freedom gimbals as described in Reference 5-2.

Supporting stringers for the PCM units are shown in Figure 5-15d. This view also shows the PCM inlets and outlets in their proper orientation for mating with the HSHX.

The elevation view (Figure 5-15f) shows some of the detail of the IRV access hatch. This hatch is also shown in Figure 5-16, exploded view. Primary access to the IRV compartment for installation and fuel capsule loading on the launch pad is obtained through this hatch. The hatch is fastened into its closed position during launch. It is jettisoned prior to Brayton cycle startup, or in the event of mission abort at any stage in the launch and startup sequence. Positive separation of the hatch from the S/C is achieved with springs, subsequent to firing pyrotechnic attachment mechanisms.

Local structural members are located around the perimeter of the hatch. These members act as part of the S/C primary load path during launch, as local stiffeners, and as attachment points for the IRV/HSHX unit support structure and hinging mechanism. Details of the IRV/HSHX support system are described in the following section.

The support system described in the previous paragraphs has been sized on a preliminary basis to facilitate generation of weight and volume penalties for a typical IRV/Brayton cycle system/spacecraft integration. Typically, the internal stringers are equivalent to 6 x 6-inch WF beams. Local stiffening box rings are 2-1/2 x 2-1/2 x 1/4-inch wall sections. The total weight of the support system members is included in the system weight summation listed in paragraph 5.2.2.

5.2.1.2 Abort and Deorbit Mechanization

Mounting and integration for the IRV is to a large degree controlled by the safety requirements described in paragraph 3.1.1. The potential abort or de-orbit event sequences that must be considered in the mechanization are shown in Figures 5-17 through 5-19, for a MORL class mission. As noted in paragraph 3.1.1 the basic difference between a MORL mission and the typical integration concept described in this section is the inclusion of a deorbit rocket engine in the MORL system. The concept shown in this section can readily accommodate a rocket motor on the nose of the IRV with a consequent requirement for greater diameter on the S/C.

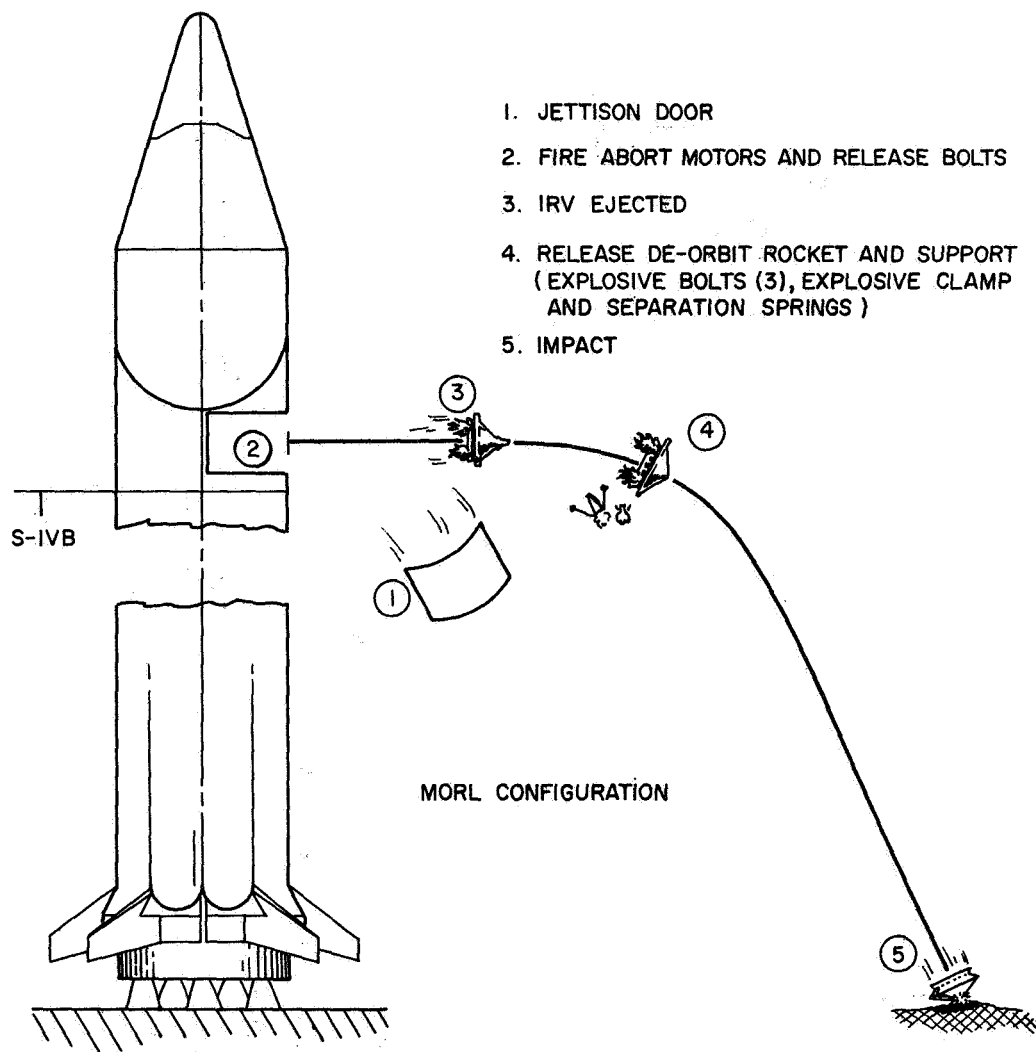
Another major factor in the installation concept is the type of emergency cooling or passive heat dump mode used in rejection of HS energy. The alternatives and approach followed are described in paragraph 5.2.1.3 following.

Mounting of the IRV/HSHX package is strongly influenced by the choice of passive cooling technique, in that the mounting system must support cooling-imposed and abort-imposed requirements simultaneously. (Figure 5-15e, a section through the IRV/HSHX centerline, shows two cooling modes: the IRV in position with the HSHX plenum doors open and the IRV deployed, looking at space.)

Figures 5-15b and 5-15d show two views of the basic IRV/HSHX support system. The support system design is complicated by the requirement for two different ejection sequences and the hinging mechanism required for initial fuel capsule loading of the IRV, and emergency cooling. (It should be noted that the hinge is sized for space operation. Fuel capsule loading on the pad necessitated provision of external support, either a crane or a cradle, for the IRV when it is swung out from its normal supported inboard position.)

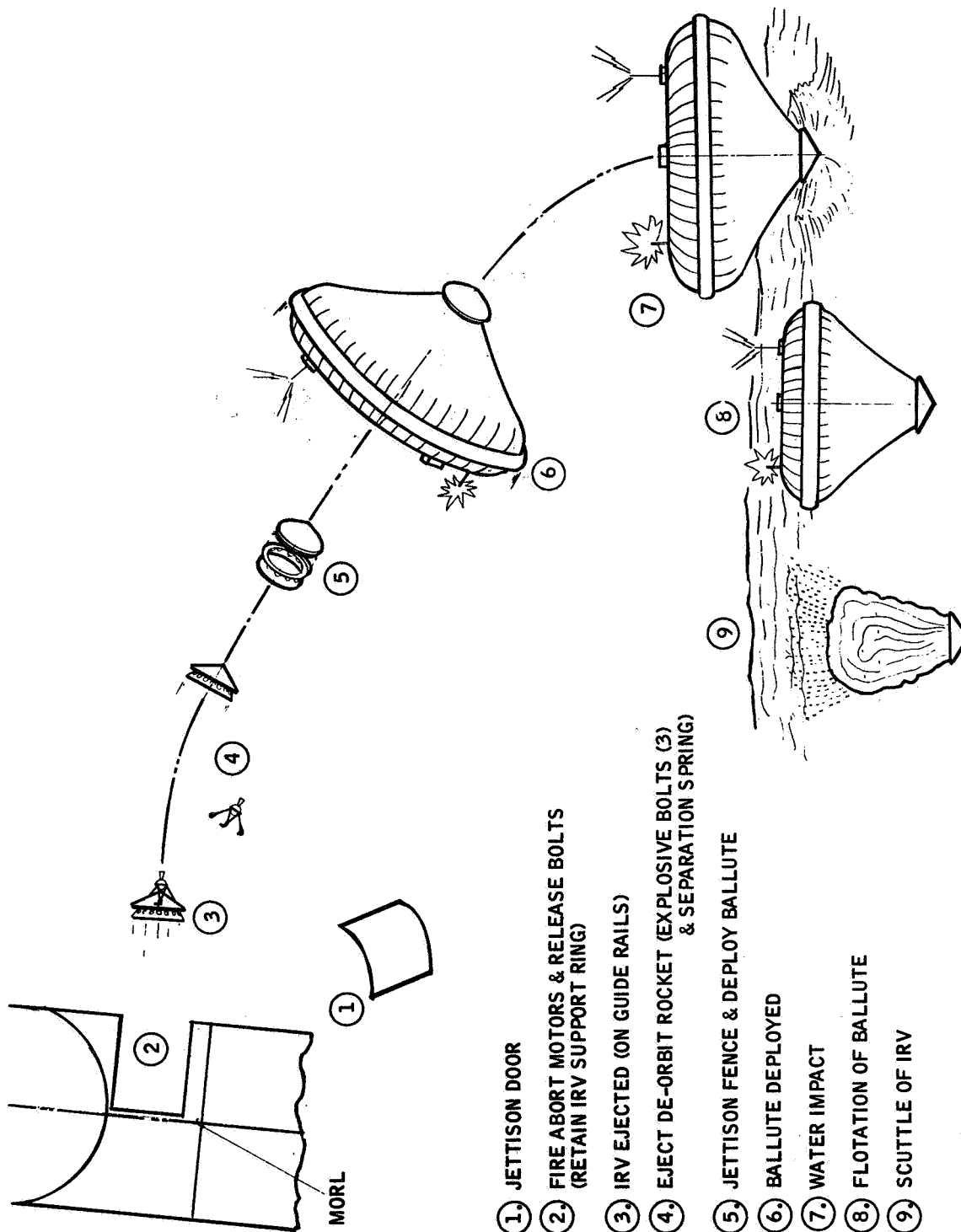
As is noted in paragraph 3.1.1, two separate ejection modes are required. In the first mode, for pad and early launch aborts, it is permissible (and desirable) that the IRV support ring with abort rockets remain attached to the IRV subsequent to ejection of the IRV. In the second mode, for late launch aborts or deorbits resulting in significant reentry heating, the IRV support ring must be left with the S/C. Detachment of the support ring during ejection minimizes potential problems of heat shield damage by the support ring during the abort/deorbit event.

Both ejection sequences must guarantee positive separation and ejection of the IRV from the S/C compartment. A track system must be supplied to ensure that the IRV is ejected in the desired attitude, with disturbing torques minimized, and without opportunity for entrapment in the S/C compartment. In developing the track system the provision of adequate clearance for the IRV and its fence during the ejection sequence and the requirement for temporary deployment of the IRV outside the S/C (Figure 5-15e) are both major considerations.



89-3335

Figure 5-17 LAUNCH PAD AND EARLY ABORT SEQUENCE



1. JETTISON DOOR

2. FIRE ABORT MOTORS & RELEASE BOLTS
(RETAIN IRV SUPPORT RING)

3. IRV EJECTED (ON GUIDE RAILS)

4. EJECT DE-ORBIT ROCKET (EXPLOSIVE BOLTS (3)
& SEPARATION SPRING)

5. JETTISON FENCE & DEPLOY BALLUTE

6. BALLUTE DEPLOYED

7. WATER IMPACT

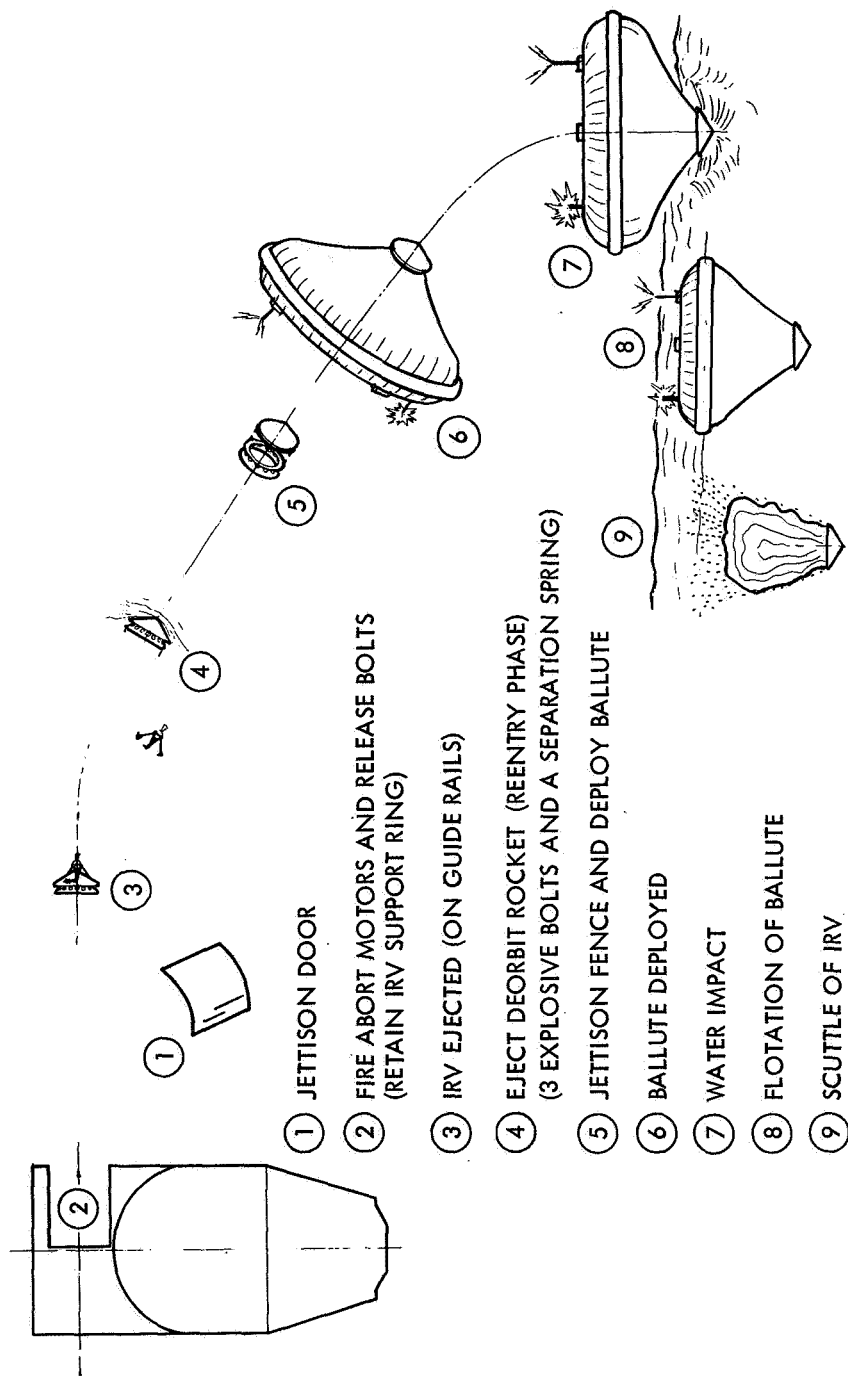
8. FLOTATION OF BALLUTE

9. SCUTTLE OF IRV

ASCENT-ABORT
MORL-CONFIGURATION

Figure 5-18 ASCENT ABORT -- MORL

78-2741



78-2747

Figure 5-19 ORBITAL ABORT AND MISSION TERMINATION -- MORL CONFIGURATION

Several possible support and ejection systems were considered prior to development of the concept used in the "typical" installation. These included:

- employing a "pull" type hook latch to the fence.
- using the fence proper as part of the main load path, ejecting the IRV by reacting on pads located on the periphery of the fence.
- ejection of the IRV without guide rails.

These concepts proved undesirable, primarily due to potential bindings or misalignments inherent in the ejection sequence.

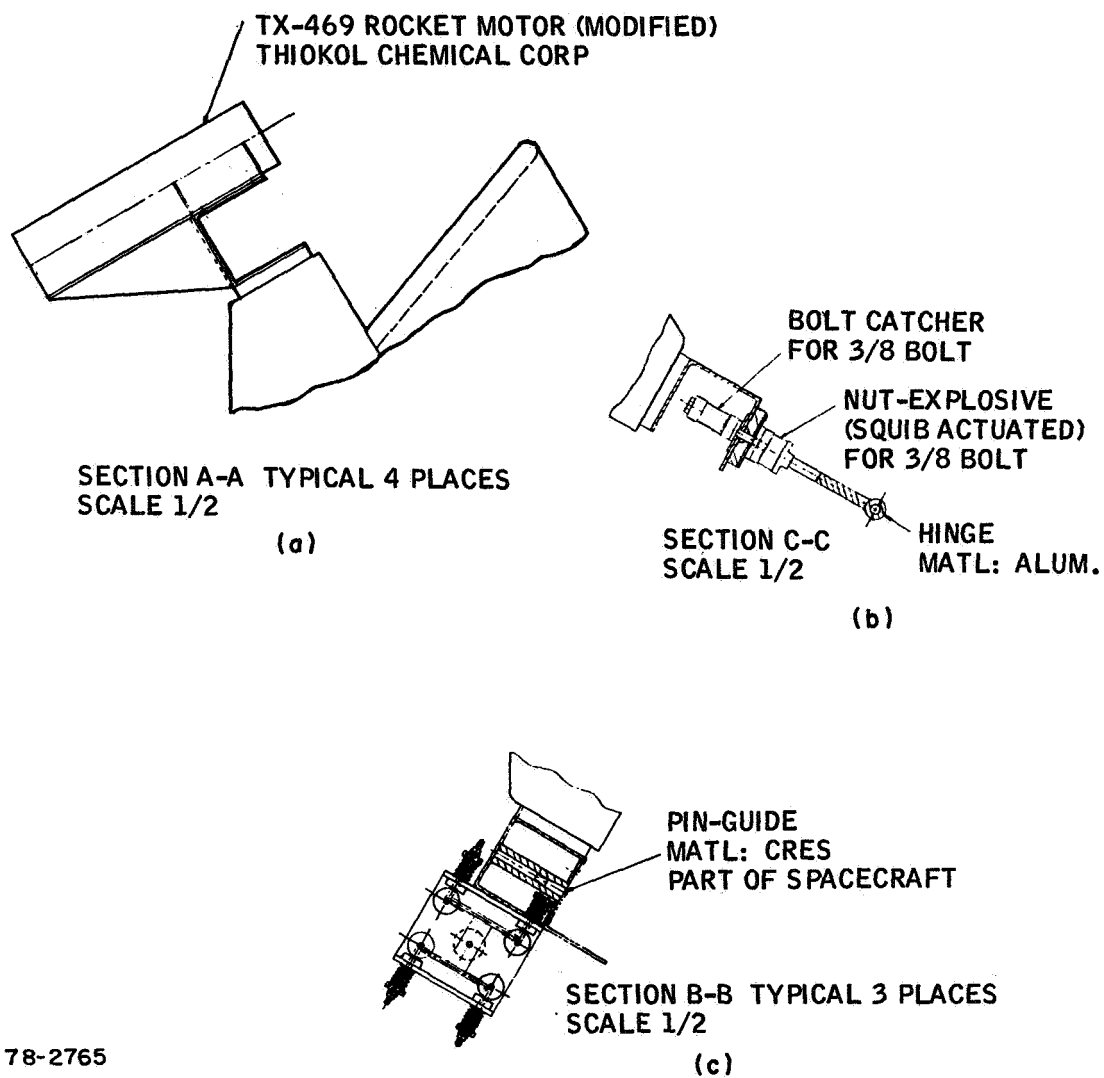
The mechanization shown in Figures 5-15b and 5-15c surmounts the combined problems arising from the various ejection requirements. This support and ejection concept is described in the following paragraphs. The structural design is consistent with the loads environments outlined in paragraph 3.2.1. Weights are included in the system weight estimate listed in paragraph 5.2.2.

Figure 5-15f shows the detail of the IRV/HSX support frame in the S/C. Basic support is achieved through a circle channel member which butts against the IRV support ring shown in Figure 5-15f. Loads from the IRV/HSX during launch are transmitted into this ring by shear pins and positioning pins as shown in the detail section, Figure 5-15g. These loads are conveyed to the S/C outer shell through the stringer tie system illustrated in Figure 5-15f. The shear pins are driven into position by a solenoid system. In the event of an abort or deployment sequence the shear pins are positively retracted. (Subsequent to launch, if S/C power is totally lost, the pins fail in the retracted position.)

The circular channel member shown in Figure 5-15f also contains the housing for the backup springs used to eject the IRV in the event of abort motor failure.

Figure 5-15g shows the IRV and the IRV support ring. This ring serves to:

- transmit structural loads to the S/C
- provide for attachment of abort rockets (Figure 5-20a).
- pick up the IRV loads (Figure 5-15g).
- pick up the hinge attachment (Figure 5-20b).
- attach the guide wheel trolleys (Figure 5-20c).



78-2765

Figure 5-20 IRV AND SUPPORT RING ASSEMBLY

The support ring is attached to the IRV by a series of explosive bolts as shown in Figure 5-21. These bolts are cut upon initiation of a late launch or orbital ejection sequence. Retention of the ring to the IRV during the remainder of the sequence is achieved through reaction with the tapered pads on the IRV described in paragraph 3.4.3. The ring is picked up by the electrically operated stops at the end of the guide rails in this class of ejection. For pad or early launch (no reentry requirement) the explosive bolts attaching the IRV and IRV support rings are not cut. Therefore, the abort rockets are allowed to fire for their full burning time, thereby achieving maximum separation range from the launch vehicle.

Details of the guide rails are depicted in Figure 5-22. The figure shows a view of the support ring and the spring loaded, wheeled trolley. During ejection the hinge connection is cut, shear pins withdrawn and the IRV and its support ring ejected in a translational motion "down" the rails out of the S/C with the ring either retained in the S/C by the electrically actuated stop or continuing in flight with the IRV. The ring stop mechanism is shown in Figure 5-22b. This view also illustrates the IRV hinging sequence. When the IRV is to be swung out for emergency cooling, the tapered wheels are disengaged from the track by retracting the tapered wheel lock, as is shown in Figure 5-22a. To reposition the IRV against the HSHX, it is rotated back into the S/C. The wheel trolley is reengaged with the guide tracks by actuating the tapered wheel lock piston. Tapered guide pins are also provided to assure proper remating of the IRV and the HSHX during this action. The safing, arming, and initiation scheme required to implement this ejection and deployment mechanization is described in paragraph 3.1.4.

5.2.1.3 Emergency Cooling Methods

As noted in paragraph 3.1.1, a major operating requirement is assurance of Heat Source generated energy rejection throughout mission life. This cooling function is accomplished on the launch pad by the ACHX system described in paragraph 3.3.3. A description of the ACHX connection and removal sequence is presented in Subsection 5.3 (Ground Handling). This discussion treats the methods used in the IRV design study to achieve rejection of the 25 kw_t of energy generated by the HS during periods when the Brayton cycle is inoperative, either by design (during launch and startup) or due to an electrical system failure.

It is apparent that provision of a heat rejection (or dump) mechanism is a vital element in assuring IRV safety throughout the postulated mission lifetime. Two basic heat rejection modes have been considered in Phase I of the study:

- Rotation of the IRV so that the HS radiates directly to space.
- Utilization of a sliding door heat "dump" to give the HS a limited view of space or of the S/C walls.

Conceptually either of these techniques is a credible heat rejection technique. They both, however, exhibit drawbacks that potentially diminish their utility. Both systems as originally developed, are dependent on mechanical action in space, i.e., the hinge must rotate, or the doors must slide. Therefore both systems are potentially vulnerable to vacuum cold welding problems. While the cold welding problem does not appear to be a problem early in the mission (the

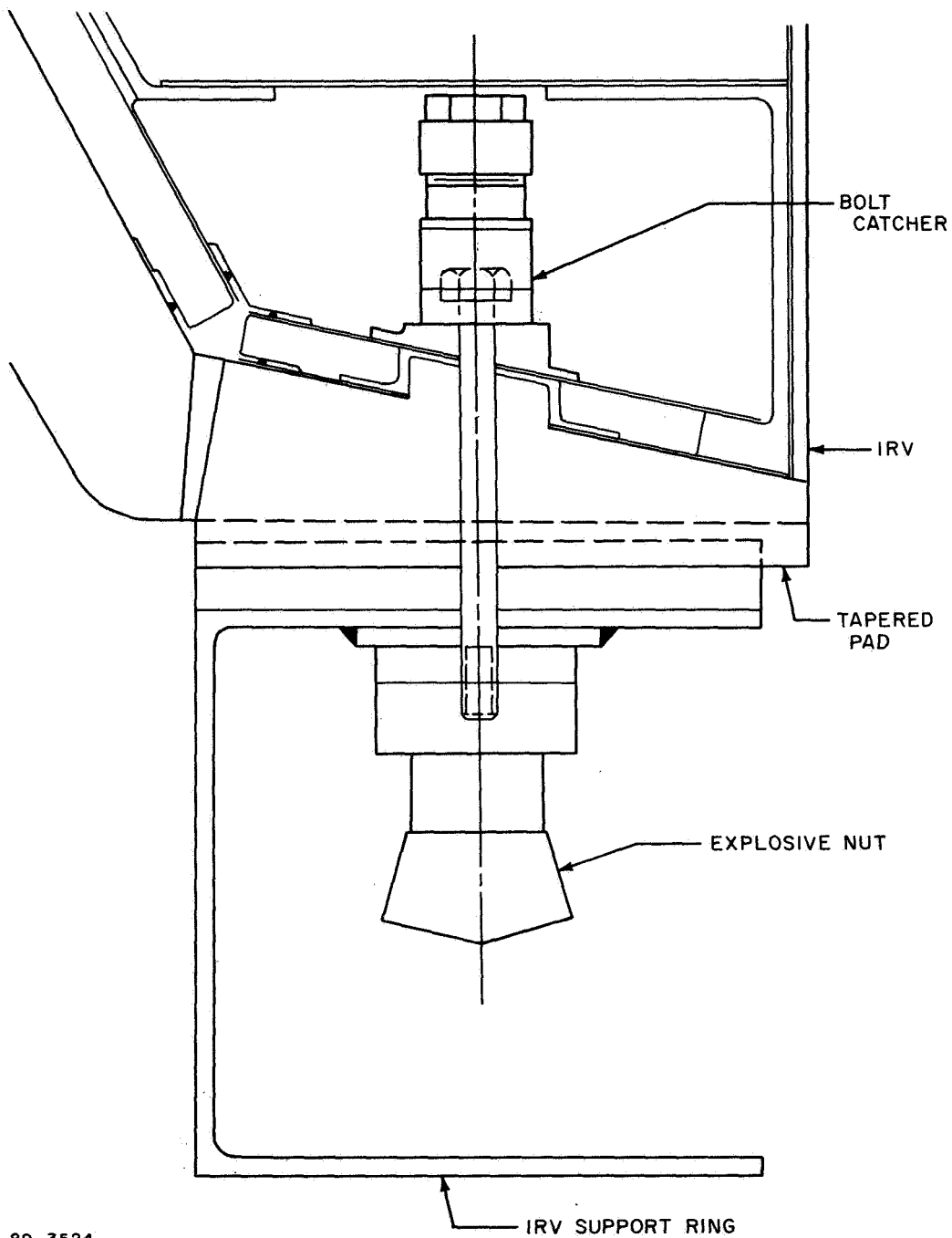


Figure 5-21 IRV/SUPPORT RING EXPLOSIVE NUT ASSEMBLY

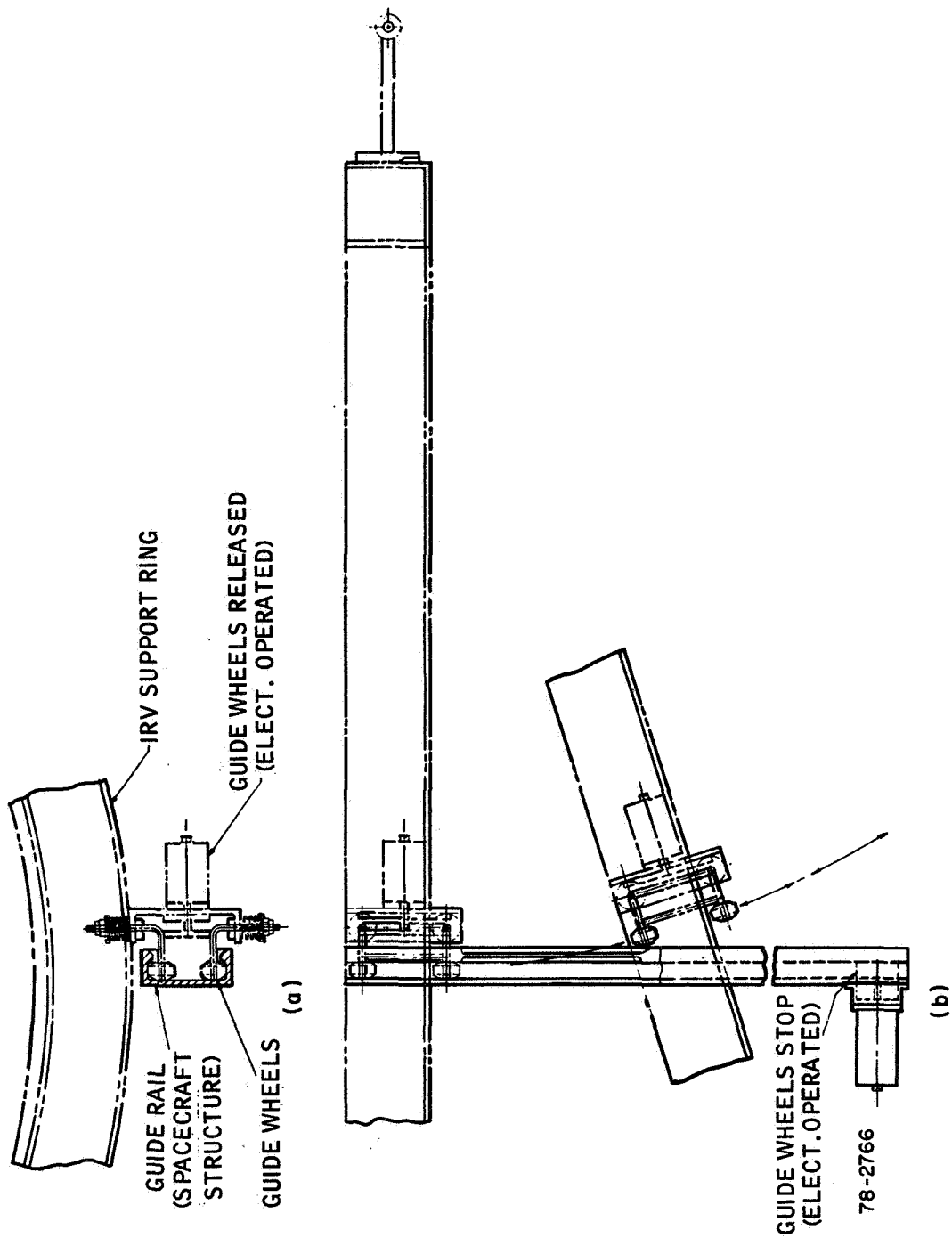


Figure 5-22 DETAIL VIEW OF GUIDE RAIL ASSEMBLY

most critical phases), and proper lubrication (e.g., use of a space lubricant) may ensure long term capability, the vital safety requirements of this mission serve to dictate a safer design than can be achieved with either concept in itself.

An absolute guarantee of fail-safe emergency cooling of the HS must be provided in the design. Extensive redundancy for this function has been provided in this integration concept. Figure 5-15e illustrates the normal operational and passive cooling modes for the two basic heat rejection systems. These are the HSHX insulation plenum and the hinge mechanism that allows rotation of the IRV out of the S/C.

This plenum has been sized to provide an adequate view factor for the HS to the S/C interior wall. Preliminary analysis indicates that the highest maximum temperature reached at the hot spot on the S/C wall is $\sim 600^{\circ}\text{F}$ with one door open, this valve falls to $< 500^{\circ}\text{F}$ with both doors open. These values are only true for the node evaluated immediately opposite the door centerline. The temperatures drop off rapidly for S/C locations further away from the peak heating point. These values are conservative in that they do not consider cooling conductivity effects (around the aeroshell) nor potential beneficial effects to be gained from circulating coolant through the radiator while the plenum chamber doors are open. Use of the circulating system could limit peak temperature values to 200°F with only one door open.

Figure 5-15e shows the plenum doors in both open (passive cooling) and shut (normal operation) modes. The plenum is fabricated from multifoil insulation supported by light honeycomb structure as required. A "house" configuration is employed to simplify fabrication and provide sufficient view factors to maintain the HS at an acceptable maximum temperature with one or two doors open. This feature is considered a necessary element in the provision of a totally safe isotope power supply. Door actuation is performed by telescoping piston mechanisms. A further safety backup is present in the IRV hinge mechanism. In the event of a total plenum door failure the capability still exists to swing the IRV into a position in which it is cooled by radiation to space.

In the normal sequence of events, the IRV/HSHX is launched with the plenum doors open, so as to provide passive cooling to the HS prior to IRV/Brayton cycle system startup. Once proper orbital parameters have been achieved, the doors are closed, the heat source allowed to rise in temperature, and at a preselected temperature the Brayton Engine startup sequence is initiated.

5.2.2 MORL Installaion

Figure 5-23 illustrates one possible mounting of the IRV/Brayton cycle system as described in the preceding section, in a MORL concept. The intent of the installation concept drawing as shown is to indicate packaging and prime component locations in the MORL storage volume. There are only two significant differences between this concept and the "typical" integration concept described in paragraph 5.2.1. These are:

- inclusion of a deorbit rocket motor mounted to the nose of the IRV.
- redistribution of the Brayton cycle components with respect to the IRV/HSHX package.

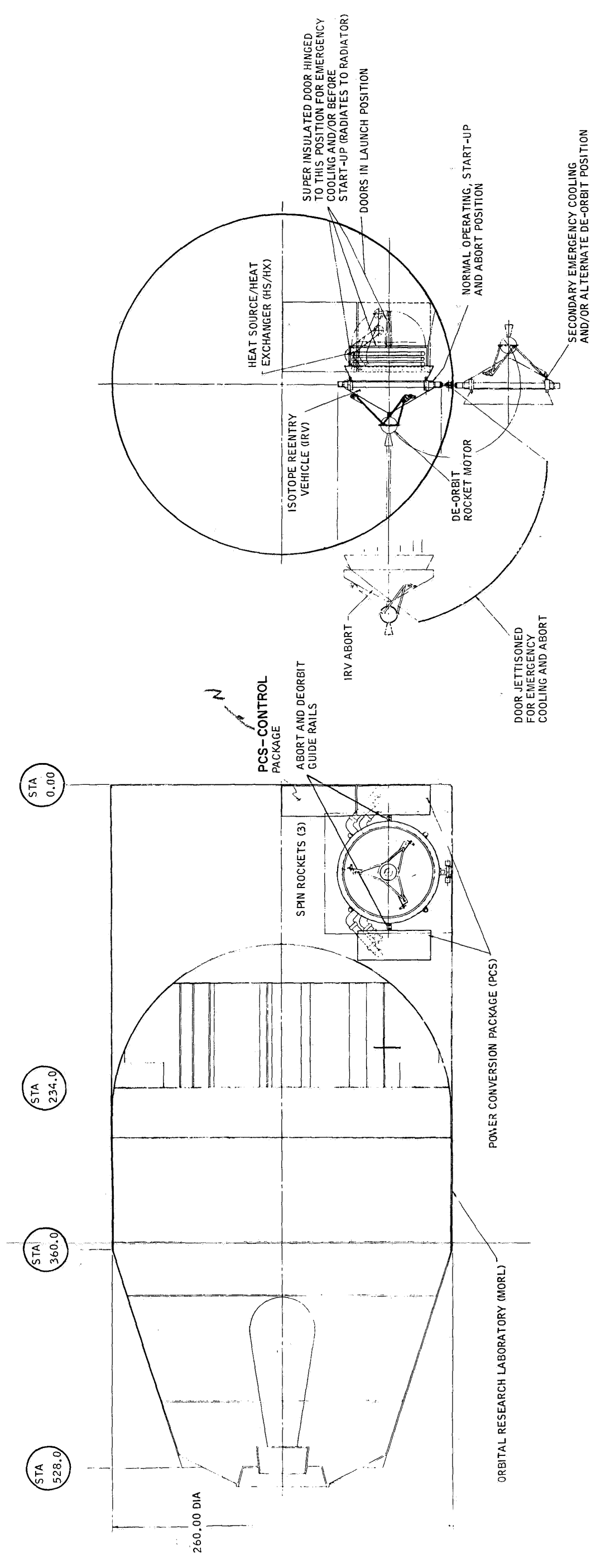


Figure 5-23 MORL/IRV INTEGRAL LAUNCH CONFIGURATION

The balance of the design features of the typical integration remain essentially unchanged. Passive cooling is achieved through the use of movable insulation doors over the HSHX or by rotating the IRV to view space. Abort or deorbit sequences of events are essentially unchanged with the exception of the peculiarities inherent in using a deorbit rocket motor to retro the IRV. The deorbit sequence of events is defined in paragraph 3.1.1. Spin motors must be fired immediately after separation to ensure maintenance of the desired attitude during deorbit rocket firing as well as crude inertial stabilization in the period elapsing between S/C separation and retro ignition.

Waste heat rejection is performed through a dual purpose radiator that serves as both an energy dissipation and as an external structural S/C shell. Estimates of structural support weight requirements have been made, based on a similar support system to that defined in paragraph 5.2.1.

Table 5-1 contains a weight summary for two installation concepts. The difference between the two is the inclusion of one or two PCM systems. Total weights for the system are approximately 4500 and 5700 pounds for the one and two PCM versions of the IRV/Brayton Cycle System. Weight estimates for the Brayton cycle components are as noted in Subsection 5.1. IRV/HSHX weight estimates are presented in Sections 3.0 and 4.0. These weight summaries do not include personnel shielding or radiator weight estimates. As noted previously, shield weights are heavily dependent on specific mission requirements. Shield design was not within the scope of this contract. It is also not possible to evaluate the radiator net weight cost without development of a valid S/C structural design. A conservative estimate of the total weight increase due to these two components is 1000 pounds. Total system weight for the two options is approximately 5500 and 6700 pounds for the one and two PCM systems.

5.3 GROUND HANDLING REQUIREMENTS

This section contains a description of the basic ground handling approach. The major events treated are:

- Fuel capsule transportation
- Heat source plate assembly and facilities
- Auxiliary cooling heat exchanger (ACHX) requirements
- Fuel capsule loading
- Launch vehicle integration
- ACHX launch pad hookup and installation.

5.3.1 Fuel Capsules

The fuel capsules, each containing 157 watts of Pu-238 radioisotope fuel, would be shipped to the launch site in fuel capsule storage casks. For the purpose of this study it is assumed that these storage casks would be designed to carry 5 to 15 fuel capsules and will attenuate radiation to acceptable levels as called out in the appropriate ICC regulations.

TABLE 5-1

WEIGHT SUMMARY IRV/BRAYTON CYCLE SYSTEM--ADVANCED MORL

	Single PCM System		Redundant PCM System	
	(lb)	(lb)	(lb)	(lb)
IRV		(2300)		(2300)
IRV	1980		1980	
Abort	90		90	
Deorbit	130		130	
Support Ring	75		75	
Springs	25		25	
HSHX		(230)		(430)
HSHX	130		260	
Ducts	35		70	
Insulation	50		70	
Support Structure	15		30	
Gas Loop		(435)		(870)
Heat Rejection		(230)		(390)
Fluid Inventory	30		60	
Cold Plates	80		90	
Pump Motor Assemblies (2)	20		(4) 40	
Accumulators (2)	20		(4) 40	
Plumbing	80		160	
Gas Management		(150)		(300)
Electrical and Control		(505)		(730)
Batteries (85 amp-hr AgZn)	180		180	
Inverters (2)	30		(4) 60	
Signal Conditions and Sensing	25		50	
VRE and Speed Control	75		125	
DC Power Supply	25		40	
Frequency Converters	25		50	
Parasitic Load Radiators	50		50	
Cable Assemblies	95		175	
System Support Structure		(690)		(690)
Insulation Plenum	200		200	
Main Hatch	50		50	
System Support Structure	440		440	
Total System Weight*		(4540)		(5710)

*Does not include radiators and radiation shield

Cooling is accomplished passively, largely by natural convection on the outside surface of the shipping cask. The steady-state fuel capsule surface temperatures in the cask are anticipated to be approximately 300° F.

The estimated weight of a typical shipping cask would be 1500 pounds.

5.3.2 Heat Source Plate Assembly and Facilities

The heat source plate assembly as described in paragraph 3.3.6 is a major functional unit in the IRV system. Although the final assembly of the heat source plate is incomplete until the fuel capsule or spacers have been installed, it will be shipped as an assembled unit, with dummy fuel capsules, positioned to permit shipment of the cover plate without distortion or scratching due to potential improper handling. Transportation of the assembled heat source plate is accomplished under normal shipping conditions with adequate protection given to the applied emissive coating.

Fuel capsule loading will be accomplished in a closed area provided at the launch site for that purpose. The closed area provides suitable conditions for receiving, storage, inspection, and other quality control functions. It has a controlled atmosphere, effluent filtering system and radiation monitoring equipment. On arrival at the ETR, the fueled capsules will undergo receiving inspection. They will be stored, in their shipping casks, in the assembly/storage area until the build up of the heat source plate assembly is completed.

Receiving inspection will consist primarily of investigation for shipping damage. This can be accomplished by inspecting individual capsules in a glove box environment. When the buildup of the heat source plate assembly is ready to proceed, the capsules will be transported to the assembly area. Operating constraints imposed by gamma and neutron radiation from Pu-238 fuel capsules are expected to be minimal with proper design and use of handling equipment. The radiation level at one meter from a single IRV capsule (157 watts) is estimated to be 3 mrem/hr, assuming use of PuO₂ enriched in O¹⁶. A handling device that provides a separation of approximately three feet between fuel capsule and trunk of the body and one foot between capsule and hand would permit fuel handling operation with virtually no restrictions from radiation exposure consideration.

Glove box handling techniques could, therefore, provide adequate protection for QC handling of the individual capsules. The dose rate is estimated to be 70 rem/hr at 4 inches from the axial centerline of the assembled 25 kw_t heat source. This level implies control of operations involving close proximity to the heat source.

Radiation shielding in the form of portable polyethylene screens 3 inches thick, located 4 feet from the heat source, will provide adequate protection from this radiation allowing controlled access to the heat source. If normal protective clothing is worn, dosimeters and film badges must be utilized and exposure for each individual must be duly noted by qualified health physics personnel. The work area must be large enough to accommodate the heat source plate assembly and transporter. It should be equipped with an overhead crane, master-slave manipulator type remote handling tools, in addition to other equipment such as fuel capsule storage casks.

The heat source plate transporter would be designed as a shielded self-contained unit with primary and backup compressors for the air required for the ACHX. After fuel capsule loading is completed the hinged shielded cover is closed and the transporter loaded onto a dolly for transfer to the launch vehicle.

5.3.3 ACHX Requirements

Cooling is mandatory during fuel capsule loading, and ground operation prior to launch.

This is primarily accomplished by the ACHX described previously. The cooling medium which has been recommended is air, and this will be controlled to maintain the heat source plate temperature to a maximum 350° F throughout the ground handling and launch pad operation. The inlet and outlet connections have been designed to accomodate quick disconnect couplings, and special features of the system will be discussed in paragraph 5.3.6.

5.3.4 Fuel Capsule Loading

Installation of the 164 radioisotope fuel capsules on the heat source support plate is completed in the closed area under a controlled atmosphere. The fuel capsules are contained in shipping casks and the heat source support plate positioned and locked by the breach lock system in the heat source transporter. Figure 5-24 shows a typical setup of the closed area with the various equipment necessary for accomplishing the loading.

After the ACHX system has been activated, individual capsules are removed from the shipping casks by a master-slave manipulator type equipment and positioned on the heat source support plate. To preclude damage to the emissive coatings on both fuel capsules and support plate, a master-slave manipulator is preferred. This operation will be performed in two stages. First the capsule is removed from the cask in its vertical orientation. Then the capsule is turned into the horizontal position on an intermediate table. From the horizontal position they are loaded into the heat source plate. As each capsule is positioned on the fuel capsule support plate, beryllium oxide capsule positioning rings are installed between capsules. These rings are designed to distribute any load which may occur as a result of launch or reentry over the entire end of the capsule rather than allow point loading.

After all the 164 capsules and capsule positioning rings have been installed, the cover plate, Figure 5-25, is positioned over the hold-down bolts, which were previously screwed into the fuel capsule support plate. At this stage a temperature differential of approximately 350° F will exist between the support plate and the cover plate. Several methods can be used to equalize temperature, the first is to position the cover plate over the hold-down bolts and wait until the temperatures of both have equalized, the second is to preheat the cover plate to the same temperature as the heat source support plate. After the cover plate temperature has equalized, it is positioned over the heads of the 194 hold-down bolts, the retaining bar is then positioned under the heads of each row of bolts. This retaining bar is a triangular bar, slotted at each bolts location; again care must be taken to ensure that the emissive coating is not damaged.

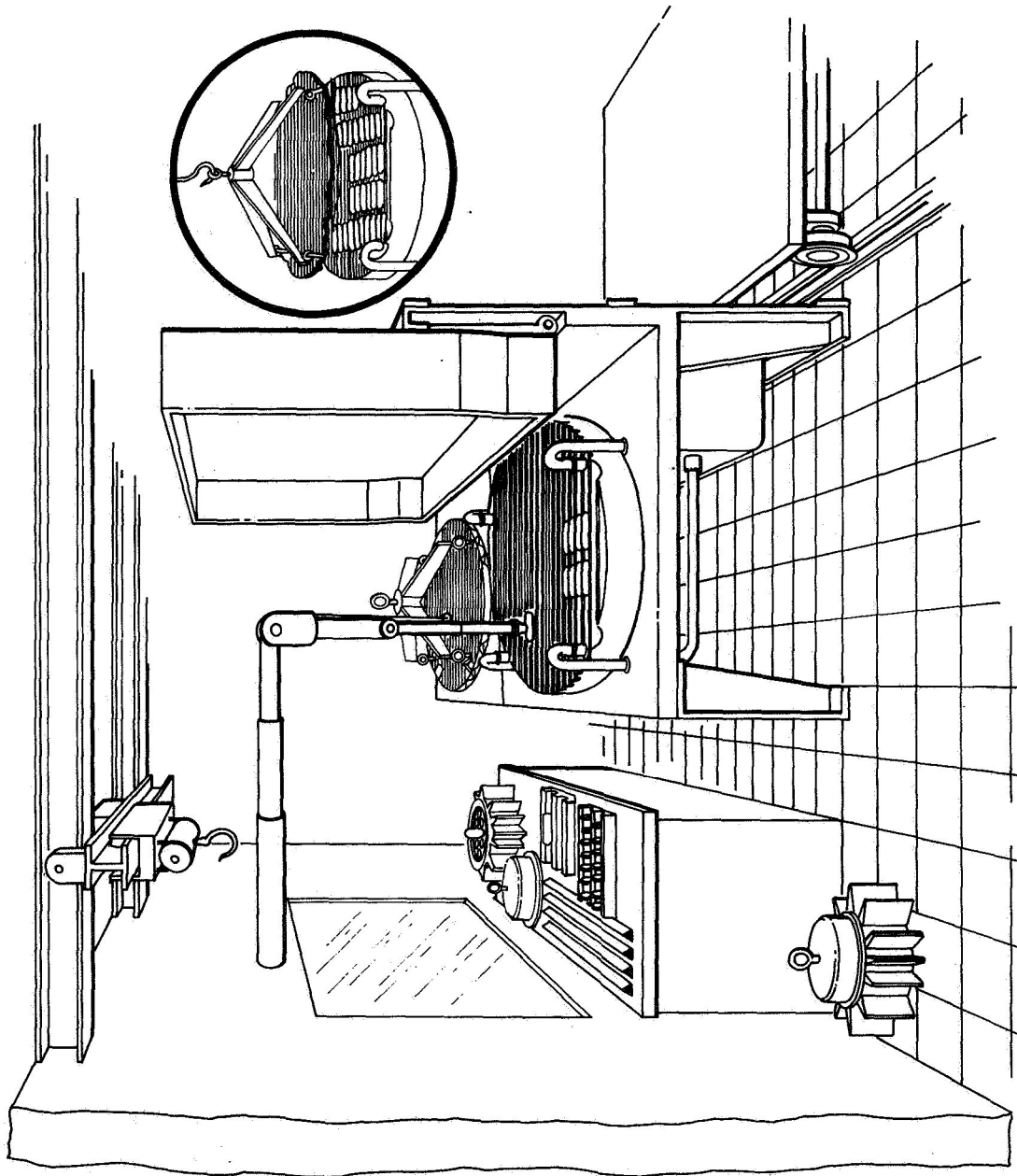


Figure 5-24 FUEL CAPSULE LOADING INSTALLATION

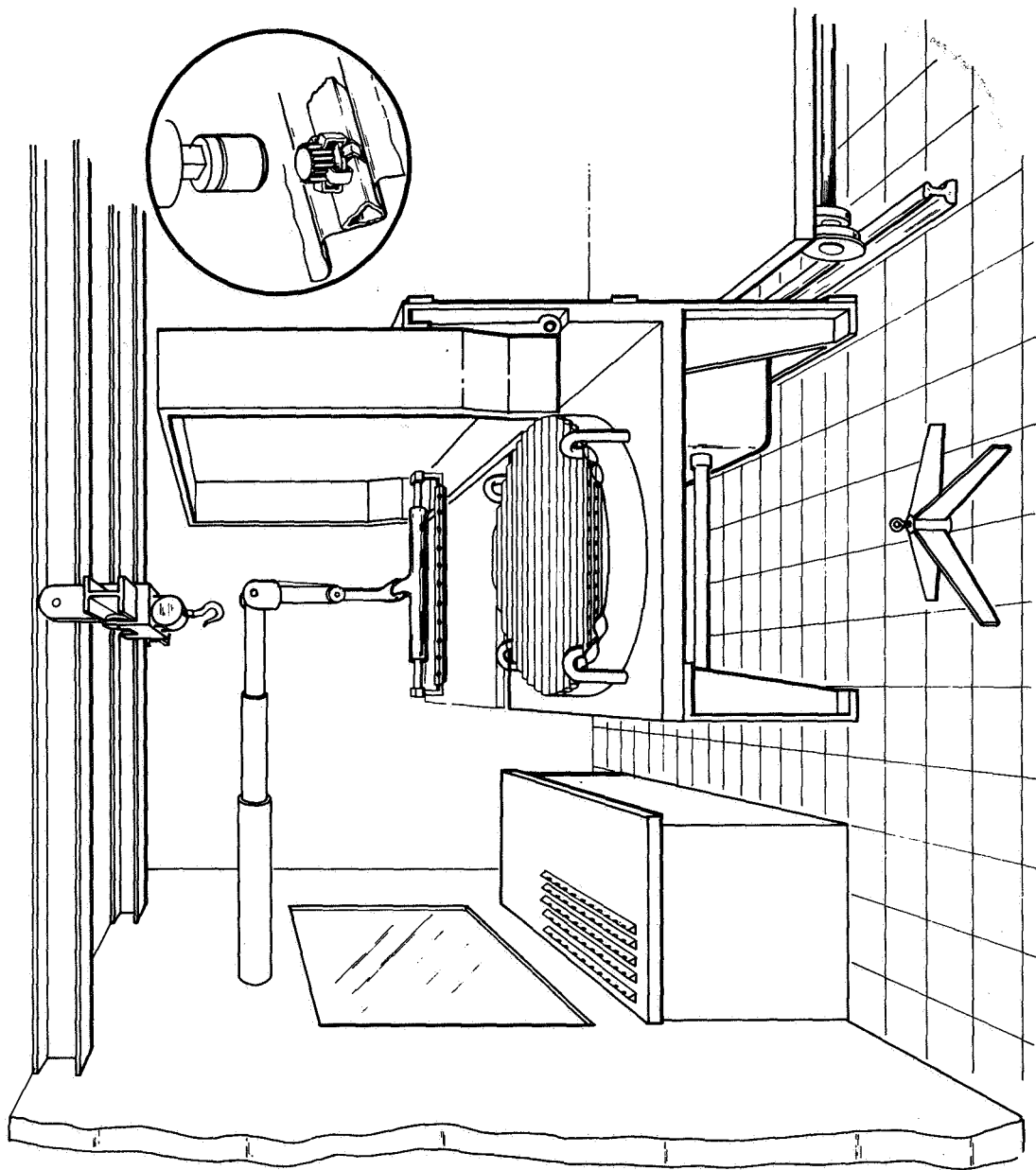


Figure 5-25 RETENTION SYSTEM ASSEMBLY

The final operation consists of tightening each bolt and locking it in position with a lock washer.

During the period after final fuel capsule loading, careful monitoring of the ACHX temperature and flow is required. Any excessive increase in temperature could cause oxidation damage to the refractory alloy structure of the heat source plate.

Following capsule loading, the cover of the transporter is closed and the unit is either stored or transferred to the launch vehicle for installation.

5.3.5 Launch Vehicle Integration

The launch vehicle integration plan has been prepared to be flexible enough to adapt to any of several launch vehicles. In all cases it is assumed that the IRV aeroshell is previously installed and in the deployed position. A major factor that must be considered is whether a manual, or fully automatic system for transferring the heat source into the launch vehicle is utilized. For the purpose of this study it is assumed that semiautomatic equipment will be used. This means that personnel will be in close proximity to the heat source during various stages of the assembly for controlled periods of time.

The actual loading of the fueled heat source assembly into the aeroshell should be accomplished late in the countdown, after the majority of personnel have been cleared from the launch pad area. This would avoid possible conflict with other operations.

Several other important factors must be considered during launch vehicle integration. These factors are basically dependent on the type of vehicle being utilized. First and most important is the support gantry and umbilical tower, and the consequent amount of work space available at the loading level. It is assumed that any operation necessary will be possible from the gantry or tower which is available.

The IRV reentry body with heat source support structure and insulation assembly would previously be installed and deployed, to affect horizontal loading of the heat source. The first stage of integration is the transportation of the assembled heat source plate in the transporter to the launch pad. Figure 5-26 shows a typical arrangement. Figure 5-27 depicts the transporter being removed from the dolly to an elevator on the gantry.

The elevator then carries the loaded transporter to the required level and work area.

The transfer mechanism required to load the heat source into the IRV must be capable of handling approximately 1500 pounds and be designed to operate semi-automatically in all directions necessary, allowing translation motion along three mutually orthogonal axes and rotational motions about these three axes, to implement installation and locking or unlocking and removal of the heat source.

Various heat source transfer systems could be considered. One system visualized is a boom-type structure which extends close to the transfer area. This boom carries a telescopic radial arm which can operate in any direction by either rack and pinion or hydraulic mechanism. Another system would consist of a monorail installed at the loading platform and a transfer mechanism unit riding this monorail.

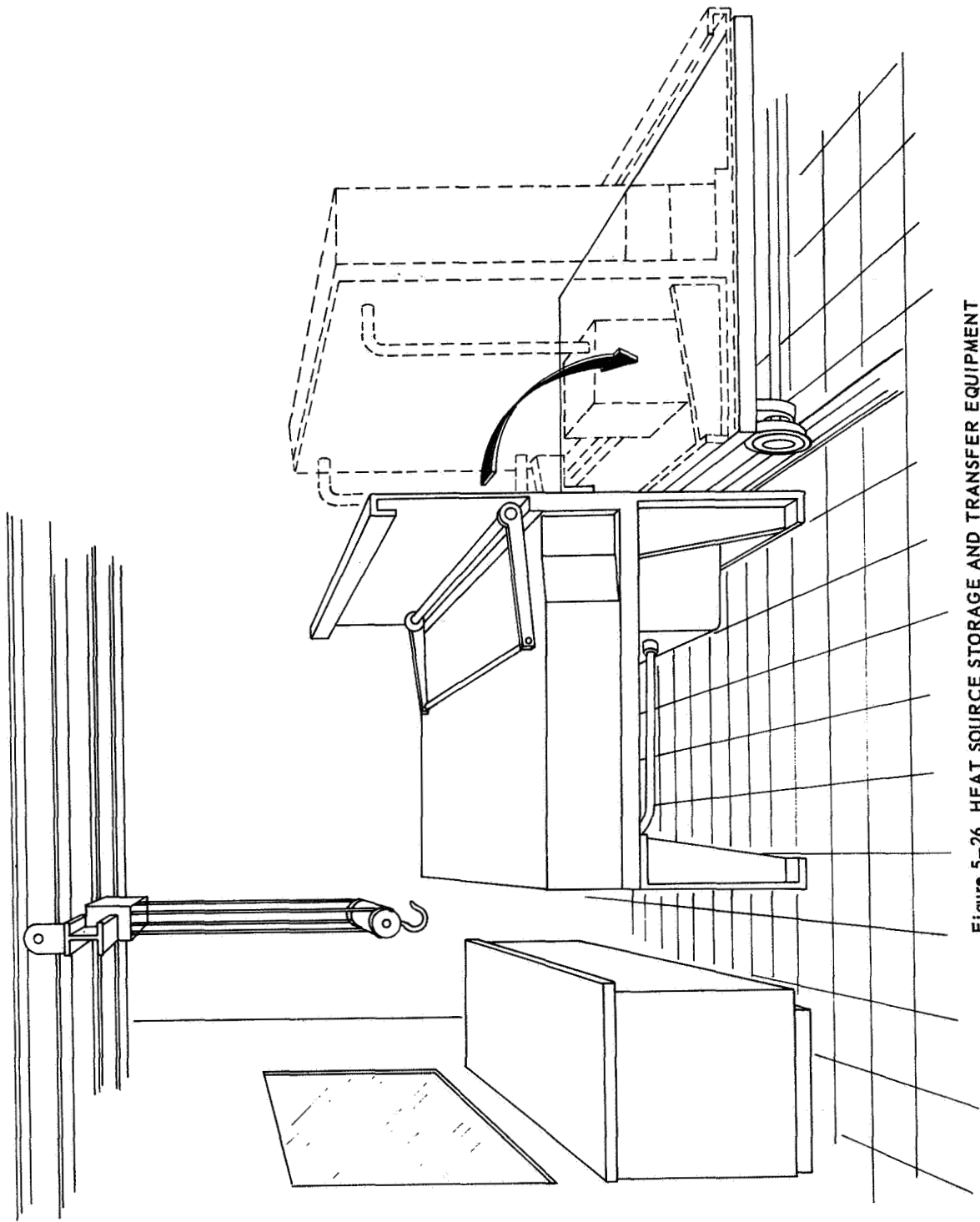


Figure 5-26 HEAT SOURCE STORAGE AND TRANSFER EQUIPMENT

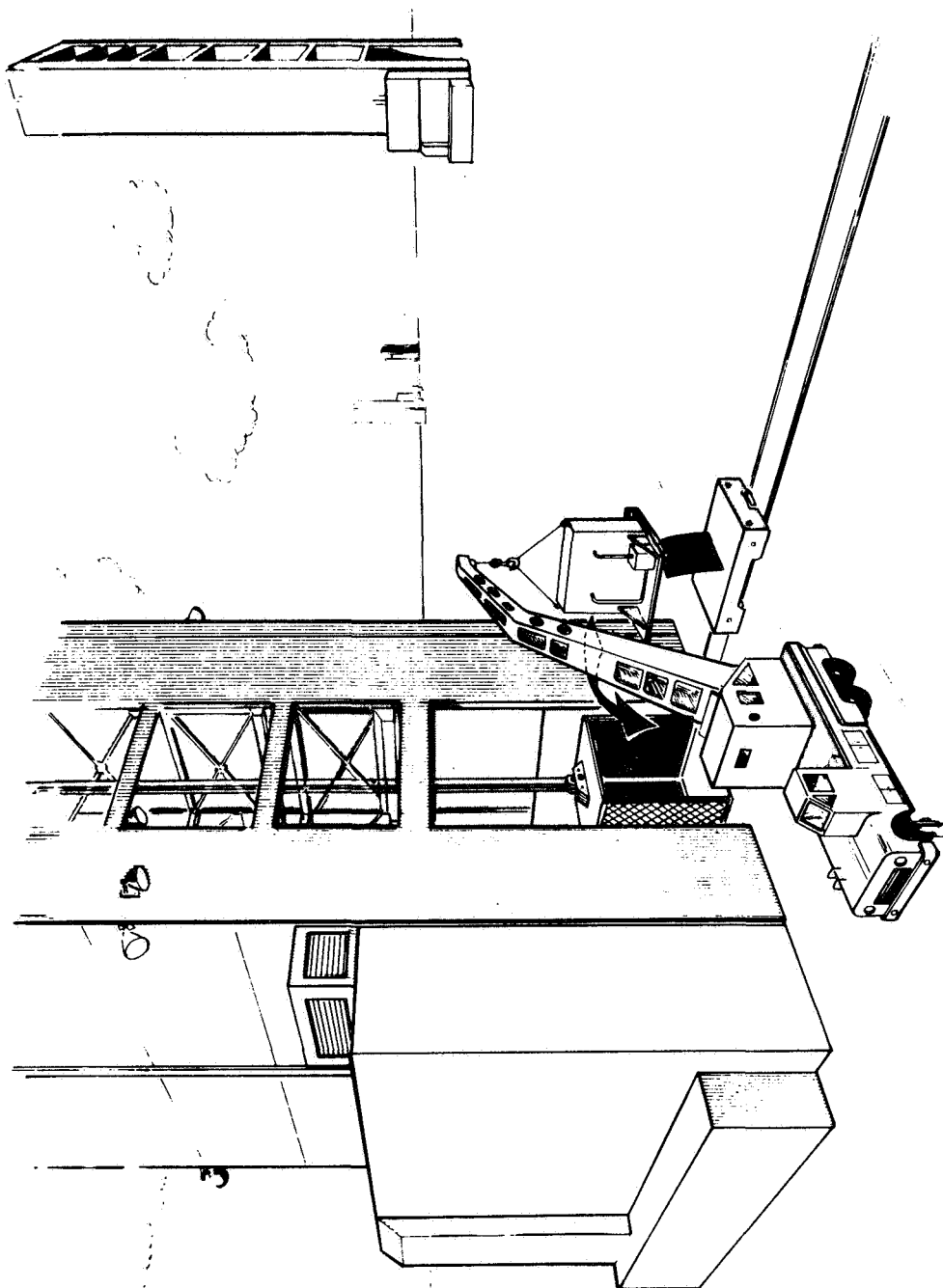


Figure 5-27 TRANSFER OF HEAT SOURCE TRANSPORTER TO GANTRY

In either case, transfer of heat source, installation, and locking in place operations would be accomplished by an operator behind a lightly shielded wall provided by the transporter.

5.3.6 ACHX Launch Pad Hook-up and Installation

The transportation of the heat source plate assembly to the launch pad and its elevation to the transfer area were accomplished with the transportable ACHX supply system operating in the closed transporter. As stated earlier the ACHX is an important element during ground handling in maintaining the refractory metal heat source plate below 350° F.

After the heat source plate has been transferred to the aeroshell as shown in Figure 5-28 and securely locked in position by the lock pins, the transportable ACHX supply lines must be replaced by the lines which are installed in the launch vehicle to permit closing of the aeroshell. As stated previously the lines have been designed with quick connect and disconnect couplings. Figure 5-29 shows five stages of ACHX connection which will be utilized on the launch pad. (The basic IRV spacecraft recounting concept is described in Section

The first operation is the locking of the heat source into the aeroshell which is in the deployed position. This cross section shows four permanent lines which pass through the Brayton cycle heat source heat exchanger cavity. Through these permanent lines are the flexible flow lines which are shown on stage two (launch pad coolant connected). Again care must be exercised in disconnecting and connecting these lines which should be controlled individually and transferred one at a time. The heat source cooling connection and the heat source plate have been designed to receive both transportable and permanent lines internally, these can be readily adapted to most available quick disconnects couplings.

Once the heat source plate has been transferred to the launch pad cooling, the closing of the IRV aeroshell can be accomplished without undue problems. It should be noted that the launch pad cooling lines pass through the insulation shutters behind the Brayton cycle heat source heat exchangers. These shutters are left open at launch, and closed prior to Brayton cycle operation once the vehicle is in orbit.

Stage three of the operation entails the closing of the IRV aeroshell to its operating position. This will be achieved mechanically with the deployment mechanism. Again care must be exercised in pulling back the flexible lines through the permanent guide tubes, and during the final stages of closing when the permanent guide tubes mate with the heat source cooling connection.

This is shown during the launch stage of operation when the launch vehicle is set ready to launch. Teflon gaskets actually make the final connection; this has been designed to ensure that after operating temperature has been reached, the Teflon gasket sublimates and a gap exists between the IRV and Brayton cycle system. It was felt that at 2000° F a possibility exists that with metal connections a space weld might have occurred which would jeopardize the deployment of the aeroshell in space.

Once this connection is made and the aeroshell locked in launch position, the flexible lines are withdrawn to the outer end of the guide tubes and again automatically connect to a quick disconnect coupling which has been designed specifically for this function.

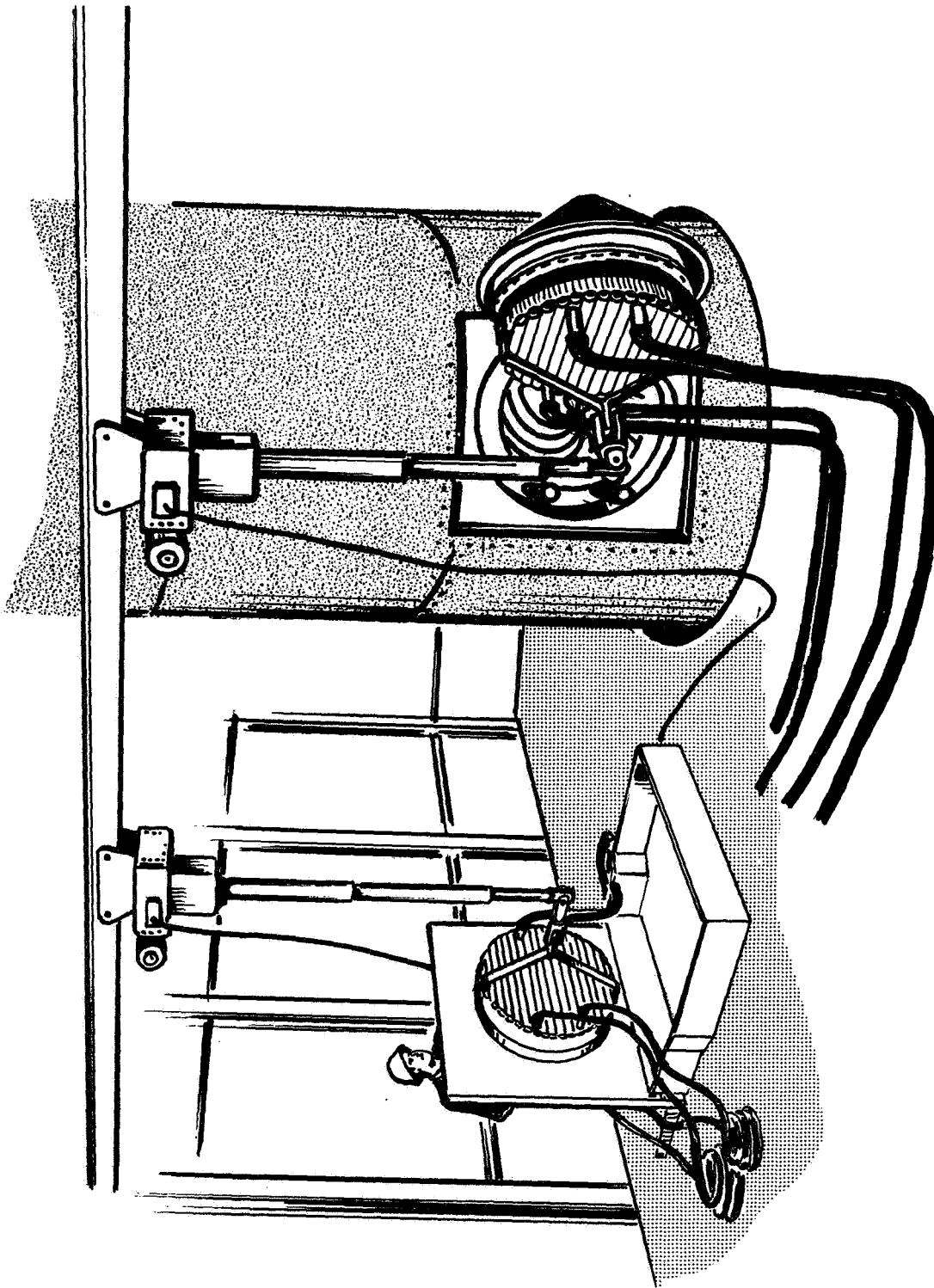
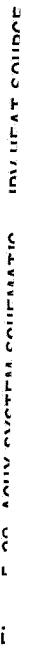


Figure 5-28 HEAT SOURCE INSTALLATION



The system can now operate for an indefinite period of time until launch, but controlled air flow and temperature monitoring is mandatory during this stage of operation.

The final stage is completed during the launch stage. At that time the ACHX lines are retracted, carrying with them the connection which was attached to the guide tubes located below the insulation shutter. This leaves clearance for the shutter doors to be closed.

5.4 REFERENCES

- 5-1 Brayton Cycle Power Conversion System for Pu-238 Fielded Electrical Power System Manned Orbital Laboratory (MORL) Volumes 1 through 4, Garrett Aircsearch Report M-2000.
- 5-2 HSHX Design Study. Topical Report, Garrett Aircsearch Report No. 68-3257 (January 31, 1968).

APPENDIX A

HEAT SOURCE AND SUPPORT SYSTEM STRUCTURAL ANALYSIS

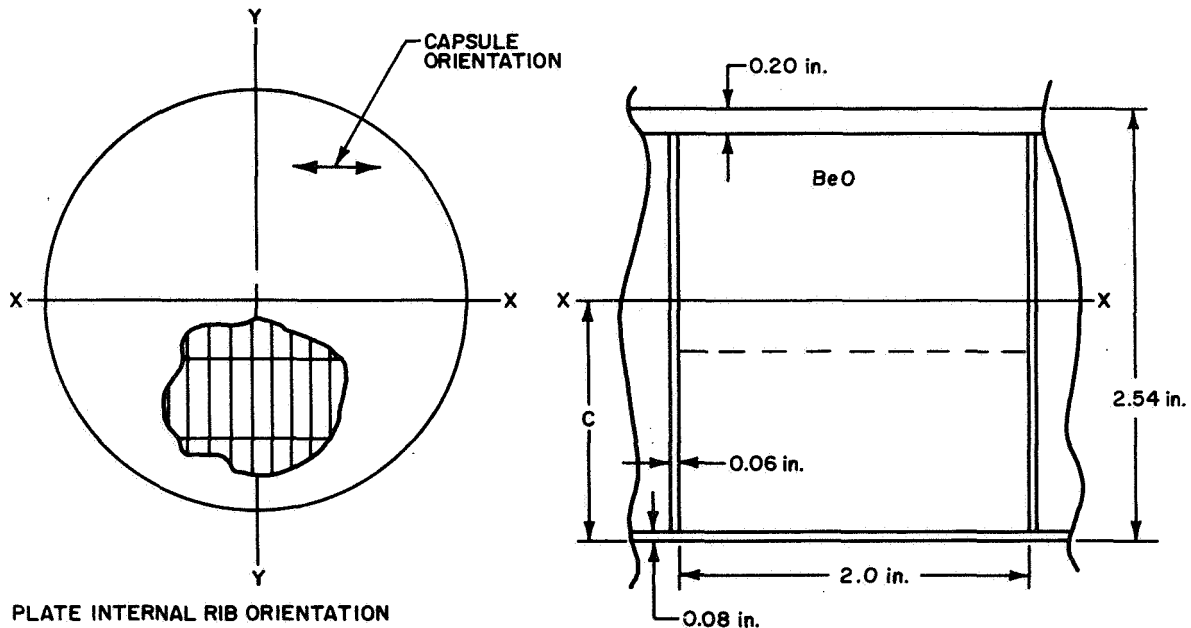
A1.0 STRUCTURAL ANALYSIS OF HEAT SOURCE PLATE

A1.1 PLATE AS A WHOLE

The plate as a whole can fail in flexure under axial g-loads. To determine its capability, the following assumptions were made:

- The BeO and its retention plate do not contribute to the plate flexural stiffness
- The capsules and cover retention plate do not contribute to the plate flexural stiffness
- Although the plate is anisotropic, a uniform flexural stiffness equal to the minimum value is assumed.
- The peripheral ACHX header, which is stiffer than the rest of the plate and which overhangs the plate support, can be neglected
- Any in-plane loads transmitted from the support ring can be neglected.

A typical cross-sectional view is shown:

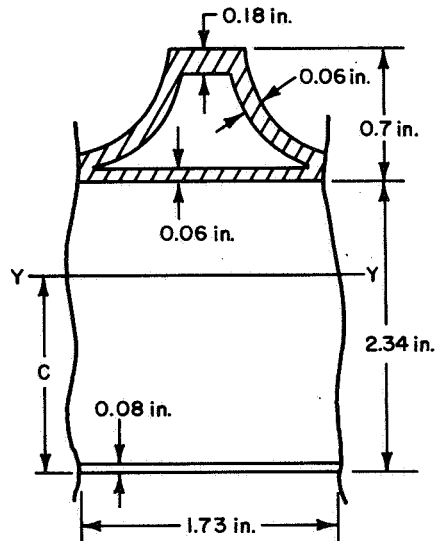


The flexural stiffness about the XX-axis is:

$$I_{XX} = 0.3024 \text{ in.}^3$$

$$Z_X = \frac{I}{C} = 0.1733 \text{ in.}^2$$

The flexural stiffness about the YY-axis can be estimated from a typical repeating cross-section as shown.

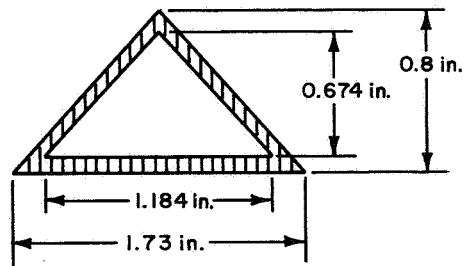


Assuming that the curved support with 0.18-inch top can be approximated by a 0.06-inch-thick triangle 0.8-inch high, the resultant flexural stiffness about the YY-axis is

$$I_{YY} = 0.3338 \text{ in.}^3$$

$$Z_Y = 0.1664 \text{ in.}^2$$

Therefore, let $Z_Y = Z_X = 0.1644 \text{ in.}^2$



For a 1300-pound heat source W , which is supported at $R = 21$ inches, the elastic load limit is given by

$$M_{\max} = 0.206 p_o R^2$$

where

$$p_o = \frac{W_g}{\pi R^2}$$

So

$$M_{\max} = 85.3 \text{ g}$$

Consider both reentry cases. Let

$$\sigma_{\max} = \sigma_{\text{yield}} \text{ at } 500^{\circ}\text{F} = 33 \text{ ksi} \begin{cases} \text{abort*} \\ \text{reentry} \end{cases} \text{ and}$$

$$\sigma_m = \sigma_y \text{ at } 1900^{\circ}\text{F} = 22 \text{ ksi} \begin{cases} \text{orbit} \\ \text{reentry} \end{cases}$$

Case 1.

$$\sigma = \frac{M}{Z}$$

$$\text{capability} = 63.6 \text{ g}$$

Thus, the factor of safety (fs) on early abort on reentry is 2.09.

Case 2.

$$\text{capability} = 42.4 \text{ g axial } \frac{42.4}{11.3}$$

The fs on normal is 3.75.

A1.2 ACHX HEADER PANELS

The header plate bending stress under 110 psig (maximum possible) header gas pressure is given by

$$\sigma = \frac{p \ell^2}{p t^2}$$

where

p = pressure, 110 psi

t = panel thickness = 0.10 inch

ℓ = panel length between fixed-end conditions

thus

$$\sigma = 26,500 \text{ lb/in.}^2$$

The allowable is the yield strength of Cb-1Zr at 200°F , which is the ACHX maximum operating temperature. The maximum operating header pressure is 110 psig (90 psig design). Allowing a 1.25 factor of safety for weld efficiency, etc., the resulting allowable stress is

* At launch the heat source temperature is 350°F ; therefore, a heat source temperature rise to 500°F prior to early launch abort is conservative.

$$\sigma_a = \frac{34,000}{1.25}$$

$$\sigma_a = 27,200 \text{ lb/in.}^2$$

Hence the 0.10 inch panel thickness is satisfactory.

A1.3 BeO RETENTION PANELS

The BeO retention panel is 0.04-inch thick, and the 50 percent perforated Cb-1Zr plate 2 x 10 inches. The weight that the panel and weld must support is

$$W = [(\rho t \ell w)_{\text{panel}} + (\rho + \ell w)_{\text{BeO}}] (g_{\text{max}})$$

which gives $W=134 \text{ lb.}$ for 38 g.

This load is mainly seen as a shear load to the panel welds as shown. The total length of tack welds required per panel can be determined as follows:



Assume that the tack weld strength is 20 ksi. (Cb-1Zr yield strength at 1800° F)

$$\text{Weld Shear Area} = (0.7) (\ell) (h) = \frac{W}{\sigma} = \frac{134}{20,000}$$

so $\ell = 0.24 \text{ inch}$ total length of tack weld is required per panel.

For a full-length peripheral weld of 24 inches length, the capability would be about 3800 g.

A1.4 INTERNAL RIBS

To yield the plate internal ribs in compression to the capsule weight, first neglect the BeO and retention reinforcement of the rib. For a uniform heat source weight distribution per panel of 0.69 lb/in². per g.

Since $\sigma_y = 33 \text{ ksi}$ at 500° F for ascent abort of 38 g, then the compressive load capability is 1147 g to yield, which gives a fs of 37.7.

To buckle in compression (reference "Introduction to Structural Stability Theory" by G. Gerard, McGraw-Hill Co.) The panel aspect ratio for a 10-inch-long, 2.28-inch-high panel, is 0.228. For fixed edges, the buckling coefficient then is approximately 20. From the stability equation:

$$\sigma_{cr} = \frac{\pi^2 KE}{12 (1 - \nu^2)} \left(\frac{t}{\ell} \right)^2$$

where

K = compressive buckling coefficient

E = Young's modulus

ν = Poisson's ratio

t = rib thickness

l = rib length,

the critical buckling stress is $\sigma_{cr} = 1450 \text{ lb/in.}^2$. Thus the g-load capability is 50.3 g.

A1.5 RETENTION BOLT FOR TOP COVER

Consider 194 bolts, evenly located approximately one per capsule, to adequately locate and retain each capsule. Vibration effects resulting in fretted surface coatings are thereby minimized. The bolt size of 0.164-inch diameter has a root diameter of 0.129 inch. A T-111 bolt has a load capability of 690 pounds during abort reentry and 480 pounds during orbit reentry, assuming the temperature environment noted in subsection A1.3. Thus, a total load capability of 133,500 and 93,000 pounds exists respectively, which is more than any structural requirements. However, the possibility of thermal stresses, nonloaded bolts, stress-relaxation effects, and dynamic loads with their stress concentration effect requires a large safety margin. The requirement of maintaining a tight interface load on the capsule to prevent fretting under vibration is of utmost importance, since the iron titanate coating would be degraded.

A1.6 SUPPORT PLATE LOCK PIN ASSEMBLY

For the heat source support plate to become free of the IRV, four lock pins would have to shear, or the retention lugs would have to shear. Four loading cases exist:

- a. Lateral loads--plate bears against support ring
- b. Angular acceleration--four pins limit load
- c. Axial loads (+)--no problem for pins
- d. Axial loads (--plate withheld by interlocking lugs.

The results of these four cases for the holddown pins are as follows:

- a. No problem for the pins
- b. Angular acceleration could cause the pins to shear at angular acceleration greater than 14.2 rad/sec.^2
- c. No problem for the pins
- d. For uniform loading on all plate and ring retention lugs, the shear stress is only 390 lb/in.^2 for a negative 9g load.

Hence, the lugs are adequate even if some nonuniform loading occurs.

A1.7 ACHX HEADER OUTLET PIPE LOAD LIMITATIONS

Header inlet-outlet tubes have design load limitations which must be noted during handling operations. These header inlets/outlets consist of 1.5-inch I.D., 1.625-inch O. D., 5-inch-long tubes integrally welded to the heat source plate structure.

The load limitations which must be noted to prevent loss of gas cooling to the ACHX are as follows:

- a. The tube-end radial load limit is 630 pounds based on yielding at the built-in end of the tube (weld) at 350°F.
- b. The axial load limit is 9800 pounds based on shear of the tube to plate weld junction.

A2.0 DYNAMIC ANALYSIS OF HEAT SOURCE AND SUPPORT SYSTEM

In the preliminary design the anticipated significant fundamental resonant frequencies were computed.

The resultant design vibratory resonant frequencies were determined for the case of the heat source mass axially resonating on the struts. This is believed to be the worst case. The areas considered with corresponding results are as follows:

- a. Heat source plate fundamental resonant frequency - $f_1 = 30.2$ Hz (umbrella mode)
- b. Strut lateral resonant frequency - $f_1 = 393$ Hz
- c. Lateral resonance of truss-heat source - $f_1 = 318$ Hz
- d. Vertical vibratory resonance of truss-heat source - $f_1 = 81$ Hz
- e. Vibratory stress level in the strut for case d - $\sigma_{\max} \leq 78$ percent of the endurance strength

It should be noted in items c, d, and e that the assumption has been made that the heat source support plate represents a mass and the truss represents a spring or beam. No consideration is given to other components or the aeroshell in this analysis.

A2.1 HEAT SOURCE PLATE FLEXURAL RESONANT FREQUENCY

The plate flexural stiffness is

$$D = \frac{EI}{1 - \nu^2} = 1.662 (10^6) \text{ lb} - \text{in.}^2$$

Now the fundamental frequency is given by

$$f = \frac{\alpha_1}{2\pi} \sqrt{\frac{D}{\mu r^4}}$$

where

$$\alpha_1 = 3.75 \text{ for the umbrella mode}$$

$$r = \text{radius}$$

$$\mu = \frac{1300}{\pi (386) r^2} = \text{mass per unit area.}$$

Result:

$$f_1 = 30.2 \text{ Hz}$$

A2.2 STRUT LATERAL RESONANT FREQUENCY

The struts are intended to approximate built-in end conditions; thus

$$f_n = \frac{a_n}{2\pi} \sqrt{\frac{EI}{\mu \ell^4}}$$

where

$$E = 25 \times 10^6 \text{ lb/in.}^2 \text{ (during launch, slightly less at temperature)}$$

$$I = 0.29 \text{ in.}^4$$

$$\ell = 19 \text{ in.}$$

$$\mu = \frac{W}{g_c \ell} = \frac{\rho A}{g_c}$$

$$\rho = 0.604 \text{ lb/in.}^3$$

$$A = 0.283 \text{ in.}^2$$

$$g_c = 386 \text{ in/sec}^2$$

$$a_1 = 22, \text{ for the first mode}$$

$$a_2 = 61.7, \text{ for the second mode.}$$

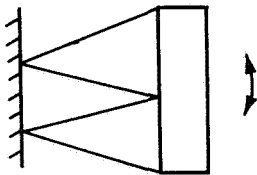
The resultant resonant frequencies are $f_1 = 393 \text{ Hz}$ and $f_2 = 1100 \text{ Hz}$.

All higher resonant frequencies are greater than 2000 Hz.

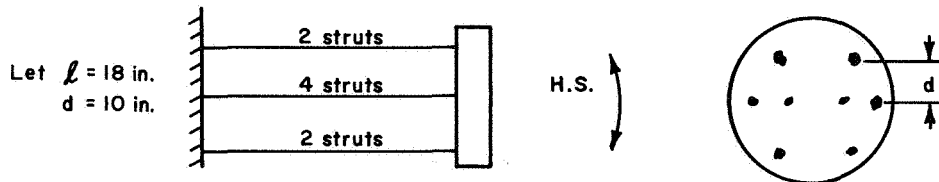
A2.3 LATERAL RESONANCE OF TRUSS HEAT SOURCE

Lateral vibratory motion can include:

1. Bending of struts (both end fixed)
2. Axial elongation of outer struts
3. Rotation of struts.



The stiffness of the system was approximated by the truss as shown.



Then the spring constant is determined from:

$$K = \frac{3EI}{\ell^3}$$

where

$$I = 8I_s + 4A_s d^2 = 1132 \text{ in.}^4$$

and

$$I_s = \text{Strut moment of inertia}$$

$$A_s = \text{Strut cross-sectional area}$$

so that

$$K = 13.4 (10^6) \text{ lb/in.}$$

Result:

$$f_r = 318 \text{ Hz}$$

A2.4 VERTICAL VIBRATORY RESONANCE OF HEAT SOURCE ON TRUSS

The total truss system spring constant is given by

$$K_T = \frac{8AE \sin^2 \alpha}{\ell}$$

Since the resonant frequency is given by

$$f_r = \frac{1}{2\pi} \sqrt{\frac{K_T g_c}{W}}$$

where

$$\alpha = 34^\circ$$

$$g_c = 386 \text{ in/sec}^2$$

$$W = 1300 \text{ lb (heat source weight)}$$

$$E = 25 (10^6) \text{ lb/in.}^2 \text{ (during launch, slightly less at temperature)}$$

consequently:

$$f_r = \frac{1}{2\pi} \left[\frac{8AE g_c \sin^2 \alpha}{W} \right]^{1/2}$$

$$f_r = 81 \text{ Hz.}$$

A2.5 VIBRATORY STRESSES IN IRV STRUT

Since most components/subassemblies have resonant frequencies less than 2000 Hz, resultant vibratory stresses occur. Consider Case A2.4 which will probably represent the worst dynamic stress.

$$\text{Define Amplification} = A_r \frac{\text{Force to Heat Source}}{0.25 \text{ g input force}} = \frac{F_{H.S.}}{F_i}$$

Where $F_i = 0.25 \text{ g}$ is specified in article 2.3.2 of Specification P1224-1, "Brayton Cycle Subsystem and Components Environmental Specification".

A_r is a function of material and system damping at resonance, and is obtainable only through experimental testing. One reference ("Shock and Vibration Handbook", Vol. II, p-36-3, C. Harris and C. Crede) gives an A_r value of 91 for a mass on a strut in which material and system damping are small. The material damping can be expected to increase as the temperature increases above room temperature since inelastic effects increase the damping associated with the material hysteresis loop:

$$\text{For } A_r = 91$$

then

$$F_{H.S.} = 22.7g$$

which will present no problem for the struts and heat source support plate. Another way of determining the vibratory stresses is by estimating only the strut material damping. Since the strut is at uniform tension-compression under vibratory loading, A_r is given by (reference Harris and Crede)

$$A_r = \frac{\pi \sigma^2}{ED}$$

where

σ = maximum stress at resonance

E = modulus of elasticity

D = specific or average damping energy.

D must be estimated for the T-111 struts since it can be found only experimentally and is a function of numerous variables, including temperature, stress history, vibratory stress level frequency of vibration, etc.

During boost, the temperature $\leq 500^\circ \text{ F}$; thus assume the endurance strength of the struts is approximately 55 ksi.

Then Harris and Crede give the following formula for D which represents most materials with sufficient accuracy.

$$D = \left(\frac{\sigma}{\sigma_e} \right)^{2.3} + 6 \left(\frac{\sigma}{\sigma_e} \right)^8$$

Assume the vibratory stress level is $\sigma = 0.779 \sigma_e = 42,800 \text{ lb/in.}^2$

At that level, the damping D is 1.379.

Thus, the amplification factor A_r is 166.

$$\text{Hence } F_{H.S.} = 0.25 (166) = 41.5 g,$$

which is the alternating load the struts would experience at takeoff.

The strut stresses are given by

$$\sigma = \frac{1300 F_{H.S.}}{8 (\sin 34) A_s}$$

where

$$A_s = \text{strut area} = 0.278 \text{ in.}^2$$

Consequently

$$\sigma = 1045 F_{H.S.}$$

$$\sigma = 43 \text{ ksi}$$

which is approximately the vibratory stress level assumed to get the damping coefficient. Therefore, the truss can withstand the axial resonant frequency during launch, when the truss amplitude may get as high as 78 percent of the endurance strength.

A3.0 STRUCTURAL ANALYSIS OF TRUSS SUBSYSTEM AND SUPPORT SYSTEM

The structural analysis of the truss subsystem includes the following components. (The greatest structural requirement each component was designed to withstand is also noted).

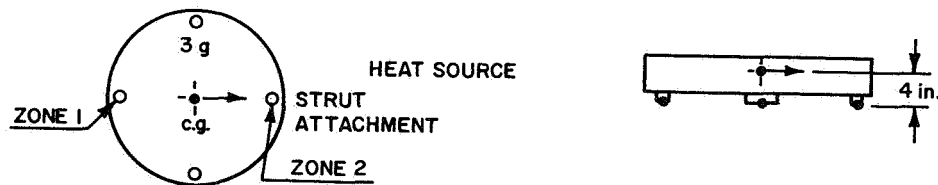
1. Struts - must survive the same abort and reentry g-loads the heat source can experience.
2. Support Ring and Tie Plate - must survive the stresses of the truss load components during reentry.
3. Truss Attachment Bolts - must withstand reentry loads but shear upon impact.

Truss bending stress due to thermal expansion/contraction of the heat source is also treated in this section.

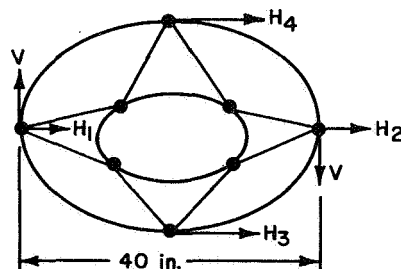
A3.1 STRUTS

The strut must survive axial compressive stresses and buckling during reentry. The worst case is the possibility of a strut sustaining an axial g-loading plus an additional load due to the lateral g-loading.

It is assumed that the heat source c.g. is 4 inches above the strut attachment to the support ring in the analysis as illustrated below.



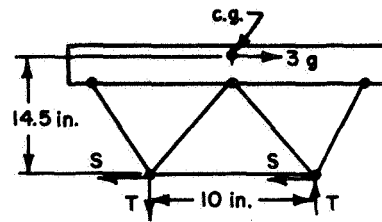
The orientation of the lateral loading is also assumed as shown. Two struts will then see an increase in axial compressive loading (i.e., the two struts at Zone 2).



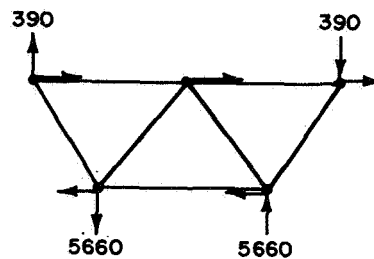
Since the horizontal shear loads H_1 , H_2 , H_3 , H_4 cannot be readily evaluated, and since they reduce the axial loading, they are neglected, and the effect of V only is evaluated. For a heat source weight of 1300 pounds, then summing the moments about Zone 1 must be equal to zero, thus for a heat source c.g. in a plane 4-inches above the truss attachment zone:

$$40 V = 4 (1300) (3)$$

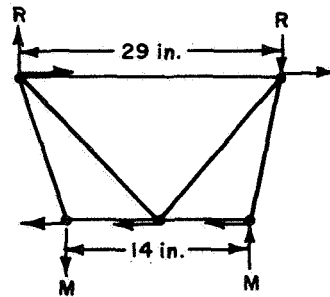
$$V = 390 \text{ lb.}$$



Looking at the bottom end of the heat source and truss and summing moments, $T = 5660 \text{ lb.}$ Hence, the truss assembly is loaded as shown below:

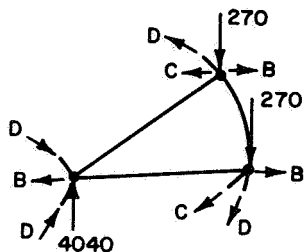


Now the truss can be loaded at other angular positions (about IRV) up to 45 degrees from the previous case, upon which the loading is shown. Proceeding as before gives $R = 539 \text{ lb}$ and $M = 4040 \text{ lb.}$



Because the truss is three-dimensional, the load, $T/2 = 2830 \text{ lb.}$ exists at four separate locations. The load $R/2 = 270 \text{ lb}$ exists at each of four joint locations, while the load $M = 4040 \text{ lb}$ exists at two joint locations. One of these two possibilities will represent the worst loading case for a strut (on compression), while all other cases of truss orientation will fall in between. Breaking the truss up will lead to a load distribution for each strut, but only the one seeing the greatest axial compressive load is of concern, since that load plus the axial g-load case will represent the worst stress and buckling case. The worst case appears to be under load $M = 4040 \text{ lb}$ as shown.

3-D LOAD DISTRIBUTION - WORST CASE

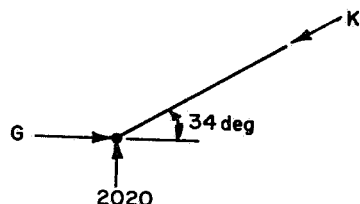


B = shear loads

C = strut load in two symmetrical adjoining struts

D = ring loads to struts

By symmetry, each of the two struts will see $4040/2 = 2020$ -lb load vertical. Hence, sectioning one of the struts and viewing it in its own vertical plane perpendicular to the heat source.



K = axial load

G = summed horizontal loads to struts

$$\Sigma F_{\text{vertical}} = 0$$

$$K = 2020 / \sin 34^\circ$$

$$\text{Thus, } K = 3610 \text{ lb.}$$

Thus, the maximum strut axial load under an IRV lateral g-load is 3610 pounds. Now the axial g-load per strut is to be added to this value.

For the worst case - abort reentry:

$$\text{Axial g-load} = 38 \text{ g}$$

$$\text{Lateral g-load} = 3 \text{ g}$$

Axial g-load strut loading:

$$L = (\text{wt})(\text{g-load}) / (\text{no. struts})(\sin 34^\circ)$$

$$L = (1300)(38) / (8)(\sin 34^\circ)$$

$$L = 11,040 \text{ lb.}$$

Total maximum axial load in a strut is

$$L_{\text{max}} = 11,040 + 3610$$

$$L_{\text{max}} = 14,650 \text{ lb.}$$

Stress Criteria

For the stress to be less than yield stress at abort temperature ($\leq 500^\circ\text{F}$), the required cross-sectional area is 0.278 in.^2 for $\sigma_y = 53 \text{ ksi}$.

Let the O.D. = 1.0 in.; then the tube I.D. can be determined.

$$\text{I.D.} = \left[1 - \frac{4}{\pi} (0.278) \right]^{1/2}$$

Hence, an I.D. of 0.8 inch minimum is required.

Buckling Criteria

The g-load capability in buckling is given by the transcendental equation:

$$\frac{\ell}{2} \sqrt{\frac{wg}{8EI \sin 34}} = \left[\tan \left(\frac{\ell}{2} \sqrt{\frac{wg}{8EI \sin 34}} \right) \right] \left[1 - \frac{w \sigma_y}{4 E \rho A D \cos 34 \sin 34} \right]$$

where:

- ℓ = strut length ≈ 19 in.
- w = heat source weight ≈ 1300 lb
- E = 25×10^6 lb/in² at 500° F
- D = strut O.D. = 1.0 in.
- d = strut I.D. = 0.8 in.
- I = $\pi/64 (D^4 - d^4) = 0.029$ in.⁴
- σ_y = 53 ksi at 500° F
- ρ = T-111 density = 0.604 lb/in.³
- A = strut cross-sectional area = 0.278 in.²

Solving by trial and error, over 200 g are required before buckling occurs.

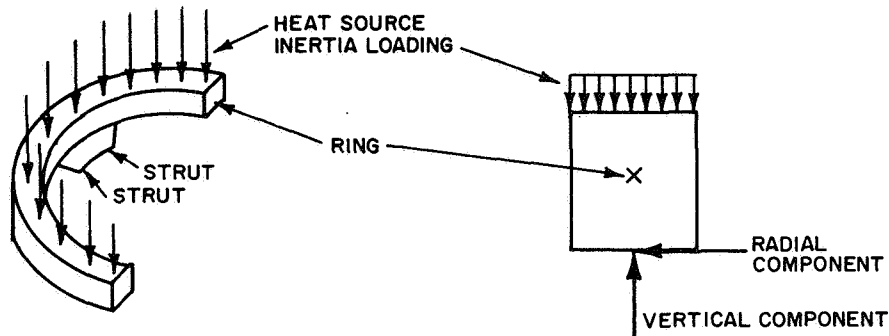
Thus, while the cross-sectional area must remain the same, it would be possible to use a smaller O.D. and I.D. for the strut. However, since the above calculations assume built-in ends which cannot be achieved in reality, allowing an additional factor of safety for this effect and an additional factor of safety for the fact that the struts may see some deflection-dependent end moments also, the estimated g-load capability would be reduced. Since the area must remain the same, however, no weight saving is possible. Hence, optimization of the diameter for buckling is unnecessary.

A3.2 SUPPORT RING AND TIE-PLATE ANALYSIS

The truss assembly supports the heat source support plate by means of a complete ring. This support ring provides peripheral support for the heat source. The ring is attached to the truss of four main separate position 90 degrees apart with four minor adjoining sections in-between. These specific positions were

selected to furnish the maximum support for the support plate and to minimize changes to the heat source plate required by the attachment pins and ring slot. The support ring must a) transpose the four-point truss support into a peripheral support of the heat source plate, b) complete the truss assemblage, c) sustain the radial loads induced by the truss design, and d) furnish an attachment re-straint for the remote assembly of the heat source assembly to the IRV. The structural design of the support ring is determined by the abort reentry loads (worst condition).

Since the struts are at an angle to the support ring, the ring undergoes a vertical and radial component load as shown.



Preliminary analysis indicated that to limit the radial deflection of the ring, a ring tie plate would be required to prevent damage to the heat source support plate. The minimum weight design would be a cross-tie which, together with the ring, must sustain the radial load, P.

The radial load P at four locations is given by

$$P = 2 (\text{strut axial load at abort reentry}) (\cos 34^\circ) \cos (\beta/2)$$

where

$$\beta = \text{Angle between struts in the plate of the ring} = 30^\circ.$$

therefore

$$P = 2 \times \left(\frac{1300 (38)}{8 \sin 34^\circ} \right) \cos 34^\circ \cos 15^\circ$$

$$P = 17,700 \text{ lb.}$$

Where the possible simultaneous lateral inertia loading is neglected since this would result in four unidirectional loads on the ring rather than four radial loads. The radial deflection of the tie plate and the ring must be equal at their interface.

Thus,

$$\Delta R)_{\text{tie}} = \Delta R)_{\text{ring}}$$

where

$$\Delta R)_{\text{tie}} = \frac{RQ}{AE}$$

$$\Delta R)_{\text{ring}} = (0.00608) \frac{WR^3}{EI}$$

where

Q = load carried by cross-tie

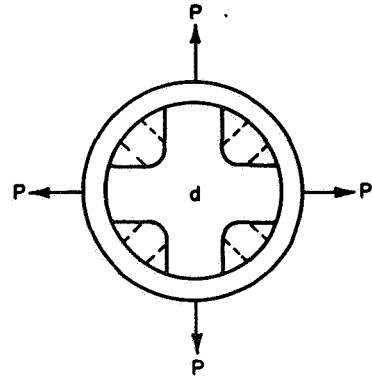
W = load carried by ring

P = Q + W = 17,700 lb

R = interface radius, 20.2 in.

A = tie cross-sectional area

I = ring cross-sectional area moment of inertia = 0.431 in.⁴ at the zones where the load is applied.



DOTTED LINES ARE OPTIONAL
TIE CONNECTIONS

Thus for a tie thickness of 0.060 in., a tie width, d, can be determined:

$$\frac{RQ}{AE} = 0.00608 \frac{WR^2}{EI}$$

or

$$Q = 0.00608 \frac{AWR^2}{I}$$

thus,

$$Q = 0.345 dW$$

where

d = tie plate section width

$$d = \frac{Q}{(0.06) \sigma_w} = \frac{Q}{1800}$$

where

σ_w = 30,000 lb/in² is the estimated weld strength for the critical weld at the tie-ring interface.

So substituting the relationships containing Q and W into

$$Q + W = 17700$$

$$17700 = 1800 d + \frac{1800 d}{0.345 d}$$

gives $d = 7$ inches which is the minimum section width required.

The resultant stress in the ring due to the load $W = 5200$ lb and is

$$\begin{aligned}\sigma &= 0.0533 \frac{WR}{I} \\ &= \frac{0.0533 (5200) (20.2)}{(0.431)}\end{aligned}$$

$$\sigma_{\text{ring}} = 13,000 \text{ psi}$$

The radial deflection is

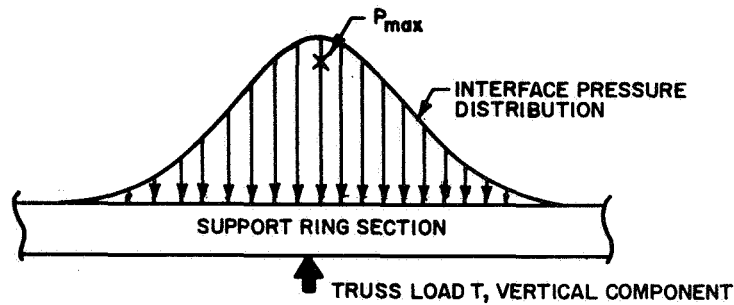
$$\Delta R = \frac{RQ}{AE}$$

$$\Delta R = 0.121 \text{ in.}$$

If the heat source support plate does not allow such localized deflections of the ring, the plate will further restrict the stresses so that the tie plate stress of 30,000 lb/in.² and the ring stress of 13,000 lb/in.² will represent the upper limit.

In addition to the $\pm 13,000$ lb/in.² bending stress, the ring will have a hoop tension stress and also experience flexure about an axis parallel to the plane of the ring. The hoop tension in the ring due to the radial loads is 1330 lb/in.².

The bending stress due to the plate load can be found by assuming the ring-plate interface loading can be approximated by beam-on-elastic foundation theory. Preliminary calculations lead to the conclusion that a very large ring would be required to convert the truss-support reactive loads into a circumferentially uniform interface loading between the ring and the support plate. Such a weight penalty is not desired, nor is it necessary to furnish such a uniform loading. Hence, it will be assumed that a circumferentially varying load will be exerted on the ring. The heat source plate will (for simplicity) be assumed to have a constant foundation modulus while in actuality the plate will deform such as to have its whole periphery supported. The following analysis considered the case shown below.



The ring section is considered to be a straight section resting on an elastic foundation ("Beams on Elastic Foundation" by M. Hetenyi, University of Michigan Press).

A ring width of 1.50 inches has been used. The desired ring thickness is that necessary to allow the truss to support the heat source support plate during reentry, so as to preclude damage to the plate from the strut support, while not allowing overstressing of the ring. Near each of the four truss loads, T, the ring has a maximum bending stress of

$$\sigma = \frac{Tt}{8I\lambda}$$

where

t = ring thickness

I = ring section moment of inertia

$$\lambda = \sqrt[4]{\frac{K}{4EI}}$$

E = Young's modulus of the ring

K = plate foundation modulus

and the maximum interface pressure, P_{max} (lb/in.²), is given by

$$P_{max} = \frac{K}{1.5} Y_{max}$$

$$= \frac{K}{1.5} \frac{T}{2K}$$

$$P_{max} = \frac{T\lambda}{3}$$

The ring must withstand the combined tensile stresses due to the vertical and radial loads exerted on the ring during abort reentry.

$$1300 + 1330 + \frac{TC}{4I_{\lambda}} = \sigma_y = 33,000 \text{ lb/in.}^2$$

or

$$\frac{TC}{4I_{\lambda}} = 18,670 \text{ lb/in.}^2$$

since

$$\lambda = \frac{3 P_{\max}}{T}$$

then

$$P_{\max} = \frac{T^2 C}{12 (18,670) I}$$

for

$$C_{\max} = 0.925 \text{ in.}$$

$$I = 0.431 \text{ in.}^4$$

$$T_{\max} = \text{axial g-load component} + \text{lateral g-load components} = 6570 \text{ lb.}$$

Then the interface compressive loading is

$$P_{\max} = 437 \text{ lb/in.}^2$$

The pressure approaches zero at a length of approximately

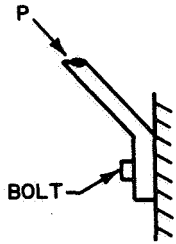
$$\ell = \frac{3\pi}{4} = \frac{\pi T}{4 P_{\max}} = 11.8 \text{ inches from } P_{\max},$$

However, at 5 inches away from the point of application of truss load, T, the interface pressure is down to one-half of P_{\max} . Hence, the ring can have a reduced section away from P_{\max} . This assumed that a plate modulus of K_p can be designed.

$$K_p = \left(\frac{3 P_{\max}}{T} \right)^4 4 EI = 69,000 \text{ lb/in.}^2$$

Now the actual foundation modulus of the plate structure could only be accurately determined experimentally. However, the desirability of having a plate with a foundation modulus in this realm is obvious. First, a low interface pressure load on the heat source support plate results, and secondly the support ring stress is limited. A very high modulus stiffness could cause failure of the plate while a very low modulus could overstress the support ring.

A3.3 STRUT-RING-BOLTS-TO-SHEAR ON IMPACT



Straight-on impact of the IRV is assumed; for 38 g minimum design failure loads, the bolt cross-sectional area required under worst reentry conditions can be determined. The vertical impact load at the four support pads due to the heat source and complete truss assembly weight combined is L.

$$L = \frac{(1300 + 140)(38)}{4}$$

$$L = 13,700 \text{ lb}$$

and using a bolt stress of 60 ksi at 350°F, which is the aeroshell's bolt temperature (estimated) for impact or abort reentry.

And P, the load required to shear the bolts but withstand reentry is

$$P > 2(14,650)(\sin 34^\circ) = 16,400 \text{ lb.}$$

Thus, the total bolt shear area at each of the four pads is

$$A > \frac{16,400}{60,000} = 0.274 \text{ in.}^2$$

and the impact g-load to shear the bolts then is 45.5 g, while on impact the struts won't fail until

$$g = \frac{N(\sigma_{ys})A \sin 34^\circ}{W} = 50.8 \text{ g}$$

where

$$N = \text{No. of struts} = 8$$

$$A = \text{strut area} = 0.278 \text{ in.}^2$$

$$\sigma_{ys} = \text{yield strength of strut material at } 500^\circ\text{F} = 53 \text{ ksi}$$

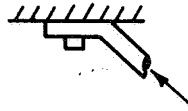
$$W = \text{heat source weight} = 1300 \text{ lb.}$$

Hence, the bolts will fail at 45.5 g load under vertical impact while the struts can survive 50.8 g vertical loads. The bolts will shear allowing the struts to fold down rather than bend or buckle which could cause penetration of the heat source. Under non-vertical impact, the bolts will still shear first, but at a lower g-load probably.

At top of struts, at 1500°F, assumed impact temperature, let

$$\sigma_s = 40 \text{ ksi}$$

Each of two strut loads, L, at a bolt location is



$$L = \frac{(1300)(38)}{8 \sin 34^\circ} = 11,040 \text{ lb.}$$

$$\begin{aligned} \text{Then, the shear load} &= 2L (\cos 34^\circ)(\cos 15^\circ) \text{ (reference support ring analysis)} \\ &= 17,700 \text{ lb.} \end{aligned}$$

Thus, the required area is 0.45 in.² (or more).

Summary:

Truss-Aeroshell Bolt Requirements: $A \geq 0.274 \text{ in}^2$. Use two bolts, 0.50 in. UNF, at each of four locations.

Truss-Support Ring V Bolt Requirements: $A \geq 0.45 \text{ in}^2$. Use three bolts, 0.5-inch diameter UNF at each of four locations.

A3.4 TRUSS BENDING STRESS DUE TO THE HEAT SOURCE PLATE EXPANSION

With the system in equilibrium on the launch pad, under loss of ACHX cooling (or during launch) the heat source will expand as it heats up from around 350° to 2000°F. Assuming the truss has not thermally adjusted, the struts will experience bending to accommodate the radial expansion of the heat source.

The heat source plate is given by

$$\Delta R = R \alpha \Delta T$$

where

R = radius

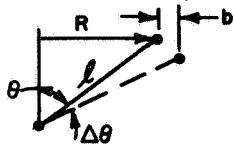
α = coefficient of thermal expansion

ΔT = temperature change.

thus,

$$\Delta T = 0.149 \text{ in.}$$

This change in radial position causes an in-plane rotation of the strut of δ , which can be found.



$$\text{Let } \theta = 56^\circ, \ell = 19.5 \text{ in, } b = \frac{\Delta R}{\cos \beta}, \text{ and } \beta = 15^\circ.$$

Now,

$$R = \sin \theta = 16.17 \text{ in.}$$

and

$$\sin(\theta + \Delta\theta) = \frac{R + 0.149/\cos \beta}{\ell}$$

$$\sin(\theta + \Delta\theta) = 0.83692$$

So,

$$\theta + \Delta\theta = 56^\circ 49'$$

Therefore,

$$\Delta\theta = 0.817^\circ$$

This is for a pinned joint with the resulting strut end deflection; then

$$\delta = \ell \Delta\theta$$

$$\delta = 0.278 \text{ in. (in-plane deflection)}$$

This deflection will cause a bending stress in the truss since both ends of the struts are built-in (worst case).

Since

$$\delta = 0.278 \text{ in.} = \frac{w \ell^3}{12 EI}$$

$$M_{\max} = \frac{w \ell}{2}$$

Then

$$\sigma_{\max} = \frac{Mc}{I} = 1.668 \frac{Ec}{\ell^2}$$

Assuming the strut pads act jointly with the struts, their bending stress is approximated by the above equation. Thus for $c = 0.125$ inch, the pad bending stress is $13,700 \text{ lb/in.}^2$. This would present no problem and would probably even relax with time at an elevated temperature.

APPENDIX B

STRUT HEAT LOSS

The truss support system, a direct mechanical linkage between the heat source support plate and the aeroshell, has a relatively poor thermal resistance and is, therefore, a major contributor to the heat losses around the system. During Phases 1A and 1B a truss system was designed that would meet stress and dynamic loading criteria with minimum thermal loss penalties. The resulting design consisted of eight T-111 and Rene-41 struts. Since it was a relatively complex structure to design and fabricate, struts consisting of all T-111 were recommended during Phase II for the preliminary design. A truss system of all T-111 struts had a larger heat loss than the bi-metal system; however, through improvements in the insulation the net change in total thermal losses was slight and did not materially alter the thermal performance.

The major components of heat transfer through the truss system consisted of conduction through the support pads and struts to the aeroshell and radiation from the surface of the struts to the aeroshell. The latter component was minimized by wrapping multifoil insulation around the struts. Analysis of the heat losses was performed based on the model shown in Figure B-1. Two struts attached from one ring pad in parallel to two aeroshell pads at the same temperature were analyzed. Thermal resistances of the various components and interfaces for the conduction path from the ring pad to the aeroshell pad were analyzed; however, the thermal resistance along the hollow section of the struts provided approximately 90 percent of this resistance. By the use of different equations for the resistance of the hollow portion of the strut, two calculations of the heat losses were performed. The first calculation was for axial conduction only along the struts, neglecting any radial conduction through the insulation. This calculation provided the minimum heat losses through the strut. At the same time, however, it provided the maximum heat flux on a centralized area of the aeroshell which is an important factor in the analysis of the aeroshell which is an important factor in the analysis of the aeroshell.

The second calculation considered the combined effect of axial conduction along the strut and radial conduction through insulation wrapped around the strut. This calculation provided a conservative estimate of the total heat losses through the base of the strut to the aeroshell pads.

Based on the equations described at the end of this section, Figure B-2 presents the total heat loss for eight struts as a function of the cold side temperature and for a hot side temperature of 1900°F. The top line presents the total truss heat loss based on the calculation including the combined effects of axial conduction in the strut and radial conduction through the insulation. The bottom line is the portion of the total heat loss that is conducted through the base of the struts to the aeroshell pad based on the above analysis. The difference in the two lines is the strut insulation loss. The middle line represents the case of axial conduction only through the struts. Total heat loss and heat conduction to the aeroshell pad for the combined axial and radial conduction will always bracket the axial conduction case. This can easily be shown by comparing the linear temperature profile of axial conduction only along a strut for a given temperature drop to the hyperbolic temperature profile for combined axial and

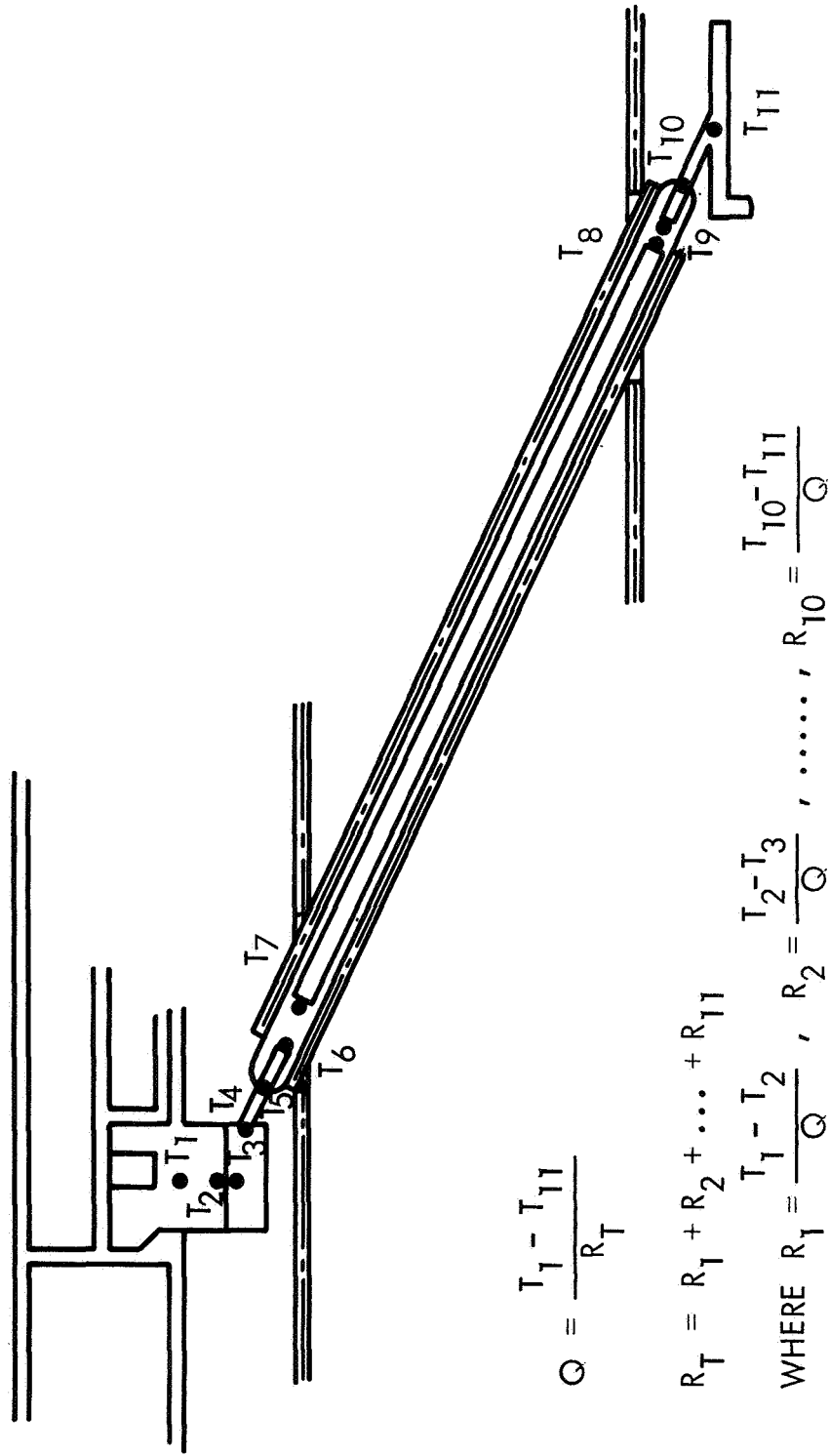


Figure B-1 STRUT HEAT LOSS MODEL

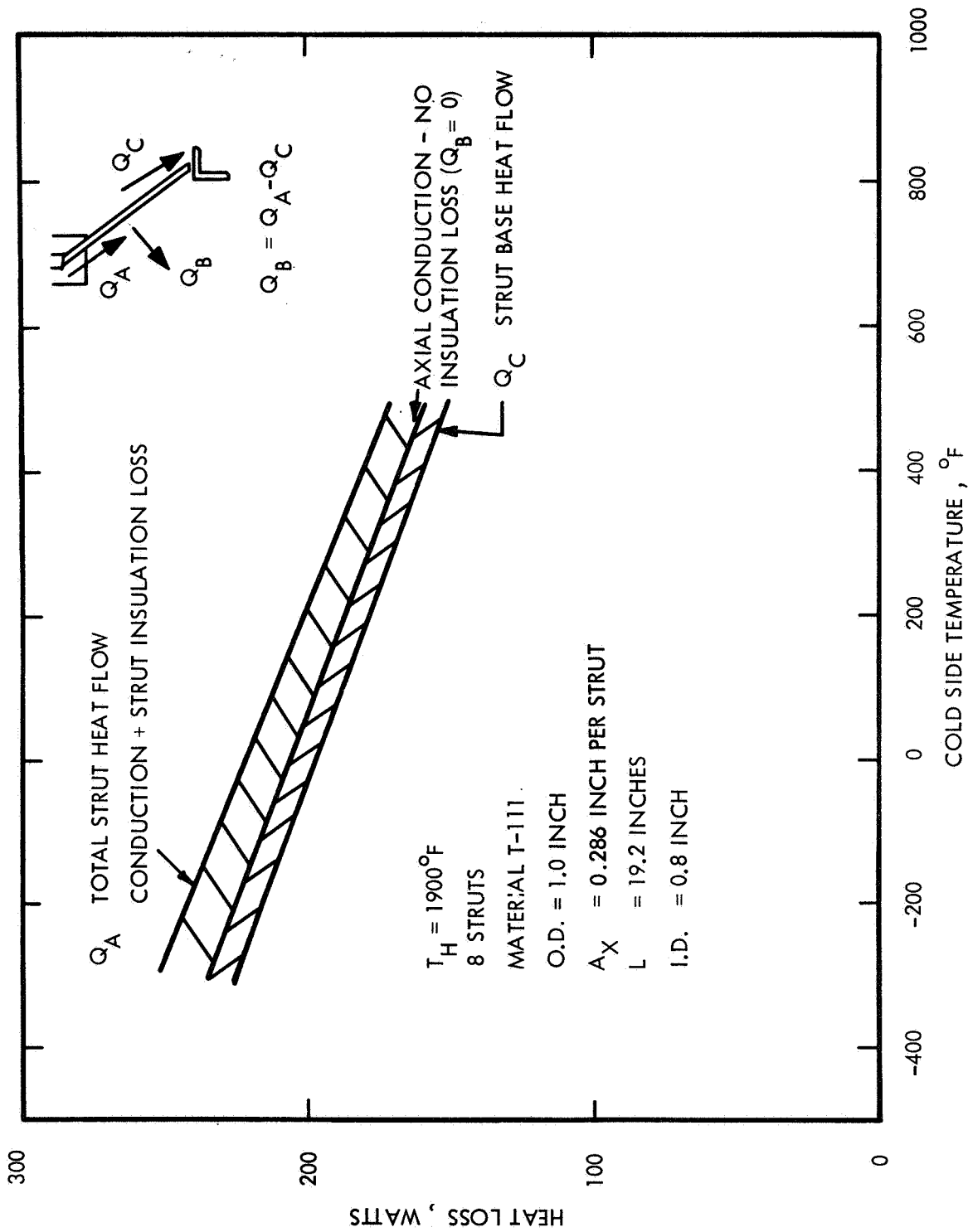


Figure B-2 STRUT HEAT LOSSES VERSUS COLD-SIDE TEMPERATURE

radial conduction along a strut. At the hot end the temperature gradient for a hyperbolic temperature profile will be steeper than the linear profile indicating a larger heat flow into the strut. At the cold end the temperature gradient will be flatter than the linear profile if the two profiles are across equal temperature drops. This indicates a smaller heat flow out of the base for a hyperbolic profile.

For evaluation of the total heat loss from the heat source a truss heat loss of 188 watts was estimated from Figure B-2 for a nominal cold side temperature of 300°F.

HEAT LOSS EQUATIONS

Heat losses through the strut pairs were calculated by the equation

$$Q = (4) \left(\frac{L}{R_T} \right) (T_h - T_c)$$

where

Q = total heat loss

R_T = total chemical resistance across strut $\left(\text{i.e., } R_T = \sum_{i=1}^{10} R_i \right)$

T_h = heat source temperature

T_c = aeroshell support ring temperature.

The resistances through each of the components for the struts are

1. Ring pad (R_1)

$$R_1 = \frac{L_1}{K_{Cb} - 1Zr A_1}$$

2. Interface between ring pad and strut pad (R_2)

$$R_2 = \frac{1}{h A_2}$$

For this calculation $h = 500 \text{ Btu/hr-ft}^2\text{-}^\circ\text{F}$

3. Strut Pad (R_3)

$$R_3 = \frac{L_3}{K_T - 111 A_3}$$

4. Strut Support (R_4)

$$R_4 = \frac{L_4}{K_T - 111 A_4}$$

5. Strut Tip (two struts in parallel) (R_5)

$$\frac{1}{R_5} = \frac{1}{R_{5a}} + \frac{1}{R_{5a}} = \frac{2}{R_{5a}}$$

where

$$R_{5a} = \frac{L_5}{K_T - 111 A_5}$$

or

$$R_5 = \left(\frac{1}{2}\right) \frac{L_5}{K_T - 111 A_5}$$

6. Strut tip (two struts in parallel) (R_6)

$$\frac{1}{R_6} = \frac{1}{R_{6a}} + \frac{1}{R_{6a}} = \frac{2}{R_{6a}}$$

where

$$R_{6a} = \frac{L_6}{K_T - 111 A_6}$$

or

$$R_6 = \left(\frac{1}{2}\right) \frac{L_6}{K_T - 111 A_6}$$

7. Hollow section of strut (R_7)

Two values of R_7 were calculated. The first is represented by pure conduction with no side losses

$$R_7 = \frac{L_7}{K_T - 111 A_7}$$

For a combination of axial conduction plus radial conduction through the multi-layer insulation, a thermal resistance may be calculated by solving the conduction equation for a constant resistance through the insulation $\left[(K/\Delta X)_{\text{insulation}} = \text{constant} \right]$. The result is similar in form to the pin fin equation for natural convection to the surroundings. The only differences is the substitution of $K/\Delta X$ for h and the selection of appropriate boundary conditions. The resulting equations are

$$R_7 = \left(\frac{1}{2} \right) R_{7a} \text{ (two struts in parallel)}$$

$$R_{7a} = \frac{\tanh(m L_7)}{m K_T - 111 A_{\text{strut}}}$$

$$m = \sqrt{\frac{2 \pi K_{\text{ins}}}{K_T - 111 A \ln \left(\frac{OD}{ID} \right)_{\text{ins}}}}$$

where K_{ins} insulation conductivity, is based on the hot side temperature of the strut and the ratio $(OD/ID)_{\text{ins}}$ corresponds to insulation thickness at the hot end of the strut.

The use of this equation requires the calculation of the ratio of heat through the base of strut to the aeroshell over the heat conducted to the strut

$$\frac{Q_b}{Q} = \frac{\tanh(m L_7)}{\sinh(m L_7)}$$

The insulation conductivity is very strongly temperature dependent, and decreases at a rate approximately equivalent to $1/L$ along the strut since the temperature varies approximately by this ratio. To maintain the above ratio the insulation thickness should, therefore, be tapered by the inverse ratio of the length. In the design the insulation is tapered linearly which provides more insulation than is necessary. Thus, the above equations yield a conservative estimate of side losses.

8. Strut Tip at Base (R_8)

$$R_8 = \left(\frac{1}{2}\right) \left(\frac{Q_b}{Q}\right) \frac{L_8}{K_T - 111 A_8}$$

9. Strut Tip at Base

$$R_9 = \left(\frac{1}{2}\right) \left(\frac{Q_b}{Q}\right) \frac{L_9}{K_T - 111 A_9}$$

10. Strut Support at Base

$$R_{10} = \frac{Q_b}{Q} \frac{L_{10}}{K_T - 111 A_{10}}$$

The total resistance for one pair of struts was calculated for a 1900°F hot side temperature to be

$$R_T = 36.42^\circ\text{F/watt} - \text{no insulation loss}$$

$$R_T = 34.56^\circ\text{F/watt} - \text{insulation loss}$$

APPENDIX C

HEAT SOURCE FABRICATION PLAN

C1.0 INTRODUCTION

The basic manufacturing approach is to provide a welded and precision machined unit into which fueled capsules can be quickly and accurately positioned and retained. Since, at the time of assembly, the fuel capsules are hot, thermally, and radioactive and remotely handled, it is imperative that the capsules and retainers accurately nest in the heat source plate and that the assembly operations be performed under strict conditions of cleanliness.

The most important items in manufacturing are welding and its related operations; cleaning, equipment, weld procedure, heat treatment, and inspection. In this particular design, the welding of the heat source plate and its components is critical. The metal Cb-1Zr is specified for this component, and this material can be successfully welded only by minimizing contamination from all sources. The purity level of the raw material must be within fixed material specification limits. All parts must be chemically cleaned prior to welding and their cleanliness retained until used within a welding chamber. The welding chamber, either vacuum or inert gas filled, should have a low leak rate which is frequently monitored.

The weld shrinkage produced by the numerous welds on the heat source plate will undoubtedly cause distortion of this item. The entire approach to the welded assembly has been aimed at reducing this distortion. The sequence of assembly of the detail parts must impart maximum rigidity to the structure during welding. Weld sequence recommendations have been developed to permit minimum distortion. Where the geometry of the heat source plate allows it, Electron Beam (EB) welding is substituted for Tungsten Inert Gas (TIG) welding. A stress-relieve is specified where it is anticipated that additional welding would cause severe distortion or where it is required prior to machining. This approach is apparent in the description which covers the detailed fabrication of the heat source plate.

The normal accepted method of inspecting weld joints of Cb-1Zr metal is the combination of visual and radiographic techniques. There are several joints (e.g., the joint between the plenum cover and support ring, Figure 3-95) on the heat source plate where the design geometry prevents any accurate inspection by radiography. A visual inspection at a magnification of 50X could be used; however, an alternate for radiography should be considered if visual only proves unsatisfactory.

In the manufacture of a unique design, such as the IRV heat source, there is always the question of equipment limitations and availability and even of the technical feasibility of some processes or operations.

All of the raw material forms of Cb-1Zr, including the cover plate, pancake forging, and the ring forging for the support ring were reviewed with Fansteel Metallurgical Corp. They can produce all items. Two companies, National Beryllia Corp. and the Brush Beryllium Co., have verified their ability to cast the BeO blocks in the specified sizes. Several companies have enclosed welding chambers in which the

TIG welding can be performed. This is also true for the EB welding. However, only one company was located, J.W. Rex Co., which has a vacuum, heated furnace in which the cover and fuel plate can be stress-relieved.

The feasibility of obtaining sound welds by electron beam welding of the joint between the capsule cradles and the top plate is questionable. Experimental work has shown that cold shuts cannot be completely eliminated from the root of the partial penetration electron beam welds in thick sections of metals. Before this welding is initiated, qualification welds should be made and examined. If cold shuts exist at the root of the weld, either the joint geometry should be changed or an alternate welding process should be substituted.

It should be understood that this is a particular manufacturing plan based on the preliminary IRV heat source design as presented and on the best of several alternate approaches. Changes in design, tolerances and materials or the results of development studies could alter specific details in this design.

C2.0 MANUFACTURING DESCRIPTION

The manufacturing description as presented here is essentially a detailed account of the operations presented on the Manufacturing Plan Charts. (Figures C-1, C-3, C-5 and C-6.)

C2.1 SUPPORT STRUCTURE (Figures C-1 and C-2)

C2.1.1 Plate

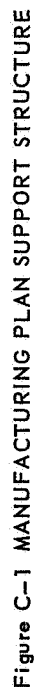
The plate is obtained by sawing a circle from a square blank of 0.060-inch-thick material, turning to the finished diameter and milling or notching the cutouts in the periphery.

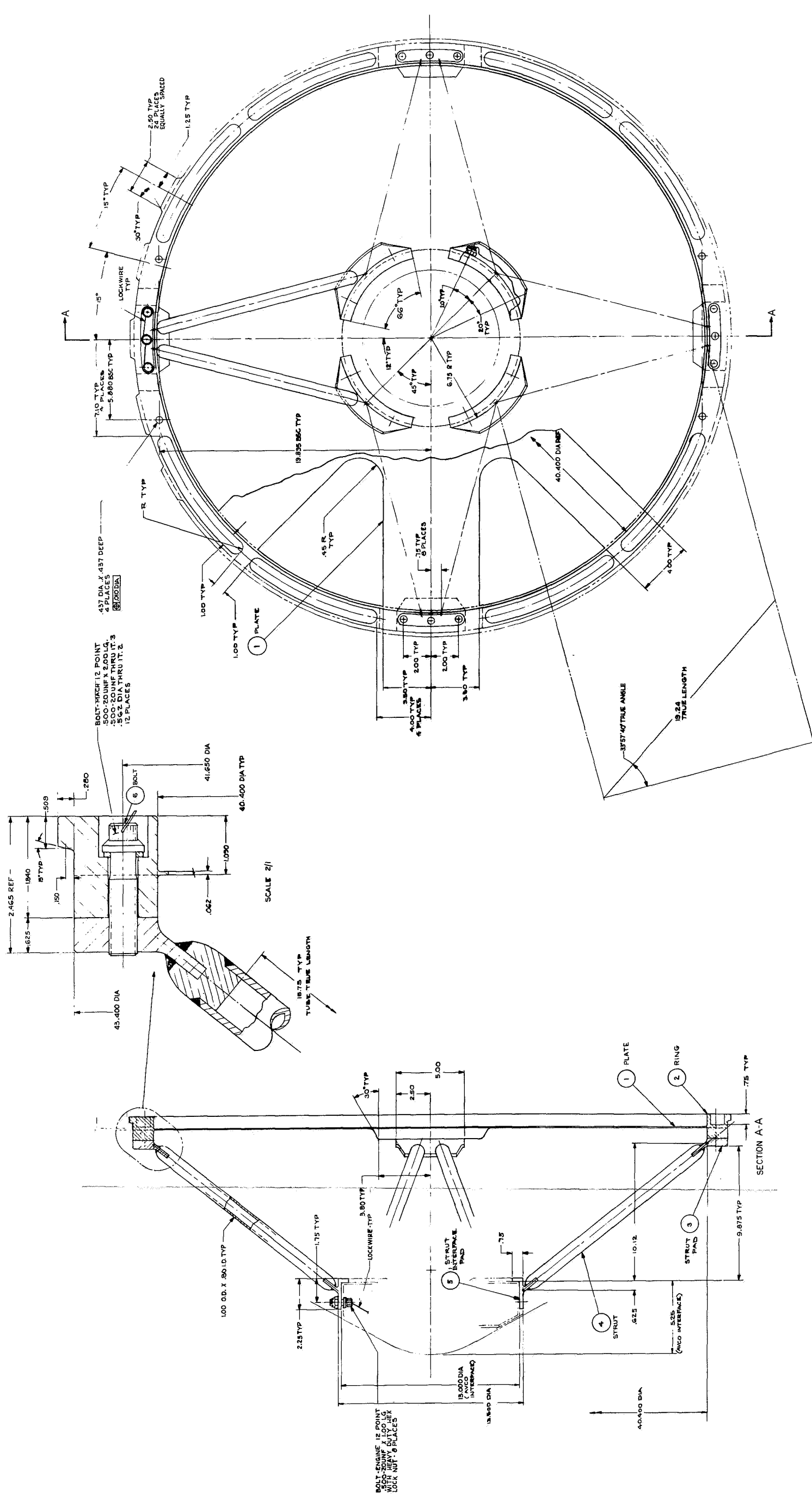
C2.1.2 Ring

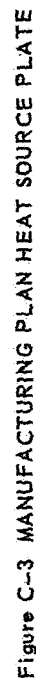
This item is made from a ring forging which receives a raw material inspection in the as-received condition. All surfaces, top, bottom, inside and outside diameters, and tangs are rough machined. The inside diameter of the projection is bored to finished size, allowing for a press fit with the plate.

C2.1.3 Subassembly, Ring and Plate

Both items are cleaned by pickling. The plate is assembled into the projection of the ring by a light press fit and the butt joint is EB (Electron Beam) welded. Since expansion of the parts during welding is restricted by the ring, a staggered sequence is used to prevent buckling or distortion of the plate. The welded assembly is stress-relieved at 2200°F for one hour in a vacuum followed by visual and radiographic inspection of the welds. The assembly is finish-machined. With the top surface down, the lower half of the inside diameter is bored, the bottom surface is faced, and the outside diameter including the tang is faced. The part is reversed and the top half of the inside diameter is bored and the top surface is faced. As a weight reduction measure, cutouts are milled in the bottom of the ring and slots are milled in the top half. The 12 holes for the assembly bolts and the two locking pin holes are then drilled.







C2.1.4 Strut Pad

The four strut pads are machined from T-111 bar stock. All exterior surfaces are milled to final dimensions. Three assembly bolt holes are drilled and tapped in each strut pad.

C2.1.5 Strut Interface Pad

The strut interface pad is manufactured from a ring forging. The bottom surface is faced and the two inside diameters are bored, allowing stock for final machining after the strut assembly is welded. The top surface is faced and the outside diameter and the tab are turned to final size. The pads are obtained by sawing the ring into four pieces.

C2.1.6 Struts

Tubing is cut to length and the ends are faced. The end plugs are cut from bar stock and only the fit for the inside diameter of the tubing is machined. The end plugs are inserted into the tubing and are butt-welded to the tube by TIG (Tungsten Inert Gas) welding process. This should be done in a vacuum-purged weld box back-filled with helium. The welds are inspected. The taper and slot are machined on both ends of the strut.

C2.1.7 Subassembly - Strut Pads, Struts and Interface Pads

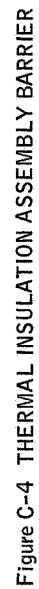
These parts are fabricated into an assembly using a locating and welding fixture. The four strut pads with the top surface down are bolted to the base of the welding fixture. The interface pads are clamped to the top of the fixture. The struts are positioned on the tabs of both pads and clamped in place. Both strut ends are tack welded to the tabs and the strut clamps are removed. The strut ends are then welded to the tabs. The joint is fillet welded, by the TIG welding process in a helium-filled weld box. The welded assembly is removed from the fixture and the welds are inspected.

The weldment is placed in a machining fixture in which the strut pads are bolted to the base of the fixture and the strut interface pads are rigidly clamped at the top. Those surfaces on the interface pads which mate with the aeroshell lower support ring are finished-machined while maintaining the height from the bottom of the strut pads to flange of the interface pads. The strut assembly is then joined to the Multi-foil thermal insulation assembly as shown on Figure C-4.

C3.0 HEAT SOURCE PLATE (Figures C-3 and C-4)

C3.1 DESCRIPTION

Starting with a flat circular plate the outside diameter of the top plate is rough turned, allowing stock for finish after welding of the fuel plate and the bottom side is faced. Two flats, diametrically opposite are milled on the edge. Since the coolant passages holes will be hidden after welding, these holes along with the inlet and outlet holes will be predrilled in the plate at this time. To assure accurate location of these holes with reference to the center of the plate, the drilling should be performed on a numerically controlled machine.



Technical drawing of a circular component, likely a fuel element, showing a cross-section and a top view.

Cross-section (Left):

- Central layer: FUEL PLATE (SEE DWG 92J617)
- Second layer: THERMAL INSULATION (100 LAYERS OF .0005 THICK ZIRCONIUM DIOXIDE)
- Third layer: .015 TITANIUM TYP
- Outer layer: FLANGE IN AEROSHELL (SEE DWG 92J617)
- Dimensions: 48.200 DIA (fuel plate), 48.200 DIA (insulation), 48.200 DIA (titanium cladding)
- Section line: A-A

Top View (Right):

- Overall diameter: 36.18 DIA
- Four smaller holes are shown, each with a diameter of .250 DIA and a 12 POINT BOLT.
- Section line: A-A

C3.1.1 End Bar

The two end bars are machined from rectangular bar stock by sawing the bar stock to length, milling the inside surface and turning the outside diameter to a rough dimension.

C3.1.2 Rib

The ribs are obtained by shearing rectangular stock to length, followed by milling the top and bottom surfaces. The ribs are milled to various length and different 90-degree notches are milled in the ends depending upon the location of the rib to the ACHX header.

C3.1.3 Support Ring

The ring forging receives a raw material inspection and all exterior surfaces are rough machined. Since this is forged material followed by considerable rough machining, a stress-relieve (2200° F for 1 hour in vacuum) is performed to reduce residual stresses. After stress-relieve the top surface, inside and outside diameter, and three weld preparations are finished-machined. The four latch mechanism holes are drilled and counterbored in the web.

C3.1.4 Cross Rib

Unlike the main ribs, all the cross ribs are identical in size. They are sheared to length, stacked and milled on each edge.

C3.1.5 Plenum Outer Wall

The plenum outer wall is obtained by butt-welding (TIG in an inert gas filled welding chamber) two semi-circular pieces which have been rolled to the proper diameter and the ends of which were milled as a weld preparation. Both welds are inspected visually and by radiography. After inspection the diameter of the plenum outer wall is sized by an expansion mandrel or by re-rolling. If a close fit-up of this part is required, it will be necessary to obtain the finished size by machining.

C3.1.6 Baffle Plate

Since it is necessary to fit the baffle plate into a welded assembly, it is preferable to mill the length and width of the baffle plate after measurements are taken from the weldment.

C3.1.7 Plenum Cover

The plenum cover consists of four circular segments of two different arc lengths. It is split in this manner to allow for the final seal weld of the baffle. The four segments are layed out on a flat plate and sawed out. The outside diameter, inside diameter, and weld preparation are finished machined. The proper arc length is obtained by milling the ends.

C3.1.8 BeO Blocks

The BeO blocks are purchased from an outside vendor from a detail drawing. Stock should be allowed on each edge for selective fitting of these blocks at assembly. National Beryllia Corp. and The Brush Beryllium Co. have verified their capability of producing the BeO blocks as designed. This includes producing a formed radius on those blocks which have peripheral locations.

C3.1.9 Retaining Plates

The retaining plates are manufactured by shearing a developed length and width from flat sheet. A radius is blanked on one end of those plates which are located at the periphery. The weight reduction holes are either punched or drilled, 90-degree notches are blanked in each corner and each side is bent 90 degrees.

C3.1.10 Bottom Cover Plate

The bottom cover plate is made by sawing a circular piece from a flat plate followed by turning the outside diameter and the weld preparation. Since this plate is plug welded to the ribs and cross ribs at various locations, the holes for plug welding are drilled prior to assembly.

C3.1.11 Capsule Cradle

Starting with rectangular bar stock, the material is sheared to length and a developed width. Using a forming die, the 90-degree circular quadrants are formed one side at a time. The ends are milled on an angle and to different lengths in order to properly arrange the cradles into a circular pattern. The edges are milled, holding an accurate dimension across the edges to ensure a close fit (metal-to-metal contact to 0.003-inch gap) into the top plate.

C3.1.12 Cradle End Plate

The two cradle end plates are produced by milling all surfaces, top, bottom, both sides of the circular quadrant, and a radius on both ends.

C3.1.13 Tube

The tube which is the guide for the locking pin is made by turning the outside diameter of round bar stock, facing both ends, and drilling and reaming the center hole.

C3.1.14 Channel Cover

The channel covers which are used as end closures on the cradles are obtained by laying out and sawing the contours from flat sheet. It is necessary to custom fit each cover at assembly since the end of each hole will have a different configuration.

C3.1.15 Weld Assembly and Machining -- Fuel Plate

The weld assembly consists of welding in position all of the detail parts described in subsection A above and as shown on the Fuel Plate Layout - Figure C-4. The

welding operations are performed in a helium or argon filled chamber. One of the required practices for obtaining sound welds with Cb-1Zr is to have thoroughly cleaned parts. Prior to welding all parts are chemically cleaned by pickling and placed in sealed polyethylene bags to prevent any contamination pickup during handling, transportation, or storage.

The assembly is started by TIG tacking and welding the end bars to the flat edges of the top plate. The numerous ribs are TIG tacked in position on the top plate and welded 3 inches from each end of the rib. The support ring is positioned by tack welding it to the top plate and the rib ends. With the aid of a template the cross ribs are located and tack welded to the ribs and the top plate. After the ribs have been tacked in place, the support ring is welded to the top plate and the ends of the ribs are welded to the support ring. The plenum outer wall is tack welded to the top plate and end bar. The baffle plate is tacked in position and welded to the support ring top plate and plenum outer wall. The four segments of the plenum cover are tack welded to the support ring and the plenum outer wall.

At this point, to minimize distortion from subsequent welding, the final welds are made on the peripheral structure. The following weld joints are completed by TIG welding: plenum outer wall to top plate and end bar, plenum cover to plenum outer wall, and plenum cover to support ring and baffle plate to plenum cover. Then a preferred developed welding sequence is used for welding the ribs and cross ribs to each other and the top plate. The assembly is then stress-relieved for one hour in vacuum at 2200° F. If during the welding of the ribs and cross ribs an abnormal amount of distortion is observed, an intermediate stress-relieve would be performed. After stress-relieve, the welds are inspected visually and by radiography.

Since the size of each compartment between the ribs and cross ribs will vary because of fabrication tolerances and distortions, the BeO blocks will be assembled by measuring the compartments and wet grinding the edges of the BeO blocks to suit. The retaining plates are placed over the BeO blocks, clamped against the blocks and welded to the ribs and cross ribs with an intermittent weld. The bottom cover plate is assembled and the location of the cross members in relation to the plug weld holes is checked. The bottom cover plate is tacked and welded to the support ring and is plug welded to the ribs and cross ribs. To prepare for the assembly of the capsule cradles, the top plate is machined by facing the top surface and form milling the pockets and steps. After machining, these surfaces are chemically cleaned by immersing approximately 1.5 inches of the weldment in the inverted position. The capsule cradles and the cradle end plates are fitted into the top plate, inspected for maximum allowable gap and electron beam welded to the top plate. The assembly is stress-relieved again in an identical manner and the EB welds are inspected. The outside diameter of the capsule cradles is machined until it is flush with the top plate periphery. The top surface of the welded assembly is milled and the holes are drilled and tapped in the capsule cradle on a tape controlled machine. Chemical cleaning of the top portion of the weldment is repeated. Four tubes are welded to the capsule cradles. To enclose the channels beneath the capsule cradles, the channel covers are custom fitted and welded to the cradles and top plate. The remainder of the welds are inspected and the machined and fabricated dimensions are inspected and recorded.

C4.0 COVER AND FUEL PLATE ASSEMBLY (Figure C-5)

C4.1 DESCRIPTION

C4.1.1 Cover

The pancake forging for the cover receives a raw material inspection prior to rough machining all surfaces, outside diameter and both sides. The semicircular grooves in the bottom side are rough milled one at a time with a form milling cutter. The top contour is rough milled in a similar manner and the cutouts in the periphery are also milled. At this point an in-process stress-relieve is performed since this is a forged material from which considerable material has been removed and the stress-relieve will eliminate distortion during final machining. The semicircular grooves are milled again, allowing stock for final machining when the cover and fuel plate are assembled. The flat bottom surface, the top contour and the peripheral cutouts are milled to finished size. The bolt holes are drilled on a numerical controlled machine with the same tape as used for the fuel plate so that the holes coincide when the plate and cover are assembled.

C4.1.2 Hold-Down Bar

The hold-down bars are manufactured by obtaining special roll-formed tubing, saw milling the tubing to various lengths, and milling the bolt slots into the side.

C4.1.3 End Plate

The end plate raw material is machined on both sides to the required thickness. The material is sheared to length and width, three sides are milled and the radial contour is milled. The end plates for the cover and fuel plate are both made in this manner.

C4.1.4 Nut

The nut is a simple screw machine item which is made by spherically turning one end, drilling and tapping the center hole and cutting-off to the proper length.

C4.1.5 Locking Pin

The locking pin is made from round bar stock on which all surfaces are machined and the two bearing surfaces are ground to a fine finish.

C4.1.6 Spring Guide and Spring

The spring guides are machined items which are obtained by turning the two outside diameters, facing both ends, reaming and counterboring the center hole and boring the steps in the center hole.

C4.1.7 ACHX Connection

The four ACHX Connections are manufactured from tubing which has been sawed to the correct length. The outside diameters and grooves are turned, the undercut is bored and the bevel is faced.

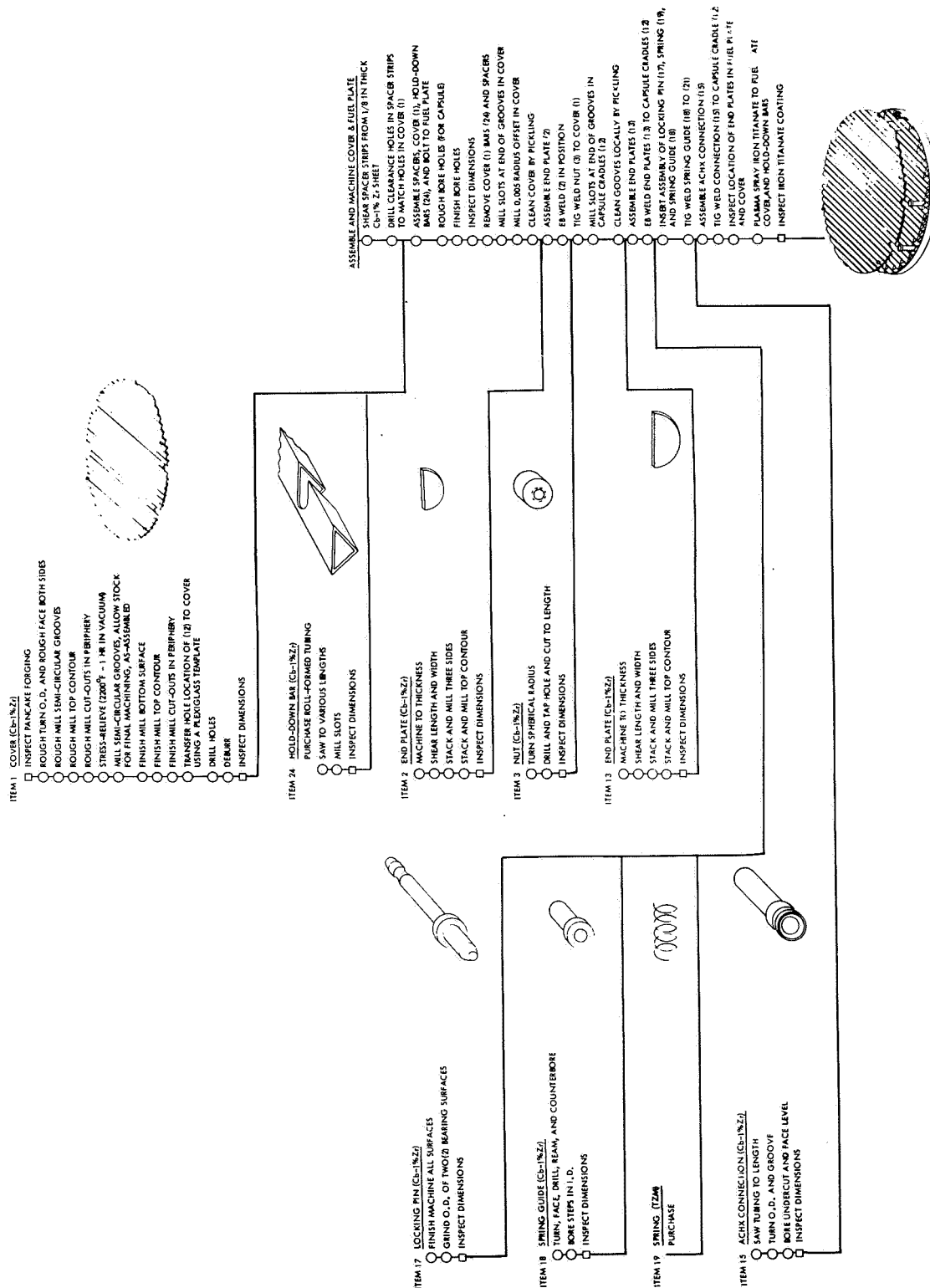


Figure C-5 MANUFACTURING PLAN COVER AND FUEL PLATE ASSEMBLY

C4.1.8 Assemble and Machine Cover and Fuel Plate

To maintain the specified gap between the cover and fuel plate, special spacers are used as the cover is bolted to the fuel plate with hold-down bars and assembly bolts. The spacers are sheared from 1/8-inch-thick sheets and drilled with bolt clearance holes which match the holes in the capsule cradles. The spacers are positioned on each capsule cradle prior to assembling the cover and fuel plate. Using a special boring bar which is supported at both ends, the capsule channels are rough and finished bored. The bolts, bars, spacers, cover and fuel plate are disassembled. Slots for the end plates are milled at the end of each capsule groove in the cover and the 0.005-inch radial thermal gap is milled in each capsule groove. The cover end plates and nuts are chemically cleaned by pickling, and the end plates are assembled into their machined slots. The end plates are electron beam welded to the cover by a small butt weld at each outside edge. The nuts which are used for lifting the cover are TIG welded to the cover. The EB and TIG welds are visually inspected. Slots for the end plates are milled at the end of each capsule groove in the fuel plate. These slots are locally cleaned, followed by electron beam welding the end plates to the fuel plate. The locking pin, spring and spring guide are assembled, inserted into the counterbored hole of the support ring and the spring guide is welded to the support ring. The four ACHX connections are assembled and welded to the capsule cradle plate and these welds are visually inspected.

An emittance coating of iron titanate is applied to the exterior surfaces of the cover, fuel plate and hold-down bars.

C5.0 INSULATION ASSEMBLY (Figure C-1)

The insulation assembly consists of multi-foil thermal insulation placed in a titanium structure which supports and protects the insulation. The titanium structure is a welded assembly of sheet metal parts which are readily fabricated by standard sheet metal forming and machining operations. The welding is accomplished with TIG welding which has become the generally accepted process for titanium. Since this design requires mostly tee joints, a filler metal of the same chemical analysis as the parent metal should be used. Because of the extreme chemical reactivity of the molten titanium, thorough cleaning and drying of joints and filler material before welding is important. Also the titanium oxide scale in the joint area should be removed by a thorough wire brushing with a clean, stainless steel brush.

C6.0 FINAL ASSEMBLY (Figure C-6)

To facilitate final assembly, an assembly stand is used and it consists of a base which holds the support structure in an identical manner as it is mounted on the aeroshell and side members which support the insulation assembly in its final location. Also the assembly stand should be an integral part of the shipping container, preferably having the assembly stand base also serve as the shipping container base and thus eliminating any disassembly prior to shipping or when the unit is received at the fuel loading facility.

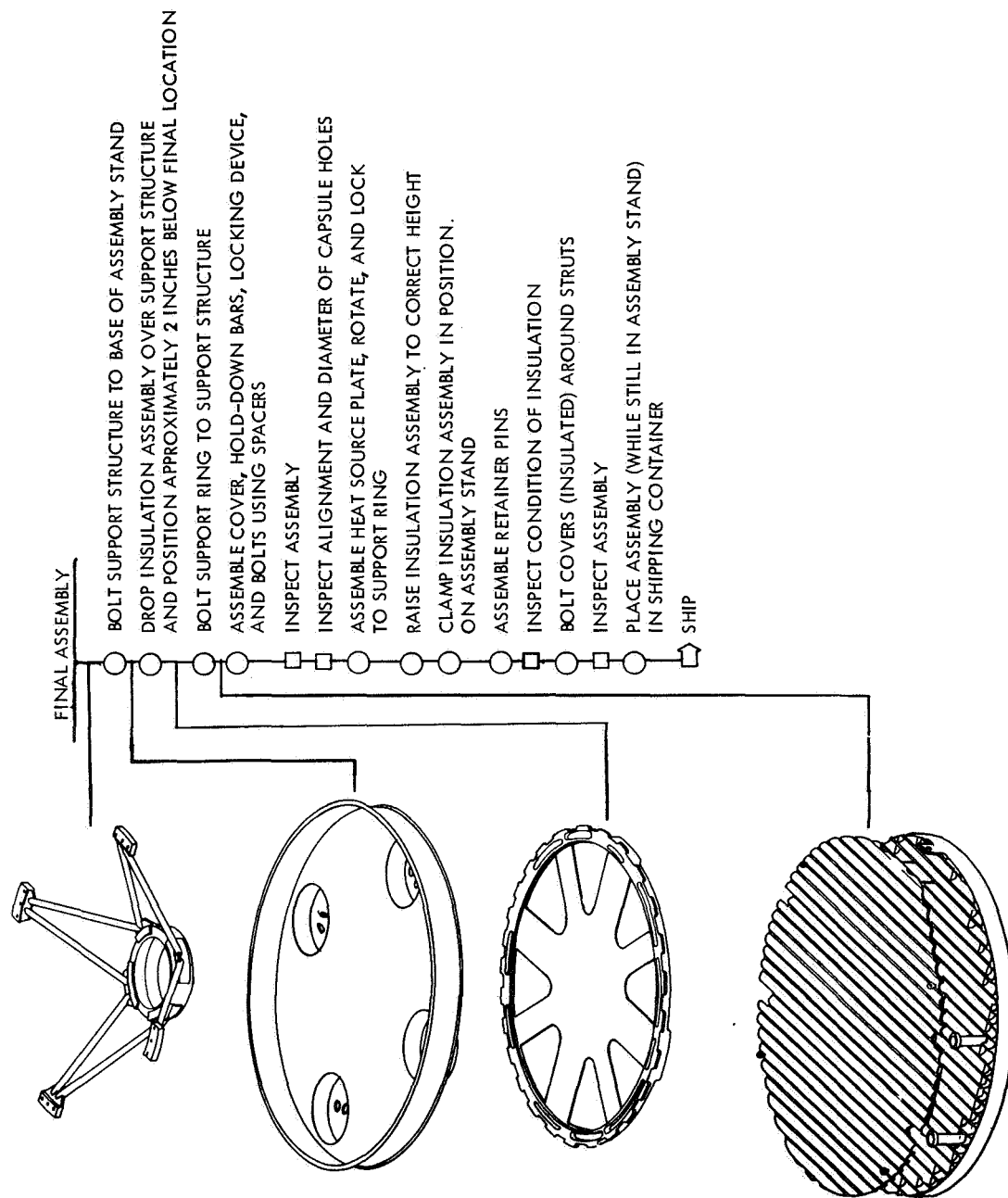


Figure C-6 MANUFACTURING PLAN FINAL ASSEMBLY

The final assembly is initiated by bolting the support structure to the assembly stand base. With the four port covers removed, the insulation assembly is lowered over the support structure and positioned approximately 2 inches below its final location. The support ring is bolted to the support structure using preset torque wrenches. The same spacers, which were used during the capsule bore machining, are placed on the fuel plate and the cover, hold-down bars and bolts are assembled. The mating of these parts is inspected and the alignment and diameter of the capsule are optically measured. The heat source plate is assembled to the support ring, rotated and locked in position. The insulation assembly is raised to the correct height and clamped to the assembly stand. After the retainer pins are inserted, the insulation is inspected for possible damage. The four port covers are placed over the insulated struts and bolted to the insulation assembly. After an inspection of the complete assembly, the unit and assembly stand are placed in a special shipping container and can be shipped to the launch facility where the fuel capsules can be installed.

DISTRIBUTION

<u>Addressee</u>	<u>No. of Copies</u>
NASA Lewis Research Center	
21000 Brookpark Road	
Cleveland, Ohio 44135	
Attn: Lloyd I. Shure, Mail Stop 500-201	3
W. T. Wintucky, Mail Stop 500-201	1
H. O. Slone, Mail Stop 500-201	1
B. Lubarsky, Mail Stop 500-201	1
D. Packe, Mail Stop 500-201	1
T. A. Moss, Mail Stop 500-201	1
R. Mather, Mail Stop 302-1	1
J. E. Dilley, Mail Stop 500-309	1
H. Bloomfield, Mail Stop 500-201	1
P. E. Foster, Mail Stop 3-19	1
R. E. English, Mail Stop 500-201	1
Library, Mail Stop 60-3	2
Report Control Office, Mail Stop 5-5	1
Technology Utilization Office, Mail Stop 3-19	1
NASA Lewis Research Center	
Plum Brook Station	
Taylor Road	
Sandusky, Ohio 44870	
Attn: J. C. Nettles, Mail Stop 7141-6	1
G. Prok, Mail Stop 7141-6	1
National Aeronautics and Space Administration	
Washington, D. C. 20546	
Attn: Dr. F. Schulman, RNP	1
B. Leefer, RNP	1
T. B. Kerr, RNS	1
T. Hagler, MTY	1
H. Roehen, RNP	1
NASA Scientific and Technical Information Facility	
Post Office Box 5700	
Bethesda, Maryland 20014	
Attn: Acquisitions Branch (SQT-34054)	1
NASA Ames Research Center	
Moffett Field, California 94035	
Attn: Library	1
V. Peterson	1
E. Katzen	1
G. Goodwin	1
NASA Manned Spacecraft Center	
Houston, Texas 77058	
Attn: Library	1

DISTRIBUTION (Cont'd)

<u>Addressee</u>	<u>No. of Copies</u>
NASA Marshall Space Flight Center Huntsville, Alabama 35812	
Attn: Library	1
L. W. Brantley/R-ASTR-AE	1
R. Boehme/R-ASTR-ED	1
 NASA Goddard Space Flight Center Greenbelt, Maryland 20771	
Attn: Library	1
 Air Force Systems Command Aeronautical Systems Division Wright-Patterson Air Force Base, Ohio 45433	
Attn: Library	1
 Power Information Center University of Pennsylvania 3401 Market Street, Room 2107 Philadelphia, Pennsylvania 19104	1
 SAMSO Los Angeles Air Force Station Los Angeles, California 90045	
Attn: Library	1
Maj. H. M. Butler	1
 NASA Langley Research Center Langley Station Hampton, Virginia 23365	
Attn: Library	1
 McDonnell Douglas Corporation Suite 620 333 West First Street Dayton, Ohio	
Attn: R. G. Donmoyer	1
 NASA Manned Spacecraft Center Houston, Texas 77058	
Attn: Tony Redding EP-5	1
Rene A. Berglund	1
 General Electric Company Flight Propulsion Division Cincinnati, Ohio 45215	
Attn: Library	1

DISTRIBUTION (Cont'd)

<u>Addressee</u>	<u>No. of Copies</u>
Jet Propulsion Laboratory 4800 Oak Grove Drive Pasadena, California 91103 Attn: Library	1 1 1
J. Mondt, Mail Stop 122-123 R. G. Ivanoff, Mail Stop 198-220	1 1
McDonnell Douglas Corporation Missile and Space Systems Division Space Systems Center 5301 Balsa Avenue Huntington Beach, California 92646 Attn: H. Coverdale R. Gervais	1 1
Battelle Memorial Institute 505 King Avenue Columbus, Ohio 43201 Attn: Library	1
General Motors Corporation Indianapolis, Indiana 46206 Attn: Library	1
Institute for Defense Analyses 400 Army-Navy Drive Arlington, Virginia 22202 Attn: Library	1
Lockheed Missiles and Space Company P. O. Box 504 Sunnyvale, California 94088 Attn: Mr. H. Greenfield	1
Aerojet-General Corporation Von Karman Center Azusa, California 91702 Attn: Library	1
Pratt & Whitney Aircraft 400 Main Street East Hartford, Connecticut 06108 Attn: Library	1
The Boeing Company Aero-Space Division Box 3707 Seattle, Washington 98124 Attn: Library S. Silverman	1 1

DISTRIBUTION (Cont'd)

<u>Addressee</u>	<u>No. of Copies</u>
Sunstrand Denver 2480 West 70 Avenue Denver, Colorado 80221 Attn: Library	1
Aerospace Corporation P. O. Box 95085 Los Angeles, California 91745 Attention: Library	1
Dr. H. Sampson	1
Martin Marietta Corporation P. O. Box 988 Baltimore, Maryland 21203 Attn: Mr. Barney Mead, Mail Stop 836	1
General Electric Company Reentry Systems Department 3198 Chestnut Street Philadelphia, Pennsylvania 19104 Attn: Mr. R. Brast	1
McDonnell-Douglas Corporation Lambert Field St. Louis, Missouri 63166 Attn: Library	1
NASA-Langley Research Center Langley Station Hampton, Virginia 23365 Attn: Mr. W. Hayes, MORL Studies Office	1
Mr. P. J. Bobbitt, Applied Mech. Br.	1
TRW Systems Division One Space Park Redondo Beach, California 90278 Attn: Library	1
A. Berman	1
U. S. Atomic Energy Commission Space Nuclear Systems Division Washington, D. C. 20545 Attn: Dr. L. Topper	1
Mr. R. L. Carpenter	1
Mr. G. Newby	1
Dr. J. A. Powers	1

DISTRIBUTION (Concl'd)

<u>Addressee</u>	<u>No. of Copies</u>
Sandia Corporation Sandia Base Albuquerque, New Mexico 87115 Attn: Library	1
Mr. A. J. Clark, Dept. 9330	1
Mr. R. W. Hunke, Dept. 9331	1
Mr. J. W. McKiernan, Dept. 9331	1
Donald Douglas Laboratories McDonnell-Douglas Corporation Richland, Washington 99352 Attn: Library	1
E. E. Warner	1
Bellcom, Incorporated 1100 17th Street N.W. Washington, D. C. 20036 Attn: Mr. C. Witze	1
Department of the Navy Naval Facilities Engineering Command Nuclear Engineering Division Washington, D. C. 20390 Attn: Mr. M. Starr	1
Atomics International P. O. Box 309 8900 DeSoto Avenue Canoqa Park, California 91304 Attn: Mr. W. Botts	1
USAF Aeropropulsion Laboratory Wright-Patterson AFB, Ohio 45433 Attn: Mr. G. Thompson (APIP-I)	1
NASA Lewis Research Center 21000 Brookpark Road Cleveland, Ohio 44135 Attn: R. N. Weltmann MS6-2	1
Mound Laboratory Miamisburg, Ohio 45342 Attn: C. Henderson	1
Navy Space Systems Activity Air Force Unit Post Office Los Angeles, California 90045 Attn: R. Silverman	1
Research Library - Lowell	3
Research Library - Wilmington	1
Reports Distribution Center	62

Unclassified
Security Classification

DOCUMENT CONTROL DATA - R & D		
(Security classification of title, body of abstract and indexing annotation must be entered when the overall report is classified)		
1. ORIGINATING ACTIVITY (Corporate author) Avco Government Products Group Avco Applied Technology Division 201 Lowell St., Wilmington, Massachusetts 01887		2a. REPORT SECURITY CLASSIFICATION None
		2b. GROUP
3. REPORT TITLE Isotope Reentry Vehicle Design Study Preliminary Design -- Phase II -- Final Report		
4. DESCRIPTIVE NOTES (Type of report and inclusive dates) Final Report		
5. AUTHOR(S) (First name, middle initial, last name)		
6. REPORT DATE August 1969	7a. TOTAL NO. OF PAGES 456	7b. NO. OF REFS 49
8a. CONTRACT OR GRANT NO. NAS 3-10938	9a. ORIGINATOR'S REPORT NUMBER(S) AVSD-0306-69-RR	
8b. PROJECT NO.		
c.	9b. OTHER REPORT NO(S) (Any other numbers that may be assigned this report)	
d.	NASA CR-72555	
10. DISTRIBUTION STATEMENT		
11. SUPPLEMENTARY NOTES	12. SPONSORING MILITARY ACTIVITY Technical Management NASA Lewis Research Center Bryton Cycle Branch Cleveland, Ohio	
13. ABSTRACT <p>This document summarizes the Phase II preliminary design effort on the Isotope Reentry Vehicle (IRV) study. The major objective of the entire study (Phases IA, IB, and II) was to develop a preliminary design of a 25 kw_t PU 238 IRV. Primary emphasis was placed on safety considerations and developability in the design.</p> <p>The Phase II study followed two previous efforts of the program, i.e., Phases IA and IB. During Phase IA various IRV, heat source, and heat source exchanger concept combinations were developed and evaluated. During Phase IB, three of the more promising combinations resulting from Phase IA were further evaluated at the conceptual design level. The results were then used to select a reference concept for preliminary design in Phase II.</p>		

DD FORM 1 NOV 55 1473

Unclassified
Security Classification

Unclassified
Security Classification

14. KEY WORDS	LINK A		LINK B		LINK C	
	ROLE	WT	ROLE	WT	ROLE	WT
Isotope Reentry Vehicle Brayton Cycle Power Supplies Plutonium 238 Fuel Capsule Heat Shields Refractory Metal Structure Impact Attenuation						

Unclassified
Security Classification